MITNE-39
(IDO-11, 107)

THE EFFECTS OF REACTOR IRRADIATION ON SANTOWAX OMP AT 610°F AND 750°F

Report Prepared
by
C. D. Sawyer
E. A. Mason

M. I. T. Organic Coolant Irradiation Project Staff:

E. A. Mason, Project Supervisor
W. N. Bley, Project Engineer

T. W. Carroll	A. H. Swan
J. P. Casey	J. F. Terrien
R. A. Chin	G. L. Woodruff
E. J. Fahimian	J. F. Howard
G. C. Nullens	A. J. Pierni
C. D. Sawyer	A. L. Seaver

DEPARTMENT OF NUCLEAR ENGINEERING
MASSACHUSETTS INSTITUTE OF TECHNOLOGY
CAMBRIDGE, MASSACHUSETTS

M. I. T. DSR PROJECT NO. 8710

Work Performed for the Idaho Operations Office,
U. S. Atomic Energy Comission Under
Contract No. AT(10-1)-1067

Issued: September, 1963

THE EFFECTS OF REACTOR IRRADIATION ON SANTOWAX OMP AT 610°F AND 750°F

ABSTRACT

Santowax OMP has been irradiated in the M.I.T. In-Pile Loop Facility at 610°F and at 750°F. At both temperatures the loop was operated in a transient phase and a steady-state-HB phase. In the transient phase, unirradiated material was allowed to degrade to 60 w/o DP. In the steady-state-HB phase, the HB content of the coolant was maintained constant at about 33 w/o by the removal and distillation of samples and the replacement of the HB by unirradiated material before returning the samples to the loop.

Neutron and gamma ray doses were measured with adiabatic calorimeters and foil monitors. The average dose rate to the coolant in the core region of the in-pile section was about 0.5 watts/gm, of which 37% was due to fast neturon interactions and 63% to gamma ray interactions.

Terphenyl concentrations were measured by gas chromatography and HB concentrations by distillation. Analysis of the transient phase terphenyl concentration and absorbed dose data showed that first order kinetics provided an adequate description of the degradation rate of the terphenyls. At 610°F no significant difference in the stabilities of the terphenyl isomers was found and the overall degradation rate of the coolant was $G^*(-omp) = G(-omp)/C_{omp} = 0.26 \pm 0.01$ molecules of terphenyl degraded per 100 ev absorbed in the terphenyls. At 750°F the terphenyl isomer stabilities were in the order para>meta>ortho. After corrections for out-of-pile pyrolysis the overall degradation rate of the coolant was $G^*(-omp) = 0.49 \pm 0.02$. The results are compared to those of other investigations.

For the 610°F irradiation the radiolytic gas generation rate was G(total gas) = 0.037 ± 0.003 molecules of gas produced per 100 ev absorbed in the coolant mixture, the principal product being hydrogen. During the 750°F irradiation the generation rate was G(total gas) = 0.105 ± 0.008, with a marked increase in the evolution of methane.

Physical property measurements included density, viscosity, specific heat, thermal conductivity, number average molecular weight, gas solubility, carbon-hydrogen content and ash content. The increase in viscosity with increasing DP concentration was significantly less for the 750°F irradiation than for the 610°F irradiation.

Heat transfer measurements showed that standard correlations could be used to determine the heat transfer rates using the physical properties of the irradiated coolant. The correlation obtained for the data of both irradiations was $Nu = 0.0079(Re)^{0.9}(Pr)^{0.4} \pm 10\%$. No evidence of scale buildup on the heat transfer surfaces was observed over the entire period of operation of the experiment. The results of preliminary measurements with a fouling probe are also reported.

PREFACE

This report is essentially divided into three parts: summary, main body and appendix. The summary (Chapter 1) provides an outline of the main conclusions drawn from the study. The main body (Chapters 2-6) discusses, in reasonable detail, all the results obtained. The appendix (Appendices A1-A4) provides supplementary detail of the procedures used and tabulates much of the data referred to in the main body.

The data presented in this report are the result of a group effort by the staff of the M. I. T. Organic Coolant Irradiation Project. The primary responsibility of each of the members of the team was as follows: E. A. Mason (project supervisor), overall supervision of the program; W. N. Bley (project engineer), supervision of all phases of the program; T. W. Carroll, supervision of loop operation; J. P. Casey, physical and chemical measurements; R. A. Chin, foil dosimetry and heat transfer measurements; E. J. Fahimian, foil dosimetry, heat transfer and physical measurements; G. C. Nullens, calorimetric dosimetry; C. D. Sawyer, data analysis and aid in all experimental measurements; A. H. Swan, supervision of loop operation; J. F. Terrien, chemical measurements; G. L. Woodruff, calorimetric dosimetry; J. F. Howard, chemical measurements and loop operation; A. J. Pierni, chemical measurements and loop operation; A. L. Seaver, physical measurements. In addition to these full time members of the staff, many graduate and undergraduate students have participated in the program.

Thanks go to the members of the M. I. T. Reactor operations staff, in particular to T. J. Thompson and D. D. Lanning, for valuable assistance in incorporation of the loop into the reactor experimental programs.

Recognition should be given to the staff of the M. I. T. Computation Center, with whose aid the data reduction codes were developed and debugged. Thanks go also to the Computation Center for the use of the IBM 7090 Computer.

TABLE OF CONTENTS

TABLE OF CONTENTS (Continued)

TABLE OF CONTENTS (Continued)

APPENDICES

TABLE OF CONTENTS (Continued)

TABLE OF CONTENTS (Continued)

TABLE OF CONTENTS (Concluded)

LIST OF TABLES

LIST OF TABLES (Continued)

LIST OF TABLES (Continued)

LIST OF TABLES (Continued)

LIST OF TABLES (Continued)

LIST OF TABLES (Continued)

APPENDIX A3

LIST OF TABLES (Concluded)

LIST OF FIGURES

LIST OF FIGURES (Continued)

LIST OF FIGURES (Continued)

CHAPTER 5

LIST OF FIGURES (Continued)

CHAPTER 6

APPENDIX A1

LIST OF FIGURES (Continued)

APPENDIX A2

APPENDIX A3

LIST OF FIGURES (Concluded)

CHAPTER 1

SUMMARY

1.1 Introduction

Organic liquids used as coolants in nuclear reactors have several desirable characteristics. These features include:

1. Low operating pressures at high coolant temperatures (100 - 200 psig at 600 - 700°F).
2. Negligible corrosion of conventional structural materials such as carbon steel.
3. Low induced activity in the coolant.
4. Feasibility of use of the organic coolant as moderator because of its hydrogen content, permitting compact and simple core designs.

There are, however, some undesirable characteristics possessed by organic coolants. First, organic coolants undergo irreversible radiolytic and thermal degradation. Aromatic hydrocarbons, particularly polyphenyls, have proven to be the most stable of the organic coolants tested to date (1.1). The main reaction induced by the radiation of polyphenyls is that of polymerization to a variety of hydrocarbons having higher molecular weights, densities, viscosities, and hence poorer heat transfer properties, than the original materials. Consequently, in the operation of an organic cooled reactor the degradation products are continually removed and fresh coolant makeup added. Makeup costs of 0.75 - 0.90 mills/kwhr(e) have been reported (1.2) for organic moderated and cooled power reactors. Second, organic coolants have relatively poor heat transfer properties due to low thermal conductivity. These coolants also tend to foul heat transfer surfaces if excessive temperatures and/or large concentrations of inorganic particulates are allowed during operation of an organic cooled reactor (1.3).

Current organic cooled nuclear reactor concepts are generally based on the use of mixtures of the isomers of terphenyl, since these

materials have been found to be the most stable of the organic coolants tested to date (1.1). Thus, Santowax OMP was the first material chosen for study at the M.I.T. In-Pile Loop Facility. Santowax OMP is a commercial mixture of terphenyls having the following nominal composition:

Less than 2 w/o biphenyl plus degradation products
~10 w/o ortho-terphenyl
~60 w/o meta-terphenyl
~30 w/o para-terphenyl.

This material was irradiated in the M.I.T. in-pile loop at 610°F and at 750°F. The principal studies performed on the irradiated material were:

1. Analyses of the chemical composition and degradation rate of the irradiated coolant.
2. Physical property measurements. Density, viscosity, specific heat, thermal conductivity, number average molecular weight, gas solubility, coolant melting point, carbon-hydrogen content and ash content of the irradiated coolant were the most important physical measurements.
3. Heat transfer measurements, including a study of the rate of fouling of the heat transfer surfaces.

1.2 Procedure

The in-pile loop at M.I.T. is an all-stainless-steel system with a total circulating volume of 5800 cc and is capable of operation to 800°F and 600 psig. Design and operating characteristics of the loop are given in Table 1.1. A detailed description of the loop has been given by Morgan and Mason (1.4).

An important aspect of the work at M.I.T. has been to correlate the changes in the chemical and physical properties of the irradiated Santowax OMP with the energy absorbed from fast neutron and gamma ray radiations. Because previous work at BEPO (1.5) and at the Curtiss-Wright Research Reactor (1.2) has indicated that fast neutrons may be more effective than gamma rays in degrading the terphenyls, an extensive calorimetry program, employing adiabatic calorimeters, was undertaken to determine both the fast neutron and the gamma ray dose rates in the in-pile

TABLE 1.1

Design and Operating Specifications of the M.I.T. In-Pile Loop

Bulk temperature	to 800°F
Loop pressure	to 600 psig
Materials of construction	Type 304 and 316 stainless steel
Volume of in-core capsule	205 cc
Circulating volume with 600 cc in surge tank	5200 cc
In-pile to out-of-pile volume ratio	0.04
Circulating flow rate	2 gallons/minute
Maximum test heater heat flux	400,000 Btu/(hr)(ft^2)
Test heater wall temperature	to 1000°F
Velocity in test heater	to 20 ft/sec
In-core capsule located along axis of central fuel element of MITR	
Specific dose rate at center of reactor to Santowax OMP	0.33 watts/gm/MW of reactor power
Ratio of fast neutron dose rate to gamma ray dose rate	0.37/0.63

section. Due to space limitations in the thimble in the reactor, it was not possible to make calorimetry measurements with the in-pile section in the reactor, so measurements were performed in 1961, before the start of the 610°F irradiation of Santowax OMP and in 1963, after the end of the 750°F irradiation of Santowax OMP.

The irradiation of Santowax OMP at 610 ± 10°F and about 100 psig was begun in August, 1961, and completed in October, 1962. The irradiation of Santowax OMP at 750 ± 5°F and about 100 psig was begun in November, 1962, and completed in April, 1963. In both irradiations, two different modes of operation were employed. At the start of each irradiation there was a transient phase, in which an initial charge of unirradiated Santowax OMP was irradiated to about 60 w/o degradation products (DP) without makeup. The DP concentration was determined by subtracting the total terphenyl concentration in the coolant from 100. Following this phase, the DP concentration was lowered to about 40 w/o by coolant withdrawal and addition of fresh Santowax OMP and a steady-state-HB phase begun. The object of this phase was to maintain a constant high boiler (HB) concentration of about 33 w/o in the coolant and to study the effects of long-term irradiation on the physical and chemical properties of the coolant. HB refers to those fractions of the irradiated coolant having higher boiling points than that of para-terphenyl. In order to maintain the HB level, samples containing about 300 grams of coolant were removed from the loop at intervals and were distilled. Each distillate was mixed with fresh Santowax OMP and returned to the loop after the next sample was taken. The still bottom fraction (i.e. HB content) of each sample was thus removed from the loop coolant.

1.3 Coolant Composition and Stability

1.3.1 Major Variables Involved

When Santowax OMP is subjected to the effects of high temperature and irradiation, a complex mixture of degradation products results. It is very difficult, if not impossible, to determine all of the components comprising the irradiated mixture, but these components can be classified into four general divisions (1.4). These are:

1. Ortho-, meta- and para-terphenyls. The terphenyls compose over 98 w/o of the unirradiated material, and in this report the

combined terphenyl content will be denoted by w/o omp.

2. High boilers (HB). This part of the coolant is composed of materials having boiling points higher than that of p-terphenyl and having molecular weights ranging from 230 (that of the terphenyls) to about 3000. The formation of these materials is the predominant and most important process occurring in the degradation of the terphenyls because of the pronounced effects of the HB on the coolant physical properties, particularly the viscosity.
3. Low and intermediate boilers (LIB). These liquid constituents have boiling points less than or equal to those of the terphenyls and have molecular weights of the order of 230. Probably no serious effect on the coolant properties results from the LIB fraction.
4. Non-condensable gases. Hydrogen, methane, ethane, ethylene and other saturated and unsaturated hydrocarbons of low molecular weight are the principal constituents. These gases dissolve to some extent in the irradiated coolant at the temperatures and pressures of the loop operation. The distinction between non-condensable gas and low boiler is not always clear.

In the work at M. I. T. it has also been found convenient to group all of the degradation products together under the label of DP. By definition, the DP concentration is (100 – w/o omp).

Previous work (1.2, 1.6, 1.7, 1.8, 1.9) has indicated that in spite of the complex mixture of degradation products formed during the irradiation of terphenyls, reasonably good correlations can be made between either the HB concentration (w/o) or the terphenyl concentration (w/o) in the irradiated mixture, and the absorbed radiation dose in the mixture. Experiments have also indicated that different types of radiation may produce different rates of damage to the coolant (1.2, 1.6, 1.10) (referred to as the LET effect). In addition, if the temperature is high enough, pyrolysis may play a significant role in the coolant decomposition (1.11, 1.12, 1.13, 1.14).

At M. I. T. only fast neutrons and gamma rays produce a significant radiation dose in the coolant (1.4). Thus the major variables considered

in the analysis of the coolant degradation data were:

1. The coolant composition measured both as weight fraction terphenyls and weight fraction HB.
2. The absorbed specific dose and its fractions of fast neutron and gamma ray doses.
3. The coolant irradiation temperature.

The weight fraction of each of the terphenyl isomers in a given sample was determined by gas chromatography. HB concentrations were determined during the steady-state-HB periods by the distillation of 300 gram samples. LIB concentrations were determined during the steady-state-HB periods by the difference between the DP and HB concentrations.

1.3.2 Measurement and Calculation of Dose Rates

Since radiolysis occurred only while the reactor was operating, it was found convenient to adopt an exposure scale based on the megawatt-hours (MWH) of reactor operation. Normal reactor operation included four days at a full thermal power of approximately 2 MW per week and a shutdown over the weekend. To reduce any pyrolytic effect on the coolant while the reactor was shut down, the loop temperature was lowered over the weekend to about 450°F. The relation between specific dose delivered to the coolant in the loop and the period of reactor operation was expressed as

$$\Delta\tau_{1-2} = \int_{MWH_1}^{MWH_2} \frac{F\rho}{M}\, d(MWH) \quad \text{watt-hr/gm} \qquad (1.1)$$

where

τ is the specific dose of fast neutron and gamma ray energy absorbed per gram of total coolant

ρ is the coolant density, gm/cc

M is the circulating coolant mass in grams

F is the in-pile dose rate factor (watt)(hr)(cc)/(MWH)(gm).

The quantity F is dependent on the carbon-hydrogen ratio of the coolant, the geometry of the irradiation capsule, the spatial distribution of the energy deposition in the capsule and on the period of reactor operation. The total in-pile dose rate factor and the fast neutron and gamma ray fractions of this factor were determined by adiabatic calorimetry (using

absorbers having widely differing fast neutron and gamma ray heating rates) both before the insertion of the in-pile section into the reactor and after its removal. The results of these determinations are given in Table 1.2. As may be seen from Table 1.2, the fast neutron fraction of the dose

TABLE 1.2

Results of Calorimetric Determination of Dose Rates

Date of Measurement	Total In-Pile Dose Rate Factor, F $\frac{(watt)(hr)(cc)}{(MWH)(gm)}$	Average Dose Rate in Core Region watts/gm	Fast Neutron Fraction of Dose Rate, f_N (%)
3/20/61	60.5 ± 2.9[a]	0.55 ± 0.02	37 ± 2
4/24/63	55.8 ± 1.9	0.51 ± 0.02	37 ± 2

a. Estimated maximum possible errors.

rate remained constant during the entire irradiation period and the total dose rate decreased only about 10% during this period. Based on supplementary foil activation measurements for the fast neutron flux, a linear decrease in the total in-pile dose rate factor was used for the calculation of the specific absorbed dose.

1.3.3 Liquid Degradation - Theory

For each of the terphenyl isomers empirical rate equations may be written, having the form

$$-\frac{dC_i}{d\tau} = k_{i,n}\left[C_i\right]^n \qquad (1.2)$$

where

i refers to a particular component

n is the reaction order

k is the reaction constant

C is the weight fraction of the component

τ is the specific dose delivered to the coolant, given by Eq. (1.1).

The stability of a particular component in the coolant may be defined simply as $k_{i,n}$, the reaction constant, but two other stability terms are also employed here. $G(-i)$, by which radiation chemistry results are frequently reported, is defined as

$$G(-i) = \frac{\text{molecules of component } i \text{ degraded}}{100 \text{ ev absorbed in the total coolant}} \qquad (1.3)$$

This stability term is just $dC_i/d\tau$ multiplied by a conversion factor (11.65 (molecules)(watt)(hr)/(100 ev)(gm of terphenyl)). The second stability term used is $G^*(-i)$ (1.4):

$$G^*(-i) = G(-i)/C_i \qquad (1.4)$$

Assuming that the dose given to component i is proportional to the concentration of i in the coolant, which should be true as long as the carbon-hydrogen ratio of the various liquid organic components is fairly constant, $G^*(-i)$ has an interesting interpretation:

$$G^*(-i) = \frac{\text{molecules of component } i \text{ degraded}}{100 \text{ ev absorbed in component } i} \qquad (1.5)$$

During the transient periods of operation Eq. (1.2) was integrated in the form

$$-k_{i,n}\tau + a = \begin{cases} \dfrac{C_i^{1-n}}{1-n} & n \neq 1 \\ \ln C_i & n = 1 \end{cases} \qquad (1.6)$$

where "a" represents a constant of integration.

These linear relations between τ and a transformed concentration variable allowed the data to be treated by the method of weighted least squares. Once a "best" value of $k_{i,n}$ was obtained, the stability criteria $G(-i)$ and $G^*(-i)$ were calculated directly from Eqs. (1.3) and (1.4) for a given component concentration.

Since the circulating coolant mass, the in-pile dose rate factor and the coolant density did not vary significantly over any steady-state-HB irradiation, the $G(-i)$ criterion during these periods could be written as (see Eqs. (1.1) and (1.3))

$$G(-i) = -11.65 \frac{d(MC_i)}{\overline{F}\,\overline{\rho}\,d(MWH)} \qquad (1.7)$$

and the quantity $-d(MC_i)/d(MWH)$ equated to the makeup rate of component i in the coolant. $G^*(-i)$ values during the steady-state-HB periods were

determined from Eqs. (1.7) and (1.5) using the average concentration of component i in the loop.

1.3.4 Liquid Degradation Results

During transient periods of operation Eqs. (1.1) and (1.6) were used to analyze the terphenyl concentration data. Weighted least squares analyses were performed with reaction orders of 0, 1, 2 and 3. The results of the analysis on the data of the first transient period of the 610°F irradiation are presented graphically in Fig. 1.1. It can be seen that the 95% confidence limit envelope (based on n = 1) encompasses both the n = 0 and n = 2 curves. The same conclusions were drawn from similar plots for the individual isomers for all transient periods of the 610°F and 750°F irradiations. It was thus concluded that statistical arguments alone could not unequivocably determine the "best" reaction order, n.

It was decided to correlate the 610°F and 750°F irradiation degradation data by first order kinetics, which appeared to fit the data at least as well as the other orders studied. Because of the choice of a first order model, the stability parameter $G^*(-i)$ takes on additional meaning, for it is just the first order rate constant (multiplied by a conversion factor) for component i and is independent of concentration. Thus, the liquid degradation results could be described by a single number for each component over the range of compositions studied.

In a loop system, such as the one at M.I.T., with auxiliary equipment and a gas-liquid interface, it is difficult to accurately determine the circulating coolant mass, M. Inspection of Eqs. (1.1) and (1.6) shows that the results obtained from transient irradiation depend directly on a knowledge of the circulating coolant mass. For this reason, and also the fact that the G and G^* values do not have to be determined from the slope of a curve during steady-state-HB irradiation, the steady-state-HB results were found to be more accurate than the transient results. Consequently, the steady-state-HB results will be summarized here. The transient results agreed with the steady-state-HB results within the possible errors involved.

During the steady-state-HB irradiations only a constant HB level in the coolant was directly maintained. However, the DP concentration

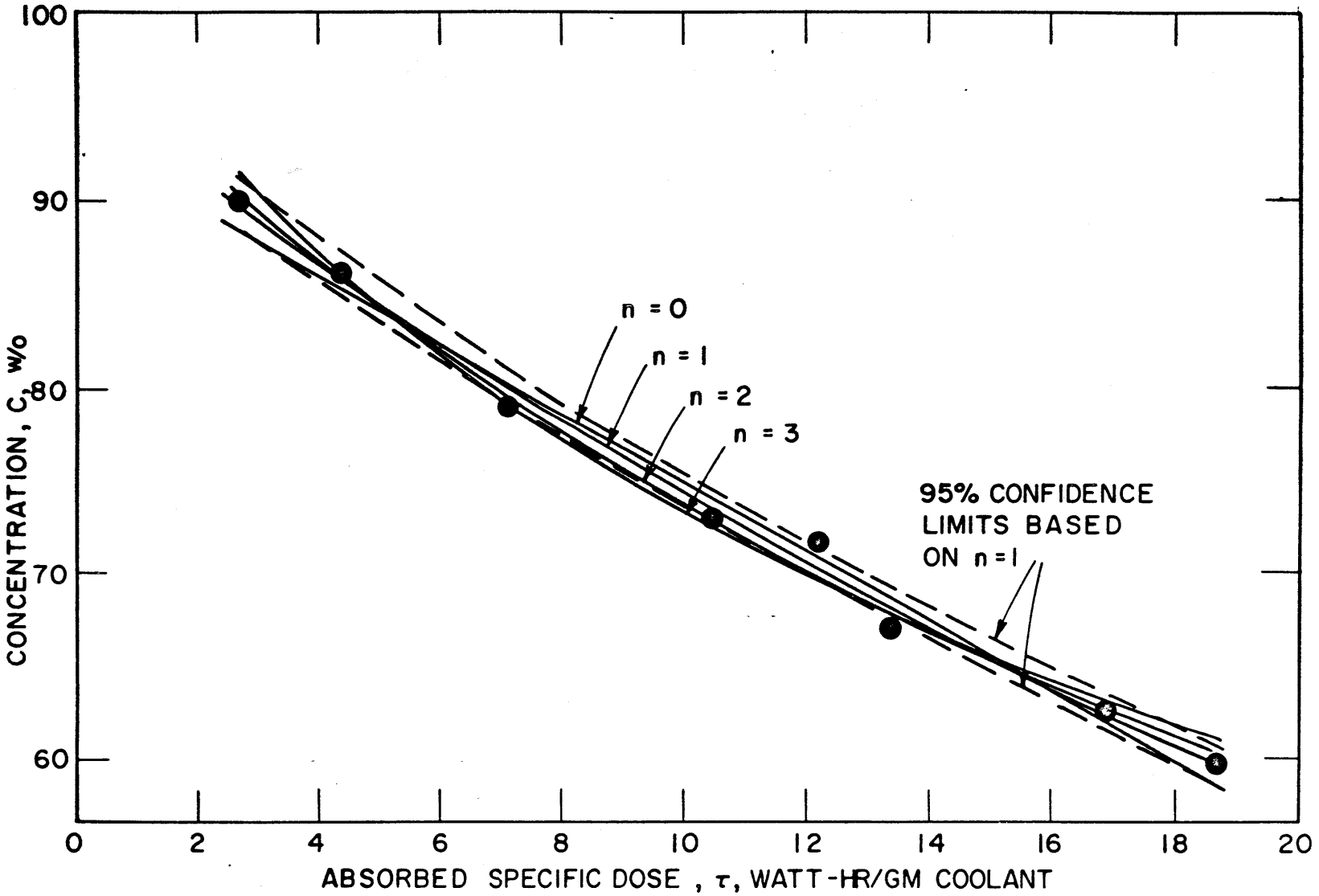

FIGURE 1.1 TOTAL TERPHENYL CONCENTRATION DURING THE FIRST TRANSIENT PERIOD OF THE 610°F IRRADIATION

and the terphenyl isomer concentrations were also observed to remain constant during the steady-state-HB irradiations. Figure 1. 2 shows as an example the variation of HB and DP concentrations during the steady-state-HB period of the 610°F irradiation.

The G^* values, based on first order kinetics, are listed in Table 1. 3 for the steady-state-HB irradiations of Santowax OMP. The quantities $G^*(\rightarrow HB)$ and $G^*(\rightarrow LIB)$ are defined in terms of the equivalent degradation of terphenyl required to form the high boiler and low and intermediate boiler fractions. Based on available data on pyrolysis of terphenyls (1. 12, 1. 13), at 610°F any pyrolytic contribution to terphenyl degradation in these studies was negligible. At 750°F the pyrolytic contribution was not negligible, but at present it is not known whether the combined effects of radiolysis and pyrolysis can be computed from their individual effects (1. 15). Corrections were therefore applied only for pyrolysis occurring in the out-of-pile volume of the loop. Essentially, these corrections involved subtracting from the observed makeup rate used in Eq. (1. 7) the amount of the terphenyls calculated to be degraded due to pyrolysis in the out-of-pile volume of the loop. Thus the G^* values reported for the 750°F irradiation are given both as measured and as corrected for out-of-pile pyrolysis. No attempt was made to correct the $G^*(\rightarrow HB)$ and $G^*(\rightarrow LIB)$ values for out-of-pile pyrolysis, since there are not sufficient data available on the pyrolytic production rates of these two groups of degradation products.

From Table 1. 3 it may be seen that at an irradiation temperature of 610°F the stabilities of each of the terphenyl isomers were not significantly different from each other, and that HB was the principal degradation product. At 750°F, the terphenyl isomer stability was found to be para> meta > ortho. A significant production rate of LIB was also observed for the 750°F irradiation. The G^* values for meta- and para-terphenyl increased by about a factor of two, while the G^* values for ortho-terphenyl increased almost three-fold due to the increase in irradiation temperature. The HB production rate almost doubled and the LIB production rate increased markedly due to the increase in irradiation temperature.

1. 3. 5 Comparison of Liquid Degradation Results with Other Work

Since previous work (1. 2, 1. 5) has indicated that combined fast neutron and gamma irradiation may be more effective in causing terphenyl

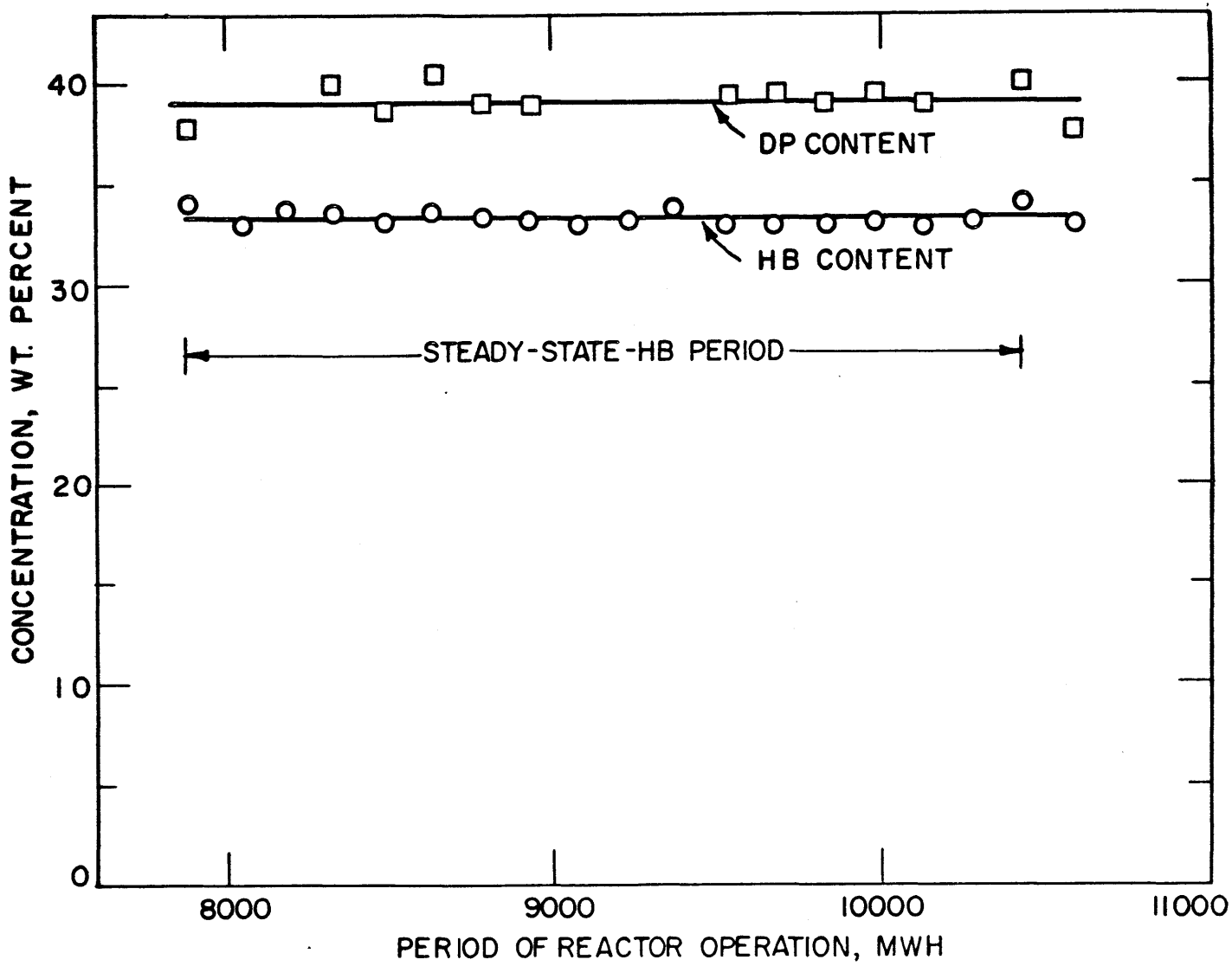

FIGURE 1.2 DP AND HB CONCENTRATIONS DURING THE STEADY-STATE-HB PERIOD OF THE 610°F IRRADIATION

TABLE 1.3

First Order G^* Values for Steady-State-HB Irradiations

Component	$G^*(-i) = G(-i)/C_i$		
	610°F	750°F	750°F[b]
Ortho-ϕ_3	0.26 ± 0.02[a]	0.79 ± 0.07	0.70 ± 0.07
Meta-ϕ_3	0.26 ± 0.02	0.52 ± 0.03	0.48 ± 0.03
Para-ϕ_3	0.28 ± 0.03	0.45 ± 0.03	0.43 ± 0.03
Total omp	0.26 ± 0.02	0.53 ± 0.04	0.49 ± 0.04
HB[c]	0.25 ± 0.01	0.47 ± 0.02	
LIB[c]	0.01 ± 0.01	0.06 ± 0.05	

a. 95% confidence limits. Standard deviations are one half of the errors quoted.

b. Corrected for pyrolysis occuring in out-of-pile circulating volume of the loop.

c. For the calculations of $G^*(\rightarrow HB)$ and $G^*(\rightarrow LIB)$, a molecular weight of 230 was used.

degradation than is gamma irradiation alone, the decomposition yields are dependent on the relative fraction of the energy absorbed due to fast neutron interactions. In order to generalize the results obtained at one laboratory with a given proportion of fast neutron dose to gamma ray dose, the approach has been to assume that the effects of fast neutron and gamma ray radiation are additive (1.6). The effects of fast neutron and gamma ray interactions are then each assigned G (or G^*) values which are assumed independent of neutron and gamma ray energy distributions. In terms of the stability criterion G^* this principle becomes

$$G^*(-i) = f_N G_N^*(-i) + (1-f_N)\, G_\gamma^*(-i) \qquad (1.8)$$

where

f_N = the fraction of absorbed energy due to fast neutron interactions

$G_N(-i) = C_i\, G_N^*(-i)$ = the molecules of component i degraded per 100 ev of fast neutron energy absorbed in the total coolant

$G_\gamma(-i) = C_i\, G_\gamma^*(-i)$ = the molecules of component i degraded per 100 ev of gamma ray energy absorbed in the total coolant.

An equivalent expression applies for $G(-i)$. In the present work 37% of the total dose is due to fast neutron interactions and 63% due to gamma ray interactions (see Table 1.2).

The results of this experiment, which was conducted in a radiation environment with a fixed fast neutron dose fraction, are not sufficient to determine both $G_N^*(-i)$ and $G_\gamma^*(-i)$, and so reliance must be placed on data obtained in other investigations with a significantly different fraction of fast neutron dose.

Due to recently reported data which show discrepancies between electron and gamma ray $G^*(-i)$ values (1.16, 1.6), it was not deemed meaningful to determine $G_N^*(-i)$ from the reported $G^*_{\text{electron}}(-i)$ or $G_\gamma^*(-i)$ values by using Eq. (1.8) with the values of f_N and $G^*(-i)$ found at M.I.T.. Instead a graphical procedure for comparing results from different irradiation facilities and at the same time for determining values of $G_N^*(-i)$ and $G_\gamma^*(-i)$ was developed. $G_N^*(-i)$ and $G_\gamma^*(-i)$ were both considered as variables in Eq. (1.8), so the use of the $G^*(-i)$ and f_N values obtained at a given

irradiation facility at a given irradiation temperature in Eq. (1.8) allowed $G_N^*(-i)$ to be plotted vs. $G_\gamma^*(-i)$ as a straight line. Thus, for a given irradiation temperature, results of various irradiation facilities would give a series of straight lines, and a common intersection of these lines would (at least in theory) determine $G_N^*(-i)$ and $G_\gamma^*(-i)$.

Figure 1.3 compares the first order $G^*(-\text{omp})$ values obtained from irradiation of terphenyl mixtures at temperatures near 610°F for various irradiation facilities. The MITR results are shown on Fig. 1.3 with the overall standard deviation being represented as shaded area on each side of the MITR line. From this plot several interesting features may be observed. First, there appears to be a discrepancy between the electron and gamma ray irradiations of encapsulated terphenyl samples. The electron irradiations were performed at Harwell, England (1.6) and at the Phillips Petroleum Company, Idaho Falls (1.17); the gamma ray irradiations were performed at the Susie reactor and at the MTR gamma canal (1.16). It can be seen that widely different values of $G_N^*(-\text{omp})/G_\gamma^*(-\text{omp})$ could be obtained from these irradiations in conjunction with the MITR results. Second, the three in-pile loop experiments for which data have been reported -- MTR (1.8), Melusine (Grenoble, France) (1.18) and the present work -- have an almost common intersection which indicates $G_N^*(-\text{omp})/G_\gamma^*(-\text{omp}) \simeq 1$. Not shown on the figure are the results obtained from operation of the OMRE at 600°F (1.19), for which only HB production rates were reported. However, the HB production rate reported for the OMRE agreed quite closely with that observed at the MITR. Third, the results of irradiations of encapsulated samples of terphenyls at various facilities -- BEPO (Harwell, England) (1.6), Oak Ridge Graphite Reactor (OGR) and Curtiss-Wright Research Reactor (CWRR) (1.9) and Susie (1.16) -- do not agree with the in-pile loop work, or with each other. Possible reasons for these discrepancies may be:

1. Electrons and gamma rays may have different effects on the degradation rate of the terphenyls.
2. Almost all of the irradiations of encapsulated samples were performed at dose rates much less than those encountered in the in-pile loop work. There may be a dose rate effect on terphenyl degradation.

---

1. f_N for OMRE = 0.28.

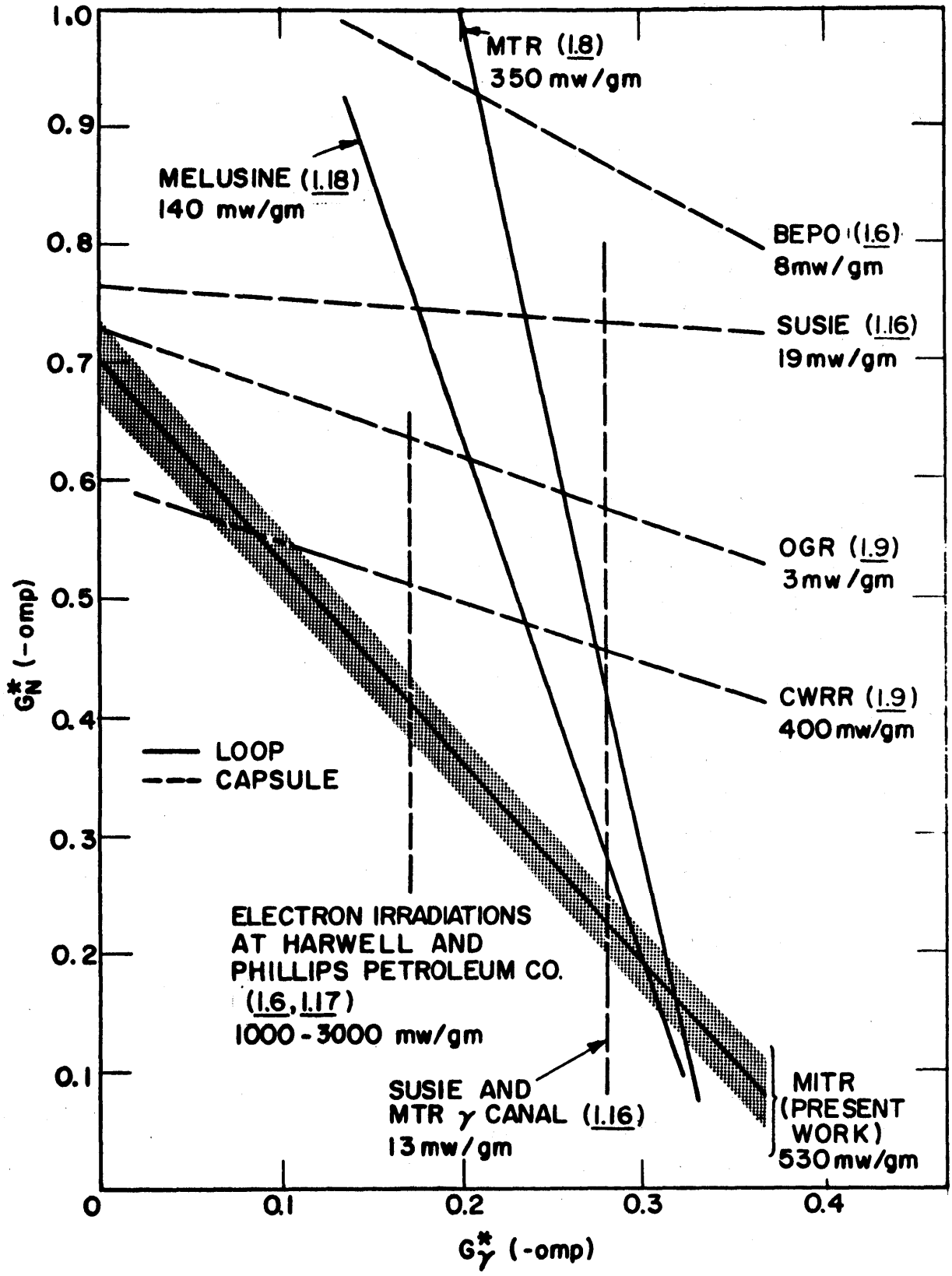

FIGURE 1.3 COMPARISON OF FIRST ORDER G^*_Λ VALUES AT 610°F

3. All irradiation experiments with encapsulated samples were carried out at fast neutron fractions reported to be 55 - 90%, whereas the loop irradiation data were obtained with fast neutron fractions of 12 - 37%. Accurate values of fast neutron dose rates are usually more difficult to obtain than accurate values of gamma ray dose rates (especially if threshold foils are used to determine the fast neutron dose rate), and errors in the fast neutron dose rate are relatively more important for the in-pile capsule irradiations. (An error in dose rate would manifest itself directly in the calculated G^* values.)
4. The mixing effect achieved in in-pile loop irradiations may serve to give a more consistent basis for terphenyl degradation.

It appears that more work must be done to more clearly establish the reasons for the present discrepancies.

Figure 1.4 compares data obtained at various irradiation facilities at temperatures near 750°F. A discrepancy between the electron irradiations at Harwell (1.6) and the gamma ray irradiations at the MTR gamma canal (1.16) also exists at this irradiation temperature. Preliminary results obtained at the Melusine loop (1.18) provide the only other in-pile loop irradiation data for comparison with the MITR work at this time. The Melusine results were not corrected for out-of-pile pyrolysis, and so the uncorrected MITR results are shown for the comparison. The two in-pile loop irradiation studies would indicate a value of $G^*_N(-omp)/G^*_\gamma(-omp) \simeq 2$. Estimates of the effect of correction of the Melusine results for out-of-pile pyrolysis and a comparison of the corrected results with the corrected MITR results indicate that about the same ratio of $G^*_N(-omp)/G^*_\gamma(-omp)$ would be obtained. The results of irradiations of encapsulated samples at BEPO (1.6) do not agree with the in-pile loop work. The same reasons postulated above for the discrepancies in the 610°F irradiation work are applicable to the 750°F irradiation work. In addition, the low dose rate irradiations are more affected by pyrolysis than the higher dose rate irradiations, making the comparison of results even more difficult.

1.3.6 Gas Generation Rates

Gas generation rates were determined during the steady-state-HB irradiations from the rates of removal of dissolved and undissolved gas

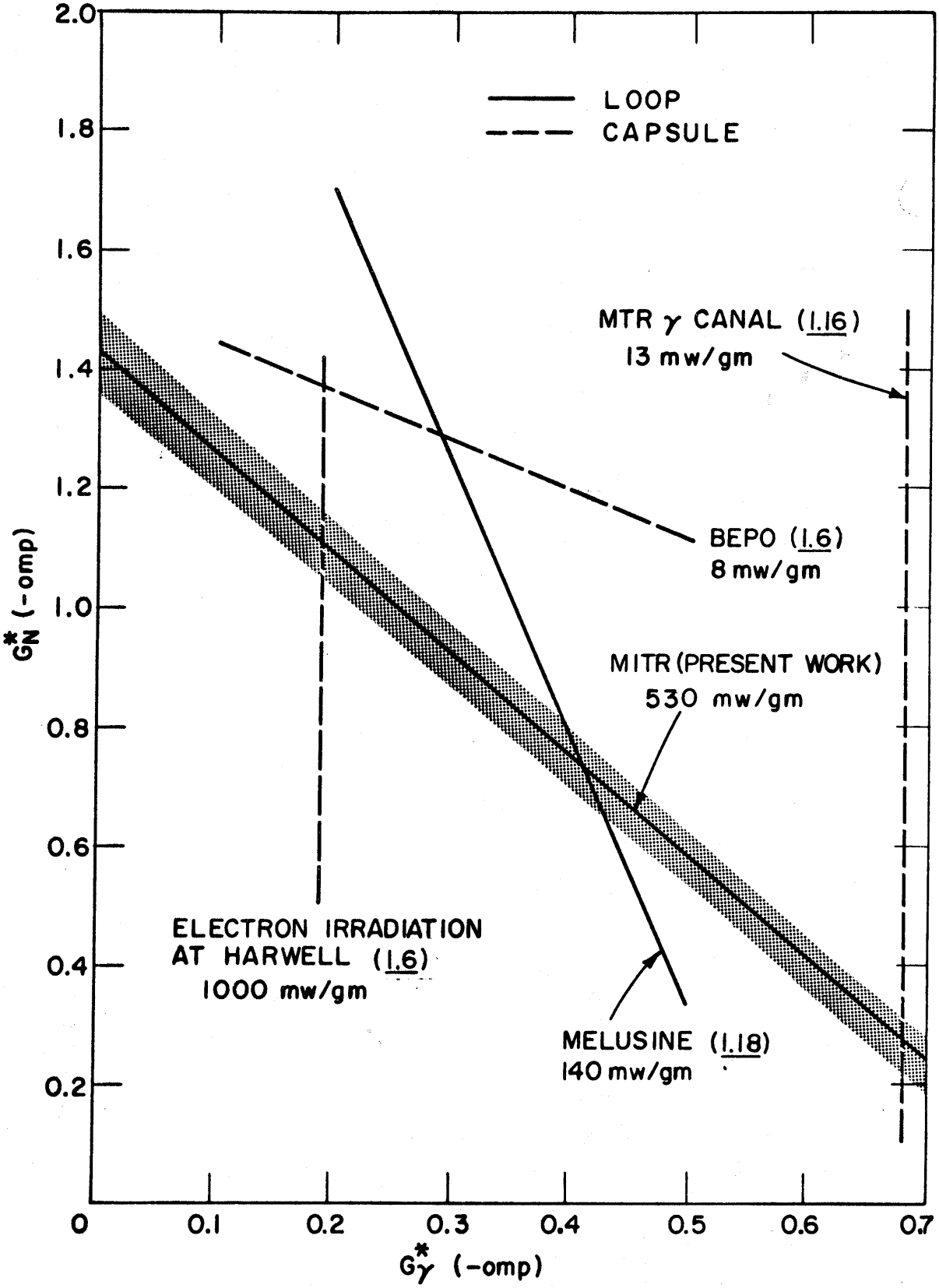

FIGURE 1.4 COMPARISON OF FIRST ORDER G^* VALUES AT 750°F

from the loop necessary to keep the total loop pressure at about 100 psig. Over 85% of the gas generated was removed as undissolved gas from the top of the surge tank in the out-of-pile section of the loop. Concentrations of various gaseous components were determined by mass spectrographic analyses of gas samples at the Petroleum Analytical Research Corporation (Houston, Texas). The method of reporting the gas generation rates follows the standard practice for net radiation yields (1.2, 1.6):

$$G(\text{gas } i) = \frac{\text{molecules of gaseous component } i \text{ generated}}{100 \text{ ev absorbed in the total coolant}} \qquad (1.9)$$

During the steady-state-HB periods of the 610°F and 750°F irradiations the concentrations of all gaseous components observed were found to be constant in both the dissolved and undissolved gas, and the total gas solubility in the coolant in the loop was found to be approximately constant, so that the net gas generation rates of each of the gaseous components could easily be determined from a knowledge of the total gas generation rate. Table 1.4 summarizes the G(gas i) values obtained for the steady-state-HB irradiations. During the 610°F irradiation hydrogen was observed to be the principal gas generated. During the 750°F irradiation hydrogen, methane and C_2 gases were the most prominent of the gases generated. The overall gas generation rate was observed to increase about a factor of three, but the hydrogen production rate only doubled while the methane production rate increased about seven-fold when the irradiation temperature was increased from 610°F to 750°F.

By comparing the G(total gas) and G(-omp) values on a weight basis it was observed that less than 1 w/o of all the degradation products formed were gases.

1.4 Physical Property Measurements

Densities of samples of irradiated Santowax OMP were measured at M.I.T. over the temperature range 400 - 800°F with calibrated pycnometers pressurized with nitrogen and immersed in a high temperature fused salt bath. Viscosities of irradiated Santowax OMP samples were also measured in the fused salt bath at M.I.T. over the temperature range 400 - 800°F by observing the efflux times in semi-micro capillary viscometers of the Ostwald type.

TABLE 1. 4

G(gas i) Values from the 610°F and 750°F Steady-State-HB Irradiations of Santowax OMP[a]

Component	G(gas i) = molecules of gaseous component i produced / 100 ev absorbed in the total coolant	
	610°F Irradiation	750°F Irradiation
Total gas	0.037 ± 0.003[b]	0.105 ± 0.008
Hydrogen (H_2)	0.020 ± 0.002	0.039 ± 0.003
Methane(C_1)	0.0057 ± 0.0005	0.040 ± 0.003
Ethane and Ethylene(C_2)	0.0060 ± 0.0005	0.018 ± 0.001
Propane and Propylene (C_3)	0.0026 ± 0.0003	0.0057 ± 0.0004
Butanes and Butenes (C_4)	0.0011 ± 0.0002	0.0013 ± 0.0001
Pentanes, Pentenes, Hexanes, Hexenes (C_{5+6})	0.0008 ± 0.0001	0.0004 ± 0.00004
Benzene, Toluene, Xylene (Aromatics)	0.0003 ± 0.00006	0.0012 ± 0.0001

a. DP concentration ~40 w/o, HB concentration ~33 w/o.

b. Standard deviations.

Specific heats of irradiated Santowax OMP samples were measured over the temperature range 400 - 800°F by the Monsanto Research Corporation (Dayton, Ohio), and at the French CEA laboratories at Grenoble, France. Data were obtained on the thermal conductivity of irradiated Santowax OMP over the temperature range 400 - 700°F for coolant samples taken during the irradiation at 610°F; the measurements were performed at Grenoble.

Table 1.5 summarizes the results of these determinations. The densities of all irradiated samples were found to have a linear temperature dependence, and the smoothed values at 0, 30 and 60 w/o DP are shown for both irradiations at two temperatures of interest to organic cooled reactor designers: 600°F and 750°F. From the table it may be observed that the densities of samples irradiated at both 610°F and 750°F agreed quite well with each other, and the densities increased less than 10% as the DP concentration increased from 0 to 60 w/o. The results obtained generally agreed to within ± 1% with the data reported at other laboratories (1.20, 1.21).

Viscosities of all irradiated samples were found to obey the relation

$$\mu = ae^{b/T} \quad \text{centipoises} \qquad (1.10)$$

where

a, b are constants

T is the temperature of measurement, °R.

over the temperature range of measurement, and the smoothed values are shown in Table 1.5. A very strong dependence on the DP concentration was observed, but a significantly lower increase in viscosity with increasing DP concentration was found for the 750°F irradiation than for the 610°F irradiation. The results obtained in general agreed with the data reported at other laboratories to within ± 5% (1.22, 1.23).

The specific heats of irradiated Santowax OMP samples were found to have a linear temperature dependence, but no dependence on the DP concentration for both the 610°F and 750°F irradiations. These data agreed with data obtained at Winfrith, England (1.24) to ± 2%.

Thermal conductivity measurements have only been performed on samples of the 610°F irradiation at DP concentrations of 0 and 40 w/o. A linear temperature dependence of the thermal conductivity data was found,

TABLE 1.5

Summary of Physical Properties of Irradiated Santowax OMP

Temperature of Irradiation →		610°F		750°F	
Temperature of Measurement →		600°F	750°F	600°F	750°F
Property	w/o DP				
Density, grams/cc	0	0.870	0.800	0.870	0.800
	30	0.896	0.830	0.896	0.830
	60	0.936	0.880	0.938	0.876
Viscosity, centipoises	0	0.36	0.23	0.37	0.23
	30	0.55	0.34	0.55	0.34
	60	1.58	0.86	1.03	0.60
Specific Heat, cal/(gm)(°C)	0	0.56	0.60	0.56	0.60
	60	0.56	0.60	0.56	0.60
Thermal Conductivity, cal/(sec)(cm)(°C) x 10^4	0	2.7	2.4	--	--
	40	3.1	2.9	--	--

and the thermal conductivities increased up to 20% as the DP concentration varied from 0 to 40 w/o. These findings are consistent with the available data on irradiated terphenyl samples (1.25, 1.26).

In addition to these physical properties, number average molecular weights of samples of irradiated Santowax OMP were measured at M.I.T. using an osmometer. Samples of irradiated coolant and of the HB fractions were dissolved in tetrahydrofuran at molal concentrations between 0.01 and 0.1 m. During the 610°F irradiation the coolant number average molecular weight increased from a value of 230 (the molecular weight of the terphenyls) at 0 w/o DP to about 350 at 60 w/o DP. During the 610°F steady-state-HB irradiation (~40 w/o DP and ~33 w/o HB) the coolant and HB number average molecular weights remained constant at values of 300 and 690 respectively. During the 750°F irradiation the coolant number average molecular weight increased less rapidly with increasing DP concentration than during the 610°F irradiation; from 230 at 0 w/o DP to about 340 at 60 w/o DP. During the 750°F steady-state-HB irradiation the coolant and HB number average molecular weights remained constant at values of 285 and 580 respectively.

Measurements of gas solubility in the irradiated coolant were also performed. The results indicate a gas solubility of $(8 \pm 3) \times 10^{-3}$(std. cc)/(gm coolant)(psia) during the 610°F steady-state-HB irradiation and a gas solubility of $(3 \pm 1) \times 10^{-3}$(std. cc)/(gm coolant)(psia) during the 750°F steady-state-HB irradiation.

The coolant melting points were found to decrease with increasing DP concentration. The 610°F irradiation samples showed an initial liquidus point and a final liquidus point of 170°F and 340°F, respectively, at 0 w/o DP, and an initial liquidus point and a final liquidus point of 100°F and 260°F, respectively, at 60 w/o DP. During the 750°F irradiation the range of the final liquidus points was about the same as for the 610°F irradiation, but the initial liquidus point decreased much more rapidly with increasing DP concentration, reaching room temperature at about 40 w/o DP.

No trend in the carbon-hydrogen ratios of all samples from the 610°F and 750°F irradiations with DP concentration was observed. The C/H ratio fluctuated within ± 7% of the value of 15.4 for pure terphenyls.

Finally, ash and inorganic content analyses were performed on irradiated Santowax OMP samples by the Monsanto Research Corporation (Dayton, Ohio). Results of these analyses indicate an ash content of less than 20 total ppm of aluminum, copper, iron, magnesium, nickel and silicon. Supplemental measurements of iron, chloride and water content at Chalk River, Ontario, indicated 2 - 20 ppm, ~3 ppm and 10 - 50 ppm for these contents, respectively. These levels of impurities are generally lower than the levels which have been maintained in other loop studies and in the OMRE (1.3).

1.5 Heat Transfer Measurements

Heat transfer measurements were performed with the aid of electric test heaters installed in the out-of-pile section of the loop. The test heaters were constructed of stainless steel (1/4 inch O.D. x 0.020 inch wall) and were heated by the passage of electrical currents of up to 450 amps A.C. along the tube walls. The coefficients of heat transfer were based on the temperature differences from the inside wall of the test heater to the bulk coolant as defined by

$$U = \frac{Q/A}{\overline{T_W^I} - \overline{T_B}} \qquad (Btu)/(hr)(ft^2)(^oF) \qquad (1.11)$$

where

(Q/A) is the heat flux into the coolant, $Btu/(hr)(ft^2)$

$\overline{T_W^I}$ is the average inside wall surface temperature, ^oF

$\overline{T_B}$ is the average coolant bulk temperature, ^oF.

No evidence of any scale formation on the test heater walls was observed over the entire period of operation of the test heaters (about 20 months). This absence of any buildup of resistance to heat transfer in the heater walls over the 20 months of operation of the loop is very encouraging and is taken to indicate that operation of nuclear reactors using terphenyl coolants will be facilitated by maintenance of a high level of coolant purity.

In view of the lack of evidence of a fouling film, the coefficient of heat transfer, U, in Eq. (1.11) was equated to the film heat transfer coefficient, h_f.

The range of variation of the major heat transfer variables involved is given in Table 1.6. Correlations of the heat transfer data by means of

TABLE 1.6

Range of Variation of Major Heat Transfer Variables During the 610°F Irradiation of Santowax OMP

Variable	Range
Heat Flux, Q/A	2×10^4 - 2×10^5 Btu/(hr)(ft^2)
Velocity, v	5-25 ft/sec
Heat Transfer Coefficient, U	340-2400 Btu/(hr)(ft^2)(°F)
Nusselt No., Nu	80-650
Reynolds No., Re	8×10^3-10^5
Prandtl No., Pr	7-32
Viscosity Ratio, μ/μ_W	1.2-2.5

the standard dimensionless parameters (Nusselt number, Reynolds number, Prandtl number) according to a Dittus-Boelter type relation (1.27), yielded the following "best" correlation for the data of both the 610°F and 750°F irradiations:

$$Nu = 0.0079\ (Re)^{0.9}\ (Pr)^{0.4} \pm 10\% \qquad (1.12)$$

The measured physical properties of the irradiated coolant (evaluated at the bulk coolant temperature) were used in the dimensionless parameters.

A fouling probe was installed in the out-of-pile section of the loop during the 750°F irradiation in order to obtain a more quantitative measure of the rate of scale formation on heated surfaces. At present, only preliminary measurements have been made, and measuring techniques are being developed. In future work, quantitative data will be available.

CHAPTER 2
EQUIPMENT AND OPERATION

2.1 Equipment

A complete description of the M.I.T. In-Pile Loop Facility has been given by Morgan and Mason (2.1). Only a summary description will be given here.

The loop is constructed entirely of stainless steel and is capable of operation to 800°F and 600 psig. The design and operating specifications of the loop are given in Table 2.1 and a schematic flow diagram of the loop in Fig. 2.1. The loop can be conveniently divided into in-pile and out-of-pile sections for further discussion.

The in-pile section is designed to fit down the axis of the central fuel element of the MITR from which eight of the normal 16 fuel plates have been removed. This section consists of a 1-1/4 inch O.D. x 0.035 inch wall aluminum thimble containing a stainless steel irradiation capsule (7/8 inch O.D. x 0.035 inch wall) which provides 205 cc of coolant holdup in the reactor core. Also in the in-pile section are the inlet-outlet lines, consisting of two annular tubes, which connect the irradiation capsule to the rest of the loop so that a continuous flow of coolant through the irradiation capsule may be maintained. The aluminum thimble is used to separate the D_2O moderator of the reactor from the hot organic material in the irradiation capsule and inlet-outlet lines. To monitor the fast and thermal neutron fluxes in the reactor core while the reactor and loop are operating, a 5/16 inch O.D. x 0.035 inch wall aluminum monitor tube is provided on the outside of the thimble beside the irradiation capsule.

The out-of-pile section (hydraulic console) consists of all loop components containing coolant which are outside the reactor shield. All of these components are enclosed in a sheet metal cabinet equipped with an automatic fire extinguisher because of the flammable nature of the organic coolant. The equipment contained in this cabinet is listed in Table 2.2 (see also the flow diagram, Fig. 2.1). Under normal operation,

TABLE 2.1

Design and Operating Specifications of the M.I.T. In-Pile Loop

Bulk temperature	to 800°F
Loop pressure	to 600 psig
Materials of construction	Type 304 and 316 stainless steel
Volume of in-core capsule	205 cc
Circulating volume with 600 cc in surge tank	5200 cc
In-pile to out-of-pile volume ratio	0.04
Circulating flow rate	2 gallons/minute
Maximum test heater heat flux	400,000 Btu/(hr)(ft^2)
Test heater wall temperature	to 1000°F
Velocity in test heater	to 20 ft/sec
In-core capsule located along axis of central fuel element of MITR	
Specific dose rate at center of reactor to Santowax OMP	0.33 watts/gm/MW of reactor power
Ratio of fast neutron dose rate to gamma ray dose rate	0.37/0.63

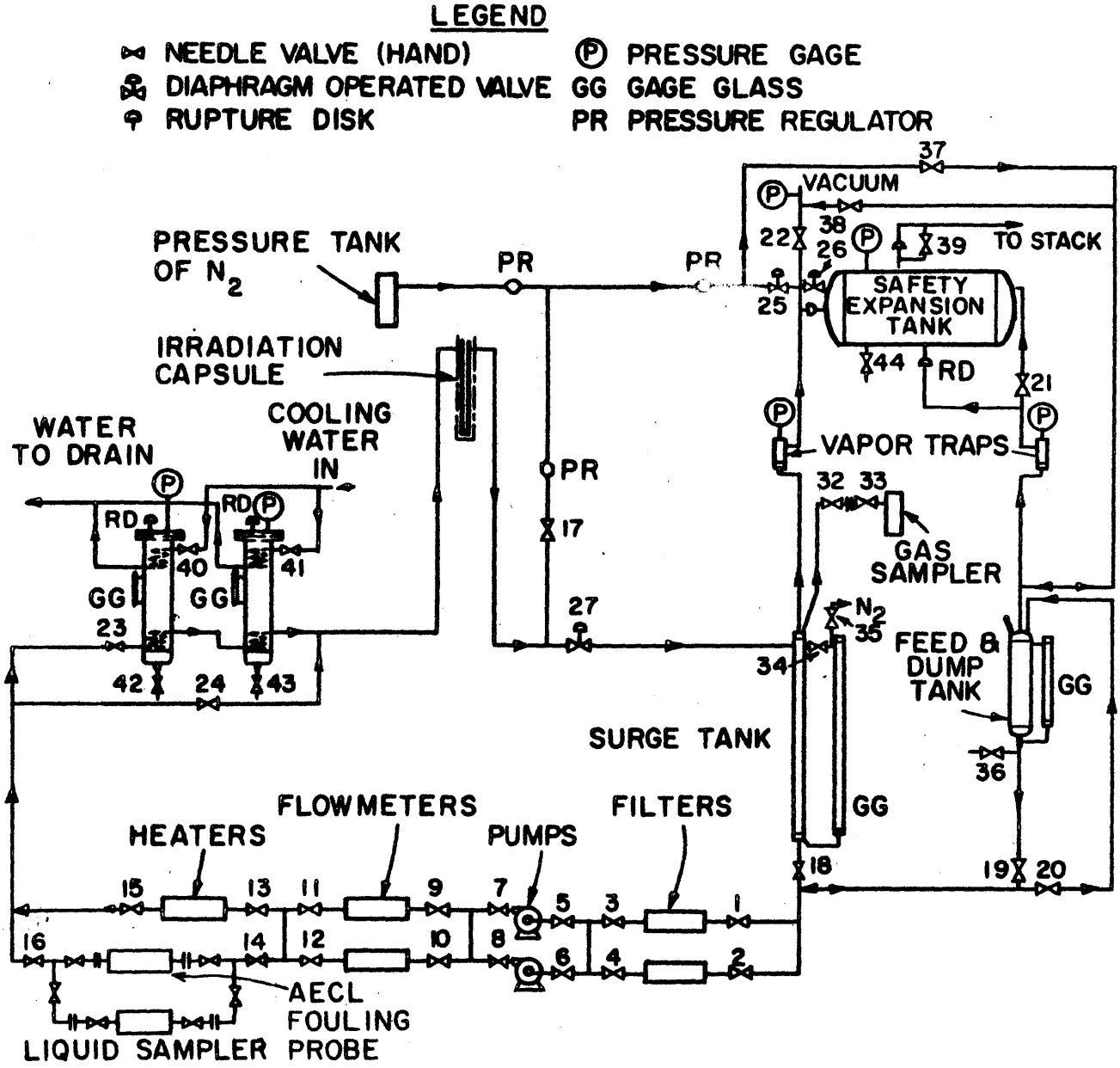

FIGURE 2.1 SCHEMATIC FLOW DIAGRAM OF M.I.T. IN-PILE LOOP

TABLE 2.2

Tabulation of Out-of-Pile Components of Loop Comprising Hydraulic Console

Component	Purpose	Description
Surge tank	Provides holdup of excess coolant for sampling and for temperature expansion. Also has gas space in which evolved gases collect.	Tank with total volume of 1450 cc and a volume per unit length of 61.1 cc/in.
Filters	Remove particulates from coolant.	Sintered stainless steel elements. One filter has 98% removal rating of 55 microns. The other has element with 98% removal rating of 2 microns.
Pumps	Circulate coolant at rates up to 2 gpm, equivalent to 20 ft/sec through test heater.	Two Chempump Model CFHT-3-3/4S canned rotor stainless steel pumps. One operating while other is stand-by.
Flowmeters	Measure volumetric rate of coolant flow.	3/8 in. Potter turbine-type volumetric flowmeter.
Test heater	Measures heat transfer coefficients and maintains loop temperature.	1/4 in. OD x 0.020 in. wall stainless steel tube heated by passage of up to 450 amps A.C. through two sections, each 12 in. in length. Thermocouples are welded to test heater wall for temperature measurements.
Main loop coolers	Remove excess energy introduced during heat transfer measurements.	Reflux condenser type using Dowtherm A as cooling medium with water-cooled coil as condenser.
Sampling stations	Take liquid and gas samples.	Liquid sample: taken in stainless steel capsule through which coolant flows before sample is collected. Gas sample: taken in stainless steel capsule from surge tank.

TABLE 2.2 (Concluded)

Tabulation of Out-of-Pile Components of Loop Comprising Hydraulic Console

Component	Purpose	Description
Feed and dump tank	Melts coolant prior to charging to loop and collects coolant drained from loop.	Tank with total volume of 5200 cc and volume per unit length of 223 cc/in.
Safety expansion tank	Rapid depressurization of loop in case of emergency involving danger to reactor or personnel.	Tank volume ~ 7 ft^3.
Pressurizing system	Provides high pressure nitrogen gas for pressurizing loop.	Purified nitrogen gas cylinder plus regulators and valves for control. Valved off after pressurization at start of an irradiation.
Valves	Control coolant flow.	Bellows-sealed stainless steel valves.
Pressure gages	Measure pressure in surge tank and feed and dump tank.	Diaphragm type pressure probes connected to gages by capillary tubes.
Trace heaters	Melt coolant for operation of loop.	Double glass insulated heating tapes.

only one pump and one flowmeter were used and flow was passed only through the coarse filter.

In addition to these two sections of the loop there is housed in a single unit all the necessary instrumentation for the control of the loop operation.

2.2 Operation

2.2.1 General

Due to space limitations inside the fuel element and thimble, it was not possible to make calorimetric dose rate measurements with the in-pile assembly in the thimble in the reactor. For this reason a special stainless steel thimble was constructed (1-1/4 inch O.D. x 0.050 inch wall) to mock up the perturbation of the neutron spectrum by the in-pile assembly. Measurements on March 20, 1961, with the Series III calorimeters formed the basis for the calorimetric measurements before the insertion of the in-pile assembly for the start of the 610°F irradiation (2.1). Measurements were again performed from April 22, 1963, to May 15, 1963, with the Series IV calorimeters after the removal of the in-pile assembly at the end of the 750°F irradiation. These measurements are discussed in detail in Chapter 3.

Two irradiations of Santowax OMP were performed in the interval between the calorimetric measurements:- one at 610 ± 10°F and the second at 750 ± 5°F.[1] The temperatures referred to, both here and in the rest of the report, are those of the coolant in the in-pile capsule in the reactor, since it is in the in-pile capsule where the coolant is subjected to irradiation. In the paragraphs that follow, operations common to both irradiations will be described.

Normally, the MITR operates for about four days at a full thermal power of approximately 2 MW and is shut down over the weekend. To match this reactor cycle, the loop was normally raised to operating temperature Monday mornings by turning on and adjusting the test heater power just before the reactor was brought up to full thermal power. Similarly, on Friday evenings the test heater was turned off when the reactor was shut down and the loop temperature lowered to about 450°F to minimize possible changes in the coolant due to pyrolysis while the reactor was shut down.

1. Loop pressure during both irradiations approximately 100 psig.

Each irradiation was performed in two distinct phases. At the outset of both irradiations there was a transient phase of operation, during which an initial amount of unirradiated Santowax OMP was allowed to degrade with periodic sampling but no makeup. Following this phase there was a steady-state-HB phase of operation. The object of this phase was to maintain a constant high boiler (HB) fraction of about 33 w/o in the coolant and to study the long-term irradiation effects on the physical and chemical properties of the coolant. An HB concentration of about 30 w/o has been used as the basis for organic reactor designs (2.2) but it remains to be demonstrated that this HB concentration level represents an economic optimum in the balance between coolant makeup costs and overall plant efficiency. In order to maintain the HB level, samples containing about 300 grams of coolant were removed at regular intervals in stainless steel capsules and were distilled. Each distillate was mixed with fresh Santowax OMP (to replace the HB removed) and returned to the loop just after the removal of the next sample to be distilled. In the next two sub-sections, the chronology of each irradiation will be presented

2.2.2 610°F Irradiation

The transient phase of operation of the 610°F irradiation began on August 9, 1961. Due to changes in density of the coolant and to sampling, it became necessary on October 5, 1961, to add fresh Santowax OMP in order to continue the irradiation. After this addition, the transient operation was resumed and continued until January 3, 1962, at which time the coolant contained about 60 w/o degradation products (DP). A period of about one month followed, during which the coolant composition was gradually changed from 60 w/o DP to about 40 w/o DP and the HB content lowered to near 33 w/o by coolant withdrawal and addition of unirradiated Santowax OMP.

The first period of steady-state-HB operation began on January 30, 1962, and lasted to March 28, 1962, at which time there was a failure of the main circulating pump (Chempump). The HB concentration varied somewhat during this period, which was thus termed the "quasi-steady-state-HB" period. When the spare pump was put on stream on March 28, 1962, the fresh Santowax OMP it contained was added to the circulating mass and the irradiated coolant in the faulty pump removed. The HB content did not level out at 33 w/o until May 24, 1962, at which time the steady-state-HB operation was resumed and continued through August 30, 1962.

From August 30, 1962, to the end of the 610°F irradiation on October 12, 1962, the HB level was kept below 40 w/o, but strict control was not maintained on the HB content, so this period was termed one of interim operation.

A summary of the operation of the loop during the 610°F irradiation is provided by Table 2.3, which lists appropriate dates, periods of reactor operation (in MWH) and DP concentration ranges.

2.2.3 750°F Irradiation

Preparations for the 750°F irradiation were not complete on the weekend of October 12, 1962, when the coolant from the 610°F irradiation was removed. To allow the reactor to continue operation, the loop was charged with unirradiated Santowax OMP on October 15, 1962. An interim period of operation followed for about one month during which preparations for the 750°F irradiation were completed.

After several flushes and drains with fresh Santowax OMP, the 750°F irradiation was begun on November 26, 1962. During the next week, rapid drops in the surge tank liquid level indicated that all parts of the loop had not been completely filled, so additional unirradiated Santowax OMP was added on December 4, 1962, to start the transient phase of the 750°F irradiation. On January 10, 1963, a coolant leak occurred at the sampling position while removing a sample from the loop, and this leak necessitated a further addition of fresh Santowax OMP to continue the irradiation. After this addition, the transient operation was resumed and continued to February 15, 1963, at which time the coolant contained about 60 w/o DP.

The coolant composition was changed from 60 w/o DP to about 40 w/o DP and the HB content lowered to near 33 w/o during the period February 15, 1963, to February 26, 1963. On this latter date the steady-state-HB phase of the 750°F irradiation was begun and continued to the end of the irradiation on April 18, 1963. Having served for 20 months of coolant irradiation, the in-pile assembly was removed on the weekend of April 18, 1963, to allow calorimetric measurements of the dose rate to be performed.

A summary of the operation of the loop during the 750°F irradiation is provided by Table 2.3.

TABLE 2.3

nmary of Loop Operation During the 610°F and 750°F Irradiations of Santowax OMP

Operation	Dates	MWH of reactor operation	Accumulated MWH of reactor operation	w/o DP
calorimetric measurements	3/20/61	−2566[a]	−2566	-
tart of 610°F irradiation	3/20/61-8/9/61	−2566-0	−2566-0	-
sient No. 1	8/9/61-10/5/61	0-1623	0-1623	0 t
sient No. 2	10/5/61-1/3/62	1623-3891	1623-3891	33 t
	1/3/62-1/30/62	3891-4630	3891-4630	60 t
i-Steady-State-HB	1/30/62-3/28/62	4630-6196	4630-6196	~4
	3/28/62-5/24/62	6196-7880	6196-7880	~4
ly-State-HB	5/24/62-8/30/62	7880-10428	7880-10428	~4
nd of 610°F irradiation	8/30/62-10/12/62	10428-11538	10428-11538	~4
tart of 750°F irradiation	10/12/62-11/26/62	0-1056	11538-12594	-
	11/26/62-12/4/62	0-253	12594-12847	0 t
sient No. 1	12/4/62-1/10/63	253-1056	12847-13650	10 t
	1/10/63-1/14/63	1056-1126	13650-13720	37 t
sient No. 2	1/14/63-2/15/63	1126-2040	13720-14634	34 t
	2/15/63-2/26/63	2040-2280	14634-14874	60 t
ly-State-HB	2/26/63-4/18/63	2280-3733	14874-16327	~4
nd of 750°F irradiation	4/18/63	3733-3748	16327-16342	~4
alorimetric measurements	4/23/63-5/10/63	0-522	16342-16864	-

bitrarily set to zero at the start of the 610°F irradiation.

CHAPTER 3
CALORIMETRY AND DOSIMETRY

3. 1 Introduction

An important aspect of the work at M. I. T. has been to correlate changes in the chemical and physical properties of the irradiated Santowax OMP with the energy absorbed from fast neutron and gamma ray radiations. Previous work at BEPO (3. 1) and at the Curtiss-Wright Research Reactor (3. 2) has suggested that fast neutrons are more effective than gamma rays in degrading the terphenyls, so that a knowledge of both the total energy deposition rate and the fast neutron and gamma ray fractions was desirable.

At M. I. T. an extensive radiation calorimetry program, employing adiabatic calorimeters, was undertaken to determine the fast neutron and gamma ray dose rates in the in-pile section. Due to space limitations it was not possible to make calorimetric measurements with the in-pile section in the reactor, so the first calorimetric measurements were made on March 20, 1961, before the insertion of the in-pile section into the reactor. These measurements employed a single calorimeter containing five separate energy absorbers operated under vacuum conditions. The measurements were made inside a special stainless steel thimble, constructed to mock-up the perturbation of the neutron spectrum by the in-pile assembly. Measurements could only be made to a reactor power level of 200 kw and had to be extrapolated to the full reactor power level (about 2 MW). The detailed design and the results obtained from these calorimeters have been reported by Morgan and Mason (3. 3).

After the removal of the in-pile assembly on April 20, 1963, the special stainless steel thimble was again inserted into position and the calorimetric measurements were again performed. A calorimeter of new and simplified design was employed at this time, allowing the measurements to be made at full reactor power. The new equipment will be described in this report.

In support of the calorimetry program to determine the fast neutron and gamma ray dose rates in the in-pile section of the loop, foil activation measurements were made in a monitor tube affixed to the in-pile assembly at intervals over the whole period of irradiation of Santowax OMP from August 9, 1961, to April 18, 1963. The major purposes of the foil measurements were:

1. To provide information on the shape of the neutron energy spectrum in the in-pile section.
2. To determine the manner in which the neutron flux changed with continuing use of the fuel element in which the in-pile section was inserted. This would help determine how to evaluate a change in the results of the calorimetric measurements made before the insertion of the in-pile section and after its removal.
3. To provide a check on the fast neutron dose rates as determined by the calorimetric measurements.

3. 2 Calorimetric Measurements

3. 2. 1 Equipment (3. 4)

A complete description of the calorimeters used before the insertion of the in-pile section (Series III) has been given by Morgan and Mason (3. 3). The equipment used following the Santowax irradiations (Series IV) will be described briefly.

Because measurements at full reactor power (about 2 MW) result in rapid temperature increases in the calorimeter absorbers, automatic recording equipment was used to measure the absorber and wall temperatures. Thus, each absorber was placed in a separate aluminum can and measurements were made with one absorber at a time. The previous designs had all absorbers in a single can (3. 3). Figures 3. 1 and 3. 2 show the detailed construction of each calorimeter assembly. Each absorber, cylindrical in shape (1/2 inch in diameter), was enclosed in a one-inch O. D. aluminum can. Thermocouples attached to the absorber and to the inside wall of the can were passed through a length of 1/2 inch O. D. polyethylene supporting tubing to the recording equipment. Figure 3. 3 shows the recording equipment and the cooling equipment in place on the reactor top. Figure 3. 4 is a schematic diagram of the vertical

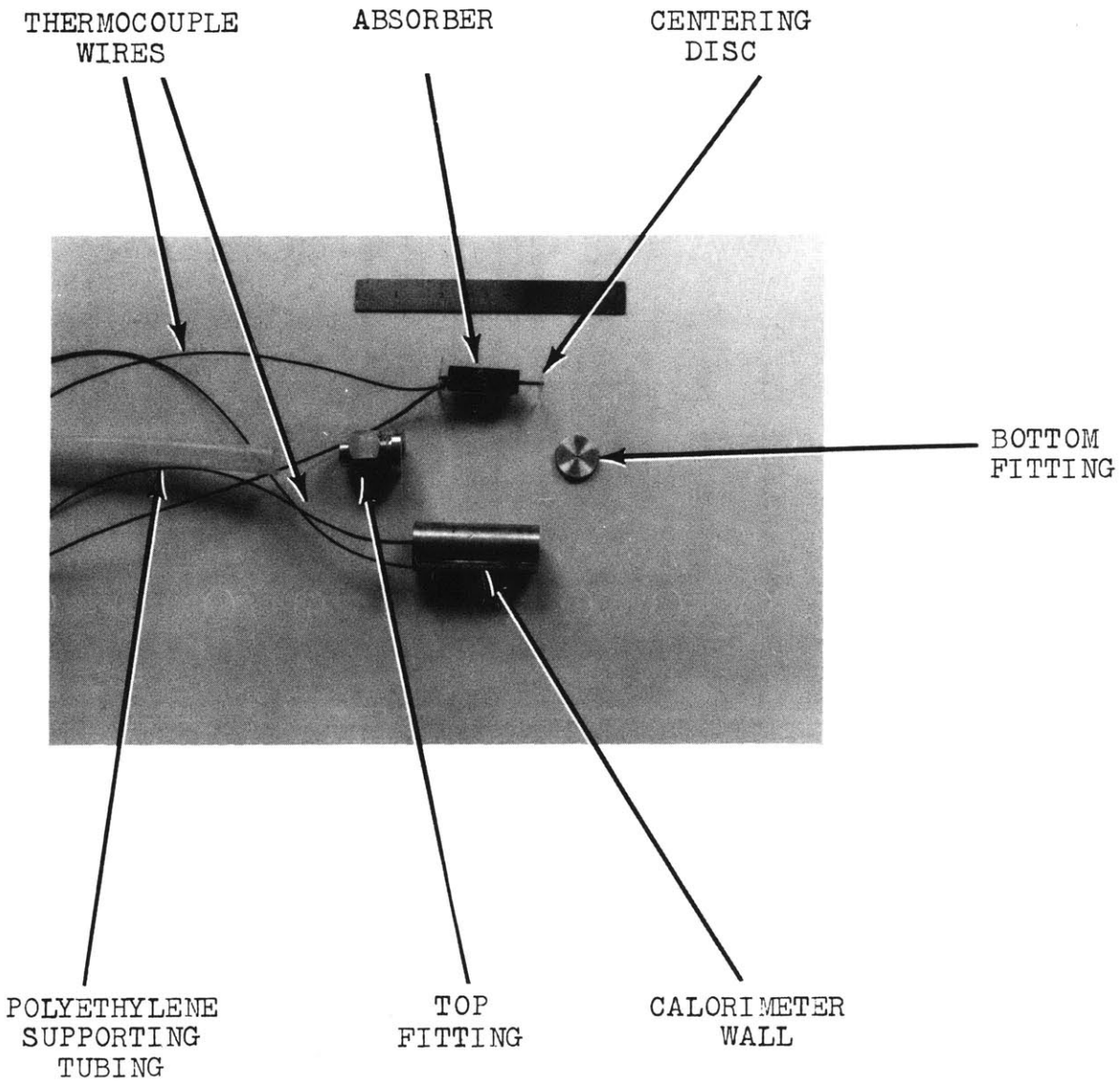

FIGURE 3.1 PHOTOGRAPH OF A SERIES IV CALORIMETER BEFORE ASSEMBLY

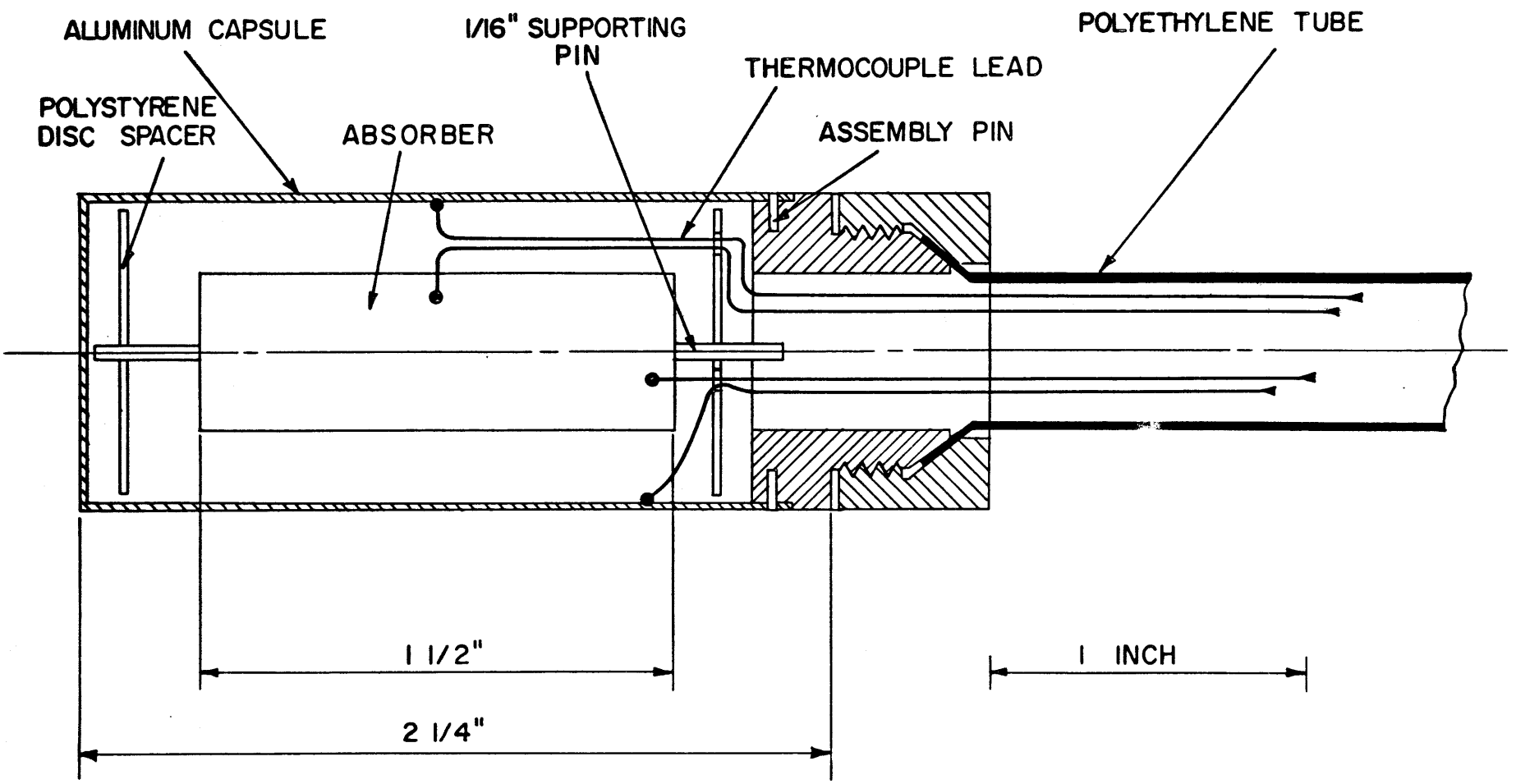

FIGURE 3.2 ASSEMBLY DRAWING OF A SERIES IV CALORIMETER

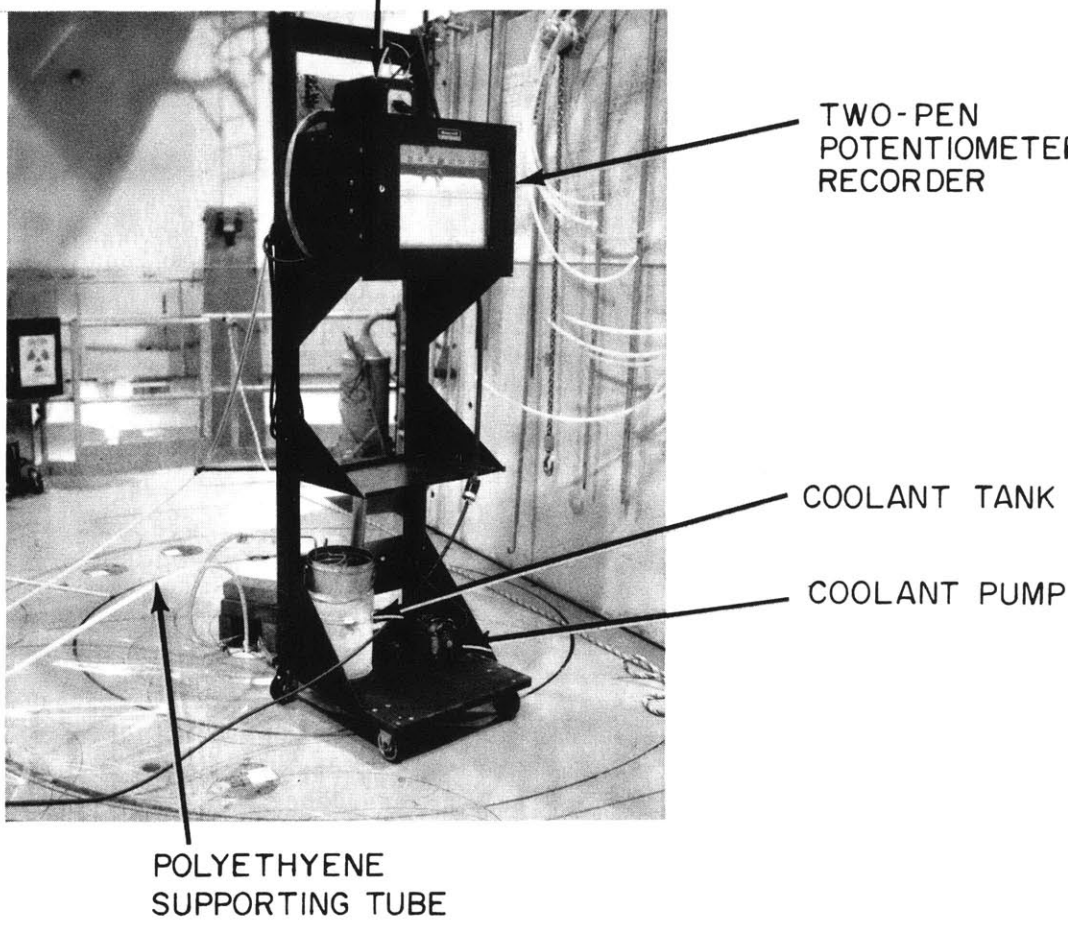

FIGURE 3.3 SERIES IV CALORIMETRIC APPARATUS

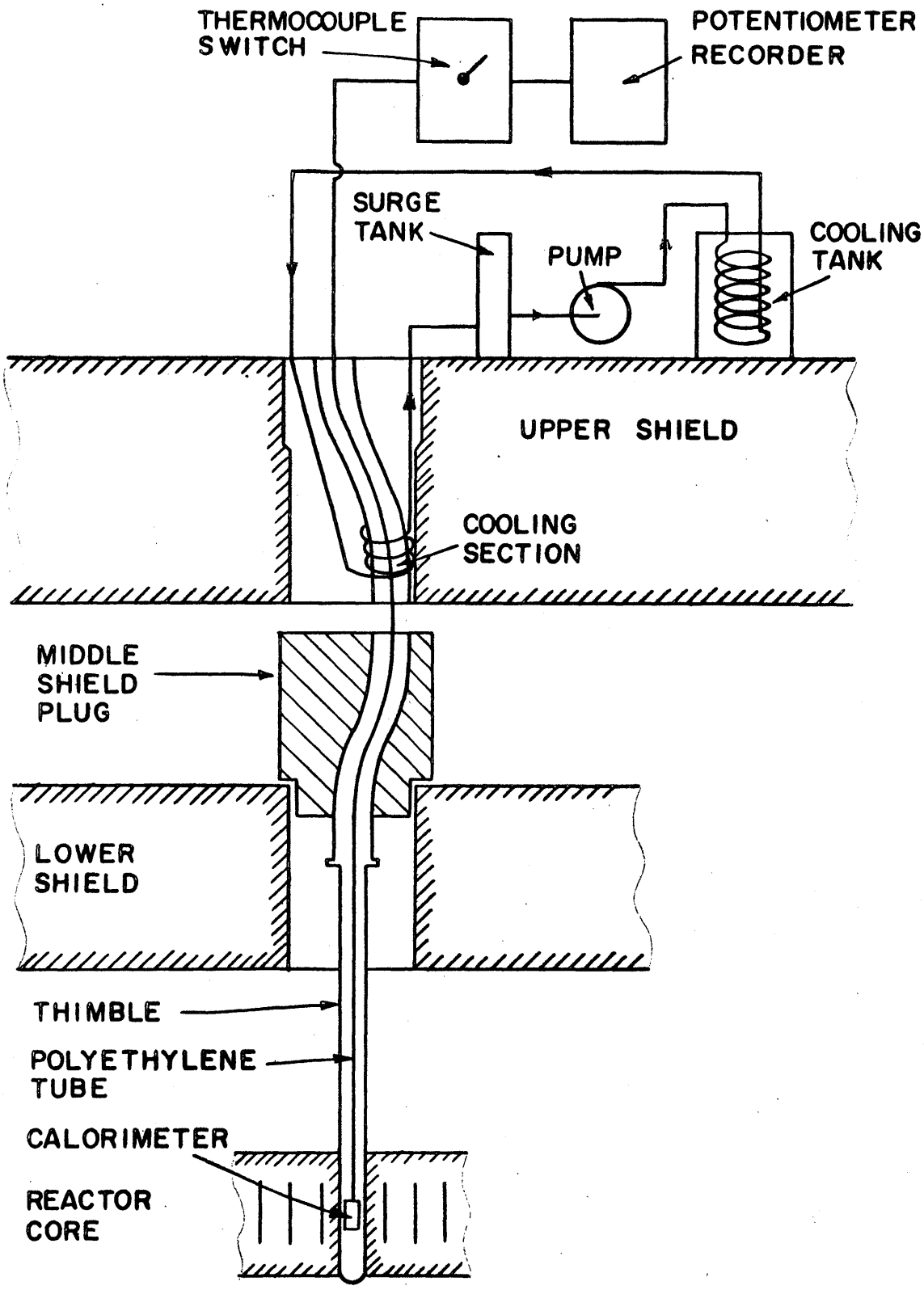

FIGURE 3.4 VERTICAL LAYOUT OF CALORIMETER EQUIPMENT

arrangement of the calorimeter equipment at the reactor. Cooling coils were placed in a specially constructed upper shield plug to permit cooling of the calorimeter between measurements.

3.2.2 Technique of Measurement

The basic method used was to observe the adiabatic rate of temperature rise in several materials having widely varying energy absorption rates due to fast neutrons and gamma rays. The absorbers used in this work were polyethylene, polystyrene, carbon, beryllium, aluminum and solid Santowax OMP. The thermal energy generation rate in a material due to radiation interactions is given by (3.3):

$$R_T^j = K\, C_p^j \left(\frac{dT^j}{dt}\right)_{q=0} \quad \text{watts/gm} \tag{3.1}$$

where

R_T^j is the total dose rate absorbed in material j, watts/gm

C_p^j is the specific heat of material j at temperature T, cal/(gm)(^{o}C)

$\left(\frac{dT^j}{dt}\right)_{q=0}$ is the adiabatic rate of temperature rise of material j, ^{o}F/min

K = 0.0387 (watt)(min)(^{o}C)/(cal)(^{o}F).

The description and specific heats of the Series IV absorber materials are given in Section A1.1.

To perform a dose rate measurement, the calorimeter was cooled in the upper shield plug to a temperature about 5^{o} - 10^{o}F lower than the ambient reactor temperature and then rapidly inserted into the radiation zone. Shortly after insertion the temperature of the calorimeter can exceeded the temperature of the absorber due to thermal contact between the can and the stainless steel thimble in the reactor. Due to the higher radiation heating rate in the absorber, however, the absorber temperature quickly rose to equal and then exceed the temperature of the can (see Fig. 3.5). At the point where these two temperatures were equal the absorber was adiabatic and the desired temperature rise in Eq. (3.1) was calculated from the slope of the line showing the absorber temperature.

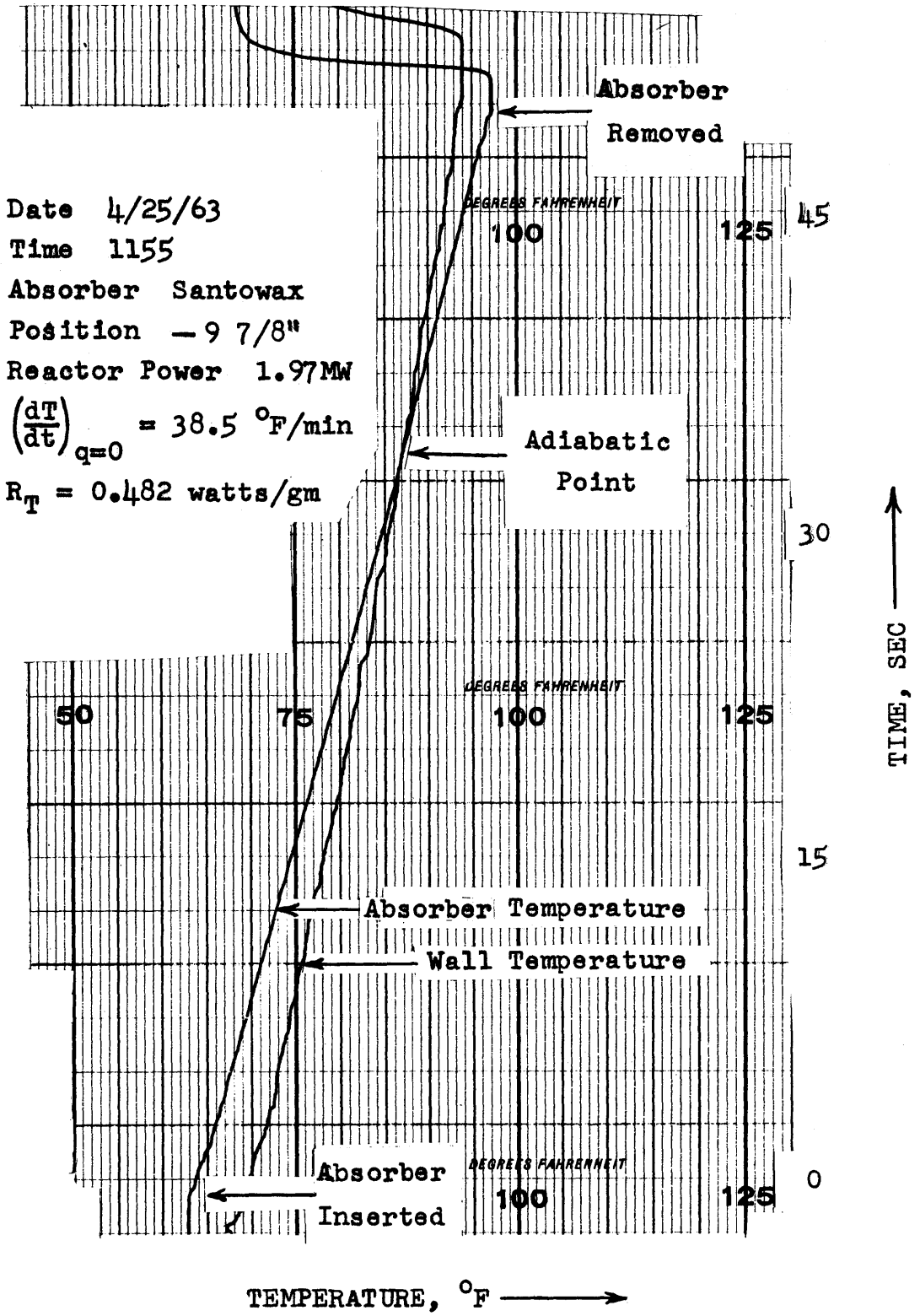

FIGURE 3.5 TYPICAL TEMPERATURE - TIME CURVES FOR A SERIES IV CALORIMETER

3.2.3 Method of Determining Fast Neutron and Gamma Ray Dose Rates

Calculations by Morgan and Mason (3.3) have shown that the only significant radiation sources of heating in the absorbers and in the Santowax OMP in the in-pile section were gamma rays, slowing down of fast neutrons and thermal neutron absorptions. Thus it is possible to write for the j^{th} absorber

$$R_T^j = \sum_i [R_{th}^i + R_\gamma^i + R_N^i] \quad \text{watts/gm} \qquad (3.2)$$

where

R_T^j is the total dose rate measured in the j^{th} absorber, watts/gm

R_{th}^i is the dose rate due to thermal neutron absorption in the i^{th} nuclide in each absorber, watts/gm

R_γ^i is the dose rate due to interactions between gamma rays and the i^{th} nuclide in the absorber, watts/gm

R_N^i is the dose rate due to slowing down of fast neutrons by the i^{th} nuclide in the absorber, watts/gm.

Of the absorbers used, only aluminum had an appreciable thermal neutron heating rate. This heating rate has been calculated at 2 - 10% of the total heating rate in aluminum, depending on the length of time the absorber was irradiated and the axial position in the reactor core (3.3, 3.4, 3.5). The calculation procedure for R_{th}^{Al} is described in Section A1.2.

For the MITR gamma spectrum the gamma ray heating in all absorbers except aluminum was found to be due primarily to Compton scattering (see Section A1.3). In aluminum it has been estimated that approximately 10% of the gamma ray heating was due to the photoelectric effect. In view of the uncertainty of the magnitude of this effect and of the effect of thermal neutron heating, aluminum is no longer used as an integral part of the calorimetry program. However, the analysis presented in this section will still include the aluminum absorber, in order to provide a means of comparison with the results obtained in 1961 before the insertion of the in-pile section into the reactor. The calorimeters used then did not contain carbon and consequently the gamma ray determinations

were based on measurements with aluminum calorimeters. Using the fact that Compton scattering provides the primary gamma heating rate in each absorber, the gamma ray dose rate in each absorber, $\sum_i R_\gamma^i$, may be related to that in carbon, R_γ^C, by:

$$\sum_i R_\gamma^i = \frac{R_\gamma^C}{(Z/A)_C} \left[\frac{\sum_i Z_i}{\sum_i A_i} \right] \quad \text{watts/gm} \tag{3. 3}$$

where

Z_i is the atomic charge of the i^{th} nuclide in the absorber

A_i is the atomic weight of the i^{th} nuclide in the absorber.

This relation was found to be valid for all absorbers except aluminum (see Section A1. 3). About a 10% error occurs in assuming Eq. (3. 3) to be valid for aluminum due to the photoelectric effect in aluminum.

The fast neutron contribution to the total heating rate in an absorber is given by:

$$\sum_i R_N^i = \sum_i N_i I_i \tag{3. 4a}$$

$$= \sum_i N_i g_i S \int_0^\infty \sigma_s^i (E)\, \phi(E)\, EdE \quad \text{watts/gm} \tag{3. 4b}$$

where

N_i is the number of atoms/gm of the i^{th} nuclide in the absorber

I_i is the neutron energy transfer integral for the i^{th} nuclide in the absorber, watts/atom

g_i is the average fraction of neutron energy lost per collision with the i^{th} nuclide in the absorber, equal to $2A_i/(A_i + 1)^2$

S is a conversion factor, $(cm^2)(watt)(sec)/(barn)(ev)$

σ_s^i is the elastic scattering cross section of the i^{th} nuclide in the absorber, barns

$\phi(E)$ is the differential neutron flux, $neutrons/(cm^2)(sec)(ev)$

E is the neutron energy, ev.

Utilizing Eqs. (3.3) and (3.4a), four equations of the form of Eq. (3.2) with $\sum R_{th}^{i} = 0$ may be written for four of the absorbers (polyethylene, polystyrene, carbon and beryllium) containing four unknowns: R_{γ}^{C} and the scattering integrals I_H, I_C and I_{Be}. (A fifth equation, introducing a fifth unknown, I_{Al}, may be written for the aluminum absorber if it is included in the data analysis. The calculation procedure for R_{th}^{Al} is given in Section A1.2). Simultaneous solution of the four equations in four unknowns involves taking the difference between quantities of similar magnitude, which results in poor precision for the values of I_i so obtained. This problem was circumvented by using the fact that although values of I_H, I_C, I_{Be} (and I_{Al}) calculated from Eq. (3.4b) with a knowledge of the neutron cross sections are dependent on the neutron spectrum used, the ratios I_C/I_H, I_{Be}/I_H (and I_{Al}/I_H) were found to be essentially independent of the neutron spectra measured at M.I.T. because the elastic scattering cross sections of the absorbers have the same general energy dependence (see Section 3.3.2). To increase the precision of the derived values, the ratios of I_C/I_H, I_{Be}/I_H (and I_{Al}/I_H) calculated from the measured spectra were therefore used to eliminate I_{Be}, I_C (and I_{Al}) from the equations found by use of Eq. (3.3) and (3.4a) in Eq. (3.2). In addition, the Santowax OMP absorber provided more information without increasing the number of unknowns, adding still further to the precision. The values obtained for I_C/I_H, I_{Be}/I_H and I_{Al}/I_H were 0.18, 0.25 and 0.12 respectively (obtained from the results of Section 3.3.2). Thus for the polyethylene, polystyrene, carbon, beryllium and Santowax OMP absorbers there resulted equations of the form

$$R_T^j = a_j R_{\gamma}^{C} + b_j I_H \text{ watts/gm} \qquad (3.5)$$

(For the aluminum absorber R_T^j in Eq. (3.5) is replaced by $[R_T^{Al} - R_{th}^{Al}]$.) The values of a_j and b_j are given in Table 3.1.

Using the experimentally determined R_T^j values, R_{γ}^{C} was expressed as a function of I_H for each absorber and a least squares analysis was used to determine the "best" values of R_{γ}^{C} and I_H consistent with all the data. The details of the least squares procedure are given in Section A1.4. Figure 3.6 shows a graphical representation of the determination of the "best" values of R_{γ}^{C} and I_H. The aluminum absorber (corrected for thermal neutron heating) was not included in the least squares analysis

1. See Section A1.4 for details of the least squares analysis.

TABLE 3. 1

Constants a_j and b_j Used for Calorimeter Absorbers

Absorber	a_j	b_j, 10^{-22} atoms/gm
Polyethylene	1. 14	9. 40
Polystyrene	1. 08	5. 48
Carbon	1. 00	0. 919
Beryllium	0. 886	1. 68
Santowax OMP	1. 06	4. 52
Aluminum	0. 964[a]	0. 263

a. Based on Compton scattering assumption.

and is shown in Fig. 3. 6 for comparison purposes only. The aluminum curve (which here assumes all Compton scattering) appears to have too high an intercept, which is consistent with the low value of a_{Al} predicted from the Compton scattering relation. (There is a significant photoelectric effect in aluminum; see above.)

3. 2. 4 Results obtained with Series IV Calorimeters (3. 5)

A detailed listing of the results obtained with the Series IV calorimeters may be found in Section A1. 6. The axial variation of the total measured dose rates in the stainless steel thimble after the removal of the in-pile assembly (4/24/63) is shown in Fig. 3. 7 for each of the absorbers used. At the time these measurements were made, the beryllium calorimeter was being repaired.

Figure 3. 8 shows the results of the least squares analysis for the "best" values of R_γ^C and I_H, using the data obtained with the polyethylene, polystyrene, carbon and Santowax OMP absorbers. The results are shown in terms of the calculated dose rates to Santowax OMP in the in-pile assembly, R_γ^{SW}, R_N^{SW} and R_T^{SW}. These values are obtained from the "best" values of R_γ^C and I_H by using the data of Table 3. 1:

$$R_\gamma^{SW} = 1.06\, R_\gamma^C \quad \text{watts/gm} \tag{3.6}$$

$$R_N^{SW} = 4.52 \times 10^{22}\, I_H \quad \text{watts/gm} \tag{3.7}$$

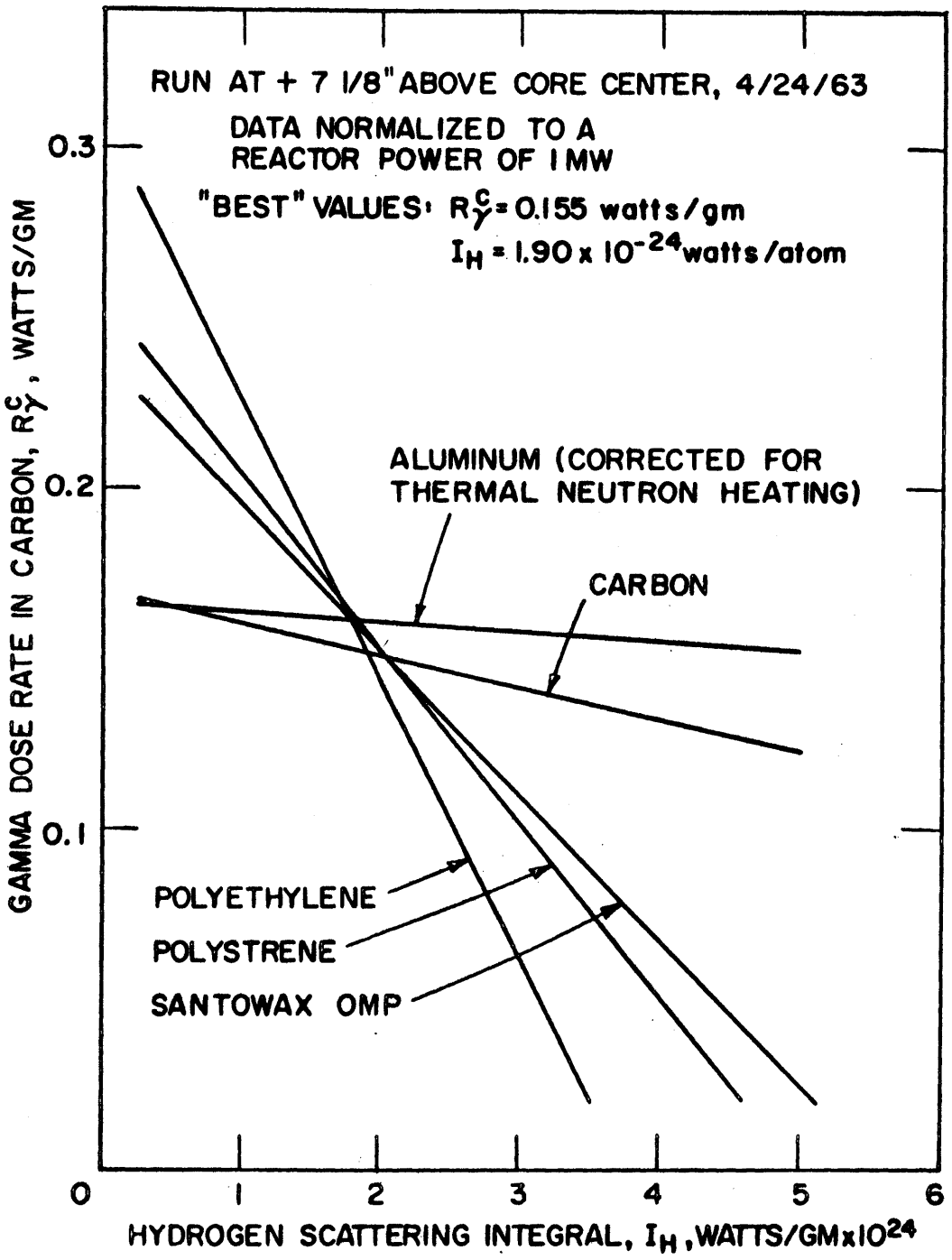

FIGURE 3.6 GRAPHICAL REPRESENTATION OF TYPICAL MEASURED DOSE RATES

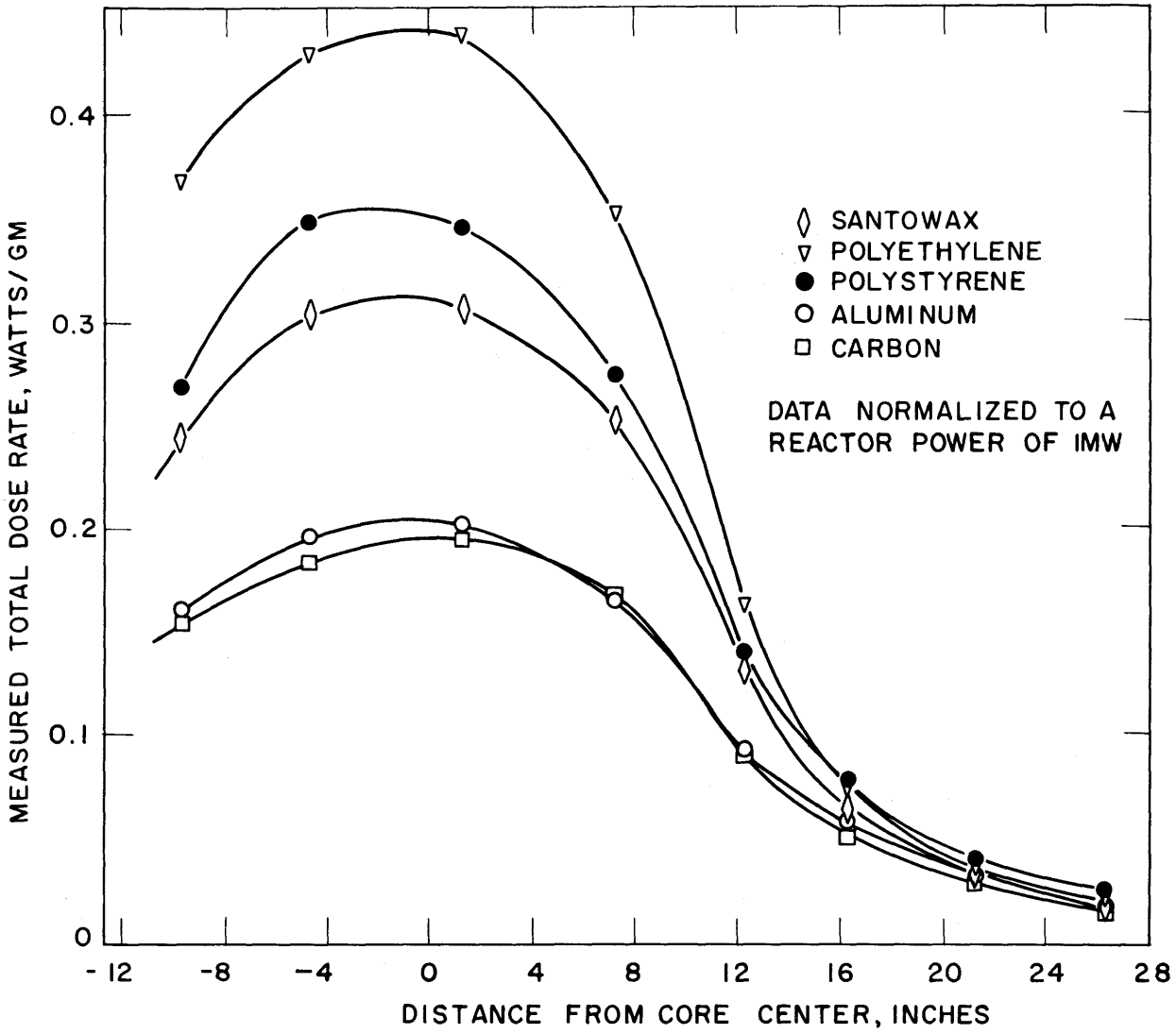

FIGURE 3.7 TOTAL MEASURED DOSE RATES IN SERIES IV CALORIMETERS (4/24/63)

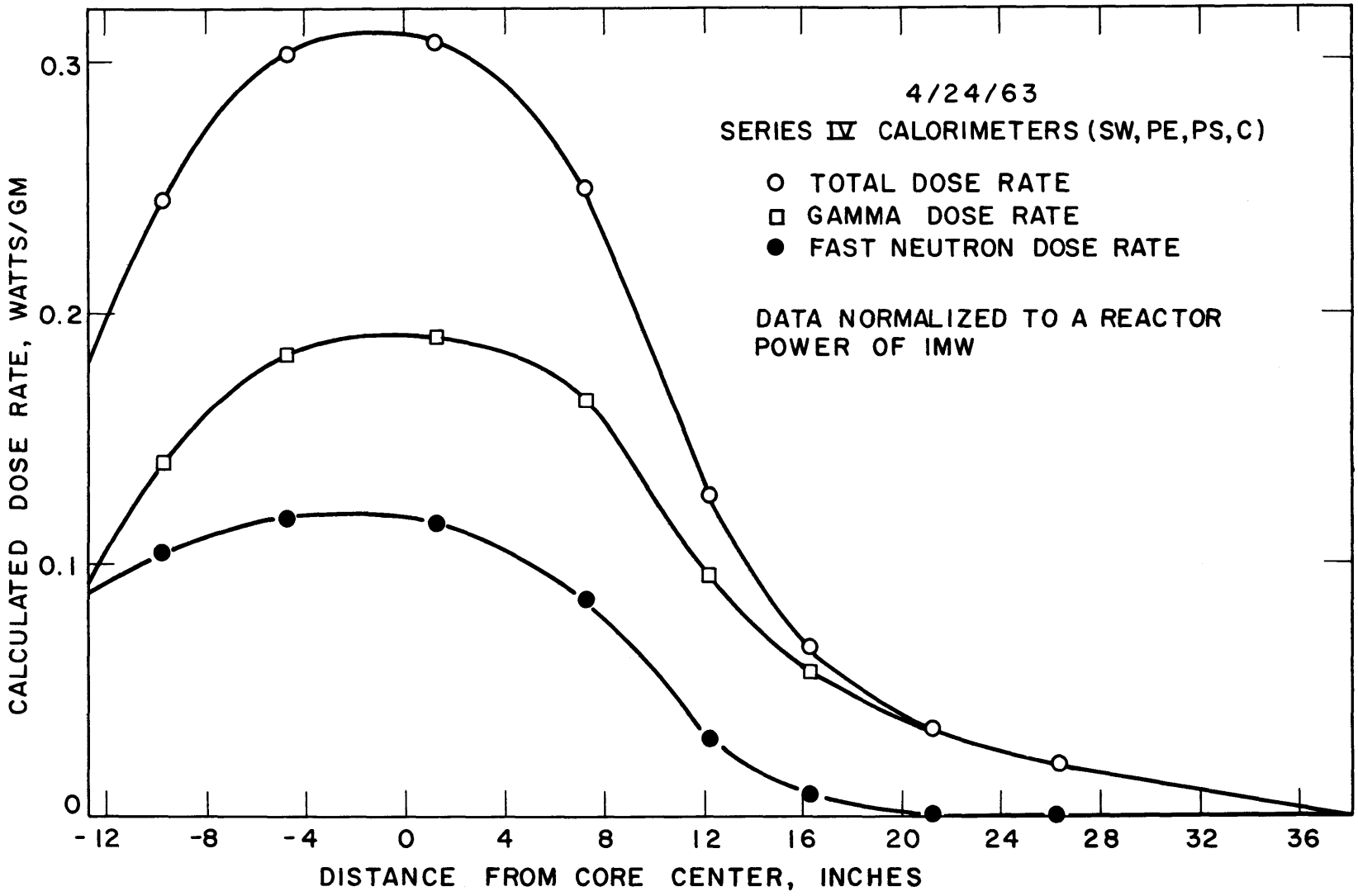

FIGURE 3.8 AXIAL VARIATION OF CALORIMETRIC DOSE RATES AFTER REMOVAL OF IN-PILE SECTION

$$R_T^{SW} = R_\gamma^{SW} + R_N^{SW} \quad \text{watts/gm} \tag{3.8}$$

The maximum possible errors in the values obtained have been estimated as follows: ± 4% for R_γ^{SW}, ± 6% for R_N^{SW} and ± 3% for R_T^{SW} (see Section A1.6). The calculated dose rate in Santowax OMP shown in Fig. 3.8 agreed with the dose rate measured in the Santowax OMP absorber (see Fig. 3.7) to within 0.5% in the core region of the reactor (−12" to +12" relative to core center).

Using the procedure given by Morgan and Mason (3.3) the integrated dose rates to Santowax OMP in the in-pile assembly were obtained. The rate at which energy is absorbed in Santowax OMP in the in-pile assembly is given by:

$$\frac{dD}{d(MWH)} = \rho F_T = \rho \int_{L_L}^{L_T} \frac{R_T^{SW}}{P_o} \, x \, dL \tag{3.9}$$

where

- D is the absorbed energy, watt-hr
- MWH is the period of reactor operation, megawatt-hours
- ρ is the organic density, gm/cc
- F_T is the total in-pile dose rate factor, (watt)(hr)(cc)(MWH)(gm)
- L_L is the bottom of the in-pile capsule, relative to the reactor core center, inches
- L_T is the top of the in-pile assembly from the reactor core center, inches
- P_o is the power level of the reactor at the time of measurement of R_T^{SW}, megawatts
- x is the volume per unit length of the capsule or tubing, cm/inch.

The period of reactor operation is given by the relation

$$\frac{d(MWH)}{dt} = P(t) \tag{3.10}$$

where

- t is the physical time elapsed, hours
- P is the reactor power level at time t, megawatts.

The definition of reactor MWH provides a convenient time scale, since no changes occur in the fuel burnup of the reactor or in the properties of Santowax OMP when the reactor is down.[1] Both the coolant density, ρ, and the in-pile dose rate factor, F_T, were considered as functions of the reactor MWH.

The quantity F_T may be evaluated using the measured volume of the irradiation capsule and tubing by the relation:

$$F_T = \int_{L_L}^{L_U} \frac{R_T^{SW}}{P_o} x_1 \, dL + \int_{L_U}^{L_T} \frac{R_T^{SW}}{P_o} x_2 \, dL \qquad (3.11)$$

where

x_1 = 8.02 cc/inch

x_2 = 3.21 cc/inch

L_L = −12 75 inches

L_U = +12.875 inches

L_T may be replaced by ∞.

Using these values and graphically integrating Fig. 3.8, the results shown in Table 3.2 were obtained. The in-pile dose rate factor has been divided

TABLE 3.2

Absorbed Dose Rates in Santowax OMP as Calculated from Series IV Calorimetric Measurements (4/24/63) with Polyethylene, Polystyrene, Santowax OMP and Carbon Absorbers

In-Pile Dose Rate Factors, $\frac{(watt)(hr)(cc)}{(MWH)(gm)}$[a]			$f_N = F_N/F_T$ (%)	$f_\gamma = F_\gamma/F_T$ (%)	f_N/f_γ
F_N	F_γ	F_T			
20.5 ± 1.2[b]	35.3 ± 1.4	55.8 ± 1.8	37 ± 2	63 ± 2	0.58 ± 0.04

a. Multiplication by the coolant density gives the absorbed dose rate.
b. Maximum possible error limits.

into the factor due to fast neutrons, F_N, and the factor due to gamma rays, F_γ. Also shown is the fast neutron fraction of the dose, f_N, the gamma ray

1. A change in fuel burnup would cause a change in the dose rate to Santowax OMP.

fraction of the dose, f_γ, and the ratio f_N/f_γ. The maximim possible errors are based on the estimates given in Section A1.6. The average total dose rate in the core region of the reactor is calculated from the data of Table 3.2 as 0.51 ± 0.02 watts/gm.

A set of measurements with Series IV calorimeters was performed over a period of a week, beginning on Monday, 4/29/63, to see whether there was any measurable difference in dose rate delivered by the reactor from startup Monday morning to shutdown Friday afternoon. The results of these measurements are shown in Fig. 3.9 in the form of calculated dose rates to Santowax OMP. The absorbers used on each day are indicated above each set of results. The error limits drawn are based on the estimates given above, but it should be noted that the calorimeters used were polyethylene, carbon and aluminum for the Monday, Tuesday and Thursday measurements and polyethylene, polystyrene and carbon for the Friday measurements. As stated above, the results obtained with aluminum are expected to give high values of R_γ^{SW} because of the photoelectric effect in aluminum. This explains why the Friday results differ somewhat from the rest of the week's measurements. In spite of the consistent error in the aluminum absorber, trends may still be observed with its use, and the Monday, Tuesday and Thursday measurements certainly display no trend. Thus it was concluded that the total dose rate to Santowax OMP, and the fast neutron and gamma ray fractions of this dose rate, did not vary significantly over the course of a cycle of reactor operation.

A final series of measurements was made on Friday, 5/10/63, with the Series IV calorimeters before the removal of the central fuel element, 2MR11, (the one which had contained the in-pile assembly). The purpose of these measurements was to check the linearity of absorbed dose in Santowax OMP with reactor power level. Previous measurements reported by Morgan and Mason (3.3) were performed at a power level of 100 kw and extrapolated to full reactor power (approximately 2 MW) so a check on the linearity of absorbed dose rate with reactor power was deemed necessary. Figure 3.10 shows the results of these measurements. Because the measurements were made in the order of decreasing reactor power level, and because only about one hour elapsed between each drop in power level and the calorimetric measurements made at the new power

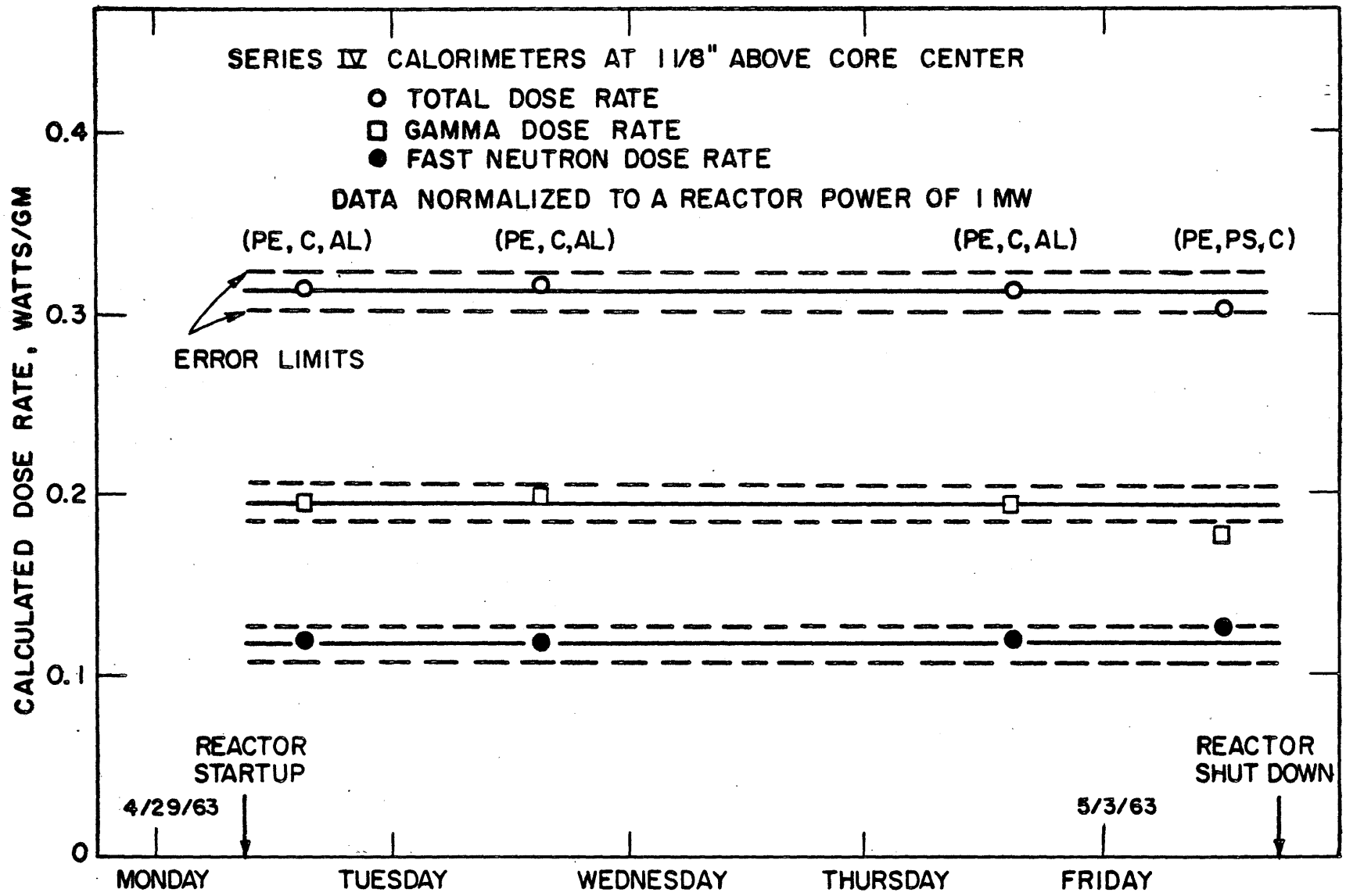

FIGURE 3.9 VARIATION OF CALORIMETRIC DOSE RATES OVER A PERIOD OF ONE WEEK

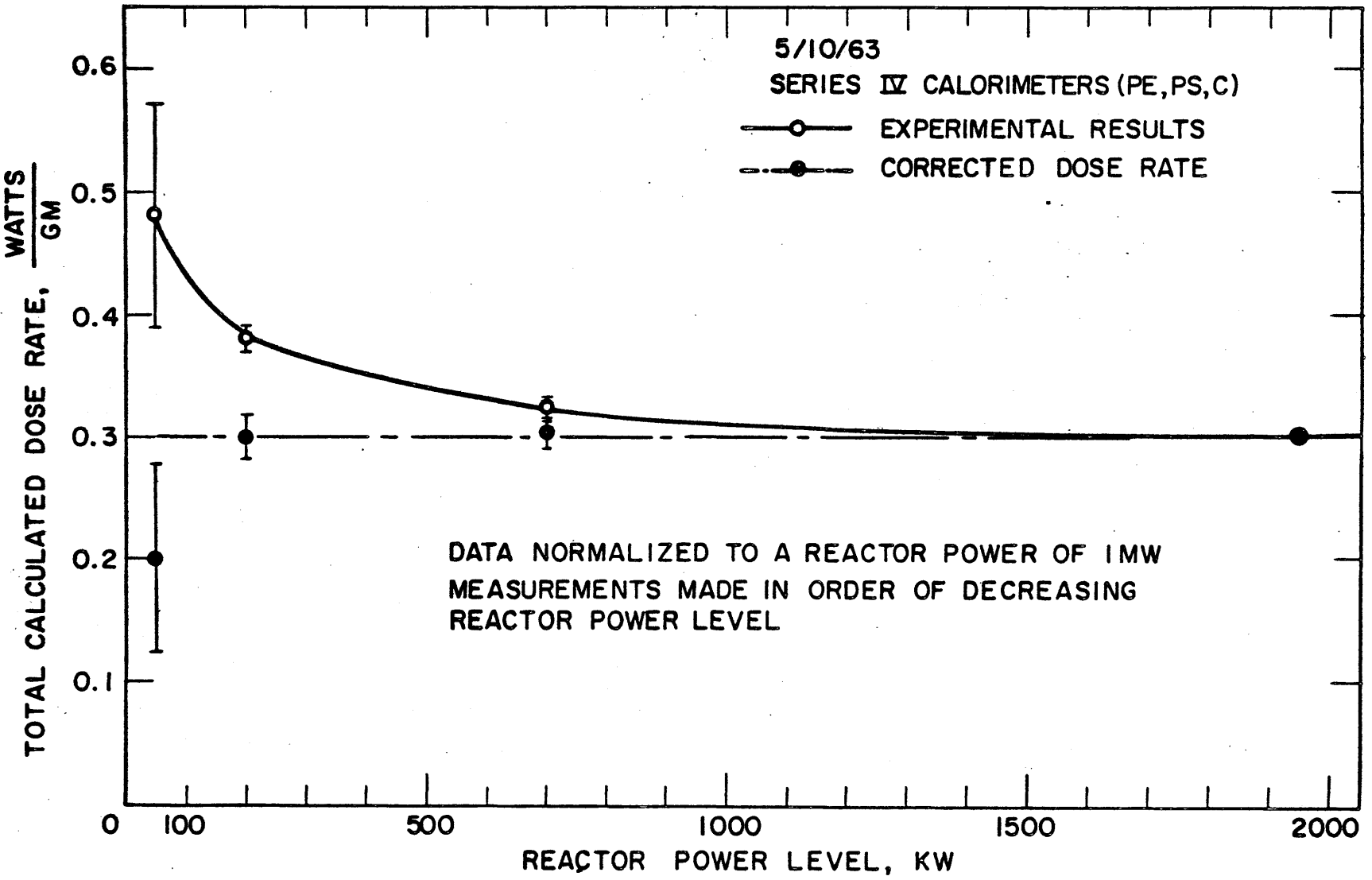

FIGURE 3.10 VARIATION OF NORMALIZED DOSE RATE AT CORE CENTER WITH REACTOR POWER LEVEL

level, there existed a significant amount of excess (above equilibrium) delayed gamma ray heating. Thus the total dose rates measured at each power level below the starting point (1.95 MW) were too large due to the excess delayed gamma dose rate. An approximate method of treating the effect of these delayed gamma rays is developed in Section A1.7. The corrected dose rates are also shown in Fig. 3.10, where it may be seen that the steady-state dose rate does indeed appear to be linear with reactor power. Error limits are shown for each data point based solely on the calculated standard deviations in the least squares analysis of the data. As may be seen the 50 kw data have a large possible error. In spite of this, the corrected dose rates for the 50 kw measurements were not expected to be very meaningful as the delayed gamma corrections were nearly as large as the measured dose rates.

The Series III calorimetric measurements reported by Morgan and Mason (3.3) were obtained at a reduced reactor power level of 100 kw on Monday mornings a few hours after reactor startup. The delayed gamma heating was measured with the calorimeters before reactor startup and the corrected dose rates obtained were extrapolated to full thermal reactor power (about 2 MW). The data shown in Fig. 3.10 clearly show the advantages of measurements made at full power without the need for extrapolation.

3.2.5 Comparison of Series IV and Series III Calorimetric Measurements

The measurements performed with Series III calorimeters on 3/20/61 before the insertion of the in-pile assembly have been reported by Morgan and Mason (3.3). Meaningful measurements were performed with only three Series III calorimeter absorbers: polyethylene, polystyrene and aluminum. These measurements have also been subjected to the least squares analysis recently developed for the Series IV calorimeters, and the detailed results of these calculations are listed in Section A1.6. The results are also shown in Fig. 3.11. A direct quantitative comparison of Fig. 3.11 with Fig. 3.8 is not completely meaningful because of the aluminum absorber used for the Series III measurements. Corrections for this fact are described below, but a glance at the two figures does show that the dose rate at core center had decreased about 10% during the period 3/20/61 to 4/24/63. Graphical integrations of Fig. 3.11 were

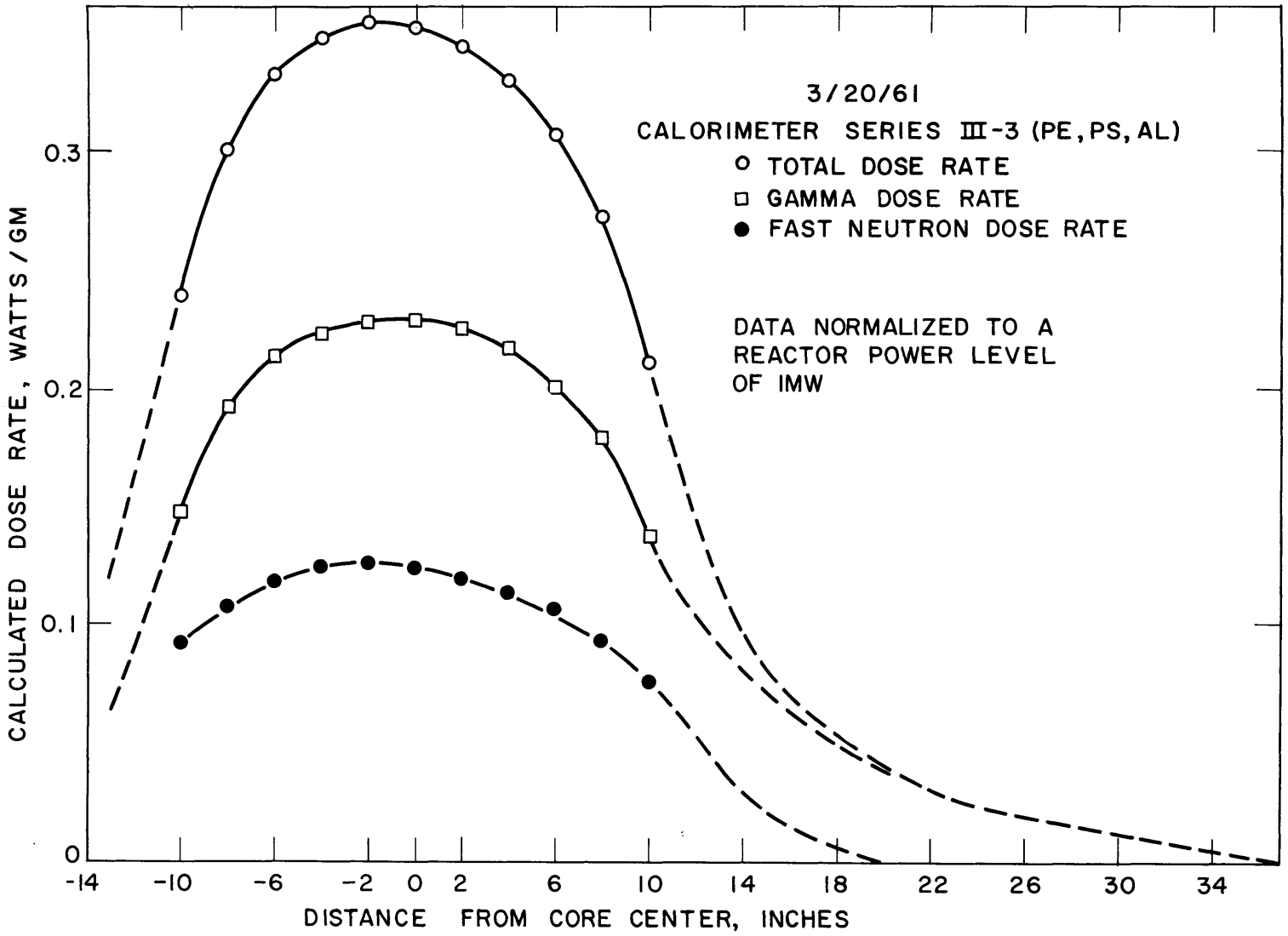

FIGURE 3.11 AXIAL VARIATION OF CALORIMETRIC DOSE RATES BEFORE INSERTION OF IN-PILE SECTION

performed with the aid of Eq. (3.11) to obtain the in-pile dose rate factors F_N, F_γ and F_T and the fast neutron and gamma ray dose fractions f_N and f_γ. The results of these calculations are summarized in Table 3.3. The error limits given are based on estimates of Morgan

TABLE 3.3

Absorbed Dose Rates in Santowax OMP as Calculated from Series III Calorimetric Measurements (3/20/61) with Polyethylene, Polystyrene and Aluminum Absorbers

In-Pile Dose Rate Factors, $\frac{(watt)(hr)(cc)}{(MWH)(gm)}$[a]			$f_N=F_N/F_T$	$f_\gamma=F_\gamma/F_T$	f_N/f_γ
F_N	F_γ	F_T	(%)	(%)	
21.1 ± 1.5	40.3 ± 2.5	61.4 ± 2.9	34 ± 2	66 ± 2	0.52 ± 0.05

a. Multiplication by coolant density gives the absorbed dose rates.

and Mason (3.3). These estimates included errors due to extrapolation of the measured dose rates, as only the range −10" to +10" relative to core center was covered by the measurements.

In order to provide a better comparison of the Series IV calorimetric dose rates to those obtained with the Series III calorimeters, calculations similar to those described above were performed with the Series IV polyethylene, polystyrene, Santowax OMP and aluminum calorimetric measurements (carbon was left out of the analysis). The replacement of the Series IV carbon calorimetric measurements by the Series IV aluminum calorimetric measurements was done for comparison purposes with the Series III calorimetric measurements only, as the Series III measurements were performed without a carbon absorber. The results of these calculations are summarized in Table 3.4.

Comparison of Tables 3.3 and 3.4 shows no statistical change in fast neutron-gamma ray ratio for the period 3/20/61 to 4/24/63. Since measurements with the aluminum absorber were known to give a high gamma ray dose rate due to the photoelectric effect in aluminum, the fractions of the absorbed dose due to gamma rays and fast neutrons used in this work were those obtained from the Series IV calorimetric measurements excluding aluminum from the analysis (see Table 3.2). The total

TABLE 3. 4

Absorbed Dose Rates in Santowax OMP as Calculated from Series IV Calorimetric Measurements (4/24/63) with Polyethylene, Polystyrene, Santowax OMP and Aluminum Calorimeters

In-Pile Dose Rate Factors, $\frac{(watt)(hr)(cc)}{(MWH)(gm)}$ [a]			$f_N = F_N/F_T$	$f_\gamma = F_\gamma/F_T$	f_N/f_γ
F_N	F_γ	F_T	(%)	(%)	
18. 3 ± 1. 1	38. 3 ± 1. 5	56. 6 ± 1. 9	32 ± 2	68 ± 2	0. 48 ± 0. 03

a. Multiplication by coolant density gives the absorbed dose rate.

absorbed dose rate in Santowax OMP measured with the Series III calorimeters was corrected for the use of an aluminum absorber by the relation

$$(R_T^{SW})_{III\ corr.} = (R_T^{SW})_{III\ uncorr.} \left[\frac{(R_T^{SW})_{IV\ using\ C}}{(R_T^{SW})_{IV\ using\ Al}} \right] \qquad (3.12)$$

The corrected total in-pile dose rate factor obtained for the Series III measurements is shown in Table 3. 5 which provides a summary of

TABLE 3. 5

Comparison of Series III and Series IV Calorimetric Measurements

Measurement	Total In-Pile Dose Rate Factor, F_T $\frac{(watt)(hr)(cc)}{(MWH)(gm)}$	Average Dose Rate in Core Region watts/gm	Fast Neutron Fraction of Dose Rate, f_N (%)
Series III-3 (3/20/61)	60. 5 ± 2. 9 [b]	0. 55 ± 0. 02	37 ± 2 [a]
Series IV (4/24/63)	55. 8 ± 1. 9	0. 51 ± 0. 02	37 ± 2

a. Best value for entire period of irradiation.
b. Maximum possible error limits.

the results of the Series III and Series IV measurements. It can be seen that the dose rate to Santowax OMP in the in-pile assembly decreased about 10% during the period 3/20/61 to 4/24/63.

3.3 Foil Activation Measurements

3.3.1 Equipment and Theory

The foil activation program was developed by Sefchovich (3.6) and has been described by Morgan and Mason (3.3). Details of the theory used are given in Sections A1.8 to A1.14.

Thermal fluxes were determined by cadmium difference measurements on Co-Al wires, utilizing the relation

$$\phi_{2200} = \frac{(Act)_B - (Act)_{Cd}}{\sigma_{2200}(1 - e^{-\lambda T})} \times 10^{24} \quad n/(cm^2)(sec) \qquad (3.13)$$

where

σ_{2200} is the 2200 m/sec cross section for Co^{59}, barns

λ is the disintegration constant for Co^{60}, min^{-1}

T is the irradiation time, min

$(Act)_B$ is the bare absolute activity per atom of the irradiated wire just after being removed from the radiation zone, dis/sec

$(Act)_{Cd}$ is the cadmium covered activity per atom of the irradiated wire just after being removed from the radiation zone, dis/sec.

The absolute activities of the irradiated Co-Al wires were determined by counting with a NaI well-type scintillation crystal of known efficiency, and the precision of the results has been estimated at ± 8% (see Section A1.11 for details of the calculation of the standard deviation).

Epithermal fluxes were determined by assuming a 1/E energy dependence from the cadmium cutoff energy (0.5 ev) through the resonance region (100-1000 ev). Cadmium ratio measurements were made with Co-Al and copper wires, and the neutron flux in this region was determined from

$$\phi(E) = \frac{\phi_o}{E} \qquad (3.14)$$

$$\phi_o = \frac{\phi_{2200}\,\sigma_{2200}}{(R_{Cd} - 1)(T.R.I.)} \qquad (3.15)$$

$$\text{T.R.I.} = \int_{E_c}^{\infty} (\sigma_{res} + \sigma_{1/v}) \frac{dE}{E} = \text{total resonance integral} \qquad (3.16)$$

where

$\phi(E)$ is the neutron flux per unit energy (differential flux) $n/(cm^2)(sec)(ev)$

ϕ_o is a constant, $n/(cm^2)(sec)$

R_{Cd} is the cadmium ratio

σ_{res} is the resonance cross section, barns

$\sigma_{1/v}$ is the 1/v cross section, barns

E_c is the cadmium cutoff energy (0.5 ev).

The resonance energies for Co^{59} and Cu^{63} are given in Table 3.6 as 120 ev and 570 ev respectively. The cross sections used are tabulated in Section A1.9. The irradiated foils were also counted with the NaI crystal, and the standard deviation of the results was estimated at ± 10% (see Section A1.11 for details).

Neutron fluxes above 2 Mev were determined by a modification of the Trice method (3.3). Four threshold detectors were used for the measurement: sulfur, nickel, magnesium and aluminum; the nuclear reactions used and the effective threshold energies are given in Table 3.6. The absolute count rates of the Ni, Mg and Al wires were determined with the NaI scintillation crystal, knowing the crystal efficiency for each species (see Section A1.10 for details). For the sulfur detectors, the irradiated material was dissolved in 2N hydrochloric acid (containing 1 g per 80 cc $(NH_4)_3PO_4$ as a carrier for the P^{32}), and the dissolved sample was placed on a planchet and dried before counting in a GM tube. A simulated P^{32} source with a known absolute count rate was used to determine the absolute count rate of the irradiated sulfur detectors. The activity of each threshold detector may be written as

$$\text{Act} = \int_{E_{th}}^{\infty} N\sigma(E)\phi(E)dE = N\overline{\sigma}_{eff} \int_{E_{eff}}^{\infty} \phi(E)dE$$

$$= N\overline{\sigma}_{eff}\phi(\geq E_{eff}) \qquad (3.17)$$

TABLE 3.6

Foils Used for Neutron Flux Measurements

Flux	Detector	Form	Resonance or Effective Threshold Energy
Thermal	Co^{59}	CoAl wire	
Epithermal	Co^{59}	CoAl wire	120 ev
	Cu^{63}	Wire	570 ev
Fast	$S^{32}[S^{32}(n,p)P^{32}]$	$MgSO_4$	3.0 Mev
	$Ni^{58}[Ni^{58}(n,p)Co^{58}]$	Cadmium-covered wire	2.9 Mev
	$Mg^{24}[Mg^{24}(n,p)Na^{24}]$	Wire	6.3 Mev
	$Al^{27}[Al^{27}(n,\alpha)Na^{24}]$	Wire	8.1 Mev

where

N	is the number of atoms in the detector
$\overline{\sigma_{eff}}$	is an effective step function cross section
E_{eff}	is an effective threshold energy
$\phi(\geq E_{eff})$	is the integral neutron flux above E_{eff}.

The cross sections used are tabulated in Section A1.9. For a first approximation $\phi(E)$ was assumed to approximate the Watt fission spectrum (see Section A1.8 for details) so that $\overline{\sigma_{eff}}$ could be determined. Thus for each detector the integral flux could be determined as

$$\phi(\geq E_{eff}) = \frac{Act}{\overline{\sigma_{eff}}(1 - e^{-\lambda T})} \tag{3.18}$$

The integral fluxes obtained by this method followed a simple exponential dependence on energy and so were fit by the method of least squares to

$$\ln \phi(\geq E) = c + dE \tag{3.19}$$

and the differential flux was determined by differentiation to be

$$\phi(E) = -de^{c + dE} \tag{3.20}$$

Using Eq. (3.20) the values of $\overline{\sigma_{eff}}$ were recomputed and an iterative process was set up. The iteration was terminated when the values of $\overline{\sigma_{eff}}$ did not change by more than 1% between iterations. The standard deviation in the fast flux determination by this method was estimated to be $\pm$ 13% (see section A1.11 for details).

3.3.2 Results

It should be pointed out before the presentation of the results obtained in this work that the results obtained from foil measurements are quite dependent on the cross section data used in the calculations. Every effort was made to obtain the best available cross section data for the isotopes used (usually the most recent), and these data are tabulated in Sections A1.9 and A1.13.

The axial distribution of the thermal neutron flux in the monitor tube is shown in Fig. 3.12 for typical runs. Runs R and S and 11 and 13 were averaged since the time elapsed between the runs was small compared to the two years of operation with the fuel element. The fluxes shown are all

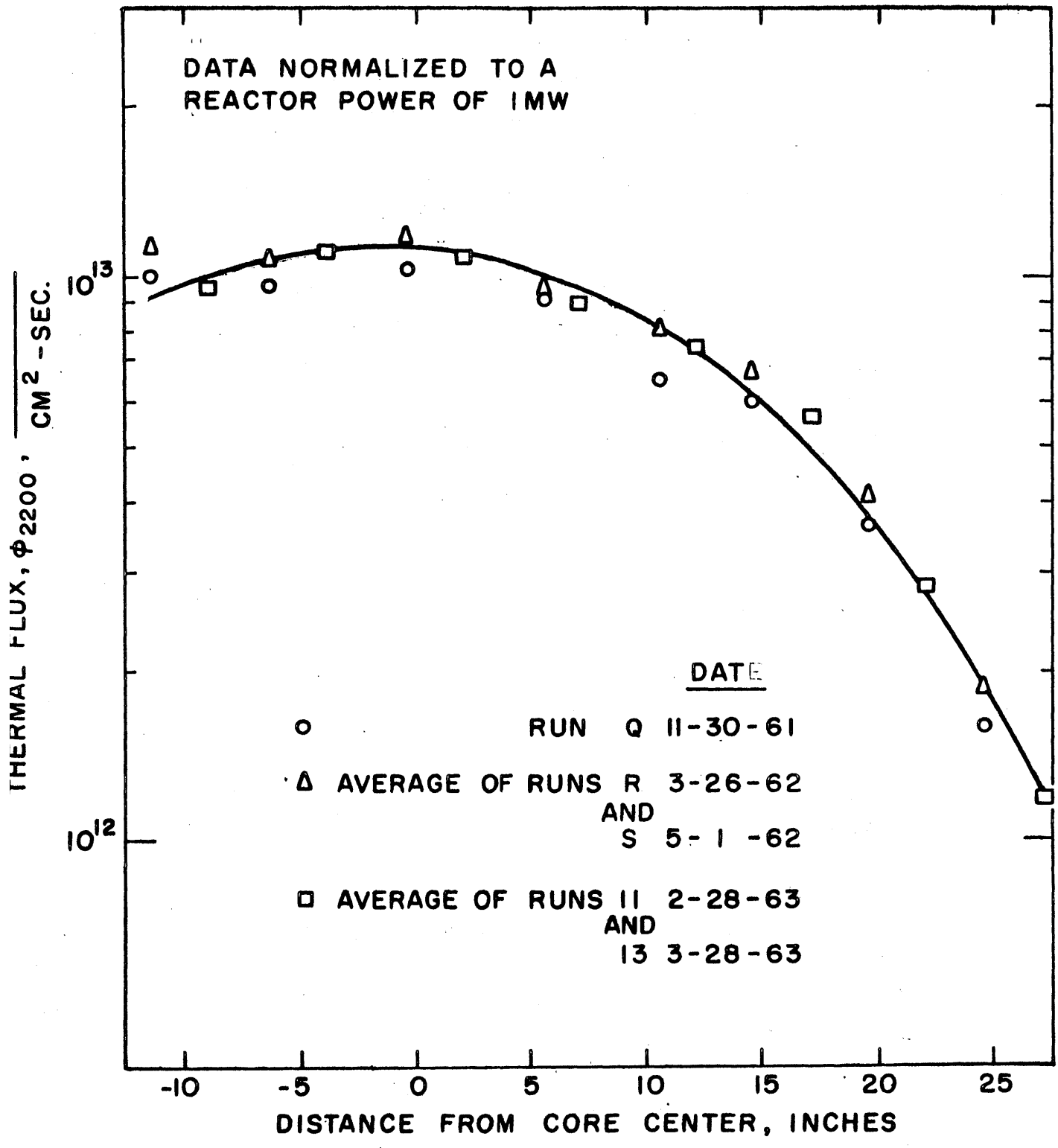

FIGURE 3.12 AXIAL VARIATION OF THERMAL NEUTRON FLUX

normalized to a reactor power level of 1 MW (the reactor normally operated near 2 MW). The change of flux with time is discussed below. The axial distribution of the differential flux at 120 ev (cobalt resonance) in the monitor tube is shown in Fig. 3. 13 and the axial variations of the differential flux at 3. 0 Mev (sulfur) and at 8. 1 Mev (aluminum) are shown in Fig. 3. 14. Again the data are normalized to a reactor power of 1 MW.

The variation of the neutron flux at a given position with time is exhibited in Fig. 3. 15 for the flux at the core center. The data are plotted against the period of reactor operation, in MWH. Zero MWH corresponds to the startup of the 610^{O}F irradiation of Santowax OMP. As may be seen from Fig. 3. 15, the thermal flux at the core center appears to have remained constant over the period of operation, while the resonance flux at 120 ev, $\phi(E)_{120\ ev}$, appears to have decreased some 15% and the fast fluxes $\phi(E)_{3\ Mev}$ some 30% and $\phi(E)_{8.1\ Mev}$ some 25%.

Morgan and Mason (3. 3) have shown that over 90% of the fast neutrons in the in-pile section come from the central fuel element, which was not replaced during the two years of irradiation. Surrounding elements were replaced at intervals to maintain a reasonably constant power distribution over the core. Therefore it is reasonable to expect a change in the fast flux but not in the thermal flux, since the mean free path for thermal neutrons in D_2O is very much larger than the slowing down length. The data are plotted on a convenient scale to show the trend. It appears that linear decreases in the resonance and fast differential fluxes fit the data as well as any other manner of decrease.

In order to compare the neutron fluxes in the monitor tube with those inside the in-pile capsule, a special experiment (run 14, 4/19/63) was performed just before the removal of the in-pile section. A small aluminum tube (1/4 inch O. D.) whose lower end was sealed was inserted into the stainless steel irradiation capsule from the top of the in-pile section, and the in-pile section was filled with isopropyldiphenyl to mock up the effect of the irradiated Santowax OMP in the in-pile section. Cobalt, nickel and aluminum detectors were attached to lengths of aluminum wire, and the wires were inserted simultaneously into the monitor tube and into the aluminum tube with the reactor operating at 500 kw. The results of this experiment (normalized to a reactor power level of 1 MW) are

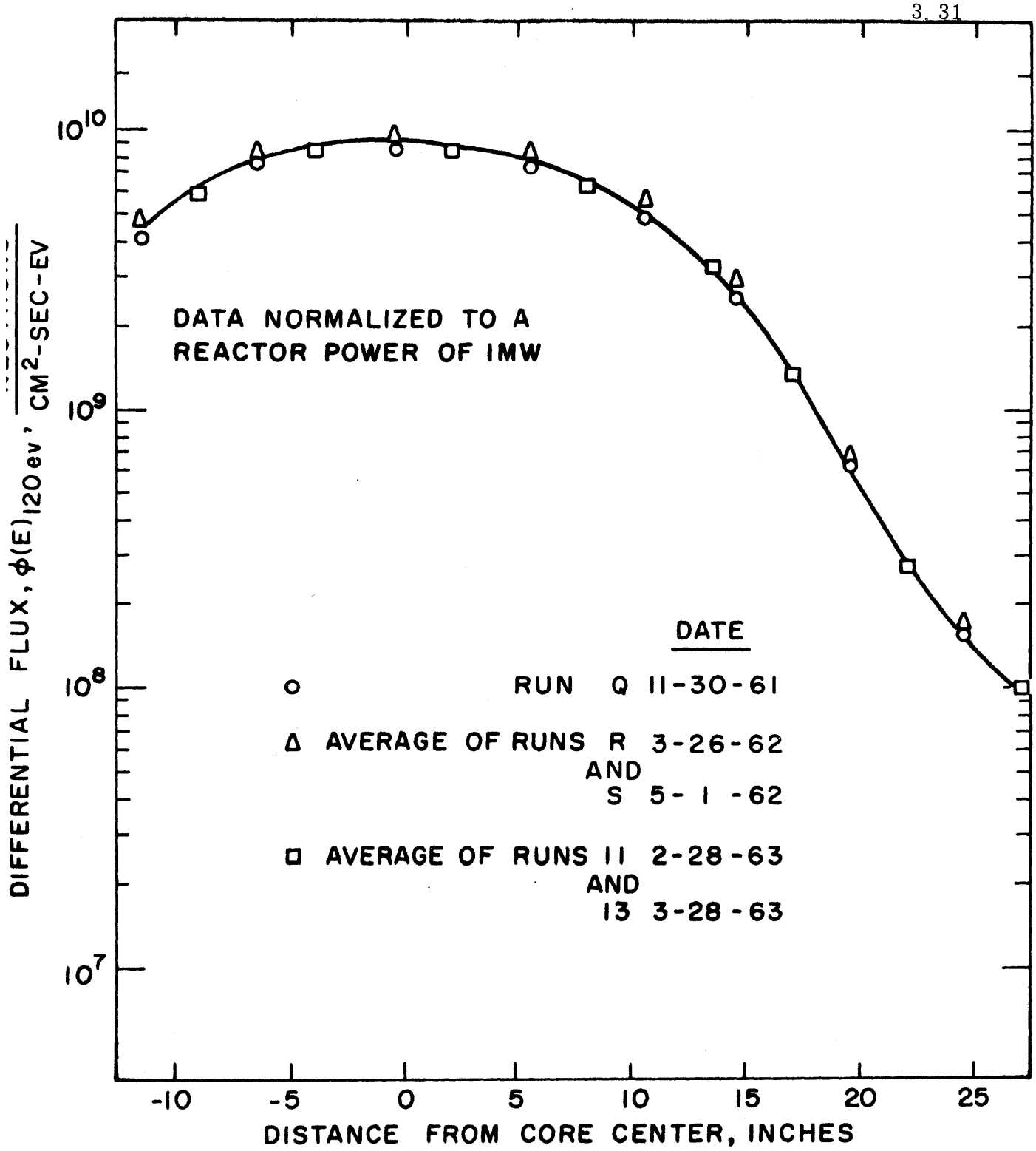

FIGURE 3.13 AXIAL VARIATION OF 120 EV NEUTRON FLUX

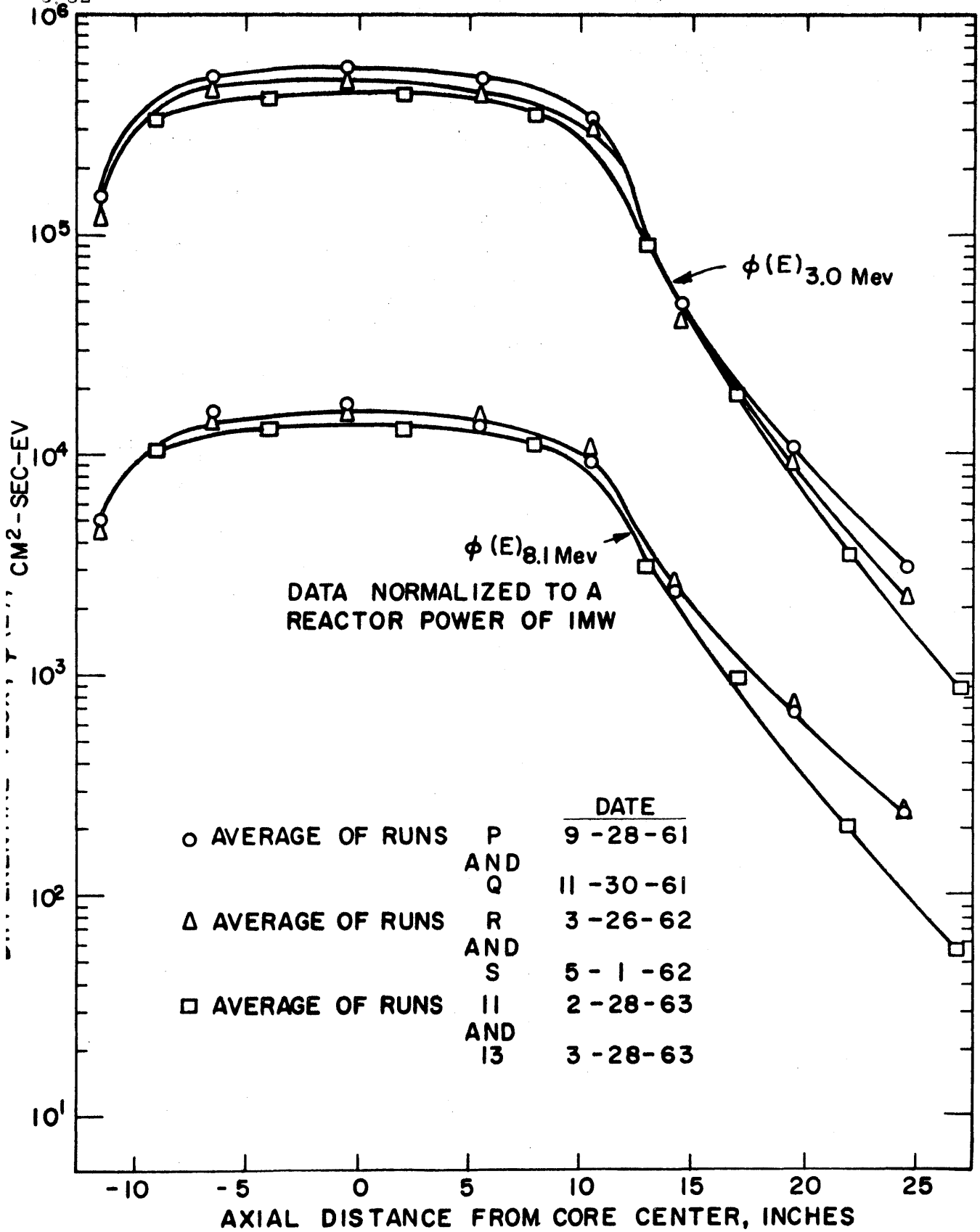

FIGURE 3.14 AXIAL VARIATION OF DIFFERENTIAL NEUTRON FLUX IN THE FAST NEUTRON ENERGY RANGE

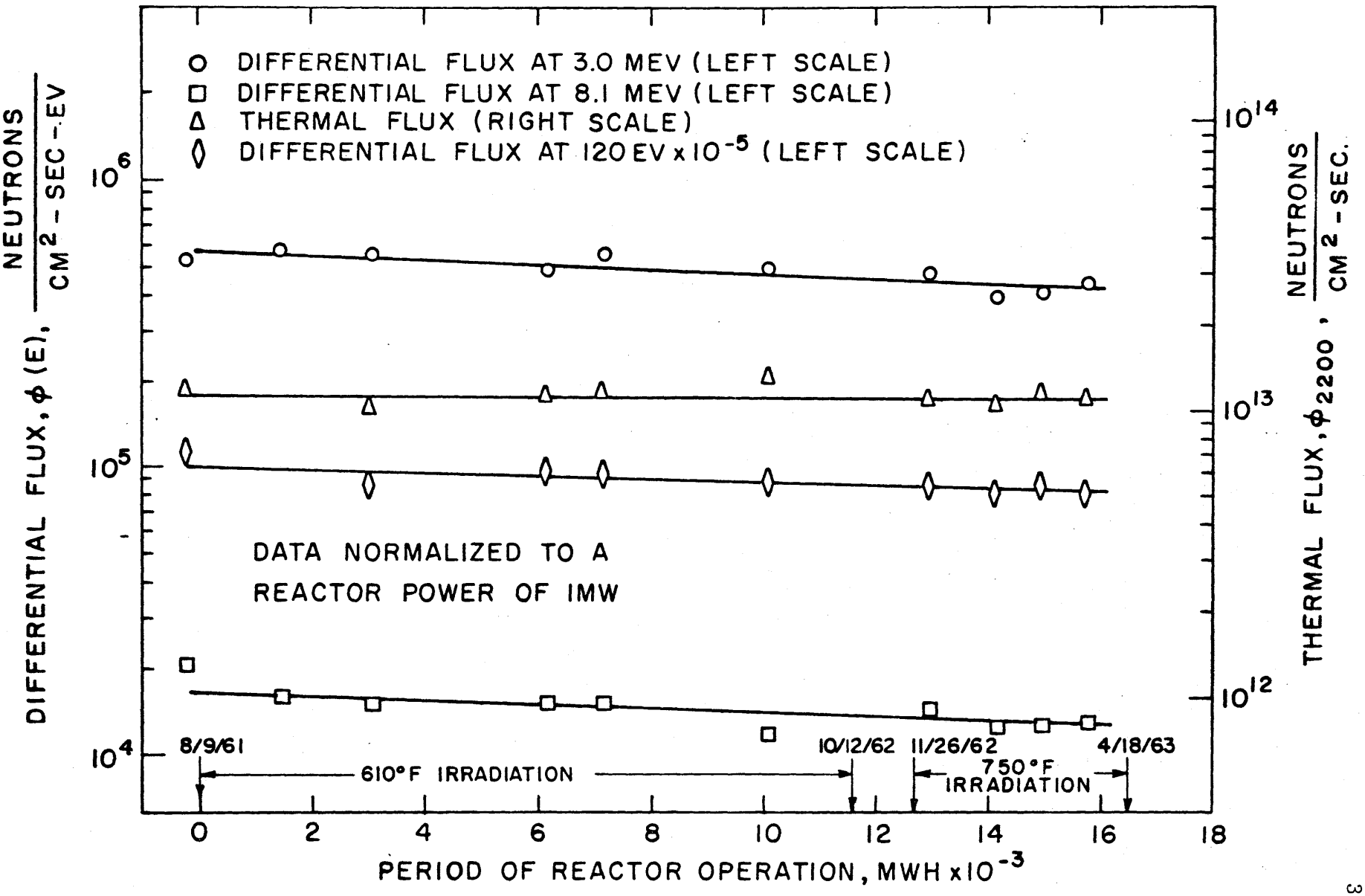

FIGURE 3.15 NEUTRON FLUXES AT CORE CENTER DURING THE 610°F AND 750° IRRADIATIONS OF SANTOWAX OMP

shown in Fig. 3. 16. The results of run 13 (run during the 750°F irradiation of Santowax OMP, 3/28/63) are shown for comparison, and it appears that the monitor tube measurements of run 14 agree quite well with those of run 13, with the exception of the 8. 1 Mev flux. However, as mentioned above, the fast flux was determined with only two detectors for run 14, (four detectors are normally used) so that the difference seen may be due to this fact. It appears that the thermal flux in the monitor tube is some 7% greater than in the capsule. The 120 ev flux is about the same for the two positions. The flux at 2. 9 Mev (nickel) appears to be some 10% higher in the capsule than in the monitor tube and the 8. 1 Mev flux (aluminum) some 7% higher in the capsule center. These data all indicate somewhat more moderation of the fission neutrons before reaching the monitor tube than before reaching the capsule centerline.

In order to calculate the fast neutron dose rate as measured by the foil measurements and to facilitate calculation of the fast neutron and gamma ray dose rates as measured by the calorimeters, it is necessary to calculate the scattering integrals I_H, I_C, I_{Al}, I_{Be} and their ratios (see Eq. (3. 4b)). Morgan and Mason (3. 3) have previously reported that while the scattering integrals are quite sensitive to the neutron spectrum used, the ratios of these integrals are quite insensitive to the neutron spectrum used (for any reasonable spectrum). Figure 3. 17 shows typical neutron spectra obtained at the core center in the monitor tube. As can be seen, there is a gap between 570 ev and 2. 9 Mev over which no foil detectors were available to measure the neutron flux. Two sets of calculations were thus made:

1. Spectrum type I. The flux between 120 ev and 0. 4 Mev was assumed to have a 1/E behavior. Above 1. 5 Mev the measured fast spectrum was used [$\phi(E) = -de^{c + dE}$, see Eq. (3. 20)]. In the region between 0. 4 and 1. 5 Mev a joining spectrum of the type $\phi(E) = pE^q$ was used.
2. Spectrum type II. The flux between 120 ev and 1. 5 Mev was assumed to be of the form $\phi(E) = pE^q$ [q will be close to −1]. The measured fast spectrum was used above 1. 5 Mev. This latter case is the one shown in Fig. 3. 18.

A comparison of spectrum types I and II is given in Fig. 3. 18 for the data of run 13. It was found that the lower limit on the scattering integral

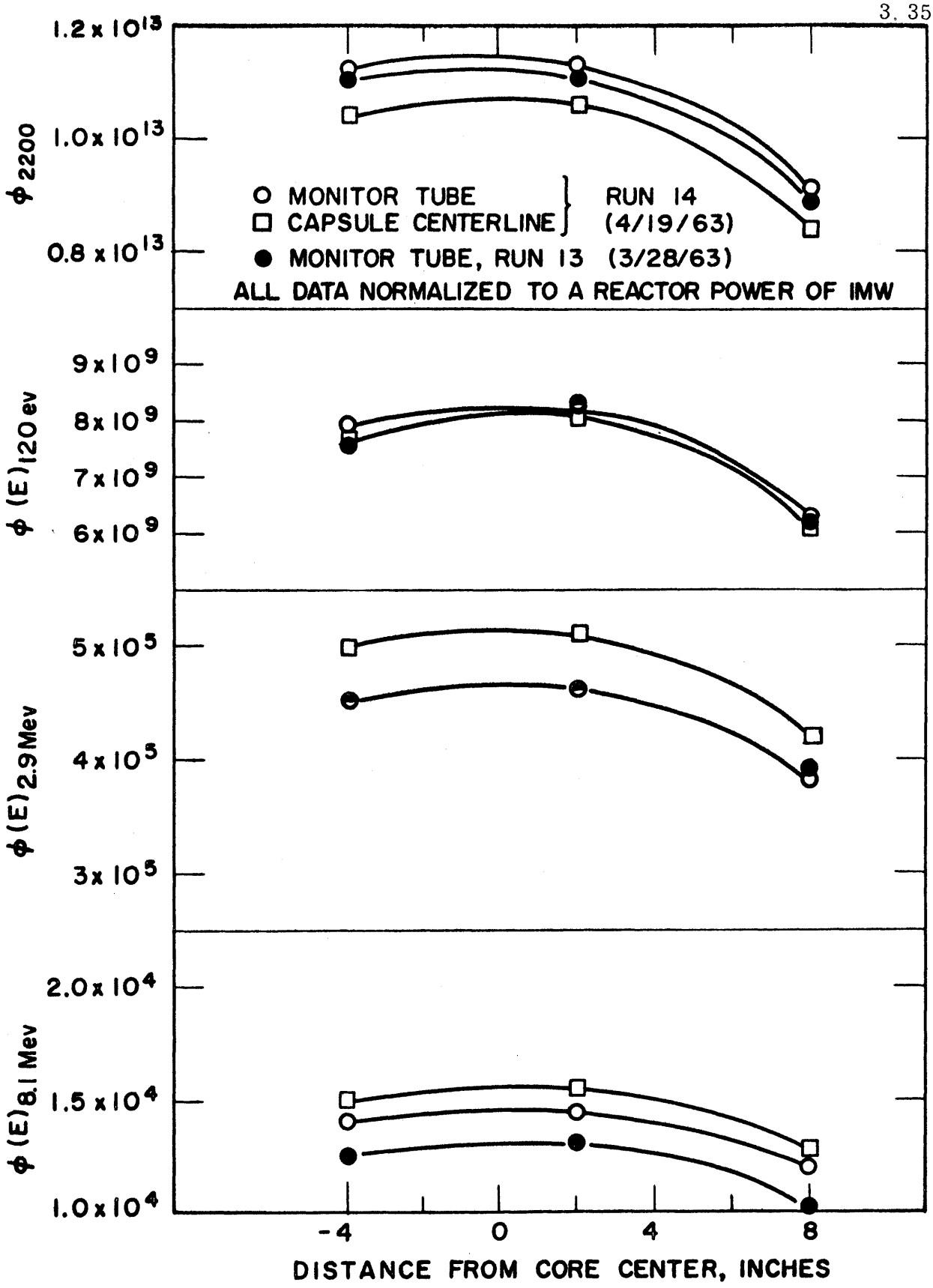

FIGURE 3.16 COMPARISON OF NEUTRON FLUXES IN MONITOR TUBE AND CAPSULE CENTERLINE

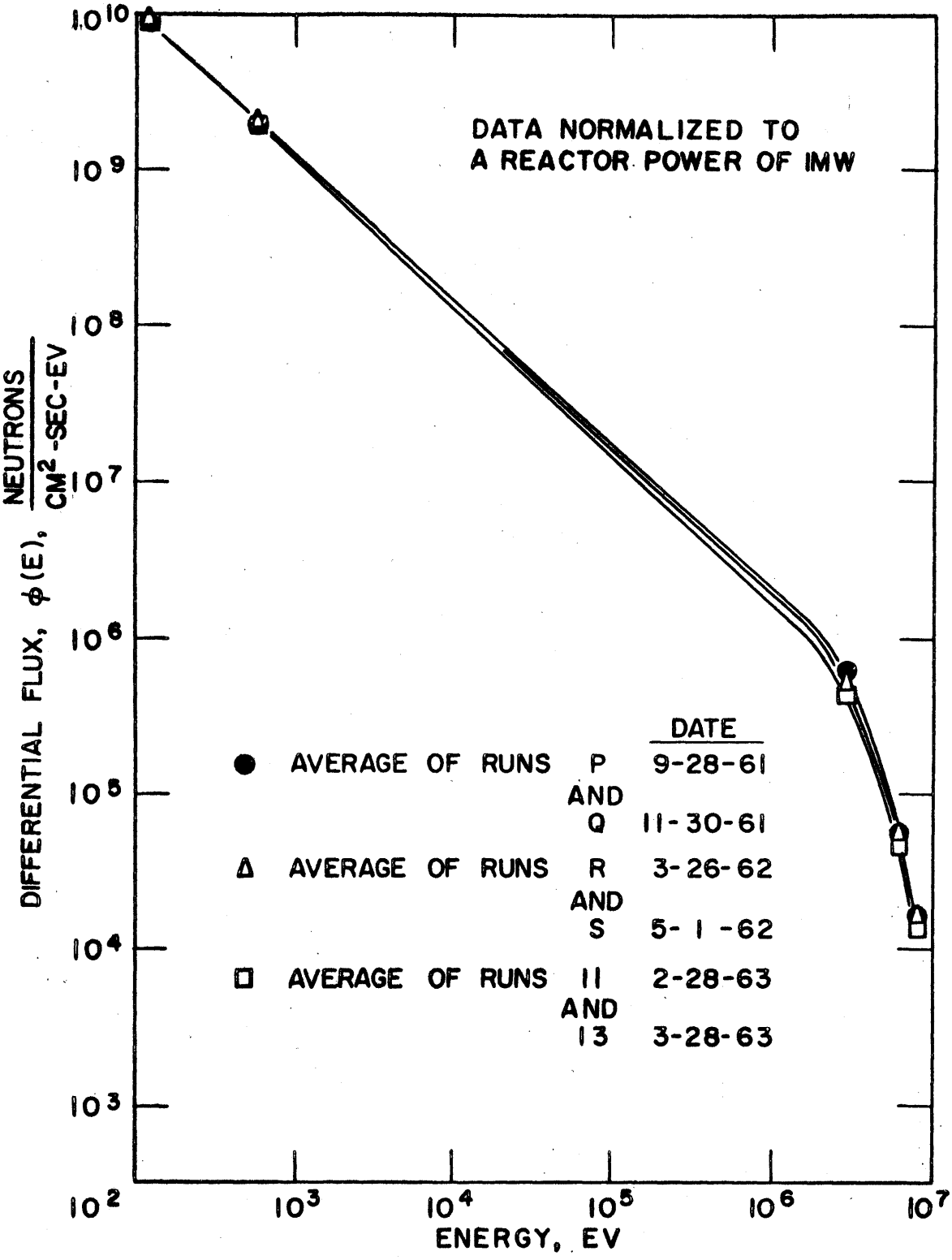

FIGURE 3.17 ENERGY DISTRIBUTION OF DIFFERENTIAL NEUTRON FLUX AT CORE CENTER

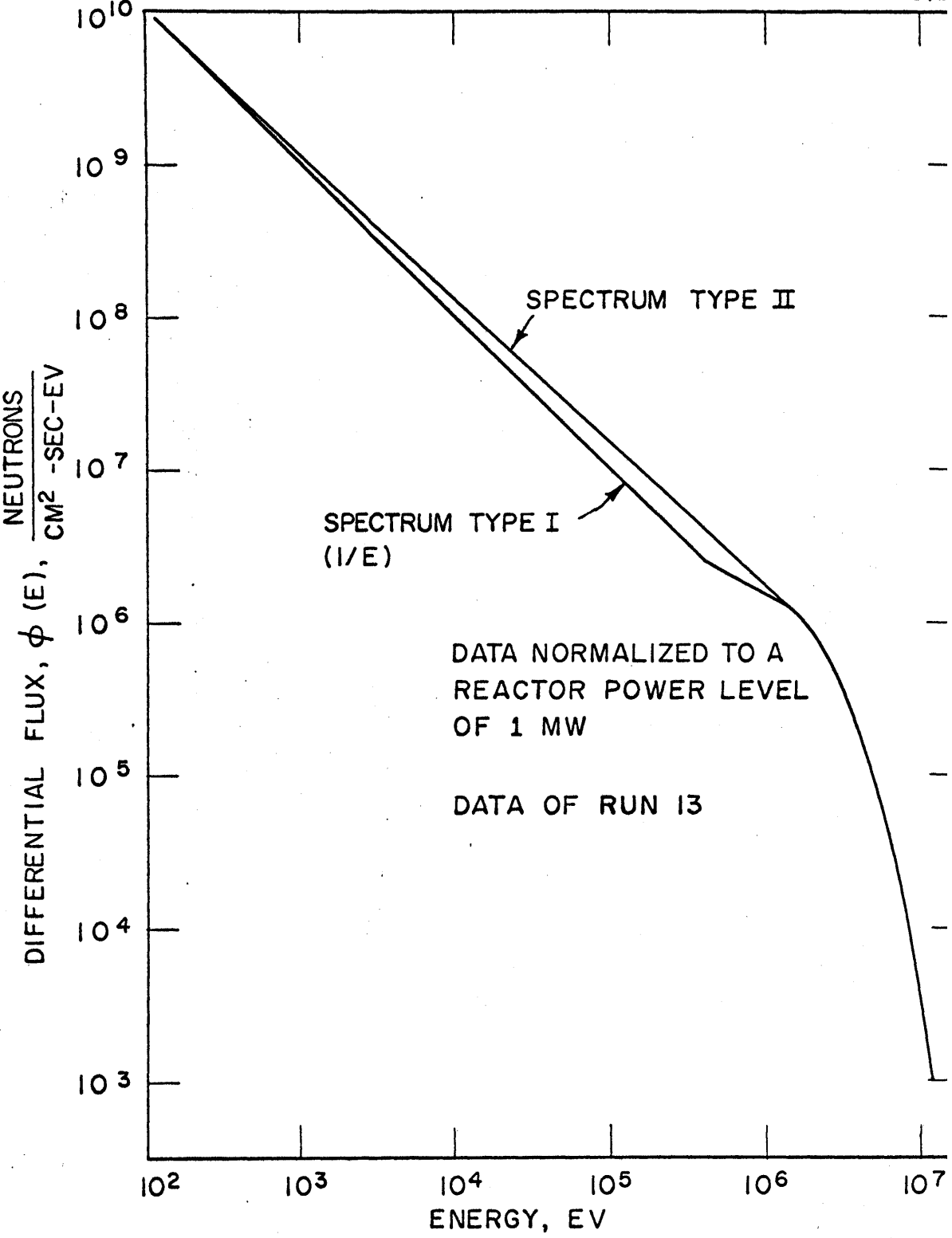

FIGURE 3.18 NEUTRON SPECTRA USED FOR THE CALCULATIC
OF SCATTERING INTEGRALS

could be set at 0.01 Mev with a negligible change in the result. Thus, only the spectrum above 10^4 ev was of interest.

Another problem in the calculation of the scattering integrals is the choice of neutron cross sections. The cross section data used are given in Section A1.13. For hydrogen and aluminum, the total cross sections (which equal the elastic scattering cross sections in the energy range of interest) were used. Carbon undergoes inelastic scattering interactions above 5 Mev, but preliminary tests showed that the difference in the values of I_C calculated from the use of the total cross section or the elastic scattering cross section was less than 2%. The total cross section was used since inelastic scattering presumably contributes something (not necessarily the same as elastic scattering) to the fast neutron heating rate. Beryllium has an (n, 2n) reaction above 2 Mev which contributes to the total cross section. The elastic scattering cross section was used for Be, and it was assumed that the (n, 2n) reaction was a negligible contributor to the fast neutron heating rate in Be. In any event preliminary calculations indicated that use of the total cross section instead of the elastic scattering cross section increased the calculated total heating rate in Be only about 3%.

Table 3.7 shows the effect (using a typical measured spectrum) of

TABLE 3.7

Comparison of Scattering Integrals and Ratios Based on Neutron Spectrum Type I and Neutron Spectrum Type II (Based on Foil Run 11, 2/28/63 at Two Inches Above Core Center)

Neutron Spectrum	I_H, $\frac{\text{watts}}{\text{atom}} \times 10^{24}$	I_C/I_H	I_{Al}/I_H	I_{Be}/I_H
I(1/E to 0.4 Mev)	1.81	.190	.125	.261
II($1/E^{0.94}$ to 1.5 Mev)	2.10	.183	.118	.251

Spectrum type I and Spectrum type II on the scattering integral calculations. Although I_H changed by 15%, the ratios changed by only 4%. With no experimental data between 570 ev and 2.9 Mev, it was felt that spectrum type II (E^q with q usually between −0.95 and −1.0) provided the better representation of the measured spectra, so that the rest of the results are presented for calculations using spectrum type II.

Table 3.8 shows the variation of the scattering integral ratios with position relative to core center for a typical measured spectra. It can be seen that while I_H varied over several orders of magnitude, the ratios of the scattering integrals were only slightly affected. For each run for which scattering integral calculations were made, an average of the scattering integral ratios over the axial positions was calculated. More weight has been given to the scattering integral ratios obtained for the core region (−12" to +12") than the reflector region in calculating the averages, since about 95% of the dose rate delivered to the coolant came from the core region. These average values are shown in Table 3.9 for various foil runs spanning the period of operation with the in-pile section. It can be seen that the scattering integral ratios did not have any significant variation with time, and so the values used for the calorimetry runs were taken as

$$I_C/I_H = 0.18$$

$$I_{Al}/I_H = 0.12$$

$$I_{Be}/I_H = 0.25$$

A plot of the calculated fast neutron dose rate in Santowax OMP ($4.52 \times 10^{22}\ I_H$) using the values of I_H calculated from two sets of foil measurements is given in Fig. 3.19. The in-pile dose rate factor due to fast neutrons, F_N, has been calculated for runs R (3/26/62) and 13 (3/28/63) for comparison with the calorimetric measurements. The results obtained using the procedure outlined in Section 3.2.4 and the data of Fig. 3.19 are tabulated and compared with the calorimetric measurements in Table 3.10. It can be seen that the foil measurements made in the monitor tube yield results which are about 15% lower than those obtained by calorimetric measurements. Part of this difference may be explained by the fact that the fast fluxes obtained in the monitor tube were apparently lower than those in the capsule center by about 10% (see Fig. 3.16). The neutron flux in the capsule should be more representative of the dose rate to Santowax OMP. In addition the fast neutron fluxes are estimated to be accurate only to ± 13% and so agree with the calorimetric results within the experimental error.

TABLE 3.8

Variation of Scattering Integral Ratios with Axial Position

(Based on Foil Run 13, 3/28/63)

Position relative to core center, inches	I_H watts/atom $\times 10^{24}$	I_C/I_H	I_{Al}/I_H	I_{Be}/I_H
−9	1.66	.183	.119	.250
−4	2.05	.183	.118	.250
+2	2.15	.182	.118	.249
+8	1.79	.183	.118	.250
+13	0.53	.180	.116	.246
+17	0.12	.179	.115	.246
+22	0.018	.181	.117	.249
+27	0.006	.179	.115	.246

TABLE 3.9

Average Scattering Integral Ratios Obtained for Various Foil Activation Runs

Run	Date	I_C/I_H	I_{Al}/I_H	I_{Be}/I_H
J-K	8/4/61	.186	.121	.256
R	3/26/62	.183	.118	.251
4	8/18/62	.181	.117	.248
10	1/29/63	.183	.119	.251
11	2/28/63	.183	.118	.251
13	3/28/63	.182	.118	.250
14 (Capsule)	4/19/63	.184	.119	.252
14 (Monitor tube)	4/19/63	.184	.119	.252
Average		.183	.118	.251

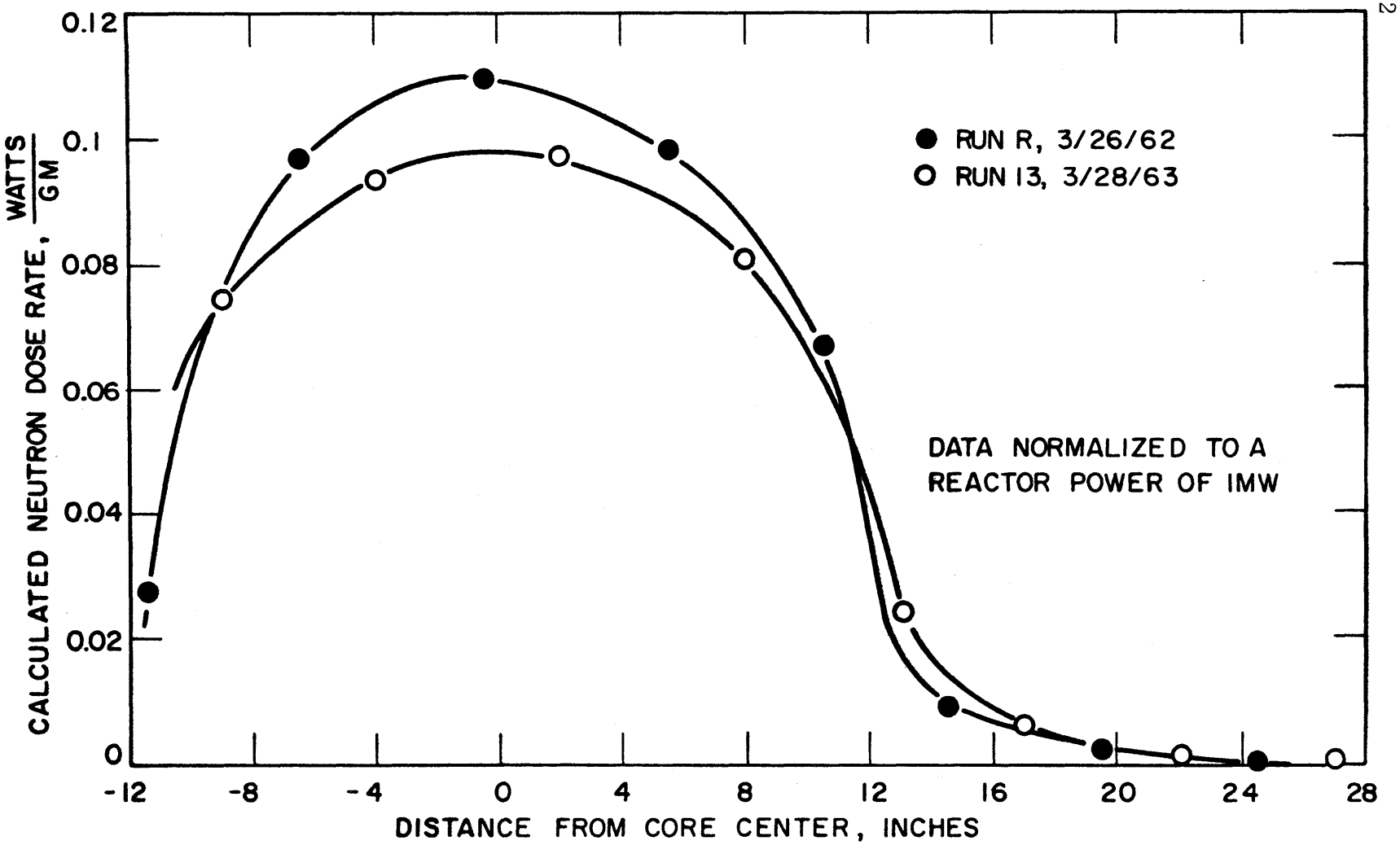

FIGURE 3.19 AXIAL VARIATION OF NEUTRON DOSE RATE IN MONITOR TUBE BASED ON FOIL MEASUREMENTS

TABLE 3.10

Comparison of the In-Pile Dose Rate Factor for Fast Neutrons Obtained by Foil Measurements and Calorimeter Measurements

Measurement	Date	F_N, (watt)(hr)(cc)/(MWH)(gm)[a]
Calorimeter Series III-3	3/20/61	21.1 ± 1.4[b]
Calorimeter Series IV	4/24/63	20.5 ± 0.6[c]
Foil Run R	3/26/62	18 ± 3
Foil Run 13	3/28/63	17 ± 3

a. Multiplication by the coolant density gives the absorbed dose rate.

b. Based on measurements with polyethylene, polystyrene and aluminum absorbers.

c. Based on measurements with polyethylene, polystyrene, Santowax OMP and carbon absorbers.

3.4 Calculation of the Specific Dose Absorbed in Santowax OMP

In Section 3.2.4 the rate at which energy was absorbed in Santowax OMP in the in-pile assembly was given as

$$\frac{dD}{d(MWH)} = \rho F_T \quad \text{(watt)(hr)/MWH} \tag{3.21}$$

The change of density with reactor MWH is given in Section A4.3. Based on the calorimetric measurements of F_T on 3/20/61 and 3/24/63 and the linear time dependence of the fast neutron fluxes found by the foil measurements, the variation of F_T with reactor MWH is given in Fig. 3.20. A linear decrease with MWH was assumed for F_T, and the maximum possible error limits were estimated as ± 4% (based on errors in the two sets of calorimetric measurements).

The energy deposited in the in-pile assembly is, in effect, absorbed by the whole circulating mass of coolant in the loop, M_{loop}. This circulating mass was defined for convenience as (see Section A2.5 for details):

$$M_{loop} = M_o + M^* \qquad , M_o >> M^* \tag{3.22}$$

where

M_o is a reference (constant) amount of circulating mass

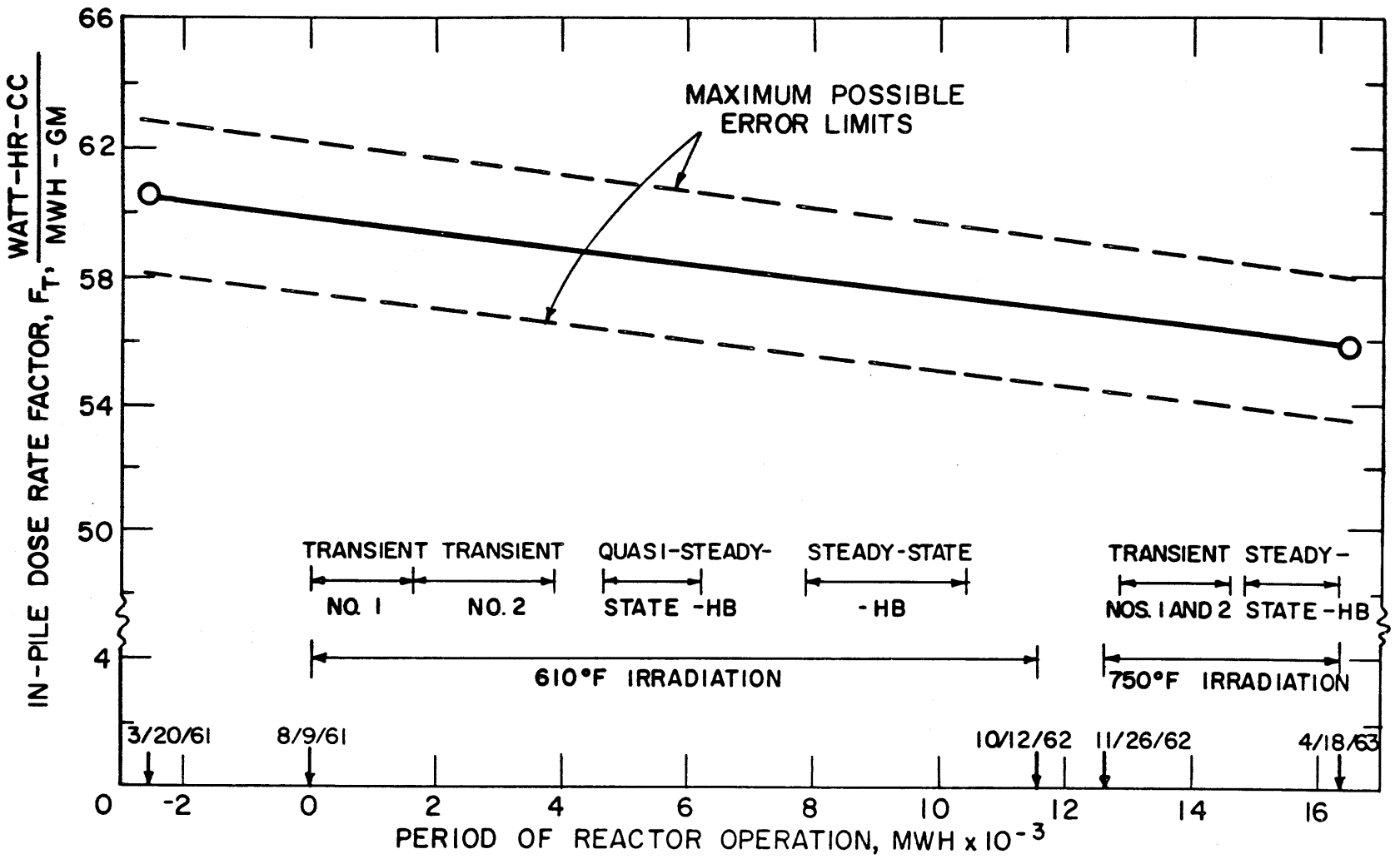

FIGURE 3.20 VARIATION OF IN-PILE DOSE RATE FACTOR WITH IRRADIATION

M^* is the relative amount of circulating mass, arranged so that $M^* = 0$ at the time when the mass in the loop during an irradiation was a minimum.

Thus the specific dose absorbed by the coolant was defined as

$$\frac{d\tau}{d(MWH)} = \frac{\rho F_T}{(M_o + M^*)} \tag{3.23}$$

where τ is the specific dose in watt hr/gm.
The variation of M^* with reactor MWH is given in Section A2.5. The specific dose absorbed by the coolant in the loop was thus

$$\Delta\tau_{1-2} = \int_{MWH_1}^{MWH_2} \frac{\rho F_T}{(M_o + M^*)} \, d(MWH) \quad \text{watt-hr/gm} \tag{3.24}$$

CHAPTER 4
COOLANT COMPOSITION AND STABILITY

4. 1 Introduction

When Santowax OMP is subjected to the effects of high temperature and irradiation, a complex mixture of degradation products results. It is very difficult, if not impossible, to determine all of the components comprising the irradiated mixture, but these components can be classified into four general divisions (4. 1). These are:

1. Ortho-, meta- and para-terphenyls. The terphenyls compose over 98 w/o of the unirradiated material, and in this report the combined terphenyl content will be denoted by w/o omp.
2. High boilers (HB). This part of the coolant is composed of materials having boiling points higher than that of p-terphenyl and having molecular weights ranging from 230 (that of the terphenyls) to about 3000. The formation of these materials is the predominant and most important process occurring in the degradation of the terphenyls because of the pronounced effects of the HB on the coolant physical properties, particularly the viscosity.
3. Low and intermediate boilers (LIB). These liquid constituents have boiling points less than or equal to those of the terphenyls and have molecular weights of the order of 230. Probably no serious effect on the coolant properties results from the LIB fraction.
4. Non-condensable gases. Hydrogen, methane, ethane, ethylene and other saturated and unsaturated hydrocarbons of low molecular weight are the principal constituents. These gases dissolve to some extent in the irradiated coolant at the temperatures and pressures of the loop operation. Morgan and Mason (4. 1) point out that the distinction between non-condensable gas and low boiler is not always clear.

In discussing the irradiated coolant composition, some laboratories refer only to the HB content of the coolant (4.2, 4.3, 4.4), but it has been found convenient to describe the coolant irradiated at M.I.T. by the degradation product content as well (4.1). The degradation product (DP) concentration is defined to be (100 - w/o omp) and differs from the HB concentration by the amount of LIB in the coolant.

Previous work (4.5, 4.6, 4.7, 4.8, 4.9) has indicated that in spite of the complex mixture of degradation products formed during the irradiation of terphenyls, reasonably good correlations can be made between either the HB concentration (w/o) or the terphenyl concentration (w/o) in the irradiated mixture and the absorbed radiation dose in the mixture. Experiments have also indicated that different types of radiation produce different rates of damage to the coolant (4.3, 4.5, 4.9) (referred to as the LET effect). In addition, if the temperature is high enough, pyrolysis may play a significant role in the coolant decomposition (4.10, 4.11, 4.12, 4.13).

At M.I.T. only fast neutrons and gamma rays produce a significant radiation dose in the coolant (see Section 3.2). Thus the major variables considered in the analysis of the data were:

1. The coolant composition, measured both as weight fraction terphenyls and as weight fraction HB.
2. The absorbed specific dose and its fractions of fast neutron and gamma ray doses.
3. The coolant irradiation temperature.

The weight fraction of each of the terphenyl isomers in a given sample was determined by gas chromatography with an F and M Model 500 chromatograph with a Model 1609 flame ionization detector.[1] The details of the column conditions are given in Section A2.1. Analyses were also performed by the Monsanto Research Corporation (Everett, Mass.) as a check, and the results of the analyses on all samples of the 610°F and 750°F irradiations are tabulated in Section A2.3. During the steady-state-HB periods the HB concentration was determined by distillation of 300 gram samples. The details of the distillation conditions and HB

---

1. F and M Research Corporation Avondale Pa.

concentration calculations are given in Section A2.2. HB analyses are tabulated in Section A2.3. Mass spectrographic analyses of radiolytic gas samples from both irradiations were performed by Petroleum Analytical Research Corporation (Houston, Texas), and the data are tabulated in Section A2.4.

4.2 Liquid Degradation - Theory

For each of the terphenyl isomers empirical rate equations may be written, having the form

$$-\frac{dC_i}{d\tau} = k_{i,n}[C_i]^n \tag{4.1}$$

where

- i refers to a particular component
- n is the reaction order
- k is the reactor constant
- C is the weight fraction of the component
- τ is the specific dose delivered to the coolant, given by Eq. (3.24).

The stability of a particular component in the coolant may be defined simply as $k_{i,n}$, the reactor constant, but two other stability terms will also be employed. $G(-i)$, by which radiation chemistry results are frequently reported, is defined as

$$G(-i) = \frac{\text{molecules of component } i \text{ degraded}}{100 \text{ ev absorbed in the total coolant}} \tag{4.2}$$

This parameter is $-dC_i/d\tau$ multiplied by $2680/A_i$ (molecules)(watt)(hr)/(100 ev)(gram of component i), where A_i is the molecular weight of component i. In the field of organic reactor coolant technology it has been conventional to use the molecular weight of the unirradiated material (terphenyl = 230) for A_i even when i does not refer to this material (4.5). Using this convention there results

$$G(-i) = -11.65\frac{dC_i}{d\tau} = 11.65k_{i,n}[C_i]^n \tag{4.3}$$

The second stability term to be defined is $G^*(-i)$ (4.1):

$$G^*(-i) = \frac{1}{C_i}G(-i) \tag{4.4}$$

Assuming that the dose given to component i is proportional to the concentration of i in the coolant, which should be true as long as the carbon-hydrogen ratio of the various liquid organic components is fairly constant (Section 5.9 has shown that it is), $G^*(-i)$ has an interesting interpretation (4.1):

$$G^*(-i) = \frac{\text{molecules of component } i \text{ degraded}}{100 \text{ ev absorbed in component } i} \tag{4.5}$$

During transient periods of operation the circulating coolant mass varied due to sampling and dilution (the addition of fresh coolant to the loop). Figure 4.1 shows the variation of circulating coolant mass with MWH of reactor operation for the transient periods of the 610°F irradiation as an example. The data are based on calculations given in Section A2.5 and assume no loss of mass due to gas formation. As may be seen, the change in mass during this period was about 8%. The variation of the in-pile dose rate factor over the transient periods of either the 610°F or 750°F irradiations was less than 2% (see Section 3.4) and the maximum variation of coolant density during the transient periods less than 7% (see Section 5.2). Thus, the specific dose delivered to the coolant as given by Eq. (3.24) may be approximately integrated for periods between dilutions as

$$\tau_{j+1} - \tau_j = \frac{F\,\rho}{M_o + M_j^*} (MWH_{j+1} - MWH_j) \tag{4.6}$$

where

j refers to the j^{th} sample (or other loss of material)

$j+1$ refers to the $j+1^{st}$ sample (or other loss of material)

$M_o + M^*$ is the circulating coolant mass in the loop ($M_o >> M^*$). M^* gives the variation of circulating coolant mass above an arbitrary level, M.

ρ is the average coolant density during the interval j to $j+1$

F is the average in-pile dose rate factor during the interval j to $j+1$ (see Section 3.4).

Since the coolant circulating mass does not vary greatly, the absorbed specific dose is nearly proportional to the reactor MWH. Also, during

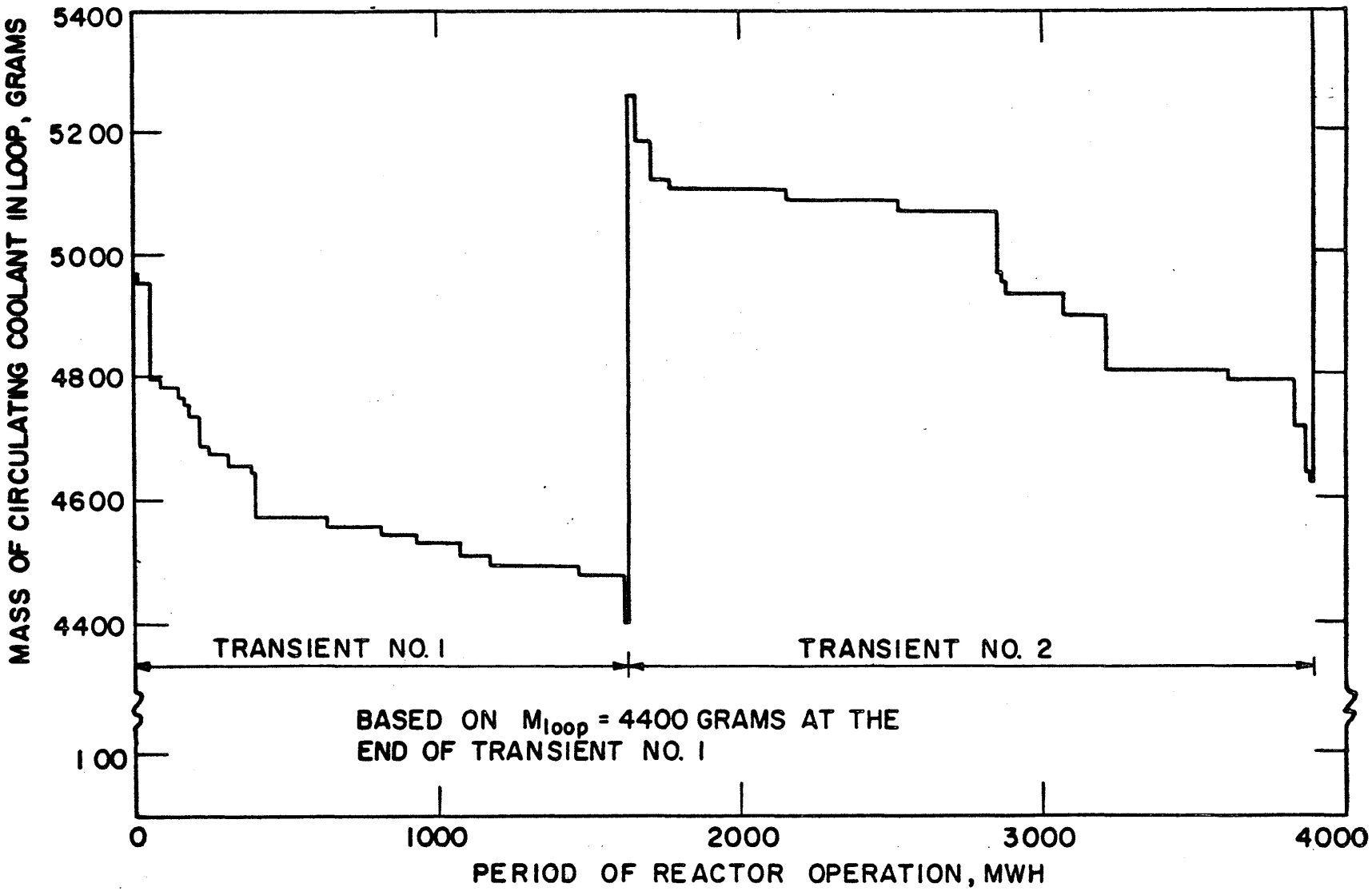

FIGURE 4.1 CIRCULATING COOLANT MASS DURING THE TRANSIENT PERIODS OF THE 610°F IRRADIATION

transient periods, Eq. (4.1) may be integrated to yield

$$-k_{i,n}\tau + a = \begin{cases} \dfrac{C_i^{1-n}}{1-n} & n \neq 1 \\ \ln C_i & n = 1 \end{cases} \tag{4.7}$$

where

a represents a constant of integration.

These linear relations between τ and a transformed concentration variable allow the experimental data to be treated by the method of weighted least squares. The details of the statistical analysis involved are given in Sections A2.6 and A2.7. Once a "best" value of $k_{i,n}$ is obtained by a least squares analysis, the stability criteria $G(-i)$ and $G^*(-i)$ may be calculated directly for a given component concentration by Eqs. (4.3) and (4.4).

During steady-state-HB operation, the $G(-i)$ criterion may be written as (see Eqs. (3.24) and (4.3)):

$$G(-i) = -11.65 \frac{MdC_i}{F\rho d(MWH)} \tag{4.8}$$

The coolant density remained quite constant during these periods (see Section 5.2). Due to continual sampling and dilution the circulating coolant mass in the loop was subject to small fluctuations. Figure 4.2 shows as an example the circulating coolant mass as a function of reactor MWH during the 610°F irradiation steady-state-HB period; on a time average basis, the circulating coolant mass may be considered as constant. The variation of the in-pile dose rate factor F during any steady-state-HB period was less than 1% (see Section 3.4). Thus Eq. (4.8) may be approximated by

$$G(-i) = -11.65 \frac{d(MC_i)}{\bar{F}\bar{\rho}d(MWH)} \tag{4.9}$$

where the bars denote averages over the steady-state-HB period. The quantity $d(MC_i)$ may be considered as the disappearance of a differential number of grams of component i and may be equated to the differential makeup by

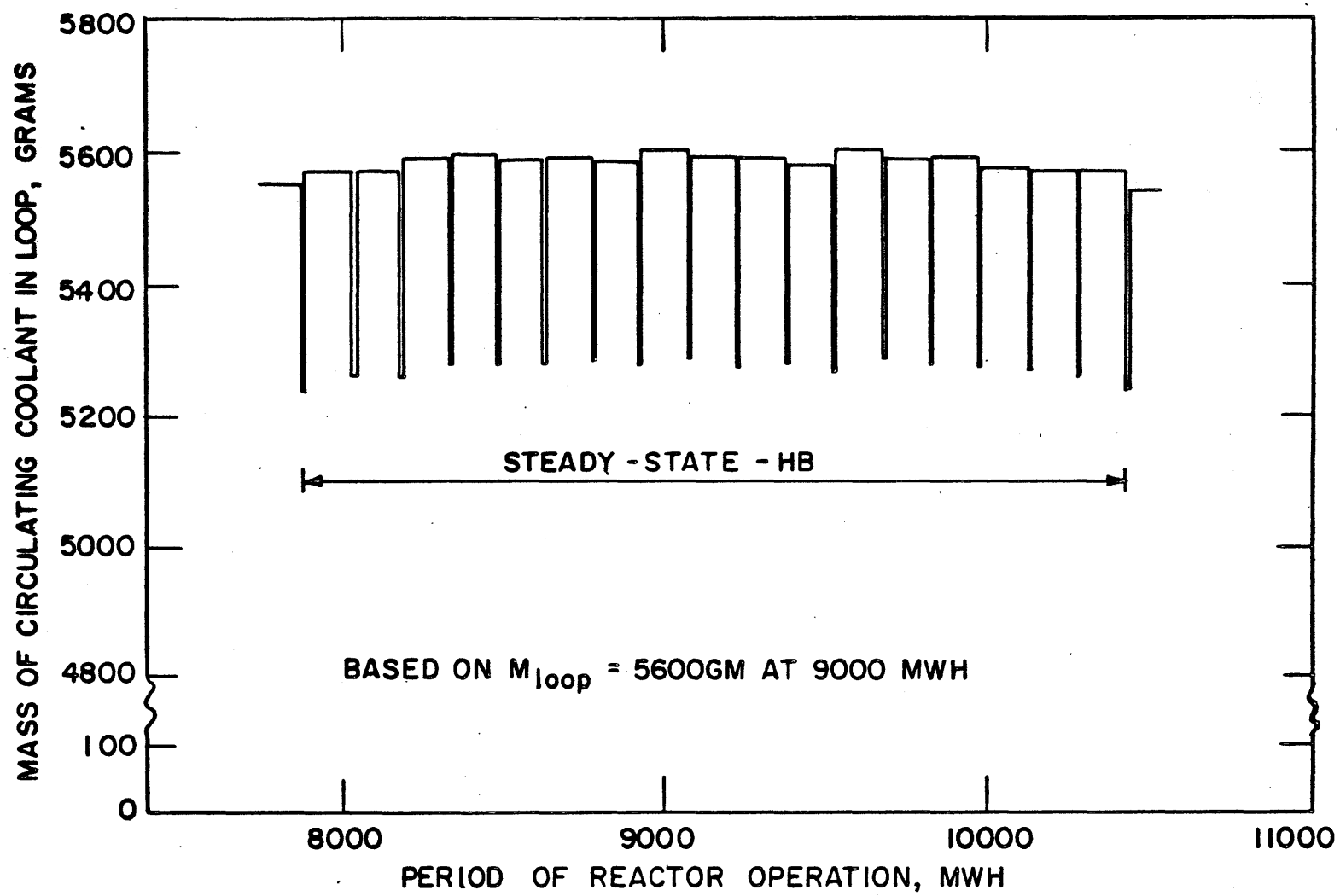

FIGURE 4.2 CIRCULATING COOLANT MASS DURING THE STEADY-STATE-HB PERIOD OF THE 610°F IRRADIATION

$$-d(MC_i) = d(makeup_i) + \delta \qquad (4.10)$$

where δ is a correction for the fact that the makeup rate may not be exactly equal to the disappearance rate. This would be manifested through a change in concentration in component i during the steady-state-HB period.

The concentration of the species under consideration is not exactly constant during the steady-state-HB period but varies as shown schematically in Fig. 4.3. In both the 610°F and 750°F irradiations

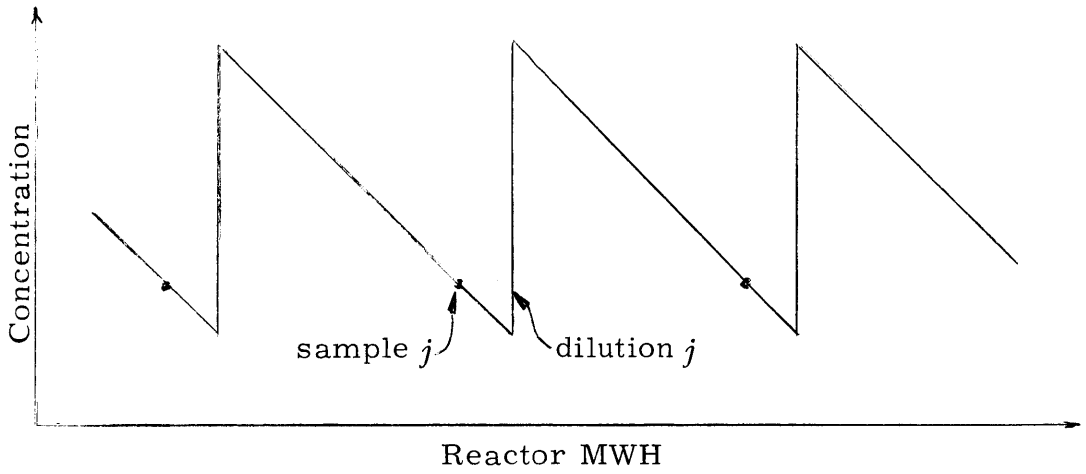

Figure 4.3 Schematic Concentration Variation During Steady-State-HB Periods

the sampling frequency was adjusted to keep the peak-to-valley difference at about 2 w/o for the HB and DP concentrations. Thus, the concentration level was considered approximately constant, and the stability criterion $G(-i)$ was considered constant during steady-state-HB operation. Integration of Eqs. (4.9) and (4.10) therefore yields

$$G(-i) = \frac{11.65\,[\text{net grams of } i \text{ makeup} + \Delta]}{\overline{F}\,\overline{\rho}\,[MWH_2 - MWH_1]} \qquad (4.11)$$

$$\Delta = M^1_{loop}\, C^1_i - M^2_{loop}\, C^2_i \qquad (4.12)$$

where

1 refers to the start of the steady-state-HB period

2 refers to the end of the steady-state-HB period.

The $G^*(-i)$ criterion is still given by Eq. (4.4), where the value of C_i used is the loop average value over the period. Note that the loop average value of C_i is not, in general, equal to the average of the concentrations in the samples removed, since the samples are removed at the bottoms of the saw-tooth shown in Fig. 4.3. The calculation of the peak-to-valley difference, and hence the difference between the loop average and sample average concentrations, may be made using the calculated values of $G(-i)$ from Eq. (4.11) or by performing a mass balance on the system at the time of dilution with unirradiated material (see Section A2.10).

4.3 Corrections for Out-of-Pile Pyrolysis

The theory discussed in Section 4.2 will yield values of G and G^* due to the combined effects of radiolysis and pyrolysis. At present, it is difficult to tell whether the combined effects of radiolysis and pyrolysis on terphenyls can be computed from the individual effects or not (4.15) but it is possible to correct the data obtained at the M.I.T. loop for out-of-pile pyrolysis, since radiation and high temperatures act together only in the in-pile capsule.

The details of the pyrolysis corrections are given in Section A2.9. Data taken at other laboratories (4.11, 4.12) were used to calculate the pyrolysis rates of the terphenyl isomers. The contribution of out-of-pile pyrolysis to the degradation of terphenyls at 610°F was found to be negligible. At 750°F the out-of-pile pyrolysis was found to contribute about 10% to the terphenyl degradation.

Briefly, during the transient periods the concentration of each terphenyl component in an irradiated sample was raised by an amount calculated to be due to out-of-pile pyrolysis. During the steady-state-HB period, the calculated number of grams of each terphenyl component pyrolyzed in the out-of-pile section was subtracted from the number of grams of makeup in Eq. (4.11).

4.4 610°F Irradiation Liquid Degradation Results

4.4.1 Transient Periods

The results from the transient periods of operation are quite dependent on the value used for the mass of circulating coolant in the

loop (see Eq. (4. 6)), or, in other words, on M_o since M_o is defined by

$$M_{loop} = M^* + M_o, \quad M_o >> M^* \tag{4. 13}$$

This consideration is of great importance in interpreting the results of the transient periods, since it has been shown in Section A2. 5 that the circulating coolant mass is subject to a sizeable discrepancy depending upon how the value of the mass was obtained. It should be pointed out that the problem of obtaining an accurate value for the circulating coolant mass is a difficult one for any circulating system which has a number of pieces of auxiliary equipment and a gas-liquid interface. The two main methods used to obtain the circulating coolant mass during the transient period were:

1. A calculation of the type described by Morgan and Mason (4. 1) at the end of the first transient period. For this calculation the volume of each section of the loop was assumed filled with coolant, and from the knowledge of the coolant density and the temperature profile around the loop, the mass in the loop was calculated. Some correction was made for dead-end lines in which not much circulation was assumed to occur.
2. The same type of calculation as described in 1. made during the steady-state-HB period. From a knowledge of the coolant masses removed and added to the loop, the circulating mass in the loop at the end of the first transient period was calculated.

These two methods gave results for the circulating coolant mass at the end of the first transient period of 4400 gm and 3700 gm (see Section A2. 5 for details). Since M^* was equal to zero at this time, $M_{loop} = M_o$ at the end of the first transient period. This discrepancy has not yet been resolved, but much useful investigation may still be pursued with the transient period data, such as an investigation of the kinetics of terphenyl degradation, since these studies are insensitive to the circulating coolant mass assumed.

Table 4. 1 shows the variation of the terphenyl isomer concentrations during the two transient periods of operation with the convenient time scale of reactor MWH. As stated previously, the absorbed specific dose is nearly proportional to the reactor MWH in each transient period. These

TABLE 4.1

Terphenyl Concentration During the Transient Periods of the 610°F Irradiation

Sample Number	Terphenyl Concentration, w/o				o:m:p Ratio	Biphenyl, w/o	Reactor MWH
	Ortho-ϕ_3	Meta-ϕ_3	Para-ϕ_3	Total omp			
1L16[a]	10.7	64.8	24.6	100.1	1:6.1:2.3	-	0
1L27	10.5	59.1	20.4	90.0	1:5.6:1.9	0.2	250
1L35	9.4	54.8	22.2	86.4	1:5.8:2.4	0.2	392
1L37	9.4	54.5	22.3	86.2	1:5.8:2.4	0.3	400
1L42	8.6	50.2	20.2	79.0	1:5.8:2.3	0.4	643
1L50	7.3	47.8	17.8	72.9	1:6.5:2.4	0.2	930
1L51	7.5	44.6	19.3	71.4	1:5.9:2.6	0.3	1076
1L52	7.5	42.3	17.0	66.8	1:5.6:2.3	0.3	1174
1L59	6.6	38.2	17.7	62.5	1:5.8:2.7	0.3	1472
1L62	6.3	37.4	16.2	59.9	1:5.9:2.6	0.3	1621
			End of Transient No. 1				
1L63	6.7	41.2	18.7	66.6	1:6.1:2.8	0.2	1659
1L66	6.8	39.4	17.8	64.0	1:5.8:2.6	0.3	1793
1L74	6.1	37.8	16.6	60.5	1:6.2:2.7	0.3	2164
1L82	5.6	34.4	15.1	55.1	1:6.0:2.6	0.3	2529
1L91	5.3	32.4	13.5	51.2	1:6.1:2.6	0.3	2869
1L92	5.3	31.9	14.5	51.7	1:6.0:2.7	0.4	2879
1L99	4.7	30.1	13.2	48.0	1:6.4:2.8	0.3	3215
1L111	4.3	24.8	11.7	40.8	1:5.8:2.7	0.4	3621
1L116	4.1	26.2	11.2	41.5	1:6.4:2.7	0.3	3839
1L118	4.1	25.1	10.4	39.6	1:6.1:2.5	0.3	3887
			End of Transient No. 2				

a. Not included in analysis due to sampling difficulties during first week of operation.

data are also plotted in Figure 4. 4 along with the analyses performed by the Monsanto Research Corporation (Everett, Mass.). In general, the agreement between the results is good, with the exception that the Monsanto analyses tend to yield higher analyses for m-terphenyl, and lower analyses for p-terphenyl. The use of a slightly impure m-terphenyl standard by Monsanto was responsible for this apparent difference.

Using Eqs. (4. 6) and (4. 7), weighted least squares treatments of the data obtained at M. I. T. have been performed with the following parameters:

1. Weighting of the transformed concentration variables (C^{1-n} or lnC) assuming two cases: (a) the relative error in the measured concentration ($\Delta C/C$) is constant and (b) the absolute error in the measured concentration (ΔC) is constant.[1]
2. Values of M_o of 4400 and 3700 gm (see Eq. (4. 6)).
3. Reaction orders of 0, 1, 2 and 3.

A statistical test based on the desire for a minimum root-mean-square deviation of the data points from the assumed correlation showed no preference for either of the assumed weightings. However, an error analysis of the terphenyl concentration data (see Section A2. 1) indicated that the relative error in the measured concentrations was constant for all samples, so that the results will be presented assuming the relative error to be constant.

Although the magnitudes of the reaction constants, $k_{i,n}$, obtained from the parameter survey depend directly on the value used for M_o, a comparison of different reaction orders with each other was found to be insensitive to the values of M_o used, so the discussion which follows is based on the higher value of M_o of 4400 gm. The variation of the circulating coolant mass in the loop for the transient periods of the 610°F irradiation is shown in Fig. 4. 1 on this basis.

---

1. Implied in the method of least squares is the assumption that the random error in the dependent variable, C, is much larger than the error in the independent variable, τ. Errors in τ due to errors in the circulating coolant mass are consistent errors. It is felt that the criterion for the least squares analysis is satisfied.

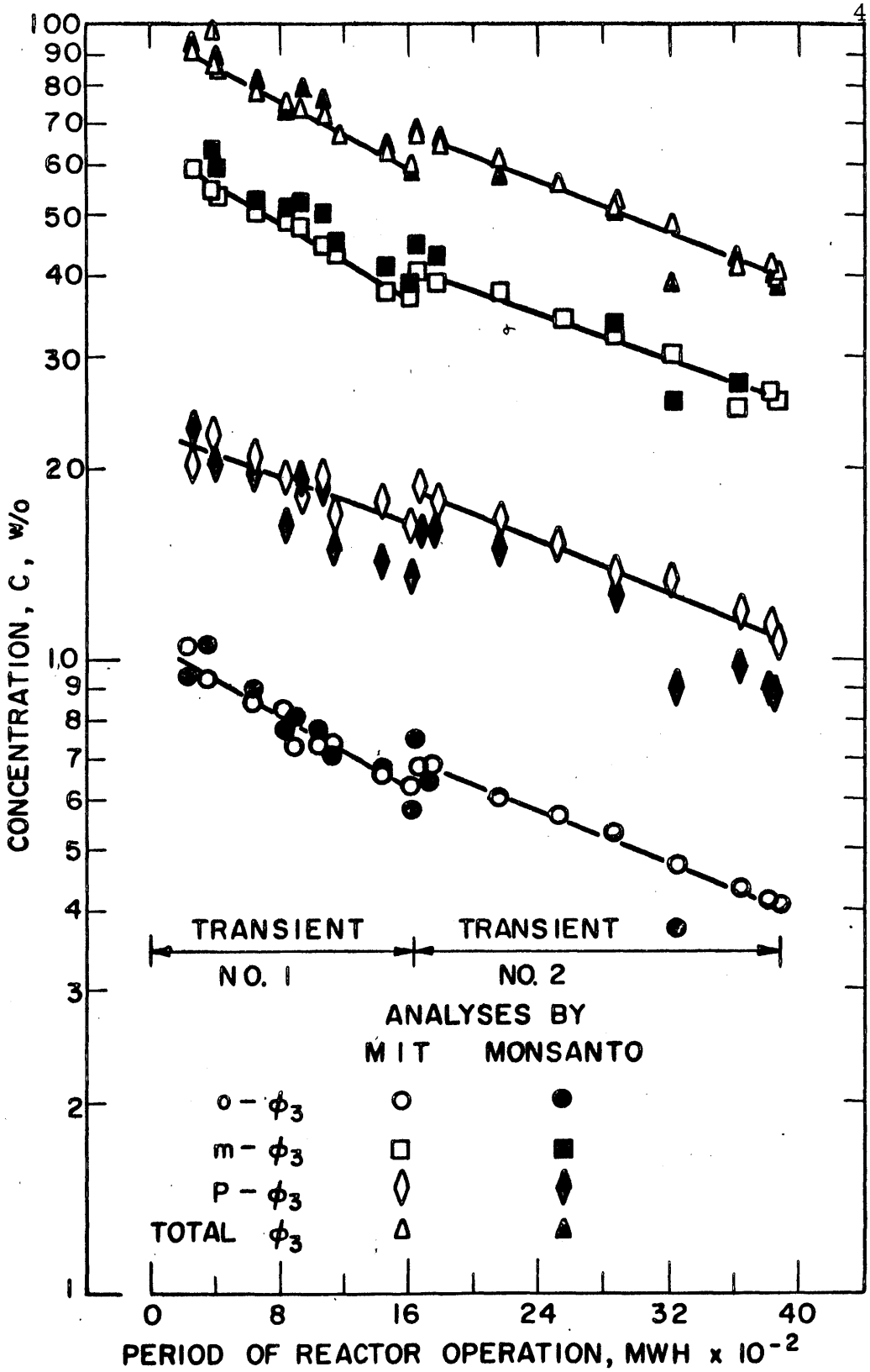

FIGURE 4.4 TERPHENYL ISOMER CONCENTRATION DURING THE TRANSIENT PERIODS OF THE 610°F IRRADIATION

The most convenient way to present the results of the reaction order parameter survey is through the reaction constants $k_{i,n}$, and Table 4. 2 presents the results in this fashion. It is quite difficult to state unequivocably which is the "best" reaction order, n. Figure 4. 5 makes this point more clear; plotted is the total terphenyl concentration versus the calculated absorbed dose (based on M_o = 4400 gm) for the first transient period with the various least squared rate laws drawn through the data points. It can be seen that the 95% confidence limit envelope (based on n = 1) encompasses both the n = 0 and n = 2 curves. The same conclusions may be drawn from similar plots for the individual isomers for both transient periods of the 610°F irradiation.

One statistical argument to determine the "best" reaction order consists of accepting as giving the "best fit" the value of n which yields the minimum relative standard deviation in the reaction constant (4. 5). On the basis of this test the data of Table 4. 2 indicate in all cases but one that the "best fit" is given by the first order rate law. However, this statistical argument cannot be regarded as conclusive.

A closer inspection of the results in Table 4. 2 reveals some interesting facts. If the rate law model (Eq. (4. 1)) is valid, the reaction constant for the i^{th} component, $k_{i,n}$, should not in any way depend on the concentration of the i^{th} component. However, there does appear to be a concentration dependence for $k_{i,n}$ for some values of n. Noticing that the o:m:p ratio in the samples obtained during each transient period remained statistically constant (see Table 4. 1) it is possible to use Eq. (4. 1) to investigate under what conditions there will be solutions which have a constant ratio of the concentrations of component i to component j. It is easy to show that the condition for constant o:m:p ratio is

$$[(C_o:C_m:C_p)_{\tau=0}]^{1-n} = k_{o,n}:k_{m,n}:k_{p,n} \qquad (4.14)$$

where the concentrations are the initial concentrations (at τ = 0), and

o refers to ortho-terphenyl

m refers to meta-terphenyl

p refers to para-terphenyl

Table 4. 3 shows the ratios of the reaction constants from Table 4. 2 and the o:m:p ratio of the terphenyl in the coolant which would be necessary to produce those ratios according to Eq. (4. 14). For zero, second and

TABLE 4.2

Reaction Constants Calculated from Data of the Transient Periods of the 610°F Irradiation

Period	Reaction Order	Reaction Constants ($-k_{i,n}$) in gm coolant/watt-hr $\times 10^2$ [a]			
		Ortho-ϕ_3	Meta-ϕ_3	Para-ϕ_3	Total omp
Transient No. 1	0	0.22 ± 0.056 [b]	1.3 ± 0.16	0.33 ± 0.15	1.9 ± 0.19
	1	2.9 ± 0.59	2.8 ± 0.27	1.8 ± 0.81	2.6 ± 0.17
	2	38.0 ± 6.5	6.0 ± 0.62	9.5 ± 4.3	3.5 ± 0.23
	3	470.0 ± 75.0	13.0 ± 1.7	50.0 ± 24.0	4.6 ± 0.46
Transient No. 2	0	0.11 ± 0.010	0.66 ± 0.094	0.31 ± 0.034	1.1 ± 0.10
	1	2.2 ± 0.12	2.1 ± 0.29	2.2 ± 0.23	2.1 ± 0.19
	2	41.0 ± 3.7	6.3 ± 1.1	15.0 ± 2.1	4.0 ± 0.51
	3	750.0 ± 110.0	19.0 ± 4.2	100.0 ± 20.0	7.5 ± 1.4

a. Based on a circulating coolant mass constant M_o = 4400 gm.

b. 95% confidence limits based on scatter in data only. Standard deviations are approximately one half the errors quoted.

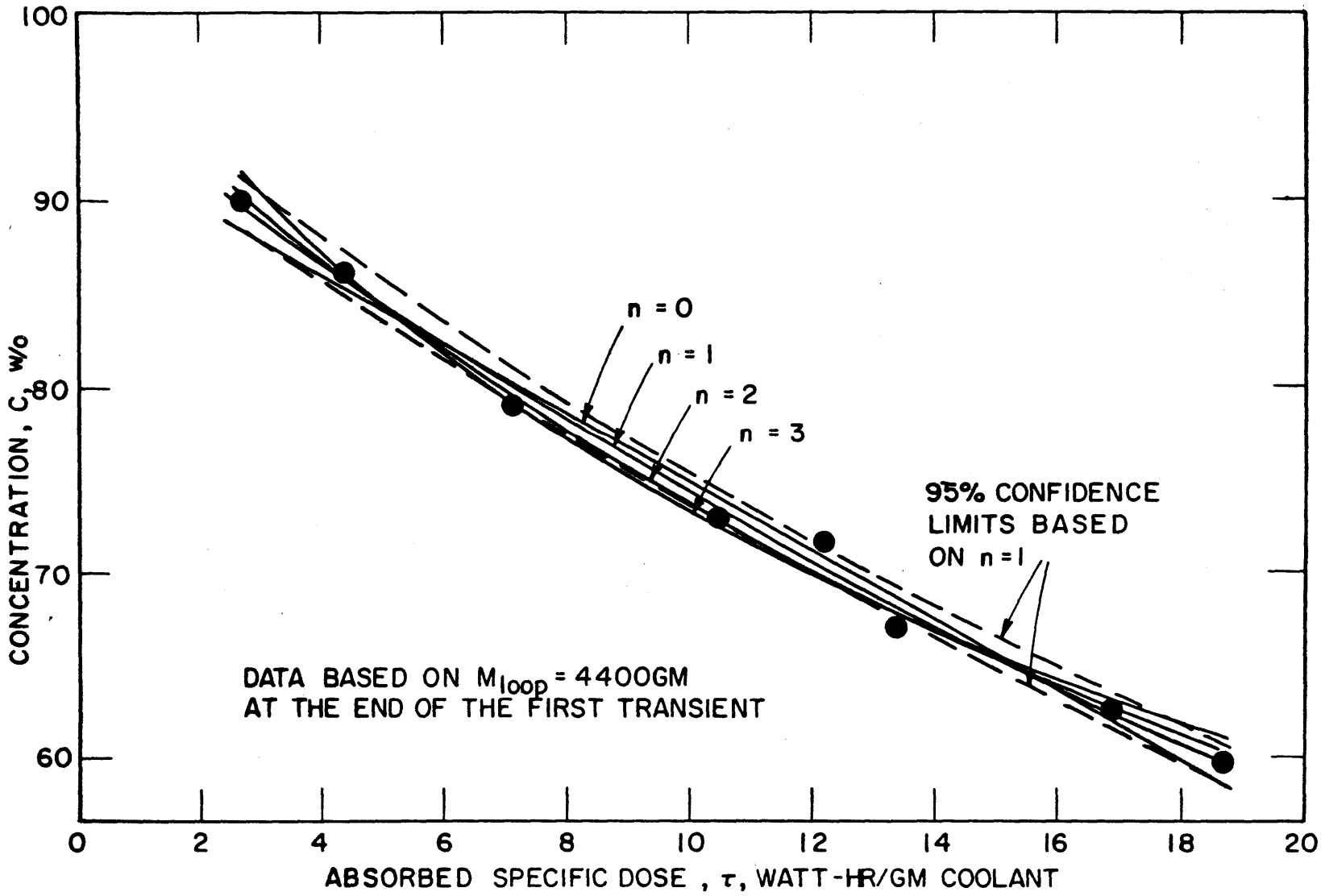

FIGURE 4.5 TOTAL TERPHENYL CONCENTRATION DURING THE FIRST TRANSIENT PERIOD OF THE 610°F IRRADIATION

TABLE 4.3

Comparison of the Ratio of Reaction Constants for Terphenyl Isomers with Terphenyl o:m:p Ratio

Reaction Order	Required o:m:p Ratio[a]	Ratio of Reaction Constants $k_{o,n}:k_{m,n}:k_{p,n}$
Transient No. 1		
0	1 : 5.8 : 1.5	1 : 5.8 : 1.5
1	1 : x : y	1 : 0.96 : 0.61
2	1 : 6.2 : 4.0	1 : 0.16 : 0.25
3	1 : 6.1 : 3.1	1 : 0.027 : 0.106
o:m:p ratio found	1 : 5.9 : 2.4	
Transient No. 2		
0	1 : 5.9 : 2.8	1 : 5.9 : 2.8
1	1 : x : y	1 : 0.95 : 1.02
2	1 : 6.5 : 2.7	1 : 0.15 : 0.38
3	1 : 6.4 : 2.7	1 : 0.025 : 0.14
o:m:p ratio found	1 : 6.1 : 2.7	

a. Required to satisfy ratio of k values and observed constant o:m:p ratio.

ıird order rate mechanisms, the rate constants calculated from the ex-
erimental data and the observed constant o:m:p ratio are compatible
ıly for the initial o:m:p ratio used. However, the rate constants are,
y definition, independent of concentration, and it is considered highly
nprobable that the initial concentrations of ortho-, meta- and para-
:rphenyl actually employed just happened to be those needed to satisfy
q. (4. 14). Since Eq. (4. 14) for the observed constant o:m:p ratio has
ıly one case in which the reaction constants are not concentration de-
endent, that of n = 1, the results of Table 4. 3 give a strong argument in
ıvor of a first order description of the data.

It has been decided to describe the 610°F irradiation data by first
rder kinetics for several reasons. The statistical and physical reasons
re stated above. In addition, it can be seen from Fig. 4. 5 that the first
rder model is at least as good as the other models allowed by Eq. (4. 1).
inally, because the first order rate constants appear to be statistically
qual for the individual terphenyl isomers (see Table 4. 2), the linearity
: the first order equation allows a consistent model; that is, the sum of
ıe rate expressions for the terphenyl isomers yields exactly the same form
: expression for the total terphenyl concentration. For second and third
rder mechanisms, the sum of the rate expressions for the individual
;omers does not form a simple second, or third, order expression of
ıe form of Eq. (4. 1).

Because of the choice of a first order model the stability parameter
$G^*(-i)$ takes on an additional meaning, for it is just the first order rate
ɔnstant (multiplied by a conversion factor) for component i and is in-
ependent of concentration. Table 4. 4 gives the $G^*(-i)$ values for the
10°F irradiation transient period data based on a first order model and
value of M_o = 4400 gm quoted above. The error limits quoted are
ıaximum possible errors and include errors in the scatter of the data, in
ıe circulating coolant mass and in the in-pile dose factor F (see Section
. 4). These latter two maximum possible errors are estimated at
16% and ± 4% respectively. As noted at the beginning of this section,
ıe possible error in the circulating coolant mass is a major error in
etermining the absolute values of $G^*(-i)$. Values of $G(-i)$ may be ob-
ıined from Table 4. 4 for any terphenyl concentration by multiplication

TABLE 4.4

$G^*(-i)$ Values for the Transient Periods of the 610°F Irradiation[a]

Component	$G^*(-i) = G(-i)/C_i$	
	Transient No. 1	Transient No. 2
Ortho-ϕ_3	0.34 ± 0.09[b]	0.25 ± 0.04
Meta-ϕ_3	0.33 ± 0.06	0.24 ± 0.04
Para-ϕ_3	0.21 ± 0.10	0.26 ± 0.05
Total omp	0.30 ± 0.05	0.25 ± 0.04

a. Based on $M_o = 4400$ gm.

b. Estimated maximum possible errors.

by the concentration C_i (see Eq. (4. 4)); this is of considerable convenience to the reactor design engineer.

From Table 4. 4 it can be seen that the $G^*(-i)$ values for each component during each transient period are about the same. The anomalously low value of $G^*(-p\phi_3)$ obtained for the first transient period is offset by the larger error which accompanies it; this is more clearly seen in the data of Table 4. 2. It is difficult to say whether the apparent reduction of $G^*(-i)$ values obtained for the second transient period is real or not.

4. 4. 2 Steady-State-HB Periods

The results obtained from the steady-state-HB periods are essentially independent of the circulating coolant mass (see Eq. (4. 11)), and so are expected to be more accurate than the transient period results. An additional piece of information on coolant degradation is available for the steady-state-HB periods since both the terphenyl concentration and HB concentration are measured during this period. In the discussion of coolant stability in terms of the formation of HB or LIB, Eq. (4. 11) still applies, except that the "makeup" term is replaced by a "removal" term for the HB and LIB fractions and the Δ term in Eq. (4. 12) must have the signs reversed. The notation used to describe the stability against the formation of HB and LIB will be $G(\rightarrow HB)$, $G(\rightarrow LIB)$, $G^*(\rightarrow HB)$ and $G^*(\rightarrow LIB)$ (4. 5). That is to say, the measured HB and LIB production rates will be converted to an equivalent amount of terphenyl degradation rate by using a molecular weight of 230 in the conversion from grams of HB and LIB formed to molecules of coolant producing these fractions. The concentration used in the calculation of $G^*(\rightarrow HB)$ and $G^*(\rightarrow LIB)$ is that of total omp. The LIB fraction is determined by difference only, i. e.

$$\text{w/o LIB} = \text{w/o HB} - \text{w/o DP} \qquad (4.15)$$

Therefore, the following relations must hold for the degradation rate of total terphenyl during the steady-state-HB period:

$$G(-\text{omp}) = G(\rightarrow HB) + G(\rightarrow LIB) \qquad (4.16)$$

and

$$G^*(-\text{omp}) = G^*(\rightarrow HB) + G^*(\rightarrow LIB) \qquad (4.17)$$

Figure 4. 6 shows the measured DP and HB concentrations of samples taken during the two steady-state-HB periods. Analyses by Monsanto

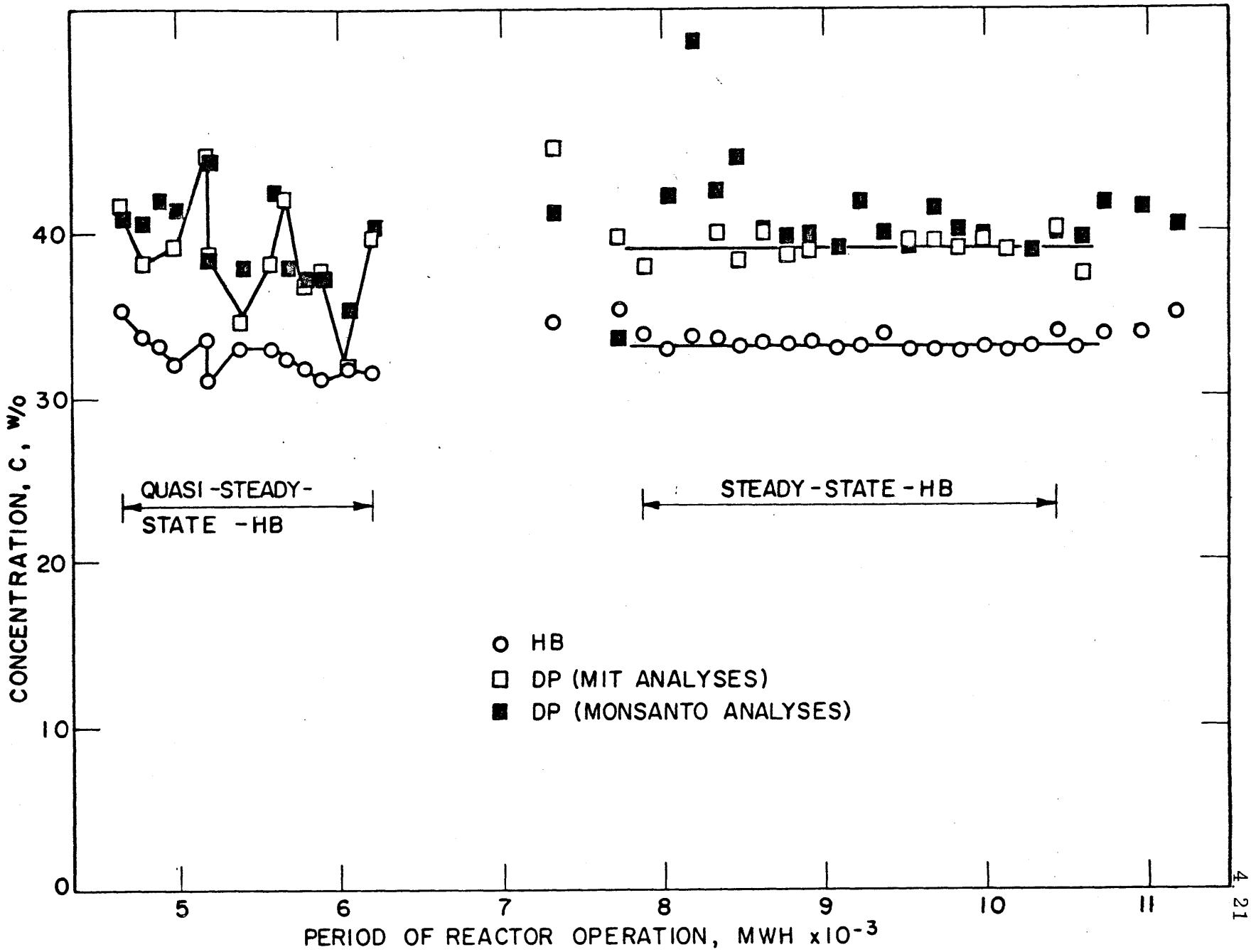

FIGURE 4.6 DP AND HB CONCENTRATIONS DURING THE STEADY-STATE-HB PERIODS

Research Corporation are shown for comparison purposes. Good control was not maintained on the HB level of the first "steady-state-HB" period. and it is therefore given the label of "quasi-steady-state-HB." During the steady-state-HB period (the second steady-state-HB period will henceforth be referred to as the "steady-state-HB period") the sample HB concentration was maintained at 33.2 ± 0.1 w/o and the DP concentration was found to be statistically constant at 39.0 ± 0.2 w/o. The error limits quoted here are based on the scatter in the data from the average value from the period. Additional consistent errors will be treated later. The terphenyl isomer concentrations during the steady-state-HB period are shown in Fig. 4.7. The isomer concentrations remained statistically constant with the averages and standard deviations based on scatter from the mean values as follows: o-ϕ_3 = 5.9 ± 0.05 w/o, m-ϕ_3 = 37.0 ± 0.01 w/o, p-ϕ_3 = 18.1 ± 0.2 w/o, total omp = 61.0 ± 0.2 w/o.

Table 4.5 summarizes the results of the G^* calculations for the steady-state-HB period. A more detailed analysis, including analysis of errors, may be found in Section A2.10. Notice that the concentrations quoted in the table are slightly higher than the sample average concentrations. This is because the samples are removed just before dilution and do not give the loop average concentrations (see Section 4.2). The results of Table 4.5 do indeed verify the transient period results in that the stabilities of the terphenyl isomers appear to be the same. From the table it is also apparent that very nearly all of the degradation products formed were HB components. This finding is consistent with the data of Mackintosh (4.8), who reports a constant LIB concentration in irradiated Santowax OM (a mixture of ortho- and meta-terphenyls) above 30 w/o HB (irradiation at 675°F). It may also be seen that the G^* values obtained in the transient periods (see Table 4.4) agree with those of the steady-state-HB period within the possible errors.

In spite of the larger fluctuations in concentration levels during the quasi-steady-state-HB period some stability information was still obtained, but the errors involved were larger due to these fluctuations. Table 4.6 summarizes the calculations performed for the quasi-steady-state-HB period; the detailed calculations are given in Section A2.10. The results obtained agree with those of the steady-state-HB period within the limits of the possible errors.

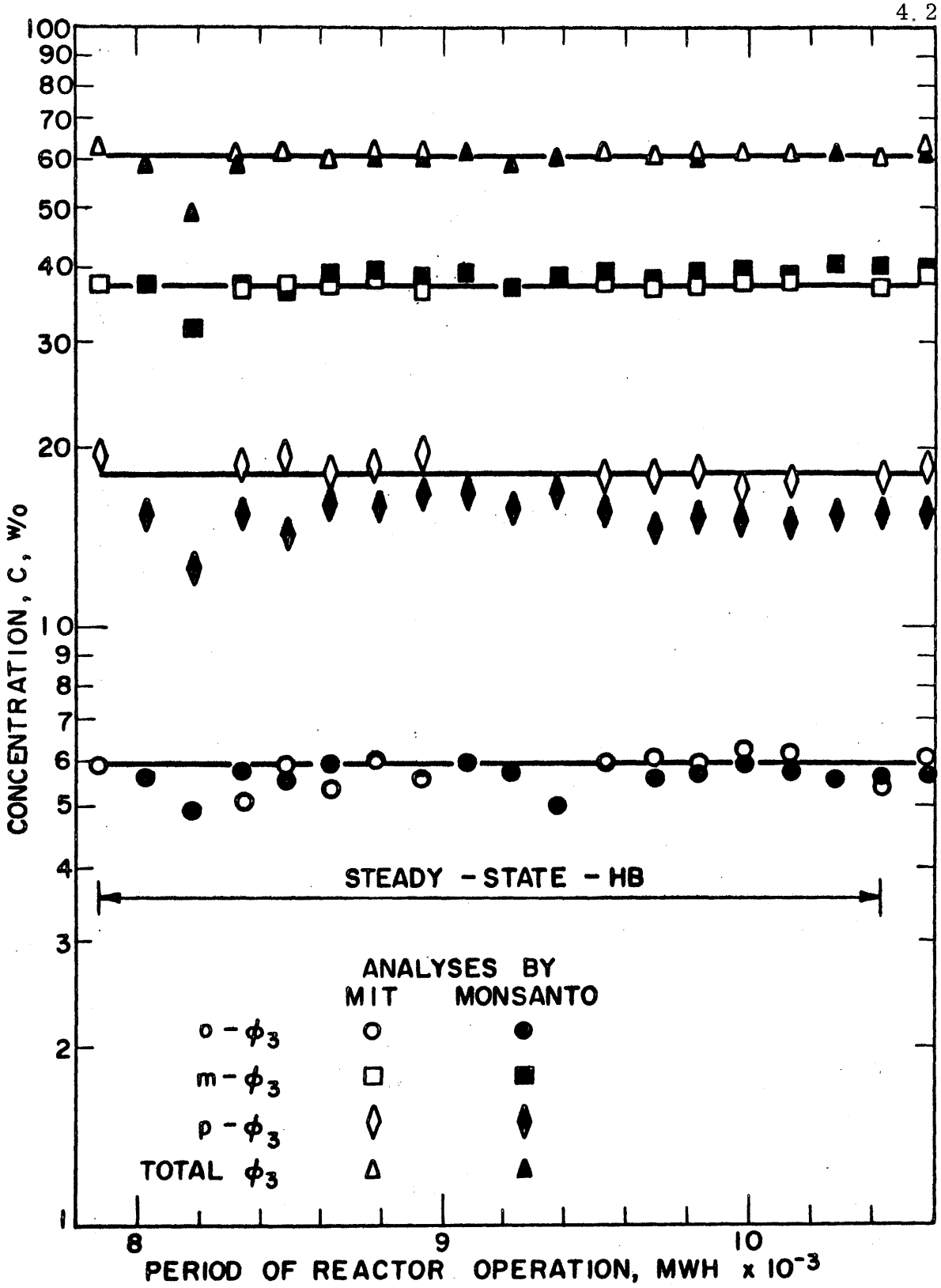

FIGURE 4.7 TERPHENYL ISOMER CONCENTRATION DURING THE STEADY-STATE-HB PERIOD OF THE 610° F IRRADIATION

TABLE 4.5

G^* Values for the Steady-State-HB Period of the 610°F Irradiation

Component	Grams Processed	Net Grams Replaced[a,d]	Loop Average Concentration, w/o	G^*
Total coolant	5361	--	--	--
Ortho-ϕ_3	318	180	6.0	0.26 ± 0.02[b]
Meta-ϕ_3	1983	1105	37.6	0.26 ± 0.02
Para-ϕ_3	968	587	18.3	0.28 ± 0.03
Total omp	3269	1872	61.9	0.26 ± 0.02
HB[c]	1778	1778	32.3	0.25 ± 0.01
LIB[c]	314	92	5.8	0.01 ± 0.01

a. Corrected for slight change in circulating coolant mass during the period.

b. 95% confidence limits. Standard deviations are one half of the errors quoted.

c. For the calculations of $G^*(\rightarrow HB)$ and $G^*(\rightarrow LIB)$, a molecular weight of 230 was used.

d. Net grams removed for HB and LIB.

TABLE 4.6

G^* Values for the Quasi-Steady-State-HB Period of the 610°F Irradiation

Component	Grams Processed	Net Grams Replaced[a,d]	Loop Average Concentration, w/o	G^*
Total Coolant	4189	-	-	-
Total ϕ_3	2575	1219	61.5	0.28 ± 0.05
HB[c]	1360	1156	32.5	0.26 ± 0.03
LIB[c]	254	63	6.0	0.02 ± 0.03

a. Corrected for changes in circulating coolant mass and concentrations during the period.

b. 95% confidence limits. Standard deviations are one half of the errors quoted.

c. For the calculations of $G^*(\rightarrow HB)$ and $G^*(\rightarrow LIB)$, a molecular weight of 230 was used.

d. Net grams removed for HB and LIB.

Although the concentrations of the various liquid components, the gas phase composition (see Section 4.9) and the physical properties of the coolant appear to have achieved constant values during the steady-state-HB periods (see Chapter 5 for physical properties) it is worth asking whether the steady-state-HB periods constituted a long-term irradiation or not. One criterion can be the number of masses equivalent to the circulating coolant mass in the loop which have been processed. In terms of this criterion the steady-state-HB and quasi-steady-state-HB periods each processed about the equivalent of one "loop mass." A second criterion can be the number of masses equivalent to the circulating coolant mass in the loop which have been replaced. In terms of this criterion the steady-state-HB periods each replaced about one-third of the circulating coolant mass. Apparently this relatively short period of time was sufficient to establish a steady-state level in the coolant composition and properties.

4.5 750°F Irradiation Liquid Degradation Results

4.5.1 Transient Periods

As discussed in Section 4.4.1 the transient period results are quite dependent on the value used for the circulating coolant in the loop. For the 750°F irradiation the results of the two methods mentioned above for calculating the circulating coolant mass yielded 3660 gm and 3170 gm respectively for the circulating coolant mass at the end of the first transient period ($M_o = M_{loop}$ at that time) (calculations are given in Section A2.5). This discrepancy amounts to about 13%, which is a smaller error than the corresponding discrepancy during the 610°F irradiation.

Figure 4.8 shows the measured terphenyl isomer concentrations during the transient periods of the 750°F irradiation. The data are also tabulated in Table 4.7 for reference. Two differences between the 750°F irradiation transient periods and those of the 610°F irradiation may be noted immediately. First, there was a significant buildup of biphenyl concentration during the 750°F irradiation transient periods, and, second, ortho-terphenyl definitely appeared less stable than the meta- and para-terphenyl isomers during the 750°F irradiation transient periods.

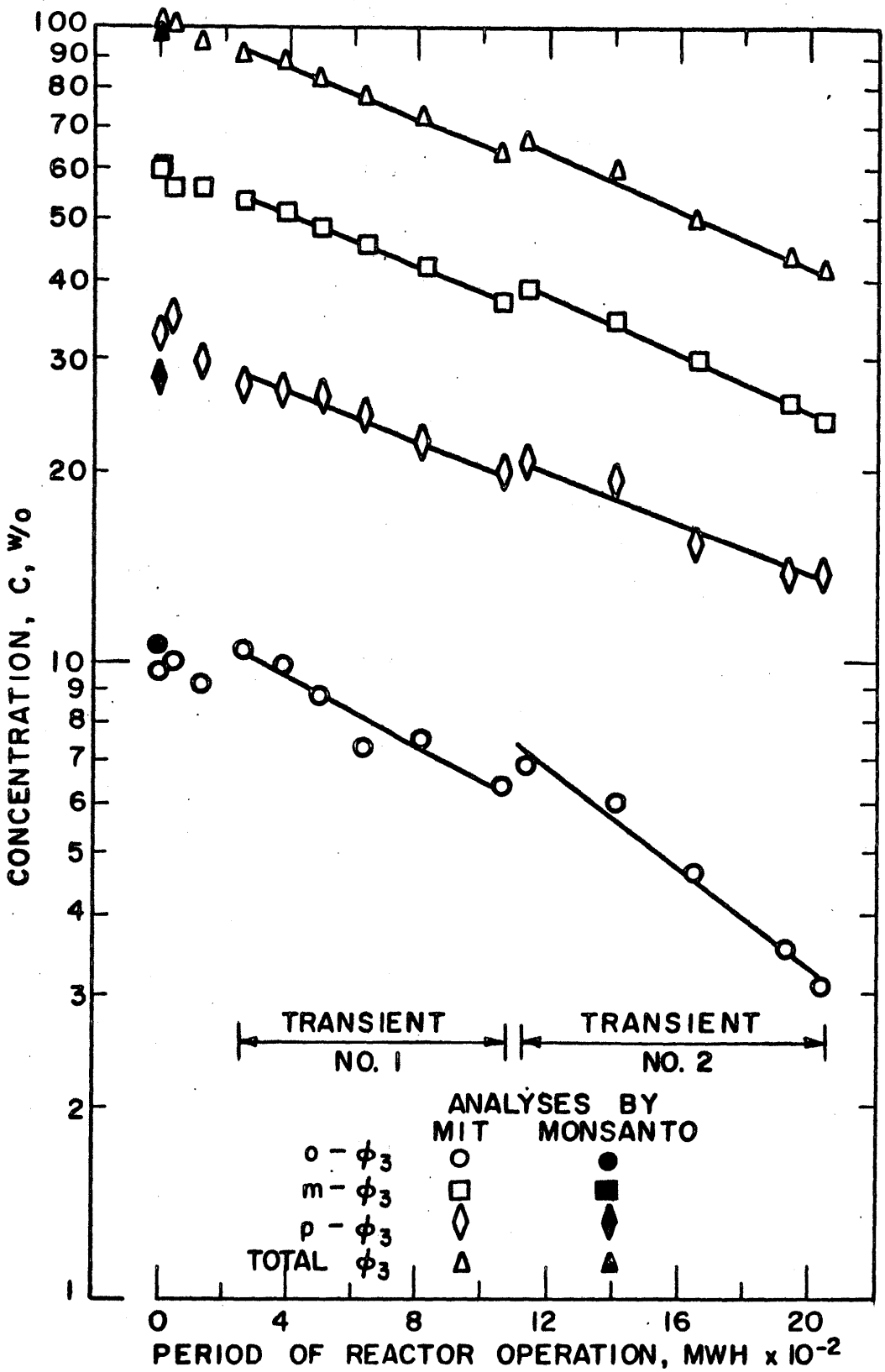

FIGURE 4.8 TERPHENYL ISOMER CONCENTRATION DURING THE TRANSIENT PERIODS OF THE 750°F IRRADIATION

TABLE 4.7

Terphenyl Concentration During the Transient Periods of the 750°F Irradiation

Sample Number	Terphenyl Concentration, w/o				Ratio o:m:p	Biphenyl, w/o	Reactor MWH
	Ortho-ϕ_3	Meta-ϕ_3	Para-ϕ_3	Total omp			
2L5	10.4	53.0	27.0	90.4	1:5.1:2.6	-	253
2L6	9.9	51.0	26.4	87.3	1:5.2:2.7	0.9	378
2L7	8.8	48.2	25.9	82.9	1:5.5:2.9	0.9	494
2L9	7.3	45.7	24.2	77.2	1:6.2:3.3	0.6	628
2L10	7.5	42.0	22.1	71.6	1:5.6:3.0	0.8	810
2L11	6.3	37.0	19.7	63.0	1:5.9:3.1	1.7	1056
			End of Transient No. 1				
2L12	6.9	38.4	20.6	65.9	1:5.6:3.0	1.7	1126
2L13	6.0	34.5	19.2	59.7	1:5.8:3.2	2.4	1406
2L14	4.6	29.8	15.3	49.7	1:6.5:3.3	2.6	1650
2L16	3.5	25.7	14.0	43.2	1:7.3:4.0	2.4	1936
2L17	3.1	24.2	13.8	41.1	1:7.8:4.4	2.9	2040
			End of Transient No. 2				

Studies similar to those performed on the 610°F transient period data showed no real statistical preference for a reaction order; the results are presented according to first order kinetics which fit the data at least as well as the other orders studied.

One item is worth discussing in view of the observed different stabilities of the terphenyl isomers. If the terphenyl isomers have different degradation rates, and if a relation of the form of Eq. (4.1) is used to describe the kinetics of the individual isomers, a first order description of the data for total terphenyl should really be given by

$$-\frac{dC_T}{d\tau} = k_{o,1} C_o + k_{m,1} C_m + k_{p,1} C_p \qquad (4.18)$$

In other words, even for first order kinetics, the relation describing the total terphenyl kinetics is not a simple one. However, a preliminary investigation for first order kinetics showed that, over the concentration range studied, Eq. (4.18) could be replaced by a relation of the form of Eq. (4.1), i.e.

$$-\frac{dC_T}{d\tau} = k_{T,1} C_T \qquad (4.19)$$

with a maximum of a 1% difference in the $G^*(-\text{omp})$ values obtained.

Table 4.8 gives the $G^*(-i)$ values for the 750°F transient periods based on a first order model and a value of the circulating mass constant, M_o, of 3660 gm. These results include the effects of out-of-pile pyrolysis and are labelled as total $G^*(-i)$ values. The maximum possible errors quoted are the result of errors of fit and maximum possible errors in the in-pile dose rate factor, F, and the circulating mass constant, M_o. It may be seen that the isomer stability appears to be para > meta > ortho.

Corrections for out-of-pile pyrolysis are described in detail in Section A2.9; studies have also been performed on the "pyrolysis corrected" data which are tabulated in that section. Again, the first order model described the data at least as well as the other models studied. Table 4.9 presents the corrected $G^*(-i)$ values.

Comparison of these results with those of the 610°F irradiation is postponed until Section 4.6.

TABLE 4.8

Total $G^*(-i)$ Values for the Transient Periods of the 750°F Irradiation[a]

Component	$G^*(-i) = G(-i)/C_i$	
	Transient No. 1	Transient No. 2
Ortho-ϕ_3	0.63 ± 0.27[b]	0.89 ± 0.25
Meta-ϕ_3	0.45 ± 0.07	0.52 ± 0.09
Para-ϕ_3	0.41 ± 0.10	0.48 ± 0.21
Total omp	0.46 ± 0.07	0.54 ± 0.13

a. Based on M_o=3660 gm.

b. Estimated maximum possible errors.

TABLE 4.9

$G^*(-i)$ Values (Corrected for Out-of-Pile Pyrolysis) for the Transient Periods of the 750°F Irradiation[a]

Component	$G^*(-i) = G(-i)/C_i$	
	Transient No. 1	Transient No. 2
Ortho-ϕ_3	0.50 ± 0.27[b]	0.58 ± 0.15
Meta-ϕ_3	0.40 ± 0.06	0.42 ± 0.07
Para-ϕ_3	0.39 ± 0.10	0.43 ± 0.21
Total omp	0.41 ± 0.07	0.44 ± 0.11

a. Based on M_o = 3660 gm.

b. Estimated maximum possible errors.

4. 5. 2 Steady-State-HB Period

Figure 4. 9 shows the measured DP and HB concentrations during the steady-state-HB period of the 750°F irradiation. Analyses by the Monsanto Research Corporation are shown for comparison. The period is divided into two parts by a 200 MWH fouling probe run (see Section 6. 4. 2) at about 3000 MWH. During the first portion the sampling rate was a little too rapid, causing both the HB and DP concentrations to decrease about 2 w/o. After the fouling probe run, the sampling rate appears to have been sufficient to maintain the HB and DP levels constant. The HB and DP concentrations at the end of the period were very nearly equal to those at the beginning of the period. There appeared to be no buildup of the LIB fraction. The terphenyl isomer concentrations during this period are shown in Fig. 4. 10 and were found to be quite constant. Ortho-terphenyl appeared to have the largest percentage change (about 8%) during the irradiation. The variation of the terphenyl isomer and HB concentrations was considered small enough to use average concentrations for the period in calculating the $G^*(-i)$ values. During the period the averages of the sample analyses were: $o\text{-}\phi_3 = 5.9 \pm 0.1$ w/o, $m\text{-}\phi_3 = 34.9 \pm 0.2$ w/o, $p\text{-}\phi_3 = 18.4 \pm 0.1$ w/o, total omp $= 59.2 \pm 0.2$ w/o, HB $= 33.3 \pm 0.2$ w/o. The errors quoted are standard deviations based on scatter from the average values for the period only. Consistent errors will be included in the error analysis of G^* values. Table 4. 10 summarizes the results of the calculations for total G^* values during the steady-state-HB period. Details of the calculations may be found in Section A2. 10.

Corrections have been made for out-of-pile pyrolysis during the steady-state-HB period (see Section A2. 9) and the "pyrolysis corrected" $G^*(-i)$ values are also tabulated in Table 4. 10. It can be seen that the out-of-pile pyrolysis correction for ortho-terphenyl amounts to about 13%, whereas the correction is only 8% for meta-terphenyl and 5% for para-terphenyl. No attempt has been made to correct the $G^*(\rightarrow HB)$ and $G^*(\rightarrow LIB)$ values for out-of-pile pyrolysis since sufficient data are not available on the pyrolytic production rates of these fractions. Wilkinson and Bates (4. 10) have noticed a significant production rate of biphenyl in the pyrolysis of para-terphenyl; this could be one reason for the six-fold

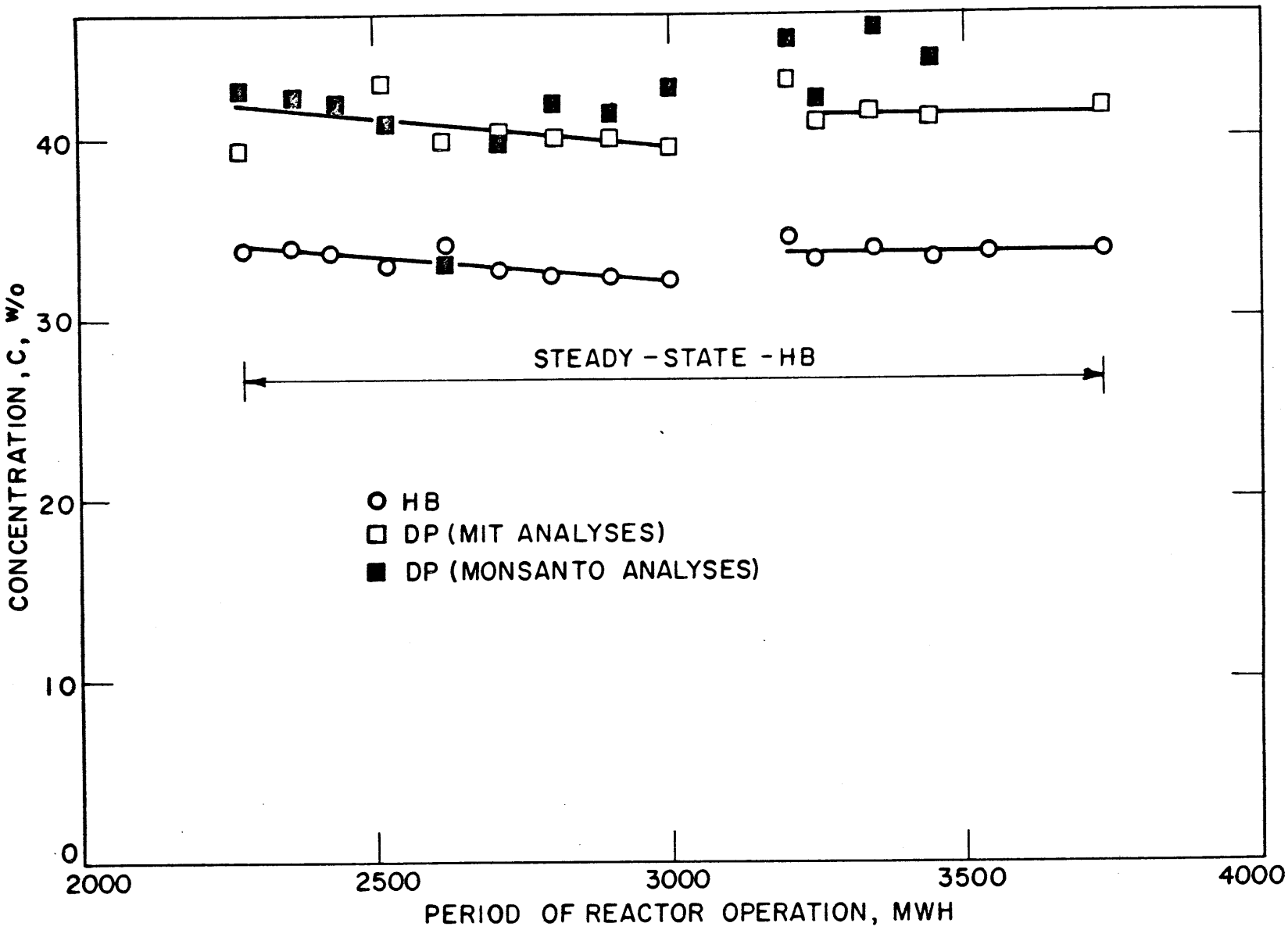

FIGURE 4.9 DP AND HB CONCENTRATIONS DURING THE STEADY-STATE-HB PERIOD

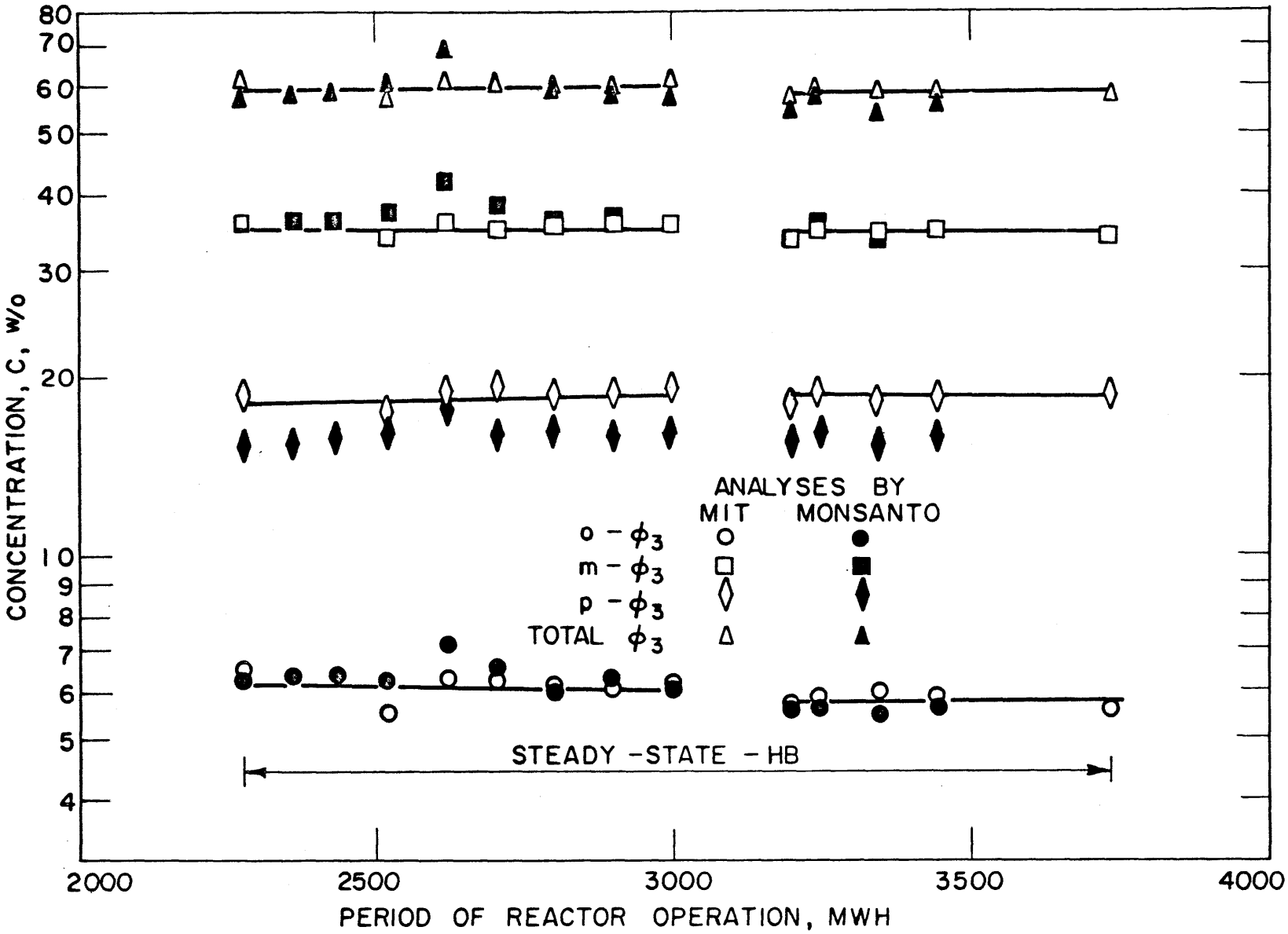

FIGURE 4.10 TERPHENYL ISOMER CONCENTRATION DURING THE STEADY-STATE-HB PERIOD OF THE 750°F IRRADIATION

TABLE 4.10

G^* Values for the Steady-State-HB Period of the 750°F Irradiation

Component	Grams Processed	Net Grams Replaced[a,d]	Loop Average Concentration, w/o	Total G^*	Pyrolysis Corrected G^*
Total coolant	5077	--	--	--	
Ortho-ϕ_3	302	283	6.1	0.79 ± 0.07[b]	0.70 ± 0.07
Meta-ϕ_3	1771	1091	35.3	0.52 ± 0.03	0.48 ± 0.03
Para-ϕ_3	932	499	18.6	0.45 ± 0.03	0.43 ± 0.03
Total omp	3005	1873	60.5	0.53 ± 0.04	0.49 ± 0.04
HB[c]	1695	1660	32.4	0.47 ± 0.02	
LIB[c]	377	213	7.1	0.06 ± 0.0	

a. Corrected for slight changes in circulating coolant mass and concentrations during the period.

b. 95% confidence limits. Standard deviations are one half of the errors quoted.

c. For the calculations of $G^*(\rightarrow HB)$ and $G^*(\rightarrow LIB)$, a molecular weight of 230 was used.

d. Net grams removed for HB and LIB.

increase in the LIB production rate from the 610°F irradiation to the 750°F irradiation (the HB production rate was not quite twice the value for the 610°F irradiation).

The length of the 750°F irradiation steady-state-HB period, as measured by number of grams processed, was more than one "loop mass." Over one-third of the circulating coolant mass in the loop was replaced during the period. This length of time appears to have been sufficient to establish a steady level in all components (except perhaps ortho-terphenyl, which should have eventually reached a steady level at a slightly lower concentration), a steady level in the gas phase composition (see Section 4.9) and a steady level in the physical properties measured (see Chapter 5).

The data of the 750°F irradiation transient periods agreed with the steady-state-HB measurements within the possible errors. For the 750°F irradiation, even after correction for out-of-pile pyrolysis, the stability of the terphenyl isomers is (to a 95% confidence level) para > meta > ortho.

4.6 Comparison of 610°F and 750°F Irradiation Liquid Degradation Results

A comparison of the 750°F irradiation data with the 610°F irradiation data is given by Table 4.11, which shows the G^* values obtained for the steady-state-HB periods of both irradiations. The transient values are not included in the comparison since they are less accurate. However, as stated above, the transient values agreed with the steady-state-HB values within the possible errors. While the 610°F irradiation data did not indicate any significant difference in the stability of the three terphenyl isomers, the stability at 750°F was para > meta > ortho. The degradation rates of meta- and para-terphenyl at 750°F were nearly twice the values at 610°F, while the degradation rate of ortho-terphenyl at 750°F was nearly three times the value at 610°F. There was a large increase in the LIB production rate during the 750°F irradiation. Some evidence of the increase was also provided by the increased biphenyl content of irradiated samples which reached about 2 w/o for the 750°F irradiation but remained at less than 0.5 w/o for the 610°F irradiation.

TABLE 4.11

First Order G^* Values for Steady-State-HB Irradiations

Component	$G^*(-i) = G(-i)/C_i$		
	610°F	750°F	750°F[b]
Ortho-ϕ_3	0.26 ± 0.02[a]	0.79 ± 0.07	0.70 ± 0.07
Meta-ϕ_3	0.26 ± 0.02	0.52 ± 0.03	0.48 ± 0.03
Para-ϕ_3	0.28 ± 0.03	0.45 ± 0.03	0.43 ± 0.03
Total omp	0.26 ± 0.02	0.53 ± 0.04	0.49 ± 0.04
HB[c]	0.25 ± 0.01	0.47 ± 0.02	
LIB[c]	0.01 ± 0.01	0.06 ± 0.05	

a. 95% confidence limits. Standard deviations = 1/2 errors quoted.

b. Corrected for pyrolysis occurring in out-of-pile circulating volume of the loop.

c. For the calculations of $G^*(\rightarrow HB)$ and $G^*(\rightarrow LIB)$, a molecular weight of 230 was used.

If it is assumed that an Arrhenius relation holds for the increase in G^* values with temperature (4. 15):

$$G^* = G_o^* e^{-\Delta E/RT} \qquad (4.20)$$

The activation energies of the various terphenyl isomers for in-pile effects only would be

ortho-terphenyl:	10 ± 2	kcal/mole
meta-terphenyl:	6 ± 2	kcal/mole
para-terphenyl:	4 ± 2	kcal/mole
total-terphenyl:	6 ± 2	kcal/mole

over the temperature range studied. In addition to the standard deviations in the G^* values, the ranges in the coolant irradiation temperatures were also considered in the computation of the standard deviations in the activation energies. These temperature ranges were ± 10°F for the 610°F irradiation and ± 5°F for the 750°F irradiation. Using Eq. (4. 20) as a guide, the variation in G^* values from the average values obtained at each temperature due to the irradiation temperature variations has been estimated as ± 0. 01 molecules degraded per 100 ev absorbed. This variation is only 2 - 5% of the absolute levels of the average G^* values found and indicates that the temperature ranges at each irradiation temperature did not significantly affect the G^* values obtained.

4. 7 Comparison of Liquid Degradation Results with Other Work

4. 7. 1 Relative Effects of Fast Neutrons and Gamma Rays on Terphenyl Degradation - Theory

Since previous work (4. 5, 4. 9) has indicated that combined fast neutron and gamma irradiation is more effective in causing terphenyl degradation than is gamma irradiation alone, the decomposition yields are dependent on the relative fraction of the energy absorbed due to fast neutron interactions. In order to generalize the results obtained at one laboratory with a given proportion of fast neutron dose to gamma ray dose, the approach has been to assume that the effects of fast neutron and gamma ray radiation are additive (4. 5). The effects of fast neutron and gamma ray interactions are then each assigned G (or G^*) values which are assumed independent of neutron and gamma ray energy distributions.

In terms of the stability criterion G^* this principle becomes

$$G^*(-i) = f_N G_N^*(-i) + (1 - f_N) G_\gamma^*(-i) \qquad (4.21)$$

where

f_N is the fraction of absorbed energy due to fast neutron interactions

$G_N(-i) = C_i G_N^*(-i)$ is the molecules of component i degraded per 100 ev of fast neutron energy absorbed in the total coolant

$G_\gamma(-i) = C_i G_\gamma^*(-i)$ is the molecules of component i degraded per 100 ev of gamma ray energy absorbed in the total coolant.

An equivalent expression applies for $G(-i)$. In the present work 37% of the total dose is due to fast neutron interactions and 63% due to gamma ray interactions (see Section 3.4).

The results of this experiment, which was conducted in a radiation environment which had a fixed fast neutron dose fraction, are not sufficient to determine both $G_N^*(-i)$ and $G_\gamma^*(-i)$, and so reliance must be placed on data obtained in other investigations with a significantly different fraction of fast neutron dose.[1]

4.7.2 Results of Electron and Gamma Ray Irradiations

In comparing results between different investigators, care must be taken to distinguish between radiation yields reported as $G(\rightarrow HB)$, which is determined from the observed rates of HB formation, and $G(-i)$, which is derived from observed rates of disappearance of the terphenyl isomers. For a given set of radiation conditions, the two yields are usually not the same due to the formation of low and intermediate boilers (LIB).

Electron irradiations using 1 Mev electrons from a Van de Graff generator have been performed on encapsulated samples of Santowax R (similar in composition to Santowax OMP) at Harwell (4.2, 4.5) and on encapsulated samples of Santowax OM (a mixture of ortho- and meta-

1. It should be noted that the results of other irradiations to be presented for comparison with the present results do not include every possible source of data. Some data (see for instance reference (4.21)) have not been included in the presentation because it has not been possible to correct the data to the first order $G^*(-i)$ values used in this report.

terphenyls) at Chalk River (4.8). The results have been reported in terms of initial G(→HB) values (i.e. G(→HB) at zero dose) determined from a second order kinetics fit to the HB concentration data. The HB concentrations were determined by a microsublimation technique (4.2) at both laboratories, but the omp concentrations were determined (by gas chromatography) only at Chalk River. The initial G(→HB) values obtained are listed in Table 4.12. Mackintosh (4.8) reports how the LIB concentration built up with dose, so that his data can be converted into results which can be compared to the results reported here. Although Mackintosh's data for HB production do appear to fit second order kinetics somewhat better than first order, his terphenyl disappearance results fit first order kinetics at least to 40 w/o DP. The conversion between (100 − w/o HB) and w/o omp was accomplished through the reported LIB concentration of about 6 w/o at 30 w/o HB. This LIB concentration is consistent with the average LIB concentration of 5.8 w/o obtained during the steady-state-HB period of the 610°F irradiation of Santowax OMP at M.I.T. (see Section 4.4.2). Thus both the results obtained at Harwell and those obtained at Chalk River were converted to terphenyl disappearance and fit by first order kinetics. The values of $G^*_{electron}$(−omp) after this conversion coincided (perhaps fortuitously) with the reported initial G(→HB) values (refer to Table 4.12).

Mackintosh also observed for the irradiated Santowax OMP that ortho-terphenyl was less stable than meta-terphenyl at 707°F. This finding is consistent with the findings at M.I.T. (see Section 4.6). The value reported in Table 4.12 is the overall value for Santowax OM.

The Phillips Petroleum Company has reported preliminary results of irradiation of encapsulated samples of Santowax OMP with 6 Mev electrons from a LINAC at 600°F (4.16). They used a microsublimation technique similar to that developed at Harwell for HB analyses and reported HB concentrations as a function of absorbed dose but made no G value calculations. Using the same conversion of (100 − w/o HB) to w/o omp mentioned above, a first order fit to their data gave a value of $G^*_{electron}$(−omp) of 0.17, in excellent agreement with the values obtained at Harwell for the same temperature.

The results of the three laboratories mentioned above for electron irradiation of terphenyls have proven to be quite consistent and show a value of $G^*_{electron}$(−omp) which increases only slightly with temperature;

TABLE 4.12

Summary of $G_{electron}$ and G_{γ} Values Obtained by Irradiation of Encapsulated Terphenyl Samples[d]

Laboratory	Material Irradiated	Irradiation Method	Dose Rate watts/gm	Irradiation Temperature °F	Reported Initial G(→HB)	G*(−omp) (First Order Kinetics)
Harwell (4.2, 4.5)	Santowax R	1 Mev electrons	~3	572	0.17[a]	0.17[b]
				662	0.17	0.17
				752	0.19	0.19
Chalk River (4.8)	Santowax OM	1 Mev electrons	7.3	707	0.18[a]	0.18[b]
Phillips Petroleum Co. (4.16)	Santowax OMP	6 Mev electrons	~1	600	--	0.17[b]
Cal. Research at Susie (4.17)	Ortho-, meta- and para-terphenyls	Reactor γ rays	up to 0.013	600	--	0.28[c]
Cal. Research at MTR γ Canal (4.17)	Ortho-, meta- and para-terphenyls	Spent fuel element γ rays	up to 0.013	425	--	0.19[c]
				600	--	0.28
				675	--	0.32
				750	--	0.68

a. Determined from second order fit to HB appearance.

b. Calculated by first order fit to omp disappearance assuming 6 - 7 w/o LIB at 30 w/o HB.

c. Assumes a terphenyl mixture containing an o:m:p ratio of 1:6:3.

d. Not included are the results from an MTR γ canal irradiation of a polyphenyl mixture at 750°F (4.21), since only a smoothed curve of G(→HB) over the range of 5 to 17 w/o HB was reported. Consequently, a valid extrapolation to an initial value of G(→HB) could not be made for these data.

0.17 at 600°F and 0.19 at 750°F (see Table 4.12). However, recent measurements by the California Research Corporation (4.17) using reactor γ rays at the "gamma rich" face of Susie (SPTF) reactor and gamma radiation from spent fuel elements in the MTR gamma canal indicate much higher G values for the terphenyls than those of the electron irradiation measurements for irradiations in the range of 600° to 750°F. For these irradiations, encapsulated samples of pure ortho-, meta- and para-terphenyl were irradiated, and the terphenyl concentrations at any time determined by gas chromatography. Isothermal calorimeters were used to determine the gamma dose rates, in much the same manner as the adiabatic calorimetric method used at M.I.T.. The results of the irradiations were analyzed by first order kinetics. At each irradiation temperature, the para- and meta-terphenyls were found to have about the same stability. Ortho-terphenyl was found to have about the same stability as meta- and para-terphenyl at 425°F, but as the irradiation temperature was increased, it became increasingly less stable than meta- and para-terphenyl. The values given in Table 4.12 are based on the linear average for a synthetic mixture of terphenyls having an o:m:p ratio of 1:6:3 (approximating Santowax OMP).

There could be two possible reasons for the discrepancy between the values obtained at California Research Corporation and by other investigators. The first is that gamma rays may be more effective than electrons in degrading terphenyls. It has previously been assumed that electron irradiations are equivalent to gamma ray irradiations because most gamma ray interactions involve Compton collisions with the atomic electrons of the material being irradiated. High energy electrons, however, undergo many types of interactions with the irradiated material (4.18) and perhaps could cause less damage than gamma rays to terphenyls for an equal amount of energy absorbed. The second possibility lies in the much lower dose rates to terphenyl (up to 0.013 watts/gm) for the California Research Corporation measurements than for the electron irradiation measurements (1 - 7 watts/gm). Possibly there is a dose rate effect on the terphenyl degradation which would cause the measurements by California Research Corporation to have higher G values than those measured by electron irradiation.

In view of these large differences in the reported values for G^*(-omp) obtained with electron and gamma irradiations, it was not

considered meaningful to select a value for $G^*_\gamma(-omp)$ from such work and then attempt to calculate $G^*_N(-omp)$ using Eq. (4.21), the selected value of $G^*_\gamma(-omp)$ and the value of $G^*(-omp)$ from the M.I.T. loop studies. An alternative procedure of comparing the results of various irradiation facilities and at the same time evaluating $G^*_N(-omp)$ and $G^*_\gamma(-omp)$ has been developed. This method involves using Eq. (4.21) to express $G^*_N(-omp)$ as a function of $G^*_\gamma(-omp)$. Thus, the results obtained at each facility (where f_N is fixed) may be represented graphically as a straight line. Presumably, the different lines obtained should have a common intersection on the $G^*_N(-omp)$ vs. $G^*_\gamma(-omp)$ plane, yielding the desired values of $G^*_N(-omp)$ and $G^*_\gamma(-omp)$.

4.7.3 Comparison with Other Irradiations Near 610°F

Figure 4.11 is the plot of $G^*_N(-omp)$ vs. $G^*_\gamma(-omp)$ for the results of different facilities performing irradiations on terphenyls at temperatures near 610°F. In the paragraphs that follow, a discussion of the data obtained at each laboratory will be given.

The results obtained from the steady-state-HB period of the 610°F irradiation at M.I.T. are shown in Fig. 4.11. The data utilized with Eq. (4.21) were: $G^*(-omp) = 0.26$ (see Section 4.6) and $f_N = 0.37$ (see Section 3.4). The shaded area on each side of the MITR line displays the overall standard deviation of the MITR results. The average dose rate in the core region of the in-pile section is also listed (~530 milliwatts/gm). The results of the electron and gamma irradiations near 610°F are also plotted in Fig. 4.11. For $G^*_{electron}(-omp)$, the value of 0.17 obtained from the Harwell and Phillips Petroleum Company data (see Table 4.12) was used. For $G^*_\gamma(-omp)$ the value of 0.28 obtained from the California Research Corporation data (see Table 4.12) was used. From these three lines it can now more clearly be seen why the determination of $G^*_N(-omp)$ and $G^*_\gamma(-omp)$ from the MITR results and the $G^*_{electron}(-omp)$ and $G^*_\gamma(-omp)$ results is inconsistent. If the Harwell and Phillips Petroleum data were taken as representative of $G^*_\gamma(-omp)$ at 610°F, a value of $G^*_N(-omp)$ of 0.41 would be obtained, yielding $G^*_N(-omp)/G^*_\gamma(-omp) = 2.4$. On the other hand, if the California Research Corporation data were taken as representative of $G^*_\gamma(-omp)$ at 610°F, a value of $G^*_N(-omp)$ of 0.23 would be obtained, yielding $G^*_N(-omp)/G^*_\gamma(-omp) = 0.9$.

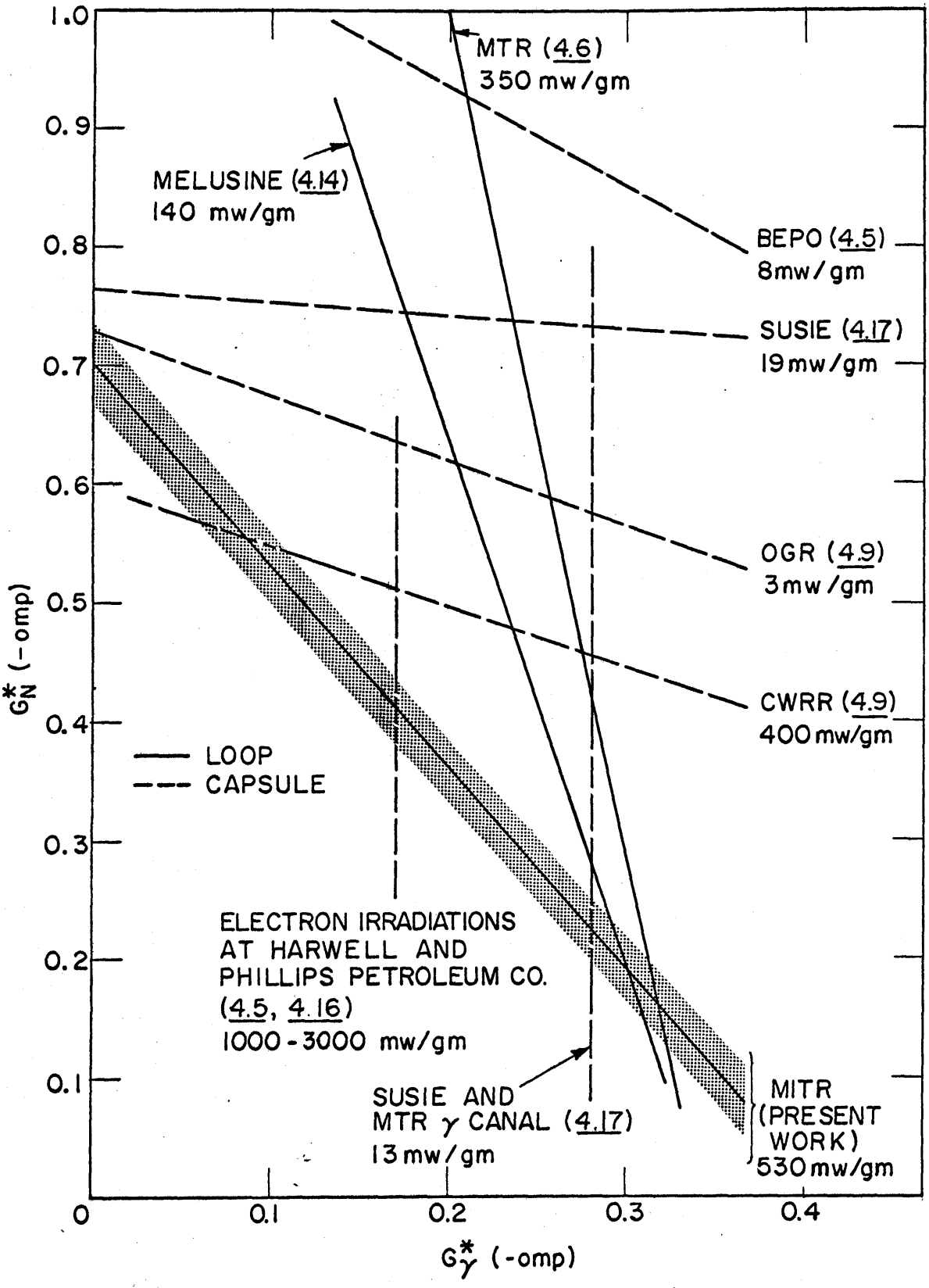

FIGURE 4.11 COMPARISON OF FIRST ORDER G^*_Λ VALUES AT 610°F

Keen et al. (4.6) report the results of transient in-pile loop irradiations of Santowax R and Santowax OM in the Materials Testing Reactor (MTR) by Bley (4.19). The measurements were performed over the temperature range 620 - 650°F. Steel isothermal calorimeters were used to measure the gamma ray dose rate, and nickel foils to measure the fast neutron dose rate. The average dose rate obtained in the in-pile section was 350 milliwatts/gm and the fast neutron fraction 0.12. Dosimetric errors have been estimated at ± 15% in the total dose rate and ± 50% in the fast neutron fraction (4.19). The data were correlated by first order kinetics and the following results reported by Keen:

$$G^*(-o\text{-}\phi_3) = 0.40 \pm 0.02$$
$$G^*(-m\text{-}\phi_3) = 0.27 \pm 0.02$$
$$G^*(-p\text{-}\phi_3) = 0.32 \pm 0.02$$

where the standard deviations are presumed to be in the fit of the first order law to the data alone. The results indicate a slightly lower stability for ortho-terphenyl than the meta- and para-terphenyl isomers. Using a synthetic mixture having an o:m:p ratio of 1:6:3 (approximating Santowax OMP) and taking into account dosimetric errors, a value of $G^*(-omp) = 0.30 \pm 0.05$ was calculated for comparison with the present data, and a graphical representation of the MTR results is also given in Fig. 4.11. Discussion of G_N^* and G_γ^* values obtainable with these results and those at the MITR is postponed until the data for the other loop irradiation of terphenyls are given below.

Van der Venne (4.14) reports the preliminary results obtained from the transient irradiation of Terphenyl OM-2 (meta-rich terphenyl mixture) in an in-pile loop at the 2 MW swimming pool reactor, Melusine (Grenoble, France). The measurements were performed at various temperatures between 392°F and 840°F; in this section only the 608°F results are considered. Dosimetric measurements were made by foil activation for fast neutron fluxes and graphite isothermal calorimeters for the gamma dose rates. The fast neutron fraction was determined as 0.18 and the overall dosimetric error was estimated as ± 10% (4.7). The total dose rate delivered to the coolant in the Melusine loop was not reported by Van der Venne, but a preliminary value of 0.14 watts/gm

has previously been stated by the Melusine staff (4.20). It is presumed that the dose rate in the Melusine loop at the time of irradiation of Terphenyl OM-2 was at least the same order of magnitude as this previously given value. By fitting the terphenyl concentration versus absorbed dose data by first order kinetics, a value of $G^*(-omp)$ of 0.28 was obtained. These data were plotted on Fig. 4.11 for comparison with the present work.

From Fig. 4.11, it is evident that the results of the three loop experiments (MITR, MTR, Melusine) indicate a value of $G_N^*(-omp)$ nearly equal to that for $G_\gamma^*(-omp)$[1]. These findings are thus more consistent with the $G_\gamma^*(-omp)$ values obtained at the California Research Corporation than the $G_{electron}^*(-omp)$ values obtained at Harwell and at Phillips Petroleum Company. However, this finding cannot be regarded as conclusive, since it will be presently demonstrated that the in-pile capsule irradiation work disagrees with the in-pile loop irradiation work.

Before describing the results of the in-pile capsule irradiations at temperatures near 610°F, comparison of the HB production rates obtained at the MITR during the steady-state-HB period of the 610°F irradiation can be made with the HB production rate observed from operation of the OMRE. Gercke and Trilling (4.21) report the results of irradiations of OMRE coolant at 600°F (primarily ortho- and meta-terphenyl) and at various HB concentration levels. The overall dose rate delivered to the coolant in the core was 1.2 watts/gm, and the fast neutron dose rate fraction in the OMRE was 0.28. At 33 w/o HB, they report a $G(\rightarrow HB)$ value of 0.14 ± 0.03. At the MITR, after converting G^* values to G values, a value of $G(\rightarrow HB)$ of 0.15 ± 0.01 was obtained for the steady-state-HB period of the 610°F irradiation, in good agreement with the OMRE data. The OMRE results would thus tend to be classed with the results of the loop experiments on Fig. 4.11; they are not plotted, however, as Fig. 4.11 is concerned with $G^*(-omp)$, not $G^*(\rightarrow HB)$.

Zack et al. (4.9) report the results of in-pile experiments at the Oak Ridge Graphite Reactor (OGR) and at the Curtiss-Wright Research Reactor (CWRR) on encapsulated samples of Santowax OMP. The irradiation temperature for the OGR experiments was 620°F, and that for the CWRR experiments was 625°F. At the OGR, threshold foils were used to determine the fast neutron dose rate and an adiabatic carbon calorimeter

1. Note that the ratio G_N^*/G_γ^* is quite sensitive to the location of the straight lines (Eq. (4.21)) for the loop data. Considering the relative slopes of the lines, the intersection in turn is sensitive to relatively small changes in the reported values of $G^*(-omp)$.

to determine the gamma ray dose rate. The average dose rate at the OGR was determined to be ~3 mw/gm, of which 63% was due to fast neutrons. No errors in the dosimetry were quoted. At the CWRR, an aluminum threshold foil was used to determine the fast neutron dose rate and a carbon calorimeter to determine the gamma ray dose rate. The dose rate was calculated as ~400 mw/g, 65% being due to fast neutrons. A possible error of ± 50% was estimated in the dosimetry (4.22) as experiments were not complete when the reactor was closed down. In both experiments gas chromatography was used to measure the terphenyl content of the irradiated material.

Both the OGR results and CWRR results have been evaluated at M.I.T., using the same least squares parameter survey as applied to the data from the transient periods of the MITR irradiations. It was found that first order kinetics could describe these data as well as other orders, so the results of these capsule irradiations are presented in Table 4.13 using first order kinetics. These results indicate an

TABLE 4.13

$G^*(-i)$ Values Obtained from OGR and CWRR Data Using First Order Kinetics

	$G^*(-i) = G(-i)/C_i$	
Component	OGR(620°F)	CWRR(625°F)
Ortho-ϕ_3	0.51 ± 0.13[a]	0.51 ± 0.07
Meta-ϕ_3	0.46 ± 0.07	0.41 ± 0.07
Para-ϕ_3	0.46 ± 0.09	0.37 ± 0.08
Total omp	0.47 ± 0.05	0.39 ± 0.07

a. 95% confidence limits based on scatter in data only.

approximately equal stability for all three terphenyl isomers, just as the results of the 610°F irradiation of Santowax OMP do. Using the $G^*(-omp)$ values found for the OGR and CWRR data, and the reported fast neutron fractions, curves have been placed on Fig. 4.11 for comparison with the other reported data. Further discussion of these data is postponed

until the other in-pile capsule irradiation work have been presented.

Bolt (4.17) reports results of in-pile irradiations of encapsulated samples of pure ortho-, meta- and para-terphenyl at the "neutron rich" face of the Susie reactor. Isothermal calorimeters were used to determine the fast neutron and gamma ray dose rates in much the same manner as the adiabatic calorimetric method used at M.I.T.. The irradiations were performed at 600°F. The measured dose rate to the terphenyl samples varied up to about 19 mw/gm, of which about 90% was due to fast neutron interactions. The terphenyl concentrations were measured by gas chromatography, and the concentration vs. absorbed dose data were analyzed by first order kinetics. The $G^*(-i)$ values obtained were:

$$G^*(-o\text{-}\phi_3) = 0.79$$

$$G^*(-m\text{-}\phi_3) = 0.70$$

$$G^*(-p\text{-}\phi_3) = 0.59$$

These results did not show an equal stability for the terphenyl isomers, and a synthetic $G^*(-omp)$ value of 0.69 is obtained by assuming an o:m:p ratio of 1:6:3 (approximating Santowax OMP) for the purpose of comparison here. The Susie results are displayed graphically on Fig. 4.11 for comparison with the other results obtained near 610°F.

In-pile irradiations have also been performed on encapsulated samples of Santowax R at BEPO and the results reported by Bates, Burns et al. (4.5). The three temperatures studied were 572°F, 662°F and 752°F. Dosimetric measurements were performed by means of calorimeters using the method described by Anderson and Waite (4.23), and the energy deposition was related to the thermal neutron dose to cobalt monitor wires in the capsules (4.24). The energy deposition rate in the samples was measured as ~ 8 mw/gm, of which 54.4% was due to fast neutron interactions. HB concentrations in the irradiated samples were measured by microsublimation and initial G(→HB) values (G(→HB) at zero dose) given. Most of the work was done at 662°F, with only one sample being irradiated at 572°F and two at 752°F. A second order kinetics fit to the 662°F irradiation data yielded $G_{initial}(\rightarrow HB) = 0.62$ to 0.70, and, based on a single irradiation at 572°F, an initial G(→HB)

value of 0.51 was given for this temperature. Conversion of the initial G(→HB) data at 662°F to first order G^*(–omp) data by the method described in Section 4.7.2 above yielded exactly the same range of first order G^*(–omp) values as the initial G(→HB) values based on second order kinetics. The same agreement between the second order initial G(→HB) values and first order G^*(–omp) values was found for the electron irradiation data reported at Harwell, so the initial G(→HB) value obtained from the single sample at 572°F was presumed to be equal to G^*(–omp). By linear interpolation in temperature, a value of G^*(–omp) at 610°F of 0.6 was used for comparison with the data of this report. This result is also shown graphically on Fig. 4.11.

It may be seen from Fig. 4.11 that the in-pile irradiation experiments on encapsulated samples of terphenyls agree neither with each other nor with the more-or-less common intersection given by the in-pile loop work. Several reasons for these discrepancies are possible. First, it may be possible that the mixing effect achieved in in-pile loop irradiations served to produce a more consistent basis for terphenyl irradiation. Second, there may be a dose rate effect on terphenyl degradation. Except for the CWRR work, all the in-pile irradiations of encapsulated samples have been performed at very low dose rates compared with the loop irradiation work and the operation of OMRE. Third, all the irradiation experiments on encapsulated samples report fast neutron dose rate fractions from 55 to 90%, whereas the loop irradiation data were obtained with fast neutron fractions of 12 to 37%. Accurate values of the fast neutron dose rates are usually more difficult to obtain than accurate values of gamma ray dose rates (especially if threshold foils are used to determine the fast neutron dose rate), and errors in the fast neutron dose rate determinations are relatively more important for the irradiations of encapsulated samples.

4.7.4 Comparison with Other Irradiations Near 750°F

Data on terphenyls irradiated near 750°F at other laboratories are meager and the data which have been published make no attempt to correct for pyrolytic damage, which makes data comparison somewhat more difficult. Figure 4.12 is the total G^*_γ(–omp) vs. G^*_N(–omp) plot for the results of different laboratories performing irradiations on terphenyls

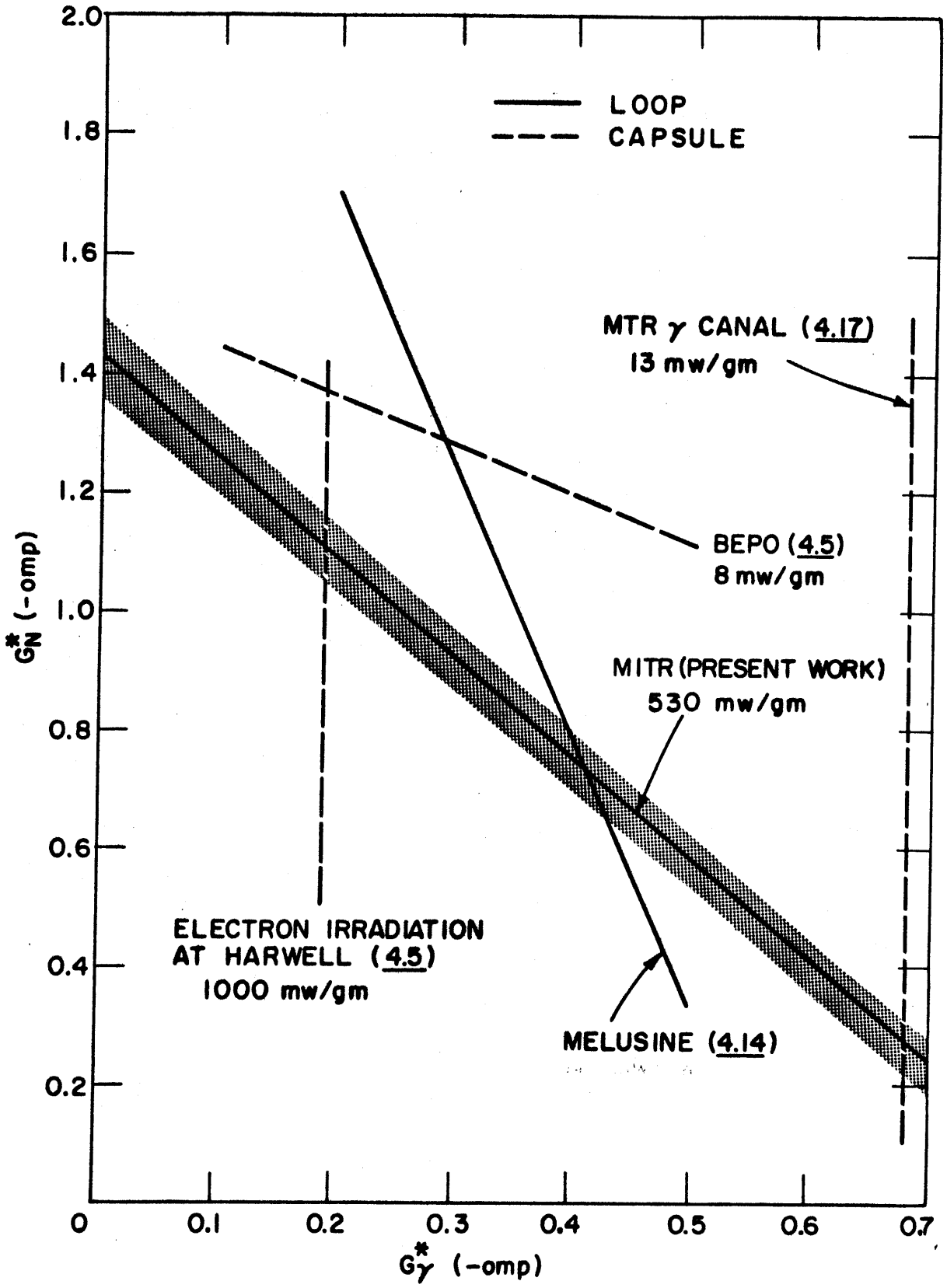

FIGURE 4.12 COMPARISON OF FIRST ORDER G^* VALUES AT 750°F

near 750°F. No data on this plot have been corrected for pyrolytic damage. In the paragraphs that follow, a discussion of the data obtained at each laboratory will be given.

The results obtained from the steady-state-HB period of the 750°F irradiation at M.I.T. are shown in Fig. 4.12. The data utilized with Eq. (4.21) were $G^*(-omp) = 0.53$ (uncorrected for out-of-pile pyrolysis; see Section 4.6) and $f_N = 0.37$ (see Section 3.4). The shaded area on each side of the MITR line displays the overall standard deviation of the MITR results. The average dose rate in the core region of the in-pile section is also listed (~ 530 mw/gm). The results of the electron and gamma irradiations near 750°F are also plotted in Fig. 4.12. For $G^*_{electron}(-omp)$, the value of 0.19 obtained from the Harwell data at 752°F (see Table 4.12) was used. For $G^*_\gamma(-omp)$ the value of 0.68 obtained from the California Research Corporation data at 750°F (see Table 4.12) was used.[1] As with the 610°F data, the wide divergence of the $G^*_{electron}(-omp)$ and $G^*_\gamma(-omp)$ values makes almost meaningless the calculation of $G^*_N(-omp)$ from these data and the MITR results; using the electron irradiation data $G^*_N(-omp)/G^*_\gamma(-omp)$ would be nearly 6, and using the gamma irradiation data $G^*_N(-omp)/G^*_\gamma(-omp)$ would be less than 0.5! Reasons for this discrepancy have been suggested in Section 4.7.3. In addition, it should be noted that because of the low dose rates used in the gamma irradiation work, the pyrolytic contribution to the degradation of the terphenyls would be relatively more important than in the electron irradiation work, thus causing the gamma irradiation work to yield higher G^* values. The data have not been corrected for pyrolytic damage since it is presently unknown whether the combined effects of radiolysis and pyrolysis in the radiation zone can be computed from the individual effects or not (4.15).

To date, there has been only one other in-pile loop irradiation of terphenyls near 750°F, and only preliminary results are available from this irradiation. Van der Venne (4.14) reports a first order $G^*(-omp)$ value for the transient irradiation of Terphenyl OM-2 at the Melusine reactor at 752°F (see Section 4.7.3 for a more complete description of the methods used at Melusine). The value reported was $G^*(-omp) = 0.47$, not corrected for out-of-pile pyrolysis. Using this value and the reported

1. At least one other irradiation at 750°F has been performed (4.21); however, see footnote d of Table 4.12.

fast neutron fraction of 0.18, the data are presented graphically in Fig. 4.12. These data, in comparison with the MITR data, would indicate a ratio of $G^*_N(-omp)/G^*_\gamma(-omp)$ equal to 1.8 at 750°F. The out-of-pile volume of the Melusine loop was reported to be about 80% of the total loop volume (4.14), but the average in-pile dose rate delivered to the coolant was not reported, and has only been inferred as about 0.14 watts/gm from previous statements by the Melusine staff (4.20). In view of this uncertainty and the uncertainty in the exact isomeric composition of the terphenyl irradiated, no formal correction was applied to the results reported. Assuming an average in-pile dose rate of 0.14 watts/gm, an out-of-pile volume fraction of 0.8, and an ortho:meta ratio of 1 in the unirradiated Terphenyl OM-2 to correct the Melusine results, and graphically comparing the corrected $G^*(-omp)$ value with the out-of-pile pyrolysis corrected value obtained at the MITR, the intersection of the two corrected lines would yield a value of $G^*_N(-omp)/G^*_\gamma(-omp)$ of about 1.7, close to the ratio obtained with the uncorrected results of the two loop irradiations.

The results of in-pile irradiations of encapsulated samples of Santowax R at BEPO at 750°F have been reported by Bates, Burns et al. (4.5). A description of the methods used at BEPO has been given in Section 4.7.3. Not enough data was available at this temperature to fit the data by a kinetic equation, so the results are quoted for initial G(→HB) values, based on the low conversions measured. Because of the previous success in equating the initial G(→HB) values to $G^*(-omp)$ values for the electron irradiations and in-pile capsule irradiations at lower temperatures, a value of $G^*(-omp) = G(\rightarrow HB) = 0.83$ was used in conjunction with the measured fast neutron fraction of 0.544 in the graphical presentation of the data on Fig. 4.12. That the BEPO results appear high is not surprising in view of the high values obtained at temperatures near 610°F (see Fig. 4.11). Again, the low dose rate may have something to do with the conversion obtained (dose rate effect). Also, because of the elevated temperature, pyrolytic decomposition would be more important in the BEPO results (due to the low dose rate at BEPO).

As with the 610°F irradiation data, it may be seen from Fig. 4.12 that the in-pile irradiation experiments on encapsulated samples of

terphenyls have no common agreement either with each other or with the results of the in-pile loop irradiation experiments. Possible reasons for these disagreements have been given above in Section 4.7.3. In addition, the effect of pyrolysis at 750°F is not negligible, especially at the low dose rates, making a meaningful comparison of the data even more difficult.

4.7.5 Conclusions and Recommendations for Future Work

At irradiation temperatures of 610°F and 750°F results obtained from irradiations of encapsulated samples of terphenyl at various irradiation facilities agree neither with each other nor with the results of in-pile loop irradiations of terphenyl. This situation is somewhat disconcerting, for it casts some doubt on the G_N^* and G_γ^* values to be used in organic cooled reactor designs. Possible reasons for these discrepancies are:

1. Electrons and gamma rays may have a different effect on the degradation rate of the coolant.
2. Almost all the in-pile irradiation work on encapsulated samples was performed at very low dose rates compared to the dose rates encountered in the in-pile loop work. There may be a dose rate effect on the degradation rate of the coolant.
3. All irradiation experiments with encapsulated samples were carried out at fast neutron fractions reported to be 55 - 90%, whereas the loop irradiation data were obtained with fast neutron fractions of 12 - 37%. Accurate values of fast neutron dose rates are usually more difficult to obtain than accurate values of gamma ray dose rates (especially if threshold foils are used to determine the fast neutron dose rate), and errors in the fast neutron dose rate determinations are relatively more important for the in-pile capsule irradiations.
4. The mixing effect achieved in in-pile loop irradiations may serve to produce a more consistent basis for terphenyl irradiation.

In view of these findings, a more complete investigation of the discrepancies between the electron and gamma ray irradiations is recommended. Research is also strongly recommended on the effects of mixed in-pile

loop irradiation of terphenyls at various temperatures in the range 600 to 800°F, at dose rates varying over several orders of magnitude and at fast neutron fractions (f_N) which vary as widely as possible. The objective of this research would be to determine the magnitudes of any dose rate effect and of the relative effects of fast neutron and gamma rays as a function of temperature under loop conditions. Based on the MITR experience, it is recommended that such future in-pile loop irradiations be carried out in a series of steady-state-HB irradiations at different HB concentrations at each irradiation temperature, since the G and G^* values obtained from steady-state-HB irradiations are more accurate than the G and G^* values obtained for transient irradiations. Such irradiations would also provide a more conclusive basis for the choice of a reaction order than is presently available with the transient irradiations.

Until further research can point out the answers to the present discrepancies in the reported degradation rates, it is recommended that design calculations for organic cooled reactors place more credence on the reported results of the in-pile irradiation work because the total dose rate, the fast neutron dose rate fractions and the continuous flow aspects of the loop irradiation work are generally similar to the conditions to be encountered in an operating organic cooled reactor. Furthermore, the loop experiments, taken alone, yield a reasonably consistent set of results.

Consequently it is recommended that design calculations for an organic reactor using terphenyl near 610°F be performed with the MITR G^* results and $G^*_N(-\text{omp})/G^*_\gamma(-\text{omp}) = 1$. Design calculations at 750°F would be influenced both by the ratio of absorbed dose to elapsed time (i.e. the dose rate) and the ratio of in-pile to out-of-pile volume because of the pyrolytic effect on the coolant at this temperature. For radiation-induced coolant degradation, using the data currently available for comparison with the MITR results, it is recommended that the G^* values from the MITR irradiation be used in conjunction with a value of $G^*_N(-\text{omp})/G^*_\gamma(-\text{omp}) \simeq 2$ (i.e. $G^*_N(-\text{omp}) \simeq 0.7$, $G^*_\gamma(-\text{omp}) \simeq 0.35$). The MITR results have been summarized in Table 4.11.

4.8 Radiolytic Gas Generation Rate - Theory

The total radiolytic gas generation rate of the irradiated coolant at any time may be written as

$$\frac{dV_i}{dD} = \frac{dV_{i,\,rem}^{undis}}{dD} + \frac{dV_{i,\,rem}^{dis}}{dD} + \frac{dV_{i,\,accum}^{undis}}{dD} + \frac{dV_{i,\,accum}^{dis}}{dD} \qquad (4.22)$$

where

D	is the total absorbed dose in the coolant, watt-hr
$\frac{dV_{i,\,rem}^{undis}}{dD}$	is the removal rate of undissolved gaseous component i in gas samples from the loop, (std. cc)/(watt)(hr)
$\frac{dV_{i,\,rem}^{dis}}{dD}$	is the removal rate of dissolved gaseous component i in liquid samples from the loop, (std. cc)/(watt)(hr)
$\frac{dV_{i,\,accum}^{undis}}{dD}$	is the rate of accumulation of undissolved gaseous component i in the loop, (std. cc)/(watt)(hr)
$\frac{dV_{i,\,accum}^{dis}}{dD}$	is the rate of accumulation of dissolved gaseous component i in the loop, (std. cc)/(watt)(hr).

Undissolved gas was removed from the top of the surge tank in the loop via stainless steel capsules at frequent intervals in order to maintain the total pressure in the loop at about 100 psig. A selected number of these samples were transferred to evacuated glass bulbs for subsequent mass spectrographic determinations of the gas phase composition. These measurements were performed by the Petroleum Analytical Research Corporation (Houston, Texas). The rest of the gas samples were vented. Dissolved gas was removed from the loop via the liquid samples. Accumulation of undissolved gas in the loop arises from a change in liquid level of the surge tank, providing more (or less) space for the undissolved gas. Accumulation of dissolved gas in the loop arises from a change in the gas solubility in the irradiated liquid and from a change in liquid inventory in the loop.

G(gas i), by which gas production rates are commonly reported (4.5, 4.2), is defined as

$$G(\text{gas } i) = \frac{\text{molecules of gaseous component } i \text{ generated}}{100 \text{ ev absorbed in the total coolant}} \quad (4.23)$$

This stability criterion is just dV_i/dD (see Eq. (4.22)) multiplied by a conversion factor (0.1195 (molecules)(watt)(hr)/(100 ev)(std. cc)).

Preliminary calculations were performed by Morgan and Mason (4.1) on the total gas generation rate of irradiated Santowax OMP during the first transient period of the 610°F irradiation. For these calculations, the integral curve of Eq. (4.22) was obtained and then differentiated to give G(total gas). With the assumption of constant gas solubility, they estimated that about 50% of the gas in the loop existed as dissolved gas. It was subsequently found that the gas solubility data obtained were only accurate to ± 30% (see Section 5.7). Furthermore, during the transient periods there were some unexplained drops in the surge tank liquid level, indicating that there may have been more gas in the loop than measured in the surge tank. These two uncertainties caused a doubtful estimate of the gas inventory in the loop during that (and all other) transient periods of operation of the loop, so that useful G(gas i) data were obtained only from the steady-state-HB periods of operation.

During the steady-state-HB periods of the 610°F and 750°F irradiations, the liquid and gas inventory in the loop remained essentially constant. The concentration of each gas component measured in both the undissolved and dissolved gas also remained fairly constant (see Section 4.9 below), so that with the assumption of constant total gas solubility during the steady-state-HB period, which appeared reasonable from the data (see Section 5.7), the two accumulation terms in Eq. (4.22) could be set to zero and the gas evolution rate set equal to the gas removal rate. Because of the constancy of the liquid density, ρ, and the in-pile dose rate factor, F, during the steady-state-HB periods, the two removal rates were evaluated as

$$\frac{dV_{i,\text{rem}}^{\text{undis}}}{dD} = \frac{\text{total amount of gas component } i \text{ removed in gas samples during steady-state-HB period}}{\bar{F}\bar{\rho}[MWH_2 - MWH_1]} \quad (4.24)$$

$$\frac{dV^{dis}_{i,rem}}{dD} = \frac{\text{total amount of gas component } i \text{ removed in liquid samples during steady-state-HB period}}{\overline{F}\,\overline{\rho}[MWH_2 - MWH_1]} \quad (4.25)$$

where

subscript 1 refers to the start of the steady-state-HB period

subscript 2 refers to the end of the steady-state-HB period.

The procedure for calculating the total gas removed via the stainless steel capsules has been described by Morgan and Mason (4.1). Essentially, the volume of gas removed was corrected to standard temperature ($32^{o}F$) and pressure (14.7 psia). The amount of each gaseous component removed was determined from the analysis of the undissolved gas composition (see Section 4.9). The total amount of dissolved gas removed in each liquid sample was determined from the relation

$$V^{dis}_{rem} = Wsp \quad (4.26)$$

where

W is the sample weight

s is the gas solubility, (std. cc)/(gm coolant)(psia)

p is the total loop pressure at the time of removal of the sample, psia.

The amount of each gaseous component removed as dissolved gas was calculated from Eq. (4.26) using the analyses of the dissolved gas samples.

4.9 Radiolytic Gas Generation Rate Results

4.9.1 $610^{o}F$ Irradiation

Figure 4.13 shows the undissolved radiolytic gas phase composition during the $610^{o}F$ irradiation of Santowax OMP. The results of the mass spectrographic analyses are shown on a nitrogen and oxygen free basis since these two components were not decomposition gases, but arose from two sources:

1. The initial pressurizing nitrogen at the beginning of the irradiation.

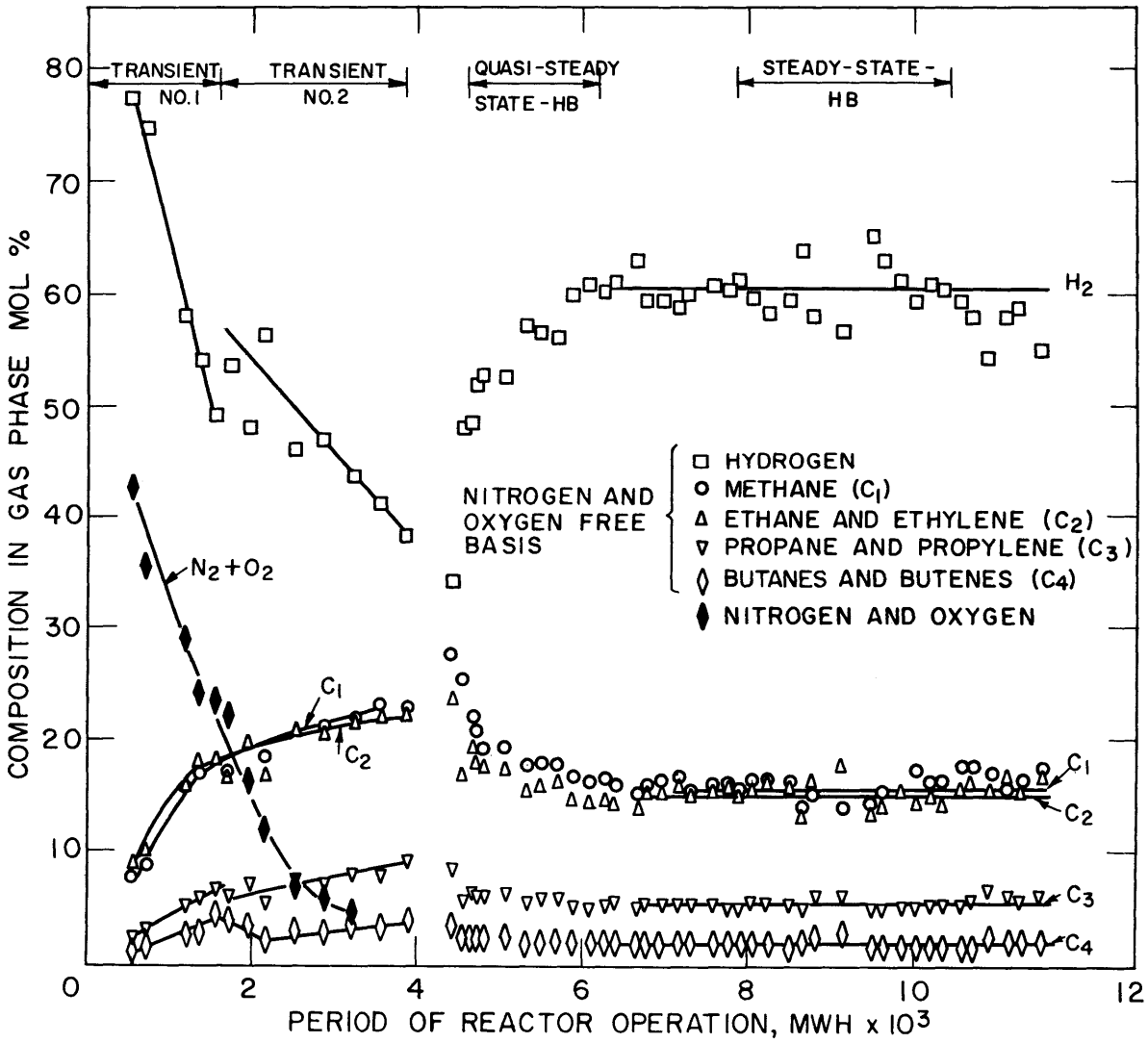

FIGURE 4.13 RADIOLYTIC GAS COMPOSITION DURING THE 610°F IRRADIATION OF SANTOWAX OMP

2. Air leakage into the gas sample during transfer or analysis. No further nitrogen was added to the loop after the start of the irradiation, and as may be seen from Fig. 4.13, the concentration of nitrogen (and some oxygen) fell to a negligible level by the end of the second transient period. After this time there continued to be about 5 mol % $N_2 + O_2$ in the sample analyses, which was presumed to come from air leakage into the samples.

The hydrogen concentration decreased very rapidly during the transient periods of operation while the concentrations of the higher molecular weight hydrocarbon gases, containing up to six carbon atoms, increased. It seems apparent from the data that the concentrations of the gas phase components are strongly dependent on the DP and HB concentration in the system. It also appears from Fig. 4.13 that at the beginning of the irradiation, when the DP concentration was nil, hydrogen was the primary gaseous product from the radiolysis of Santowax OMP.

During the steady-state-HB period, the concentrations of the gas phase components remained essentially constant. Table 4.14 lists the average concentrations of each component in the undissolved gas during the steady-state-HB period, together with the standard deviations based on the deviations from the mean concentrations during the period. Of the C_2 gases produced, about 98% were ethane and only 2% ethylene. For the C_3 and C_4 gases produced, about 85% were saturated hydrocarbons and 15% unsaturated. About 50% of the C_{5+6} gases were pentanes, and about 60% of the aromatic gases were benzene. For more details refer to Section A2.4.

Also listed in Table 4.14 are the dissolved gas compositions during the steady-state-HB period. No gas solubility samples were taken during this period, but the dissolved gas compositions of samples 1L118 (composition 60 w/o DP and taken at the end of the transient irradiation) and 1L195 (composition 30 w/o DP and taken at the end of the quasi-steady-state-HB irradiation) were not radically different, so the average of these two sets of analyses is given. For the detailed analyses of dissolved gas samples, see Section A2.4. Again, the preponderance of the gases formed at each number of carbon atoms were the saturated hydrocarbons.

TABLE 4.14

Undissolved and Dissolved Radiolytic Gas Composition During the Steady-State-HB Period of the 610°F Irradiation of Santowax OMP

Component	Nitrogen and Oxygen Free Composition, Mole %	
	Undissolved Gas	Dissolved Gas
Hydrogen (H_2)	60.5 ± 0.7[a]	20.6 ± 4.7
Methane (C_1)	15.6 ± 0.3	15.8 ± 0.4
Ethane and Ethylene (C_2)	14.9 ± 0.4	25.6 ± 2.1
Propane and Propylene (C_3)	5.5 ± 0.1	16.6 ± 1.8
Butanes and Butenes (C_4)	2.0 ± 0.1	9.7 ± 0.2
Pentanes, Pentenes, Hexanes (C_{5+6})	1.0 ± 0.07	8.6 ± 0.1
Benzene, Toluene, Xylene (Aromatics)	0.5 ± 0.08	3.1 ± 0.05

a. Standard deviation based on deviation from mean value during the period.

During the steady-state-HB period the radiolytic gas removal rates were determined as

undissolved gas:	13.9 ± 1.0 (std. cc)/MWH
dissolved gas:	2.2 ± 0.7 (std. cc)/MWH
total gas:	16.1 ± 1.2 (std. cc)/MWH

The gas solubility used was the average of 1L118 and 1L195 (see Section 5.7):- 8.5×10^{-3} (std. cc)/(gm coolant)(psia). A standard deviation of ± 7% was assigned to the undissolved gas production rate (4.1). Since over 85% of the total gas removed from the loop was in the form of undissolved gas, the overall standard deviation was still only about 10% in spite of the ± 30% possible error in the gas solubility data. Using the data of Table 4.14 and Eqs. (4.22), (4.23), (4.24) and (4.25) there resulted the data tabulated in Table 4.15. The standard deviations quoted include errors in dosimetry (± 2%) as well as the other errors quoted in the section.

By comparing the G(total gas) value with the G(-omp) value during the steady-state-HB period, it can be seen that about 15% of the degradation products formed were gases on a molecule basis. However, on a weight basis, since the average molecular weight of the degradation products in the coolant was probably close to 600 (the number average molecular weight of the HB; see Section 5.6) and that of the gases about 14 (see Table 4.14), only about 0.5 w/o of the degradation products were in the form of gases.

4.9.2 750°F Irradiation

Figure 4.14 shows the undissolved radiolytic gas composition during the 750°F irradiation. As with the 610°F irradiation data the compositions have been plotted on a nitrogen and oxygen free basis. Again the composition seems to be a function of the DP concentration. It is interesting to note that for this irradiation, extrapolation back to the start of the irradiation (0 w/o DP) did not show just hydrogen to be the principal initial component as with the 610°F irradiation data, but both methane and the C_2's were present in appreciable amounts as well.

During the steady-state-HB period, the composition of the undissolved gas remained essentially constant. Of note was the large increase in the methane content over the 610°F steady-state-HB irradiation

TABLE 4.15

G(gas i) Values for the Steady-State-HB Period of the 610°F Irradiation of Santowax OMP[a]

Component	$G(\text{gas } i) = \frac{\text{molecules of gaseous component } i \text{ produced}}{100 \text{ ev absorbed in the total coolant}}$
Total gas	0.037 ± 0.003[b]
Hydrogen (H_2)	0.020 ± 0.002
Methane (C_1)	0.0057 ± 0.0005
Ethane and Ethylene (C_2)	0.0060 ± 0.0005
Propane and Propylene (C_3)	0.0026 ± 0.0003
Butanes and Butenes (C_4)	0.0011 ± 0.0002
Pentanes, Pentenes, Hexanes (C_{5+6})	0.0008 ± 0.0001
Benzene, Toluene, Xylene (Aromatics)	0.0003 ± 0.00006

a. DP concentration ~40 w/o, HB concentration ~33 w/o.

b. Standard deviations.

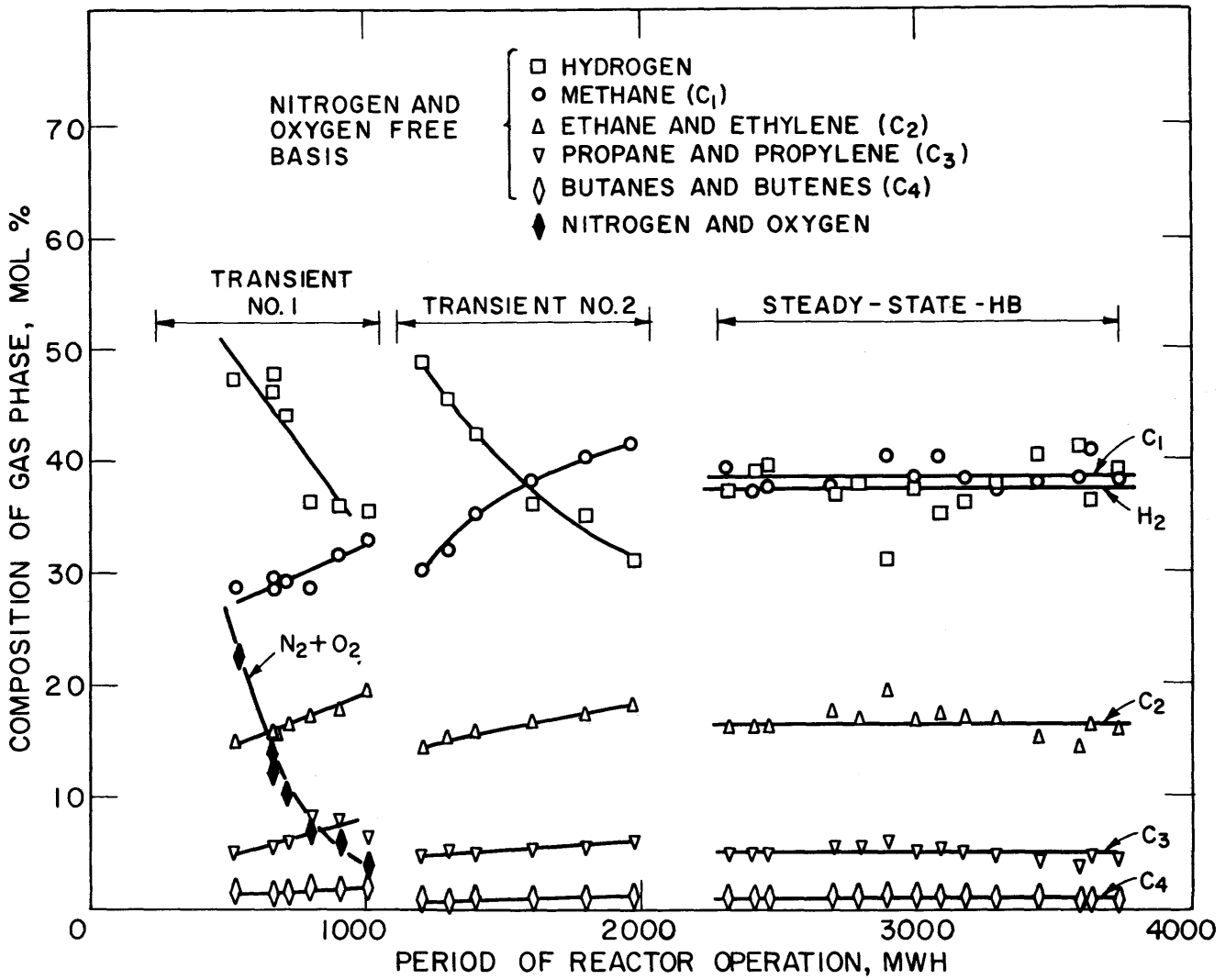

FIGURE 4.14 RADIOLYTIC GAS COMPOSITION DURING THE 750°F IRRADIATION OF SANTOWAX OMP

data (see Fig. 4.13). Table 4.16 tabulates the average composition of the undissolved gas during the steady-state-HB period. The errors quoted were based on deviations from the mean values for the period. The C_2 composition during this period was about 99% ethane, while the C_3 and C_4 compositions were about 95% saturated hydrocarbons, a significant increase over the 610°F steady-state-HB irradiation saturated hydrocarbon composition. Another significant difference between the 750°F and 610°F irradiation data was the 80% pentenes and hexenes found in the C_{5+6} composition. The aromatic composition was found to be about 90% benzene. For further details, see Section A2.4.

The dissolved gas composition during the steady-state-HB period of the 750°F irradiation is also listed in Table 4.16. This composition is the average of the three dissolved gas samples obtained during the steady-state-HB period, as there appeared to be no significant trend of the composition with irradiation. The dissolved gas samples, like the undissolved samples, showed a preponderance of unsaturated hydrocarbons for each number of carbon atoms, with the exception of the pentenes and hexenes. For a detailed listing of these data see Section A2.4. Using an average gas solubility of 2.5×10^{-3} (std. cc)/(gm coolant)(psia) during the steady-state-HB period (see Section 5.7) the following gas removal rates from the loop were obtained:

undissolved gas:	40.4 ± 2.8 (std. cc)/MWH
dissolved gas:	1.0 ± 0.3 (std. cc)/MWH
total removed:	41.4 ± 2.8 (std. cc)/MWH

A standard deviation of ± 7% was set on the undissolved gas removal rate (4.1). Since only about 2.5% of the gas removed was via the dissolved gas, the ± 30% possible error in the gas solubility had almost no effect on the results. Using the data of Table 4.16 together with Eqs. (4.22), (4.23), (4.24) and (4.25) the data of Table 4.17 resulted. The standard deviations quoted include the errors in dosimetry (± 2%) as well as the other errors mentioned in this section. By comparison with the liquid degradation data, it was observed that on a weight basis about 1 w/o of the degradation products was radiolytic gases.

TABLE 4.16

Undissolved and Dissolved Radiolytic Gas Composition During the Steady-State-HB Period of the 750°F Irradiation of Santowax OMP

Component	Nitrogen and Oxygen Free Composition, Mole %	
	Undissolved Gas	Dissolved Gas
Hydrogen (H_2)	37.5 ± 0.4[a]	14.0 ± 1.6
Methane (C_1)	38.4 ± 0.3	26.9 ± 0.4
Ethane and Ethylene (C_2)	16.5 ± 0.3	26.9 ± 1.1
Propane and Propylene (C_3)	5.1 ± 0.1	19.1 ± 0.8
Butanes and Butenes (C_4)	1.1 ± 0.1	6.1 ± 0.1
Pentanes, Pentenes, Hexenes (C_{5+6})	0.3 ± 0.02	4.2 ± 0.2
Benzene, Toluene, Xylene (Aromatics)	1.1 ± 0.08	2.8 ± 0.3

a. Standard deviation based on deviation from mean value during the period.

TABLE 4.17

G(gas i) Values for the Steady-State-HB Period of the 750°F Irradiation of Santowax OMP[a]

Component	$G(\text{gas } i) = \frac{\text{molecules of gaseous component } i \text{ produced}}{100 \text{ ev absorbed in the total coolant}}$
Total gas	0.105 ± 0.008[b]
Hydrogen (H_2)	0.039 ± 0.003
Methane (C_1)	0.040 ± 0.003
Ethane and Ethylene (C_2)	0.018 ± 0.001
Propane and Propylene (C_3)	0.0057 ± 0.0004
Butanes and Butenes (C_4)	0.0013 ± 0.0001
Pentanes, Pentenes, Hexenes (C_{5+6})	0.0004 ± 0.00004
Benzene, Toluene, Xylene (Aromatics)	0.0012 ± 0.0001

a. DP concentration ~40 w/o, HB concentration ~33 w/o.

b. Standard deviations.

4.9.3 Comparison of 610°F and 750°F Irradiation Results

Table 4.18 summarizes the results obtained during the 610°F and 750°F steady-state-HB irradiations of Santowax OMP. The total gas evolution rate increased almost three-fold from 610°F to 750°F. The hydrogen evolution rate, however, only doubled, while the methane production increased about seven-fold.

4.9.4 Comparison with Other Irradiations

Comparison with other work is made more difficult by the fact that the gas production rates were obtained at M.I.T. only for a liquid composition of ~ 40 w/o DP and ~ 33 w/o HB. Based on the varying compositions obtained during the transient periods the production rates for the individual components might vary significantly if the DP concentration were changed. However, in-pile capsule measurements by Berg et al. (4.22) and Bates, Burns et al. (4.2, 4.5) indicated that the G(total gas) value was approximately independent of the DP concentration, at least at the lower irradiation temperatures. Thus, the data at M.I.T. will be compared to these data using the assumption that G(total gas) is independent of DP concentration.

Morgan and Mason (4.1) have previously suggested using a relation similar to that for the liquid degradation G values, i.e.

$$G(\text{total gas}) = f_N G_N(\text{total gas}) + (1 - f_N) G_\gamma(\text{total gas}) \qquad (4.27)$$

where

f_N is the fast neutron dose rate fraction

$G_N(\text{total gas})$ is the total gas generation rate due to fast neutron interactions

$G_\gamma(\text{total gas})$ is the total gas generation rate due to gamma ray interactions.

As with the liquid degradation calculations, results obtained in a single irradiation facility cannot alone determine $G_N(\text{total gas})$, and so the same graphical procedure devised for the liquid degradation results was applied. Figure 4.15 shows the graphical representation of the MITR results at 610°F on the $G_N(\text{total gas})$ vs. $G_\gamma(\text{total gas})$ plane, using Eq. (4.27) with a fast neutron fraction of 0.37 (see Section 3.4)

TABLE 4.18

G(gas *i*) Values from the 610°F and 750°F Steady-State-HB Irradiations of Santowax OMP[a]

Component	$G(\text{gas } i) = \frac{\text{molecules of gaseous component } i \text{ produced}}{100 \text{ ev absorbed in the total coolant}}$	
	610°F Irradiation	750°F Irradiation
Total gas	0.037 ± 0.003[b]	0.105 ± 0.008
Hydrogen (H_2)	0.020 ± 0.002	0.039 ± 0.003
Methane (C_1)	0.0057 ± 0.0005	0.040 ± 0.003
Ethane and Ethylene (C_2)	0.0060 ± 0.0005	0.018 ± 0.001
Propane and Propylene (C_3)	0.0026 ± 0.0003	0.0057 ± 0.0004
Butanes and Butenes (C_4)	0.0011 ± 0.0002	0.0013 ± 0.0001
Pentanes, Pentenes, Hexanes, Hexenes (C_{5+6})	0.0008 ± 0.0001	0.0004 ± 0.00004
Benzene, Toluene, Xylene (Aromatics)	0.0003 ± 0.00006	0.0012 ± 0.0001

a. DP concentration ~40 w/o, HB concentration ~33 w/o.

b. Standard deviations.

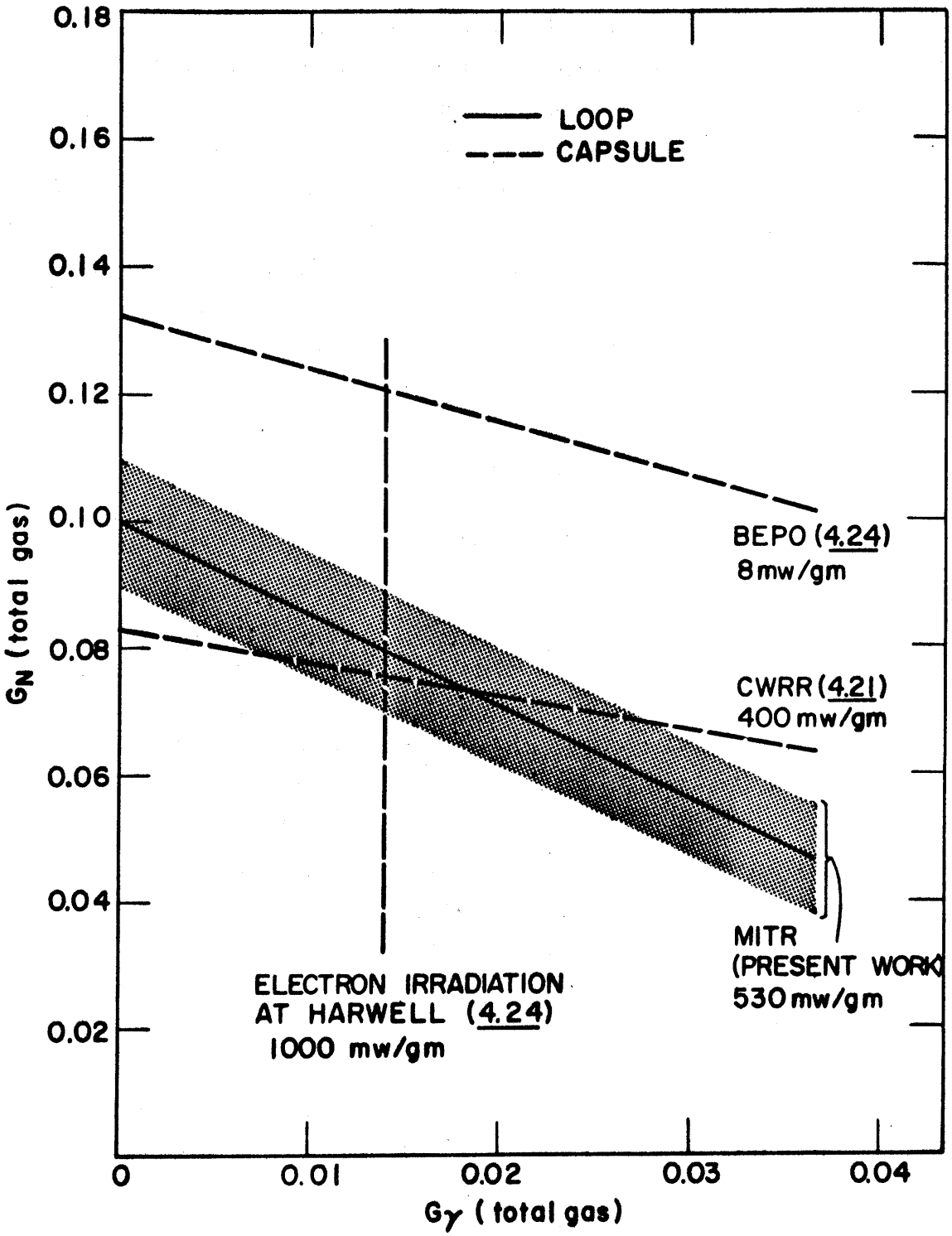

FIGURE 4.15 COMPARISON OF G(TOTAL GAS) VALUES NEAR 610° F

and a G(total gas) value of 0.037 (see Table 4.18). The shaded area represents the standard deviation of the results. Also shown is the average dose rate in the core region in-pile section (~530 mw/gm).

Initial G(total gas) values have been reported by Bates, Burns et al. (4.24) for the electron irradiation work on encapsulated samples of Santowax R at Harwell. The procedures used at Harwell have been described in Section 4.7.2 above. The total amount of gas produced was nearly linear with absorbed dose, at least to 50 w/o HB (4.2) so that G(total gas) at any DP concentration was about equal to the initial G(total gas) value. At 572°F a value of 0.011 was reported, and at 662°F a value of 0.016 was reported for the initial G(total gas). The composition of the evolved gas for both these irradiations was reported at over 90% H_2 initially, with an increase in the CH_4 and C_2 concentrations as the irradiations proceeded (4.2). This observation is in keeping with the MITR results for the transient periods of operation. A value of 0.014 for 610°F obtained by linear interpolation between the two irradiation temperatures is shown in Fig. 4.15.

Berg et al. (4.22) report an average G(total gas) value of 0.054 for the experiments on encapsulated samples of Santowax OMP in the CWRR at 625°F with no trend of the G(total gas) value with increasing irradiation (i.e. total gas produced was linear with irradiation). No gas phase composition was reported. The procedures used at the CWRR have been described in Section 4.7.3. Using the value of 0.054 found, and the fast neutron fraction of 0.65, the data are plotted in Fig. 4.15. It can be seen that the CWRR, MITR and electron irradiation results have an almost common intersection point.

Bates, Burns et al. (4.5) also report initial G(total gas) values for in-pile irradiations of encapsulated samples of Santowax R at BEPO at 572°F and 662°F. The procedures used at BEPO have been described in Section 4.7.3. It was found that the total gas evolved was linear with absorbed dose to 30 w/o HB (the extent of the measurements) (4.24). Later work on Santowax R at 662°F confirmed this linearity to about 50 w/o HB (4.5). Again hydrogen was observed as the principal product, consistent with the MITR results. The data obtained were G(total gas) = 0.064 at 572°F and G(total gas) = 0.080 at 662°F. Using a linearly interpolated

value of 0.072 at 610°F and the fast neutron fraction of 0.544, the results are presented graphically on Fig. 4.15. The results (as with the results of liquid degradation studies made in capsules at BEPO) appear to be higher than predicted by the three other irradiations.

Figure 4.16 graphically presents the results of the 750°F steady-state-HB irradiation of Santowax OMP at M.I.T.. A value of G(total gas) = 0 105 (see Table 4.18) in conjunction with a fast neutron fraction of 0.37 (see Section 3.4) was used for this plot. The shaded area represents the standard deviation of the MITR results. Also indicated is the dose rate in the core region of the in-pile section (~ 530 mw/gm).

Bates, Burns et al. (4.24) report the results of electron irradiations of encapsulated samples of Santowax R at 752°F. The total gas generated was linear with absorbed dose to 30 w/o HB (the extent of the measurements) (4.2), so that the reported initial G(total gas) value of 0.023 was placed on Fig. 4.16 for comparison with the present data. Hydrogen still composed the largest fraction of the gas, but an increased amount of the CH_4 and C_2 concentrations were observed (4.2), consistent with the MITR findings.

In 1962, Bates, Burns et al. (4.5) also reported initial G(total gas) values for in-pile capsule irradiations of Santowax R at 752°F in BEPO. Preliminary work by them (4.24), reported in 1959, had indicated that G(total gas) increased with irradiation and that there was initially very appreciable amounts of CH_4 and C_2 as well as H_2. Subsequent determinations of initial G(total gas) with better temperature control on the samples were reported but the variation of the gas production rate with observed dose (or with w/o DP) was not reported. Measurements on pure meta-terphenyl at 752°F reported in 1962 (4.5) indicated an increase in G(total gas) with irradiation. Using the initial G(total gas) value of 0.119 reported for Santowax R and the fast neutron fraction of 0.544, the data are shown graphically in Fig. 4.16. The data appear lower than the electron irradiation measurements and the MITR measurements, but, as mentioned above, this may be due to an (unreported) increase in G(total gas) with increasing DP concentration (only the value at 0 w/o DP was available).

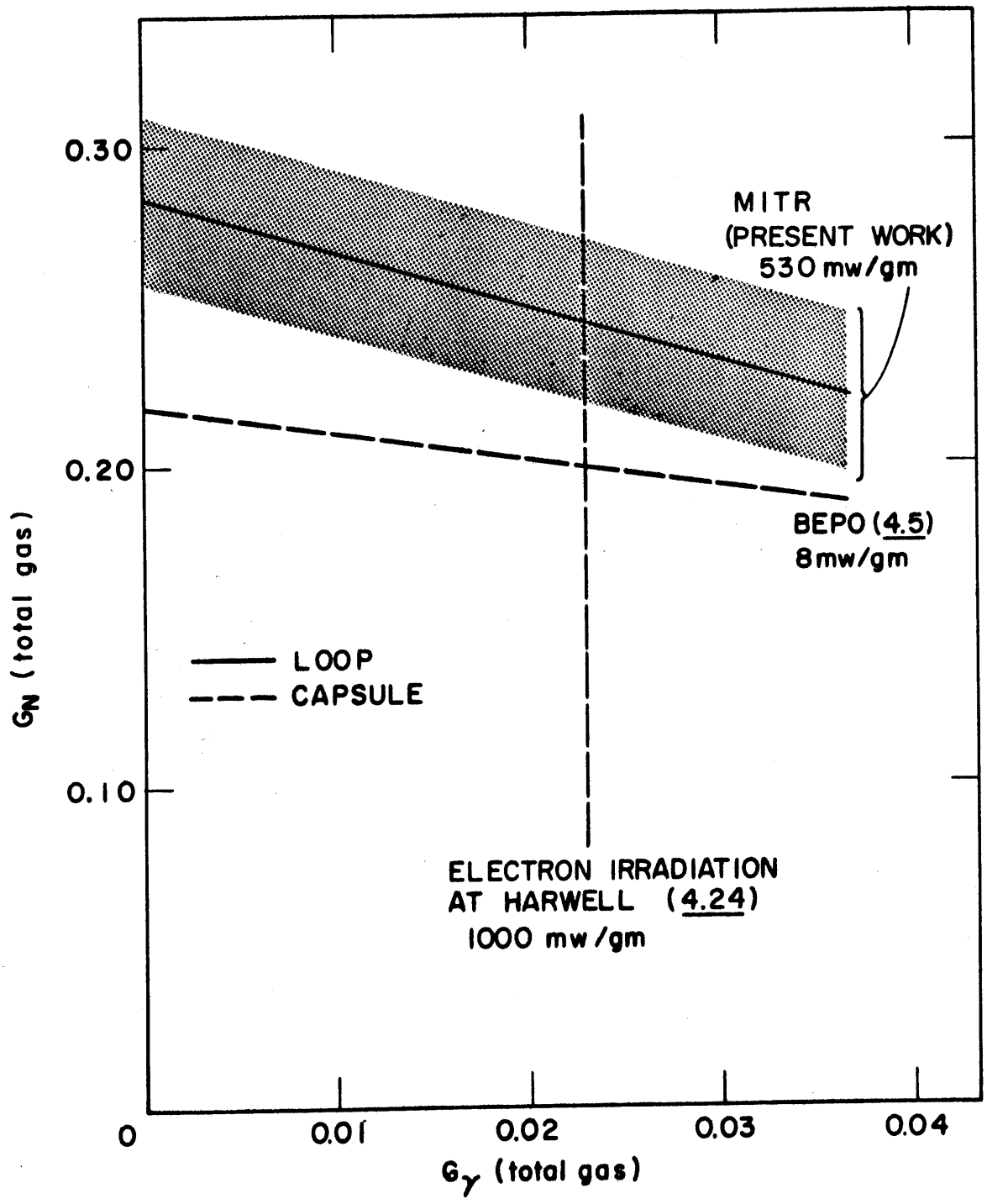

FIGURE 4.16 COMPARISON OF G (TOTAL GAS) VALUES NEAR 750°F

4.9.5 Conclusions

In view of the fact that less than 1 w/o of the degradation products formed during the irradiation of Santowax OMP in the MITR at 610°F and at 750°F was in the form of radiolytic gases, it is not as important to know accurately this gas generation rate as it is to know accurately the liquid degradation rate. However, the following tentative conclusions have been reached in comparing the MITR gas generation data with the available results of other work:

1. At 610°F: G_N(total gas) $\simeq$ 0.076, G_γ(total gas) $\simeq$ 0.015, G_N(total gas)/G_γ(total gas) $\simeq$ 5.
2. At 750°F: G_N(total gas) $\simeq$ 0.24, G_γ(total gas) $\simeq$ 0.023, G_N(total gas)/G_γ(total gas) $\simeq$ 10.

It should be noted that comparisons were made entirely with irradiations of encapsulated samples, as no gas generation data are currently available from in-pile loop irradiations. The values for the 750°F irradiation are subject to extra doubt due to the lack of available data on the pyrolytic gas generation rate.

CHAPTER 5
PHYSICAL PROPERTY MEASUREMENTS

5. 1 Introduction

One of the important aspects of the work at M. I. T. has been the determination of the effects of temperature and irradiation on some of the physical properties of Santowax OMP. A knowledge of how some of these properties vary with irradiation is essential. For instance, in heat transfer and pumping power design calculations, the effect of irradiation on the coolant density, viscosity, heat capacity and thermal conductivity would have to be known.

The results of density, viscosity, specific heat, thermal conductivity number average molecular weight, gas solubility, coolant melting point, carbon-hydrogen content and inorganic content measurements on irradiated Santowax OMP are discussed. The results of miscellaneous other physical measurements are also presented.

5. 2 Density

Densities of samples of irradiated Santowax OMP were determined using calibrated pycnometers. The pycnometers were pressurized with nitrogen and immersed in a high temperature fused salt bath for measurements at temperatures ranging from 400^{o}F to 800^{o}F. Details of the apparatus used are given by Morgan and Mason (5. 1).

The theory of the use of the pycnometers is discussed in Section A3. 1. The data obtained for each sample have been found to closely follow a linear temperature dependence and were fit by the method of least squares to a relation of the form

$$\rho = A + BT \qquad (5.1)$$

where

ρ is the sample density, gm/cc

A, B are constants

T is the sample temperature, ^{o}F.

The results of this smoothing process for the individual samples for both the 610°F and 750°F irradiation are listed in Section A3.4. The data obtained for each sample are believed accurate to an average standard deviation of ± 0.3%.

Figure 5.1 shows the variation of the smoothed density data obtained from the 610°F irradiation of Santowax OMP with the concentration of degradation products (DP). For each sample, the smoothed density data at 400, 500, 600, 700 and 800°F are plotted. The DP concentration of each sample has a standard deviation of about ± 2 w/o at 0 w/o DP and to about ± 1 w/o at 50 w/o DP (see Section A2.1). The coolant density can be seen to have increased about 10% during the two transient periods of operation of the loop, when the DP concentration increased from 0 to 60 w/o. During the steady-state-HB period the density remained approximately constant (see below) as did the DP concentration (see Section 4.4). Thus, the average density is shown for the average DP concentration for the steady-state-HB period in Fig. 5.1. The data indicate about a 1% higher density for a given temperature and DP concentration during the steady-state-HB period than during the transient period. A slight increase in number average molecular weight of the degradation products (at the same DP concentration) from the transient to the steady-state-HB periods was observed for the irradiated coolant (see Section 5.6), and it appears that this observed increase was responsible for the density increase from transient to steady-state-HB periods.

Figure 5.2 presents the density data of the steady-state-HB period plotted against the period of reactor operation in MWH. The quasi-steady-state-HB data are also shown and agree within 0.5% with the steady-state-HB data. The data show no change with increasing irradiation, indicating little or no change of average molecular weight of the coolant during these periods (see Section 5.6).

An overall correlation of the density data for the transient periods of the 610°F irradiation (valid over the temperature range 400 - 800°F) is given graphically in Fig. 5.3. The data are presented as

$$\rho = \rho_o - \rho_1(T - 400) \qquad (5.2)$$

with the functional dependence of ρ_o and ρ_1 on the concentration of

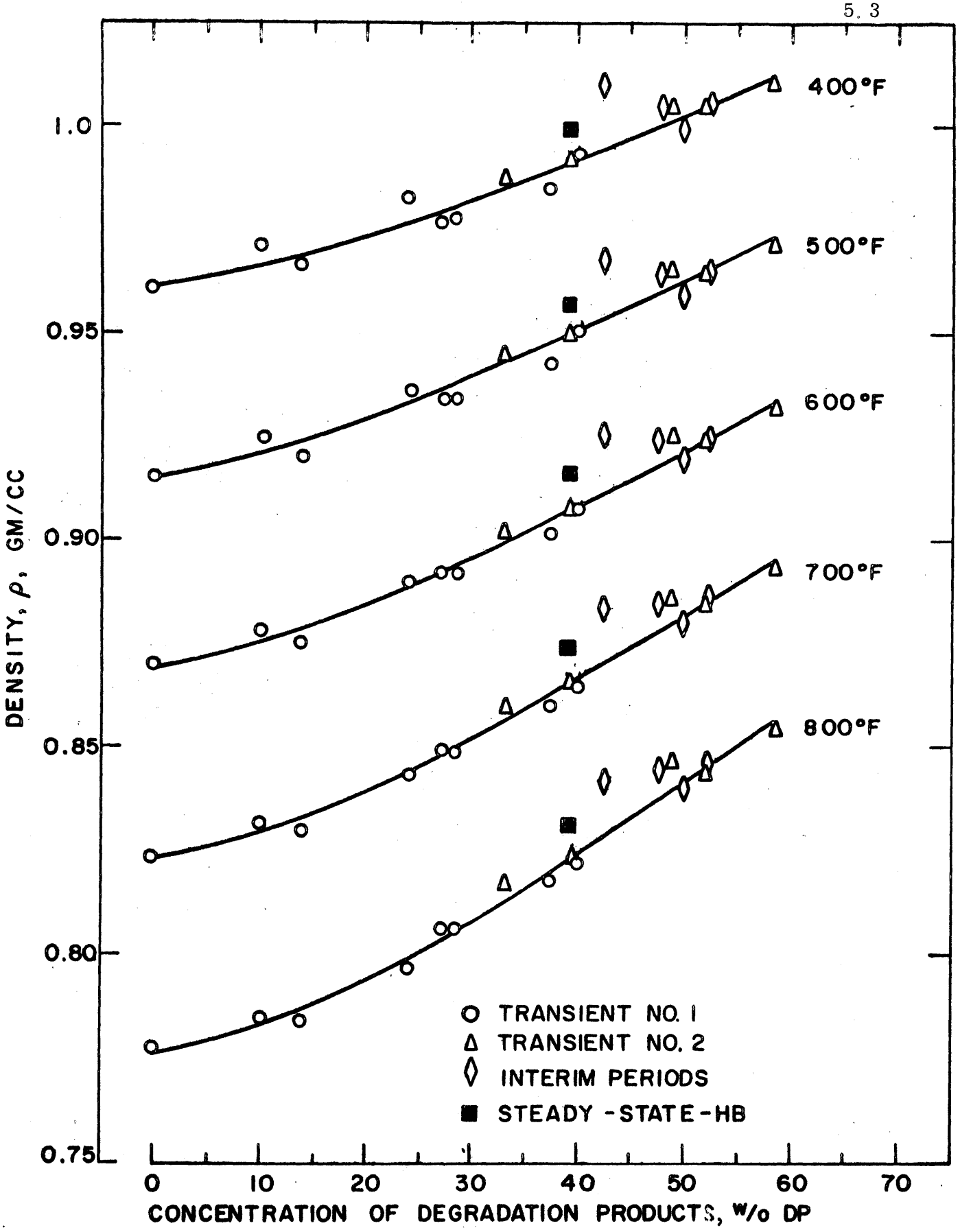

FIGURE 5.1 DENSITY OF IRRADIATED SANTOWAX OMP FOR THE 610°F IRRADIATION

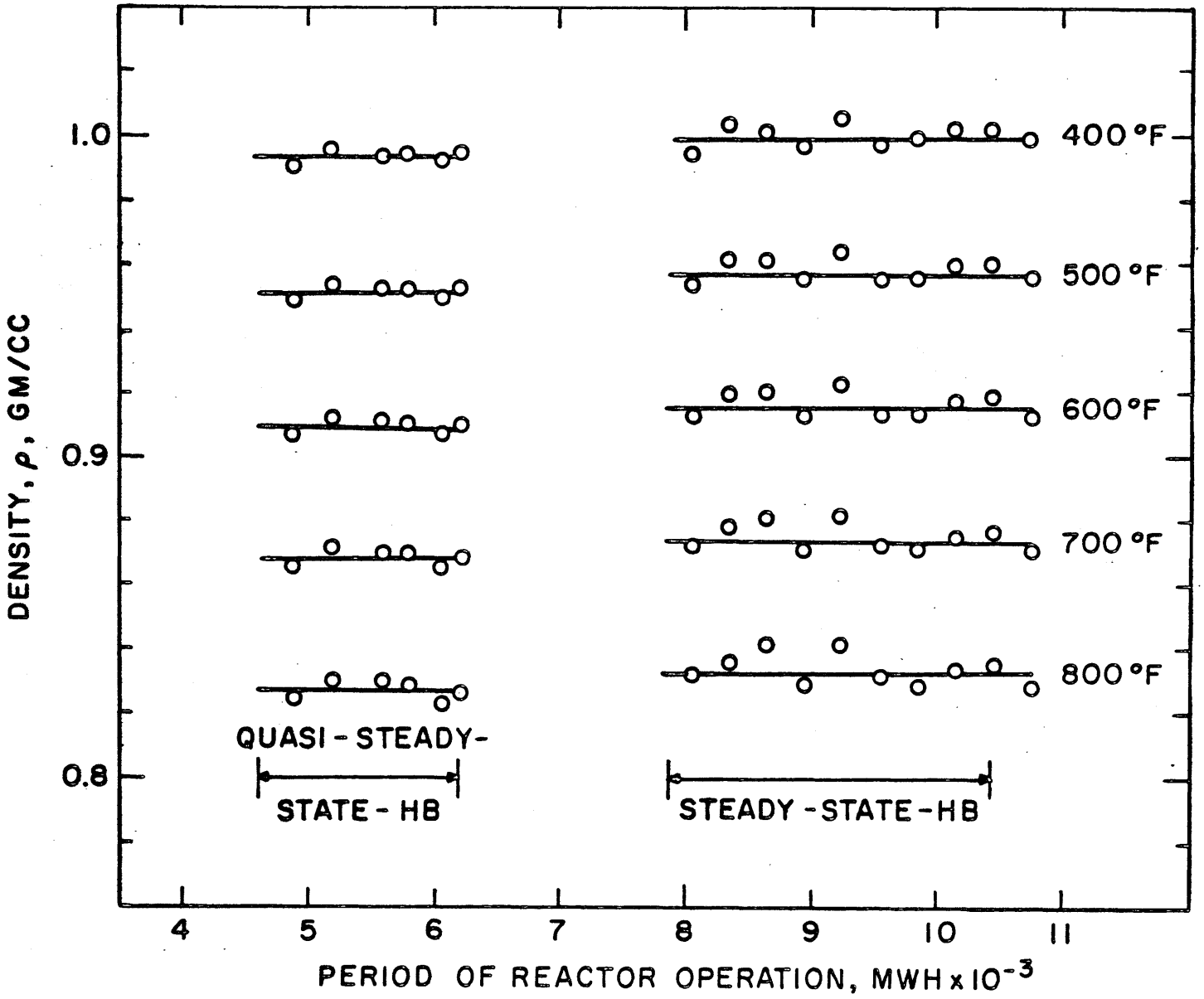

FIGURE 5.2 DENSITY OF IRRADIATED SANTOWAX OMP DURING THE STEADY-STATE-HB PERIODS OF THE 610 °F IRRADIATION

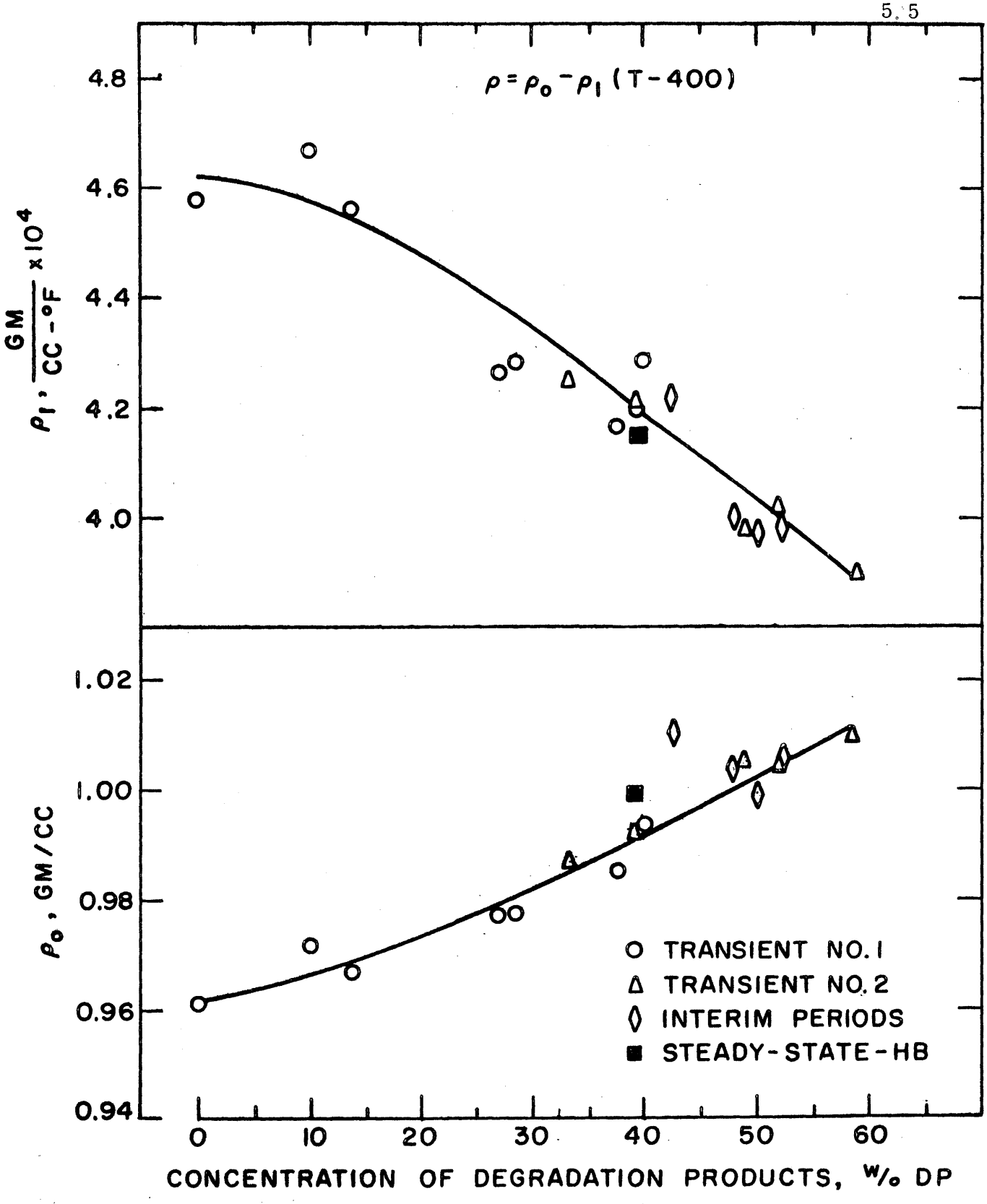

FIGURE 5.3 CORRELATION OF IRRADIATED SANTOWAX OMP DENSITY DATA FROM THE 610°F IRRADIATION

degradation products being given in Fig. 5.3. T is the temperature in ^{o}F. As stated above, the data for the steady-state-HB periods indicate slightly higher densities than those given by the correlation.

The density data from the 750^{o}F irradiation of Santowax OMP are given in Fig. 5.4 as a function of DP concentration. In contrast to the 610^{o}F irradiation results, the steady-state-HB data agree quite well with the data of the transient periods. A good agreement of number average molecular weight of the coolant for the steady-state-HB period with the transient periods of the 750^{o}F irradiation at the same DP concentration was also observed (see Section 5.6). During the steady-state-HB period of the 750^{o}F irradiation the densities remained quite constant, as shown in Fig. 5.5. An overall correlation of the density data from the transient periods of the 750^{o}F irradiation (valid from 400 - 800^{o}F) using an equation of the form of Eq. (5.2) is given in Fig. 5.6.

A comparison of the density data from the 610^{o}F and 750^{o}F irradiations with each other and with the results of other laboratories is given in Fig. 5.7. The data of the two irradiations agree quite well with each other over the temperature range of interest, but the change in density with temperature for the higher DP concentrations is greater for the 750^{o}F irradiation than for the 610^{o}F irradiation (compare Figs. 5.3, 5.6 and 5.7). For the 750^{o}F irradiation a slower increase in number average molecular weight of the coolant with DP concentration than for the 610^{o}F irradiation was observed (see Section 5.6). These two phenomena appear to be related.

Gercke and Asanovich (5.2) report the results of measurements made at Atomics International with pycnometers on samples of Santowax R irradiated in the MTR (5.3). Their data are shown for comparison with the present data in Fig. 5.7. The fact that the data appear to be 1 - 2% lower than the present results is somewhat misleading since the material used for their report, Santowax R, contained about 18 w/o low and intermediate boilers (LIB) even before irradiation, and these products probably have densities close to those of o-, m-, and p-terphenyl.

Density measurements on a sample of the charge material for the 750^{o}F irradiation were also made at Grenoble, France (5.4), using a Mohr balance (5.5), and the smoothed values obtained are shown for

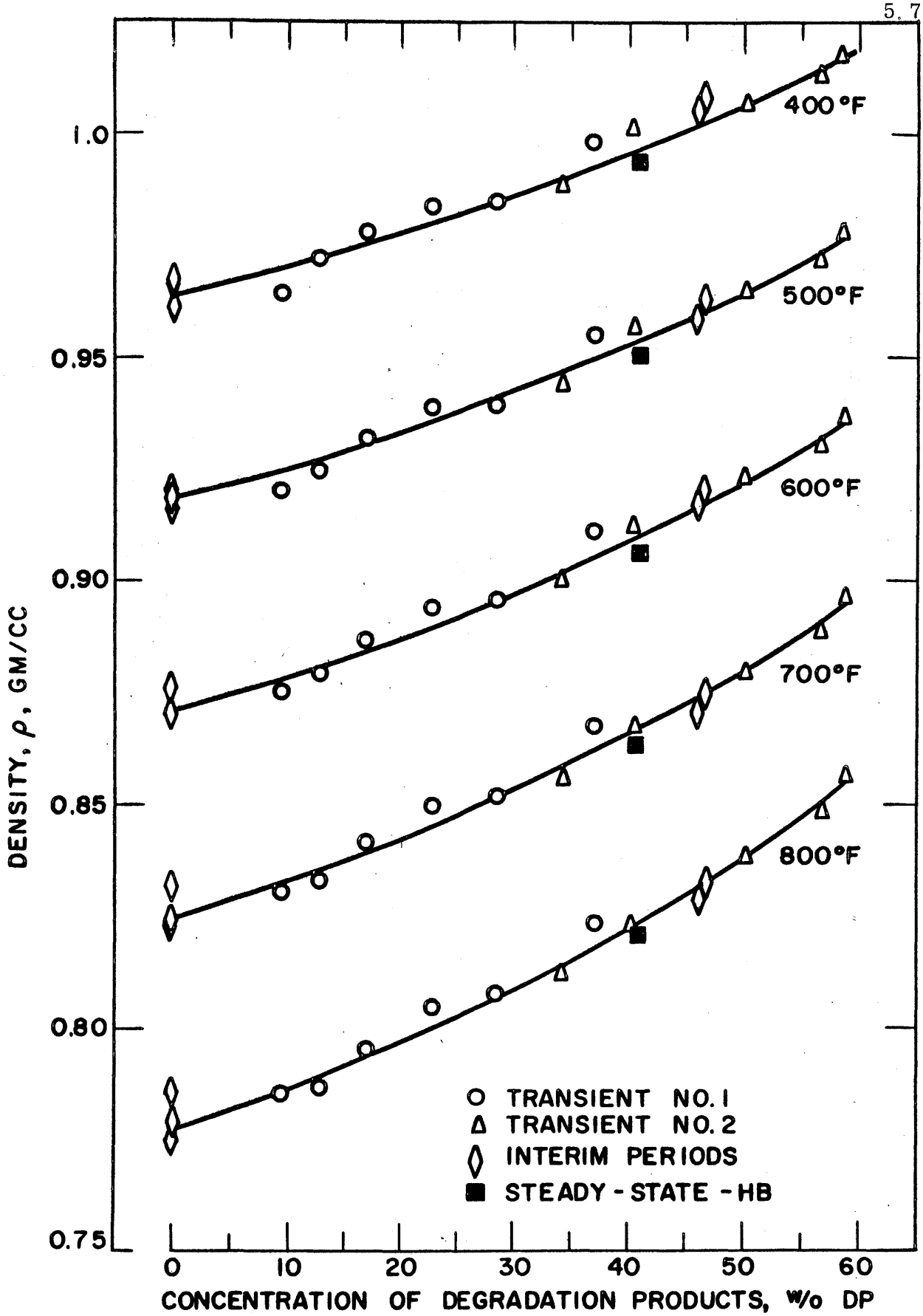

FIGURE 5.4 DENSITY OF IRRADIATED SANTOWAX OMP FOR THE 750°F IRRADIATION

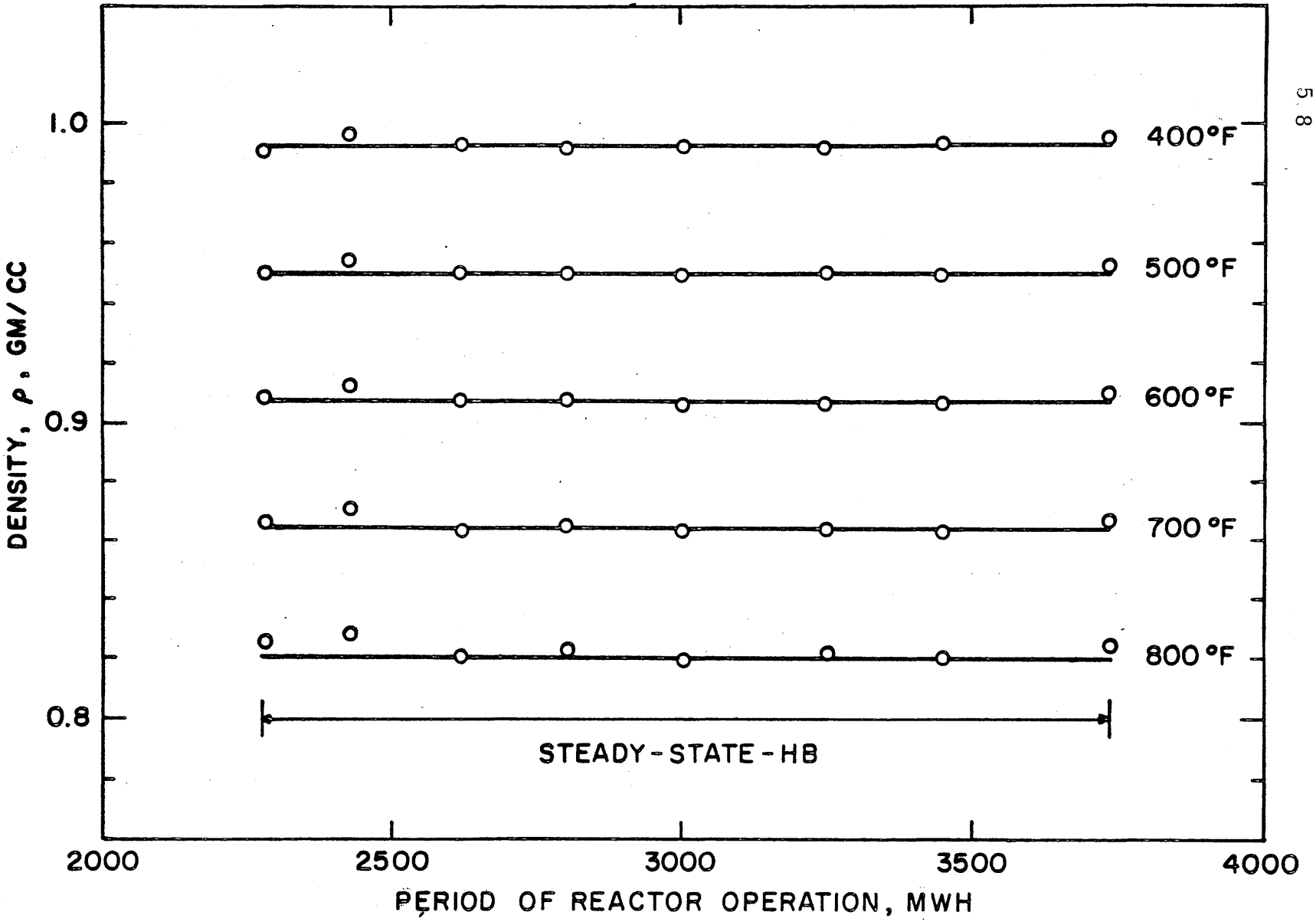

FIGURE 5.5 DENSITY OF IRRADIATED SANTOWAX OMP DURING THE STEADY-STATE-HB PERIOD OF THE 750°F IRRADIATION

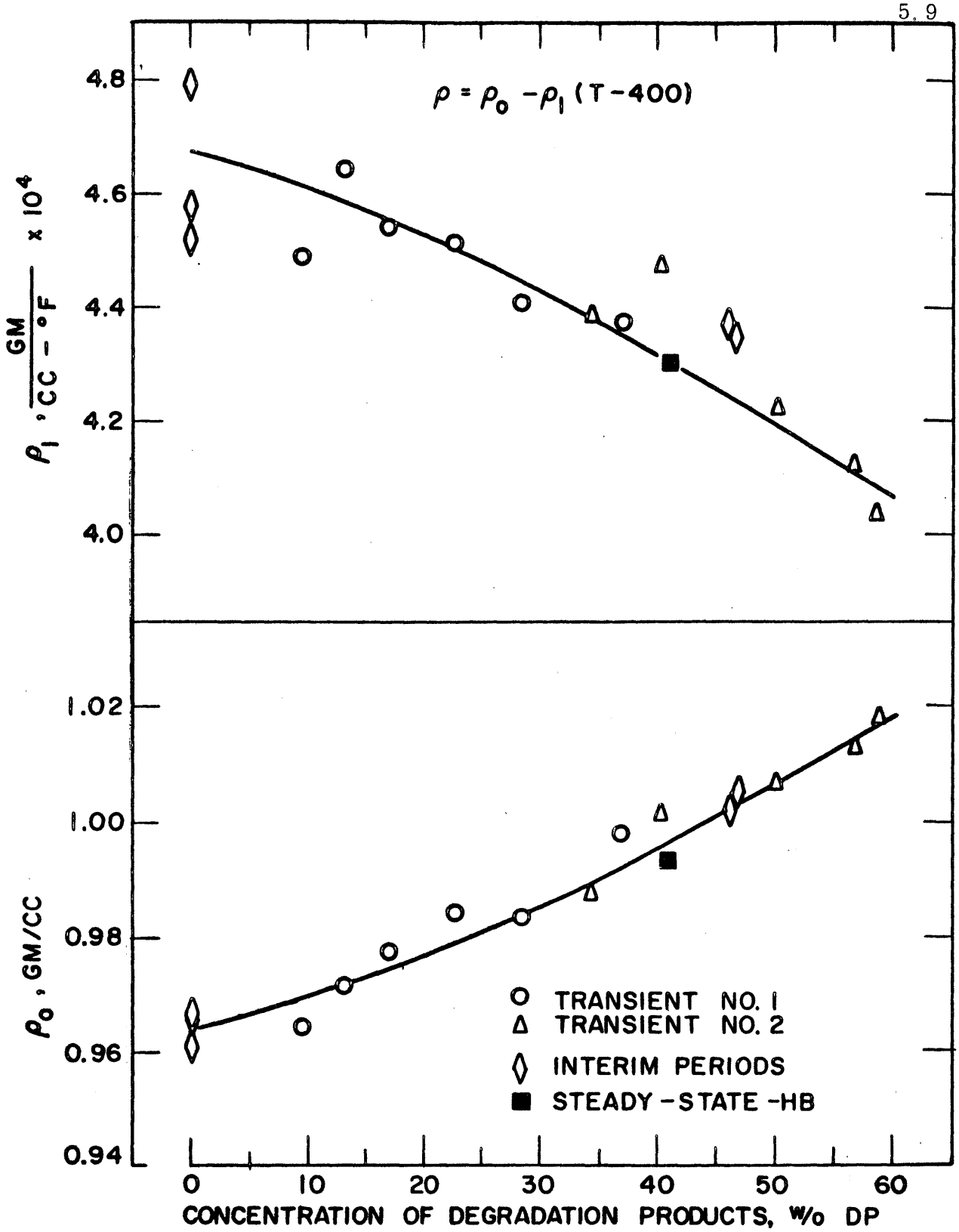

FIGURE 5.6 CORRELATION OF IRRADIATED SANTOWAX OMP DENSITY DATA FROM THE 750°F IRRADIATION

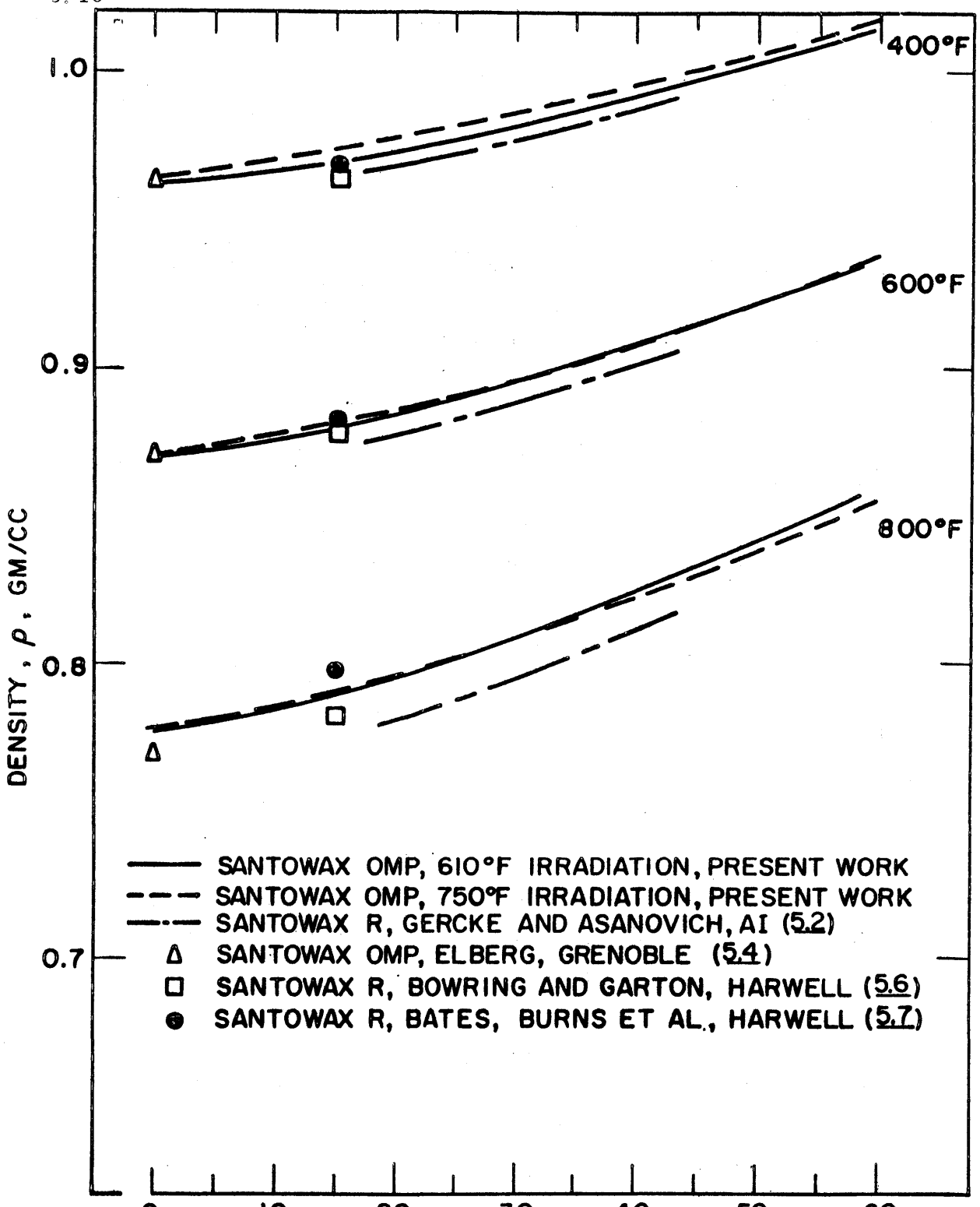

FIGURE 5.7 COMPARISON OF DENSITY DATA

comparison with the present data in Fig. 5.7. The data obtained were not fit to a linear temperature dependence but still agree almost exactly with the present data to 600°F. At 800°F the results appear to be about 1% lower than those obtained at M.I.T..

Bowring and Garton (5.6) made measurements on unirradiated Santowax R at Harwell using a glass dilatometer. The p-terphenyl and HB compositions of the material were reported as one value, so that the DP concentration is not exactly known but is believed to lie between 10 and 20 w/o. The data were fitted to a parabolic temperature dependence and are shown in Fig. 5.7 at a DP concentration of 15 ± 5 w/o. For 600°F their data agree quite well with the present results, but their data appear to be about 1% lower than the present data both at 400 and 800°F. Bates, Burns et al. (5.7), who also made measurements on unirradiated Santowax R with glass dilatometers, report values in agreement with those of Bowring and Garton, except at temperatures approaching 800°F, where their results are about 1% higher than those of this work and 2% higher than those of Bowring and Garton.

In general, the agreement of the density data of this work with those obtained at other laboratories is within about 1%, which is quite good.

5.3 Viscosity

Viscosities of irradiated Santowax OMP samples were determined over the temperature range 400 - 800°F by measuring efflux times in semi-micro capillary viscometers of the Ostwald type. As with the density measurements, the viscometers were pressurized with nitrogen and immersed in a high temperature fused salt bath. Morgan and Mason (5.1) describe the equipment in detail, and the theory of the use of viscometers is described in Section A3.2.

The viscosity data obtained for each sample were fit by the method of least squares to the relation

$$\mu = \mu_o e^{\frac{\Delta E}{RT}} \qquad (5.3)$$

where

μ, μ_o are in centipoises

ΔE is an "activation energy," kcal/mole

R is the gas constant, kcal/mole ^{o}R

T is the sample temperature, ^{o}R.

The data have been found to fit this type of relation over the temperature range of interest (400 - 800^{o}F), even for DP concentrations approaching 60 w/o. The smoothed constants μ_o and ΔE are reported for all samples from the 610^{o}F and 750^{o}F irradiation in Section A3.4, and the viscosities for each sample are believed accurate to an average standard deviation of ± 3%.

Figure 5.8 shows the variation of the smoothed viscosity data obtained from the 610^{o}F irradiation of Santowax OMP with DP concentration. For each sample the smoothed viscosities at 400^{o}F, 600^{o}F and 800^{o}F are plotted. As stated above, the DP concentration of each sample has a standard deviation of 1 - 2 w/o. The viscosities increased about four-fold through the two transient periods when the DP concentration increased from 0 to 60 w/o. This strong DP concentration dependence becomes very important in heat transfer and pumping power calculations. As with the density measurements the averaged steady-state-HB data are higher than the transient data for the same w/o DP, the difference amounting to about 10% at 600^{o}F. This implies a buildup of high molecular weight compounds in the HB fraction from the transient to steady-state-HB periods (see Section 5.6). During both steady-state-HB periods, the coolant viscosity seems to have remained fairly constant, as shown in Fig. 5.9, implying little change of the molecular weight distribution during these periods. The number average molecular weight data support this conclusion (see Section 5.6).

An overall correlation of the viscosity data from transient periods of the 610^{o}F irradiation (valid over the temperature range 400 - 800^{o}F) is given in Fig. 5.10. The correlation is of the form

$$\mu = \mu_1 \exp\left[\frac{\Delta E}{R}\left(\frac{1}{T} - 1.163 \times 10^{-3}\right)\right] \qquad (5.4)$$

where T is in ^{o}R and the variations of μ_1 and ΔE with DP concentration are displayed graphically.

The viscosity data from the 750^{o}F irradiation are shown in Fig. 5.11 as a function of DP concentration. As with the density data for the

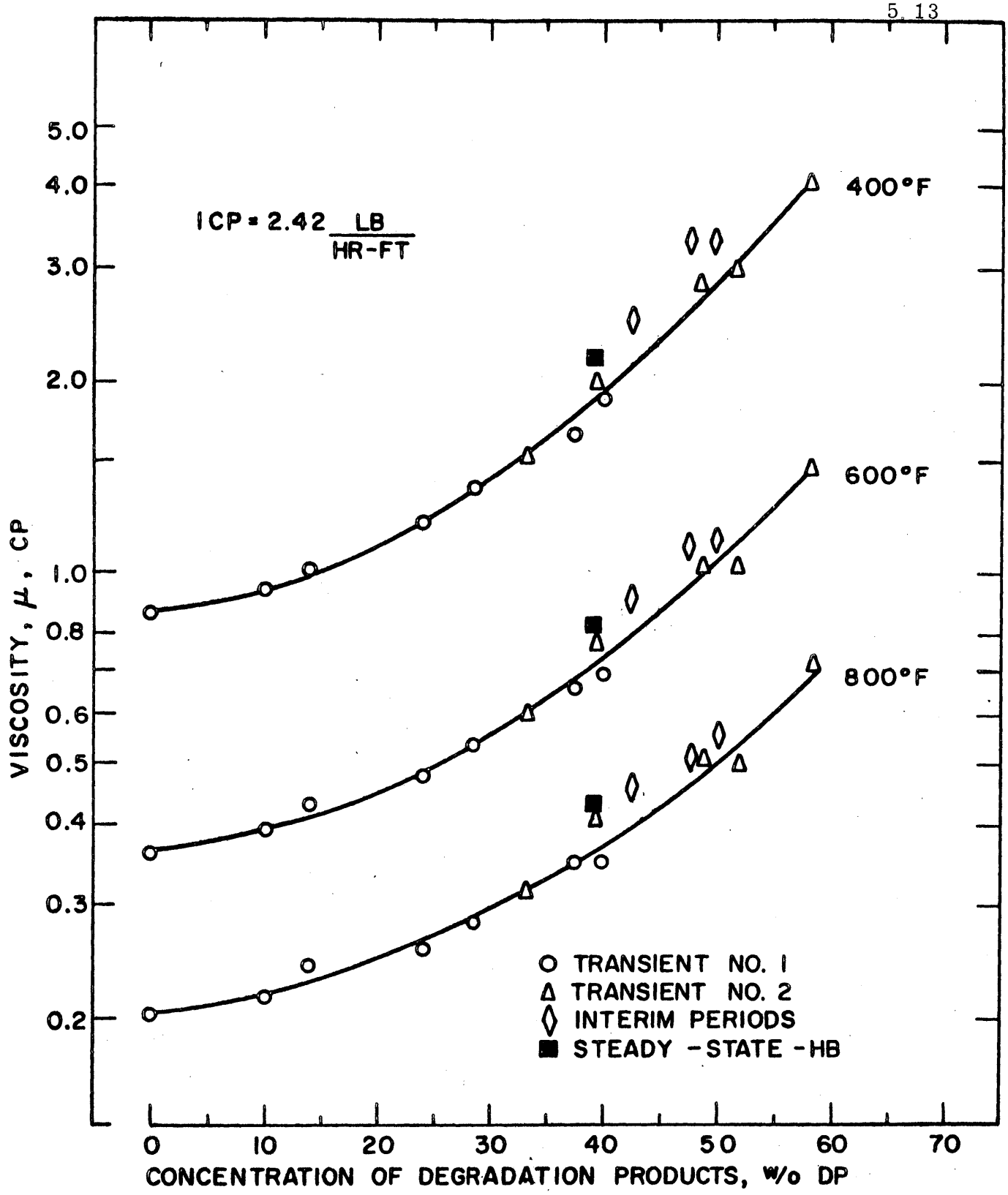

FIGURE 5.8 VISCOSITY OF IRRADIATED SANTOWAX OMP FOR THE 610°F IRRADIATION

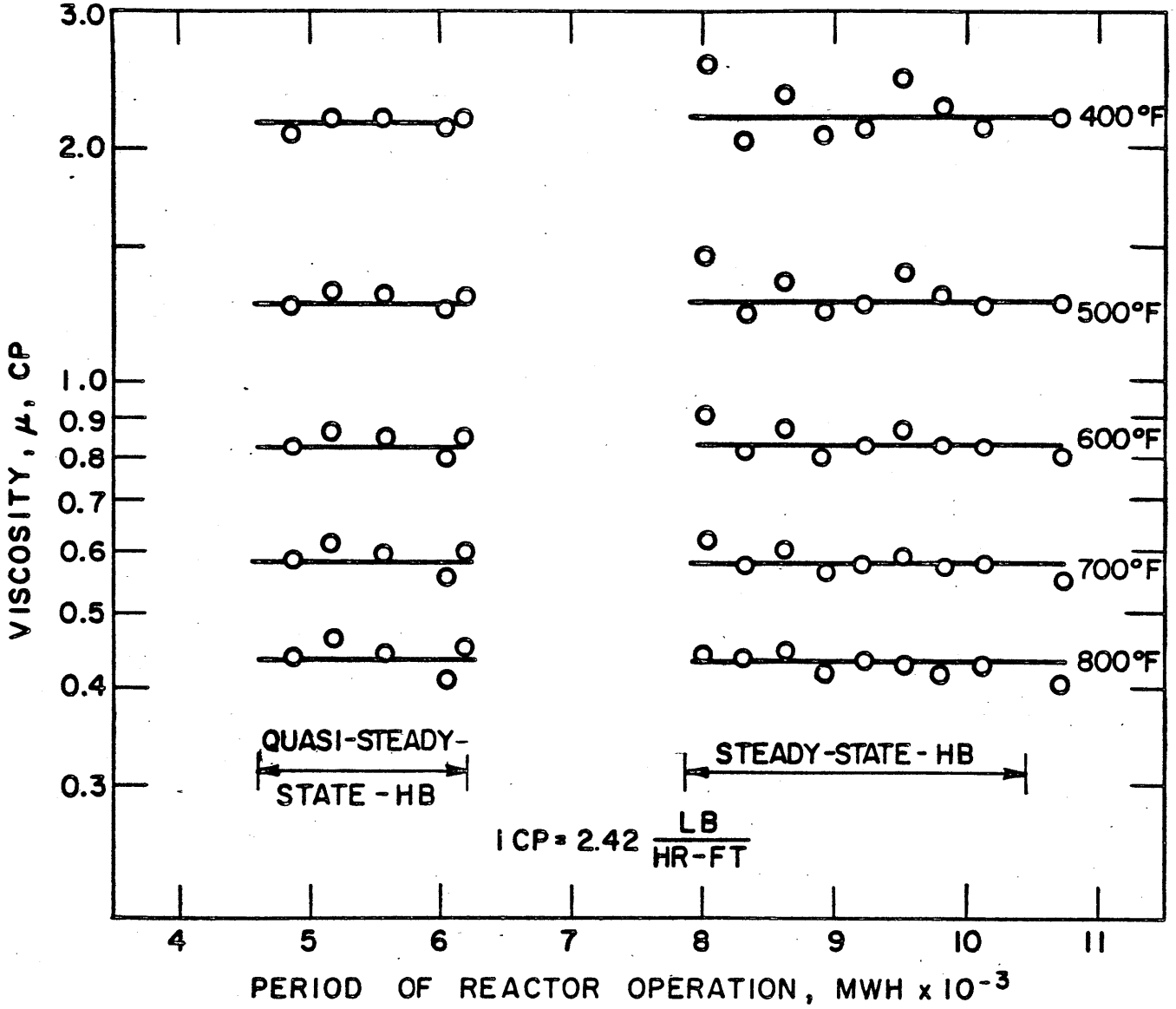

FIGURE 5.9 VISCOSITY OF IRRADIATED SANTOWAX OMP DURING THE STEADY-STATE-HB PERIODS OF THE 610°F IRRADIATION

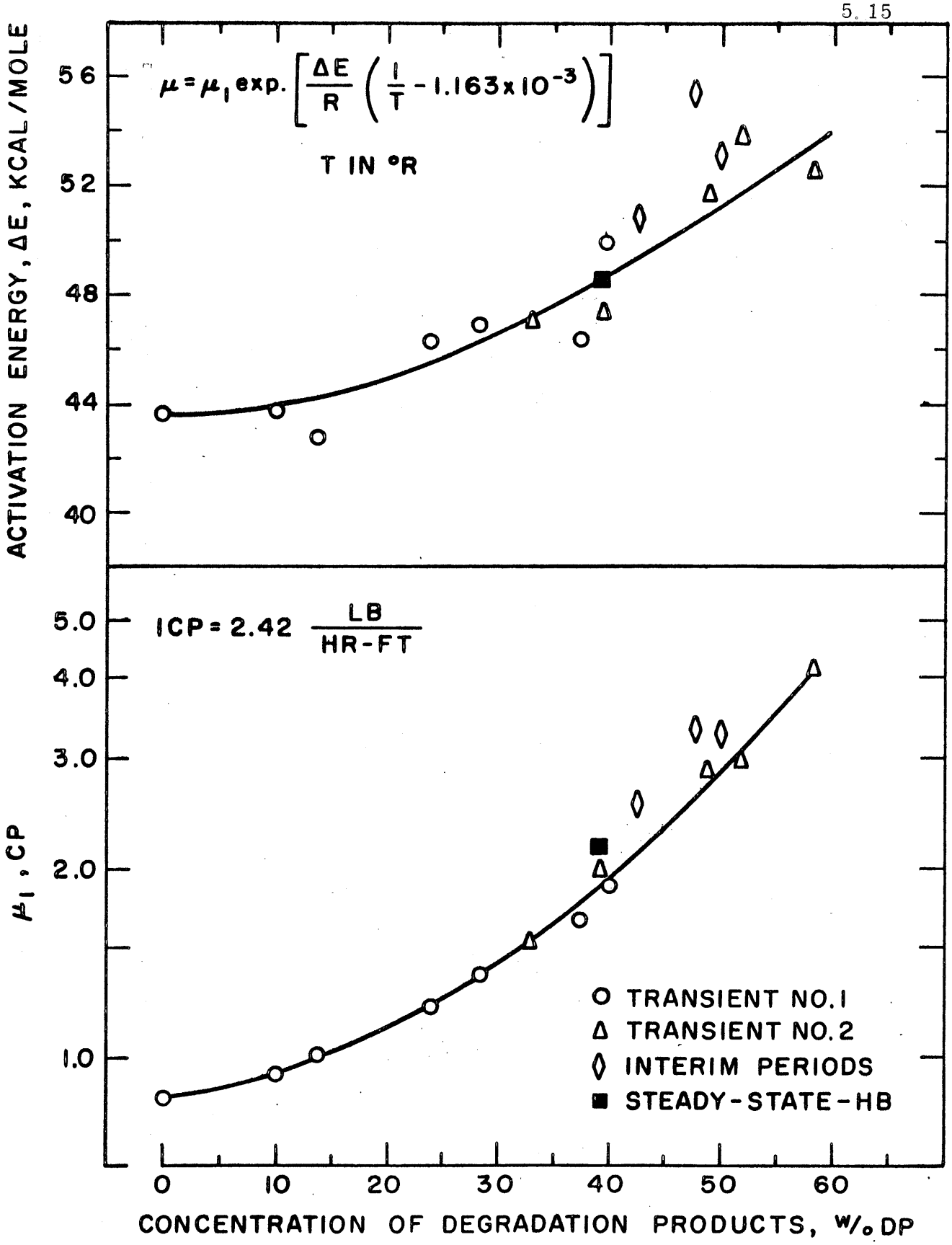

FIGURE 5.10 CORRELATION OF IRRADIATED SANTOWAX OMP VISCOSITY DATA FROM THE 610°F IRRADIATION

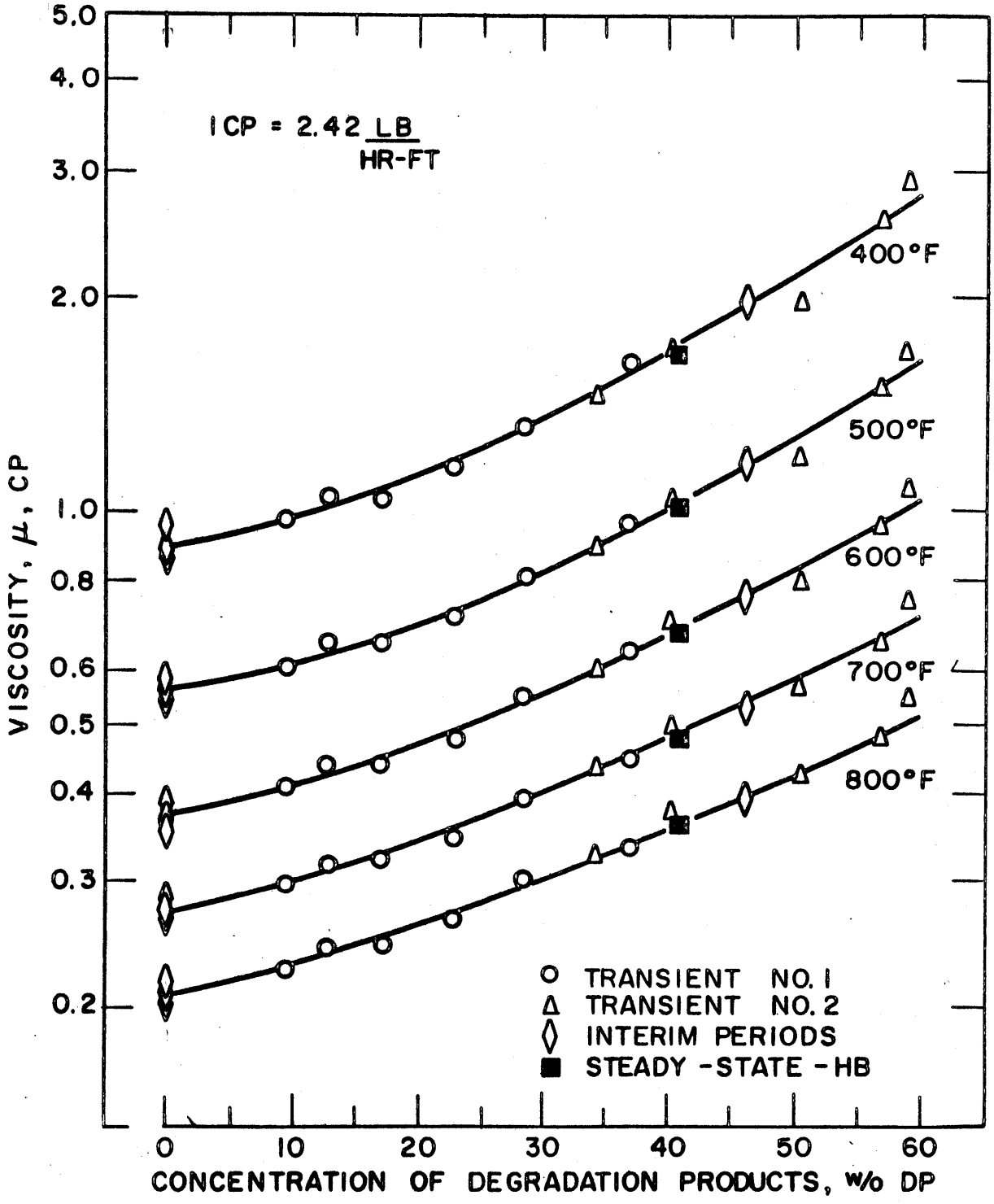

FIGURE 5.11 VISCOSITY OF IRRADIATED SANTOWAX OMP FOR THE 750°F IRRADIATION

750°F irradiation, the steady-state-HB data agreed with those of the transient period for the same DP concentration, in contrast to the results of the 610°F irradiation. The viscosities during the steady-state-HB period of the 750°F irradiation remained quite constant, as shown in Fig. 5. 12.

An overall correlation of the viscosity data from the transient periods of the 750°F irradiation (valid over 400 - 800°F) by a relation of the form of Eq. (5. 4) is given in Fig. 5. 13.

A comparison of the viscosity data from the two irradiations together with data of other laboratories is provided by Fig. 5. 14. To about 20 w/o DP the viscosity data of the two irradiations agree with each other within the possible errors in the viscosities and the DP concentrations, but at higher conversions the 750°F irradiation viscosities are significantly lower than the 610°F irradiation viscosities. Also, as shown in Figs. 5. 10 and 5. 13, the "activation energy," ΔE, did not increase as rapidly with DP concentration for the 750°F irradiation as for the 610°F irradiation. The number average molecular weight of the HB fraction of the coolant was found to be significantly lower for the steady-state-HB periods of the 750°F irradiation than for the steady-state-HB period of the 610°F irradiation (see Section 5. 6). The coolant viscosity thus appears to be more influenced by the molecular weight distribution in the coolant than by the average molecular weight of the coolant, and apparently the higher irradiation temperature hinders the buildup of high molecular weight compounds.

Corrected viscosity data of Santowax R samples irradiated in the MTR (5. 3) are reported by Atomics International (5. 8). The viscosities were also measured with Ostwald-type viscometers and are shown in Fig. 5. 14. As mentioned in Section 5. 2, the fact that the data seem low compared to the present results is somewhat misleading since the unirradiated Santowax R composition contained about 18 w/o LIB.

Bessouat et al. (5. 5) report measurements on unirradiated Santowax OMP (composition not given but assumed 0 w/o DP) made at Grenoble. The method utilized was to time the fall of a cylindrical plummet through a given distance in the liquid. Their results are shown in Fig. 5. 14 and agree within 5% with the present results.

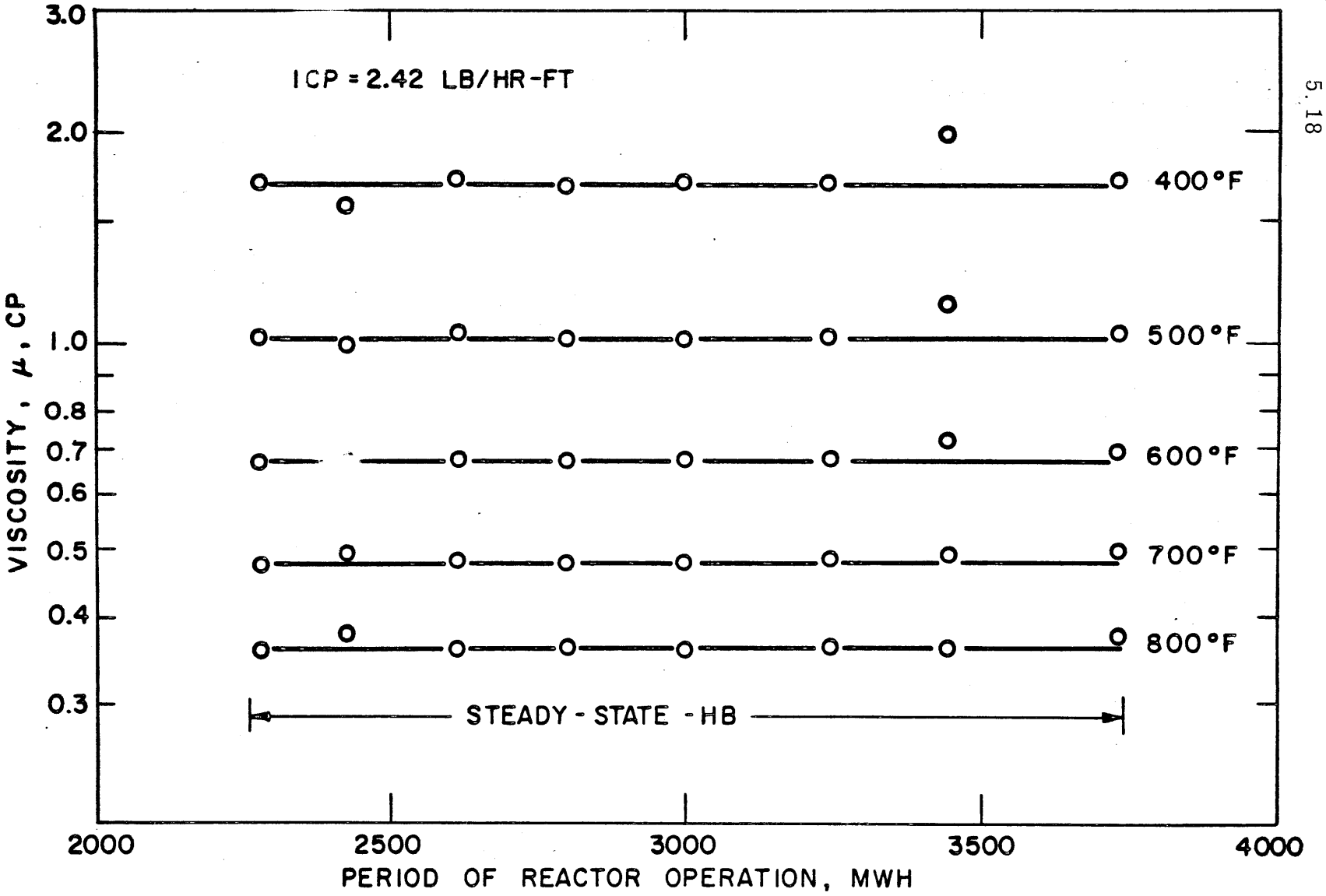

FIGURE 5.12 VISCOSITY OF IRRADIATED SANTOWAX OMP DURING THE STEADY-STATE-HB PERIOD OF THE 750°F IRRADIATION

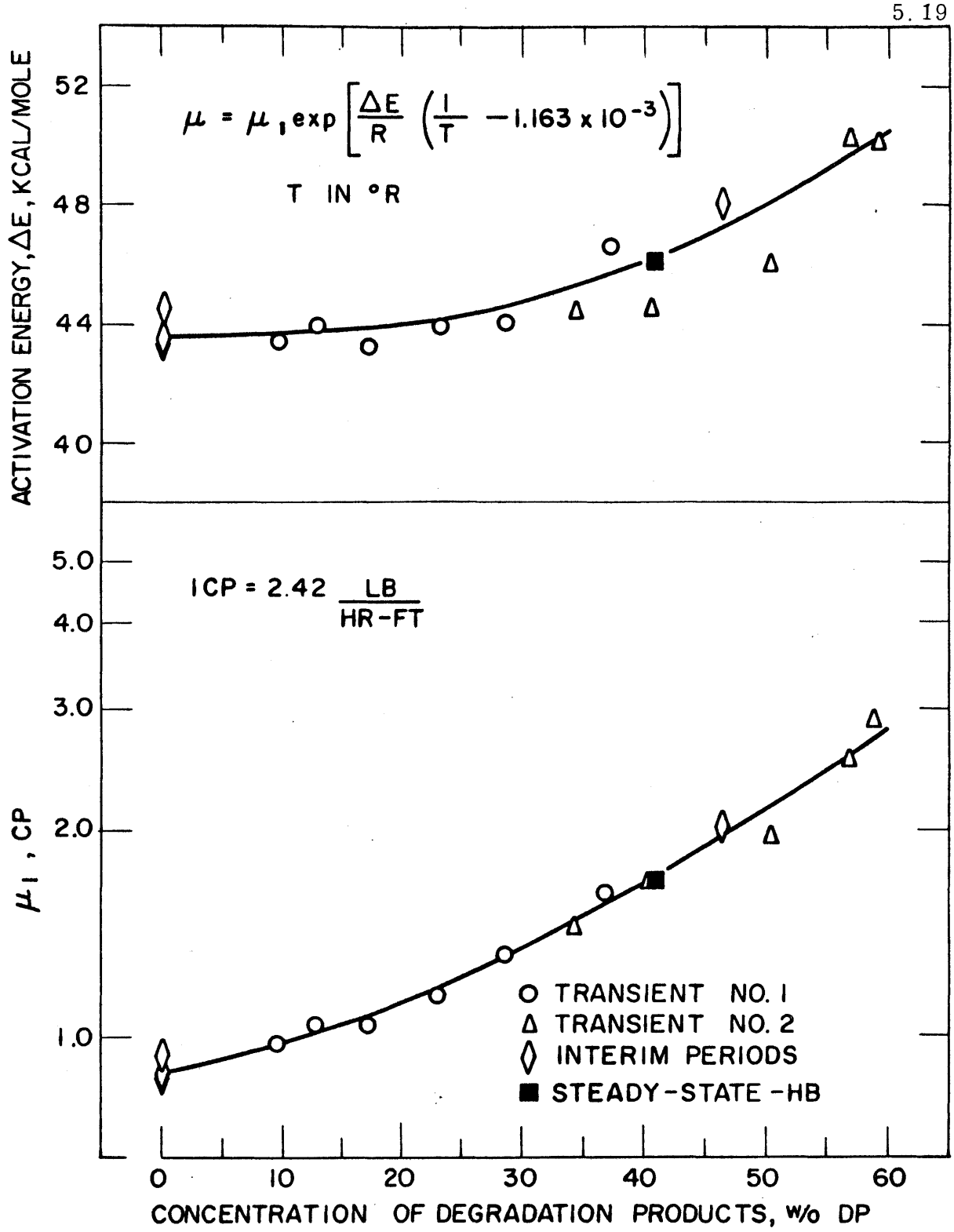

FIGURE 5.13 CORRELATION OF IRRADIATED SANTOWAX OMP VISCOSITY DATA FROM THE 750°F IRRADIATION

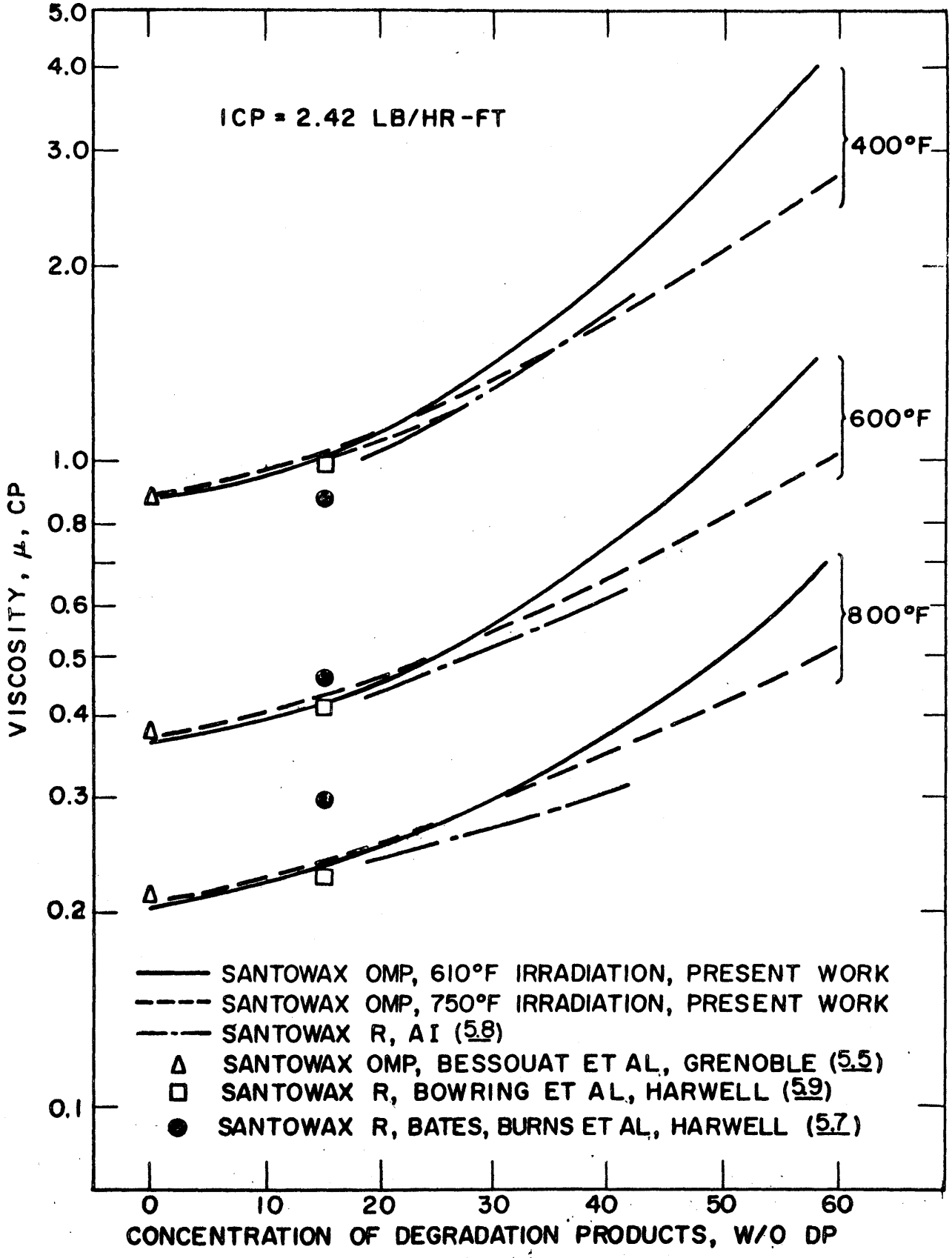

FIGURE 5.14 COMPARISON OF VISCOSITY DATA

The viscosity of unirradiated Santowax R was also measured by Bowring et al. (5.9) at Harwell using the same method as Bessouat et al.. Since the p-terphenyl and HB concentrations were reported together, the DP concentration is not exactly known but is believed to be 15 ± 5 w/o. The agreement with the present results is good (within 4%) over the whole temperature range 400 - 800°F. Measurements made by Bates, Burns et al. (5.7) at Harwell on unirradiated Santowax R did not agree very well with either those of Bowring et al. or those of this work.

In general the data obtained at other laboratories agree with those of M.I.T. to within ± 5%

5.4 Specific Heat

Specific heat measurements were made on selected samples from the 610°F and 750°F irradiations by the Monsanto Research Corporation at Dayton, Ohio (5.10). The method used was to find the heat content (enthalpy) of the samples at three temperatures -- near 400°F, 600°F and 800°F -- by drop calorimetry and to fit the heat content versus temperature curves by parabolas. Upon differentiation of these fitted curves, the specific heat as a (linear) function of temperature was obtained. The method is estimated accurate to ± 4% (see Section A3.5).

Measurements were also made on a mixture of two samples (having about the same composition) from the 610°F irradiation at Grenoble (5.4). The method used for this measurement was to deduce the specific heat of the sample at a given temperature from the observed temperature rise of the sample in an adiabatic calorimeter after a known amount of heat had been added. This method is said to yield results good to ± 1% (5.11). These data, together with the data from Monsanto, are given in detail in Section A3.5, and smoothed values at 400, 600 and 800°F are shown in Fig. 5.15 as a function of w/o DP.

As may be seen from Fig. 5.15, the Monsanto and Grenoble data seem to agree quite well. There is no significant variation of specific heat with DP concentration or temperature of irradiation.

A comparison of the data obtained for this report with data of other laboratories is given in Fig. 5.16. Bowring et al. (5.12) report the results of specific heat measurements on unirradiated Santowax R at

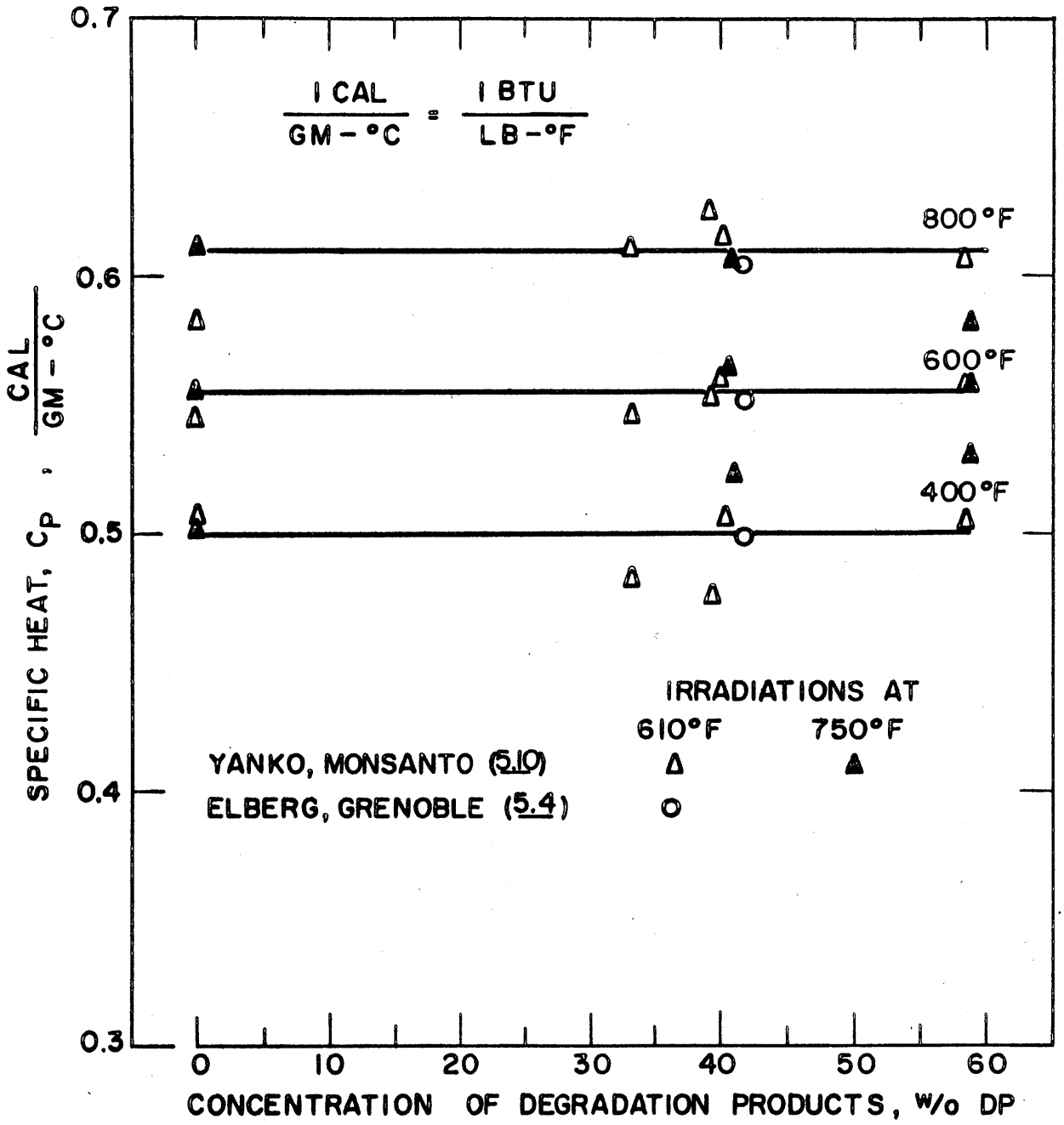

FIGURE 5.15 SPECIFIC HEAT OF IRRADIATED SANTOWAX OMP FOR THE 610°F AND 750°F IRRADIATIONS

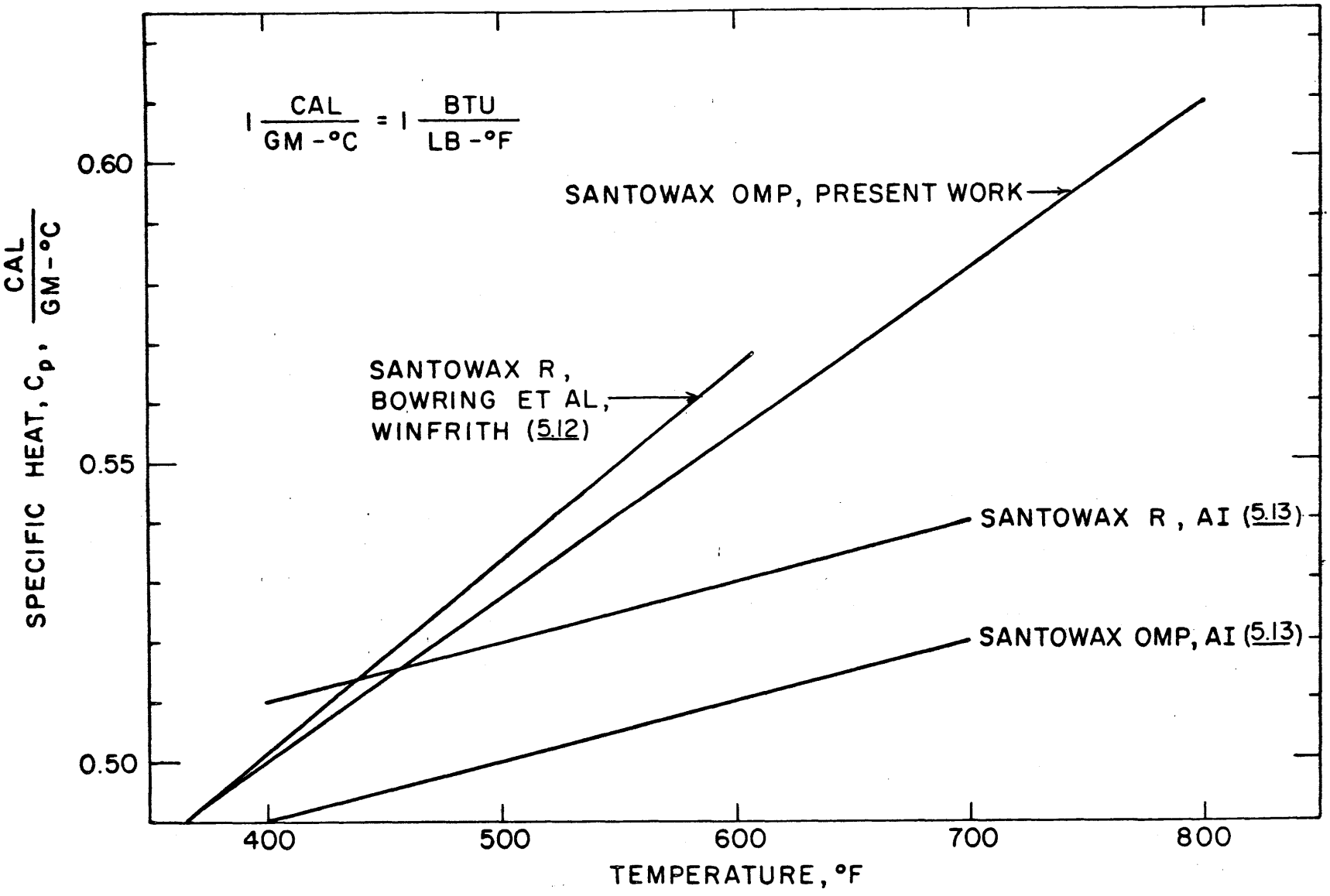

FIGURE 5.16 COMPARISON OF SPECIFIC HEAT DATA

Winfrith, England. The method used was the same as the method used at Grenoble, and their data cover the range 350 - 600°F. As seen from Fig. 5. 16 their data appear to agree with the results of this study at about 400°F but have a larger slope with temperature. However, for the calibration experiments at Winfrith, Bowring et al. measured the specific heat of diphenyl ether over the range 100 - 400°F and compared their measurements to those of the National Bureau of Standards (5. 18). Their comparison showed higher specific heats for diphenyl ether than measured by the National Bureau of Standards. If the percentage discrepancy between the Bowring et al. data and those of the National Bureau of Standards were extrapolated to 600°F, it would account for the difference between the Bowring et al. results for Santowax R and those of the present study. In any event, these two sets of data agree within 2% at 600°F.

Specific heat data have been reported over the temperature range 400 - 700°F for unirradiated Santowax OMP and Santowax R by Atomics International (5. 13). Their measurement techniques were similar to those used by Monsanto. The data are shown in Fig. 5. 16 and are somewhat lower than the present data, the discrepancy amounting to about 10% at 700°F. This discrepancy is greater than the reported accuracy of ± 5%.

5. 5 Thermal Conductivity

Thermal conductivity measurements have been made over the temperature range 400 - 700°F on two samples from the 610°F irradiation of Santowax OMP and on the charge material for the 750°F irradiation of Santowax OMP. These measurements have been made at Grenoble, and the results are reported by Elberg (5. 4). The method used was to pass a step change in current through a thin platinum wire submerged in the liquid at a certain temperature. The rate of rise of temperature of the wire can be related to the thermal conductivity of the liquid (5. 5). The data for each sample were smoothed by assuming a linear dependence of thermal conductivity on temperature. The measured data are tabulated in Section A3. 5 and are stated as accurate to ± 2% (5. 5).

The smoothed data are shown in Fig. 5. 17 as a function of DP concentration at 400, 600 and 800°F. Straight lines were drawn through the

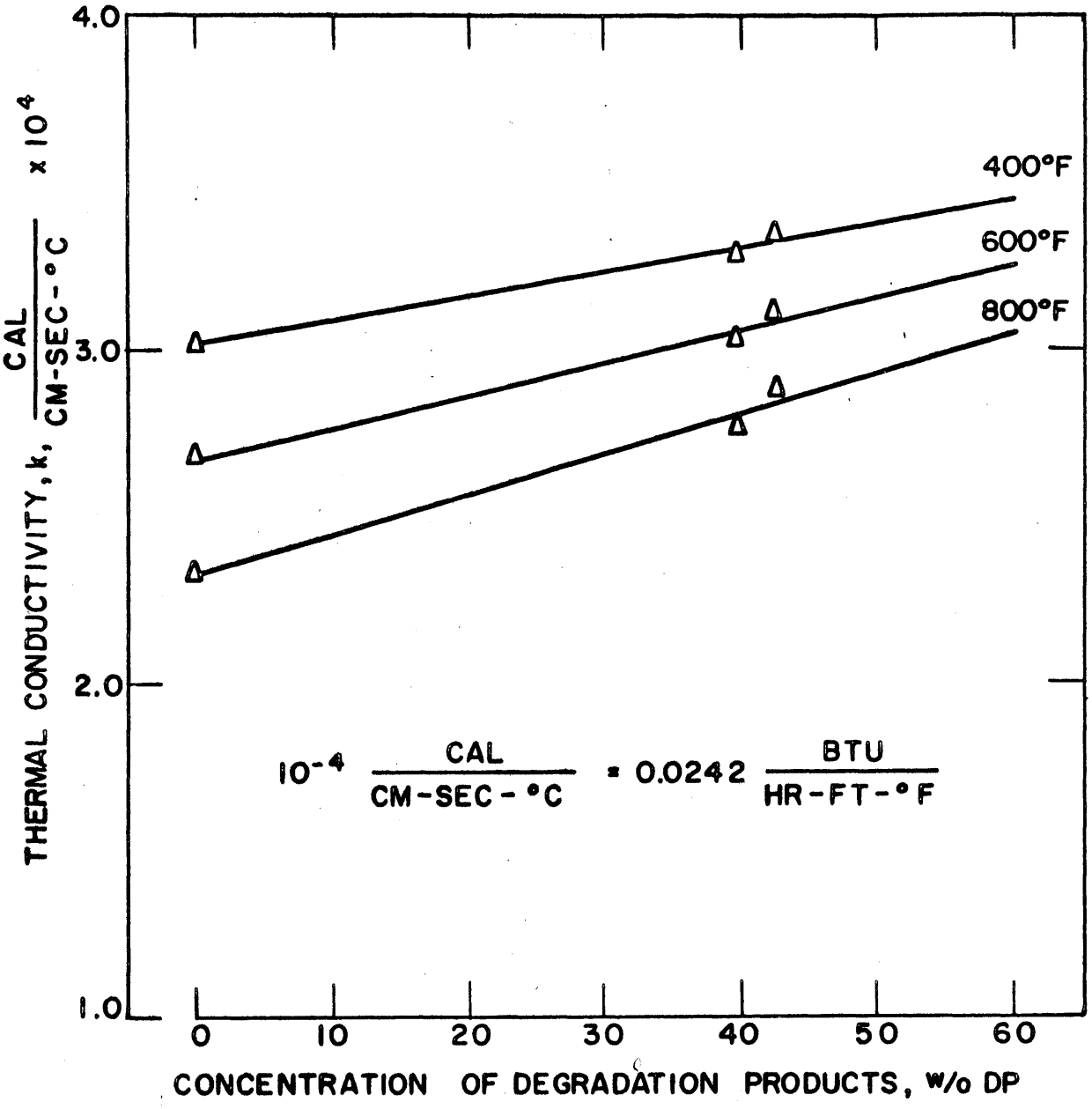

FIGURE 5.17 THERMAL CONDUCTIVITY OF IRRADIATED SANTOWAX OMP FOR THE 610°F IRRADIATION

data due to lack of better information. It appears from the data that the thermal conductivity may increase by over 20% as the DP concentration increases from 0 to 60 w/o.

A comparison of the present results with those of other laboratories is given in Fig. 5.18. The data obtained at Grenoble are shown in the figure, together with the DP concentration for the three samples analyzed. Ziebland and Burton (5.14) report the results of thermal conductivity measurements on unirradiated Santowax R over the temperature range 300 - 750°F. The p-terphenyl and HB compositions were reported together so that the DP concentration was estimated to be between 10 - 20 w/o, since unirradiated Santowax R usually contains some degradation products. Their method was to place the liquid between two coaxial cylinders and to heat the inner cylinder. At steady-state, the thermal conductivity can be calculated from the heat input, the temperature drop across the gap and the geometry of the system. Their results, stated as accurate to ± 2%, are shown on Fig. 5.18 and can be seen to agree quite well with the results of this work.

Measurements on the thermal conductivity of irradiated OMRE coolant have been reported over the temperature range 350 - 650°F by Atomics International (5.15), and their data are shown in Fig. 5.18. The concentration of degradation products for the OMRE coolant was defined as 100 − w/o omp − w/o biphenyl, since biphenyl was a significant fraction of the unirradiated coolant, and the values are shown in the figure for the two sets of measurements reported. The data are seen to agree with the present data with a maximum deviation of 6% over the range covered.

In general, the thermal conductivity data agree with those of other laboratories; however, the data are somewhat sparse, and more measurements should be made in the future to more accurately determine this property.

5.6 Number Average Molecular Weight

During the 610°F and 750°F irradiations number average molecular weight measurements were made on both coolant and HB (bottoms) samples. Measurements were made at M.I.T., using a Mechrolab Model 301A

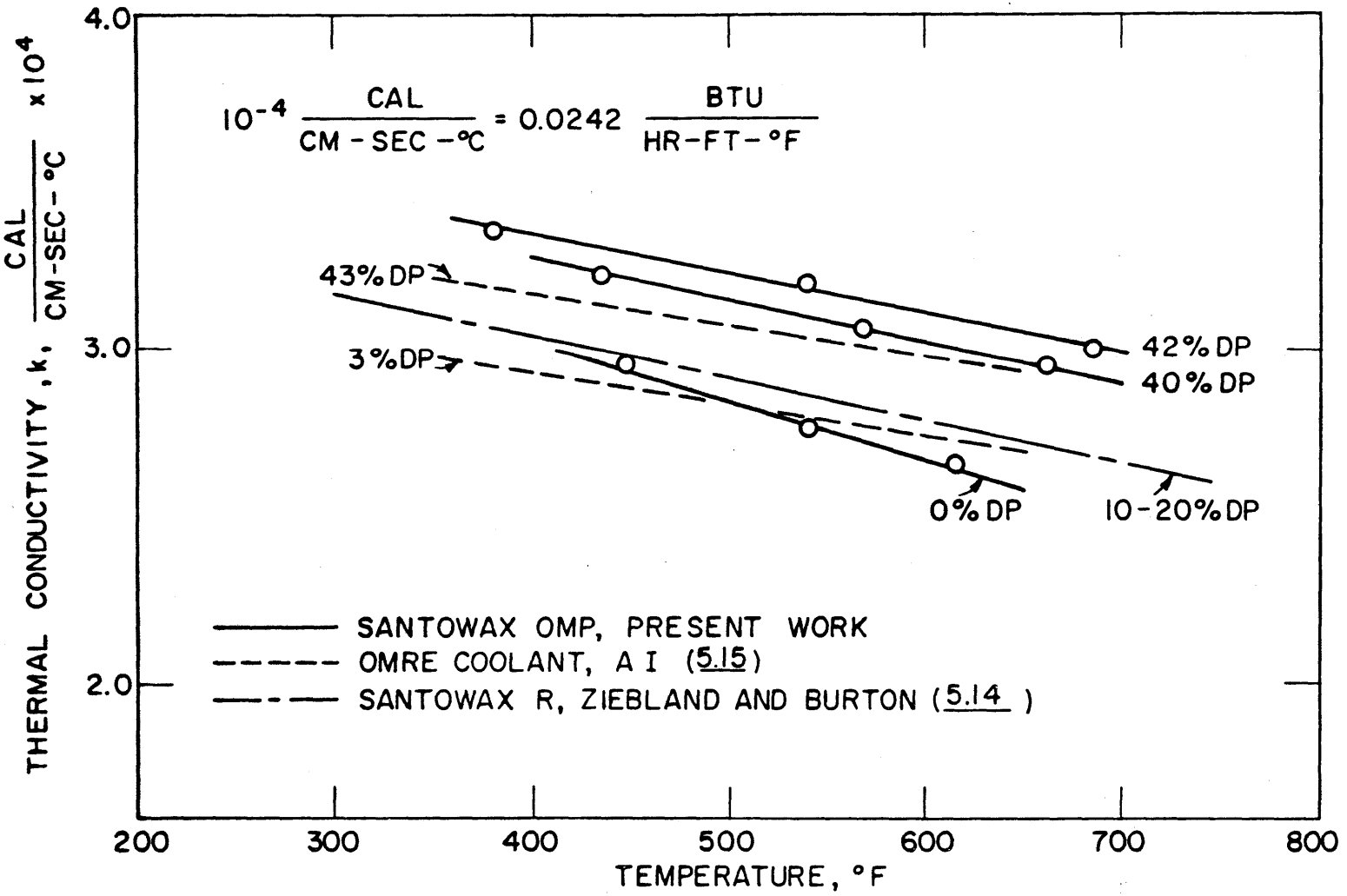

FIGURE 5.18 COMPARISON OF THERMAL CONDUCTIVITY DATA

osmometer,[1] and at the Monsanto Research Corporation (Everett, Mass.) using a cryoscopic method. The procedures used at M.I.T. are described in detail in Section A3.6 and the standard deviation of the measurements has been estimated to be + 3% to − 2%. A tabulation of the data may be found in Section A3.7.

The number average molecular weight is defined as

$$MW_N = \frac{\sum C_i}{\sum C_i / A_i} \tag{5.5}$$

where

C_i is the weight fraction of species i in the mixture

A_i is the molecular weight of species i.

and gives emphasis to low molecular weight species. The HB samples were therefore corrected for the small amount of m- and p-terphenyl in them by applying the formula

$$MW_N^{corrected} = \left[\frac{1 - y}{\frac{1}{MW_N^{uncorrected}} - \frac{y}{230}} \right] \tag{5.6}$$

where y is the weight fraction of omp in the HB samples.

Figure 5.19 shows the number average molecular weight of the coolant and HB fraction (distillation bottoms) as a function of the DP concentration for the 610°F irradiation. As stated above, the DP concentration of each sample has a standard deviation of 1 - 2 w/o. The MW_N of the coolant increased with increasing DP concentration from a value of 230 at 0 w/o DP to about 350 at 60 w/o DP. The number average molecular weight of the coolant was about 5% higher during the steady-state-HB periods for the same DP concentration, implying a slight buildup of higher molecular weight species. During the steady-state-HB period the average bottoms MW_N was near 690.

During the steady-state-HB period of the 610°F irradiation the coolant MW_N values remained quite constant (see Fig. 5.20) with an average near 300. The HB results were much more scattered, and it is

1. Mechrolab, Inc., Mountain View, California.

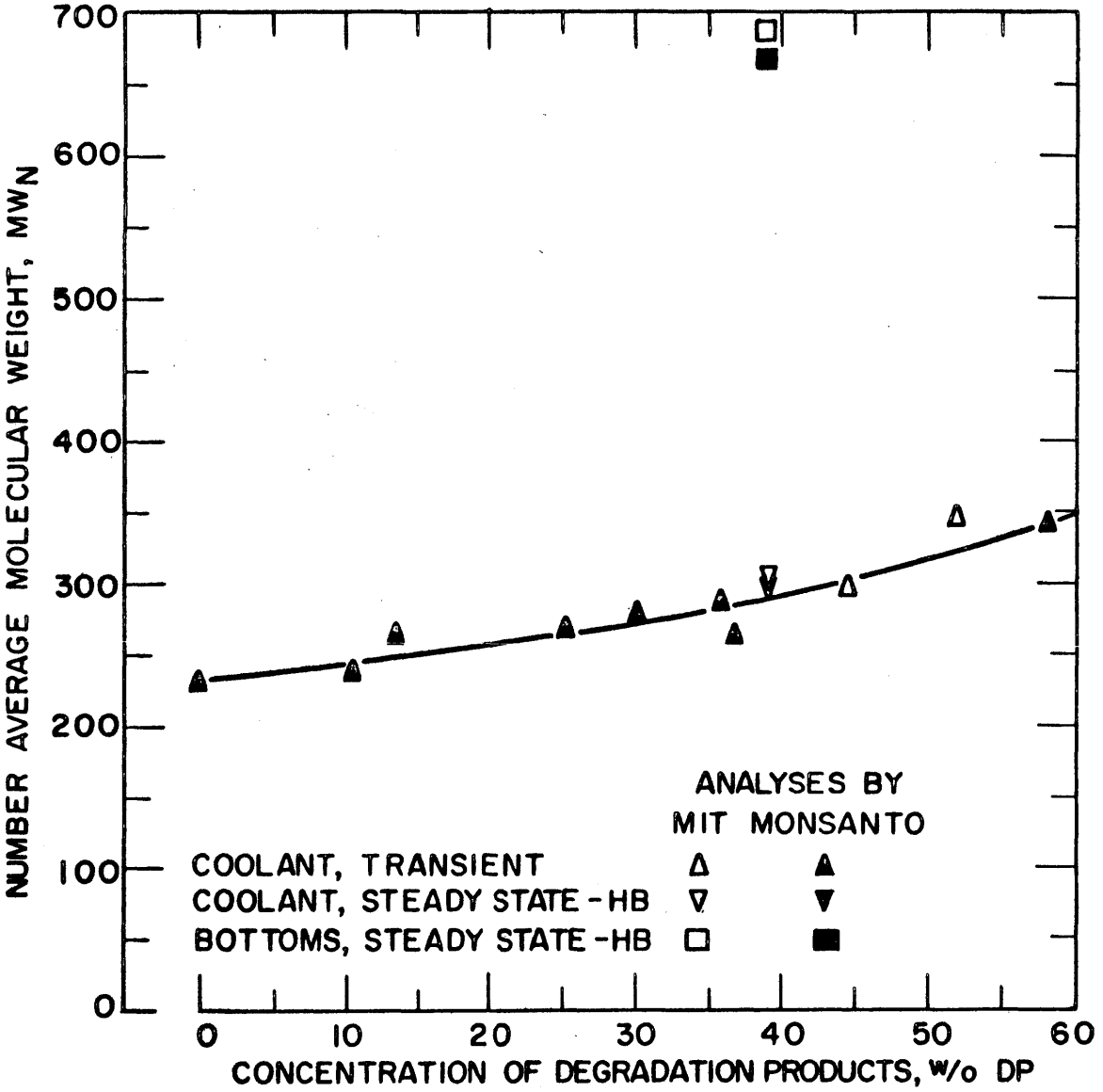

FIGURE 5.19 NUMBER AVERAGE MOLECULAR WEIGHT OF IRRADIATED SANTOWAX OMP FOR THE 610°F IRRADIATION

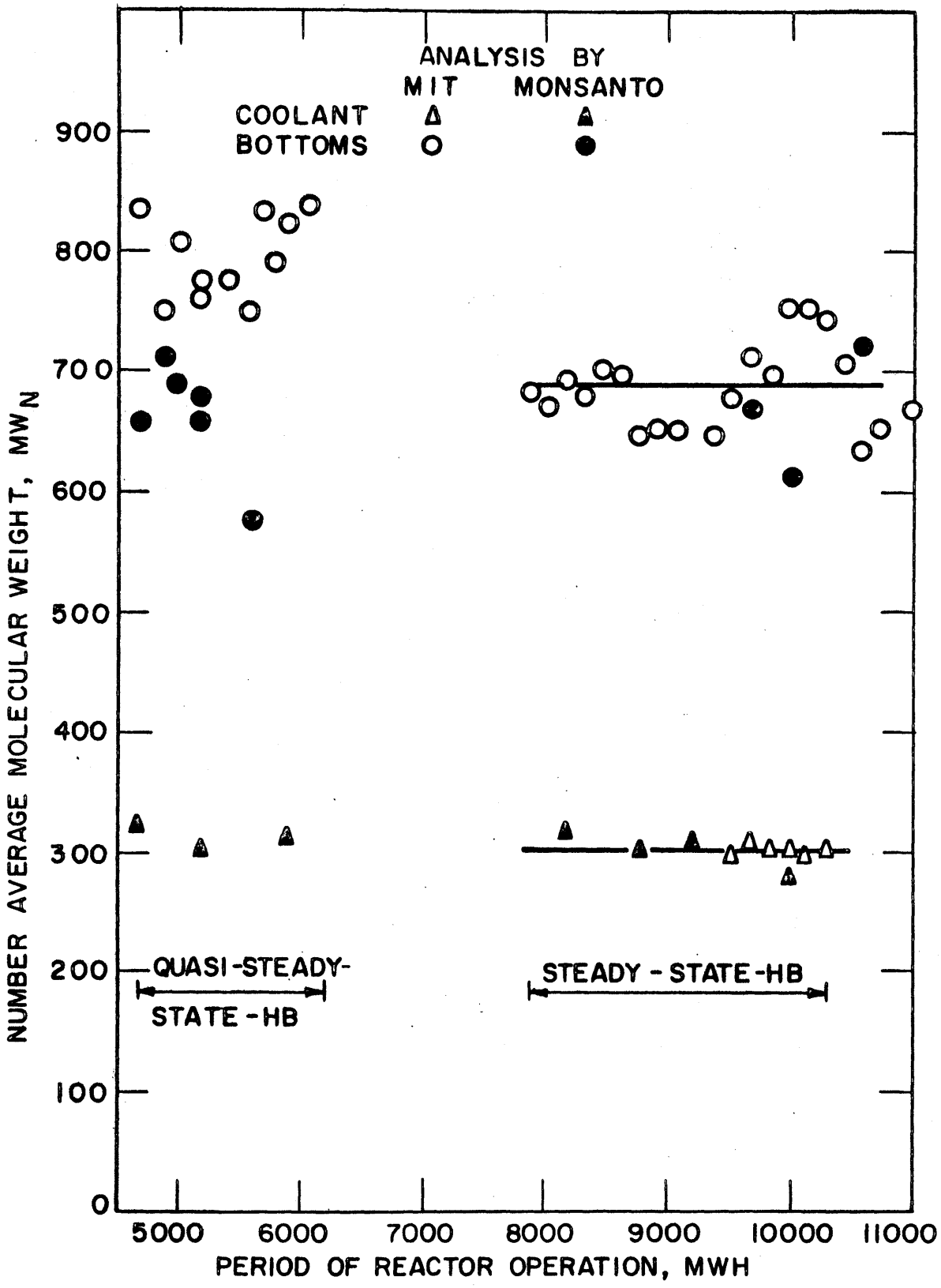

FIGURE 5.20 NUMBER AVERAGE MOLECULAR WEIGHT OF IRRADIATED SANTOWAX OMP FOR THE STEADY-STATE - HB PERIODS OF THE 610°F IRRADIATION

difficult to tell whether there was a trend during the irradiation or not. Some of this scattering may be due to insolubility effects (see Section A3.6) of the HB material. Since the number average molecular weights give emphasis to low molecular weight compounds, the coolant MW_N data would be expected to show less scatter than the HB MW_N data, in view of the 60 w/o terphenyl concentration in the coolant.

Figure 5.21 shows the coolant and bottoms MW_N data obtained during the 750°F irradiation of Santowax OMP as a function of the DP concentration. The steady-state-HB coolant data agreed quite well with those of the transient period for the same DP concentration. The coolant and HB MW_N data remained constant within experimental error during the steady-state-HB period (see Fig. 5.22) with the coolant MW_N averaging about 285 and the bottoms MW_N averaging 580.

The data for the two irradiations indicate a fairly good agreement of the MW_N's of the coolant during the transient periods. The MW_N data for the 750°F irradiation appeared to be only 2% lower at 40 w/o DP for the 750°F irradiation. However, the HB data show that the MW_N of the bottoms was about 15% lower for the 750°F irradiation. This would indicate that the increase in irradiation temperature either inhibits formation or promotes breakdown of high molecular weight compounds.

Number average molecular weight data have been reported for OMRE coolant by Atomics International for the 30 w/o HB phase of the Core II operation at 600°F (5.15). Their HB data show an average of 600, which is about 12% lower than the average for the 610°F irradiation at M.I.T.. Considering the differences of coolant (unirradiated OMRE Core II coolant contained about 15 w/o diphenyl) and the slightly lower HB level at Atomics International, the molecular weight results of the OMRE and M.I.T. irradiations appear to be consistent.

5.7 Gas Solubility

Measurements on the solubility of radiolytic gas in irradiated Santowax OMP were performed at intervals during the 610°F and 750°F irradiations. The purpose of these measurements was to determine the amount and composition of dissolved gas in the loop during the irradiations in order to complete the gas balance for the determination of the

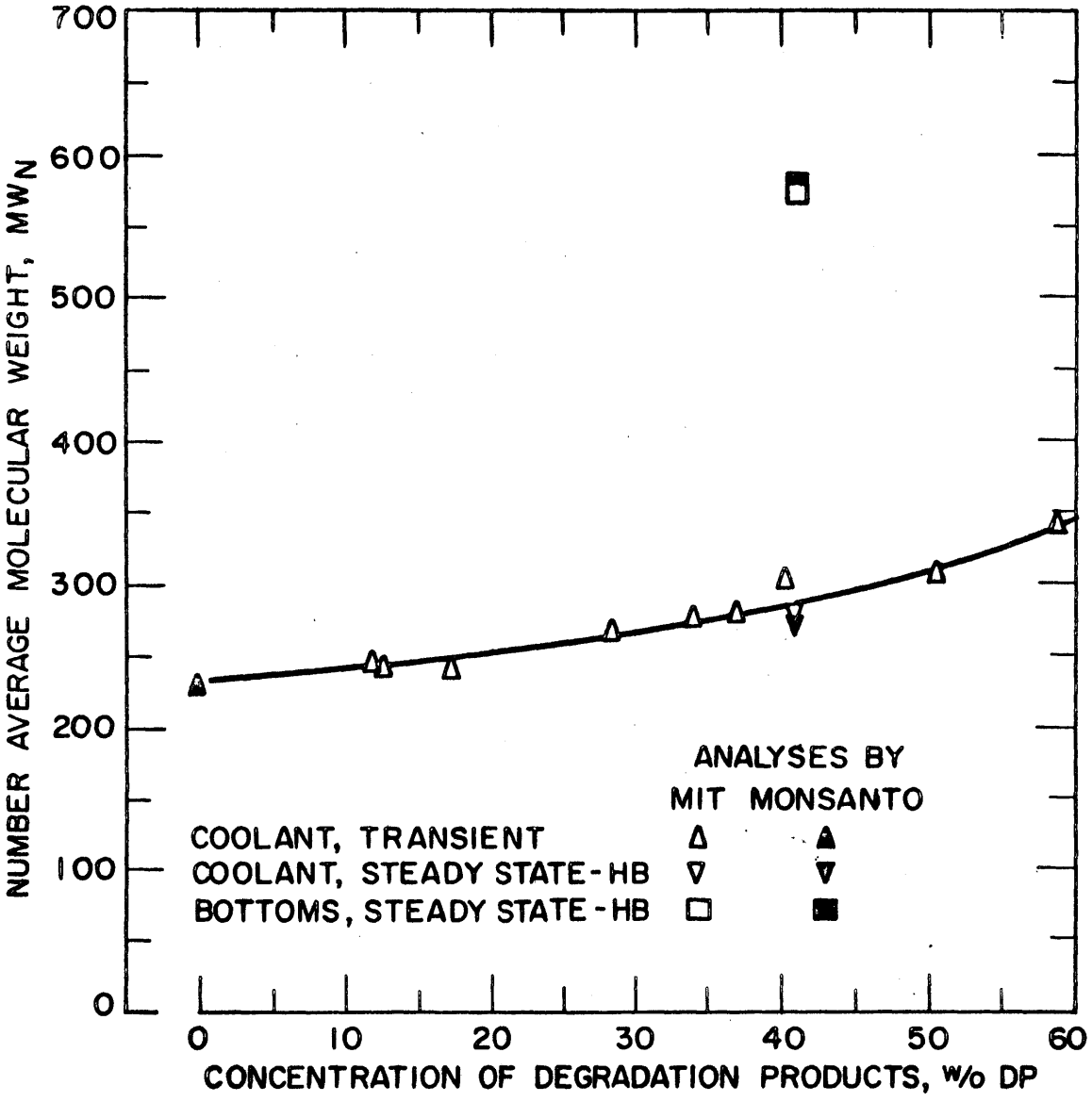

FIGURE 5.21 NUMBER AVERAGE MOLECULAR WEIGHT OF IRRADIATED SANTOWAX OMP FOR THE 750°F IRRADIATION

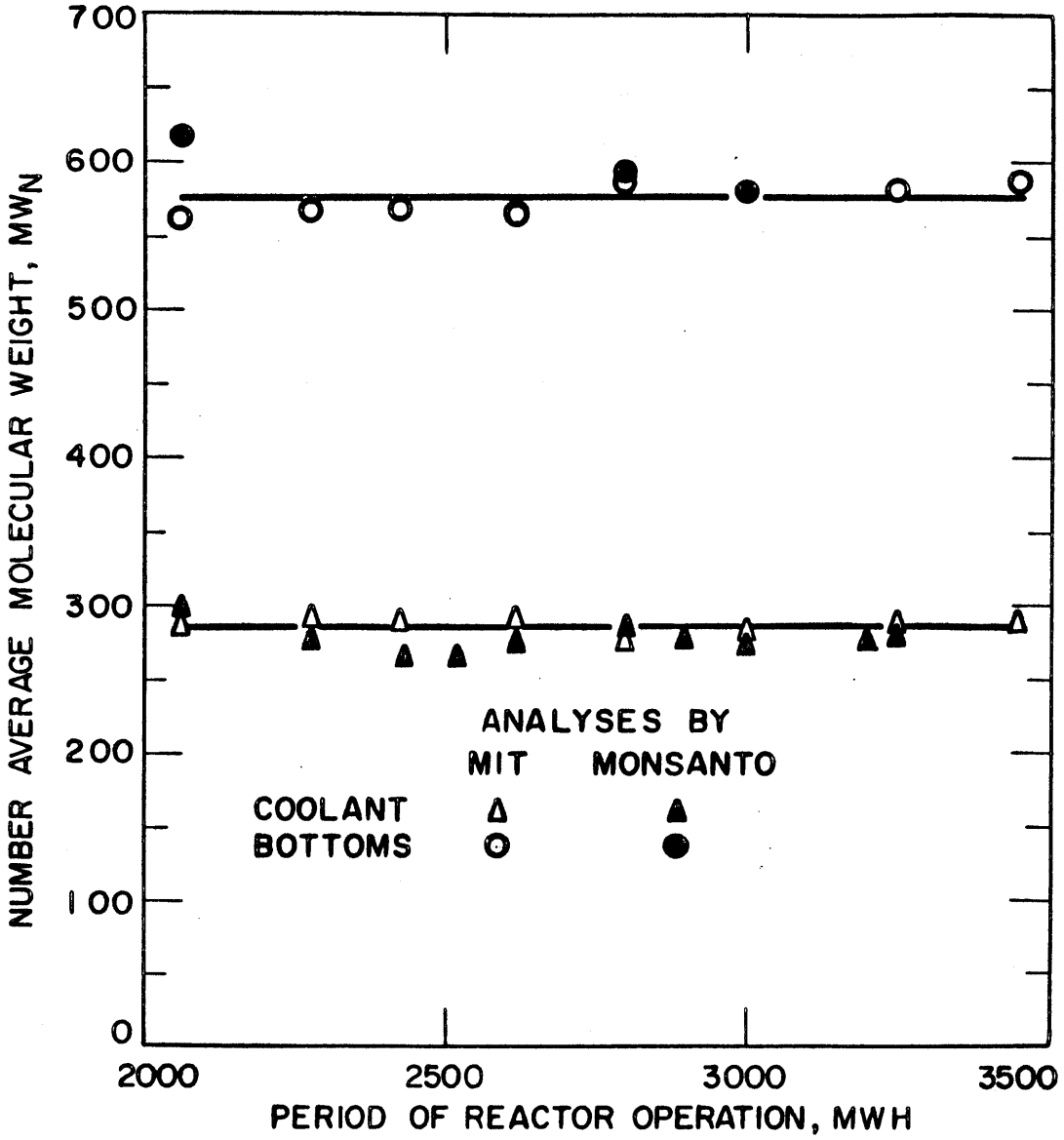

FIGURE 5.22 NUMBER AVERAGE MOLECULAR WEIGHT OF IRRADIATED SANTOWAX OMP FOR THE STEADY STATE-HB PERIOD OF THE 750°F IRRADIATION

gas generation rate in irradiated Santowax OMP (see Section 4.8).

The procedure for these measurements has been described in detail by Morgan and Mason (5.1). Briefly, the capsule containing the sample to be analyzed was connected directly to a reflux boiler and the organic material boiled under a vacuum. A cold trap on the condensing side of the boiler prevented low boilers from entering a collecting buret, which collected the gas evolved.

It should be remembered that these measurements are inherently more difficult to make in a loop system than in a batch system, due to the greater chance for gas leakage from the irradiated sample while it is being transferred to the gas solubility apparatus from the loop. Another source of error arose from the leakage of air into the gas solubility apparatus during the measurement. This latter error was partially corrected by assuming that all the oxygen and nitrogen found in the mass spectrographic analysis of the dissolved gas came from this air leak and not from a leak in transfer to the mass spectrometer. (Mass spectrographic analyses of dissolved gas from the gas solubility samples are listed in Section A2.4.)

The overall error in the gas solubility has been estimated at ± 30%. Fortunately, this large error did not affect the gas production rate analysis much, since most of the gas removed from the loop was via samples of undissolved gas and not through the dissolved gas in the liquid samples (see Section 4.9).

A summary of the data obtained is presented in Table 3.1.[1] As is evident from the table, there is considerable scatter in the data, but the data do indicate a greater gas solubility during the 610°F irradiation (range 3 to 9 x 10^{-3} (std. cc)/(gm coolant)(psia) over the course of the irradiation) than during the 750°F irradiation (range 1 to 4 x 10^{-3} (std. cc)/(gm coolant)(psia) over the course of the irradiation). These findings were consistent with the data reported by Atomics International (5.16), who reported a value of about 5 x 10^{-3} (std. cc)/(gm coolant)(psia) for OMRE coolant irradiated at 400 - 600°F.

---

1. In this report, the designation "1L" refers to liquid samples from the 610°F irradiation, and the designation "2L" refers to liquid samples from the 750°F irradiation.

TABLE 3. 1

Gas Solubility in Irradiated Santowax OMP Samples from the 610°F and 750°F Irradiations

Sample	w/o DP	Solubility, (std. cc)/(gm coolant)(psia) x 10^3
1L52	33	3
1L118	60	8
1L195	31	9
2L8	17	2
2L14	50	1
2L30	40	4
2L35	41	3
2L39	41	2

5. 8 Coolant Melting Point

As pointed out by Morgan and Mason (5. 1) the coolant melting point is a nebulous quantity due to the large range in melting points of the components comprising the irradiated Santowax OMP; for instance, pure o-terphenyl melts at 134°F and pure p-terphenyl at 416°F. Two melting points were defined:

1. The initial liquidus point, which is the temperature at which the first liquid drop appears.
2. The final liquidus point, which is the temperature at which the last crystal disappears.

These temperatures were measured visually using a Fisher-Johns apparatus (5. 1). The determinations were difficult to make because of the tarry black color of the samples; this is particularly true of the initial liquidus point. The data for the individual samples are tabulated in Section A3. 8.

The data obtained for the 610°F irradiation of Santowax OMP are shown in Fig. 5. 23, where the melting points are seen to decrease with increasing DP concentration. The data for the steady-state-HB periods appear to be lower than those of the transient periods for the same DP concentration, which is probably due to the buildup of the LIB fraction in the coolant.

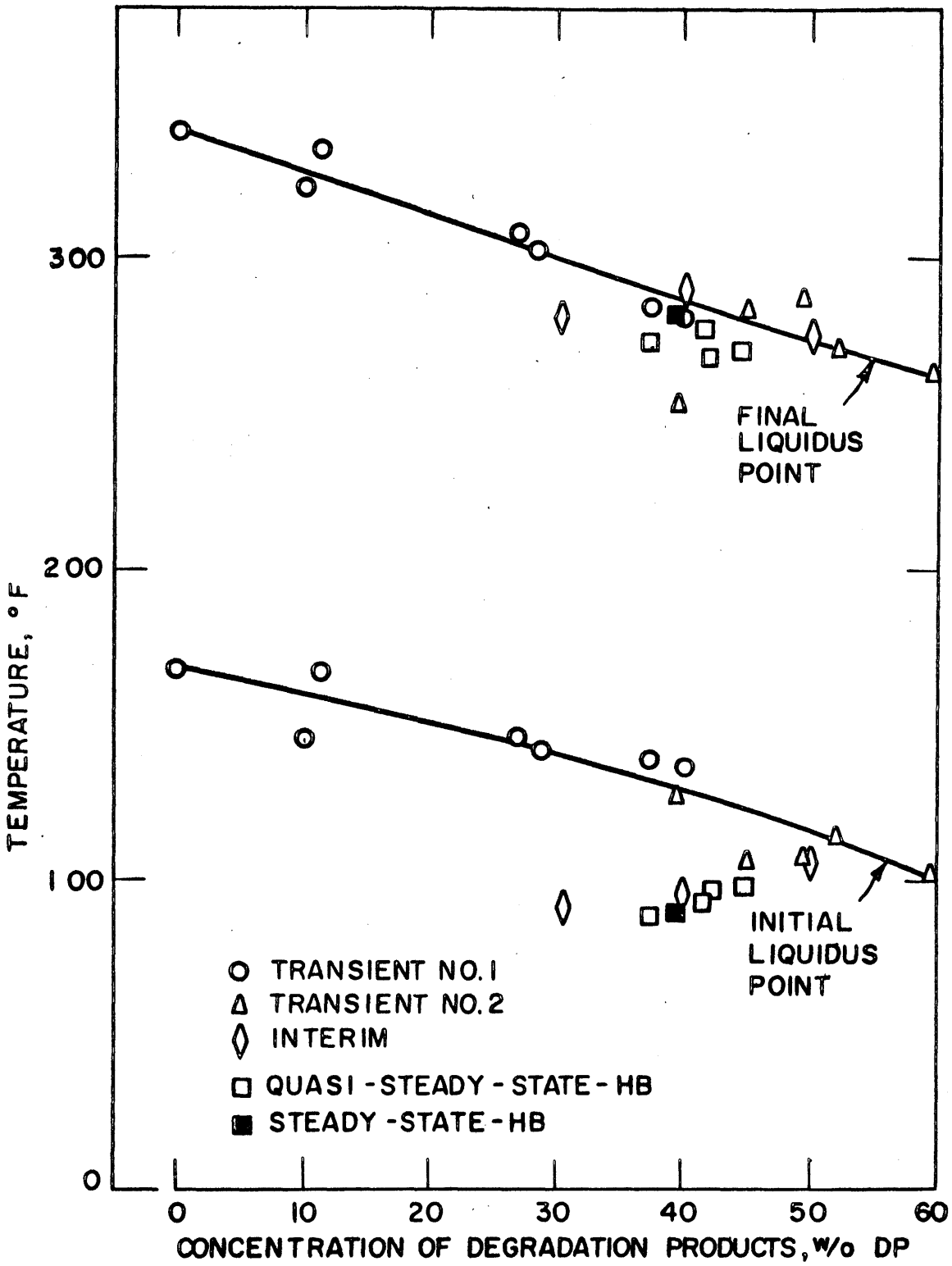

FIGURE 5.23 MELTING POINTS OF IRRADIATED SANTOWAX OMP DURING THE 610°F IRRADIATION

The data obtained for the 750°F irradiation are presented in Fig. 5.24. It may be seen that the melting points of the 750°F irradiation are lower than those of the 610°F irradiation. This is particularly true of the initial liquidus point, which reached room temperature around 40 w/o DP. All samples with a DP concentration of 40 w/o DP or more contained some liquid at room temperature.

5.9 Carbon-Hydrogen Content

Carbon-hydrogen content measurements on samples of irradiated Santowax OMP have been performed by the Monsanto Research Corporation (Everett, Mass.) using a standard combustion technique, and the results are said to be accurate to ± 0.5 w/o (5.1). A summary of the results for the 610°F and 750°F irradiations is presented in Table 5.2. A more detailed listing may be found in Section A3.9. For comparison, the carbon-hydrogen content of the pure terphenyls is 93.88 w/o carbon and 6.12 w/o hydrogen with a C/H ratio of 15.4.

TABLE 5.2

Carbon-Hydrogen Content of Irradiated Santowax OMP Samples from the 610°F and 750°F Irradiations

Sample No.	w/o DP	w/o Carbon	w/o Hydrogen	C/H Ratio
1L16	0.0	93.8	6.2	15.1
1L50	27.1	93.7	6.3	14.9
1L66	36.0	94.2	5.9	16.0
1L91	48.8	94.0	6.0	15.7
Average 610°F Steady-State-HB	39.0	94.2	6.1	15.5
2L1	0.0	93.9	6.1	15.4
Average 750°F Steady-State-HB	40.8	93.9	5.7	16.5

In view of the experimental accuracy and the lack of a definite trend of the data, it appears that no change in the carbon-hydrogen content occurred during the irradiation of Santowax OMP at both 610°F and

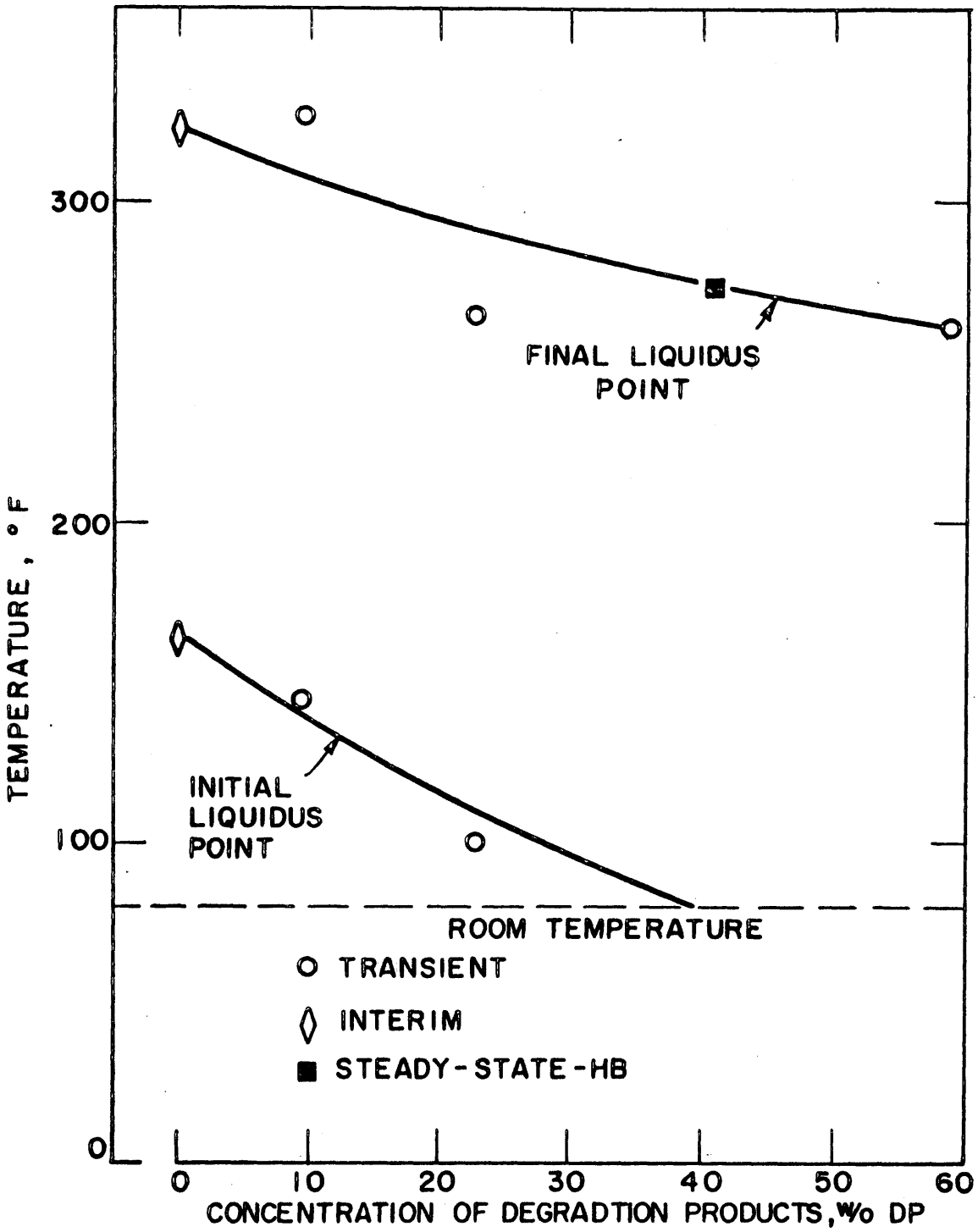

FIGURE 5.24 MELTING POINTS OF IRRADIATED SANTOWAX OMP DURING THE 750°F IRRADIATION

750°F. This result is not surprising, since the primary cause of a change in the C-H content would be the evolution of a substantial mass of gas having a widely different carbon-hydrogen content than that of the pure terphenyls. Since the weight of gas formed during the irradiations was less than 0. 5 w/o of the original coolant, the C/H ratio could not change greatly even if all the gas was hydrogen.

5. 10 Ash and Semi-Quantitative Emission Spectroscopy

Since it has been suggested that inorganic particulate matter in the coolant is responsible for the eventual fouling of heat transfer surfaces (5. 18), the ash or inorganic content of the irradiated coolant is of interest. The Monsanto Research Corporation (Dayton, Ohio) has performed ash analyses on five gram samples of irradiated Santowax OMP from the 610°F and 750°F irradiation. The residue of the ashing was subsequently analyzed by emission spectroscopy for individual components. A summary of the results of these analyses is given in Table 5. 3. A

TABLE 5. 3

Ash and Semi-Quantitative Emission Spectroscopy Analyses on Irradiated Santowax OMP Samples from the 610°F and 750°F Irradiations

Sample Number	Reactor MWH	Ash ppm	Concentration of Inorganic Material, ppm (by wt) Al	Cu	Fe	Mg	Mn	Mo	Na	Ni	Si
1L35	392	90	<2			<2		1-3			3-9
1L116	3839	15	2-4		2-7	<3	<3		<3		2-7
1L180	5785	20	3-8	3-8	3-8	<3	<3		3-9		9-28
1L269	10579	0	<2	2-5	<2	<2	<2			<2	2-5
2L5	253	20	2-5	2-5	3-8	2-6				2-5	5-15
2L22	2278	40	<3	<3	2-5	<3				<3	8-25
2L36	3445	20	<3	<3	3-9	<3				2-6	6-19

more detailed listing may be found in Section A3. 10.

The quantity of ash obtained was apparently quite sensitive to the ashing procedure used. The conditions used for the samples listed in

Table 5.3 are 1000°C for 90 minutes. Morgan and Mason (5.1) have reported results up to 1 w/o ash for 750°C for 3 minutes. Furthermore, it is believed that because of the small sample size (five grams), determinations to better than ± 100 ppm cannot be expected, so that the major conclusion to be drawn from the ashing analyses is that there seems to be no significant amount present.

The major inorganic constituents in the ash residue were found to be silicon (Si), iron (Fe), copper (Cu), aluminum (Al), magnesium (Mg) and nickel (Ni), all of which appear to be present in amounts < 10 ppm.

In connection with the study of fouling in the M.I.T. In-Pile Loop, analyses for iron (Fe), chloride (Cl) and water content of several samples from the 610°F irradiation of Santowax OMP have been performed at Chalk River, Ontario. The results of these analyses are tabulated in Section 6.4.1, where it is shown that the analyses yield

Fe	2 - 20 ppm
Cl	~3 ppm
Water	10 - 50 ppm

These trace amounts are consistent with the findings of the Monsanto Research Corporation and indicate that the coolant under irradiation was quite "clean."

5.11 Other Physical Measurements

Other physical measurements on the irradiated coolant were: ultraviolet (UV) and infrared (IR) transmission analyses (both performed by the Monsanto Research Corporation (Everett, Mass.); and mass spectrographic analyses on some liquid samples from the first transient phase of the 610°F irradiation (performed by the California Research Corporation, (Richmond, California).

The only distinguishing feature in the UV spectra for samples of irradiated and unirradiated coolant was a large peak at 370 mμ.

The IR analyses were performed over the range 2 - 15 μ, and many peaks were observed. Some changes in the spectra were noted as the irradiation progressed. A typical IR spectrum is shown in Fig. 5.25. At present no meaningful interpretation of these data has

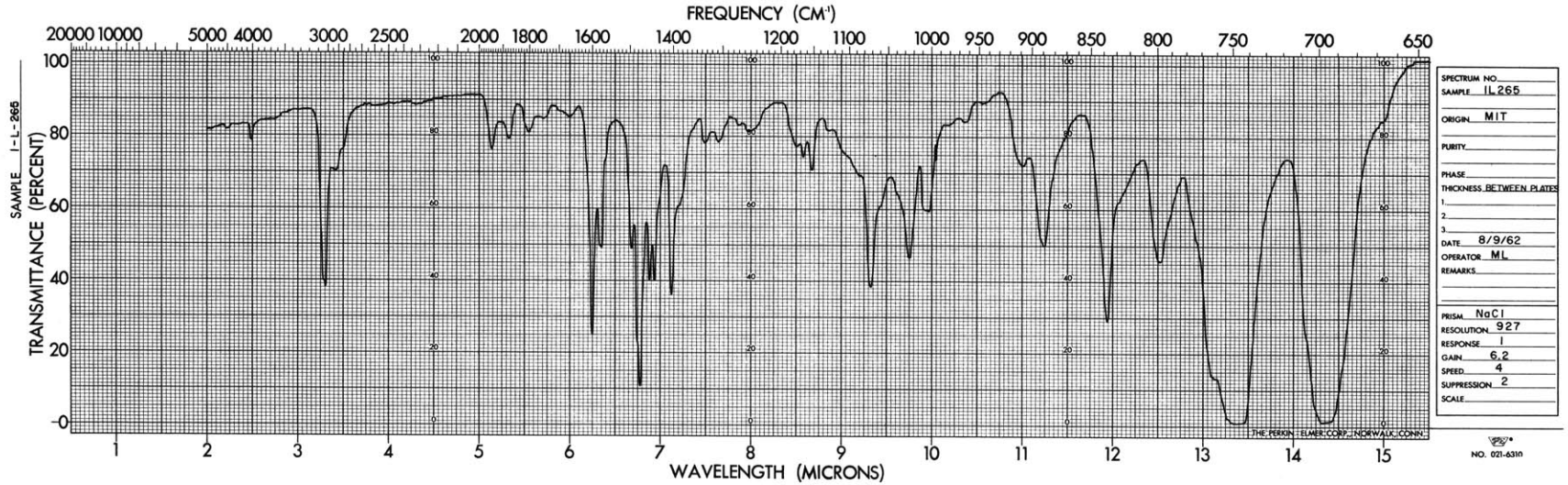

FIGURE 5.25 SAMPLE IR SPECTRUM OF IRRADIATED SANTOWAX OMP

been made, and it is doubted that much useful information will be obtained due to the complexity of the irradiated samples.

Mass spectrographic analyses on irradiated liquid samples yielded only qualitative information about the coolant composition. Molecular weights were assigned to the peaks reported, and suggestions were made as to the possible compounds in the coolant. In a qualitative way the analyses showed the buildup of aromatic linked compounds with irradiation up to nonaphenyl at the end of the first transient period of the 610^{o}F irradiation. The results were not found to be useful, and analyses were not performed after this period.

CHAPTER 6
HEAT TRANSFER MEASUREMENTS

6. 1 Introduction

The heat transfer properties of an irradiated coolant are important considerations in the use of organic liquids in nuclear reactor systems. Two test heaters, installed in the out-of-pile section of the M. I. T. loop, were used to measure the changes in heat transfer properties of Santowax OMP with irradiation during both the 610°F and 750°F irradiations. A complete description of the test heaters has been given by Morgan and Mason (6. 1). Briefly, the heat transfer measurements were performed in two 1/4 inch O. D. stainless steel tubes (wall thickness 0. 020 inches) with thermocouples spot welded to the outsides of the tubes. The tubes were heated by the passage of AC currents up to 450 amps along the test heater walls and heat transfer coefficients determined from the net electrical heat input and the difference between the wall temperatures and bulk liquid temperatures.

Correlations of the heat transfer data obtained with changes in physical properties of the irradiated Santowax OMP were performed; the data analysis and results obtained are reported in Sections 6. 2 and 6. 3.

During the latter half of the 750°F irradiation of Santowax OMP a fouling probe obtained from the AECL (Chalk River, Ontario) was installed in the out-of-pile section of the loop, and preliminary measurements have been performed with the probe. The results of this and other fouling tests are reported in Section 6. 4.

6. 2 Theory

Details of the theory behind the heat transfer measurements are given in Sections A4. 1 - A4. 5. A summary will be given here.

Thermocouples spot welded at intervals along a test heater tube were used to measure the outside wall temperature of the tube.

Immersion thermocouples inserted in mixing chambers at the upstream and downstream ends of a test heater served to measure the bulk liquid temperature. The outside wall thermocouples and the bulk thermocouples were read on a precision potentiometer. A typical temperature profile along the test heater is shown in Fig. 6.1.

The heat flux in the test heater being utilized was determined from the voltage drop in each half of the heater and the electrical resistance of the stainless steel tube which was known as a function of the temperature of the tube (6.1). Small corrections for heat losses from the tube were applied.

A turbine type flowmeter was used to measure the volumetric flow rate of the coolant through the test heater.

From the inside wall temperature, which was obtained by correcting the outer (measured) wall temperature for internal heat generation (and heat loss) in the tube (see Section A4.1) the total heat transfer coefficient from the inside surface of the wall to the bulk of the fluid was expressed as

$$U = \frac{Q_{in}}{A(\overline{T_W^I} - \overline{T_B})} \quad \frac{\text{Btu}}{(\text{hr})(\text{ft}^2)(^\circ\text{F})} \qquad (6.1)$$

where

Q_{in} is the heat transfer rate into the coolant, Btu/hr

A is the wall surface through which the heat flows, ft^2

$\overline{T_W^I}$ is the average temperature of the inside surface of the test heater wall, $^\circ\text{F}$

$\overline{T_B}$ is the average coolant bulk temperature, $^\circ\text{F}$.

If the heat transfer resistance due to scale on the test heater wall is small compared with the overall heat transfer resistance, U is equivalent to h_f, the film heat transfer coefficient. (This has indeed proven to be the case; see Section 6.4).

For a series of measurements in a given day, the physical properties (density, viscosity, specific heat and thermal conductivity) of the coolant were known (see Chapter 5 and Section A4.3), and with the

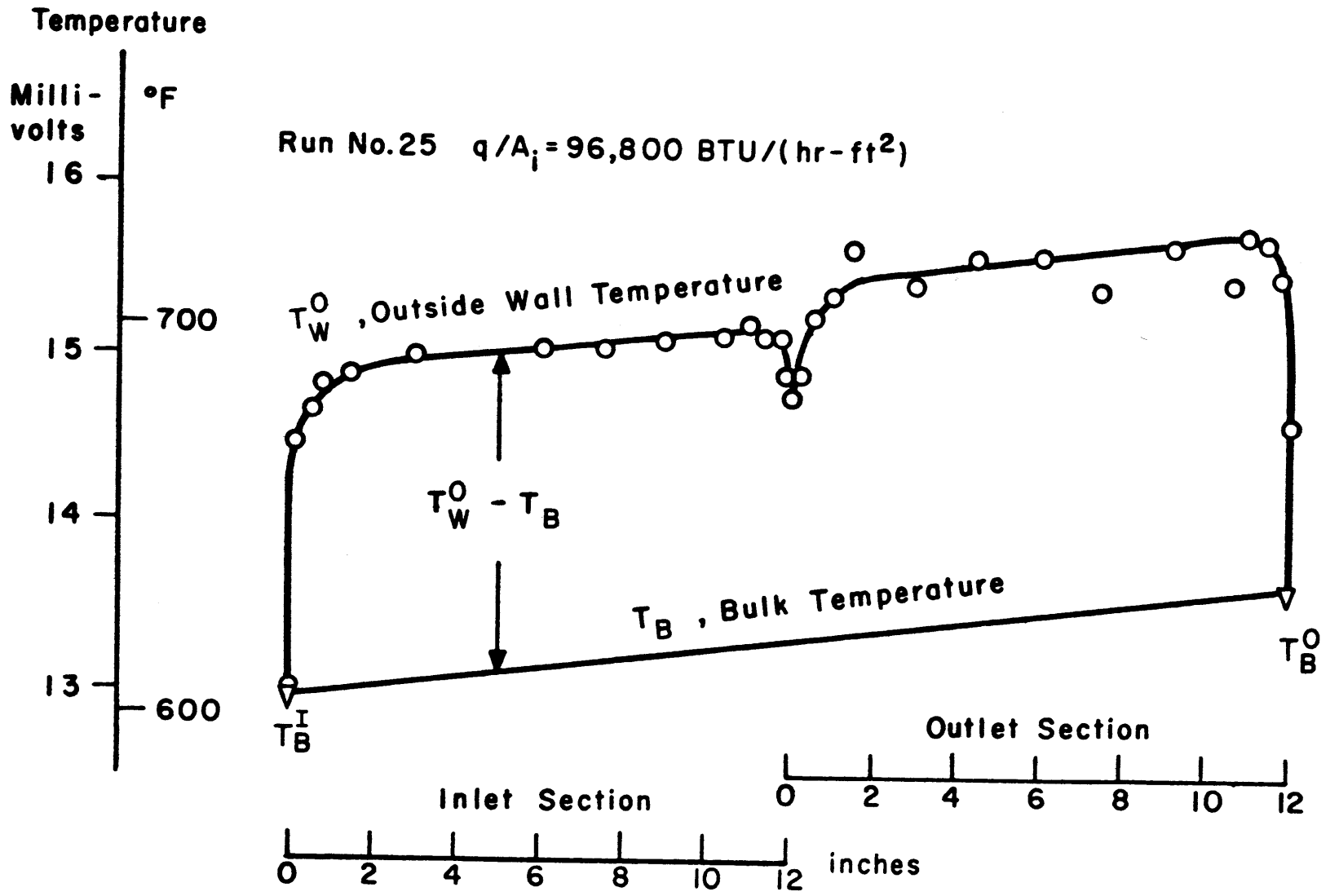

FIGURE 6.1 TYPICAL TEST HEATER TEMPERATURE PROFILE

knowledge of the coolant velocity, v, and the inside diameter of the test heater, D, the following dimensionless parameters were calculated:

1. Nusselt number $= Nu = \frac{UD}{k}$ (6.2)

2. Reynolds number $= Re = \frac{Dv\rho}{\mu}$ (6.3)

3. Prandtl number $= Pr = \frac{C_p \mu}{k}$ (6.4)

4. Viscosity Ratio $= \frac{\mu}{\mu_W}$ (6.5)

All physical properties except μ_W were evaluated at the coolant bulk temperature. μ_W is the viscosity of the coolant evaluated at the inside test heater surface temperature. The heat transfer data were correlated in terms of the dimensionless parameters described above by relations of the form

$$Nu = A(Re)^B (Pr)^C \left(\frac{\mu}{\mu_W}\right)^D \quad (6.6)$$

This type of relation has proved valuable in the correlation of heat transfer data (6.2, 6.3). Each of the constants A, B, C and D were determined from a least squares analysis of the data (see Section A4.4 for details). The least squares method allowed any of the constants (A, B, C or D) to be fixed at certain values and the remainder determined from the least squares analysis.

One of the methods used to determine the buildup of scale on the test heater walls is due to Wilson (6.1). The general relation between the overall heat transfer coefficient from test heater surface to bulk coolant and the film heat transfer coefficient is

$$\frac{1}{U} = \frac{1}{h_f} + R_S \quad (6.7)$$

where R_S is a scale resistance to heat transfer.
The film heat transfer coefficient is related to the fluid velocity by (6.2):

$$h_f = av^B \qquad (0.8 < B < 1.0) \quad (6.8)$$

where the constant "a" is dependent on the geometry of the system and the physical properties of the coolant. On a given day, heat transfer coefficients were determined at several velocities. Since the constant "a" did not vary over this short period of time, a plot of 1/U versus $1/v^B$ for the data of that day should be a straight line yielding R_S as an intercept. Various values of B were used, including the value obtained from a least squares analysis of Eq. (6.6). The results of these Wilson plots are reported in Section 6.4. Briefly, it was found that U could be replaced by h_f in Eq. (6.2) within the accuracy to which these determinations of R_S could be made. This indicates that the amount of resistance to heat transfer due to scale buildup was insignificant over the period of the two irradiations at 610°F and 750°F.

6.3 Results

6.3.1 M.I.T. Results

The ranges of variation of the major variables associated with the heat transfer data obtained during the 610°F and 750°F irradiations of Santowax OMP are given in Tables 6.1 and 6.2 respectively. The more restricted range on the variables for the 750°F irradiation data was a result of the higher bulk temperature of the coolant and the desire to keep the maximum wall temperature under 900°F. A more detailed listing of the heat transfer data may be found in Section A4.6.

The heat transfer data from the two irradiations were subdivided into several categories. All the data obtained during the 610°F irradiation of Santowax OMP were placed in category 1. These data were also divided into three further categories. Category 2 data were data obtained during the 610°F irradiation using test heater no. 5 (TH5) at a nominal heat flux of 2×10^5 Btu/(hr)(ft^2) Category 3 data were data obtained during the 610°F irradiation using TH5 at a nominal heat flux of 10^5 Btu/(hr)(ft^2). Category 4 data were obtained during the 610°F irradiation using TH6 at a nominal heat flux of 10^5 Btu/(hr)(ft^2).

All the data obtained from TH6 during the 750°F irradiation of Santowax OMP at a nominal heat flux of 1.3×10^5 Btu/(hr)(ft^2) were placed in category 5. Some of these data were obtained from a special run at a constant velocity and a variation in bulk temperature to provide

TABLE 6.1

Range of Variation of Major Heat Transfer Variables
During the 610°F Irradiation of Santowax OMP

Variable	Range
Heat Flux, Q/A	2×10^4-2×10^5 Btu/(hr)(ft^2)
Velocity, v	5-25 ft/sec
Heat Transfer Coefficient, U	340-2400 Btu/(hr)(ft^2)(°F)
Nusselt No., Nu	80-650
Reynolds No., Re	8×10^3-10^5
Prandtl No., Pr	7-32
Viscosity Ratio, μ/μ_W	1.2-2.5

TABLE 6.2

Range of Variation of Major Heat Transfer Variables
During the 750°F Irradiation of Santowax OMP

Variable	Range
Heat Flux, Q/A	4×10^4-1.5×10^5 Btu/(hr)(ft^2)
Velocity, v	9-22 ft/sec
Heat Transfer Coefficient, U	550-2000 Btu/(hr)(ft^2)(°F)
Nusselt No., Nu	150-570
Reynolds No., Re	2×10^4-10^5
Prandtl No., Pr	6-19
Viscosity Ratio, μ/μ_W	1.2-1.9

a variation in the dimensionless parameters. These special data, run with a nominal heat flux of 1.3×10^5 Btu/(hr)(ft^2), were also placed in category 6. Category 7 contains further special runs during the 750°F irradiation at a constant velocity with a nominal heat flux of 4.5×10^4 Btu/(hr)(ft^2).

The first analyses were performed using Eq. (6.6) in two forms:

1. $Nu = A(Re)^B (Pr)^C$ [Dittus-Boelter type (6.3)]
2. $Nu = A(Re)^B (Pr)^C (\mu/\mu_W)^D$ [Sieder-Tate type (6.2)]

with all constants to be determined from a least squares analysis of the data. The results of these analyses are shown in Table 6.3. The exponent on the Reynolds number using a least squares analysis for A, B and C on the Dittus-Boelter type relation was higher than the normally used 0.8 value reported in the literature (6.2, 6.3), and so least squares analyses were performed on the Sieder-Tate type relation to see if the viscosity effect (μ/μ_W) would lower the exponential dependence on the Reynolds number. The results tabulated in Table 6.3 show that the inclusion of this term only served to raise the magnitude of the exponential dependence on the Reynolds number. From a statistical analysis of the fit to the data, the power D had errors-of-fit alone of the order of 100%. Because of this error and two other facts -- the viscosity data had to be extrapolated to the wall temperatures (800 - 900°F) and the range on the variable (μ/μ_W) was much less than on the other dimensionless variables studied -- it was felt that the Dittus-Boelter type correlation gave a better representation of the data.

Based on the fits of the data to the Dittus-Boelter type correlation reported in Table 6.3, a Reynolds number power dependence of 0.9 was chosen as the "best" value to characterize all the data. To obtain the "best" value of the Prandtl number power dependence, C, the power, B, was fixed at 0.9 and a least squares analysis performed on the relation $Nu = A(Re)^{0.9} (Pr)^C$. The results of these analyses are given in Table 6.4. On the basis of these results a Prandtl number power dependence of 0.4 was chosen as the "best" value for all the data.

Thus, all data were characterized by an equation of the form

TABLE 6.3

Least Squares Analysis of Heat Transfer Data Using the Correlation $Nu = A(Re)^B(Pr)^C(\mu/\mu_W)^D$

Category	Irradiation Temperature °F	Test Heater	Nominal Heat Flux Btu/(hr)(ft^2)	$Nu = A(Re)^B(Pr)^C$			$Nu = A(Re)^B(Pr)^C(\mu/\mu_W)^D$			
				A	B	C	A	B	C	D
1	610	TH5+TH6	10^5-2 x 10^5	0.0068	0.93	0.37	0.0037	0.97	0.40	0.19
2	610	TH5	2 x 10^5	0.0029	0.98	0.48	0.13	0.69	0.35	−0.76
3	610	TH5	10^5	0.0053	0.93	0.45	0.0055	0.93	0.45	−0.008
4	610	TH6	10^5	0.0074	0.89	0.45	0.0037	0.95	0.47	0.20
5	750	TH6	1.3 x 10^5	0.0073	0.90	0.41	0.0058	0.92	0.41	0.08
6[a]	750	TH6	1.3 x 10^5	0.0072	0.88	0.51	0.0057	0.90	0.51	0.07
7[a]	750	TH6	4.5 x 10^5	0.012	0.86	0.30	0.0079	0.90	0.31	0.19

a. Special runs with constant velocity and varying bulk temperature.

TABLE 6.4

Least Squares Analysis of Heat Transfer Data
Using the Correlation $Nu = A(Re)^{0.9}(Pr)^{C}$

Category	Irradiation Temperature °F	Test Heater	Nominal Heat Flux Btu/(hr)(ft^2)	$Nu = A(Re)^{0.9}(Pr)^{C}$	
				A	C
1	610	TH5+TH6	10^5-2 x 10^5	0.0096	0.34
2	610	TH5	2 x 10^5	0.0093	0.37
3	610	TH5	10^5	0.0081	0.41
4	610	TH6	10^5	0.0069	0.45
5	750	TH6	1.3 x 10^5	0.0071	0.41
6[a]	750	TH6	1.3 x 10^5	0.0053	0.54
7[a]	750	TH6	4.5 x 10^5	0.0074	0.34

a. Special runs with constant velocity and varying bulk temperature.

$$Nu = A(Re)^{0.9} (Pr)^{0.4} \quad (6.9)$$

Comparison of the various categories of data with each other has been postponed until this point, as the constant A may now be used as a direct measure of comparison. The value of A depends strongly on the values of the powers B and C used, and so the values of A obtained while B and C were being least squared could not give as meaningful a comparison of the data. Table 6.5 presents the results of correlations using Eq (6.9) and also the results of correlations using the Dittus-Boelter relation (6.3):

$$Nu = A(Re)^{0.8} (Pr)^{0.4} \quad (6.10)$$

It can be seen that in all cases but one, the preferred fit on the basis of the root-mean-square deviation of the data points from the correlation would be given by Eq. (6.9).

Figure 6.2 shows graphically the results of Table 6.5 for all the data of the 610°F irradiation of Santowax OMP (category 1). It can be seen that a 0.9 Reynolds number power dependence is preferred to a 0.8 power dependence but that the correlation obtained with the 0.8 power dependence still has a maximum deviation of 20% from the dependence data over the range studied. The value of 0.023 obtained for this 0.8 power dependence agrees very well with the literature (6.2, 6.3). The effect of the heat flux, Q/A, on the heat transfer rate is compared graphically in Fig. 6.3 for measurements using TH5 during the 610°F irradiation of Santowax OMP at nominal heat fluxes of 2×10^5 and 10^5 Btu/(hr)(ft^2) (categories 2 and 3 in Table 6.5) Morgan and Mason (6.1) have pointed out that consistent errors in the measurement of heat transfer coefficients amount to about ± 10% for heat fluxes above 10^5 Btu/(hr)(ft^2). These errors would not be taken into account by the RMS errors quoted in Table 6.5, which assume only random errors in the data. However, based on the RMS errors alone, it can be stated that no effect of Q/A on the data of the 610°F irradiation was observed.

The data obtained by TH6 for the 610°F irradiation of Santowax OMP (category 4) are shown graphically in Fig. 6.4. The correlation obtained agreed with those obtained with TH5 within the errors set by Morgan and Mason.

TABLE 6.5

Least Squares Analysis of Heat Transfer Data Using the Correlations $Nu = A(Re)^{0.9}(Pr)^{0.4}$ and $Nu = A(Re)^{0.8}(Pr)^{0.4}$

Category	Irradiation Temperature °F	Test Heater	Nominal Heat Flux Btu/(hr)(ft^2)	$Nu = A(Re)^{0.9}(Pr)^{0.4}$		$Nu = A(Re)^{0.8}(Pr)^{0.4}$	
				A	RMS Error, %[a]	A	RMS Error, %
1	610	TH5+TH6	10^5-2 x 10^5	0.0081	5.0	0.023	8.2
2	610	TH5	2 x 10^5	0.0086	2.8	0.025	5.2
3	610	TH5	10^5	0.0084	2.1	0.024	4.7
4	610	TH6	10^5	0.0079	4.3	0.021	5.2
5	750	TH6	1.3 x 10^5	0.0073	3.6	0.021	5.0
6[b]	750	TH6	1.3 x 10^5	0.0074	2.8	0.021	2.1
7[b]	750	TH6	4.5 x 10^4	0.0063	1.5	0.017	2.5

a. Root-mean-square deviation of data points from assumed correlation.

b. Special runs with constant velocity and varying bulk temperature.

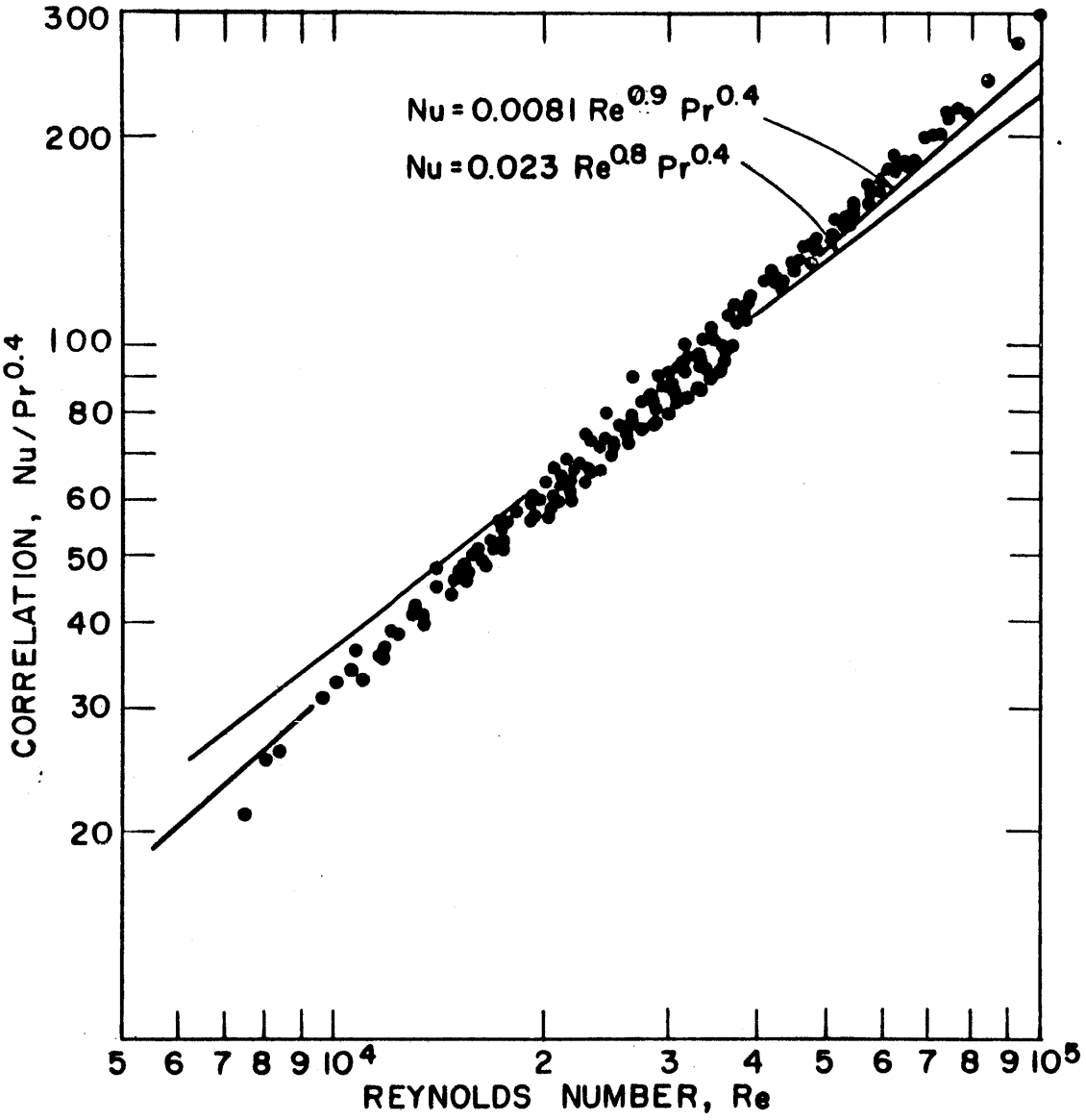

FIGURE 6.2 ALL HEAT TRANSFER DATA FOR SANTOWAX OMP IRRADIATED AT 610°F

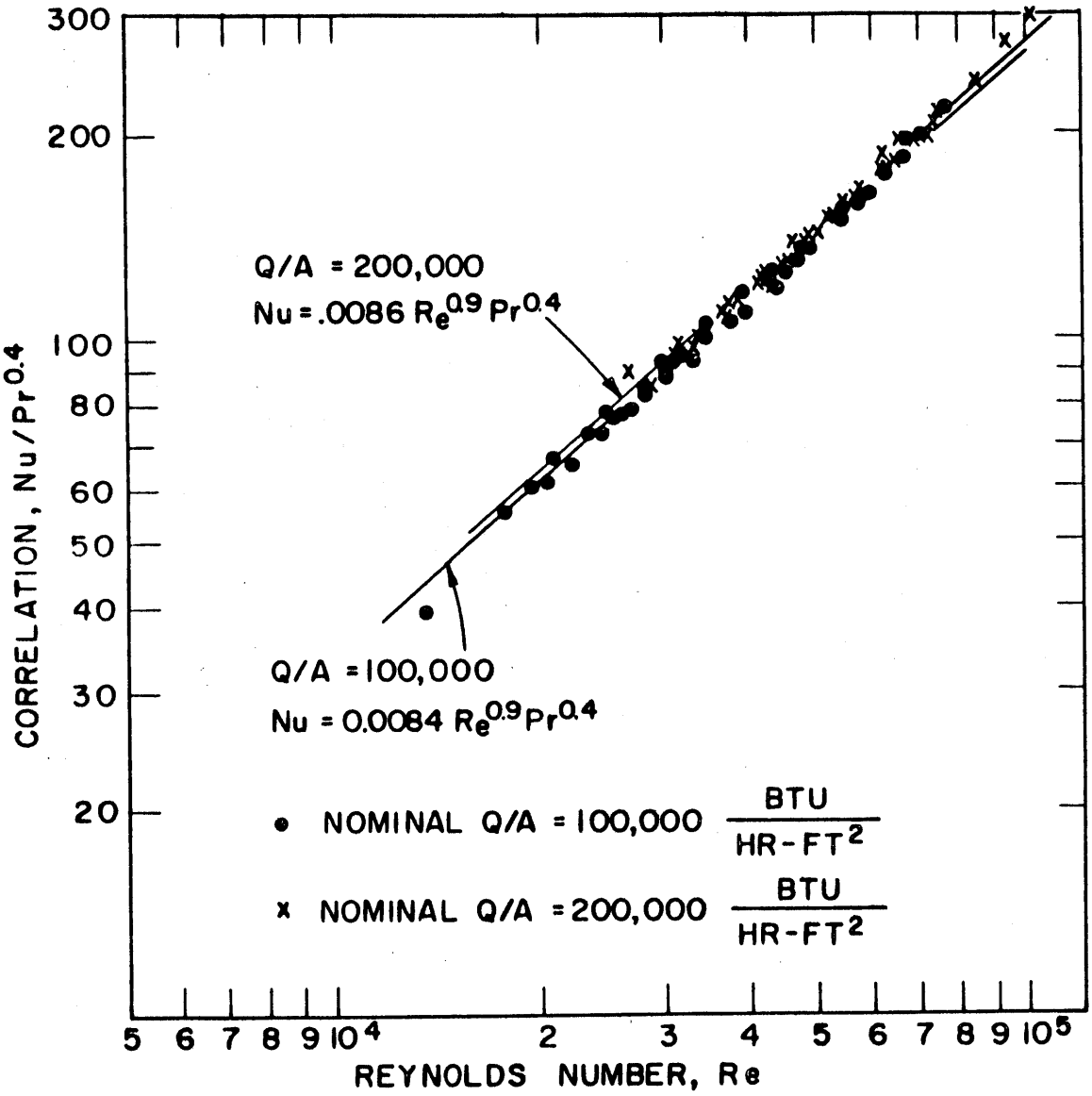

FIGURE 6.3 TH5 DATA FOR SANTOWAX OMP IRRADIATED AT 610°F

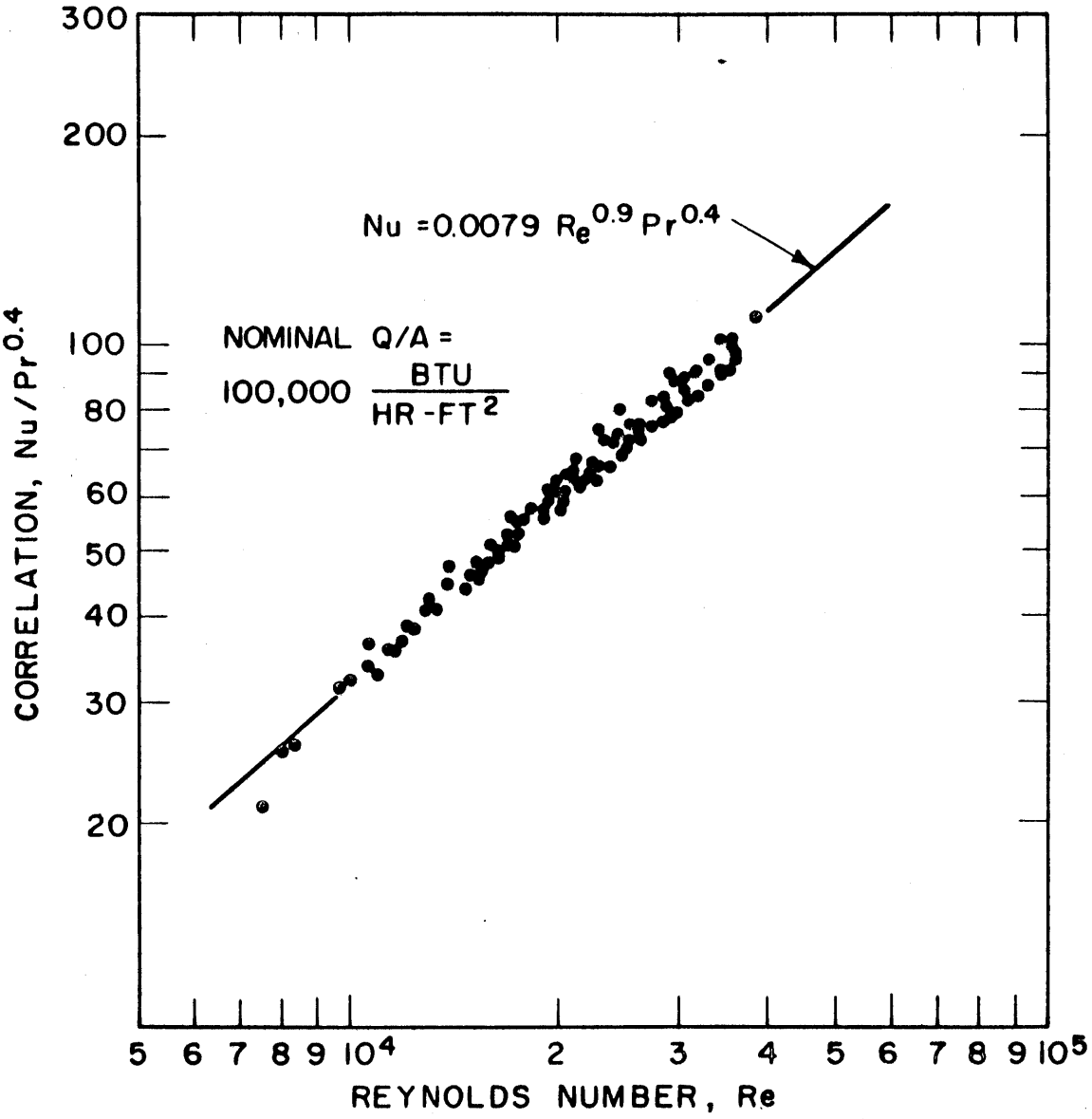

FIGURE 6.4 TH6 DATA FOR SANTOWAX OMP IRRADIATED AT 610°F

The correlations obtained for the 750°F irradiation Santowax OMP data (categories 5 and 7) are shown in Fig. 6.5. The data obtained at a nominal heat flux of 1.3×10^5 Btu/(hr)(ft^2) agreed both with the overall correlation obtained for the 610°F irradiation data (category 1) and with the data obtained just using TH6 during the 610°F irradiation (category 4) within the possible error limits set by Morgan and Mason. The apparently lower value of A obtained for the 750°F data can be explained by the fact that the calibration data, originally obtained only for a bulk coolant temperature of near 600°F, had to be extrapolated for the 750°F irradiation data.

As the heat flux is lowered below 10^5 Btu/(hr)(ft^2) consistent errors in the calibration of the test heater thermocouples, in the calculation of outside to inside wall temperature and in the measured heat losses become much more important. The correlations obtained with a heat flux of 4.5×10^4 Btu/(hr)(ft^2) during the 750°F irradiation differ from the other correlations obtained by as much as 20% and it is felt that the increase in importance of the possible consistent errors was responsible for this discrepancy.

In summary, the recommended correlation for heat transfer studies based on all of the data obtained for both irradiations of Santowax OMP is

$$Nu = 0.0079\ (Re)^{0.9}\ (Pr)^{0.4} \pm 10\% \qquad (6.11)$$

6.3.2 Comparison with Other Work

It has been mentioned above that the 0.9 Reynolds number power dependence observed in this work is somewhat higher than the 0.8 power dependence predicted by the correlation of Dittus and Boelter (6.3). Other recent work on organic fluids has also indicated a Reynolds number power dependence greater than 0.8 (6.4, 6.5, 6.6).

Stone et al. (6.4) have reported the results of heat transfer measurements on biphenyl, isopropylbiphenyl (unirradiated and about 40 w/o HB), a mixture of ortho-terphenyl, meta-terphenyl and biphenyl (unirradiated and about 30 w/o HB) and two aliphatic compounds The measurements were made with bulk liquid temperatures of 200 to 600°F, heat fluxes of 4×10^4 to 3×10^5 Btu/(hr)(ft^2) and a Reynolds number range of 1.2×10^4 to 4×10^5. Their best correlation was given by

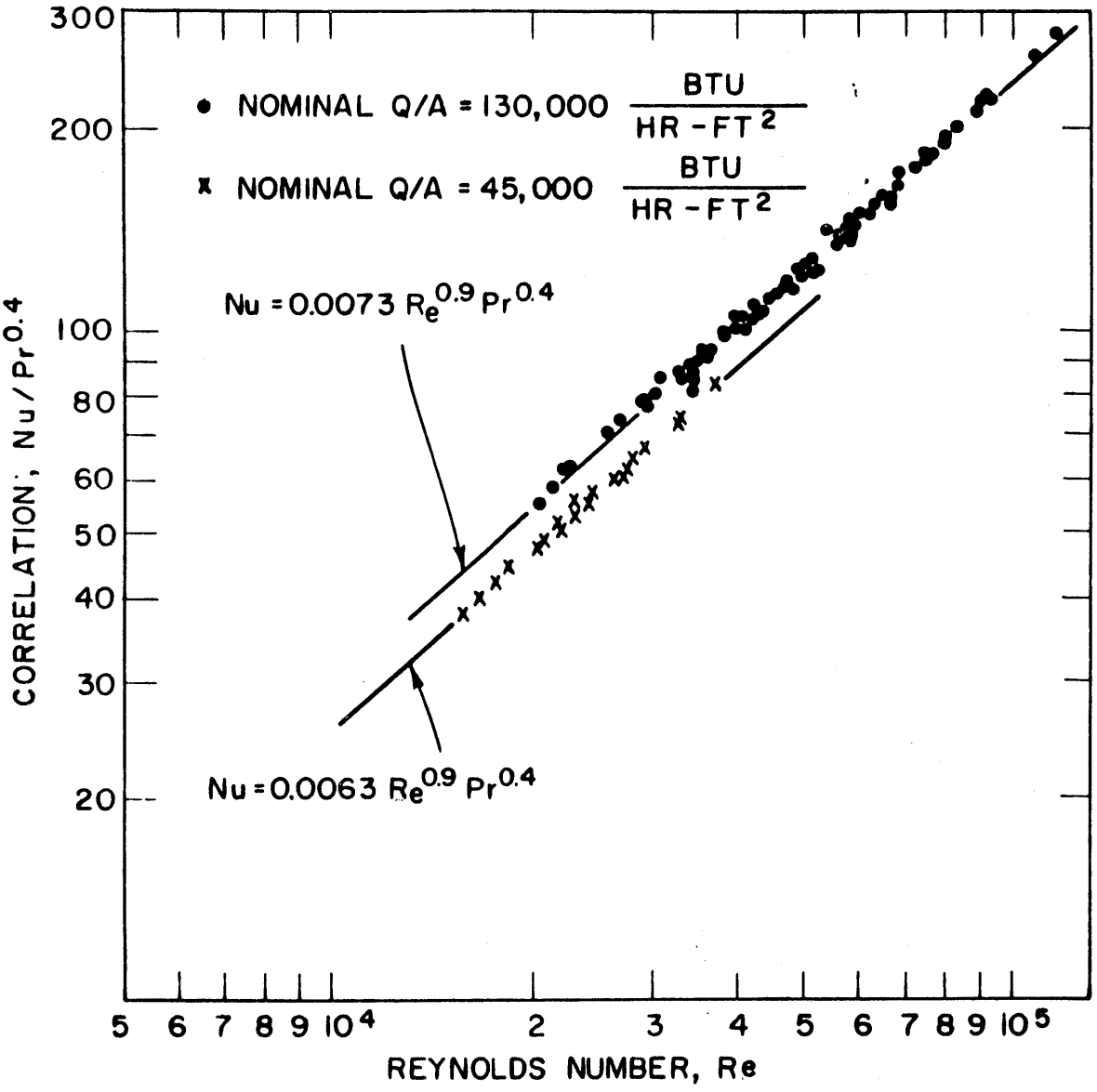

FIGURE 6.5 TH6 DATA FOR SANTOWAX OMP IRRADIATED AT 750° F

$Nu = 0.0175\ (Re)^{0.84}\ (Pr)^{0.4} \pm 5.5\%$, and the correlation is compared with that of the present work in Fig. 6.6. Their results are about 20% higher at a Reynolds number of 10^4 and about 10% higher at a Reynolds number of 10^5 than the correlation obtained in the present work.

Stone et al. also report another interesting aspect of their work. Using the irradiated terphenyl-biphenyl mixture, they increased the temperature difference between the heater wall and the bulk fluid from 78°F to 322°F by increasing the heat flux and noticed no change in the film heat transfer coefficient. The Sieder-Tate type of relation [using (μ/μ_W)] would have predicted an 11% increase in the heat transfer coefficient.

Bessouat et al. (6.5) have reported the results of heat transfer measurements on unirradiated Santowax OMP and Santowax OM (unirradiated and containing 24 w/o HB). The measurements were made with bulk liquid temperatures of 550 to 770°F, heat fluxes of 1.5 to 3×10^5 Btu/(hr)(ft^2) and a Reynolds number range of 7.5×10^4 to 4×10^5. Their best correlation was given by $Nu = 0.0098\ (Re)^{0.88}\ (Pr)^{0.4} \pm 6\%$ and is compared with that of the present work in Fig. 6.6. At a Reynolds number of 10^5 their correlation is lower than that of the present work by only 2%. If their correlation were extrapolated to a Reynolds number of 10^4, it would agree almost exactly with the one obtained in the present work.

Silverberg and Huber (6.6) report the results of heat transfer measurements on biphenyl, Santowax R and Santowax OM. Measurements were made with bulk liquid temperatures of 480 to 770°F, heat fluxes of 4×10^4 to 3×10^5 Btu/(hr)(ft^2) and a Reynolds number range of 2×10^4 to 3×10^5. Their best correlation was given as $Nu = 0.015(Re)^{0.85}\ (Pr)^{0.3} \pm 9\%$ Since the exponent on the Prandtl number differed from the one used in this work, the results of the present work were least squared with the following type of equation to compare the results with those of Silverberg and Huber:

$$Nu = A(Re)^{0.85}\ (Pr)^{0.3} \qquad (6.12)$$

The "best" value of A obtained by this procedure for all the data obtained during both irradiations of Santowax OMP was 0.017, some 12% higher than that obtained by Silverberg and Huber, but within the possible errors in both correlations.

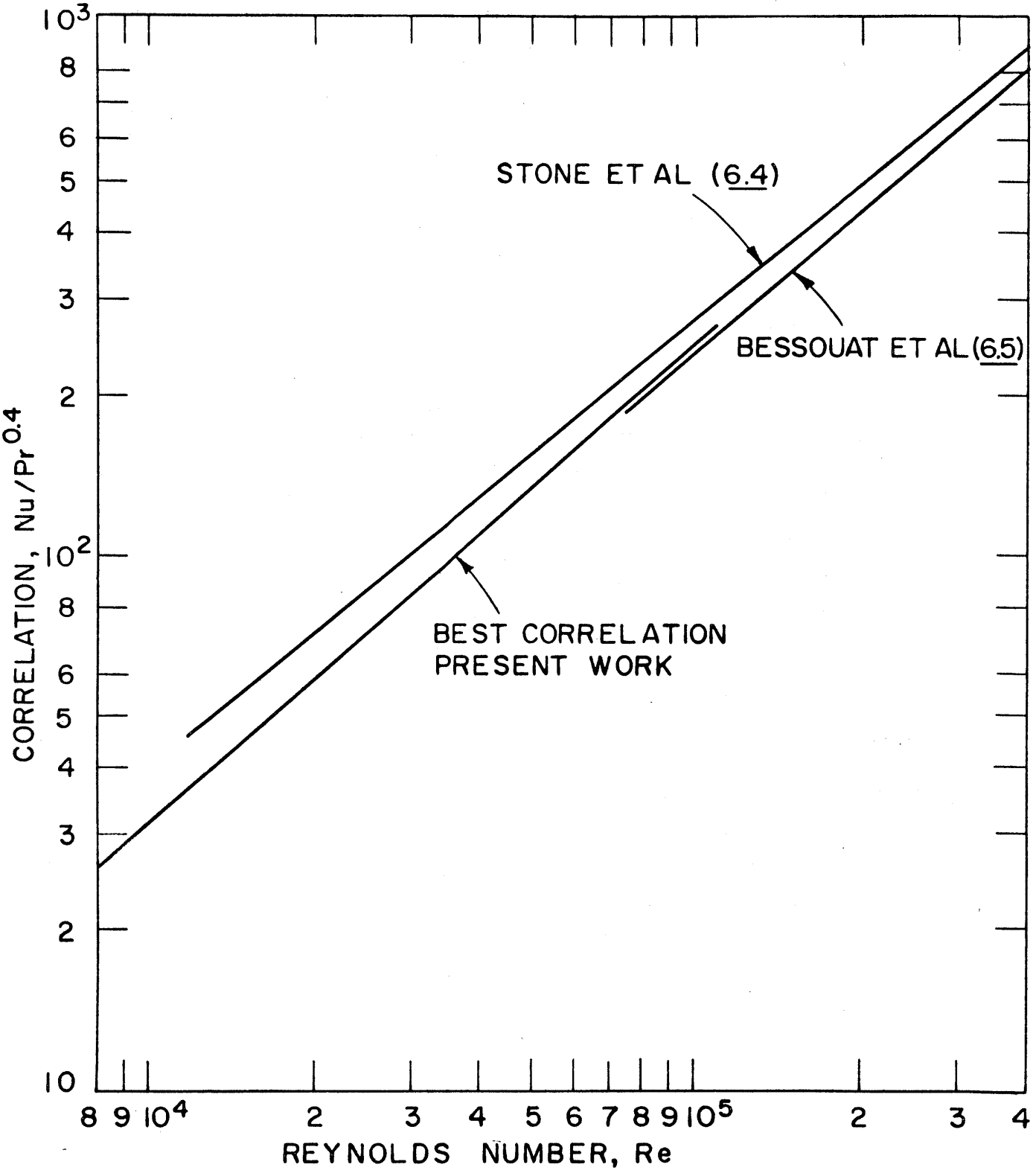

FIGURE 6.6 COMPARISON OF HEAT TRANSFER CORRELATIONS

Thus, the results obtained at M. I. T. were found to generally agree with those obtained by other investigators of polyphenyl coolants.

6.4 Fouling Studies

6.4.1 Introduction

In addition to the heat transfer properties of an organic coolant, a major consideration in the selection of such a coolant is the extent to which it fouls, or forms scale on the high temperature surfaces.

Previous investigators have noted gradual fouling of heat transfer surfaces in organic reactors and in organic loops (6.7, 6.8). However, it is generally agreed that the impurities in the coolant are prime factors in causing scaling or fouling of heat transfer surfaces (6.7). To eliminate this cause of fouling considerable effort was made to maintain the coolant purity in the MITR in-pile loop. All materials charged and used for makeup in the loop were vacuum distilled in glass equipment in the laboratory. After distillation, atmospheric contamination of the charge and makeup material was minimized by keeping the material blanketed with high-purity nitrogen whenever in the liquid state, and by keeping the material tightly stoppered at other times. The loop itself is an all stainless steel system with bellows seal valves and with two sintered stainless steel filters provided in the loop main stream to keep the organic material clean after charging it to the loop. One filter has a mean pore opening of 165 microns and a 98% removal rating of 55 microns. The other filter has a mean pore opening of 5 microns and a 98% removal rating of 2 microns. The fine filter was used only at the start of an irradiation and the coarse filter was used continually during normal operation.

Activation of the coolant in the loop was very low, about 0.05 microcuries/gm. Gamma ray spectrometry indicated the contaminants to be primarily Mn^{56} and Na^{24}. Total ash and X-ray emission spectroscopy analyses were performed by the Monsanto Research Corporation (Dayton, Ohio) on several liquid samples taken from both the 610°F and 750°F irradiations of Santowax OMP. These analyses indicated the ash content to be on the order of 20 ppm total of aluminum, copper, iron, magnesium, manganese, sodium, nickel and silicon (see Section 5.10

for more details of these analyses). Analyses for water, iron and chloride were performed by the AECL at Chalk River, Ontario (6.9, 6.10), and the results are reported in Table 6.6. Three samples of the irradiated coolant were run in a special out-of-pile fouling test loop at Chalk River (6.9) before the analytic determinations were made. Results of fouling rates observed will be discussed in Section 6.4.2 below together with preliminary measurements made at M.I.T. using a fouling probe obtained from the AECL. These results corroborate the findings by the Monsanto Research Corporation and indicate that the coolant in the MITR in-pile loop was quite "clean."

Operating procedures were separated into three distinct portions. The major portion (more than 60%) of the operating time was spent in maintaining the irradiation temperature in the in-pile capsule of the loop, and during this period the test heater was used continuously as a heat source. Heat fluxes were at about 8×10^4 Btu/(hr)(ft^2) for the 610°F irradiation and about 1.2×10^5 Btu/(hr)(ft^2) for the 750°F irradiation. The fluid was pumped at maximum velocity (about 20 ft/sec). Under these conditions the average wall temperature on the test heater was about 700°F for the 610°F irradiation and about 850°F for the 750°F irradiation. On weekends, when the reactor was shut down, the test heater was shut off and the loop temperature lowered to about 450°F. About 35% of the total operating time was spent at this low temperature.

A third set of conditions existed when heat transfer measurements were being made. The range of conditions for these measurements has been given in Tables 6.1 and 6.2. Less than 5% of the total operating time was spent in making heat transfer measurements. At the low velocities and high heat fluxes one or two wall thermocouples registered temperatures of 900°F for approximately 20 minutes per week (measurements were normally performed weekly).

The precautions taken at M.I.T. to keep a clean coolant have resulted in the operation of the loop for 14 months at an irradiation temperature of 610°F and for five months at an irradiation temperature of 750°F with no evidence of fouling of the test heater surface.

TABLE 6. 6

AECL Inorganic Content Analyses on Samples of Irradiated Santowax OMP from the 610°F and 750°F Irradiations

Sample Number	Reactor MWH Exposure[a]	Inorganic Content, ppm by wt.		
		H_2O	Fe	Cl
1L121[b]	3999		2. 5	3. 1
1L123	4083			
1L131[b]	4379	~10	2. 5	2. 7
1L275	11538	19		
1L278	11538	54	4. 5	
2L0	0	22	20	
2L5	253	46	6	

a. The MITR normally operates at a power level of 2 MW.

b. Samples run in a special fouling test loop before analysis (6. 9).

6.4.2 Fouling Probe Work

During the 750°F irradiation of Santowax OMP, a fouling probe was obtained from the AECL, Chalk River, Ontario, and was incorporated into the out-of-pile section of the loop. The fouling probe was installed in a by-pass line parallel to the liquid sampling position, and this by-pass line was equipped with a turbine-type flowmeter similar to the one used to measure the main loop flow rate.

A photograph of the fouling probe is shown in Fig. 6.7. The test section of the probe consists of a three inch long piece of type 316 stainless steel tubing (1/16 inch O.D. x 0.006 inch wall) which is heated by the passage of A.C. currents up to 50 amp (at 6 volts) along the tube wall.

The test section is cooled by the flow of organic coolant in the annular region between the outside wall of the tube and the inside wall of the probe assembly. This annular region (1/16 inch I.D. x 3/16 inch O.D.) allows coolant flow rates up to 10 ft/sec. The fouling probe assembly consists of a heavy-walled tube made from a piece of hexagonal stainless steel stock (one inch x six inches long) which has an axial 3/16 inch hole bored through it to receive the test section and which is machined to receive Autoclave[1] seals at both electrodes.

The high voltage electrode is sealed with a combination Autoclave-Conax[2] fitting and has a 1/16 inch I.D. hole for the insertion of a test section thermocouple. This stainless steel clad thermocouple is 0.027 inch O.D. and is used to measure the temperature profile of the inside wall of the test section tube and to monitor the maximum temperature during a fouling probe run.

The grounded electrode is sealed with a combination Autoclave fitting and Teflon packed seal. While the test section is being heated, a spring on the ground electrode provides approximately five pounds of tension to prevent the test section from bowing and grounding out to the 3/16 inch outer diameter of the annulus.

A preliminary run with the fouling probe was made over a 78 hour period from March 26, 1963, to March 29, 1963. (This was during the steady-state-HB period of the 750°F irradiation of Santowax OMP.)

---

1. Autoclave Engineers Sales Corporation, Erie, Penn.
2. Conax Corporation, Buffalo, New York.

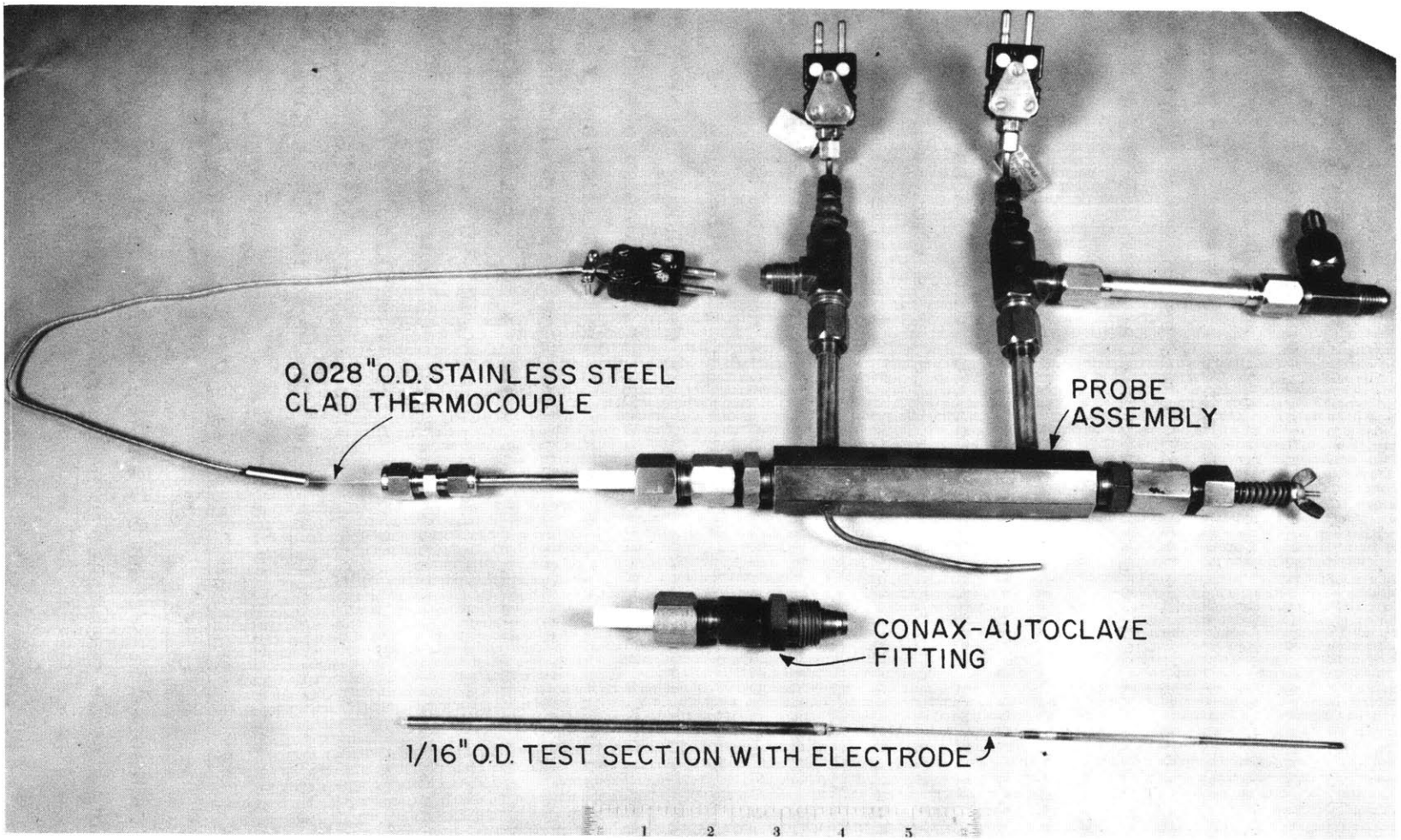

FIGURE 6.7 AECL FOULING PROBE

Figure 6.8 shows the temperature profile of the inside tube wall of the test section for this run. The temperature was quite level at about 895°F except near the ends of the test section where the wall temperature rapidly approached the coolant bulk temperature of 730°F. The maximum temperature of the inner wall was maintained constant at 895 ± 5°F throughout this run by varying the power input, and the coolant flow by the outer wall of the test section was kept constant at 7.5 ft/sec. The temperature drop through the wall of the test section was estimated at about 5°F, so that the wall exposed to coolant was kept at about 890°F for the duration of the run.

At the end of the run, the fouling probe was taken from the loop and the center inch of the test section removed, carefully cleaned with tetrahydrofuran and weighed on a precision balance. A hard, dull-edged knife was used to scrape the weighed test section, which was then weighed again on the precision balance. The total amount removed in the scraping performed on the preliminary run was 0.5 milligrams out of a total test section weight of about 250 milligrams. Because of the lack of experience in scraping the test section, it is not known how much stainless steel was removed along with the scale, and techniques are currently being developed to improve the precision of the method. Bancroft (6.9) has suggested that a good method of estimating the amount of stainless steel removed in the scraping is to scrape the test section several times to get a "background" removal of stainless steel. The preliminary result would indicate a scale buildup rate of about 3×10^{-6} grams/(cm^2)(hr); no error limits have been assigned to this result since the reproducibility of the scraping technique has not yet been demonstrated. However, the result does appear high, in view of two careful fouling probe measurements performed at Chalk River on samples of irradiated Santowax OMP from the 610°F irradiation (6.9). The results of the Chalk River determinations are summarized in Table 6.7.

6.4.3 Wilson Plot and Other Tests for Scale Formation on Test Heater Surfaces

As mentioned in Section 6.2 above, the Wilson plot method for determining a scale resistance to heat transfer makes use of the following relations:

$$\frac{1}{U} = \frac{1}{h_f} + R_S \qquad (6.13)$$

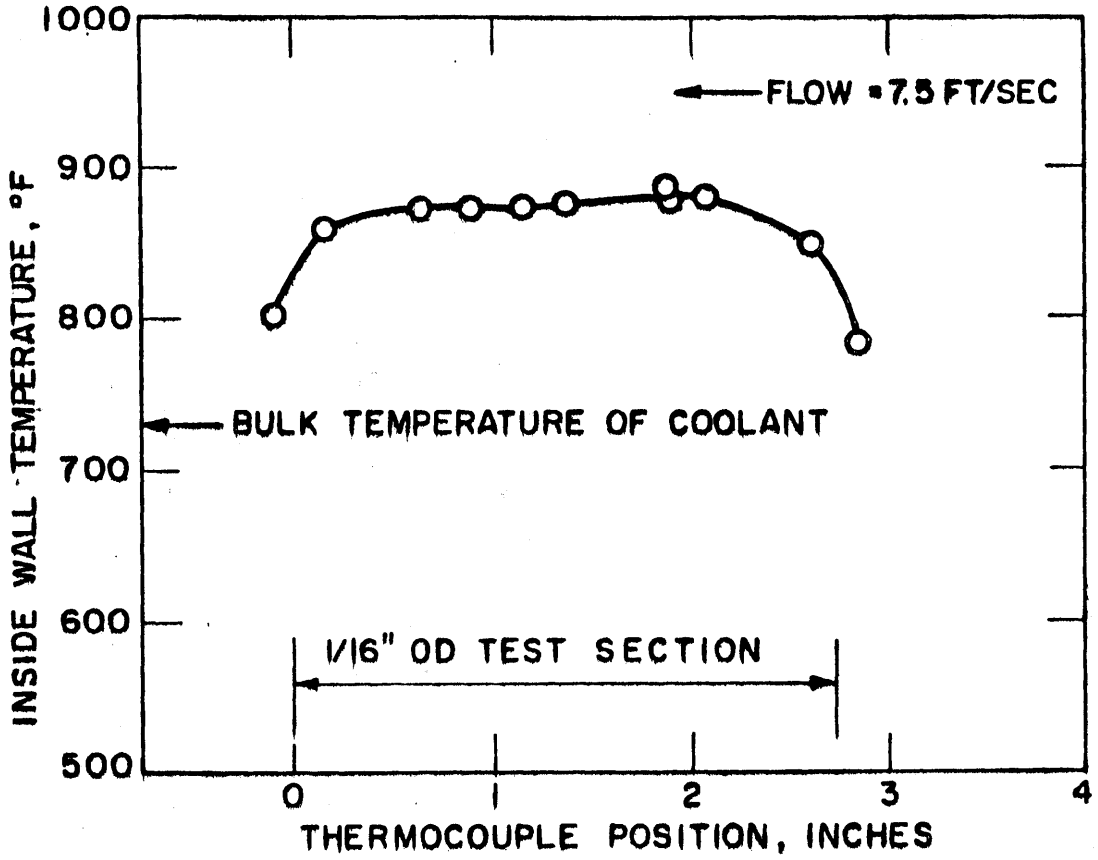

FIGURE 6.8 TYPICAL TEMPERATURE PROFILE OF AECL FOULING PROBE

TABLE 6.7

Results of Fouling Probe Studies at Chalk River
on Samples of Irradiated Santowax OMP from the 610°F Irradiation

Sample	w/o DP	Inside Wall Temperature, °F	Coolant Bulk Temperature, °F	Deposition Rate gm/(cm^2)(hr) x 10^6
1L121+ 1L123	50	895	725	0.8 ± 0.3
1L121+ 1L123+ 1L131	50	895	725	0.5 ± 0.3

and

$$h_f = av^B \quad (0.8 < B < 1.0) \qquad (6.14)$$

For a set of heat transfer measurements on a given day, the physical properties of the coolant and the scale resistance (if any) would not change appreciably, so that by plotting 1/U versus $1/v^B$, the scale resistance could be determined by a least squares fit of a straight line through the data.

One problem involved in this method is the choice of the power B. Since the Nusselt number defined in this work is based on U, the overall heat transfer coefficient from test heater surface to bulk coolant, it might be argued that the 0.9 Reynolds number power dependence observed in this work was the result of there being some scale resistance on the test heater surface, so that U was not equal to h_f, the film coefficient of heat transfer. In Section A2.7 the results of various tests of hypothetical scale buildup on the test heater walls are discussed. In all tests, the Reynolds number power dependence for correlations based on the hypothetical h_f was found to be higher than those actually obtained for U (assuming no scale resistance). The results of these tests indicated that the value of the Reynolds number power dependence of 0.9 observed for all the M.I.T. data (which was higher than the Dittus-Boelter value of 0.8) was <u>not</u> a direct cause of there being any scale resistance on the test heater walls.

In view of the results of the tests of hypothetical scale on the test heater walls, it was decided to use the value of B = 0.9 obtained in the correlation of the data (using U in the Nusselt number) for the Wilson plot analyses. Plots were also constructed with values of B = 0.8 and 1.0 to see what differences in conclusions might result. Figure 6.9 shows typical Wilson plots for the heat transfer data of the 610°F and 750°F irradiation of Santowax OMP based on a Reynolds number power dependence of 0.9. All of the data analyzed by this method gave intercepts of -1 to $+1 \times 10^{-4}$ (hr)(ft^2)(°F)/Btu. Considering a possible consistent error of ± 10% in the measurement of U and the necessary extrapolations to obtain the intercepts, the Wilson plot results indicate little or no scale buildup at all for the entire periods of irradiation. Using Reynolds number powers of 0.8 and 1.0 served only to shift the range of intercepts on the Wilson plots down or up respectively, with about the same spread in the intercepts. Thus, it was concluded that within the accuracy of this technique, no appreciable fouling of the test heaters used was observed.

One final test of scale buildup was provided by the changeover from test heater TH5 to test heater TH6. It has been emphasized to this point that no changes in the overall heat transfer coefficients obtained could be attributed to scaling or fouling of the test heater tube surface throughout the period of irradiation of Santowax OMP. However, a highly abnormal situation developed after three and one half months of operation with TH5 when the test heater was accidentally overheated by a drastic reduction in coolant flow rate for a brief period (less than a minute) while the heat flux through the tube was 2×10^5 Btu/(hr)(ft^2). As a result, a coke deposit was formed in the heater tube which reduced the maximum flow rate attainable in the loop by about 10% and the overall heat transfer coefficient by about a factor of two. Continued operation with this heater in the coked state under normal operating conditions for a period of about a month showed no further changes in the flow or heat transfer rates. When this heater was replaced by TH6, the heat transfer rates and Wilson plot intercepts obtained with the new heater agreed with those obtained in TH5 before the coking incident, indicating that little or no scale had been formed on the inside walls of TH5. The coked test heater was cut apart, and inspection showed

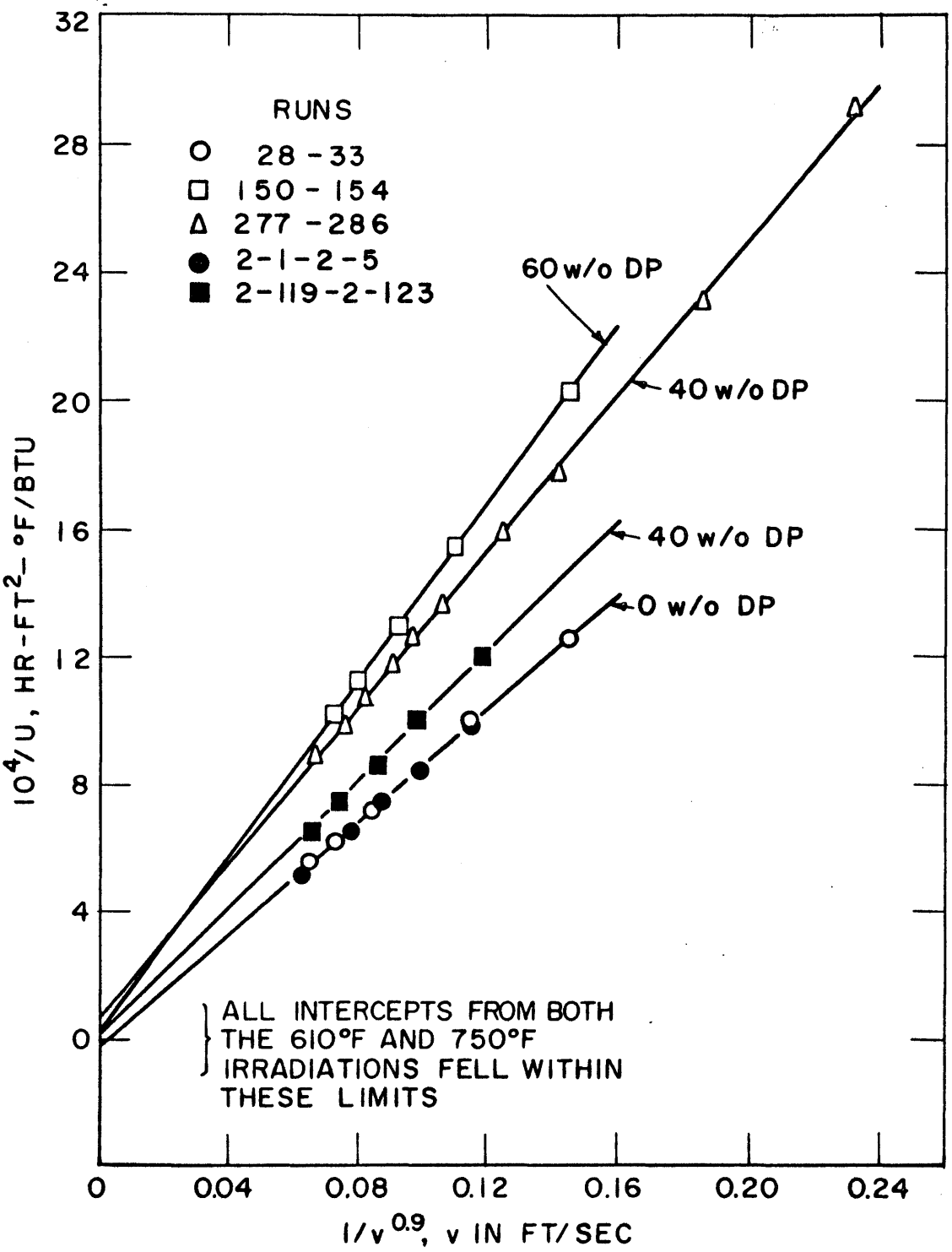

FIGURE 6.9 TYPICAL WILSON PLOTS FROM THE 610°F AND 750°F IRRADIATIONS OF SANTOWAX OMP

carbon-like material which easily flaked off the walls, indicating that the material on the walls of the coked test heater was coked coolant and not the adherent scale reported by other investigators (6.7).

APPENDIX A1
CALORIMETRY AND DOSIMETRY

A1.1 Description and Specific Heats of Series IV Calorimeter Absorbers (A1.1)

The materials used in the calorimeters were aluminum, polyethylene, polystyrene, carbon, beryllium, and Santowax OMP. The aluminum used was type 1100 which is more than 99% pure. It was purchased as solid one-half inch diameter rod from American Steel and Aluminum Company. The polyethylene and polystyrene samples were cut from standard one-half inch commercial rods purchased from Forest Products, Inc., Cambridge, Mass. The carbon used was pyrolytic graphite made in a furnace by vapor deposition of natural gas. It was purchased from High Temperature Materials, Inc., Brighton, Mass. The beryllium used was furnished by Nuclear Metals, Inc., Concord, Mass. No specifications regarding the amounts or nature of impurities of the beryllium were available.

The Santowax OMP used came from a portion of the makeup used for the steady-state-HB period of the 610° F irradiation, labelled Makeup M-3. The composition of this material was 9.4 w/o ortho-terphenyl, 58.7 w/o meta-terphenyl and 31.9 w/o para-terphenyl. The sample was prepared in the following way: The Santowax was melted, then poured into a one-half inch inside diameter, stainless steel cylinder fitted with pistons at either end. Immediately after the cylinder was filled, it was placed in a vise and compressed. The compression was gradually increased for a period of approximately thirty minutes when the cylinder was placed into dry ice and frozen. The resulting Santowax rod was then pushed out of the cylinder. This procedure evolved from a series of tests of various techniques and produced the maximum in structural strength and homogeneity of all the methods tried.

The specific heat of a portion of each absorber was measured by the Dynatech Corporation, Cambridge, Mass., using the method of mixtures and a drop calorimeter. The results are plotted in Fig. A1.1. The data points represent average temperatures. In particular, the Santowax data

point at 150°F represents an average value for the range 125°F-175°F. Since phase changes in some of the components in Santowax may occur in this region, the curve presented for this absorber is not expected to be very accurate in this region. An overall assignment of a ±2% uncertainty, based on the reproducibility at a given temperature, was given the data.

A1.2 Calculation of the Thermal Neutron Heating Rate in Aluminum (A1.1, A1.2)

The thermal neutron heating rate in aluminum results from self-absorption from the following sources:

1. Prompt gamma radiation from the reaction $Al^{27}(n,\gamma)\ Al^{28}$.
2. Gamma radiation from the decay of Al^{28}.
3. Beta radiation from the decay of Al^{28}.

The calculation of each of these effects has been reported by Morgan and Mason (A1.2) for the Series III calorimeters. Due to slight changes in the geometry of the absorbers the calculations were again performed for the Series IV calorimeters with the following result (A1.1):

$$R_{th}^{Al} = \phi_{2200} \times 10^{-16}[3.2+9.3(1-e^{-0.3t})] \text{ watts/gm} \qquad (A1.1)$$

where

ϕ_{2200} is the thermal neutron flux, neutrons/(cm^2)(sec)

t is the length of time the calorimeter has been exposed to the thermal flux, min.

It is estimated that Eq. (A1.1) is accurate to ±15% (A1.2) because of the approximations made in deriving the relation.

A1.3 Assumption of Compton Scattering for Absorbers

In Section 3.2.3 it was assumed that all interactions between gamma rays and the calorimeter absorbers were Compton interactions. This allowed allowed the gamma dose rate in any material to be related to that in carbon by a simple formula:

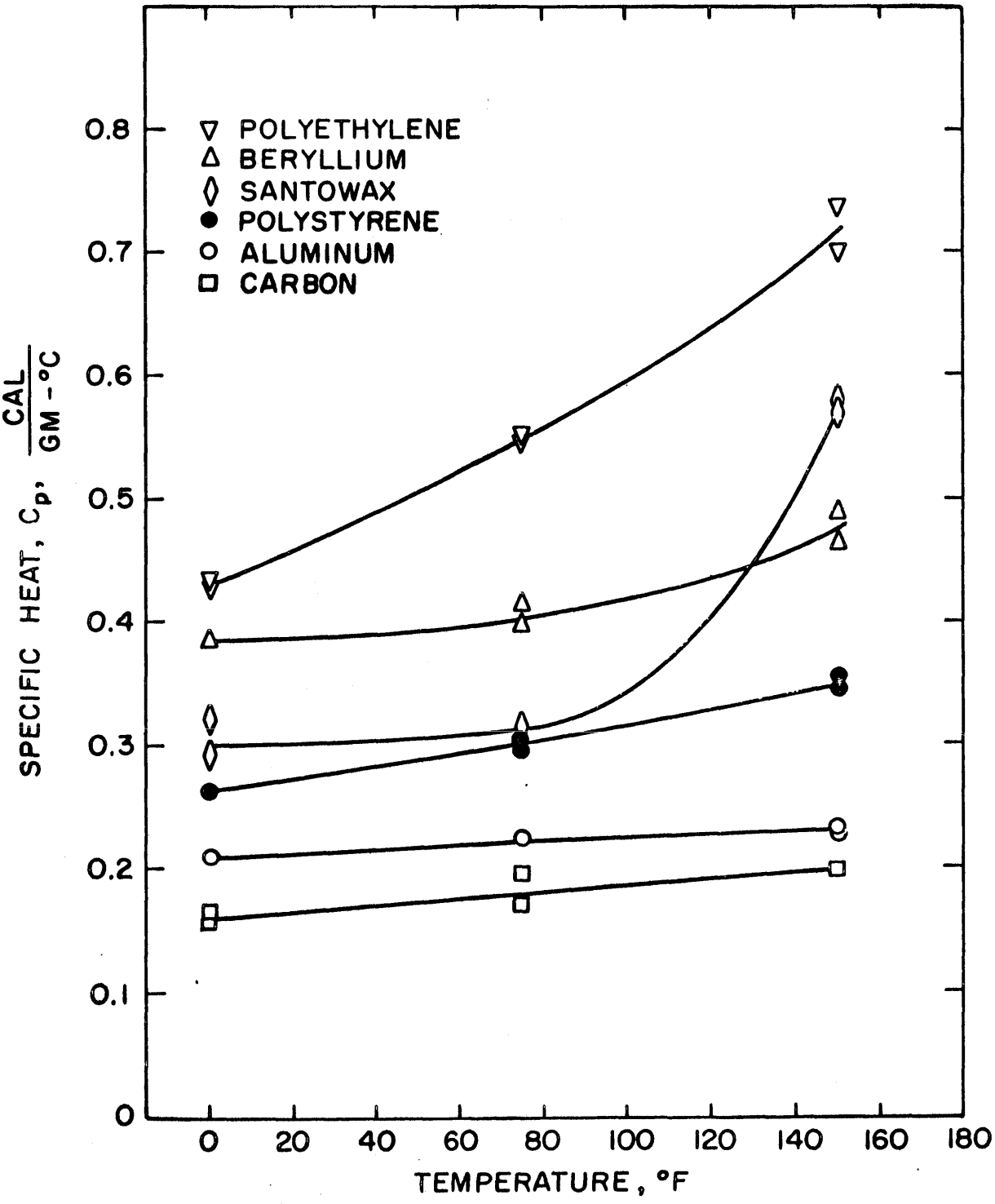

FIGURE A1.1 SPECIFIC HEAT DATA FOR CALORIMETER SERIES IV

$$R_\gamma^j = R_\gamma^C \frac{(Z/A)_j}{(Z/A)_C} \qquad \text{(A1.2)}$$

where

Z/A for compounds is the weighted average Z/A.

The fission gamma ray spectrum extends from 0 to 10 Mev, and, for the low Z materials used in the absorbers (hydrogen Z = 1, beryllium Z = 4, carbon Z = 6, aluminum Z = 13), Compton interactions are predominant over most of this energy range. However, there are also some photoelectric and pair production interactions which should be taken into account. These two effects do not follow the simple law given by Eq. (A1.2) and, furthermore, do not occur at the same energy in all the absorbers.

The gamma ray dose rate in any material is given by (A1.2):

$$R_\gamma^j = \int_0^\infty g(E)\, I(E)\, E \left[\frac{\tau_a}{\rho} + \frac{\sigma_a}{\rho} + \frac{\kappa_a}{\rho}\right] dE \; \frac{\text{Mev}}{(\text{gm})(\text{sec})} \qquad \text{(A1.3)}$$

where

g(E) is an attenuation coefficient taking into account the absorption of gamma rays by materials separating the calorimeter absorber from the radiation field

I(E) is the intensity of the gamma field, photons/(cm^2)(sec)(Mev)

E is the gamma ray energy, Mev

τ_a is the photoelectric energy absorption coefficient of the absorber, cm^{-1}

σ_a is the Compton energy absorption coefficient of the absorber, cm^{-1}

κ_a is the pair production energy absorption coefficient of the absorber, cm^{-1}

ρ is the absorber density, gm/cc.

Morgan and Mason (A1.2) have made calculations of R_γ^j/R_γ^C using Eq. (A1.3) with a prompt gamma fission spectrum:

$$\begin{aligned} N(E) &= 14e^{-1.1E}\ \text{Mev}^{-1} \quad \text{if } E > 1 \text{ Mev} \\ &= 46.9e^{-2.3E}\ \text{Mev}^{-1} \quad \text{if } E < 1 \text{ Mev} \end{aligned} \qquad \text{(A1.4)}$$

where

N(E) is the number of photons of energy E emitted per Mev and per fission, and is proportional to I(E).

For the calculations, they also used an attenuation coefficient of the form

$$g(E) = e^{-\mu_1 X_1} e^{-\mu_2 X_2} \qquad \text{(A1.5)}$$

where

$\mu = \sigma_a + \tau_a + \kappa_a$

X is the thickness of the attenuating material (stainless steel and aluminum)

and

subscript 1 refers to the stainless steel thimble

subscript 2 refers to the aluminum can of the calorimeter.

It should be noted that this type of attenuation coefficient does not take into account the replacement of attenuated low energy gamma rays by scattered higher energy gamma rays. Their results are listed in the second column of Table A1.1, where it can be seen that the only significant deviation from the Compton scattering relation occurred for aluminum, which had about a 3% higher calculated R_γ ratio than Z/A ratio. The photoelectric effect in aluminum was responsible for this increase.

TABLE A1.1

Comparison of (Z/A) Ratios to Calculated R_γ Ratios

Material	$(Z/A)_j/(Z/A)_C$	R_γ^j/R_γ^C (A1.2)[a]	R_γ/R_γ^C [b]
Carbon (Z = 6)	1.00	1.00	1.00
Hydrogen (Z = 1)	1.99	1.99	1.99
Aluminum (Z = 13)	0.964	0.990	1.058

a. Prompt gamma fission spectrum with attenuation in stainless steel thimble and aluminum can.

b. Measured gamma spectrum (A1.4) and no attenuation in stainless steel thimble and aluminum can.

When the series IV calorimeters were employed for dose rate measurements in the stainless steel thimble after the removal of the in-pile section, discrepancies between the carbon and aluminum calorimetric measurements of the order of 10% indicated that there were more low energy gamma rays in the thimble than given by the attenuated fission gamma spectrum used by Morgan and Mason. More recently, gamma ray spectra have been measured at the M.I.T. reactor by Kaiz (A1.4). Figure A1.2 shows two measured gamma spectra from a beam port at the M.I.T. reactor. The first spectrum was measured as the beam came out of the port, and the second after it had passed through 12" of polyethylene and 0.5" of boral (an alloy of aluminum containing a small amount of boron). The unattenuated fission spectrum used by Morgan and Mason [see Eq. (A1.4)] is shown for comparison (not normalized). Even after traversing 0.5" of boral the spectrum appears to have a greater slope for low energies than given by the fission spectrum. It is precisely this portion of the spectrum which leads to deviations from the Compton scattering relation for the aluminum absorber, because the photoelectric effect in aluminum is important in this low energy range.

For gamma rays with energies of 0.05 Mev or less, 0.5" of aluminum is equivalent to 0.05" of stainless steel (the thickness of the stainless steel thimble) in absorbing gamma rays. Thus it appears that there should be a considerable buildup of low energy gamma rays in the stainless steel thimble.

Calculations using Eq. (A1.3) were therefore made using the measured spectrum of Kaiz (A1.4) [the spectrum after crossing 12" of polyethylene and 0.5" of boral] and these calculations are also shown in the third column of Table A1.1. It can be seen that aluminum was the only material with a deviation from the Compton scattering relation (calculations for beryllium were not performed inasmuch as the photoelectric effect is very strongly dependent on Z and the Z for beryllium is less than that for carbon). Based on these calculations, aluminum had about a 10% greater gamma dose rate than predicted from the Compton scattering relation, but the other absorbers followed the Compton scattering relation quite well.

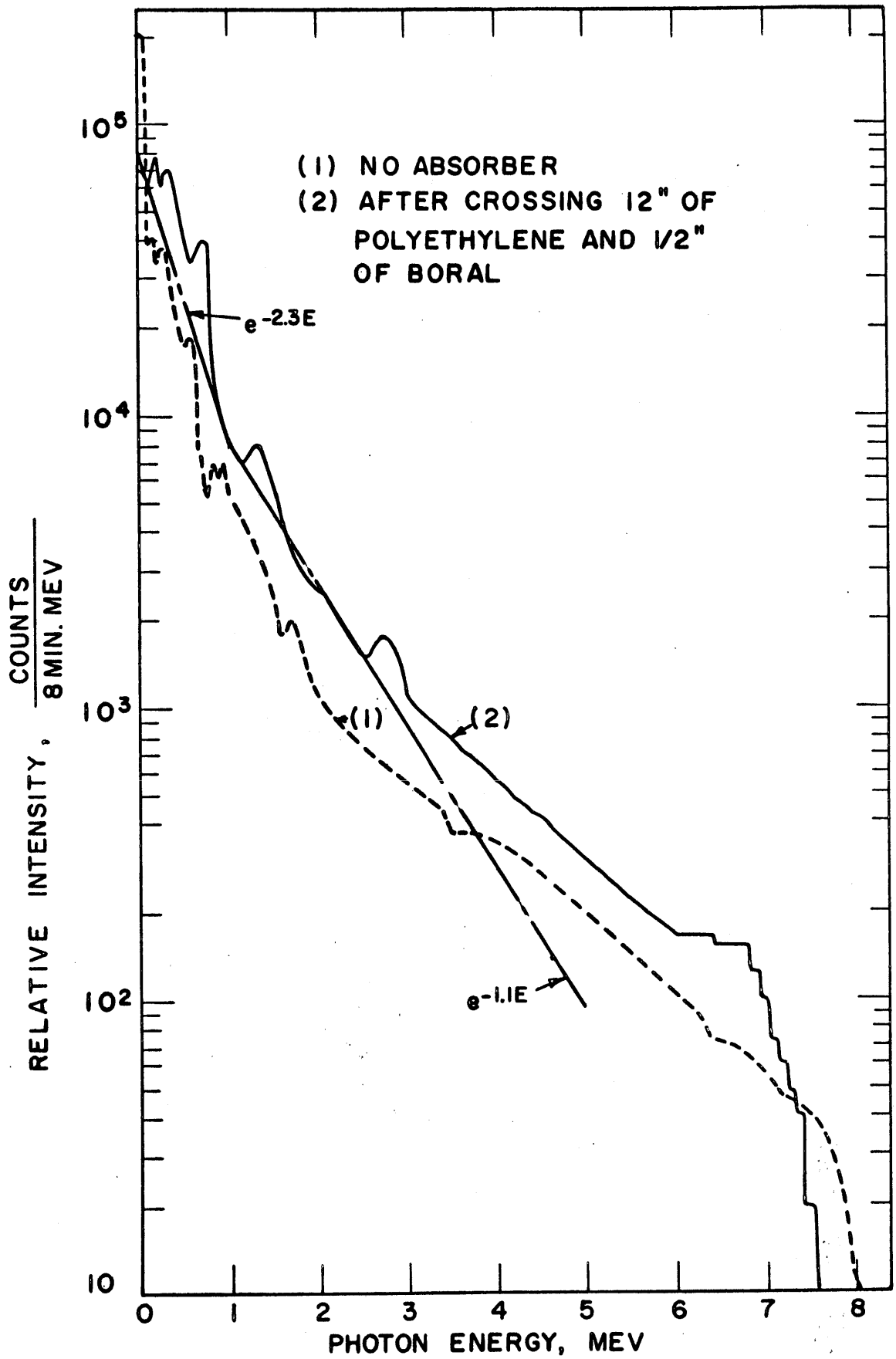

FIGURE A1.2 RELATIVE INTENSITY OF THE GAMMA RAY SPECTRA AT THE MIT REACTOR FACE (A14)

A1.4 A Least Squares Method for Determining R_γ^C and I_H from Calorimeter Measurements

As stated in Section 3.2.3, the calorimetric measurements may be substituted into a set of N (N greater than 2) equations with only two unknowns: R_γ^C, the gamma energy absorption rate in carbon and I_H, the neutron scattering integral for hydrogen.

The equations for the absorbers used in this experiment are described in detail in Section 3.2.3 and may be written in the form

$$R_T^j = a_j\, R_\gamma^C + b_j\, I_H \tag{A1.6}$$

where

j may refer to Santowax OMP, polyethylene, polystyrene, carbon, and beryllium. (For aluminum, R_T^j must be replaced by $[R_T^{Al} - R_{th}^{Al}]$.)

What is desired are the values of R_γ^C and I_H which would give a minimum variance in the calculated total dose rate in the organic liquid (Santowax OMP) being irradiated in the in-pile section. The variance in the total dose rate to Santowax may be expressed as

$$\sigma^2\left(R_T^{SW}\right) = (a_{SW})^2\, \sigma^2\left(R_\gamma^{C*}\right) + (b_{SW})^2\, \sigma^2\left(I_H^*\right) \tag{A1.7}$$

where the asterisks denote the "best" values of R_γ^C and I_H by the propagation of variance rule, and the variances in R_γ^C and I_H may be approximated by

$$\sigma^2\left(R_\gamma^{C*}\right) = \frac{\sum_{j=1}^{N_\gamma} \left(R_\gamma^{Cj} - R_\gamma^{C*}\right)^2}{N_\gamma(N_\gamma - 1)} \tag{A1.8}$$

$$\sigma^2\left(I_H^*\right) = \frac{\sum_{j=1}^{N_N} \left(I_H^j - I_H^*\right)^2}{N_N(N_N - 1)} \tag{A1.9}$$

where

R_γ^{Cj}, I_H^j are the values of R_γ^C and I_H predicted by absorber j

R_γ^{C*}, I_H^* are the "best" values of R_γ^C and I_H

N_γ is the number of absorbers considered to have a sufficient gamma dose rate to provide a reasonable estimate of the error in R_γ^C. In this experiment all absorbers used are considered to meet this qualification.

N_N is the number of absorbers considered to have a sufficient fast neutron dose rate to provide a reasonable estimate of the error in I_H. Only the polyethylene, polystyrene and Santowax absorbers meet this qualification.

An illustration of how these variances are formed is given in Fig. A1.3.

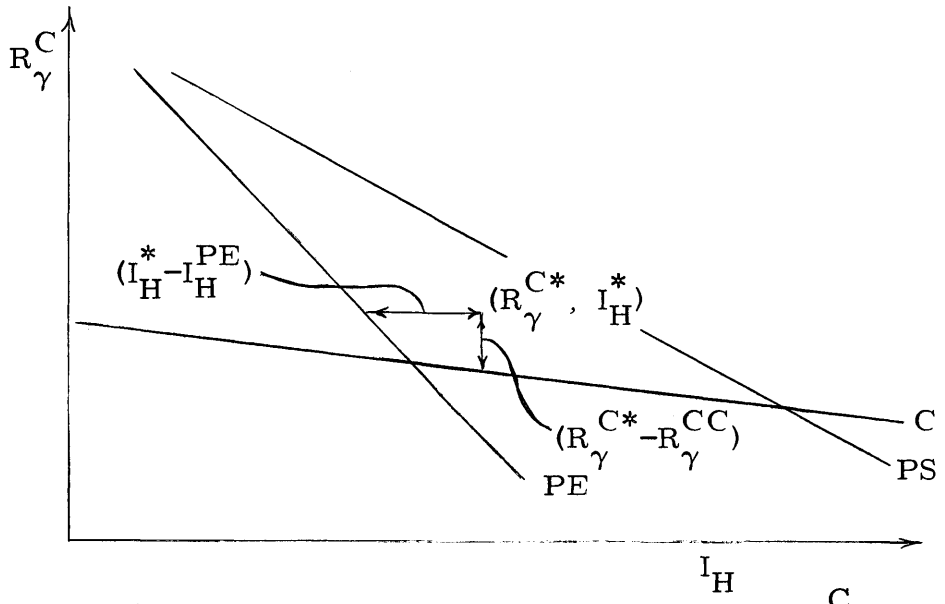

Figure A1.3 Graphical Representation of Errors in R_γ^C and I_H

The variances estimated thus far have been variances of the mean, and if N_γ and N_N were equal a least squares analysis could be applied directly to Eq. (A1.7) after substituting in the analytic expressions given by Eqs. (A1.6), (A1.8) and (A1.9). Since in this experiment N_γ is always greater than N_N and since it is desirable to assign equal weight to the variances of the fast neutron and gamma dose rates, it is important to note that the quantities to be minimized should really be the population variances. Thus, after substitution, the expression to be minimized is

$$\sum_{j=1}^{N_\gamma}\left(R_\gamma^{C*}-\frac{R_T^j}{a_j}+\frac{b_j}{a_j}I_H^*\right)^2+\sum_{j=1}^{N_N}\left(I_H^*-\frac{R_T^j}{b_j}+\frac{a_j}{b_j}R_\gamma^{C*}\right)^2=\text{minimum} \tag{A1.10}$$

where

$D=\left(\frac{b_{SW}}{a_{SW}}\right)^2\frac{N_\gamma}{N_N}$ and supplies the necessary weighting of the two sums.

By taking the partial derivatives of Eq. (A1.10) with respect to R_γ^{C*} and I_H^* and setting them equal to zero there result two equations for the solution of R_γ^{C*} and I_H^*:

$$\left[N_\gamma+D\sum_{j=1}^{N_N}\left(\frac{a_j}{b_j}\right)^2\right]R_\gamma^{C*}+\left[\sum_{j=1}^{N_\gamma}\left(\frac{b_j}{a_j}\right)+D\sum_{j=1}^{N_N}\left(\frac{a_j}{b_j}\right)\right]I_H^*$$

$$=\sum_{j=1}^{N_\gamma}\left(\frac{R_T^j}{a_j}\right)+D\sum_{j=1}^{N_N}\left(\frac{R_T^j a_j}{b_j^2}\right) \tag{A1.11}$$

$$\left[\sum_{j=1}^{N_\gamma}\left(\frac{b_j}{a_j}\right)+D\sum_{j=1}^{N_N}\left(\frac{a_j}{b_j}\right)\right]R_\gamma^{C*}+\left[\sum_{j=1}^{N_\gamma}\left(\frac{b_j}{a_j}\right)^2+DN_N\right]I_H^*$$

$$=\sum_{j=1}^{N_\gamma}\frac{R_T^j b_j}{a_j^2}+D\sum_{j=1}^{N_N}\frac{R_T^j}{b_j} \tag{A1.12}$$

The coefficients on the left sides of Eqs. (A1.11) and (A1.12) are constant for any set of calorimetric runs; only the dose rates R_T^j vary. Once the "best" values, R_j^{C*} and I_H^*, are computed Eqs. (A1.7), (A1.8) and (A1.9) may be used to compute the variances in R_T^{SW}, R_γ^{C*} and I_H^*. If it is desired only to minimize $\sigma^2\left(R_\gamma^{C*}\right)$, then D may be set equal to zero.

A1.5 Calorimetry Computer Program, MNCAL

MNCAL is an IBM 709/7090 FORTRAN program (for use with a 32K storage) which takes the measured dose rates in the calorimeter absorbers

(aluminum corrected for thermal neutron dose rate) and finds the "best" values of R_γ^C, I_H and R_T^{SW} using the equations described in Section A1.4. The FORTRAN listing of MNCAL is given in Table A1.2 and a logic flowsheet is given in Fig. A1.4. The program has the option of minimizing the variance in R_γ^C alone, the variance in R_γ^C, or both. In the paragraphs that follow a brief description of how to use the program will be given; a sample input and sample output are given in Tables A1.3 and A1.4, respectively, as an aid. Some familiarity with FORTRAN input/output format is assumed; for details see the IBM 709/7090 FORTRAN reference manual (A1.5).

The input is arranged as a series of tables, each headed by a card upon which any desired information may be placed. All fixed point data use I4 format and all floating point data E12.5 format. Alphanumeric data, used to describe the run numbers, use A6 format.

The first table supplies two control constants:

1. The number of absorbers for which the constants a_j and b_j will be supplied. In this work there are six such absorbers: Santowax, polyethylene, polystyrene, aluminum, carbon and beryllium.
2. The number of absorbers having a sufficient fast neutron dose to provide an estimate of the error in I_H. In this experiment there are three: Santowax, polyethylene and polystyrene.

The second table gives the constants a_j and b_j for the absorbers in the form a_1, b_1, a_2, b_2 .... The input to the program as shown in Table A1.3 is arbitrarily arranged in the order: Santowax, polyethylene, polystyrene, aluminum, carbon, beryllium. Since Santowax is both an absorber and the material being irradiated in the actual experiment, the arrangement of data given is correct. If some material other than Santowax were being irradiated, a_1 and b_1 would be the constants for this material, and all absorber data would have to be shifted one place to the right.

The third table is headed by a "free" card upon which any information punched will be printed as a heading for the output. The card after the heading contains the following control data:

1. The number of runs in the group of data to follow.

TABLE A1.2
FORTRAN LISTING OF MNCAL

```
*       LIST 8
*       LABEL
*       SYMBOL TABLE
C MNCAL HAS 108 CARDS          7-8-63
        DIMENSION A(20),B(20),DOSE(20),NC(20)
        NOT=2
        NIT=4
        READINPUTTAPE NIT,1,NCALS,NCALG
     1  FORMAT(/(18I4))
        SENSE LIGHT 0
    42  READINPUTTAPE NIT,2,(A(I),B(I),I=1,NCALS)
     2  FORMAT(/(6E12.5))
    39  READINPUTTAPE NIT,3
     3  FORMAT(80H
       1                          )
        READINPUTTAPE NIT,4,NRUNS,N2,(NC(J),J=1,NCALS),NOVER,KPUNCH
     4  FORMAT(18I4)
        READINPUTTAPE NIT,6,FAC
     6  FORMAT(6E12.5)
        WRITEOUTPUTTAPE NOT,3
        WRITEOUTPUTTAPE NOT,10
    10  FORMAT(1H0,3X3HRUN,3X9HR GAMMA C,3X10HS.D.(RG C),6X2HIH,7X8HS.D.(I
       1H),3X9HRTOTAL SW,3X10HS.D.(RTSW))
        IF(KPUNCH)100,100,101
   100  PUNCH 3
        PUNCH 10
   101  C1=NCALS
        C10=NCALG
        C2=0.
        C3=0.
        C4=0.
        C5=0.
        DO 17 J=1,NCALS
        IF(NC(J))18,18,19
    19  C1=C1-1.
        IF(J-NCALG)50,50,17
    50  C10=C10-1.
        GO TO 17
    18  C3=C3+B(J)/A(J)
        C5=C5+(B(J)/A(J))**2
        IF(J-NCALG)20,20,17
    20  C2=C2+(A(J)/B(J))**2
        C4=C4+A(J)/B(J)
    17  CONTINUE
        ENCALS=C1*(C1-1.)
        IF(ABSF(C10-1.)-1.0E-7)60,60,61
    60  ENCALG=1.
        GO TO 62
    61  ENCALG=C10*(C10-1.)
    62  DO 38 I=1,NRUNS
        IF(NCALS-6)200,200,201
   200  READINPUTTAPE NIT,202,RUN,(DOSE(J),J=1,NCALS)
   202  FORMAT(A6,6E12.5)
        GO TO 203
   201  READINPUTTAPE NIT,5,RUN,(DOSE(J),J=1,NCALS)
     5  FORMAT(A6,6E12.5/(6E12.5))
   203  C6=0.
```

TABLE A1.2 (CONCLUDED)

```
      C7=0.
      C8=0.
      C9=0.
      DO 21 J=1,NCALS
      IF(NC(J))15,15,21
   15 C6=C6+DOSE(J)/A(J)
      C8=C8+DOSE(J)*B(J)/A(J)**2
      IF(N2)16,16,21
   16 IF(J-NCALG)22,22,21
   22 C7=C7+DOSE(J)*A(J)/B(J)**2
      C9=C9+DOSE(J)/B(J)
   21 CONTINUE
      IF(N2)25,25,29
   25 D=(B(1)/A(1))**2*C1/C10*FAC
    9 C11=C1+D*C2
      C12=C3+D*C4
      C22=C5+D*C10
      DELTA=C11*C22-C12**2
      C13=C6+D*C7
      C23=C8+D*C9
      RGAL=(C13*C22-C23*C12)/DELTA
      EYEH=(C11*C23-C12*C13)/DELTA
      RTOTAL=A(1)*RGAL+B(1)*EYEH
      SIG2X=0.
      SIG2Y=0.
      DO 12 J=1,NCALS
      IF(NC(J))11,11,12
   11 DELTAY=RGAL-(DOSE(J)-B(J)*EYEH)/A(J)
      SIG2Y=SIG2Y+DELTAY**2
   12 CONTINUE
      DO 14 J=1,NCALG
      IF(NC(J))13,13,14
   13 DELTAX=EYEH-(DOSE(J)-A(J)*RGAL)/B(J)
      SIG2X=SIG2X+DELTAX**2
   14 CONTINUE
      SIGX=SQRTF(SIG2X/ENCALG)
      SIGY=SQRTF(SIG2Y/ENCALS)
      SIGRT=SQRTF(SIG2X/ENCALG*B(1)**2+SIG2Y/ENCALS*A(1)**2)
      WRITEOUTPUTTAPE NOT,37,RUN,RGAL,SIGY,EYEH,SIGX,RTOTAL,SIGRT
   37 FORMAT(2XA6,6E12.4)
      IF(KPUNCH)102,102,29
  102 PUNCH 37,RUN,RGAL,SIGY,EYEH,SIGX, RTOTAL,SIGRT
   29 IF(SENSE LIGHT 1)38,8
    8 IF(N2)38,31,31
   31 SENSE LIGHT 1
      D=0.
      GO TO 9
   38 CONTINUE
      IF(NOVER)42,39,41
   41 CALL EXIT
      END
```

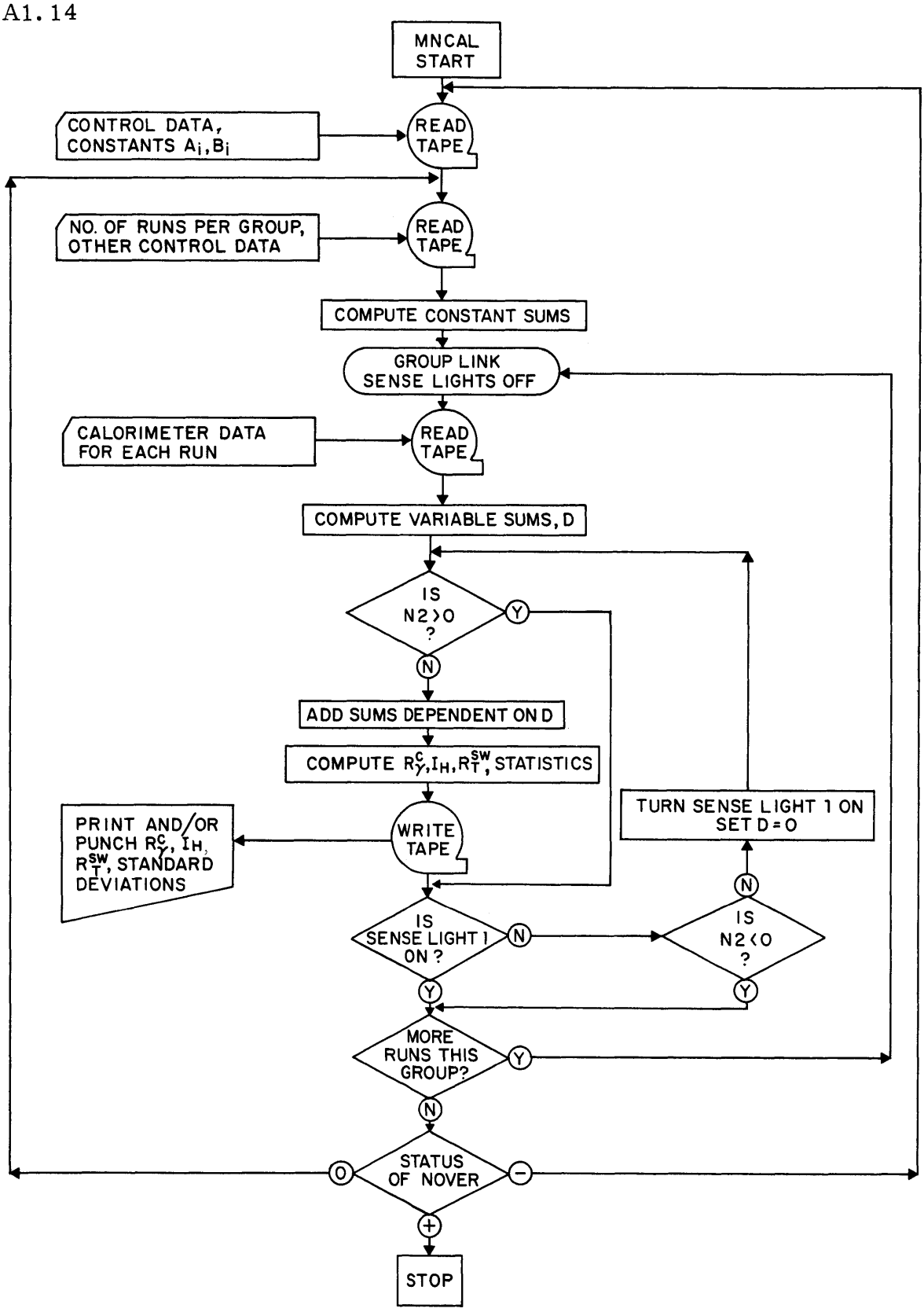

FIGURE A1.4 LOGIC FLOWSHEET FOR MNCAL

TABLE A1.3
SAMPLE INPUT TO MNCAL

```
                                NUMBER OF CALORIMETERS
  6   3
                                 SLOPES AND INTERCEPTS
 1.060          0.0452          1.141          0.094          1.078          0.0548
 0.9639         0.00263         1.             0.00919        0.886          0.0168
1                          DOSE AT 2 MW    G. NULLENS  NO AL
  8   0   0   0   0   1   0   1
 1.
 5      0.2443          0.3681          0.2691          0.1539          0.1538
 6      0.3024          0.4284          0.348           0.1903          0.1837
 7      0.306           0.4369          0.3449          0.1961          0.1951
 8      0.2523          0.3516          0.2746          0.1601          0.1684
 9      0.1303          0.1618          0.1392          0.08725         0.0894
 10     0.0644          0.07435         0.07915         0.05305         0.05115
 11     0.0331          0.03555         0.04025         0.03075         0.0301
 12     0.01745         0.02085         0.02625         0.01725         0.01725
```

TABLE A1.4
SAMPLE OUTPUT FROM MNCAL

DOSE AT 2 MW G. NULLENS NO AL

RUN	R GAMMA C	S.D.(RG C)	IH	S.D.(IH)	RTOTAL SW	S.D.(RTSW)
5	0.1323E-00	0.1209E-03	0.2308E 01	0.2448E-02	0.2446E-00	0.1693E-03
5	0.1324E-00	0.1140E-03	0.2307E 01	0.3045E-02	0.2446E-00	0.1831E-03
6	0.1736E-00	0.7319E-02	0.2613E 01	0.1473E-00	0.3022E-00	0.1022E-01
6	0.1691E-00	0.7127E-02	0.2652E 01	0.1657E-00	0.2991E-00	0.1064E-01
7	0.1796E-00	0.4357E-02	0.2564E 01	0.8949E-01	0.3063E-00	0.6139E-02
7	0.1770E-00	0.4251E-02	0.2586E 01	0.9953E-01	0.3045E-00	0.6368E-02
8	0.1554E-00	0.1913E-02	0.1897E 01	0.3305E-01	0.2505E-00	0.2518E-02
8	0.1538E-00	0.1826E-02	0.1913E 01	0.4192E-01	0.2495E-00	0.2709E-02
9	0.9015E-01	0.2959E-02	0.6939E 00	0.5059E-01	0.1269E-00	0.3881E-02
9	0.8751E-01	0.2813E-02	0.7199E 00	0.6544E-01	0.1253E-00	0.4200E-02
10	0.5419E-01	0.3424E-02	0.2021E-00	0.7973E-01	0.6657E-01	0.5115E-02
10	0.5285E-01	0.3380E-02	0.2113E-00	0.8358E-01	0.6557E-01	0.5207E-02
11	0.3173E-01	0.1617E-02	0.2276E-01	0.4029E-01	0.3467E-01	0.2501E-02
11	0.3131E-01	0.1605E-02	0.2476E-01	0.4128E-01	0.3431E-01	0.2525E-02
12	0.1783E-01	0.1751E-02	0.2973E-01	0.4852E-01	0.2024E-01	0.2873E-02
12	0.1785E-01	0.1749E-02	0.2664E-01	0.4867E-01	0.2013E-01	0.2877E-02

2. A least square control, called N2 in Fig. A1.4. If this constant is positive, only the variance in R_γ^C will be minimized; if it is zero, both methods will be used.
3. Calorimeter control constants telling the computer which of the absorbers to use in the least squares analysis. For each of the absorbers for which a_j and b_j data were given a constant must appear. If the constant is greater than zero the computer will not use any data supplied for that absorber; otherwise the computer will include the data from that absorber in the analysis. Thus, in the example given in Table A1.3, the aluminum data are not used; and since there are no beryllium data, no beryllium data are used.
4. A repeat control, called NOVER in Fig. A1.4. If this constant is zero, the computer will expect another group of data to follow this one; if it is less than zero, the computer will start from the beginning again after completing the analysis of this group; if it is positive, the computer will stop upon completion of the analysis of this group.
5. A punch control. If the constant is ≤ 0, a punched record of the output will appear along with the printed record. If it is >0, no punched record will be given.

The card after the control data card contains a factor by which to multiply the constant D (see Eq. (A1.10)) to attain other than equal weighting between the variance in the gamma dose rate and the fast neutron dose rate. Normally this factor is 1.0. Next the calorimeter data for all the runs in the group to be analyzed are given. Each run has the following information:

1. The run number, format A6.
2. The measured dose rates, format E12.5 for each. The data must be given the order: Santowax, polyethylene, polystyrene, aluminum, carbon, beryllium. If an absorber is not used, a zero is placed in the appropriate place.

Each group of data which follows the first (the repeat control being selected above) must have the format described above. In addition, if it is desired to run data with different values of a_j and b_j the formats must be as described for the second table and following for each such group of data.

The output needs almost no explanation. As can be seen in Table A1.4 the I_H results are to be multiplied by 10^{-24}. In addition, when the same run is printed out twice, the first is the result of minimizing the variances of both the gamma dose rate and the fast neutron dose rate, and the second is the result of minimizing the variance of the gamma dose rate alone.

The loading time for an IBM 7090 type computer is 0.13 minutes and running time is about 0.007 minutes per printed line of output desired.

A1.6 Tabulation of Results of Series IV and Series III Calorimetric Measurements

Measurements with the Series IV calorimeters have been performed by Nullens (A1.3). The measured dose rates obtained just after the removal of the in-pile section (4/23/63 to 4/25/63) are given in Table A1.5. Also shown in Table A1.5 are the thermal neutron dose rate corrections in aluminum, calculated with the aid of Eq. (A1.1).

The results of the computer least squares analyses for the "best" solutions for R_γ^C and I_H are shown in Table A1.6 in terms of R_N^{SW} ($4.52 \times 10^{22} I_H$), R_γ^{SW} $\left(1.06\ R_\gamma^C\right)$ and R_T^{SW} $\left(R_N^{SW} + R_\gamma^{SW}\right)$. Two sets of analyses were performed – one set with the Santowax, polyethylene, polystyrene, and carbon calorimeters, and one set with the Santowax, polyethylene, polystyrene and aluminum calorimeters. This latter set was calculated for comparison with the Series III-3 calorimetric measurements (see below).

Table A1.7 lists the results of the dose rate measurements with Series IV calorimeters during the week of 4/29/63. Dose rate measurements were also performed with the Series IV calorimeters at various reactor power levels, and the results of these measurements are given in Table A1.8. Corrections for delayed gamma heating in the data taken at different reactor power levels are discussed in Section A1.7.

Error limits must still be placed on the results obtained from the Series IV calorimetric measurements at full reactor power. Errors are from two main sources: random errors in the measured dose rates giving rise to random errors in the "best" values of R_γ^C and I_H; and errors inherent in each calorimeter, such as the error in the specific heat of each

TABLE A1.5

Measured Dose Rates in Series IV Calorimeters, 4/23/63-4/25/63[a]

Position Relative to Core Center inches	R_T^{SW} watts/gm	R_T^{PE} watts/gm	R_T^{PS} watts/gm	R_T^{C} watts/gm	R_T^{Al} watts/gm	R_{th}^{Al}[b] watts/gm	R_T^{Al} (corrected) watts/gm
-9-7/8	0.244	0.368	0.269	0.154	0.159	0.005	0.154
-4-7/8	0.302	0.428	0.348	0.184	0.195	0.005	0.190
1-1/8	0.306	0.437	0.345	0.195	0.201	0.005	0.196
7-1/8	0.252	0.352	0.275	0.168	0.165	0.005	0.160
12-1/8	0.130	0.162	0.139	0.0894	0.0919	0.0046	0.0873
16-1/8	0.0644	0.0744	0.0792	0.0512	0.0582	0.0051	0.0531
21-1/8	0.0331	0.0356	0.0403	0.0301	0.0349	0.0041	0.0308
26-1/8	0.0175	0.0208	0.0263	0.0173	0.0193	0.0020	0.0173

a. Data normalized to a reactor power of 1 MW.

b. Calculated from Eq. (A1.1).

TABLE A1.6

Calculated Dose Rates in Santowax OMP in the In-Pile Assembly Based on the Data of Table A1.5[a]

Position Relative to Core Center inches	Based on SW, PE, PS, C Calorimeters			Based on SW, PE, PS, Al Calorimeters		
	R_N^{SW} watts/gm	R_γ^{SW} watts/gm	R_T^{SW} watts/gm	R_N^{SW} watts/gm	R_γ^{SW} watts/gm	R_T^{SW} watts/gm
-9-7/8	0.105	0.140	0.245	0.093	0.156	0.249
-4-7/8	0.118	0.184	0.302	0.103	0.206	0.309
1-1/8	0.116	0.190	0.306	0.103	0.209	0.312
7-1/8	0.086	0.165	0.251	0.081	0.172	0.253
12-1/8	0.031	0.096	0.127	0.029	0.099	0.128
16-1/8	0.009	0.057	0.066	0.007	0.061	0.068
21-1/8	0.001	0.034	0.035	0.000	0.035	0.035
26-1/8	0.001	0.019	0.020	0.001	0.019	0.020

a. Data normalized to a reactor power of 1 MW.

TABLE A1.7

Dose Rate Measurements with Series IV Calorimeters, Week of 4/29/63[a]

Date and Time	Measured Dose Rates, watts/gm[b]					Calculated Dose Rates in Santowax, watts/gm		
	R_T^{PE}	R_T^{PS}	R_T^{C}	R_T^{Al}	$R_T^{Al}-R_{th}^{Al}$	R_N^{SW}	R_γ^{SW}	R_T^{SW}
Monday (1500)	0.458	–	0.197	0.198	0.194	0.119	0.194	0.313
Tuesday (1500)	0.456	–	0.199	0.199	0.195	0.117	0.197	0.314
Thursday (1500)	0.454	–	0.191	0.199	0.195	0.118	0.193	0.311
Friday (1230)	0.451	0.331	0.193	–	–	0.125	0.177	0.302

a. Date normalized to a reactor power of 1 MW.

b. Measured at 1-1/8 inches above core center.

TABLE A1.8

Dose Rate Measurements with Series IV Calorimeters at Different Power Levels, 5/10/63[a]

Reactor Power kw	Measured Dose Rates, watts/gm[b]			Calculated Dose Rates in Santowax, watts/gm		
	R_T^{PE}	R_T^{PS}	R_T^{C}	R_N^{SW}	R_γ^{SW}	R_T^{SW}
1950	0.450	0.330	0.193	0.124±0.0006[c]	0.177±0.0006	0.301±0.001
700	0.457	0.361	0.214	0.114±0.005	0.210±0.006	0.324±0.008
193	0.521	0.422	0.259	0.122±0.007	0.258±0.007	0.380±0.011
50	0.522	0.608	0.308	0.089±0.063	0.394±0.065	0.483±0.090

a. Data normalized to a reactor power of 1 MW.

b. Measured at 1-1/8 inches above core center.

c. Standard deviation based on calculations of "best" values from the data above.

absorber. Unfortunately, these two errors are coupled, since the "best" values of R_γ^C and I_H are determined through the simultaneous use of the measured rates of temperature rise and the specific heats of the absorbers. Thus an approximate method of estimating the errors in the results was used. Errors in the "best" values of R_γ^C, I_H and R_T^{SW} were determined by the computer program MNCAL. For the data of Table A1.6, the largest relative error in the computed "best" value of R_T^{SW} obtained in the reactor core (-12" to 12") was chosen as the possible error in the results. This criterion led to the following maximum possible errors:

$$R_T^{SW} = \pm 3\%, \quad R_\gamma^{SW} = \pm 4\%, \quad R_N^{SW} = \pm 6\%.$$

The data reported by Morgan and Mason (A1.2) and Turricchia (A1.6) (calorimeter Series III-3) are shown in Fig. A1.5. These data were also analyzed by the computer program MNCAL. As is evident from Fig. A1.5 the measurements for each calorimeter could not be made at the same position in the core, since all the calorimeter absorbers were housed in a single unit. Thus calculations were made using the smoothed data, and the results are given in Table A1.9.

A1.7 Calculation of the Effect of Delayed Gamma Rays on the Dose Rate Measurements Made at Different Reactor Power Levels (A1.3)

As noted in Section 3.2.4, the experimental measurements of reactor dose rate at various reactor powers made with the Series IV calorimeters were not linear with reactor power. This was due to the fact that the equilibrium fission product concentration in the reactor existed only for the first full power measurement which was made on a Friday, following four days of continuous reactor operation at full power. Subsequent measurements made a few hours after a power reduction were too high as a result of the fission product gammas from the previous higher power levels. An approximate method of correcting the data for this delayed gamma heating is presented in this section.

It was assumed that at full power (1.95 MW) on Friday, 5/10/63, the reactor was operating at a steady-state level. Under these conditions, the measurements of Table A1.8 yielded a value of $R_\gamma^C = 0.326$ watts/gm.

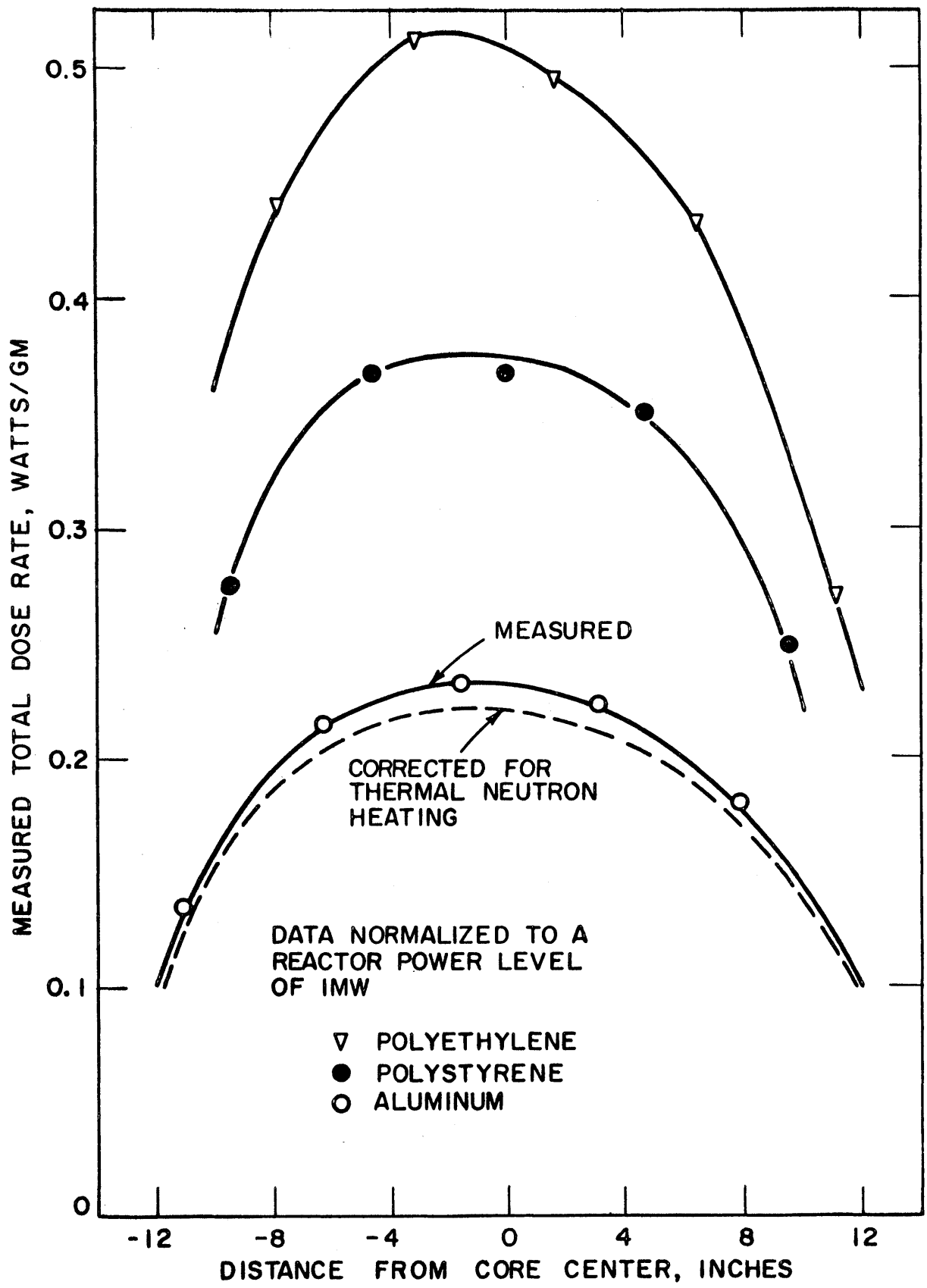

FIGURE A1.5 MEASURED DOSE RATES IN SERIES III-3 CALORIMETERS (3/20/61)

TABLE A1.9

Calculated Dose Rates in Santowax OMP in the In-Pile Assembly Based on Series III-3 Measurements, 3/20/61[a,b]

Position Relative to Core Center inches	R_N^{SW} watts/gm	R_γ^{SW} watts/gm	R_T^{SW} watts/gm
-10	0.091	0.148	0.239
-8	0.107	0.193	0.300
-6	0.117	0.215	0.332
-4	0.124	0.223	0.347
-2	0.125	0.228	0.353
0	0.123	0.229	0.352
2	0.119	0.225	0.344
4	0.113	0.217	0.330
6	0.106	0.201	0.307
8	0.092	0.180	0.272
10	0.075	0.137	0.212

a. Data normalized to a reactor power of 1 MW.

b. Smoothed data from Fig. A1.5 used.

The period of time elapsing between the moment the reactor power was reduced and the dose rate measurement was different for each absorber, and so each was corrected separately. A fission of one atom of U^{235} yields on the average 193.5 Mev of thermal energy (excluding the energy of the neutrons) (A1.7). Of this energy 7% comes from gamma rays, and 46% of the delayed energy ($\gamma+\beta$) comes from delayed gamma rays. Untermeyer and Weills (A1.8) have tabulated the fraction of operating power, f, left at time t after shutdown of a pure U^{235} fissioning system.

Thus, assuming that all gamma rays have the same effect on the dose rate, when the reactor was reduced in power from 1950 kw to 700 kw the excess delayed gamma ray dose rate in carbon was approximately

$$\left(R_\gamma^C\right)^{\text{excess}}_{1950\,\text{kw}} = \frac{(1950-700)\times f\times 46}{1950\times 7}\times 0.326 \text{ watts/gm}$$

and the corrected dose rate in each absorber used for the 700 kw measurements was thus

$$\left(R_T^j\right)_{cor.} = \left(R_T^j\right)_{measured} - a_j \left(R_\gamma^C\right)^{excess}_{1950\,kw} \qquad (A1.13)$$

where

a_j is the ratio $(Z/A)_j/(Z/A)_C$.

For the 193 kw and 50 kw runs the corrections follow from the above discussion. For instance, the 50 kw run included the effect of delayed gamma rays from the reduction 1950 - 700 kw, plus the effect due to the reduction 700 - 193 kw, plus the effect due to the reduction 193 - 50 kw.

One problem remained in these calculations. Untermeyer and Weills (A1.8) have a series of curves for the factor f, depending on the length of time the reactor had been operating at full power. Since the reactor is normally shut down over the weekend, it is difficult to say whether four days is an appropriate operating time to use, or whether, since the fuel elements have been exposed to this cycle continually, some longer time should be used. Turricchia (A1.6) has measured the residual background heating rate at the axial center of the core in stainless steel thimble after 72 hours of shutdown as 9.5% of the total dose rate in aluminum. Using the data of Table A1.9 at core center together with the data procided by Fig. A1.5 it is possible to calculate f (the reactor operated at a power level of 1 MW in March, 1961).

$$R_T^{Al} = 0.232 \text{ watts/(gm)(MW)}$$

$$R_\gamma^{Al} = 0.208 \text{ watts/(gm)(MW)}$$

$$\frac{1000 \times f \times 46}{1000 \times 7} \times 0.208 = 0.095 \times 0.1 \times 0.232$$

which gives $f = 1.6 \times 10^{-3}$. This value corresponds to an irradiation time of about one week in the curves of Untermeyer and Weills, so one week was the value used for the corrections.

The corrected results of these measurements are given in Table A1.10 (compare with Table A1.8). The corrected results show the dose rate to be linear with reactor power at least down to 200 kw. For the 50 kw measurements the corrections were almost as large as the measured values so

TABLE A1.10

Corrected Dose Rate Measurements with Series IV Calorimeters at Different Power Levels, 5/10/63[a, b]

Reactor Power kw	Measured Dose Rates watts/gm			Calculated Dose Rates in Santowax watts/gm		
	R_T^{PE}	R_T^{PS}	R_T^{C}	R_N^{SW}	R_γ^{SW}	R_T^{SW}
1950	0.450	0.330	0.193	0.124±0.0006[c]	0.177±0.0006	0.301±0.001
700	0.439	0.340	0.194	0.118±0.005	0.186±0.005	0.304±0.007
193	0.439	0.348	0.178	0.126±0.010	0.176±0.010	0.302±0.014
50	0.220	0.306	0.060	0.079±0.057	0.122±0.054	0.201±0.078

a. Data normalized to a reactor power level of 1 MW.

b. Measured at 1-1/8 inches above core center.

c. Standard deviation based on calculations of "best" values from the data alone.

that the corrected results were not expected to be meaningful. In view of the errors computed for the "best" values by the computer program MNCAL, the results for the 50 kw run appear to be not statistically different from the others.

A1. 8 Measurement of the Differential Neutron Flux $\phi(E)$ – Theory

The techniques used in this report for determining the differential neutron flux were, with minor modifications, the same as those reported by Morgan and Mason (A1. 2) and Sefchovich (A1. 9). This section summarizes the theory used.

In the thermal energy range, high purity cobalt-aluminum (Co-Al) wires (0. 595 w/o Co) were irradiated. The 2200 m/sec flux was calculated from the relation (A1. 2):

$$\phi_{2200} = \frac{(Act)_B - (Act)_{Cd}}{\sigma_{2200}(1 - e^{-\lambda T})} \qquad (A1.14)$$

where

σ_{2200} is the 2200 m/sec cross section for Co^{59}, barns
λ is the disintegration constant for Co^{60}, min^{-1}
T is the irradiation time, min
$(Act)_B$ is the bare absolute activity per atom, disintegrations/sec
$(Act)_{Cd}$ is the cadmium covered absolute activity per atom, disintegrations/sec

and

$$Act = \frac{(C - C_b)\, A\, e^{\lambda t}}{W N_o \epsilon} \qquad (A1.15)$$

where

C is the measured count rate of the detector, disintegration/sec
C_b is the background count rate of the detector, disintegration/sec
A is the atomic weight of the detector
W is the weight of the detector, grams
N_o is Avogadro's Number

t is the time elapsed between irradiation and counting (waiting time)

ϵ is the overall counting efficiency for the wire.

The count rates of irradiated Co-Al wires were measured in a NaI well-type scintillation system (A1. 2).

The neutron flux in the resonance region was determined by the Co-Al measurements since Co^{59} has a resonance at 120 ev. Cu^{63}, which has a resonance at 570 ev, was also used to determine the resonance flux. In this region, the flux was presumed to have a 1/E behavior, i. e.,

$$\phi(E) = \frac{\phi_o}{E} \tag{A1.16}$$

where

ϕ_o = constant, $n/(cm^2)(sec)$

E = neutron energy, ev.

For the determination of ϕ_o the following relation was used:

$$\phi_o = \frac{\phi_{2200}\sigma_{2200}}{(R_{Cd} - 1)(T.R.I.)} \tag{A1.17}$$

where

$$R_{Cd} = \frac{(Act)_B}{(Act)_{Cd}} = \text{cadmium ratio}$$

and T. R. I. is the total resonance integral, given by

$$T.R.I. = \int_{E_c}^{\infty} (\sigma_{res} + \sigma_{1/v}) \frac{dE}{E} \text{ barns} \tag{A1.18}$$

where

σ_{res} is the resonance cross section, barns

$\sigma_{1/v}$ is the 1/v cross section, barns

E_c is the cadmium cutoff energy, assumed to be 0. 5 ev in this work.

The cadmium ratios were determined by irradiating bare and cadmium covered Co-Al and copper wires, counting them in the NaI system and applying Eq. (A1. 15).

For the determination of the fast neutron flux (above about 1 Mev) detectors undergoing threshold reactions were used. Following the Trice method (A1.10) the reaction rate for a threshold reaction with a threshold of energy E_{th} may be written as

$$\text{Reaction Rate} = \int_{E_{th}}^{\infty} N\sigma(E)\,\phi(E)\,dE = N\overline{\sigma}_{eff}\int_{E_{eff}}^{\infty}\phi(E)\,dE = N\overline{\sigma}_{eff}\,\phi(\geq E_{eff}) \qquad \text{(A1.19)}$$

where

N is the number of atoms in the detector

$\overline{\sigma}_{eff}$ is an effective step function cross section

E_{eff} is an effective threshold energy.

Thus, if $\phi(E)$ were known so that $\overline{\sigma}_{eff}$ could be determined from Eq. (A1.19), the integral flux, $\phi(\geq E_{eff})$, could be determined from

$$\phi(\geq E_{eff}) = \frac{\text{Act}}{\overline{\sigma}_{eff}(1 - e^{-\lambda T})} \qquad \text{(A1.20)}$$

where the detector activity, Act, is evaluated from Eq. (A1.15).

From a set of measurements of the integral flux with different detectors having different values of E_{eff} the derivative may be taken with respect to energy to determine the differential flux in the fast neutron energy region. However, $\phi(E)$ had to be assumed to determine the integral fluxes, so an iterative procedure was set up for determining $\phi(E)$. For an initial estimate of the fast flux shape the fission spectrum of Watt (A1.11),

$$X(E) = \sqrt{\frac{2}{\pi e}}\, e^{-E} \sinh\sqrt{2E} \qquad \text{(A1.21)}$$

was used. However, for E > 2 Mev the fission spectrum may be approximated very closely by an exponential (e^{dE}), and, furthermore, the results obtained suggested that the actual spectrum in the in-pile section did have an exponential form in the fast region. Thus, the technique applied was to use the Watt spectrum to obtain a first approximation to the flux shape and to fit the integral flux versus energy curve by means of the relation

$$\ln\phi(\geq E) = c + dE \qquad \text{(A1.22)}$$

by the method of least squares. Once the constants c and d were found

Eq. (A1.22) was differentiated to give the differential flux:

$$\phi(E) = -de^{c+dE} \qquad \text{(A1.23)}$$

and the effective threshold cross sections were re-evaluated using Eqs (A1.19), (A1.23), and the previously calculated integral flux, $\phi(\geq E_{th})$. The iteration on the flux shape was continued until $\overline{\sigma}_{eff}$ for each detector did not change significantly. The threshold detectors used in this experiment were sulfur in the form of $MgSO_4(S^{32}(n,p)P^{32})$, nickel wire $(Ni^{58}(n,p)Co^{58})$, magnesium wire $(Mg^{24}(n,p)Na^{24})$ and aluminum wire $(Al^{27}(n,\alpha)Na^{24})$. The NaI system was also used to count all threshold detectors but sulfur. A brief description of the counting procedure for the sulfur detectors is given in Section A1.10.

The data used for all detectors are given in the next section.

A1.9 Neutron Cross Sections Used for the Calculation of the Differential Neutron Flux $\phi(E)$

The cross sections for the thermal and resonance activation foils, Co^{59} and Cu^{63}, have been obtained from the data of Dahlberg et al. (A1.12). Table A1.11 summarizes the data. A cadmium cutoff energy of 0.5 ev has

TABLE A1.11

Cross Sections for Thermal and Resonance Foils Co^{59} and Cu^{63}

Isotope	Resonance ev	σ_{2200} barns	$\int_{0.5ev}^{\infty} \sigma_{res} \frac{dE}{E}$ barns	$\int_{0.5}^{\infty} (\sigma_{res} + \sigma_{1/v}) \frac{dE}{E}$ barns
Co^{59}	120	38.0 ± 0.7	55.2 ± 4.5	72 ± 4.5
Cu^{63}	570	4.50 ± 0.15	3.09 ± 0.15	5.1 ± 0.2

been assumed. Eq. (A1.16) may be written in the form

$$\phi_o = \frac{K\,\phi_{2200}}{(R_{Cd}-1)} \qquad \text{(A1.24)}$$

where K, determined from Table A1.11, is 0.528 for Co^{59} and 0.887 for Cu^{63}. It is desirable to have as large a ratio of the resonance integral, $\int_{E_c}^{\infty} \sigma_{res} \frac{dE}{E}$, to the 1/v contribution, $\int_{E_c}^{\infty} \sigma_{1/v} \frac{dE}{E}$, as possible so that

the error introduced by the assumed cadmium cutoff energy, E_c, is as small as possible. For instance, if the cadmium cutoff were actually 0.4 ev there would be a 3% error introduced into the Co^{59} measurements, but a 5% error in the Cu^{63} measurements, since its resonance integral is relatively smaller than that of Co^{59}. For this reason the Co^{59} data are believed to be more accurate.

The cross section data for the $S^{32}(n,p)P^{32}$ reaction have been taken from Howerton (A1.13) and are plotted in Fig. A1.6. The data appear to be quite reliable.

The data used for the $Ni^{58}(n,p)Co^{58}$ reaction are those of Passell and Heath (A1.14) and are plotted in Fig. A1.7. Their best curve is based on theory and the experimental results of Gonzales et al. (A1.15), Preiss and Fink (A1.16) and Howerton (A1.13). More recent data in the low energy range (A1.17) agree fairly well with the best curve shown by Passell and Heath, but the data of Barry (A1.18) in the 4-9 Mev range appear to be somewhat higher than the theoretical curve shown. The data presented show considerable scatter and are therefore considered somewhat unreliable.

The data used for the $Mg^{24}(n,p)Na^{24}$ reaction are plotted in Fig. A1.8. The curve shown is the theoretical curve of Bullock and Moore (A1.19), and it can be seen that not much experimental data are available to support the theory. The available data of Hughes (A1.20) and Howerton (A1.13) are also plotted in Fig. A1.8. It appears that there is some scatter in these data, but the error limits are unknown due to the lack of experimental data, especially in the lower energy region.

The data of Bayhurst and Prestwood (A1.21) and Howerton (A1.13) are used for the $Al^{27}(n,\alpha)Na^{24}$ reaction and are plotted in Fig. A1.9. The data appear to be quite reliable.

In using the Trice method (A1.10), explained in the previous section, it is necessary to make an initial estimate of the effective threshold cross section for a given threshold foil by assuming that the fast flux distribution approximates that of a fission spectrum. Table A1.12 lists the effective threshold energies used for the threshold detectors in this work (A1.14, A1.22) together with the values of $\overline{\sigma}_{eff}$ calculated using the Watt spectrum (A1.11).

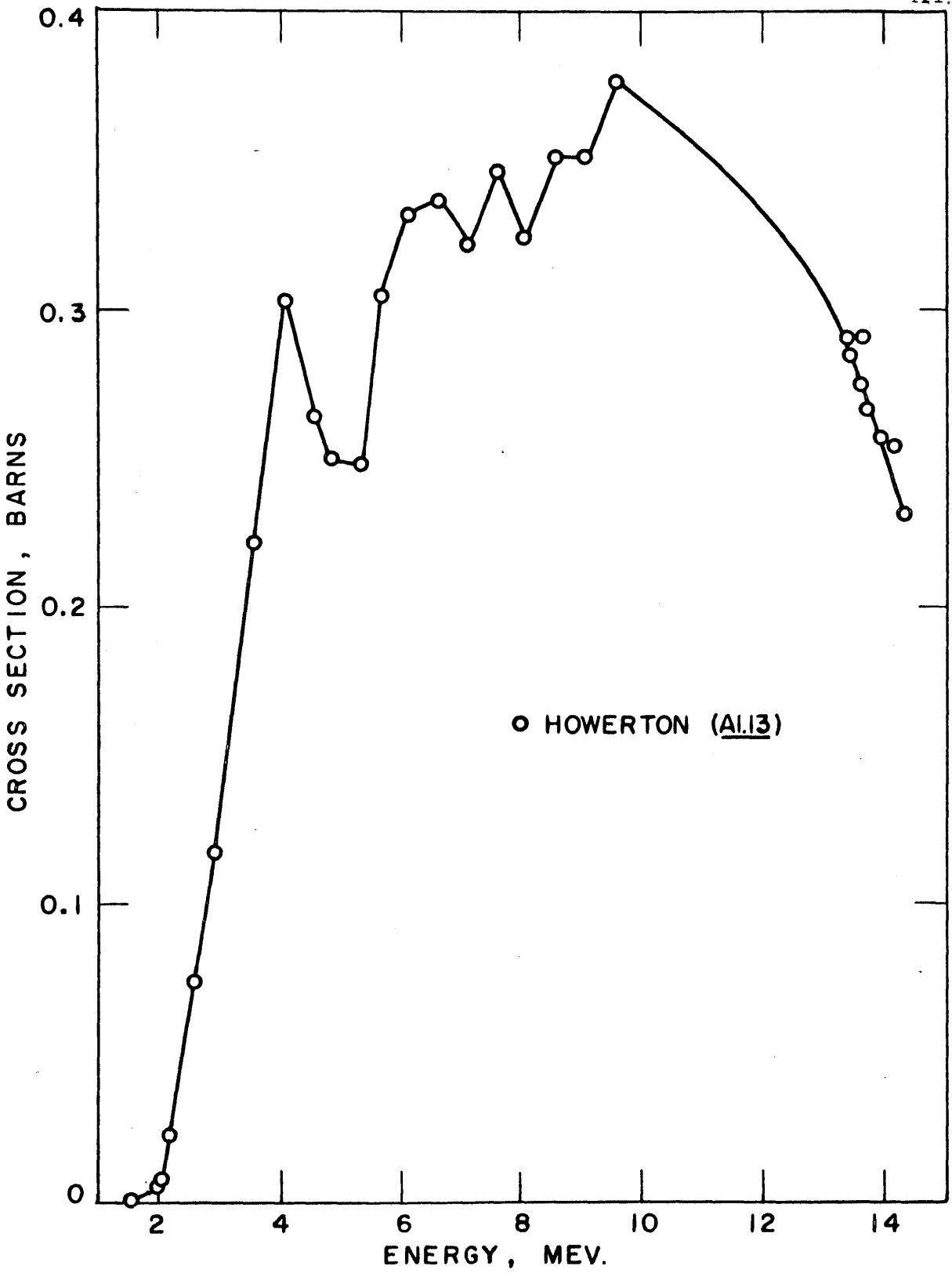

FIGURE A1.6 S^{32} (n,p) P^{32} CROSS SECTION

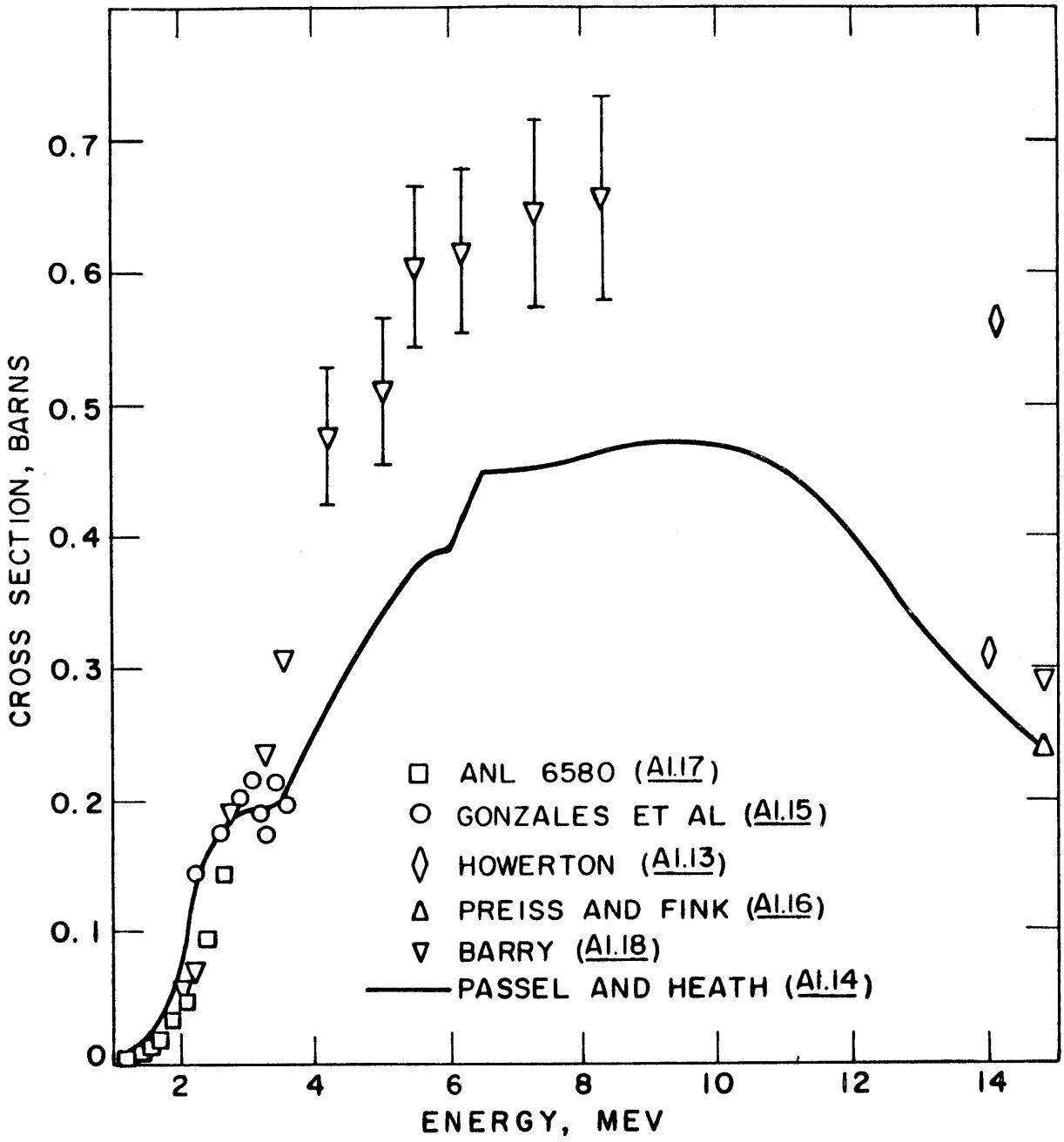

FIGURE A1.7 $Ni^{58}(n,p)\,Co^{58}$ CROSS SECTION

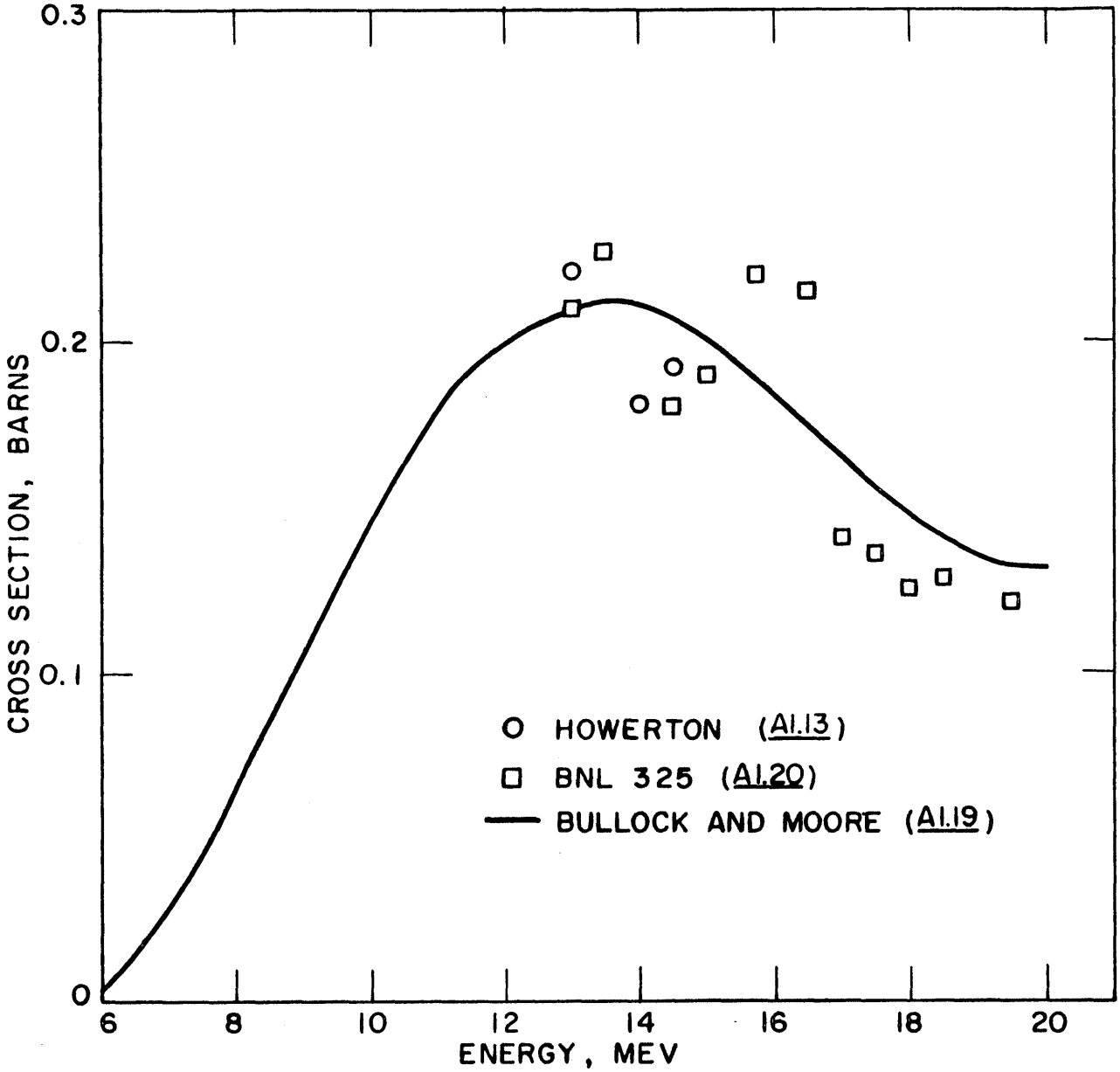

FIGURE A1.8 Mg^{24} (n,p) Na^{24} CROSS SECTION

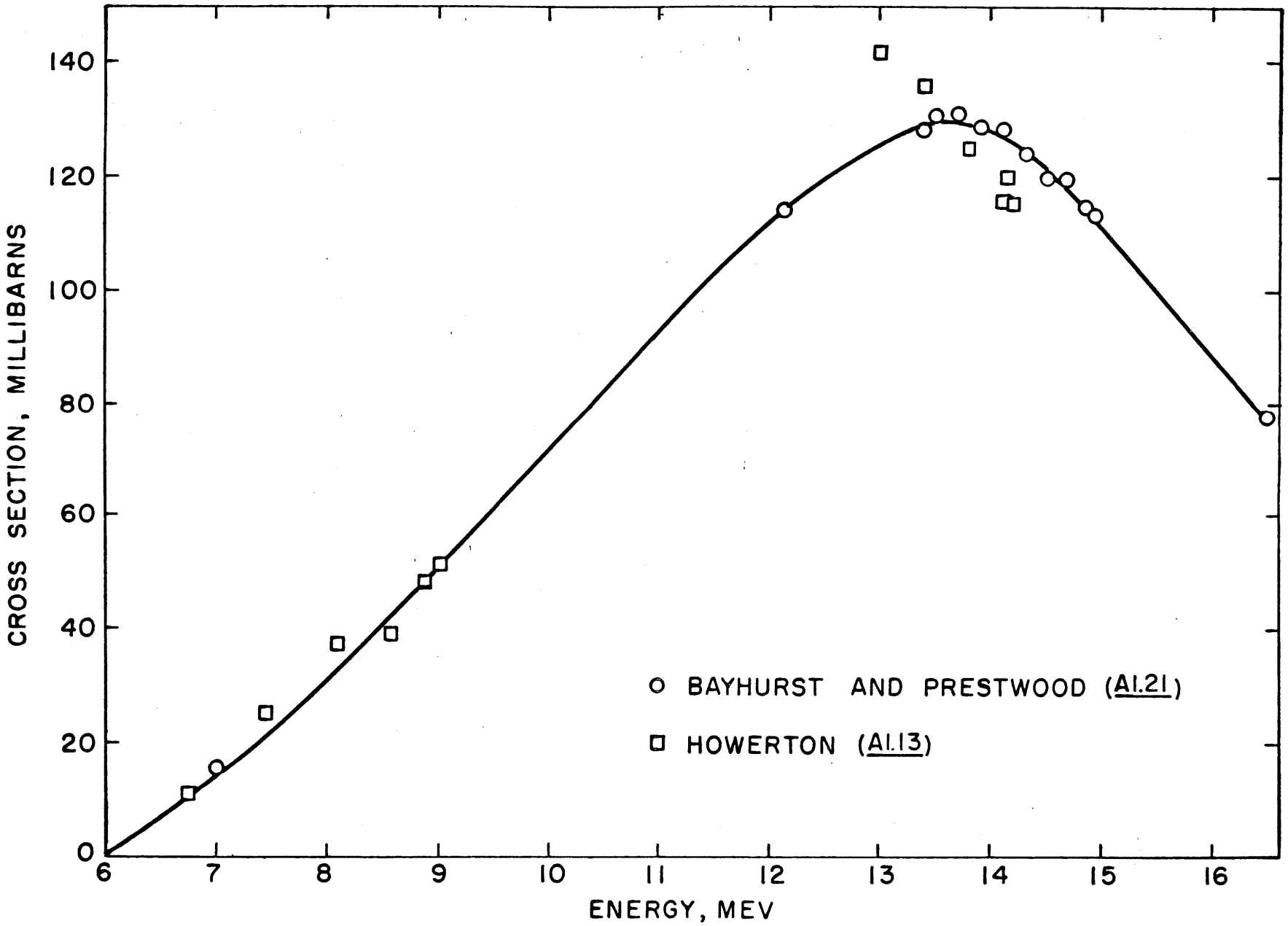

FIGURE A1.9 $Al^{27}(n,\alpha)Na^{24}$ CROSS SECTION

TABLE A1.12

Threshold Energies and Effective Cross Sections for S^{32}, Ni^{58}, Mg^{24} and Al^{27}[a]

Isotope	E_{eff} (Mev)	$\overline{\sigma}_{eff}$ (barns)
S^{32}	3.0	0.3
Ni^{58}	2.9	0.41
Mg^{24}	6.3	0.051
Al^{27}	8.1	0.1

a. Watt fission spectrum used for initial iteration. $\overline{\sigma}_{eff}$ values represent those calculated using the Watt spectrum.

A1.10 Counting Efficiency, ϵ, for Foil Measurements

The procedure for determining the counting efficiencies for the various foils used in this experiment has been described in detail by Sefchovich (A1.9). For the sulfur detectors the sulfur was irradiated as $MgSO_4$, then dissolved in 2N-hydrochloric acid (containing 1 g/80 cc $(NH_4)_3PO_4$ as a carrier for the P^{32}). The dissolved sample was placed on a planchet and dried before counting by a GM tube. A simulated P^{32} Reference Source Kit from the Tracerlab Co., Waltham, Mass. with a known absolute count rate was used as a reference to determine the absolute count rate of the irradiated samples.

The nickel, magnesium, aluminum, cobalt and copper detectors were in the form of wires of lengths varying from 1/8" to 1", and were counted in a NaI well-type scintillation crystal. The efficiency of the crystal for all detectors but the copper was determined by the use of coincidence counting. The coincidence counting procedure is nearly the same as described by Sefchovich (A1.19), except that only one of the gamma photo peaks was allowed in each channel (Sefchovich counted both photo peaks in each channel). For the calibration, the absolute count rate of each wire was determined by the coincidence method, and then the wire was counted in the NaI crystal used for this experiment. The ratio of

the two count rates determined the efficiency of the crystal. Coincidence counting cannot determine the absolute count rate of the copper detector, so the copper measurements were used only to determine the resonance flux (at 570 ev), since only the cadmium ratio is needed for this calculation.

The efficiency of the NaI crystal used for the nickel, magnesium, aluminum and cobalt detectors is given in Table A1.13. The error limits are calculated from the counting statistics. Also shown are the corrected values obtained by Sefchovich (A1.9). In general, the results compare favorably with the previous measurements, and there seems to be no effect of wire size on the crystal efficiency. The present measurements are believed more accurate.

Using the data of Table A1.13 and the weight precent of the desired isotope in each detector, the overall counting efficiency of the NaI system for the foils used was calculated. The results are given in Table A1.14.

TABLE A1.13

NaI Crystal Efficiency for Foil Measurements

Foil	Efficiency (this work)	Efficiency [Previous Measurements at MIT] (A1.9)[a]
Ni-1 cm	0.37±0.01	0.41
Ni-1/4 cm	0.38±0.01	
Mg-1 in.	–	0.50
Mg-1/4 in.	0.53±0.02	
Al-1 in.	0.53±0.02	0.50
Al-1/4 in.	0.53±0.02	
Co-1 in.	0.46±0.01	0.47
Co-1/4 in.	0.45±0.01	

a. Corrected values.

TABLE A1.14

Overall Counting Efficiency for Foil Measurements

Foil	ϵ
Ni	0.25
Mg	0.42
Al	0.53
Co	0.0027

A1.11 Accuracy of Absolute Neutron Flux Measurements

In general, the largest sources of error in the absolute flux measurements were in the counting efficiencies (see Table A1.13) and in the cross sections (reported in Section A1.9). Table A1.15 lists the standard deviations assigned to the individual detectors.

TABLE A1.15

Errors in Absolute Neutron Flux Measurements

Flux	Detector	Standard Deviation, %
Thermal	Cobalt	±8
Epithermal	Cobalt	±10
	Copper	±11
Fast	Sulfur	±13
	Nickel	±20
	Magnesium	±13
	Aluminum	±10

For the thermal flux measurements the standard deviation in the counting efficiency was about 3% and the standard deviation in the cross section about 2%. However, there is also a possible error in the weight percent cobalt in the Co-Al wires. Sefchovich (A1.9) has reported a standard deviation of 6.7% in the weight percent determination, so that the overall standard deviation was about 8%.

The epithermal flux was not affected by errors in counting efficiency or weight percent cobalt directly, since the cadmium ratio was the quantity measured. However, it was affected by errors in the thermal flux, errors in the cross sections used, and a possible error in the cadmium cutoff energy (see Section A1.9).

For all fast flux measurements a standard deviation of 5% was assigned to the iterative method for determining the differential fluxes, since these fluxes were determined by differentiating an exponential curve fitted to the integral flux measurements. For the sulfur detectors, the counting standard used was accurate to ±10% (A1.2), and a standard deviation of 5% was assigned to the cross section data. For the nickel detectors, the counting efficiency had a standard deviation of 4% (see Table A1.13) but the cross section data seem to be quite scattered (see Fig. A1.7) so a standard deviation of 20% was assigned to these data. The magnesium and aluminum detectors had a counting efficiency error of ±6%. An error of ±10% was assigned to the cross section data for magnesium, as the data are based mostly on theory. An error of ±5% was assigned to the aluminum cross section data, which seem reliable.

In the reflector region of the reactor additional errors in the fast flux were possible due to small amounts of impurities in the detectors and low count rates. This was because of the large ratio of thermal to fast flux in the reflector region. No formal error can be assigned to the effect of impurities, since the amounts and types of impurities are unknown at present. Therefore the fast flux data in the reflector region are subject to some doubt.

A1.12 Foil Activation Computer Program, MNFOIL

MNFOIL is an IBM 709/7090 FORTRAN program (for use with a 32K storage) which uses the theory of Section A1.8 to determine the differential flux $\phi(E)$ from the foil activation measurements. The FORTRAN listing of MNFOIL is given in Table A1.16, and a logic flowsheet is given in Fig. A1.10. In the paragraphs that follow a brief description of how to use the program will be given; a sample input and sample output are given in Tables A1.17 and A.18, respectively, as an aid. Some familiarity with

TABLE A1.16
FORTRAN LISTING OF MNFOIL

```
*      LIST 8
*      LABEL
*      SYMBOL TABLE
CMNFOIL
C      MNFOIL HAS SUBPROGRAMS MAIN,LINLSQ(2) IN FORTRAN, LINLAG IN FAP
C      MAIN HAS 156 CARDS      2.28.63
       COMMON SUMX,SUMY,SUMX2,SUMXY,SUMY2,SLOPE,ENTCPT,SIG2E,SIG2P,SIGA,S
      1IGB,RLIN,NOT,KPUNCH
       DIMENSION NENG(50),H(50),EFFIC(50),ATWT(50),SIGAV(50),ELAMB(50),ET
      1H(50),SIGENG(100,50),ENG(100,50),SIGAV1(50),POS(100),RUN(50),PHIIN
      2T(50),Y(50),PHIDIP(50),SIGAV2(50),NLAST(50),FACTOR(50),N(50),SL(10
      30),SIGS(100),ENT(100),SIGE(100),RL(100)
       NOT=2
       NIT=4
       READINPUTTAPE NIT,2,NFOT,NFOR,KPUNCH,(NENG(I),I=1,NFOT)
       NFO=NFOT+NFOR
       NF=NFOT+1
       DO 42 I=1,NFOT
       NE=NENG(I)
       READINPUTTAPE NIT,5,(SIGENG(J,I),ENG(J,I),J=1,NE)
    42 CONTINUE
       READINPUTTAPE NIT,5,TAU,ERROR1,ERROR2,(FACTOR(I),I=NF,NFO),(ATWT(I
      1),SIGAV(I),ELAMB(I),ETH(I),I=1,NFO),(EFFIC(I),I=2,NFO),(H(I),I=1,N
      2FOT)
       DO 6 I=1,NFOT
       SIGAV1(I)=SIGAV(I)
     6 CONTINUE
    41 READINPUTTAPE NIT,1
     1 FORMAT(80H
      1                              )
       READINPUTTAPE NIT,2,NFOILT,NFOILR,NPOS,(N(I),I=1,NFO),KEND
     2 FORMAT(/(18I4))
       WRITEOUTPUTTAPE NOT,1
       WRITEOUTPUTTAPE NOT,30
    30 FORMAT(/8X8HPOSITION,2X8HDETECTOR,3X5HETH/R,2X37HSIGMA AV/CR PHI I
      1NT/F2200 PHI DIFF/FO)
       IF(KPUNCH)3,3,4
     3 PUNCH 1
       PUNCH 30
     4 NFOIL=NFOT+NFOILR
     5 FORMAT(/(6E12.5))
       DO 23 J=1,NPOS
       READINPUTTAPE NIT,5,POS(J)
       IF(NFOILT)99,99,98
    98 DO 9 I=1,NFOT
       IF(N(I))63,63,64
    64 Y(I)=0.
       PHIINT(I)=0.
       GO TO 9
    63 IF(I-1)60,60,61
    60 READINPUTTAPE NIT,8,COUNT,TCOUNT,BACK,TBACK,WT,EMW,RUN(I),TIRR,TWA
      1IT,EFFIC(I)
       GO TO 62
    61 READINPUTTAPE NIT,8,COUNT,TCOUNT,BACK,TBACK,WT,EMW,RUN(I),TIRR,TWA
      1IT
     8 FORMAT(6E12.5,A6/(6E12.5))
    62 COUNT=COUNT/(TCOUNT-TAU*COUNT)
```

TABLE A1.16 (CONTINUED)

```
      BACK=BACK/(TBACK-TAU*BACK)
      PHIINT(I)=(COUNT-BACK)*ATWT(I)*EXPF(ELAMB(I)*TWAIT*1440.0)/(EFFIC(
     1I)*36.138*EMW*WT*SIGAV1(I)*(1.0-EXPF(-ELAMB(I)*TIRR)))
      Y(I)=LOGF(PHIINT(I))
    9 CONTINUE
   26 CALL LINLSQ(1,NFOT,ETH,Y,-1)
      IF(SLOPE)101,19,19
  101 DO 10 I=1,NFOT
      NLAST(I)=1
      PHIDIP(I)=-SLOPE*1.0E-6*EXPF(ENTCPT+SLOPE*ETH(I))
   10 CONTINUE
      KTEST=0
      DO 18 I=1,NFOT
      IF(N(I))81,81,18
   81 SENSE LIGHT 0
      ENTGRL=0.0
      E=ENG(1,I)
      NE=NENG(I)
      NSTEPS=(ENG(NE,I)-ENG(1,I))/H(I)-0.99999
      CRIT=(ENG(NE,I)-ENG(1,I))/SIGAV1(I)/PHIINT(I)
      PHISG1=0.0
      DO 15 K=1,NSTEPS
      E=E+H(I)
      CALL LINLAG(NENG(I),NLAST(I),0,ENG(1,I),SIGENG(1,I),E,SIGMA)
      PHISIG=-SLOPE*EXPF(ENTCPT+SLOPE*E)*SIGMA
      IF(PHISIG*CRIT-ERROR1)11,11,12
   11 IF(PHISIG-PHISG1)24,12,12
   12 PHISG1=PHISIG
      IF(SENSE LIGHT 1)14,13
   13 ENTGRL=ENTGRL+4.0*PHISIG
      SENSE LIGHT 1
      GO TO 15
   14 ENTGRL=ENTGRL+2.0*PHISIG
   15 CONTINUE
   24 SIGAV2(I)=H(I)*ENTGRL/3.0/EXPF(SLOPE*ETH(I)+ENTCPT)
      IF(ABSF((SIGAV1(I)-SIGAV2(I))/SIGAV1(I))-ERROR2)18,18,16
   16 KTEST=1
   18 CONTINUE
      IF(KTEST)19,19,7
   19 SL(J)=SLOPE
      ENT(J)=ENTCPT
      SIGS(J)=SIGB
      SIGE(J)=SIGA
      RL(J)=RLIN
   99 IF(NFOILR)65,65,66
   66 DO 21 I=NF,NFOIL
      READINPUTTAPE NIT,8,COUNT,TCOUNT,BACK,TBACK,WT,TIRR,RUN(I),TWAIT,C
     1OUNTC,TCOUNC,BACKC,TBACKC,WTC,TIRRC,TWAITC,EMW
      BACK=BACK/(TBACK-TAU*BACK)
      BACKC=BACKC/(TBACKC-TAU*BACKC)
      COUNT=(COUNT/(TCOUNT-TAU*COUNT)-BACK)*EXPF(ELAMB(I)*TWAIT*1440.0)/
     1(1.0-EXPF(-ELAMB(I)*TIRR))/WT
      COUNTC=(COUNTC/(TCOUNC-TAU*COUNTC)-BACKC)*EXPF(ELAMB(I)*TWAITC*144
     10.0)/(1.0-EXPF(-ELAMB(I)*TIRRC))/WTC
      SIGAV1(I)=COUNT/COUNTC
      IF(I-NF)50,50,51
   50 PHIINT(I)=(COUNT-COUNTC)*ATWT(I)/(EFFIC(I)*36.138*EMW    *SIGAV(I))
      P=PHIINT(I)*EMW
   51 PHIDIP(I)=FACTOR(I)*P/(SIGAV1(I)-1.0)/EMW
```

TABLE A1.16 (CONTINUED)

```
 21 CONTINUE
 65 WRITEOUTPUTTAPE NOT,33,POS(J)
 33 FORMAT(F15.2)
    IF(KPUNCH)34,34,35
 34 PUNCH 33,POS(J)
 35 IF(J-1)31,31,32
 31 DO 36 I=1,NFO
    IF(N(I))37,37,36
 37 WRITEOUTPUTTAPE NOT,38,RUN(I),ETH(I),SIGAV1(I),PHIINT(I),PHIDIP(I)
 38 FORMAT(19XA6,0PF10.5,1PE12.5,1P2E13.5)
    IF(KPUNCH)39,39,36
 39 PUNCH 38,RUN(I),ETH(I),SIGAV1(I),PHIINT(I),PHIDIP(I)
 36 CONTINUE
    GO TO 23
 32 DO 90 I=1,NFO
    IF(N(I))91,91,90
 91 WRITEOUTPUTTAPE NOT,92,SIGAV1(I),PHIINT(I),PHIDIP(I)
 92 FORMAT(34X1P3E13.5)
    IF(KPUNCH)93,93,90
 93 PUNCH 92,SIGAV1(I),PHIINT(I),PHIDIP(I)
 90 CONTINUE
    GO TO 23
  7 DO 17 I=1,NFOT
    IF(N(I))100,100,17
100 PHIINT(I)=PHIINT(I)*SIGAV1(I)/SIGAV2(I)
    SIGAV1(I)=SIGAV2(I)
    Y(I)=LOGF(PHIINT(I))
 17 CONTINUE
    GO TO 26
 23 CONTINUE
    IF(NFOILT)96,96,97
 97 WRITEOUTPUTTAPE NOT,94,(POS(J),SL(J),SIGS(J),ENT(J),SIGE(J),RL(J),
   1J=1,NPOS)
 94 FORMAT(1H-,5X8HPOSITION,5X5HSLOPE,5X11HS.D.(SLOPE),2X9HINTERCEPT,3
   1X11HS.D.(INTCP),2X11HCORR. COEF./(0PF12.2,1X1P5E13.5))
    IF(KPUNCH)95,95,96
 95 PUNCH 94,(POS(J),SL(J),SIGS(J),ENT(J),SIGE(J),RL(J),J=1,NPOS)
 96 IF(KEND)41,41,40
 40 CALL EXIT
    END
```

TABLE A1.16 (CONTINUED)

```
*       LIST 8
*       LABEL
*       SYMBOL TABLE
        SUBROUTINE LINLSQ(N1,N2,X,Y,N3)
CLINLS2
C       LINLSQ(2) HAS 47 CARDS              7-26-63
        COMMON SUMX,SUMY,SUMX2,SUMXY,SUMY2,SLOPE,ENTCPT,SIG2E,SIG2P,SIGA,S
       1IGB,RLIN,NOT,KPUNCH
        DIMENSION X(300),Y(300)
        SUMX=0.0
        SUMY=0.0
        SUMX2=0.0
        SUMXY=0.0
        SUMY2=0.0
        EN=N2-N1+1
        DO 1 I=N1,N2
        IF(Y(I))12,11,12
   11   EN=EN-1.0
        GO TO 1
   12   SUMX=SUMX+X(I)
        SUMY=SUMY+Y(I)
        SUMX2=SUMX2+X(I)**2
        SUMXY=SUMXY+X(I)*Y(I)
        SUMY2=SUMY2+Y(I)**2
    1   CONTINUE
        DEN=EN*SUMX2-SUMX**2
        SLOPE=(EN*SUMXY-SUMX*SUMY)/DEN
        ENTCPT=(SUMY*SUMX2-SUMX*SUMXY)/DEN
        SIG2E=(SUMY2-ENTCPT*SUMY-SLOPE*SUMXY)/(EN-2.0)
        IF(SIG2E)9,9,10
    9   SIG2E=0.0
   10   SIG2P=(SUMY2-SUMY**2/EN)/(EN-1.0)
        SIGB=SQRTF(EN*SIG2E/DEN)
        SIGA=SQRTF(SUMX2*SIG2E/DEN)
        RLIN=SQRTF(1.0-SIG2E*(EN-2.0)/SIG2P/(EN-1.0))
        IF(N3)8,2,5
    2   WRITEOUTPUTTAPE NOT,3
    3   FORMAT(75H      SLOPE      S.D.(SLOPE)    INTERCEPT    S.D.(INTCP)  CO
       1RR. COEFF      SIG2E)
        IF(KPUNCH)4,4,5
    4   PUNCH 3
    5   WRITEOUTPUTTAPE NOT,6,SLOPE,SIGB,ENTCPT,SIGA,RLIN,SIG2E
    6   FORMAT(1P6E13.5)
        IF(KPUNCH)7,7,8
    7   PUNCH 6,SLOPE,SIGB,ENTCPT,SIGA,RLIN,SIG2E
    8   RETURN
        END
```

TABLE A1.16 (CONTINUED)

```
*       LINLAG HAS 141 CARDS
*       FAP
        COUNT   140
      1 TTL     LINEAR AND LAGRANGIAN INTERPOLATION SUBROUTINE
        LBL     LINLAG
        ENTRY   LINLAG
        REM     THE FORTRAN CALLING SEQUENCE IS . . .
        REM     CALL LINLAG(N,NLAST,MOR,A,B,P,Q)
        REM
        REM     N IS THE NUMBER OF ELEMENTS IN A AND B
        REM     NLAST IS LAST TIMESS CORRECT INTERVAL
        REM     MOR IS THE NUMBER OF POINTS TO BE USED IN INTERPOLATION.
        REM     A FASTER LINEAR INTERPOLATION RESULTS WITH MOR=0
        REM     A IS THE INDEPENDENT VARIABLE (1D MATRIX)
        REM     B IS THE DEPENDENT VARIABLE (1D MATRIX)
        REM     P IS THE PARTICULAR VALUE OF A
        REM     Q IS THE ANSWER RETURNED BY THE SUBROUTINE
        REM
LINLAG  CLA*    1,4
        SUB     =01000000
        TZE     ONEEL                   TEST NO. OF ELEMENTS
        STD     NLOOP                   SET UPPER BOUND ON THE A TABLE
        SXA     BACK,1                  SAVE INDEX REGISTERS
        SXA     BACK+1,2
        SXD     LINLAG-2,4
        CLA     4,4
        STA     SETA1                   SET UP A
        STA     SETA2
        ADD     =1
        STA     SETA3                   SET UP A+1
        CLA*    2,4                     LAST TIMES CLOSEST
        PDX     0,1                     ELEMENT NO. TO IR1
LOOP1   CLA*    6,4
SETA1   FSB     **,1                    P-A(IR1)
        TPL     TEST1
        NZT     CONST                   IS CONST=0
        TRA     FOUND
        TXI     *+1,1,-1                NO. DECREASE IR1 BY 1
        TXL     LOOP1,1,-2              IS P LESS THAN A(1)
        TRA     OUT                     YES. ERROR IN CALLING PROGRAM
FOUND   ZET*    3,4                     IS INTERPOLATION TO BE LINEAR
        TRA     LGRNG                   NO. GO TO LAGRANGIAN
        STO     DATA                    YES. STORE P-A(L) IN DATA
        CLA     5,4
        STA     SETB1                   SET UP B
        STA     SETB2
        ADD     =1
        STA     SETB3                   SET UP B+1
SETA2   CLA     **,1
SETA3   FSB     **,1                    A(L)-A(L-1)
        STO     Q
SETB1   CLA     **,1
SETB3   FSB     **,1                    B(L)-B(L-1)
        FDP     Q
        FMP     DATA
SETB2   FAD     **,1                    B(L)
        STO*    7,4                     ANSWER
        PXD     0,1
        SUB     =01000000
```

TABLE A1.16 (CONTINUED)

```
        STO*    2,4                     STORE NEW NEAR ELEMENT NO.
 BACK   AXT     **,1
        AXT     **,2                    RESTORE INDEX REGISTERS
        SXD     CONST,4
        TRA     8,4                     RETURN TO CALLING PROGRAM
TEST1   STZ     CONST
        TXI     *+1,1,1                 INCREASE IR1 BY 1
NLOOP   TXL     LOOP1,1,**
  OUT   TSX     $ERROR,4                ERROR SUBROUTINE
        PZE     ALPHA
        TXI     *+2,0,0
        PZE     LINLAG-2,0,0
        TSX     $EXIT,4
LGRNG   PXD     0,1
        SUB     =01000000
        STO*    2,4                     STORE NEW NEAR ELEMENT NO.
        CLA*    3,4
        PDX     0,1                     M1 TO IR1
        STO     M1
        ARS     19
        ALS     18                      INTEGER DIVISION BY TWO
        SUB*    2,4
        TZE     NOW+1
        TPL     SETLO                   CHECK LOW END OF TABLE
        STO     LOW
        ADD*    1,4
        SUB     M1
        SUB     =01000000
        TMI     SETHI                   CHECK HIGH END OF TABLE
        CLA     LOW
  NOW   ARS     18
        ADD     4,4
        STA     ALOW1                   SET UP A+LOW
        STA     ALOW2
        STA     ALOW3
        SUB     4,4
        ADD     5,4
        STA     BLOW                    SET UP B+LOW
        CLA     6,4
        STA     SETP
        STZ     Q                       Q=0.0 INITIALLY
LOOP2   SXD     K,1
        CLA     =1.0
        STO     PK                      PK=1.0 INITIALLY
        LXD     M1,2                    M1 TO IR2
LOOP3   PXD     0,2
        SUB     K
        TZE     TEST3                   COMPARE IR1 WITH IR2
ALOW2   CLA     **,1
ALOW3   FSB     **,2                    A(-LOW+IR1)-A(-LOW+IR2)
        STO     DATA
 SETP   CLA     **
ALOW1   FSB     **,2                    P-A(-LOW+IR2)
        FDP     DATA
        FMP     PK
        STO     PK                      PK=PK*(P-A(-LOW+IR2))
TEST3   TIX     LOOP3,2,1               DECREASE IR2 BY 1
 BLOW   LDQ     **,1                    B(-LOW+IR1)
        FMP     PK
```

TABLE A1.16 (CONCLUDED)

```
        FAD     Q
        STO     Q
        TIX     LOOP2,1,1                DECREASE IR1 BY 1
        STO*    7,4
        TRA     BACK
SETLO   CLA     =01000000
        TRA     NOW
SETHI   SSP
        ADD     LOW
        TRA     NOW
ONEEL   CLA*    5,4
        STO*    7,4                      ANSWER IS SINGLE ELEMENT
        TRA     8,4
 DATA   PZE
   M1   PZE
  LOW   PZE
   PK   PZE
    K   PZE
    Q   PZE
CONST   OCT     1
ALPHA   BCI     5, EXTRAPOLATION IS NOT POSSIBLE
        OCT     777777777777
        END
```

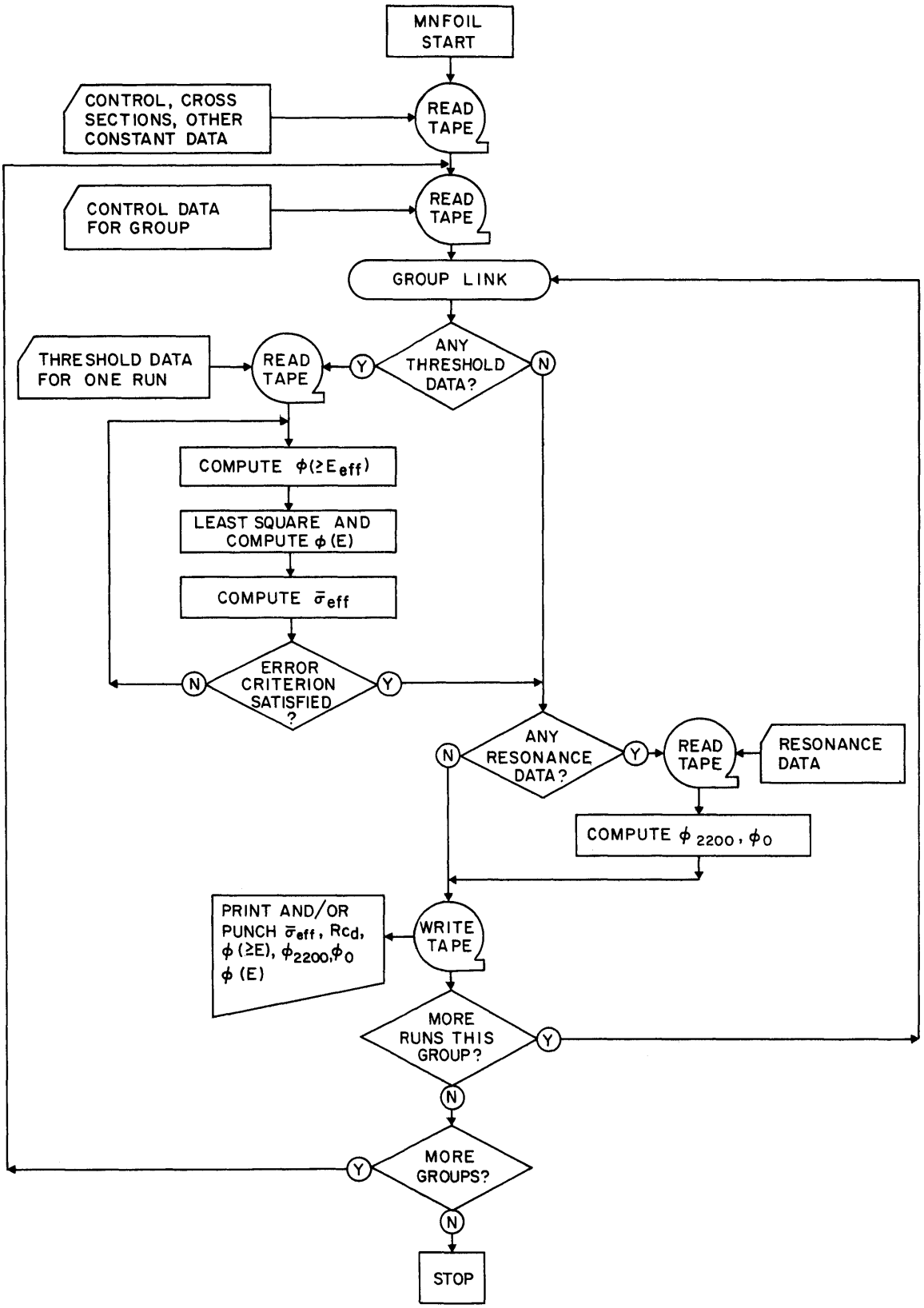

FIGURE A1.10 LOGIC FLOWSHEET FOR MNFOIL

TABLE A1.17
SAMPLE INPUT TO MNFOIL

```
                                CONTROL CONSTANTS
  4   2   0  24  24  16  18
                S32 (N,P) P32          DATA OF HOWERTON
0.0             1.59            0.0052          1.98            0.0072          2.08
0.022           2.18            0.073           2.57            0.117           2.92
0.221           3.56            0.302           4.04            0.263           4.54
0.25            4.82            0.248           5.33            0.304           5.69
0.331           6.11            0.336           6.61            0.322           7.11
0.346           7.61            0.324           8.09            0.351           8.58
0.351           9.07            0.376           9.56            0.333           12.0
0.3             13.1            0.28            13.5            0.23            14.3
                 NI58 (N,P) CO58        DATA OF PASSELL AND HEATH
0.              .999            0.              1.              .011            1.5
.07             2.              .14             2.25            .17             2.5
.187            2.75            .195            3.              .2              3.5
.25             4.              .3              4.5             .34             5.
.38             5.5             .39             6.              .45             6.5
.45             7.              .46             8.              .47             9.
.47             10.             .45             11.             .4              12.
.33             13.             .275            14.             .23             15.
                MG24 (N,P) NA24        THEORY OF BULLOCK AND MOORE
0.0             5.85            0.0147          6.5             0.029           7.0
0.0665          8.0             0.1075          9.0             0.146           10.0
0.180           11.0            0.191           11.5            0.199           12.0
0.205           12.5            0.21            13.0            0.212           13.5
0.21            14.3            0.201           15.0            0.184           16.0
0.165           17.0
                 AL27 (N,ALPHA) NA24            LA 2493
0.0             6.0             0.0145          7.0             0.0305          8.0
0.050           9.0             0.071           10.0            0.093           11.0
0.112           12.0            0.120           12.5            0.123           12.75
0.126           13.0            0.128           13.25           0.1295          13.5
0.1295          13.75           0.128           14.0            0.1205          14.5
0.111           15.0            0.088           16.0            0.065           17.0
                EFFICIENCIES, ATOMIC WTS, CROSS SECTIONS ETC
1.2300E-07      0.0005          0.01            0.528           0.887           32.07
0.3             3.37100E-5      3.0             58.69           0.43            6.69700E-6
2.9             24.32           0.06            7.70200E-4      6.3             26.98
0.098           7.70200E-4      8.1             58.94           38.0            2.50300E-7
1.20000E-4      63.57           4.5             9.01130E-4      5.70000E-4      0.254
0.417           0.530           0.00270                         0.1             0.1
0.1             0.1
1                       THIS IS RUN SERIES 13  3.28.63
                            CONTROL TABLE
  4   2   8
                      RUN 13 IN POSITION -9.
-9.
45386.          20.             19719.          90.             0.000954        1.95            13S
30.             7.8562          0.01006
906683.         4.              7003.           7.              0.01750         1.95            13NI
30.             11.1569
140067.         4.              48036.          60.             0.00498         1.94            13MG
25.             2.0424
313974.         4.              8431.           10.             0.02154         1.95            13AL
23.             2.0271
506833.         4.              10077.          12.             0.01342         30.             13CO
11.             69469.          4.              29579.          30.             0.01398
```

TABLE A1.17 (CONTINUED)

30. 11. 1.95
558783. 4. 62267. 60. 0.01085 30. 13CU
6.9972 52947. 4. 50993. 60. 0.01166
31. 6.7069 1.95
RUN 13 IN POSITION -4.
-4.
25602. 10. 19719. 90. 0.000859 1.95 13S
30. 7.8472 0.01006
1100957. 4. 7003. 7. 0.01776 1.95 13NI
30. 11.1375
174078. 4. 48036. 60. 0.005 1.94 13MG
25. 2.0576
330647. 4. 26255. 30. 0.02154 1.95 13AL
21. 2.1125
622582. 4. 29579. 30. 0.01357 30. 13CO
11. 91072. 4. 10077. 12. 0.014
30. 11. 1.95
803962. 4. 50993. 60. 0.01087 31. 13CU
6.7104 59513. 4. 62267. 60. 0.01174
30. 6.9924 1.95
RUN 13 IN POSITION 2.
2.
27739. 10. 19719. 90. 0.0009 1.95 13S
30. 7.8382 0.01006
1020441. 4. 7003. 7. 0.01602 1.95 13NI
30. 11.1597
174368. 4. 48036. 60. 0.00498 1.94 13MG
25. 2.0667
399458. 4. 8431. 10. 0.02152 1.95 13AL
23. 2.0214
583252. 4. 10077. 12. 0.01339 30. 13CO
11. 98692. 4. 29579. 30. 0.01398
30. 11. 1.95
645759. 4. 62267. 60. 0.01073 30. 13CU
6.9861 71017. 4. 50993. 60. 0.01159
31. 6.7153 1.95
RUN 13 IN POSITION 8.
8.
40955. 20. 19719. 90. 0.000774 1.95 13S
30. 7.8236 0.01006
990177. 4. 7003. 7. 0.01832 1.95 13NI
30. 11.141
148862. 4. 48036. 60. 0.00502 1.94 13MG
25. 2.0715
280294. 4. 26255. 30. 0.02163 1.95 13AL
21. 2.1056
506620. 4. 29579. 30. 0.01359 30. 13CO
11. 76690. 4. 10077. 12. 0.01428
30. 11. 1.95
645737. 4. 50993. 60. 0.01092 31. 13CU
6.7188 47943. 4. 62267. 60. 0.01175
30. 6.9806 1.95
RUN 13 IN POSITION 13.
13.
17145. 20. 19719. 90. 0.000931 1.95 13S
30. 7.8090 0.01006
298888. 4. 7003. 7. 0.01855 1.95 13NI
30. 11.1632
46627. 4. 48036. 60. 0.00513 1.94 13MG

TABLE A1.17 (CONCLUDED)

25.	2.0757					
111657.	4.	8431.	10.	0.02192	1.95	13AL
23.	2.0125					
389717.	4.	10077.	12.	0.01363	30.	13CO
11.	42674.	4.	29579.	30.	0.01428	
30.	11.	1.95				
457977.	4.	62267.	60.	0.01117	30.	13CU
6.9771	29268.	4.	50993.	60.	0.01176	
31.	6.7215	1.95				
	RUN 13 IN POSITION 17.					
17.						
7322.	20.	19719.	90.	0.000977	1.95	13S
30.	7.7938	0.01006				
71070.	4.	7003.	7.	0.02084	1.95	13NI
30.	11.1456					
23160.	4.	48036.	60.	0.00516	1.94	13MG
25.	2.0792					
23957.	4.	26255.	30.	0.02212	1.95	13AL
21.	2.0993					
297469.	4.	29579.	30.	0.01382	30.	13CO
11.	30377.	6.	10077.	12.	0.01446	
30.	11.	1.95				
390039.	4.	50993.	60.	0.01126	31.	13CU
6.7257	26436.	8.	62267.	60.	0.01198	
30.	6.9708	1.95				
	RUN 13 IN POSITION 22.					
22.						
4919.	20.	19719.	90.	0.001006	1.95	13S
30.	7.7792	0.01006				
25461.	6.	7003.	7.	0.02142	1.95	13NI
30.	11.1667					
20203.	12.	48036.	60.	0.00518	1.94	13MG
25.	2.0826					
25307.	10.	8431.	10.	0.02237	1.95	13AL
23.	2.0021					
148906.	4.	10077.	12.	0.01385	30.	13CO
11.	21676.	12.	29579.	30.	0.0145	
30.	11.	1.95				
165906.	4.	62267.	60.	0.01130	30.	13CU
6.9507	26248.	16.	50993.	60.	0.01223	
31.	6.7285	1.95				
	RUN 13 IN POSITION 27.					
27.						
4532.	20.	19719.	90.	0.000919	1.95	13S
30.	7.7625	0.01006				
22712.	12.	7003.	7.	0.02269	1.95	13NI
30.	11.1479					
23079.	20.	48036.	60.	0.00539	1.94	13MG
25.	2.0875					
24616.	20.	26255.	30.	0.02329	1.95	13AL
21.	2.0813					
66058.	4.	29579.	30.	0.01393	30.	13CO
11.	23143.	20.	10077.	12.	0.01460	
30.	11.	1.95				
84331.	4.	50993.	60.	0.01131	31.	13CU
6.7403	23965.	20.	62267.	60.	0.01250	
30.	6.9507	1.95				

TABLE A1.18
SAMPLE OUTPUT FROM MNFOIL

THIS IS RUN SERIES 13 3.28.63

POSITION	DETECTOR	ETH/R	SIGMA AV/CR	PHI INT/F2200	PHI DIFF/FO
-9.00					
	13S	3.00000	3.03473E-01	4.64228E 11	3.39064E 05
	13NI	2.90000	4.36504E-01	5.52457E 11	3.63419E 05
	13MG	6.30000	5.89627E-02	4.91812E 10	3.43648E 04
	13AL	8.10000	9.92332E-02	1.42946E 10	9.85916E 03
	13CO	0.00012	8.11352E 00	9.12230E 12	6.77102E 11
	13CU	0.00057	1.83961E 01	0.	4.65163E 11
-4.00					
			3.03473E-01	5.88485E 11	4.15993E 05
			4.36504E-01	6.65494E 11	4.45625E 05
			5.89627E-02	6.22623E 10	4.29450E 04
			9.92332E-02	1.81237E 10	1.24452E 04
			7.39785E 00	1.09741E 13	9.05671E 11
			1.07330E 01	0.	1.00018E 12
2.00					
			3.03473E-01	6.12696E 11	4.33111E 05
			4.36504E-01	6.82022E 11	4.64218E 05
			5.89627E-02	6.32542E 10	4.39068E 04
			9.92332E-02	1.81790E 10	1.25984E 04
			6.48688E 00	1.01836E 13	9.79959E 11
			1.53152E 01	0.	6.31041E 11
8.00					
			3.03473E-01	5.09534E 11	3.64685E 05
			4.36504E-01	5.77980E 11	3.90907E 05
			5.89627E-02	5.36423E 10	3.68797E 04
			9.92332E-02	1.51303E 10	1.05679E 04
			7.29980E 00	8.85307E 12	7.41996E 11
			1.10831E 01	0.	7.78850E 11
13.00					
			3.02838E-01	1.48011E 11	1.03187E 05
			4.33109E-01	1.68368E 11	1.10456E 05
			5.99755E-02	1.54080E 10	1.09131E 04
			9.83213E-02	4.83278E 09	3.20451E 03
			1.05641E 01	7.09127E 12	3.91485E 11
			2.69365E 01	0.	2.42531E 11
17.00					
			3.00811E-01	3.26824E 10	2.18518E 04
			4.21584E-01	3.47655E 10	2.32597E 04
			6.41077E-02	6.60729E 09	2.78371E 03
			9.52923E-02	1.12180E 09	9.04725E 02
			1.83377E 01	5.53306E 12	1.68503E 11
			3.23332E 01	0.	1.56644E 11
22.00					
			2.99420E-01	5.82019E 09	3.54957E 03
			4.12648E-01	6.67415E 09	3.75810E 03
			6.83904E-02	1.09542E 09	5.39537E 02
			9.30150E-02	3.07511E 08	1.93088E 02
			4.66383E 01	2.82043E 12	3.26303E 10
			7.66637E 01	0.	3.30660E 10
27.00					
			2.99420E-01	1.77821E 09	1.05479E 03
			4.12648E-01	1.73261E 09	1.11712E 03
			6.83904E-02	4.23552E 08	1.58601E 02
			9.30150E-02	7.43611E 07	5.64251E 01

TABLE A1.18 (CONCLUDED)

5.13753E 01 1.19612E 12 1.25370E 10
1.02933E 02 0. 1.04091E 10

POSITION	SLOPE	S.D.(SLOPE)	INTERCEPT	S.D.(INTCP)	CORR. COEF.
-9.00	-6.93684E-01	1.20268E-02	2.89962E 01	6.66131E-02	9.99700E-01
-4.00	-6.88105E-01	6.07550E-03	2.91921E 01	3.36506E-02	9.99922E-01
2.00	-6.93613E-01	4.85202E-03	2.92409E 01	2.68740E-02	9.99951E-01
8.00	-6.94356E-01	6.47685E-03	2.90701E 01	3.58735E-02	9.99913E-01
13.00	-6.80780E-01	1.03794E-02	2.77867E 01	5.74887E-02	9.99768E-01
17.00	-6.24394E-01	7.63971E-02	2.61517E 01	4.23142E-01	9.85357E-01
22.00	-5.70870E-01	3.00230E-02	2.42633E 01	1.66289E-01	9.97246E-01
27.00	-5.74153E-01	8.35849E-02	2.30539E 01	4.62954E-01	9.79457E-01

FORTRAN input/output format is assumed; for details see the IBM 709/7090 FORTRAN reference manual (A1. 5).

The input is arranged as a series of tables, each headed by a card upon which any desired information may be placed. All fixed point data use I4 format and all floating point data E12.5 format. Alphanumeric data, used to describe the run numbers, use A6 format.

The first table supplies control data for the program. It must contain the following information:

1. The total number of threshold detectors for which data will be supplied; in the present case, 4.
2. The total number of thermal and resonance foils for which data will be supplied; in the present case, 2. It is assumed that only one thermal detector will be used to calculate the thermal flux, and that this detector can also be used to calculate an epithermal flux.
3. A punch control. If the constant is ≤ 0, a punched record of the output will be given along with the printed copy. If it is >0, only a printed record will be given.
4. For each threshold detector, the number of pairs of entries in the cross section-energy tables to be supplied. The order has been arbitrarily arranged as sulfur, nickel, magnesium, aluminum.

The next series of tables supplies the cross section-energy data for each threshold detector in the form σ_1, E_1, σ_2, E_2 ..., where the cross sections are in barns and the energies in Mev. The order of threshold foils must be the same as mentioned in the first table.

The table following the threshold detector cross section data must contain the following information:

1. The dead time for the counting system used, min.
2. An error criterion which will allow the computer to stop integrating in the calculation of each $\overline{\sigma}_{eff}$ before the maximum energy specified in the cross section table has been reached. The error specified is a fraction of the average value of the integrand, $\overline{\phi(E)\sigma(E)}$, which can be easily approximated from the input $\overline{\sigma}_{eff}$ (see below), the first approximation of the integral flux $\phi(\geq E_{eff})$ and the total range of integration given in the cross section tables.

For example, a typical curve of $\phi(E)\sigma(E)$ versus energy might look schematically as shown in Fig. A1.11.

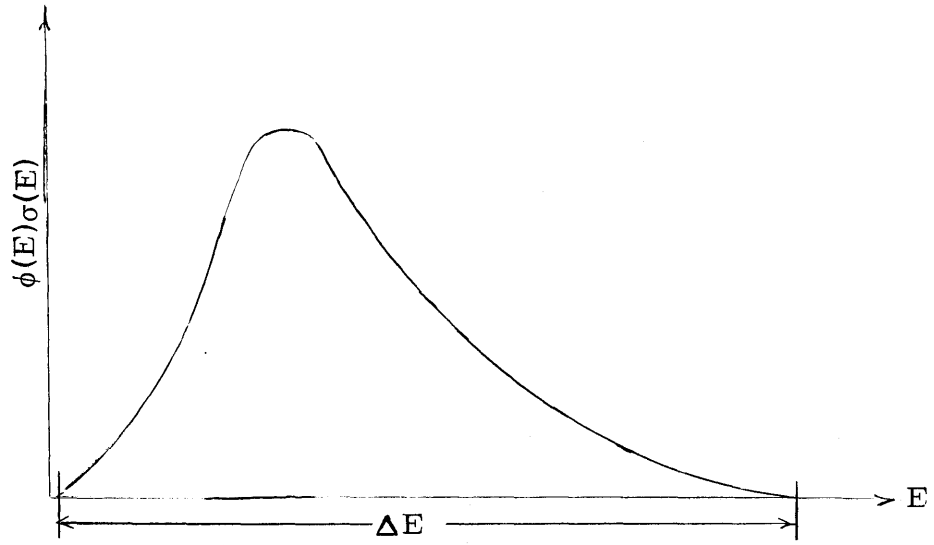

Figure A1.11 Typical Curve of $\phi(E)\sigma(E)$ versus Energy for a Threshold Detector

A good approximation of the average value of $\phi(E)\sigma(E)$ may be calculated by

$$\overline{\phi(E)\sigma(E)} \approx \frac{\overline{\sigma}_{eff}\,\phi(\geq E_{eff})}{\Delta E} \qquad \text{(A1.25)}$$

The computer, which uses Simpson's Parabolic Rule (A1.23) to evaluate the integral $\int_0^\infty \phi(E)\sigma(E)\,dE$, should be allowed to stop once the integrand becomes very small with respect to the value calculated by Eq. (A1.25), since conservative values of ΔE are usually supplied in the cross section tables. The error criterion used for the data of this experiment is 0.0005, meaning that when the ratio of $\phi(E)\sigma(E)$ calculated at a point past the maximum to Eq. (A1.25) is less than 0.0005 the computer will consider the integration complete.

3. An error criterion specifying the allowable fractional change of $\overline{\sigma}_{eff}$ for each detector between iterations on the flux shape. In this experiment the criterion chosen was 0.01, meaning that once the fractional change in the $\overline{\sigma}_{eff}$ for every threshold

detector is less than 0.01 between iterations, the computer will consider the iteration to have converged.

4. The factors, K, needed for use in Eq. (A1. 24) for the resonance detections.
5. i) Isotope atomic weight.
   ii) Cross section, barns; initial approximation to $\overline{\sigma}_{eff}$ for threshold detector, σ_{2200} for the thermal detector.
   iii) Decay constant, min^{-1}.
   iv) Detector energy, Mev; effective threshold energy for threshold detectors, resonance energy for resonance detectors.

   The threshold detector data must be given first, and the data are arbitrarily ordered as sulfur, nickel, magnesium, aluminum, cobalt, copper in this work.
6. The counter efficiency for all but the first threshold detector, sulfur. The order is nickel, magnesium, aluminum, cobalt, copper. The copper efficiency will not be used since only its cadmium ratio will be computed.
7. The integration step size for the threshold detectors, Mev. In the present case a step size of 0.1 Mev was used for all threshold detectors.

Next, the measured data are given the computer in groups. Normally, a group will consist of a series of measurements made at one time at different positions in the in-pile section. Heading each group is a "free" card upon which any desired information may be printed; the computer will re-print the information on this card to head the output from the group of data. Also, a control table must be given for each group, supplying the following information:

1. The number of threshold detectors in the group. There must be a minimum of 2 for the least squares analysis, but a zero may be typed if only thermal and resonance data are to be evaluated.
2. The number of thermal and resonance detectors in the group. There is assumed to be one thermal detector which also provides data in the resonance region. A zero may be typed if there are no data in this energy region.
3. The number of runs in the group.

4. A series of control constants for each detector. If the constant is ≤ 0 the computer will expect data for the detector; if it is >0, the computer will not expect data for the detector. The order for this experiment is, as stated above, sulfur, nickel, magnesium, aluminum, cobalt, copper. For example, the data of Table A1.17 include all the detectors used in this work.
5. A repeat control. If it is ≤ 0, the computer will search for more groups of data to analyze after the present one has been completed. If it is >0, the computer will halt after analyzing the present group.

For each run included in the group, a table of data will be given with the following information

1. The position relative to the core center where the run was made.
   i) The number of constants measured.
   ii) The counting time, min.
   iii) The number of background counts measured.
   iv) The background counting time, min.
   v) The detector weight, gm.
   vi) The reactor power level in MW at the time of the run.
   vii) In columns 73-78 of the first card for each detector, alphanumeric information describing the run number.
   viii) The irradiation time, min.
   ix) The waiting time, days.

   The first threshold detector must also supply the counting efficiency. This is because the counting efficiency for sulfur, the first detector used in this experiment, must be evaluated in a special way (A1.9) and may vary from run to run. The order for this work is sulfur, nickel, magnesium, aluminum.
3. For the thermal and resonance detectors for which data were taken
   i) The number of counts measured for the bare foil.
   ii) The counting time for the bare foil, min.
   iii) The number of background counts for the bare foil.
   iv) The background counting time for the bare foil, min.
   v) The weight of the bare foil, gm.
   vi) The irradiation time for the bare foil, min.

vii) In columns 73-80 of the first card for each detector, alphanumeric information describing the run number.

viii) The waiting time for the bare foil, days.

ix through xv) Data for the cadmium covered foil in the same position in the same order as for the bare foil, i) to vi) and viii).

xvi) The reactor power level in MW at the time of the run.

The order for this work is cobalt, copper.

For each group of data which follows the first (the repeat control being selected above), the format must follow that described above.

The output from MNFOIL needs some explanation (refer to Table A1.18). In the column marked "DETECTOR," the alphanumeric data used in the input are printed. As can be seen, it is advantageous to give both the run number and the detector name to unambiguously define the results quoted. The results given for every position have the same format, so that it is necessary to fill in the "DETECTOR" column only once. In the column marked "ETH/R" the effective threshold energy is printed for the threshold foils and the resonance energy for the resonance foils (in Mev) for reference. The column headed by "SIGMA AV/CR" serves two purposes: for the threshold detectors the values of $\overline{\sigma}_{eff}$ after convergence of the Trice method are printed, and for the resonance foils the cadmium ratios are given. In the column headed by "PHI INT/F2200" the integral fluxes in $n/(cm^2)(sec)$ are given for the threshold detectors and the 2200 m/sec flux in $n/(cm^2)(sec)$ is given for the thermal detector (cobalt). In the final column, marked "PHI DIFF/F0" the differential flux, $\phi(E)$, in $n/(cm^2)(sec)(ev)$ is given for the threshold detectors, and the 1/E flux constant ϕ_o (see Eq. (A1.16)) is given for the resonance foils.

After the results quoted above for every run in the series have been printed, the least square constants c and d for the integral fast flux shape (see Eq. (A1.23)) and their standard deviations are given for each run. The constant d has the units of Mev^{-1}.

The loading time for MNFOIL in an IBM 7090 type computer is 0.14 min. and the running time is about 0.02 min. per set of detectors in a given position.

A1. 13 Neutron Cross Sections Used for the Calculation of the Energy Transfer Integrals I_H, I_C, I_{Al}, I_{BE}

As defined in Section 3. 2. 3 the energy transfer integral is given by

$$I_i = \frac{A_i}{(A_i + 1)^2} S \int_0^\infty \sigma_s^i(E)\, \phi(E)\, E\, dE \text{ watts/atom} \qquad \text{(A1. 26)}$$

where

A_i is the atomic weight of atom i

S is a conversion factor, $(cm^2)(watt)(sec)/(barn)(ev)$

σ_s^i is the elastic scattering cross section of atom i, barns.

For the neutron spectra observed in the in-pile section the lower limit on the integral was replaced by 0. 01 Mev without any significant change in the result (A1. 2), since the scattering contributions below this energy were insignificant. In order to evaluate the integral, the scattering cross section must be known as a function of energy.

The data for hydrogen were obtained from Hughes (A1. 20) and are plotted in Fig. A1. 12. The data are given for the total cross section of hydrogen, and it is presumed that the elastic scattering cross section is equal to the total cross section in the region $E \geq 0.01$ Mev.

The carbon data were obtained from Parker (A1. 24) and are plotted in Fig. A1. 13. The total cross section is equal to the elastic scattering cross section in the range $0.01 \text{ Mev} \leq E \leq 4.8$ Mev. Above 4. 8 Mev carbon also undergoes inelastic scattering interactions with neutrons.

The data for aluminum were obtained from Howerton (A1. 13). The elastic scattering cross section is very nearly equal to the total cross section in the range $0.01 \leq E \leq 13$ Mev. Aluminum has so many resonances in the energy region of interest that an integration scheme, such as Simpson's Parabolic Rule (A1. 23), would give results which depend strongly on the step size used if the fine structure of the data were used. To avoid this problem, the cross section data were averaged for use with an integration step size of 0. 01 Mev beginning at 0. 01 Mev. For instance, the cross section used for 0. 31 Mev was the average cross section of the energy range 0. 26-0. 36 Mev. The resultant averaged cross section data are presented in Fig. A1. 14, and are intended for use only with Simpson's

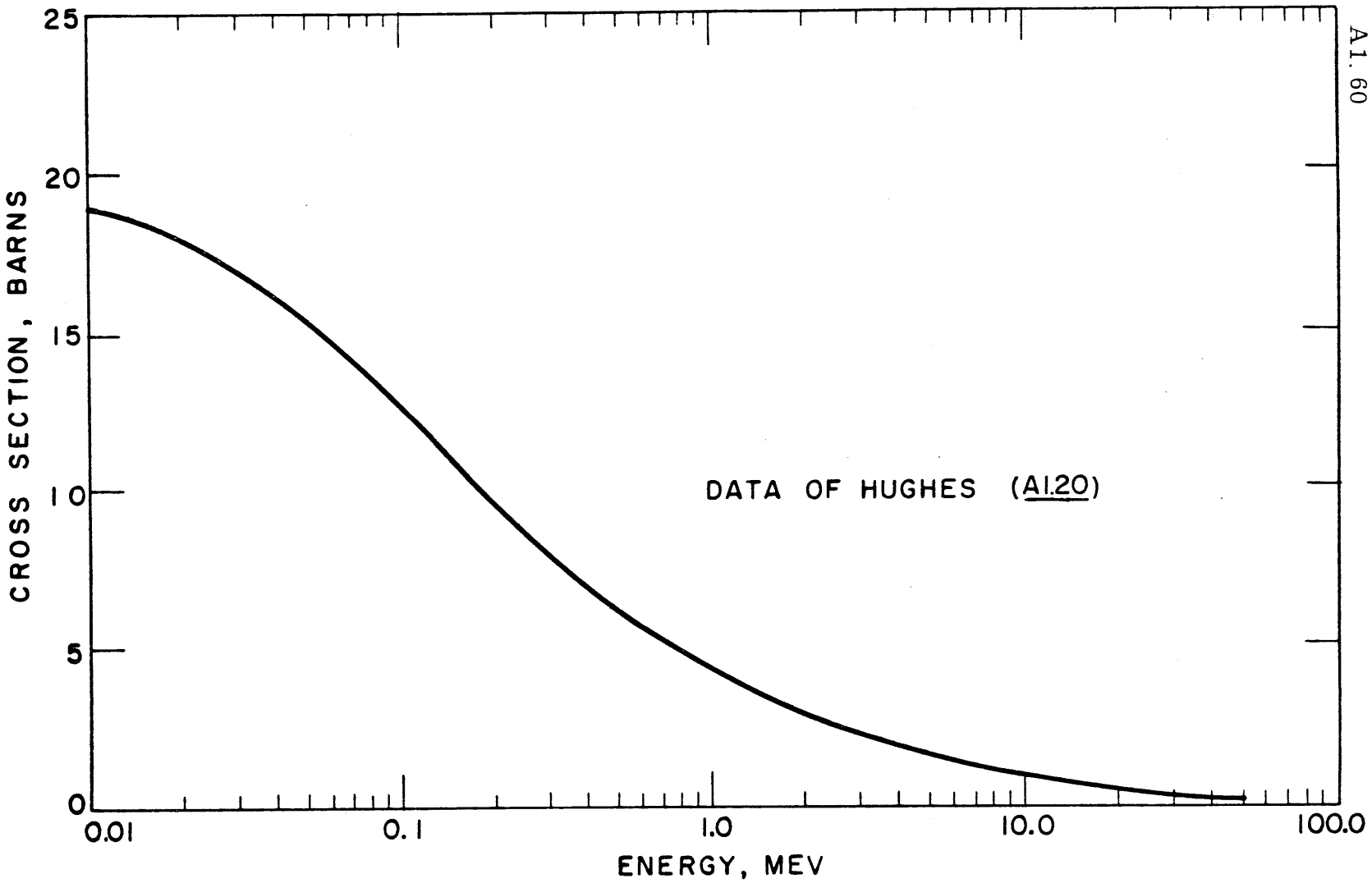

FIGURE A1.12 TOTAL CROSS SECTION OF HYDROGEN

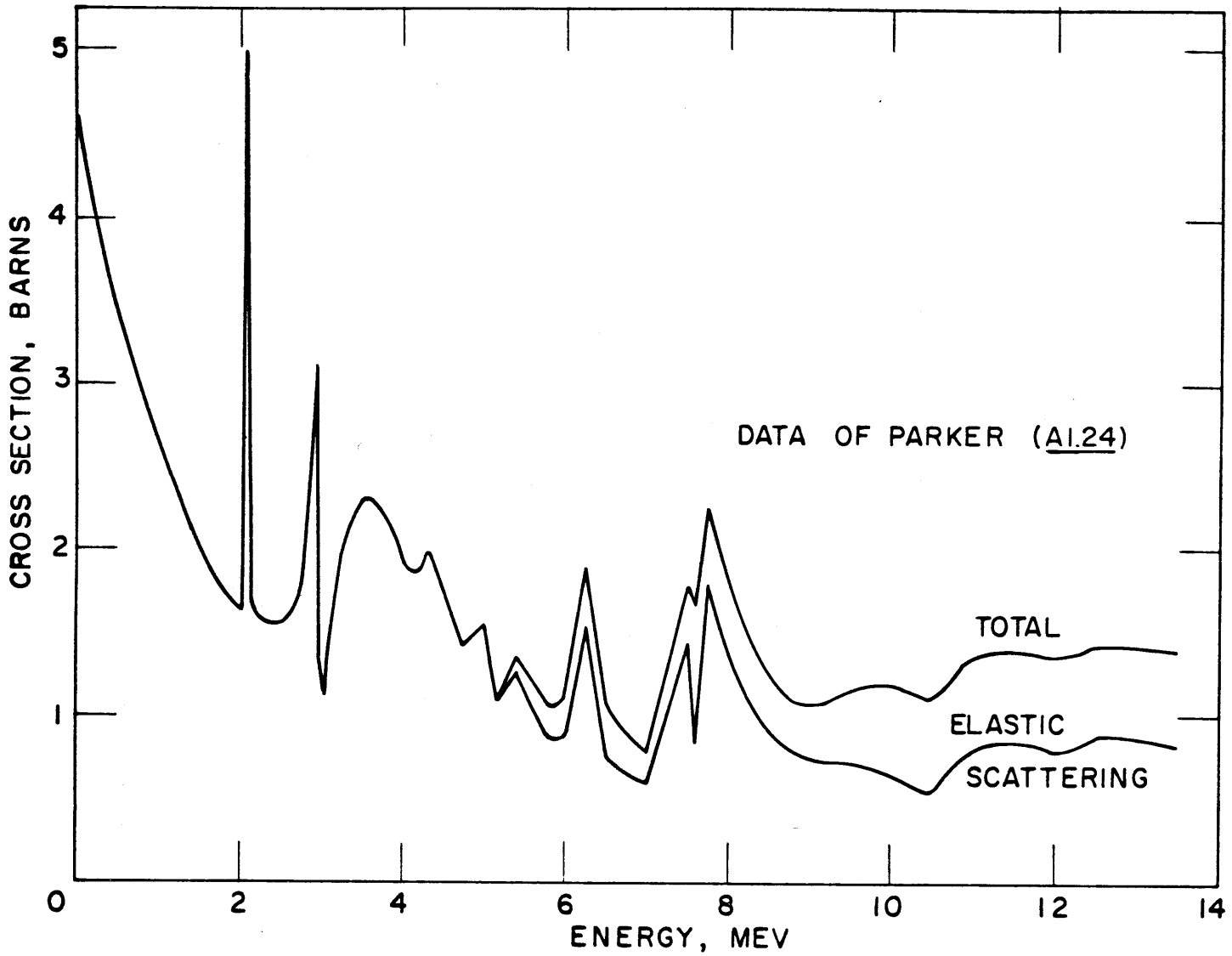

FIGURE A1.13 CROSS SECTION OF CARBON

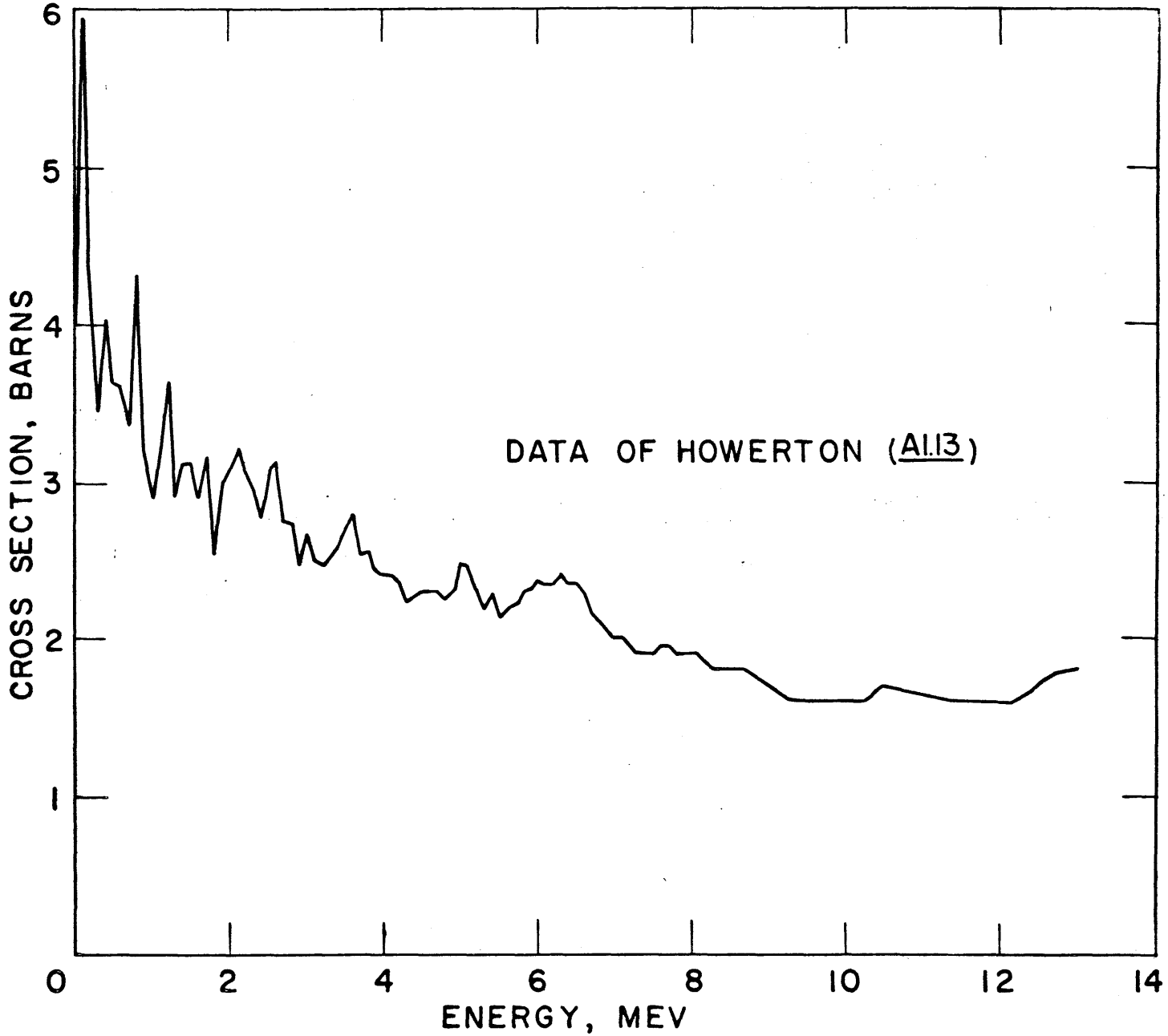

FIGURE A1.14 "AVERAGED" TOTAL CROSS SECTION OF ALUMINUM

Rule applied to Eq. (A1.25) with an energy step size of 0.1 Mev beginning at 0.1 Mev.

The data for beryllium are taken from Parker (A1.25) and are plotted in Fig. A1.15. For the two resonances below 1 Mev an averaging procedure identical to that used for aluminum was applied. From 0.01 Mev to 2 Mev the elastic scattering and total cross sections are identical. Above 2 Mev the (n, 2n) reaction becomes an important contributor to the total cross section.

A1.14 Dosimetry Computer Program, MNDOS

MNDOS is an IBM 709/7090 FORTRAN program (for use with a 32K storage) which evaluates the energy transfer integrals, Eq. (A1.26), by means of Simpson's Parabolic Rule and calculates the ratio I_j/I_H for use in the calorimetry program. The neutron flux data are taken from the results of MNFOIL, and the program has the option of using two flux shapes. The first assumes a 1/E energy dependence to a specified cutoff energy from the resonance region, and then a joining function of the form $\phi(E) = pE^q$ between the cutoff energy specified and the beginning of the fast neutron energy spectrum (about 2 Mev). The second assumes that the epithermal part of the spectrum does not quite behave a 1/E and assumes that $\phi(E) = pE^q$ describes the flux shape between the resonance region and the fast region. Both assume the fast flux shape is the exponential shape given by Eq. (A1.23). Table A1.19 gives the FORTRAN listing of the program, and a logic flowsheet is given in Fig. A1.16. In the paragraphs that follow a brief description of how to use the program will be given; a sample input and sample output are given in Tables A1.20 and A1.21, respectively, as an aid. Some familiarity with FORTRAN input/output format is assumed; for details see the IBM 709/7090 FORTRAN reference manual (A1.5).

The input is arranged as a series of tables, each headed by a card upon which any desired information may be typed. All fixed point data use I4 format and all floating point data E12.5 format.

The first table supplies control data for the program. It contains the following information:

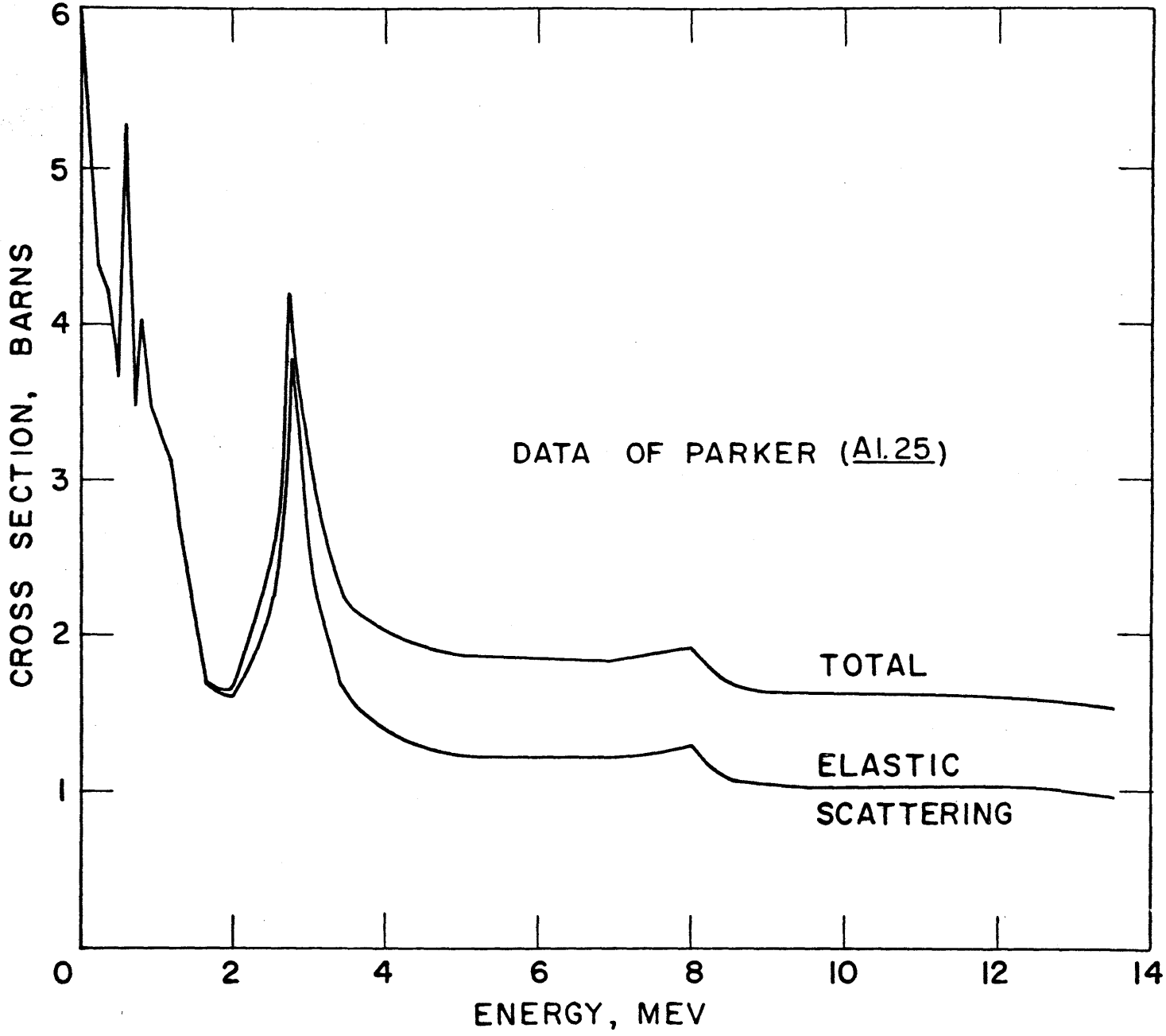

FIGURE A1.15 CROSS SECTION OF BERYLLIUM

1. A punch control. If the constant is ≤ 0, a punched record on the output will be given along with the printed record. If it is >0, only the printed record will be given.
2. The number of atomic species for which the energy transfer integrals will be computed. The program expects at least 3 – hydrogen, carbon and aluminum.
3. For each atomic species, the number of pairs of entries in the cross-section-energy tables to be supplied. The data must be given in the order hydrogen, carbon, aluminum. The data for any other species may be arranged in any order after aluminum.

The next table appears only if data for more than 3 atomic species are given. If this is the case, then using format A4 (left adjust in each field), the name of each species after aluminum must be given. In Table A1.20 the data for beryllium are given, so the label BE appears in the atom table.

The next table must contain the following "constant" data

1. The minimum energy at which integration is to begin. For this experiment 0.01 Mev was chosen as the lower limit.
2. The energy at which integration will be considered complete. In this experiment 13 Mev was chosen as the upper limit.
3. For each integral I_j to be computed:
   i) The integration step size (0.1 Mev was chosen for this experiment).
   ii) A factor equal to $2A_j/(A_j+1)^2 \times 1.60 \times 10^{-13}$ (see Eq. (A1.26)) to obtain the results in units of watts/atom $\times$ 10^{24}.

   The order must be as stated above.

The next series of tables supplies the cross section-energy data for each atomic species in the form $\sigma_1, E_1, \sigma_2, E_2 \ldots$, where the cross sections are in barns and the energies in Mev. The order of these tables must be as stated above.

Last, the flux shape data are given the computer in groups. Each group must be headed by a "free" card upon which any desired information may be punched, and the computer will re-print this information to head the output for the group. Before the flux data are given, a control table must also be supplied, containing:

TABLE A1.19
FORTRAN LISTING OF MNDOS

```
*       LIST 8
*       LABEL
*       SYMBOL TABLE
C MNDOS
C       MNDOS HAS SUBPROGRAM MAIN IN FORTRAN, LINLAG IN FAP
C       MAIN HAS 104 CARDS      1-3-63
        DIMENSION NSIG(10),H(10),FAC(10),NLASTS(10),SIG(200,10),ESIG(200,1
       10),ENTGRL(10),ENTRAT(10),ATOM(10)
        NOT=2
        NIT=4
        READINPUTTAPE NIT,2,KPUNCH,NATOM,(NSIG(I),I=1,NATOM)
    2   FORMAT(/(18I4))
        IF(NATOM-3)18,18,17
   17   READINPUTTAPE NIT,19,(ATOM(I),I=4,NATOM)
   19   FORMAT(/(18A4))
   18   READINPUTTAPE NIT,5,EMIN,EMAX,(H(I),FAC(I),I=1,NATOM)
    5   FORMAT(/(6E12.5))
        DO 6 I=1,NATOM
        NS=NSIG(I)
        NLASTS(I)=1
        READINPUTTAPE NIT,5,(SIG(J,I),ESIG(J,I),J=1,NS)
    6   CONTINUE
   41   READINPUTTAPE NIT,1
    1   FORMAT(80H
       1                          )
        WRITEOUTPUTTAPE NOT,1
        IF(KPUNCH)3,3,4
    3   PUNCH 1
    4   READINPUTTAPE NIT,2,NPOS,KEND
        DO 16 K=1,NPOS
        READINPUTTAPE NIT,7,EMAXE,EMINF,PHIZER,A,B,BLANK,RUN
    7   FORMAT( (6E12.5,A6))
        DO 11 I=1,NATOM
        SENSE LIGHT 0
        E=EMIN
        NSTEPS=(EMAXE-EMIN)/H(I)-0.99999
        IF(NSTEPS-1)36,31,31
   31   CALL LINLAG(NSIG(I),NLASTS(I),0,ESIG(1,I),SIG(1,I),E,SIGC)
        ENTGRL(I)=SIGC
        DO 10 J=1,NSTEPS
        E=E+H(I)
        CALL LINLAG(NSIG(I),NLASTS(I),0,ESIG(1,I),SIG(1,I),E,SIGC)
        IF(SENSE LIGHT 1)9,8
    8   ENTGRL(I)=ENTGRL(I)+4.0*SIGC
        SENSE LIGHT 1
        GO TO 10
    9   ENTGRL(I)=ENTGRL(I)+2.0*SIGC
   10   CONTINUE
        E=E+H(I)
        CALL LINLAG(NSIG(I),NLASTS(I),0,ESIG(1,I),SIG(1,I),E,SIGC)
        ENTGRL(I)=(ENTGRL(I)+2.0*SIGC)*PHIZER
   36   SLOPE=(A+B*EMINF-LOGF(PHIZER/EMAXE/(-B)))/LOGF(EMINF/EMAXE)
        ENTCPT=A+B*EMINF-SLOPE*LOGF(EMINF)+LOGF(-B)
        IF(NSTEPS-1)32,33,33
   32   CALL LINLAG(NSIG(I),NLASTS(I),0,ESIG(1,I),SIG(1,I),E,SIGC)
        ENTGRL(I)=SIGC*E*EXPF(ENTCPT+SLOPE*LOGF(E))
        NSTEPS=(EMAX-EMIN)/H(I)-0.99999
```

TABLE A1.19 (CONTINUED)

```
      GO TO 34
   33 NSTEPS=(EMAX-EMAXE)/H(I)-0.99999
   34 DO 60 J=1,NSTEPS
      E=E+H(I)
      CALL LINLAG(NSIG(I),NLASTS(I),0,ESIG(1,I),SIG(1,I),E,SIGC)
      IF(SENSE LIGHT 3)65,66
   66 IF(SENSE LIGHT 2) 62,61
   61 ENTGRL(I)=ENTGRL(I)+4.0*SIGC*E*EXPF(ENTCPT+SLOPE*LOGF(E))
      SENSE LIGHT 2
      GO TO 63
   62 ENTGRL(I)=ENTGRL(I)+2.0*SIGC*E*EXPF(ENTCPT+SLOPE*LOGF(E))
   63 IF(E-EMINF)60,64,64
   64 SENSE LIGHT 3
      GO TO 60
   65 SENSE LIGHT 3
      IF(SENSE LIGHT 2)68,67
   67 ENTGRL(I)=ENTGRL(I)-4.0*SIGC*E*EXPF(A+B*E)*B
      SENSE LIGHT 2
      GO TO 60
   68 ENTGRL(I)=ENTGRL(I)-2.0*SIGC*E*EXPF(A+B*E)*B
   60 CONTINUE
      ENTGRL(I)=ENTGRL(I)*H(I)/3.0*FAC(I)
   11 CONTINUE
      DO 12 I=2,NATOM
      ENTRAT(I)=ENTGRL(I)/ENTGRL(1)
   12 CONTINUE
      WRITEOUTPUTTAPE NOT,13,ENTGRL(1),RUN,SLOPE,ENTGRL(2),ENTRAT(2),ENT
     1GRL(3),ENTRAT(3)
   13 FORMAT(1H0,30X3H***/31X5H*IH =1PE11.4,11H WATTS/ATOM/2X8HRUN NO. A
     16,2X6HSLOPE=0PF6.3,6H *IC =1PE11.4,5X2H--,5X7HIC /IH=0PE11.4/31X5H
     2*IAL=1PE11.4,5X2H--,5X7HIAL/IH=1PE11.4)
      IF(NATOM-3)20,20,21
   21 WRITEOUTPUTTAPE NOT,30,(ATOM(I),ENTGRL(I),ATOM(I),ENTRAT(I),I=4,NA
     1TOM)
   30 FORMAT((31X2H*I,A2,1H=1PE11.4,5X2H--,5X1HI,A2,4H/IH=1PE11.4))
   20 WRITEOUTPUTTAPE NOT,14
   14 FORMAT(31X3H***)
      IF(KPUNCH)15,15,16
   15 PUNCH 13,ENTGRL(1),RUN,SLOPE,ENTGRL(2),ENTRAT(2),ENTGRL(3),ENTRAT(
     13)
      IF(NATOM-3)22,22,23
   23 PUNCH 30,(ATOM(I),ENTGRL(I),ATOM(I),ENTRAT(I),I=4,NATOM)
   22 PUNCH 14
   16 CONTINUE
      IF(KEND)41,41,40
   40 CALL EXIT
      END
```

TABLE A1.19 (CONTINUED)

```
*       LINLAG HAS 141 CARDS
*       FAP
        COUNT   140
     1  TTL     LINEAR AND LAGRANGIAN INTERPOLATION SUBROUTINE
        LBL     LINLAG
        ENTRY   LINLAG
        REM     THE FORTRAN CALLING SEQUENCE IS . . .
        REM     CALL LINLAG(N,NLAST,MOR,A,B,P,Q)
        REM
        REM     N IS THE NUMBER OF ELEMENTS IN A AND B
        REM     NLAST IS LAST TIMESS CORRECT INTERVAL
        REM     MOR IS THE NUMBER OF POINTS TO BE USED IN INTERPOLATION.
        REM     A FASTER LINEAR INTERPOLATION RESULTS WITH MOR=0
        REM     A IS THE INDEPENDENT VARIABLE (1D MATRIX)
        REM     B IS THE DEPENDENT VARIABLE (1D MATRIX)
        REM     P IS THE PARTICULAR VALUE OF A
        REM     Q IS THE ANSWER RETURNED BY THE SUBROUTINE
        REM
LINLAG  CLA*    1,4
        SUB     =01000000
        TZE     ONEEL                   TEST NO. OF ELEMENTS
        STD     NLOOP                   SET UPPER BOUND ON THE A TABLE
        SXA     BACK,1                  SAVE INDEX REGISTERS
        SXA     BACK+1,2
        SXD     LINLAG-2,4
        CLA     4,4
        STA     SETA1                   SET UP A
        STA     SETA2
        ADD     =1
        STA     SETA3                   SET UP A+1
        CLA*    2,4                     LAST TIMES CLOSEST
        PDX     0,1                     ELEMENT NO. TO IR1
LOOP1   CLA*    6,4
SETA1   FSB     **,1                    P-A(IR1)
        TPL     TEST1
        NZT     CONST                   IS CONST=0
        TRA     FOUND
        TXI     *+1,1,-1                NO. DECREASE IR1 BY 1
        TXL     LOOP1,1,-2              IS P LESS THAN A(1)
        TRA     OUT                     YES. ERROR IN CALLING PROGRAM
FOUND   ZET*    3,4                     IS INTERPOLATION TO BE LINEAR
        TRA     LGRNG                   NO. GO TO LAGRANGIAN
        STO     DATA                    YES. STORE P-A(L) IN DATA
        CLA     5,4
        STA     SETB1                   SET UP B
        STA     SETB2
        ADD     =1
        STA     SETB3                   SET UP B+1
SETA2   CLA     **,1
SETA3   FSB     **,1                    A(L)-A(L-1)
        STO     Q
SETB1   CLA     **,1
SETB3   FSB     **,1                    B(L)-B(L-1)
        FDP     Q
        FMP     DATA
SETB2   FAD     **,1                    B(L)
        STO*    7,4                     ANSWER
        PXD     0,1
        SUB     =01000000
```

TABLE A1.19 (CONTINUED)

```
        STO*    2,4                     STORE NEW NEAR ELEMENT NO.
  BACK  AXT     **,1
        AXT     **,2                    RESTORE INDEX REGISTERS
        SXD     CONST,4
        TRA     8,4                     RETURN TO CALLING PROGRAM
 TEST1  STZ     CONST
        TXI     *+1,1,1                 INCREASE IR1 BY 1
 NLOOP  TXL     LOOP1,1,**
   OUT  TSX     $ERROR,4                ERROR SUBROUTINE
        PZE     ALPHA
        TXI     *+2,0,0
        PZE     LINLAG-2,0,0
        TSX     $EXIT,4
 LGRNG  PXD     0,1
        SUB     =01000000
        STO*    2,4                     STORE NEW NEAR ELEMENT NO.
        CLA*    3,4
        PDX     0,1                     M1 TO IR1
        STO     M1
        ARS     19
        ALS     18                      INTEGER DIVISION BY TWO
        SUB*    2,4
        TZE     NOW+1
        TPL     SETLO                   CHECK LOW END OF TABLE
        STO     LOW
        ADD*    1,4
        SUB     M1
        SUB     =01000000
        TMI     SETHI                   CHECK HIGH END OF TABLE
        CLA     LOW
   NOW  ARS     18
        ADD     4,4
        STA     ALOW1                   SET UP A+LOW
        STA     ALOW2
        STA     ALOW3
        SUB     4,4
        ADD     5,4
        STA     BLOW                    SET UP B+LOW
        CLA     6,4
        STA     SETP
        STZ     Q                       Q=0.0 INITIALLY
 LOOP2  SXD     K,1
        CLA     =1.0
        STO     PK                      PK=1.0 INITIALLY
        LXD     M1,2                    M1 TO IR2
 LOOP3  PXD     0,2
        SUB     K
        TZE     TEST3                   COMPARE IR1 WITH IR2
 ALOW2  CLA     **,1
 ALOW3  FSB     **,2                    A(-LOW+IR1)-A(-LOW+IR2)
        STO     DATA
  SETP  CLA     **
 ALOW1  FSB     **,2                    P-A(-LOW+IR2)
        FDP     DATA
        FMP     PK
        STO     PK                      PK=PK*(P-A(-LOW+IR2))
 TEST3  TIX     LOOP3,2,1               DECREASE IR2 BY 1
  BLOW  LDQ     **,1                    B(-LOW+IR1)
        FMP     PK
```

TABLE A1.19 (CONCLUDED)

```
       FAD     Q
       STO     Q
       TIX     LOOP2,1,1              DECREASE IR1 BY 1
       STO*    7,4
       TRA     BACK
SETLO  CLA     =01000000
       TRA     NOW
SETHI  SSP
       ADD     LOW
       TRA     NOW
ONEEL  CLA*    5,4
       STO*    7,4                    ANSWER IS SINGLE ELEMENT
       TRA     8,4
 DATA  PZE
   M1  PZE
  LOW  PZE
   PK  PZE
    K  PZE
    Q  PZE
CONST  OCT     1
ALPHA  BCI     5, EXTRAPOLATION IS NOT POSSIBLE
       OCT     777777777777
       END
```

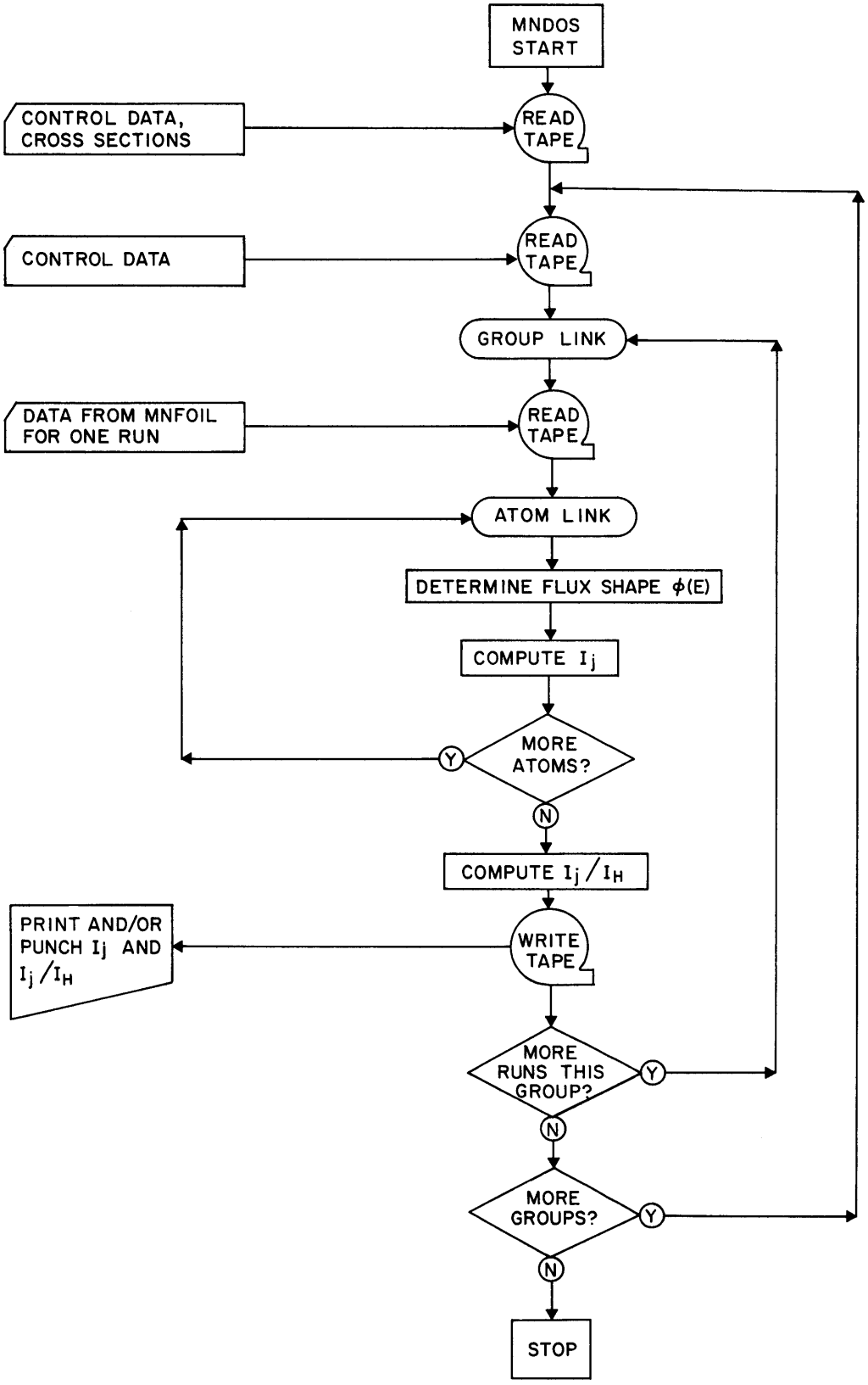

FIGURE A1.16 LOGIC FLOWSHEET FOR MNDOS

TABLE A1.20
SAMPLE INPUT TO MNDOS

```
                                CONTROL TABLE
   0   4  33  56  96  32
                                ATOM TABLE
BE
                              INTEGRATION DATA
  0.01          13.0          0.1          0.8010E-13   0.1          0.2273E-13
  0.1           0.1104E-13    0.1          0.2880E-13
          TOTAL HYDROGEN CROSS SECTION    BNL325
 19.0           0.00999       17.4         0.025        15.4         0.05
 13.8           0.075         12.6         0.1          10.8         0.15
  9.5           0.20           8.6         0.25          7.95        0.3
  6.9           0.4            6.15        0.5           5.6         0.6
  5.15          0.7            4.8         0.8           4.5         0.9
  4.25          1.0            3.75        1.25          3.4         1.5
  3.1           1.75           2.9         2.0           2.5         2.5
  2.25          3.0            2.05        3.5           1.9         4.0
  1.6           5.0            1.4         6.0           1.25        7.0
  1.15          8.0            1.05        9.0           0.95        10.0
  0.85          11.0           0.8         12.0          0.74        13.01
          TOTAL CARBON CROSS SECTION   ANRE 0-71/60
  4.71          0.001          4.68        0.01          4.38        0.1
  3.4           0.5            2.68        1.0           2.01        1.5
  1.835         1.66           1.61        2.0           1.62        2.02
  5.0           2.08           1.67        2.15          1.57        2.28
  1.54          2.4            1.55        2.51          1.635       2.65
  1.695         2.7            1.795       2.76          1.815       2.77
  2.615         2.93           3.1         2.95          1.31        3.0
  1.105         3.05           1.38        3.1           1.96        3.25
  2.3           3.51           2.295       3.62          2.225       3.76
  1.93          4.0            1.865       4.1           1.86        4.21
  1.975         4.3            1.76        4.5           1.43        4.7
  1.55          5.0            1.08        5.15          1.35        5.4
  1.26          5.5            1.05        5.8           1.11        6.0
  1.9           6.25           1.09        6.5           0.78        7.0
  1.79          7.5            1.66        7.6           2.25        7.75
  1.82          8.0            1.22        8.5           1.06        9.0
  1.17          9.5            1.2         10.0          1.1         10.5
  1.36          11.0           1.4         11.5          1.35        12.0
  1.42          12.5           1.40        13.5
          TOTAL ALUMINUM CROSS SECTION     HOWERTON
  3.52          0.00999        5.95        0.11          4.40        0.21
  3.43          0.31           4.05        0.41          3.63        0.51
  3.61          0.61           3.37        0.71          4.34        0.81
  3.21          0.91           2.9         1.01          3.28        1.11
  3.65          1.21           2.91        1.31          3.13        1.41
  3.13          1.51           2.89        1.61          3.16        1.71
  2.53          1.81           2.96        1.91          3.12        2.01
  3.22          2.11           3.06        2.21          2.96        2.31
  2.51          2.41           3.06        2.51          3.15        2.61
  2.74          2.71           2.73        2.81          2.47        2.91
  2.68          3.01           2.49        3.11          2.47        3.21
  2.51          3.31           2.59        3.41          2.72        3.51
  2.82          3.61           2.53        3.71          2.55        3.81
  2.43          3.91           2.40        4.01          2.40        4.11
  2.34          4.21           2.24        4.31          2.27        4.41
  2.3           4.51           2.3         4.71          2.25        4.81
  2.3           4.91           2.47        5.01          2.45        5.11
```

TABLE A1.20 (CONCLUDED)

```
 2.32          5.21          2.18          5.31          2.29          5.41
 2.14          5.51          2.19          5.61          2.22          5.71
 2.29          5.81          2.31          5.91          2.37          6.01
 2.35          6.11          2.35          6.21          2.4           6.31
 2.35          6.41          2.35          6.51          2.3           6.61
 2.17          6.71          2.12          6.81          2.04          6.91
 2.0           7.01          2.0           7.11          1.95          7.21
 1.9           7.31          1.9           7.51          1.95          7.61
 1.95          7.71          1.9           7.81          1.9           8.01
 1.88          8.11          1.83          8.21          1.8           8.31
 1.8           8.71          1.6           9.31          1.6           10.21
 1.61          10.31         1.67          10.41         1.69          10.51
 1.6           11.31         1.6           12.11         1.61          12.21
 1.64          12.31         1.67          12.41         1.71          12.51
 1.74          12.61         1.77          12.71         1.8           13.011
      ELASTIC CROSS SECTION OF BERYLLIUM     AWRE O-27/60
 6.0           0.001         6.0           0.01          5.8           0.06
 5.4           0.1           4.9           0.15          4.35          0.25
 4.2           0.38          3.88          0.46          3.65          0.51
 5.27          0.61          3.48          0.71          4.03          0.81
 3.49          0.91          3.4           1.0           3.1           1.2
 2.09          1.5           1.66          1.7           1.59          2.0
 2.18          2.5           2.36          2.6           3.8           2.72
 2.55          3.0           1.57          3.5           1.37          4.0
 1.26          4.5           1.21          5.0           1.21          7.0
 1.28          8.0           1.07          8.5           1.03          9.5
 1.03          12.0          0.983         13.5
1                          RUN R DATA
                           CONTROL TABLE
  8
 0.00012       1.51          6.3609E 11    27.8319       -0.629953              RB
 0.00012       1.51          1.0287E 12    29.2196       -0.671276              RL
 0.00012       1.51          1.1593E 12    29.3330       -0.675573              RC
 0.00012       1.51          9.8309E 11    29.2414       -0.675929              RU
 0.00012       1.51          6.6351E 11    28.8497       -0.669772              RT
 0.00012       1.51          3.4139E 11    26.6296       -0.533503              RR1
 0.00012       1.51          8.0995E 10    25.1465       -0.508718              RR2
 0.00012       1.51          1.8064E 10    23.6719       -0.448205              RR3
```

TABLE A1.21
SAMPLE OUTPUT FROM MNDOS

RUN R DATA

```
                                  ***
                                  *IH = 5.9928E-01 WATTS/ATOM
RUN NO.   RB   SLOPE=-1.037       *IC = 1.0828E-01      --      IC /IH= 0.1807E-00
                                  *IAL= 6.9876E-02      --      IAL/IH= 1.1660E-01
                                  *IBE= 1.4885E-01      --      IBE/IH= 2.4839E-01
                                  ***

                                  ***
                                  *IH = 2.1497E 00 WATTS/ATOM
RUN NO.   RL   SLOPE=-0.941       *IC = 3.9397E-01      --      IC /IH= 0.1833E-00
                                  *IAL= 2.5544E-01      --      IAL/IH= 1.1883E-01
                                  *IBE= 5.4233E-01      --      IBE/IH= 2.5229E-01
                                  ***

                                  ***
                                  *IH = 2.4012E 00 WATTS/ATOM
RUN NO.   RC   SLOPE=-0.941       *IC = 4.3935E-01      --      IC /IH= 0.1830E-00
                                  *IAL= 2.8474E-01      --      IAL/IH= 1.1858E-01
                                  *IBE= 6.0522E-01      --      IBE/IH= 2.5205E-01
                                  ***

                                  ***
                                  *IH = 2.1772E 00 WATTS/ATOM
RUN NO.   RU   SLOPE=-0.934       *IC = 3.9916E-01      --      IC /IH= 0.1833E-00
                                  *IAL= 2.5885E-01      --      IAL/IH= 1.1889E-01
                                  *IBE= 5.4967E-01      --      IBE/IH= 2.5247E-01
                                  ***

                                  ***
                                  *IH = 1.4783E 00 WATTS/ATOM
RUN NO.   RT   SLOPE=-0.933       *IC = 2.7160E-01      --      IC /IH= 0.1837E-00
                                  *IAL= 1.7624E-01      --      IAL/IH= 1.1922E-01
                                  *IBE= 3.7366E-01      --      IBE/IH= 2.5277E-01
                                  ***

                                  ***
                                  *IH = 2.0272E-01 WATTS/ATOM
RUN NO.   RR1  SLOPE=-1.100       *IC = 3.7343E-02      --      IC /IH= 0.1842E-00
                                  *IAL= 2.4207E-02      --      IAL/IH= 1.1941E-01
                                  *IBE= 5.0607E-02      --      IBE/IH= 2.4963E-01
                                  ***

                                  ***
                                  *IH = 4.6892E-02 WATTS/ATOM
RUN NO.   RR2  SLOPE=-1.106       *IC = 8.7285E-03      --      IC /IH= 0.1861E-00
                                  *IAL= 5.6717E-03      --      IAL/IH= 1.2095E-01
                                  *IBE= 1.1768E-02      --      IBE/IH= 2.5096E-01
                                  ***

                                  ***
                                  *IH = 1.1081E-02 WATTS/ATOM
RUN NO.   RR3  SLOPE=-1.107       *IC = 2.1346E-03      --      IC /IH= 0.1926E-00
                                  *IAL= 1.3973E-03      --      IAL/IH= 1.2609E-01
                                  *IBE= 2.8347E-03      --      IBE/IH= 2.5581E-01
                                  ***
```

1. The number of runs in the present group.
2. A repeat control. If the control is ≤ 0, the computer will expect more data after analyzing the present group of data. If it is >0, the computer will halt after the completion of computations on the group of data.

For every run in the group the following data must be given:

1. The maximum energy at which the flux can be assumed to follow a 1/E law. If this energy is less than the lower limit on the integral given above, the computer will assume no 1/E dependence, but one of a form $\phi(E) = pE^q$ between the energy stated and the minimum energy at which the fast flux exponential shape is assumed (see Step 2 below). Because of the nature of the Simpson's Rule used, if a 1/E dependence is to be assumed at all it must hold for a minimum of five integration steps (A1.23). That is, in the present case it must hold to 0.41 Mev. Thereafter, to retain the accuracy of Simpson's Rule, the integration over the 1/E part of the spectrum should terminate on any odd number of steps. For instance, possible numbers for the input of this work would be 0.41, 0.61, 0.81, ... Mev.
2. The minimum energy at which the fast flux spectrum, given by $\phi(E) = -de^{c+dE}$ (Eq. (A1.23)), describes the flux shape. The only restriction on this number is that it ought to coincide with one of the energies used for Simpson's Rule, i.e., 0.01 + 0.1n Mev (n integer) for the input used in this work.
3. ϕ_o as computed by MNFOIL, $n/(cm^2)(sec)$.
4. and 5. The values of c and d (see Eq. (A1.23)) as given by MNFOIL for use in the fast flux shape.
6. In columns 72-78, according to format A6, an alphanumeric description of the run being analyzed.

For each group of data to be analyzed (the repeat control being selected above) the format must be as described above.

The output needs very little explanation. The quantity SLOPE refers to the exponent, q, on the energy dependence of the joining function $\phi(E) = pE^q$. The integrals as given have the units of watts/atom$\times 10^{24}$.

The loading time for MNDOS is 0.14 min. and the running time is about 0.005 min. per integration.

APPENDIX A2

COOLANT COMPOSITION AND STABILITY

A2.1 Gas Chromatographic Analysis of Irradiated Santowax OMP Samples

Samples of irradiated Santowax OMP were analyzed for biphenyl, o-, m- and p-terphenyl by high temperature gas phase chromatography. Two chromatographs were used during the course of the 610°F and 750°F irradiations: a Burrell K-7 (A2. 1) and an F and M 500 with a Model 1609 flame ionization attachment.[1] The operating conditions for the Burrell have been described by Morgan and Mason (A2. 1), and all samples analyzed on this equipment have since been re-analyzed on the F and M, the operating conditions for which are given in Table A2. 1. Although not recorded in Table A2. 1, some samples were originally run with a temperature programming technique. However, it was found that this technique produced less reproducible results than did isothermal operation, and it was abandoned.

Figure A2. 1 shows a typical chromatogram of an irradiated Santowax OMP sample. The peaks are, in order: benzene (solvent), biphenyl, o-terphenyl, triphenylmethane (standard), m-terphenyl and p-terphenyl. Meta- and para-terphenyl are not completely separated; this phenomenon was observed for all of the Apiezon L columns used.

Quantitative determinations of the various components were made through the use of standard solutions with known amounts of the components and of triphenylmethane (TPM). The o:m:p ratio in the standards were chosen to closely approximate those of the irradiated samples and the meta-terphenyl: TPM ratio was chosen to give the same peak height for both components. For the standard solutions, "f" factors may be defined as (A2. 1):

$$f_i = \frac{X_i}{X_{TPM}} \frac{A_{TPM}}{A_i} \qquad \text{(A2. 1)}$$

1. F and M Research Corp., Avondale, Pa.

TABLE A2.1

Operating Conditions for F and M Model 500 Chromatograph

Column	5-8 w/o Apiezon L on 30-50 and 40-60 mesh firebrick; column lengths 6-8 feet, 1/4" OD
Column Temperature	200-250°C (isothermal)
Column Life	About 2 months
Detector	Flame ionization
He Flowrate	35-40 cm^3/min at 60 psig
Detector Temperature	350°C-450°C
Injection Block Temperature	350°C-450°C
Internal Standard	Triphenylmethane (TPM)
Solvent	Benzene
Nominal Concentration	0.004 grams of TPM and 0.03 grams of sample per cc of solution
Sample Size Injected	4-8 μliters

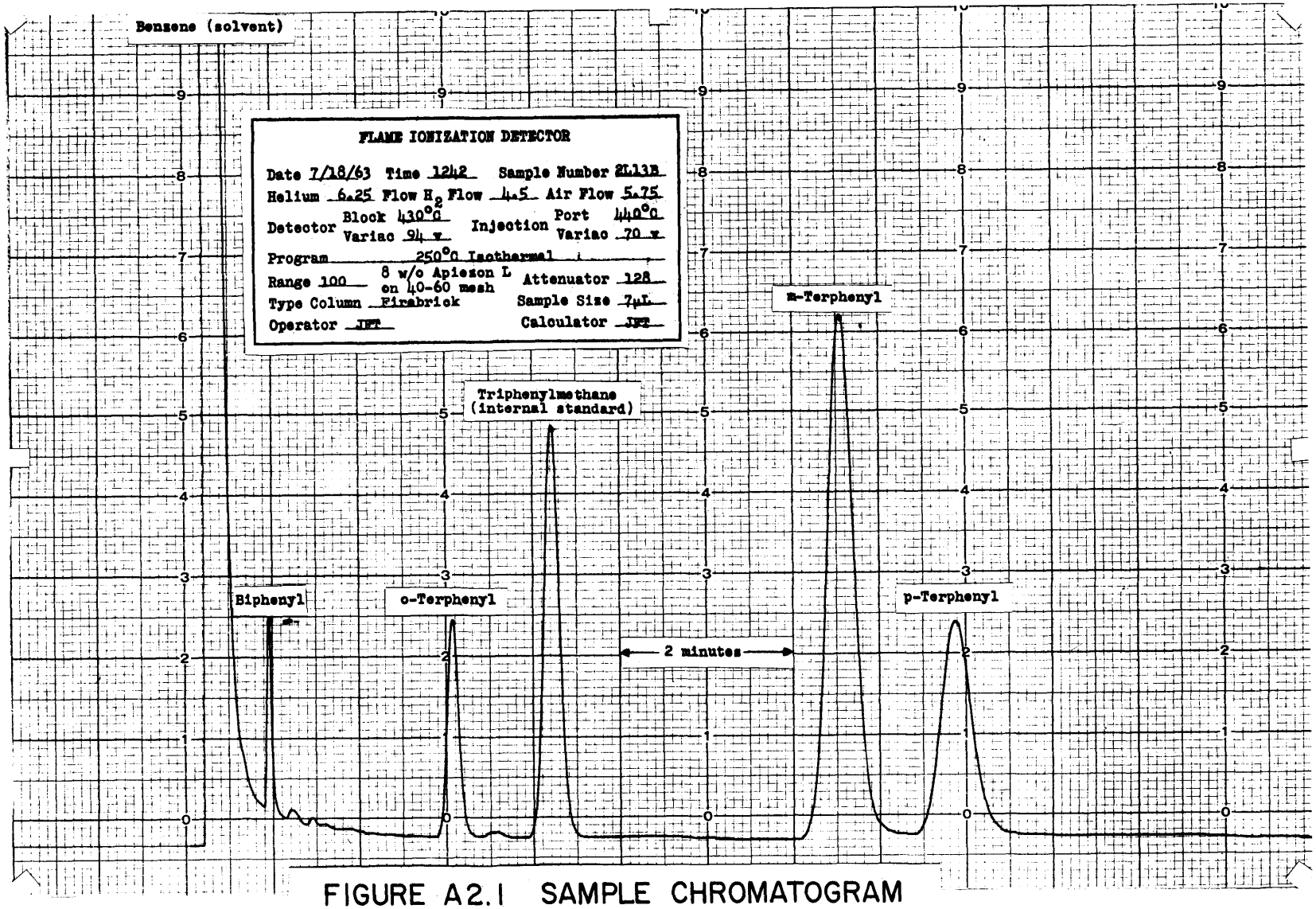

FIGURE A2.1 SAMPLE CHROMATOGRAM

where

i refers to biphenyl, o-, m- and p-terphenyl

X_i is the weight of component i in the standard

A_i is the chromatogram area of component i in the standard.

The overlapping area between m- and p-terphenyl was divided equally between the two components. For each column many standard samples were injected, and the average "f" factor for each component was used for computational purposes as long as no trend of the "f" factor with time was observed. For the irradiated samples the weight fraction of each component was calculated from

$$C_i = \overline{f_i} \frac{X_{TPM}}{X_T} \frac{A_i}{A_{TPM}} \qquad \text{(A2.2)}$$

where

$\overline{f_i}$ is the average "f" factor of component i

X_{TPM} is the weight of TPM in the irradiated sample solution

X_T is the total irradiated sample weight

A_i is the chromatogram area of component i in the irradiated sample solution.

At least four injections of each irradiated sample were made to reduce the error in the determination.

Errors in the chromatographic analyses can be divided into three categories: errors in the preparation of standards and "f" factors; errors in the preparation of irradiated samples and the calculation of C_i; and errors due to non-representative sampling. In view of the form of Eqs.(A2.1) and (A2.2), and the fact that chromatogram areas were made about the same for all samples via sample injection size, no matter what the omp concentration of the samples, it was felt that the relative error in the measured concentrations was a constant for each component (i.e., $\Delta C_i / C_i$ was a constant) for the concentration ranges covered in this work.

Relative standard deviations ($\Delta C/C$) in the preparation of standards and the "f" factors have been determined for a typical column as: biphenyl ±1%, o-terphenyl ±0.2%, m-terphenyl ±0.2%, p-terphenyl ±0.9%. Typical relative standard deviations in the preparation of irradiated samples and the calculation of C_i were: biphenyl ±4%, o-terphenyl ±0.9%, m-terphenyl ±0.4%, p-terphenyl ±1.1%. The third type of error, that due to nonrepresentative sampling, was difficult to assess. It was found that the LIB

content of some samples changed due to repeated heating for sampling purposes, as witnessed by the gradual disappearance of biphenyl (in extreme cases o-terphenyl) in chromatograms of those samples. Also, there is a small probability that the sample taken at the loop may not have been completely representative of the circulating coolant in the loop. An estimate of the combined effects of errors due to nonrepresentative sampling and the calculation of C_i was provided by the samples analyzed for the 610°F irradiation steady-state-HB period in which the HB level remained essentially constant. There appeared to be no trend of the terphenyl and biphenyl concentrations with irradiation (see Section 4. 4. 2) so that the standard deviation of the results from the average value for the period provided the estimate. Thus, these relative standard deviations were estimated as: biphenyl ±10%, o-terphenyl ±3%, m-terphenyl ±1%, p-terphenyl ±4%. Propagation of these errors led to the results tabulated in Table A2. 2. The error for total terphenyl was calculated

TABLE A2. 2

Estimated Relative Standard Deviations in Gas Chromatographic Analysis

Component	Estimated Relative Standard Deviation (% of value reported)
Biphenyl	±12
Ortho-terphenyl	± 3
Meta-terphenyl	± 1
Para-terphenyl	± 4
Total terphenyl	± 2

assuming an o:m:p ratio of 1:6:3, which was typical of the irradiated Santowax OMP samples.

A2. 2 HB Determination by Distillation

A procedure for the distillation of samples weighing approximately 300 g was developed by TeStrake (A2. 2). The distillation apparatus is

shown in Fig. A2.2 and consisted principally of a pot, an air cooled condenser, a distillation receiver, a cold trap, and N_2 and vacuum lines. Samples were distilled under 10-20 mm Hg of N_2, and the progress of a distillation was determined from its temperature-distillate yield curves. Typical curves are shown in Fig. A2.3, displaying the sharp cutoff after the distillation of p-terphenyl. For the irradiated Santowax OMP samples of this experiment, typical operating variables are given in Table A2.3.

The HB content of the sample was defined as

$$\text{w/o HB} = \frac{\text{wt. of bottoms}\,[100-\text{w/o omp in bottoms}]}{\text{wt. of charge}} \qquad \text{(A2.3)}$$

where the weight percent omp (actually just m- and p-terphenyl for the samples of this work) was determined by gas chromatography and usually amounted to a very small (<1%) correction. A series of distillations on samples taken from a large homogeneous batch of OMRE coolant (containing about 18 w/o HB) was performed and a standard deviation of 0.2 w/o was calculated for the accuracy of an HB determination.

A2.3 Results of Chemical Analyses on Irradiated Santowax OMP Samples from the 610°F and 750°F Irradiations

The results of the gas chromatographic analyses on loop samples from the 610°F irradiation are listed in Table A2.4. The Monsanto Research Corp. (Everett, Mass.) performed similar analyses on many of these samples, and their findings are also listed in Table A2.4. Their results for total w/o omp generally agreed with those obtained at M.I.T., but their analyses usually showed a higher w/o m-terphenyl and a correspondingly lower w/o p-terphenyl. The Monsanto analyses were performed with Eastman White Label m-terphenyl[1] which has been discovered at M.I.T. to contain about 4 w/o p-terphenyl in it. Where possible, the samples were re-analyzed at M.I.T. using a fractionally crystallyzed 99.9 w/o pure m-terphenyl standard; otherwise, corrections were applied to the old analyses. Monsanto made no such corrections, thus accounting for the differences in the results.

Table A2.5 lists the results of gas chromatographic analyses on sample distillates and bottoms from distilled samples of the 610°F irradiation, and these analyses, together with the analysis of the makeup material

1. Eastman Kodak Co., Rochester, N.Y.

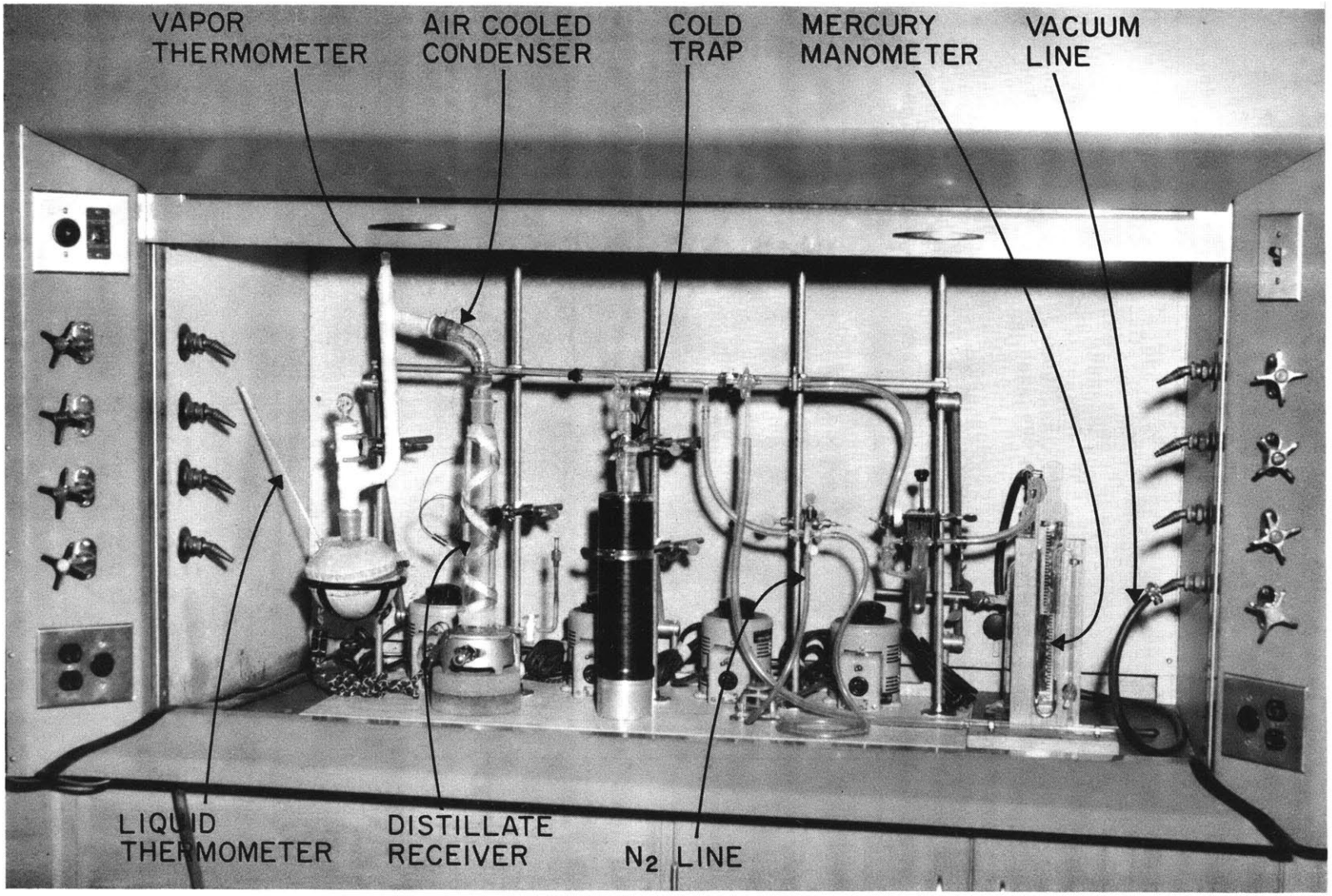

FIGURE A2.2 DISTILLATION APPARATUS

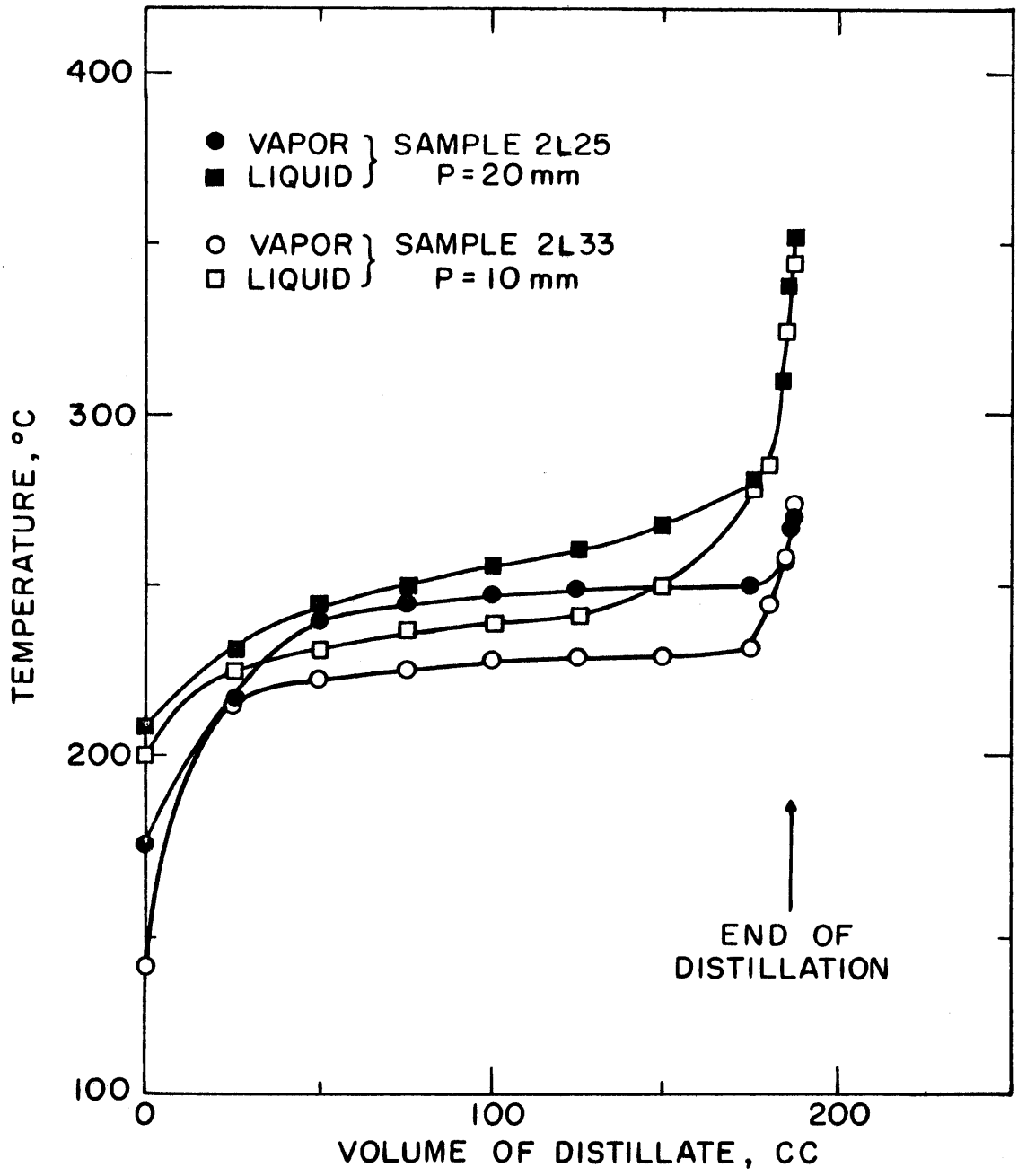

FIGURE A2.3 TYPICAL TEMPERATURE - YIELD CURVES FOR SAMPLE DISTILLATIONS

TABLE A2.3

Typical Operating Variables for Distillation of Irradiated Santowax OMP

Pressure	10-20 mm Hg of N_2
Liquid temperature range	200-350°C
Vapor temperature range	150-270°C
Charge	300 g containing approximately: 60 w/o omp 33 w/o HB 7 w/o LIB
Distillate	200 g containing approximately: 90 w/o omp 10 w/o LIB
Cold trap	< 2 g containing approximately: 100 w/o LIB
Bottoms	100 g containing approximately: 99.5 w/o HB 0.5 w/o omp

TABLE A2.4

Gas Chromatographic Analyses of Loop Samples from the 610°F Irradiation of Santowax OMP

SAMPLE NUMBER	REACTOR MWH	POLYPHENYL COMPOSITION, WT%									
		MIT ANALYSES					MONSANTO ANALYSES				
		o-ϕ_3	m-ϕ_3	p-ϕ_3	TOTAL omp	ϕ_2	o-ϕ_3	m-ϕ_3	p-ϕ_3	TOTAL omp	ϕ_2
1L16	0	10.7	64.8	24.6	100.1	-	10.0	61.3	22.7	94.0	0.3
1L18	58	9.5	56.8	27.4	93.7	-	12.9	73.0	8.5	94.4	1.4
1L22	148	10.5	59.4	25.1	95.0	-	9.9	61.7	23.4	95.0	0.5
1L24	172	10.1	57.9	20.8	88.8	-	9.7	61.5	20.5	91.7	0.3
1L27	250	10.5	59.1	20.4	90.0	0.2	9.4	60.0	22.8	92.2	0.3
1L35	392	9.4	54.8	22.2	86.4	0.2	10.6	63.4	22.7	96.7	0.4
1L37	400	9.4	54.5	22.3	86.2	0.3	9.5	57.6	20.3	87.4	0.08
1L42	643	8.6	50.2	20.2	79.0	0.4	8.9	52.8	19.1	80.8	0.4
1L47	816	8.3	48.5	19.3	76.1	0.3	7.9	49.8	16.1	73.8	0.4
1L50	930	7.3	47.8	17.8	72.9	0.2	8.2	52.5	19.1	79.8	0.6
1L51	1076	7.5	44.6	19.3	71.4	0.3	7.8	48.7	18.1	74.6	0.3
1L52	1174	7.5	42.3	17.0	66.8	0.3	7.0	44.6	14.8	66.4	0.3
1L59	1472	6.6	38.2	17.7	62.5	0.3	6.7	42.9	14.3	63.9	0.3
1L62	1621	6.3	37.4	16.2	59.9	0.3	5.8	39.6	13.4	58.8	0.2
1L63	1659	6.7	41.2	18.7	66.6	0.2	7.4	44.2	15.5	67.1	0.3
1L66	1793	6.8	39.4	17.8	64.0	0.3	6.5	42.7	16.1	65.3	0.2
1L74	2164	6.1	37.8	16.6	60.5	0.3	6.0	37.9	13.5	57.4	0.3
1L82	2529	5.6	34.4	15.1	55.1	0.3					
1L91	2869	5.3	32.4	13.5	51.2	0.3					
1L92	2879	5.3	31.9	14.5	51.7	0.4	5.3	33.5	12.6	51.4	0.4
1L99	3215	4.7	30.1	13.2	48.0	0.3	3.7	25.7	9.0	38.4	0.1
1L111	3621	4.3	24.8	11.7	40.8	0.4	4.3	28.5	9.9	42.7	0.3
1L116	3839	4.1	26.2	11.2	41.5	0.3	4.1	26.2	9.0	39.3	0.5
1L117	3880	4.2	25.7	10.2	40.1	0.3	4.2	25.6	8.8	38.6	0.5
1L118	3887	4.1	25.1	10.4	39.6	0.3					
1L120	3985	5.1	32.0	14.6	51.7	0.3	5.3	31.2	11.5	48.0	0.4
1L121	3999	5.3	30.9	13.5	49.7	0.3	5.3	31.4	12.6	49.3	0.3
1L123	4083	5.1	30.9	13.9	49.9	0.3	5.0	30.6	11.9	47.5	0.3
1L124	4140						7.0	42.1	17.1	66.2	0.3
1L126	4243	5.5	33.9	16.0	55.4	0.3	5.7	33.6	12.9	52.2	0.2
1L131	4379	5.6	32.4	14.4	52.4	0.3					
1L134	4476	6.0	36.9	14.0	56.9	0.3	6.3	36.7	13.2	56.2	0.3
1L136	4621	5.9	33.7	16.6	56.2	0.3	5.9	36.1	15.5	57.5	0.9
1L137	4662	6.2	35.2	17.1	58.5	0.2	6.2	37.1	15.9	59.2	0.3
1L146	4779	6.5	37.8	17.5	61.8	0.2	6.2	37.1	16.2	59.5	0.4
1L151	4875						6.2	35.9	15.9	58.0	0.2
1L152	4980	6.4	36.6	17.9	60.9	0.3	6.3	36.6	15.8	58.7	0.3
1L159	5179	5.3	33.7	16.4	55.4	0.1	5.9	34.9	15.0	55.8	0.2
1L160	5179	6.2	35.1	19.9	61.2	0.2	6.4	37.6	17.6	61.6	0.3
1L167	5381	6.7	38.8	20.0	65.5	0.2	6.2	38.2	17.9	62.3	0.3
1L172	5578	6.0	37.2	18.7	61.9	0.1	6.1	36.0	16.5	58.6	0.3
1L176	5668	6.1	34.6	17.3	58.0	0.1	6.2	38.4	17.6	62.2	0.3
1L180	5785	6.4	37.1	19.7	63.2	0.3	6.2	38.9	17.9	63.0	0.3
1L183	5886	5.8	37.1	19.6	62.5	0.2	6.2	38.6	17.9	62.7	0.3
1L186	6047	6.2	41.3	20.9	68.4	0.3	5.7	40.4	18.7	64.8	0.4

TABLE A2.4 (Concluded)
Gas Chromatographic Analyses of Loop Samples from the 610°F Irradiation of Santowax OMP

SAMPLE NUMBER	REACTOR MWH	POLYPHENYL COMPOSITION, WT %									
		MIT ANALYSES					MONSANTO ANALYSES				
		o-ϕ_3	m-ϕ_3	p-ϕ_3	TOTAL omp	ϕ_2	o-ϕ_3	m-ϕ_3	p-ϕ_3	TOTAL omp	ϕ_2
1L192	6196	6.4	34.9	19.1	60.4	0.2	5.6	36.7	17.4	59.7	0.2
1L195	6290	6.0	41.0	22.3	69.4	0.2	5.8	41.5	18.7	66.0	0.06
1L208	6742	5.8	36.1	18.0	59.9	0.1	5.6	37.9	16.5	60.0	0.3
1L214	6928	5.4	32.6	17.6	55.6	0.2	5.5	34.3	16.2	56.0	0.3
1L223	7075	6.4	38.0	20.0	64.4	0.2	6.1	39.0	17.2	62.3	0.3
1L231	7317	5.9	33.7	15.5	55.1	0.2	6.0	37.2	15.6	58.8	0.3
1L238	7524	6.1	35.6	17.2	58.9	0.1					
1L245	7723	6.1	36.5	17.8	60.4	0.1	6.6	42.4	17.5	66.5	0.4
1L251	7880	5.8	37.2	19.1	62.1	0.2					
1L252	8030						5.6	36.8	15.4	57.8	0.3
1L253	8180						4.8	31.3	12.4	48.5	0.3
1L254	8336	5.1	36.6	18.4	60.1	0.1	5.7	36.6	15.3	57.6	0.3
1L255	8481	5.8	36.8	19.0	61.6	-	5.5	35.9	14.0	55.4	0.3
1L256	8628	5.3	36.6	17.7	59.6	-	5.8	38.0	16.3	60.1	0.1
1L257	8781	5.9	37.2	18.2	61.3	0.2	6.0	39.0	15.3	60.3	0.3
1L258	8928	5.6	36.4	19.2	61.2	0.1	5.6	38.1	16.5	60.2	0.2
1L259	9081						5.9	38.3	16.8	61.0	0.3
1L260	9231						5.7	36.9	15.7	58.3	0.3
1L261	9381						5.0	38.6	16.6	60.2	0.2
1L262	9530	5.9	37.1	17.6	60.6	0.2	5.9	39.3	15.6	60.8	0.3
1L263	9683	6.0	36.9	17.6	60.5	-	5.5	38.6	14.4	58.5	0.3
1L264	9831	5.9	37.0	18.1	61.0	-	5.7	39.2	15.0	59.9	0.3
1L265	9979	6.2	37.6	16.8	60.6	-	5.8	39.7	15.0	60.5	0.3
1L266	10130	6.1	37.6	17.4	61.1	-	5.7	39.2	14.6	59.5	0.2
1L267	10280						5.6	40.2	15.2	61.0	0.2
1L268	10428	5.4	37.0	17.5	59.9	-	5.6	39.2	15.3	60.1	0.3
1L269	10579	6.1	38.2	18.3	62.6	-	5.6	39.4	15.3	60.3	0.2
1L270	10730						5.6	38.0	14.8	58.4	0.3
1L271	10983						5.5	38.2	14.8	58.5	0.2
1L272	11180						5.4	39.2	15.1	59.7	0.3
1L278	11538	4.9	34.6	18.1	57.6	0.1					
M3L1	11538	8.4	54.1	25.7	88.2	-					

used during these periods, are listed in Table A2. 6.

Table A2. 7 lists the weights of the various input and output streams during the steady-state-HB periods of the 610°F irradiation. From this table, an overall mass balance on the loop and mass balances around the distillation column and makeup flask were performed.

The HB determinations on samples from the 610°F irradiation of Santowax OMP are given in Table A2. 8. The DP contents, determined from the M. I. T. results listed in Table A2. 4, are also listed in order to determine the LIB content by difference. From Table A2. 2 it may be seen that the standard deviation of a DP (gas chromatographic) analysis in the 40 w/o range was ±1 w/o. The standard deviation of an HB (distillation) analysis was ±0. 2 w/o (see Section A2. 2). By the propagation of variances rule the LIB contents have standard deviations of ±1 w/o or ±14% of the values quoted.

The results obtained on the samples of the 750°F irradiation are listed in Tables A2. 9-A2. 12 in the same order as for the 610°F irradiation samples. Table A2. 9 lists the results of the M. I. T. and Monsanto gas chromatographic analyses on loop samples, and Table A2. 10 lists the distillate and bottoms analyses. Table A2. 6 lists the return and makeup analyses. Table A2. 11 gives the mass balance information for the steady-state-HB period of the 750°F irradiation. Finally, the HB and LIB determinations are listed in Table A2. 12.

Some of the samples from the 610°F and 750°F irradiations were analyzed for HB content by microsublimation at Chalk River (A2. 3). Their results are listed in Table A2. 13 together with the HB and DP determinations made at M. I. T. As may be seen from the table the agreement between the Chalk River determinations and those at M. I. T. is only fair.

Since the microsublimation techniques are dependent upon the HB content and must be calibrated by distillation of large (~300 gm) samples of the coolant to be sublimated, the M. I. T. results are believed to be more accurate.

A2. 4 Tabulation of Radiolytic Gas Analyses

Mass spectrographic analyses were performed on undissolved and dissolved radiolytic gas samples from both the 610°F and 750°F irradiations by the Petroleum Analytical Research Corp. (Houston, Texas). The results of analyses on 610°F and 750°F irradiation undissolved gas samples are tabulated in Table A2. 14 and Table A2. 15 respectively.

The actual mole % of nitrogen plus oxygen in the samples is given

TABLE A2.5

Gas Chromatographic Analyses of Sample Bottoms and Distillates from the Steady-State-HB Periods of the 610°F Irradiation of Santowax OMP

SAMPLE NUMBER	REACTOR MWH	POLYPHENYL COMPOSITION, WT%									
		BOTTOMS					DISTILLATE				
		o-ϕ_3	m-ϕ_3	p-ϕ_3	TOTAL omp	ϕ_2	o-ϕ_3	m-ϕ_3	p-ϕ_3	TOTAL omp	ϕ_2
1L137	4662	-	5.5	5.1	10.6	-	10.7	59.4	24.2	94.3	0.3
1L146	4779	-	3.6	4.7	8.3	-	9.9	59.4	22.3	91.6	0.2
1L151	4875	-	2.2	3.1	5.3	-	9.6	55.2	26.5	91.3	0.3
1L152	4980	-	2.6	3.5	6.1	-					
1L159	5179	-	2.7	3.6	6.3	-					
1L160	5179	-	1.9	3.3	5.2	-	9.3	52.3	24.7	86.3	0.3
1L167	5381	-	3.0	3.8	6.8	-					
1L172	5578	-	1.8	2.6	4.4	-					
1L176	5668	-	2.4	3.3	5.7	-					
1L180	5785	-	2.1	3.2	5.3	-					
1L183	5886	-	1.8	2.7	4.5	-					
1L186	6047	-	2.1	3.0	5.1	-					
1L192	6196	-	1.6	2.8	4.4	-					
1L245	7723	-	1.4	1.6	3.0	-	10.0	61.7	27.8	99.5	0.3
1L251	7880	-	0.2	0.3	0.5	-	8.9	54.3	28.5	91.7	0.2
1L252	8030	-	0.1	0.2	0.3	-	9.0	54.1	25.9	89.0	0.1
1L253	8180	-	0.2	0.2	0.4	-	9.0	54.8	26.4	90.2	0.1
1L255	8481						8.9	57.4	26.9	93.2	0.08
1L256	8628	-	0.2	0.2	0.4	-	9.2	55.4	24.5	89.1	-
1L257	8781	-	0.1	0.2	0.3	-	8.8	52.8	24.9	86.5	0.2
1L258	8928	-	0.1	0.2	0.3	-	8.9	56.3	26.5	91.7	-
1L259	9081	-	0.2	0.3	0.5	-	9.2	56.1	25.6	90.9	-
1L260	9231	-	0.1	0.2	0.3	-					
1L261	9381	-	0.6	0.8	1.4	-	9.3	56.8	24.6	90.7	-
1L262	9530	-	0.2	0.2	0.4	-					
1L263	9683	-	0.3	0.2	0.5	-	9.0	57.0	26.3	92.3	-
1L264	9831	-	0.1	0.3	0.4	-	9.4	55.2	24.4	89.0	-
1L265	9979	-	0.3	0.3	0.6	-	9.2	56.4	23.7	89.3	-
1L266	10130	-	0.1	0.2	0.3	-	9.2	57.7	24.3	91.2	-
1L267	10280	-	0.2	0.2	0.4	-	9.4	57.6	25.1	92.1	-

TABLE A2.6

Gas Chromatographic Analyses of Makeup and Return Samples for the Steady-State-HB Periods of the 610°F and 750°F Irradiations of Santowax OMP

Sample Number	Polyphenyl Composition, Wt %				
	o-ϕ_3	m-ϕ_3	p-ϕ_3	Total omp	ϕ_2
1L186R	10.6	60.2	26.1	96.9	-
1D28	8.9	58.3	26.6	93.8	-
1D31	10.0	56.8	27.3	94.1	0.1
Makeup M-3	9.4	58.7	31.9	100.0	-
2D8	11.0	53.1	28.2	92.3	1.5
2D11	11.0	52.4	28.6	92.0	1.4
2D17	11.3	56.9	28.6	96.7	1.3
2D23	11.3	56.6	28.6	96.5	1.8
750°F charge	12.7	58.3	29.4	100.4	-

TABLE A2.7
Masses Removed and Returned for the Steady-State-HB Periods of the 610°F Irradiation of Santowax OMP

SAMPLE NUMBER	SAMPLE WEIGHT, GRAMS	REACTOR MWH REMOVED	DISTILLATION WEIGHTS, GRAMS				MAKEUP WEIGHTS, GRAMS		RETURN WEIGHT, GRAMS	REACTOR MWH RETURNED	RETURN NUMBER
			CHARGE	DISTILLATE	BOTTOMS	COLD TRAP	DISTILLATE	MAKEUP			
BEGINNING OF QUASI-STEADY-STATE-HB AT 4630 MWH WITH 1D6											
-	-	-	-	-	-	-	-	282.0	282.0	4630	1D6
1L137	317.0	4662	304.0	180.6	119.6	0.2	171.0	263.0	296.0	4678	1D7
Drop in surge tank	60.0	4730	-	-	-	-	-	-	-	-	-
1L146	320.0	4779	310.3	195.6	114.0	-	185.0	221.5	317.0	4830	1D8
1L151	314.0	4874	304.5	196.1	106.5	-	185.1	250.9	308.0	4920	1D9
1L152	317.0	4980	307.0	200.1	104.6	-	192.6	202.3	301.0	5028	1D10
1L159	319.0	5179	308.0	196.4	109.7	-	188.8	220.8	308.0	5233	1D12
-	-	-	-	-	-	-	-	332.0	332.0	5179	1D11
1L160	317.0	5179	306.9	204.9	100.0	-	197.2	209.3	334.0	5465	1D13
1L167	320.0	5382	310.8	196.5	109.5	-	189.6	191.5	318.0	5623	1D14
1L172	316.0	5579	307.3	200.0	105.6	-	192.4	221.1	340.0	5715	1D15
1L176	317.0	5668	306.5	199.3	105.0	-	193.0	206.8	331.0	5804	1D16
1L180	318.0	5784	306.7	201.8	102.7	-	194.6	213.3	339.0	5898	1D17
1L183	317.0	5886	286.1	-	93.3	-	181.5	214.2	315.0	6131	1D18
1L186	317.0	6046	306.2	201.2	101.8	-	-	-	-	-	-
1L192	320.0	6196	305.9	202.3	100.5	-	-	-	-	-	-
END OF QUASI-STEADY-STATE-HB AT 6196 MWH WITH 1L192											
1L231	314.0	7317	297.7	193.9	102.3	-	188.1	240.4	344.0	7546	1D24
1L238	319.3	7526	309.1	-	-	0.4	154.7	228.0	340.5	7792	1D25
1L245	316.0	7723	301.3	189.1	109.8	2.4	182.4	235.1	333.3	7882	1D26
1L251	314.7	7880	301.7	197.3	102.4	2.1	190.1	241.1	312.9	8049	1D27

TABLE A2.7 (Concluded)
Masses Removed and Returned for the Steady-State-HB Periods of the 610°F Irradiation of Santowax OMP

SAMPLE NUMBER	SAMPLE WEIGHT, GRAMS	REACTOR MWH REMOVED	DISTILLATION WEIGHTS, GRAMS				MAKEUP WEIGHTS, GRAMS		RETURN WEIGHT, GRAMS	REACTOR MWH RETURNED	RETURN NUMBER
			CHARGE	DISTILLATE	BOTTOMS	COLD TRAP	DISTILLATE	MAKEUP			
BEGINNING OF STEADY-STATE-HB AT 7880 MWH AFTER 1L251											
1L252	311.0	8030	299.0	199.3	98.8	1.8	191.9	247.7	332.5	8189	1D28
1L253	316.0	8180	303.9	201.0	102.5	3.4	193.4	247.1	316.0	8340	1D29
1L254	310.8	8336	293.0	189.9	98.5	2.9	183.9	233.0	313.0	8490	1D30
1L255	318.8	8481	306.3	200.3	101.6	3.3	193.8	243.0	315.3	8642	1D31
1L256	310.8	8628	298.3	196.2	99.6	1.3	188.9	225.0	310.0	8787	1D32
1L257	316.6	8781	302.8	199.8	100.8	1.4	195.4	245.0	326.0	8932	1D33
1L258	311.0	8928	297.9	194.3	99.2	3.2	187.3	211.0	302.5	9086	1D34
1L259	313.5	9081	299.0	195.5	98.9	2.7	188.6	211.9	316.0	9234	1D35
1L260	314.0	9232	300.2	195.6	99.6	2.8	189.2	212.3	306.0	9388	1D36
1L261	316.5	9381	301.4	194.8	103.2	2.2	187.4	199.0	334.2	9533	1D37
1L262	311.1	9530	298.1	198.9	98.4	2.0	191.7	211.2	303.0	9688	1D38
1L263	318.5	9683	305.4	201.8	100.8	2.0	196.7	197.9	314.0	9836	1D39
1L264	312.0	9832	298.8	197.9	98.0	1.5	189.7	168.6	304.0	9986	1D40
1L265	319.5	9979	296.3	195.5	98.4	1.4	188.2	189.0	313.0	10132	1D41
1L266	311.0	10130	290.0	191.2	95.3	1.9	183.4	199.5	314.0	10284	1D42
1L267	321.0	10279	303.9	199.5	100.7	2.0	198.1	181.0	299.5	10442	1D43
1L268	328.5	10428	318.3	197.7	108.4	1.3	190.2	199.5	326.5	10590	1D44
END OF STEADY-STATE-HB AT 10428 MWH WITH 1L268											
1L269	350.5	10578	327.6	215.8	108.0	1.2	209.5	187.9	317.0	10783	1D45
1L270	323.5	10730	308.8	199.5	104.7	0.3	190.9	196.3	325.5	10850	1D46
1L271	321.1	10983	214.3	137.1	72.8	-	130.3	278.5	333.6	11186	1D47
1L272	333.5	11180	320.1	202.2	112.8	0.5	189.4	186.3	-	-	-
1L278	FINAL	DRAIN	300.0	186.8	110.9	1.8	-	-	-	-	-

TABLE A2.8

HB and LIB Content of Samples

from the 610°F Irradiation of Santowax OMP

Sample Number	HB Content Wt %	DP Content Wt %	LIB Content (By Difference) Wt %
1L137	35.2	41.5	6.3
1L146	33.7	38.2	4.5
1L151	33.1		
1L152	32.0	39.1	7.1
1L159	33.4	44.6	11.2
1L160	30.9	38.8	7.9
1L167	32.8	34.5	1.7
1L172	32.9	38.1	5.2
1L176	32.3	42.0	9.7
1L180	31.7	36.8	5.1
1L183	31.1	37.5	6.4
1L186	31.6	31.6	-
1L192	31.4	39.6	8.2
1L231	34.4**	44.9	10.5
1L245	35.3	39.6	4.3
1L251	33.8	37.9	4.1
1L252	33.0		
1L253	33.6		
1L254	33.5*	39.9	6.4
1L255	33.0*	38.4	5.4
1L256	33.3	40.4	7.1
1L257	33.2	38.7	5.5
1L258	33.2	38.8	5.6
1L259	32.9		
1L260	33.1		
1L261	33.8		
1L262	32.9	39.4	6.5
1L263	32.8	39.5	6.7
1L264	32.7	39.0	6.3

TABLE A2.8 (Concluded)

HB and LIB Content of Samples

from the 610°F Irradiation of Santowax OMP

Sample Number	HB Content Wt %	LP Content Wt %	LIB Content (By Difference) Wt %
1L265	33.0	39.4	6.4
1L266	32.8	38.9	6.1
1L267	33.0		
1L268	33.9*	40.1	6.2
1L269	32.8*	37.4	4.6
1L270	33.8*		
1L271	33.8*		
1L272	35.1*		
1L278	36.8*	42.4	5.6

*No bottoms analysis available. Average correction of 0.4 w/o omp used.

**Uncorrected for omp content in bottoms.

TABLE A2.9

Gas Chromatographic Analyses of Loop Samples from the 750°F Irradiation of Santowax OMP

SAMPLE NUMBER	REACTOR MWH	POLYPHENYL COMPOSITION, WT%									
		MIT ANALYSES					MONSANTO ANALYSES				
		o-ϕ_3	m-ϕ_3	p-ϕ_3	TOTAL omp	ϕ_2	o-ϕ_3	m-ϕ_3	p-ϕ_3	TOTAL omp	ϕ_2
2L1	0	9.7	59.5	32.6	101.8	0.2	10.6	60.1	27.7	98.4	0.2
2L2	41	10.0	55.5	34.9	100.4	-					
2L3	122	9.2	55.6	29.3	94.1	0.6					
2L4	240	7.6	51.8	28.7	88.1	0.6					
2L5	253	10.4	53.0	27.0	90.4	-					
2L6	378	9.9	51.0	26.4	87.3	0.9					
2L7	494	8.8	48.2	25.9	82.9	0.9					
2L9	628	7.3	45.7	24.2	77.2	0.6					
2L10	810	7.5	42.0	22.1	71.6	0.8					
2L11	1056	6.3	37.0	19.7	63.0	1.7					
2L12	1126	6.9	38.4	20.6	65.9	1.7					
2L13	1406	6.0	34.5	19.2	59.7	2.4					
2L14	1650	4.6	29.8	15.3	49.7	2.6					
2L16	1936	3.5	25.7	14.0	43.2	2.4					
2L17	2040	3.1	24.2	13.8	41.1	2.9					
2L18	2060	5.8	31.2	16.7	53.7	2.0	5.8	33.0	13.8	52.6	2.4
2L19	2145	5.9	31.1	17.1	54.1	1.9	5.4	33.7	14.4	53.5	2.5
2L22	2278	6.4	35.7	18.6	60.7	1.9	6.3	35.9	15.1	57.3	2.5
2L23	2360						6.3	36.2	15.4	57.9	2.7
2L24	2424						6.4	36.1	15.6	58.1	2.5
2L25	2520	5.5	33.9	17.3	56.7	1.8	6.2	37.3	15.8	59.3	2.6
2L26	2618	6.3	35.7	18.3	60.3	2.0	7.1	42.2	17.7	67.0	3.1
2L27	2707	6.2	34.8	18.8	59.8	2.1	6.5	37.9	15.8	60.2	2.6
2L28	2800	6.1	35.3	18.5	60.0	2.0	6.0	36.2	15.9	58.1	2.4
2L29	2900	6.0	35.5	18.4	59.9	2.3	6.2	36.7	15.8	58.7	2.7
2L31	3000	6.1	35.5	18.9	60.5	2.2	6.0	35.6	15.8	57.4	2.3
2L32	3200	5.7	33.8	17.9	57.4	2.4	5.6	33.7	15.4	54.7	2.8
2L33	3245	5.8	34.8	18.6	59.2	2.5	5.6	36.1	16.2	57.9	2.6
2L34	3344	5.9	34.7	18.1	58.7	2.6	5.5	33.5	15.2	54.2	2.8
2L36	3445	5.8	34.7	18.5	59.0	2.3	5.6	34.5	15.8	55.9	2.7
2L40	3733	5.6	34.3	18.4	58.3	2.3					
2L41	3748	5.4	34.0	18.9	58.3	2.2					
2L42	3748	11.0	51.9	26.1	89.0	0.9					

TABLE A2.10

Gas Chromatographic Analyses of Sample Bottoms and Distillates from the Steady-State-HB Period of the 750°F Irradiation

Sample Number	Reactor MWH	Polyphenyl Composition, Wt%									
		Bottoms					Distillate				
		o-ϕ_3	m-ϕ_3	p-ϕ_3	Total omp	ϕ_2	o-ϕ_3	m-ϕ_3	p-ϕ_3	Total omp	ϕ_2
2L18	2060	-	0.3	0.6	0.9	-	9.7	54.6	28.6	92.9	3.3
2L19	2145	-	1.1	1.7	2.8	-	9.6	54.6	28.2	92.4	2.9
2L22	2278	-	0.7	1.0	1.7	-	9.7	53.3	26.8	89.8	2.6
2L23	2360	-	0.3	0.5	0.8	-	10.6	55.1	27.4	93.1	2.7
2L24	2424	-	0.5	0.8	1.3	-	9.8	55.0	28.1	92.9	2.2
2L25	2520	-	0.3	0.5	0.8	-	9.5	55.2	27.6	92.3	2.7
2L26	2618	-	0.9	1.6	2.5	-					
2L27	2707	-	0.7	0.7	1.4	-	10.5	58.6	30.2	99.3	3.4
2L28	2800	-	0.2	0.3	0.5	-	10.1	54.3	27.1	91.5	2.7
2L29	2900	-	0.5	1.1	1.6	-	10.2	56.4	29.0	95.6	3.4
2L31	3000	-	0.1	0.1	0.3	-	9.4	53.3	27.3	90.0	3.4
2L32	3200	-	-	-	-	-	9.0	52.7	27.0	88.7	3.5
2L33	3245	-	-	-	-	-	8.9	51.2	26.8	86.9	2.7
2L34	3344	-	-	-	-	-	9.8	56.0	30.3	96.1	4.3
2L36	3445	-	-	-	-	-	9.0	53.7	29.2	91.9	3.4
2L37	3544	-	-	-	-	-	9.4	51.4	26.9	87.7	3.9
2L40	3733	-	0.4	1.1	1.5	-					

TABLE A2.11

Masses Removed and Returned for the Steady-State-HB Period of the 750°F Irradiation of Santowax OMP

SAMPLE NUMBER	SAMPLE WEIGHT, GRAMS	REACTOR MWH REMOVED	DISTILLATION WEIGHTS, GRAMS				MAKEUP WEIGHTS, GRAMS		RETURN WEIGHT, GRAMS	REACTOR MWH RETURNED	RETURN NUMBER
			CHARGE	DISTILLATE	BOTTOMS	COLD TRAP	DISTILLATE	MAKEUP			
2L18	302.0	2060	279.2	171.5	104.7	0.5	163.5	192.7	332.0	2150	2D7
-	-	-	-	-	-	-	-	323.0	323.0	2066	2D6
Fouling probe out	50.0	2110	-	-	-	-	-	-	-	-	-
2L19	299.5	2145	285.3	174.6	108.1	0.4	166.9	211.9	330.5	2253	2D8
-	-	-	-	-	-	-	-	-	335.0	2190	Opened 5μ filter
2L20	303.0	2250	-	-	-	-	-	-	-	-	-
2L21	308.0	2253	-	-	-	-	-	-	-	-	-
-	-	-	-	-	-	-	-	-	330.0	2253	2D9
2L22	297.0	2278	272.6	176.5	93.7	0.2	168.9	204.5	342.5	2368	2D11
Closed 5μ filter	335.0	2280	-	-	-	-	-	-	-	-	-
BEGINNING OF STEADY-STATE-HB AT 2280 MWH WITH 2D10											
-	-	-	-	-	-	-	-	-	312.0	2280	2D10
2L23	355.0	2360	344.8	223.4	118.0	0.7	211.8	161.6	341.0	2427	2D12
Fouling probe leak	50.0	2412	-	-	-	-	-	-	-	-	-
2L24	318.0	2424	300.7	195.2	102.7	0.4	186.3	204.4	344.0	2526	2D13
2L25	299.5	2520	285.3	186.6	94.6	1.1	178.0	207.3	349.0	2623	2D14
Fouling probe leak	50.0	2566	-	-	-	-	-	-	-	-	-
2L26	308.0	2618	280.6	179.0	98.2	0.7	171.8	207.8	335.0	2712	2D15
Fouling probe leak	50.0	2620	-	-	-	-	-	-	-	-	-
2L27	301.0	2707	285.0	186.2	94.9	0.7	179.3	215.8	364.0	2804	2D16

TABLE A2.11 (Concluded)
Masses Removed and Returned for the Steady-State-HB Period of the 750°F Irradiation of Santowax OMP

SAMPLE NUMBER	SAMPLE WEIGHT, GRAMS	REACTOR MWH REMOVED	DISTILLATION WEIGHTS, GRAMS				MAKEUP WEIGHTS, GRAMS		RETURN WEIGHT, GRAMS	REACTOR MWH RETURNED	RETURN NUMBER
			CHARGE	DISTILLATE	BOTTOMS	COLD TRAP	DISTILLATE	MAKEUP			
Fouling probe leak	50.0	2746	-	-	-	-	-	-	-	-	-
2L28	303.0	2800	285.9	187.4	93.2	0.8	180.7	203.7	355.5	2908	2D17
2L29	299.5	2900	285.5	187.8	93.9	0.5	180.6	222.9	365.5	3006	2D18
2L30	25.5	2902	-	-	-	-	-	-	-	-	-
2L31	297.5	3000	270.8	180.8	87.2	0.5	173.2	167.0	325.0	3200	2D19
Fouling probe out	35.0	3199	-	-	-	-	-	-	-	-	-
2L32	339.2	3200	318.3	204.7	109.3	0.6	196.6	157.4	312.4	3250	2D20
2L33	301.0	3245	284.6	186.3	94.9	0.8	178.3	171.6	291.0	3354	2D21
2L34	377.5	3344	360.7	234.8	121.9	0.9	226.7	133.7	332.0	3448	2D22
2L35	25.5	3350	-	-	-	-	-	-	-	-	-
2L36	323.5	3445	294.9	195.9	98.1	0.1	189.6	180.8	300.5	3546	2D23
2L37	302.2	3544	281.5	182.2	94.9	0.7	173.9	174.8	303.2	3656	2D24
2L38	296.0	3645	-	-	-	-	-	-	-	-	-
2L39	27.0	3651	-	-	-	-	-	-	-	-	-
2L40	343.0	3733	331.5	215.6	113.4	0.4	-	-	-	-	-
END OF STEADY-STATE-HB AT 3733 MWH WITH 2L40											
2L41	FINAL DRAIN										

TABLE A2.12

HB and LIB Content of Samples

from the 750°F Irradiation of Santowax OMP

Sample Number	HB Content Wt %	DP Content Wt %	LIB Content (By Difference) Wt %
2L18	37.2	46.3	9.1
2L19	36.8	45.9	9.1
2L22	33.8	39.3	5.5
2L23	33.9		
2L24	33.7		
2L25	32.9	43.3	10.4
2L26	34.1	39.7	5.6
2L27	32.8	40.2	7.4
2L28	32.4	40.0	7.6
2L29	32.4	40.1	7.7
2L31	32.1	39.5	7.4
2L32	34.4	42.6	8.2
2L33	33.4	40.8	7.4
2L34	33.8	41.3	7.5
2L36	33.3	41.0	7.7
2L37	33.7		
2L40	33.7	41.7	8.0

TABLE A2.13

Comparison of Chalk River and M.I.T. HB Determinations

Sample Number	DP Content (M.I.T.)	HB Content	
		M.I.T.[a]	Chalk River[b]
1L92	48.3		45.2
1L254	39.9	33.5	38.5
1L268	40.1	33.9	33.7
2L1	~0		1.0
2L5	9.6		7.8
2L14	50.3		40.4
2L22	39.3	33.8	33.5
2L31	39.5	32.1	34.6
2L41	41.7	33.7[c]	42.5

a. By distillation.

b. By microsublimation.

c. Analysis for 2L40 given.

TABLE A2.14
Mass Spectrographic Analyses of Gas Samples from the 610°F Irradiation of Santowax OMP

SAMPLE NUMBER	REACTOR MWH	NITROGEN AND OXYGEN FREE COMPOSITION, MOLE %							NITROGEN + OXYGEN MOLE %
		HYDROGEN	METHANE (C_1)	ETHANE ETHYLENE (C_2)	PROPANE PROPYLENE (C_3)	BUTANES BUTYLENES (C_4)	PENTANES PENTENES HEXANES (C_{5+6})	BENZENE TOLUENE XYLENE	
1G39	562	77.3	7.6	8.9	2.5	1.3	0.6	1.8	42.5
1G43	735	74.8	8.9	9.7	3.2	1.4	0.5	1.5	35.5
1G54	1207	57.9	15.7	15.7	5.6	2.5	1.2	1.4	28.4
1G56	1386	53.9	16.8	17.7	5.9	2.9	1.2	1.6	23.9
1G61	1586	49.1	18.1	18.0	6.8	4.6	2.1	1.3	23.3
1G64	1726	53.8	17.0	16.5	6.2	4.0	1.3	1.2	22.0
1G70	1972	48.6	19.3	19.3	7.1	3.2	1.4	1.1	16.3
1G73	2164	56.3	18.4	16.7	5.6	2.0	0.7	0.3	11.8
1G83	2529	46.2	20.6	20.7	7.7	2.8	1.3	0.7	7.0
1G90	2860	46.9	21.0	20.2	7.3	2.8	1.2	0.6	5.8
1G101	3220	43.6	21.7	21.3	8.1	3.2	1.4	0.7	4.5
1G110	3574	41.3	22.9	21.8	8.2	3.3	1.6	0.9	4.4
1G119	3887	38.2	22.5	22.0	9.1	3.9	2.5	1.8	4.7
1G127	4243	34.2	27.4	23.6	8.7	3.5	1.7	0.9	5.0
1G135	4555	48.2	25.3	17.0	5.9	2.2	1.0	0.4	9.5
1G142	4678	48.5	22.0	19.1	6.5	2.5	1.1	0.3	31.1
1G143	4712	51.8	20.8	17.9	6.2	2.2	0.9	0.2	8.5
1G147	4817	52.8	19.3	17.4	6.4	2.5	1.2	0.4	7.1
1G156	5075	52.6	19.4	17.2	6.4	2.5	1.3	0.6	13.9
1G163	5358	57.2	17.7	15.4	5.8	2.0	1.2	0.7	5.4
1G170	5510	56.7	17.7	15.8	5.8	2.2	1.2	0.6	7.5
1G177	5710	56.2	17.6	16.1	5.9	2.3	1.2	0.7	6.8
1G182	5884	60.0	16.7	14.6	5.2	2.0	1.0	0.5	6.3
1G187	6085	61.0	16.4	14.3	5.1	1.9	0.8	0.5	5.3
1G194	6282	60.3	16.5	14.5	5.2	2.0	1.0	0.5	4.4

TABLE A2.14 (Concluded)
Mass Spectrographic Analyses of Gas Samples from the 610°F Irradiation of Santowax OMP

SAMPLE NUMBER	REACTOR MWH	NITROGEN AND OXYGEN FREE COMPOSITION, MOLE %							NITROGEN + OXYGEN MOLE %
		HYDROGEN	METHANE (C_1)	ETHANE ETHYLENE (C_2)	PROPANE PROPYLENE (C_3)	BUTANES BUTYLENES (C_4)	PENTANES PENTENES HEXANES (C_{5+6})	BENZENE TOLUENE XYLENE	
1G197	6391	60.8	15.8	14.2	5.7	2.0	1.0	0.5	4.9
1G203	6649	62.9	15.1	13.9	5.1	1.9	0.8	0.3	2.5
1G209	6777	59.5	15.7	15.3	5.6	2.3	1.1	0.5	2.2
1G220	6976	59.5	16.2	15.2	5.4	2.1	1.2	0.4	10.8
1G225	7180	59.0	16.5	15.8	5.5	2.0	0.9	0.3	2.0
1G230	7316	60.0	15.7	14.9	5.5	2.1	1.3	0.5	1.8
1G239	7586	60.7	16.0	15.2	5.3	1.9	0.7	0.2	2.9
1G246	7784	60.4	16.1	15.7	5.0	1.8	0.7	0.3	5.6
1G251	7880	61.4	15.7	14.8	5.2	1.7	0.8	0.4	4.3
1G254	8052	59.6	16.4	15.4	5.5	1.9	0.8	0.4	5.1
1G260	8244	58.3	16.6	16.2	5.7	2.1	0.8	0.3	4.3
1G267	8502	59.5	16.3	15.6	5.3	1.6	1.2	0.5	3.7
1G270	8652	63.9	13.9	13.0	5.0	2.1	0.8	1.3	8.1
1G273	8782	58.1	15.1	16.3	6.2	2.4	1.3	0.6	14.5
1G283	9134	56.8	14.0	17.6	6.5	2.9	1.5	0.7	3.0
1G289	9481	65.0	14.3	13.1	5.0	1.7	0.7	0.2	8.1
1G293	9635	62.9	15.2	13.9	5.0	1.7	0.9	0.4	8.3
1G299	9847	61.1	15.3	15.3	5.3	1.8	0.8	0.4	7.7
1G304	10033	59.5	17.1	14.3	5.2	1.9	1.1	0.9	4.4
1G308	10204	60.8	16.3	14.8	5.6	1.7	0.6	0.2	18.9
1G311	10350	60.3	16.4	14.0	5.5	2.0	1.1	0.7	13.7
1G318	10596	59.4	17.6	15.3	5.3	1.7	0.6	0.1	10.1
1G321	10685	57.9	17.6	16.0	5.7	1.8	0.7	0.3	2.5
1G325	10895	54.3	16.7	15.4	6.8	2.7	2.1	2.0	2.9
1G333	11142	58.0	15.9	16.5	6.2	2.1	1.0	0.3	7.0
1G336	11282	58.7	16.4	15.3	5.8	2.1	1.0	0.7	5.4
1G342	11538	55.0	17.2	16.9	6.5	2.3	1.3	0.8	9.9

TABLE A2.15

Mass Spectrographic Analyses of Gas Samples from the 750°F Irradiation of Santowax OMP

SAMPLE NUMBER	REACTOR MWH	NITROGEN AND OXYGEN FREE COMPOSITION, MOLE %							NITROGEN + OXYGEN MOLE %
		HYDROGEN	METHANE (C_1)	ETHANE ETHYLENE (C_2)	PROPANE PROPYLENE (C_3)	BUTANES BUTYLENES (C_4)	PENTANES PENTENES HEXANES (C_{5+6})	BENZENE TOLUENE XYLENE	
2G28	531	47.4	28.8	14.7	5.4	1.6	0.7	1.4	22.4
2G38	669	46.2	29.5	15.8	5.6	1.5	0.5	0.9	11.8
2G39	673	47.7	28.6	15.5	5.5	1.5	0.4	0.8	14.0
2G45	720	44.0	29.3	16.4	6.0	1.6	0.5	2.2	10.0
2G47	805	36.1	28.8	17.1	8.8	2.0	2.2	5.0	7.2
2G56	905	36.0	31.7	17.8	8.0	2.0	0.7	3.8	6.1
2G67	1010	35.4	32.8	19.5	6.6	2.1	0.9	2.7	3.6
2G98	1208	48.8	30.2	14.4	4.8	0.9	0.3	0.6	23.0
2G108	1300	45.4	32.0	15.3	5.4	0.6	0.5	0.8	15.3
2G110	1400	42.1	35.2	15.7	5.1	1.1	0.09	0.7	10.9
2G124	1607	36.4	38.2	16.8	5.5	1.0	0.4	1.7	6.1
2G138	1800	34.9	40.2	17.1	5.5	1.0	0.3	1.0	3.1
2G153	1970	31.3	41.2	18.0	6.2	1.3	0.5	1.5	2.8
2G194	2311	37.4	39.4	16.1	4.9	1.0	0.3	0.9	14.0
2G207	2404	39.0	37.2	16.0	5.1	1.0	0.4	1.2	10.5
2G208	2462	39.5	37.5	16.0	4.9	1.0	0.2	0.9	8.7
2G229	2697	37.1	37.2	17.4	5.5	1.1	0.4	1.3	2.7
2G231	2787	37.8	37.8	16.8	5.4	1.1	0.3	0.8	1.9
2G233	2895	31.0	40.1	19.5	6.3	1.3	0.4	1.4	3.1
2G244	2999	37.4	38.1	16.7	5.2	1.0	0.3	1.3	1.9
2G246	3084	35.1	40.1	17.2	5.4	1.0	0.3	0.9	2.7
2G260	3176	36.2	38.3	17.0	5.1	2.2	0.3	0.9	2.1
2G272	3287	37.9	37.2	16.8	5.1	1.0	0.3	1.7	3.6
2G274	3440	40.2	37.7	15.2	4.6	1.1	0.2	1.0	3.0
2G286	3590	41.0	38.5	14.4	4.0	0.7	0.3	1.1	1.8
2G287	3634	36.5	40.9	16.4	4.7	0.8	0.1	0.6	1.7
2G305	3730	39.2	38.1	16.0	4.7	0.8	0.2	1.0	1.6

in the tables. Some oxygen was identified in the forms of CO and CO_2. The hydrocarbon gases are listed as mole % on an oxygen and nitrogen free basis, since oxygen and nitrogen are not radiolytic gas products but come from two sources:

1. The original pressurizing nitrogen at the start of the irradiation
2. Air leakage into the gas samples.

Above methane the analyses are ordered according to the number of carbon atoms in the species. A typical mole % split of the analyses for samples from the steady-state-HB period of the 610°F irradiation was

C_2: 98% ethane, 2% ethylene
C_3: 85% propane, 15% propylene
C_4: 85% butanes, 15% butylenes
C_{5+6}: 48% pentanes, 39% pentenes, 8% hexanes, 5% hexenes
Aromatics: 61% benzene, 23% toluene, 16% xylene.

Samples from the 750°F irradiation tended to show a higher percentage of saturated hydrocarbons (C_{5+6} is an exception). A typical mole % split for samples from the steady-state-HB period of the 750°F irradiation was

C_2: 99% ethane, 1% ethylene
C_3: 94% propane, 6% propylene
C_4: 95% butanes, 5% butylenes
C_{5+6}: 21% pentanes, 62% pentenes, 17% hexenes
Aromatics: 89% benzene, 10% toluene, 1% xylene.

Analyses have also been performed on dissolved gas samples recovered from the gas solubility experiments (see Section 5.7). The results of these analyses for both irradiations are given in Table A2.16. For the 610°F irradiation dissolved gas samples, a typical mole % split of the hydrocarbon gases was

C_2: 100% ethane
C_3: 65% propane, 35% propylene
C_4: 80% butanes, 20% butylenes
C_{5+6}: 35% pentanes, 37% pentenes, 15% hexanes, 12% hexenes, 1% heptenes
Aromatics: 94% benzene, 6% toluene, trace xylene.

As with the samples of gas produced, the 750°F irradiation dissolved gas samples tended to show a higher percentage of saturated hydrocarbons. A typical mole % split, taken from the 750°F steady-state-HB samples, was

TABLE A2.16

Mass Spectrographic Analysis of Dissolved Gas Samples from the 610°F and 750°F Irradiations of Santowax OMP

Sample Number	Reactor MWH	Nitrogen and Oxygen Free Composition, Mole %							Nitrogen + Oxygen Mole %
		Hydrogen	Methane (C_1)	Ethane Ethylene (C_2)	Propane Propylene (C_3)	Butanes Butylenes (C_4)	Pentanes Pentenes Hexanes (C_{5+6})	Benzene Toluene Xylene	
1L52	1174	-	11.7	34.8	23.7	17.5	7.4	4.9	23.9
1L118	3887	16.0	16.2	27.8	18.4	9.9	8.7	3.0	1.4
1L195	6290	25.3	15.4	23.6	14.7	9.4	8.5	3.1	36.8
2L8	522	17.4	22.9	27.4	16.6	6.0	3.9	5.8	20.6
2L14	1650	18.5	19.4	22.8	19.0	5.7	5.5	9.1	84.5
2L30	2902	16.5	26.7	25.2	18.2	6.2	4.5	2.7	7.0
2L35	3350	14.5	27.6	26.6	18.3	5.8	3.9	3.3	3.8
2L39	3651	11.1	26.4	29.0	20.7	6.3	4.2	2.3	22.9

C_2: 100% ethane
C_3: 74% propane, 26% propylene
C_4: 92% butanes, 8% butylenes
C_{5+6}: 23% pentanes, 70% pentenes, 7% hexenes
Aromatics: 97% benzene, 3% toluene, trace xylene.

No error limits have been quoted on the above samples. Errors could be due both to analyses and representation of gas samples. An overall standard deviation estimate was provided by the assumption of constancy of undissolved gas composition during the steady-state-HB period of the 750°F irradiation (Section 4. 9 shows no trend of the concentration of any species). The standard deviation from the average value provided the estimate. The results of this error analysis are given in Table A2. 17.

It may be seen that the relative standard deviation in measurement ($\Delta C/C$) tends to increase as the concentration of the desired species decreases. The absolute standard deviation (ΔC) tends to decrease with decreasing concentration. Assuming the above results to be independent

TABLE A2. 17

Estimated Standard Deviation in Mass Spectrographic Analyses

Component	Average Undissolved Gas Composition, 750°F Irradiation Steady-State-HB, mole %	Estimated Relative Standard Deviation (% of value reported)
H_2	37. 5	4
C_1	38. 4	3
C_2	16. 5	7
C_3	5. 1	10
C_4	1. 1	33
C_{5+6}	0. 3	26
Aromatics	1. 1	27

of the species being studied, Table A2. 17 gives an indication of the precision with which high and low concentrations were measured.

A2.5 Calculations of Circulating Coolant Mass in the Loop

Three basically different methods were employed to calculate the circulating coolant mass in the loop during both the 610°F and 750°F irradiations. These were:

1. Calculations based on the known volume of various sections of the loop.
2. Calculations based on the amount of coolant drained at the termination of the irradiation.
3. Dilution calculations, employing the change in concentration of the terphenyls and HB across a dilution with fresh material. A special tritium dilution was also employed, in which a known amount of tritiated terphenyl was added to the loop just before the drain from the 610°F irradiation.

Each method will be described in turn.

Calculations of the volume in the loop in which the coolant may be considered to have good mixing have been performed by Morgan and Mason (A2.1). These calculations were based on measurements with acetone. A fraction of the volume of some loop sections not in the direct line of flow was included in the circulating volume. A summary of these calculations for the normal circulating volume (which includes flow through only one filter and one flowmeter) together with the temperature profiles around the loop for the 610°F and 750°F irradiations is given in Table A2.18. The circulating volume is divided into sections which are shown schematically in Fig. A2.4. To facilitate the identification of each section in the figure, the sections were not joined together.

Using the data of Table A2.18 together with the density of the coolant in the loop (see Section 5.2) and the measured surge tank level, it was possible to calculate the circulating coolant mass in the system at any time. Errors in this method of determining the circulating coolant mass arose for two reasons. First, the assignment of circulating and non-circulating volume to sections was somewhat arbitrary. Morgan and Mason (A2.1) have estimated this error at ±200 cc. Second, the underlying assumption in this method is that the sections tabulated in Table A2.18 are filled with coolant. There is no way at present of checking this assumption and, probably more important, estimating this as a source of error.

TABLE A2.18

Circulating Volumes and Temperatures of Loop Sections

Section	Circulating Volume, cc	Temperature, °F	
		610°F Irradiation	750°F Irradiation
1. In-pile section to right angle bend below upper shield plug	500	610	750
2. Right angle bend to surge tank	407	605	745
3. Surge tank above 0" in lower sight glass	$61.1y \frac{\rho_{\text{gage glass}}}{\rho_{\text{surge tank}}}$ [a]	GG = 400 ST = 600	GG = 530 ST = 740
4. 0" lower in surge tank to pump	788	590	725
5. Pump impeller section through upstream half test heater	1030	585	720
6. Pump motor section	660	400	450
7. Downstream half test heater to coolers	444	615	760
8. Volume of sampler (and AECL fouling probe when in use)	173 + capsule volume (+ volume of AECL fouling probe[b])	585	720
9. Coolers	341	500	500
10. Coolers to right angle bend	246	615	755

a. y is the measured surge tank level in inches.

b. Fouling probe volume = 35 cc.

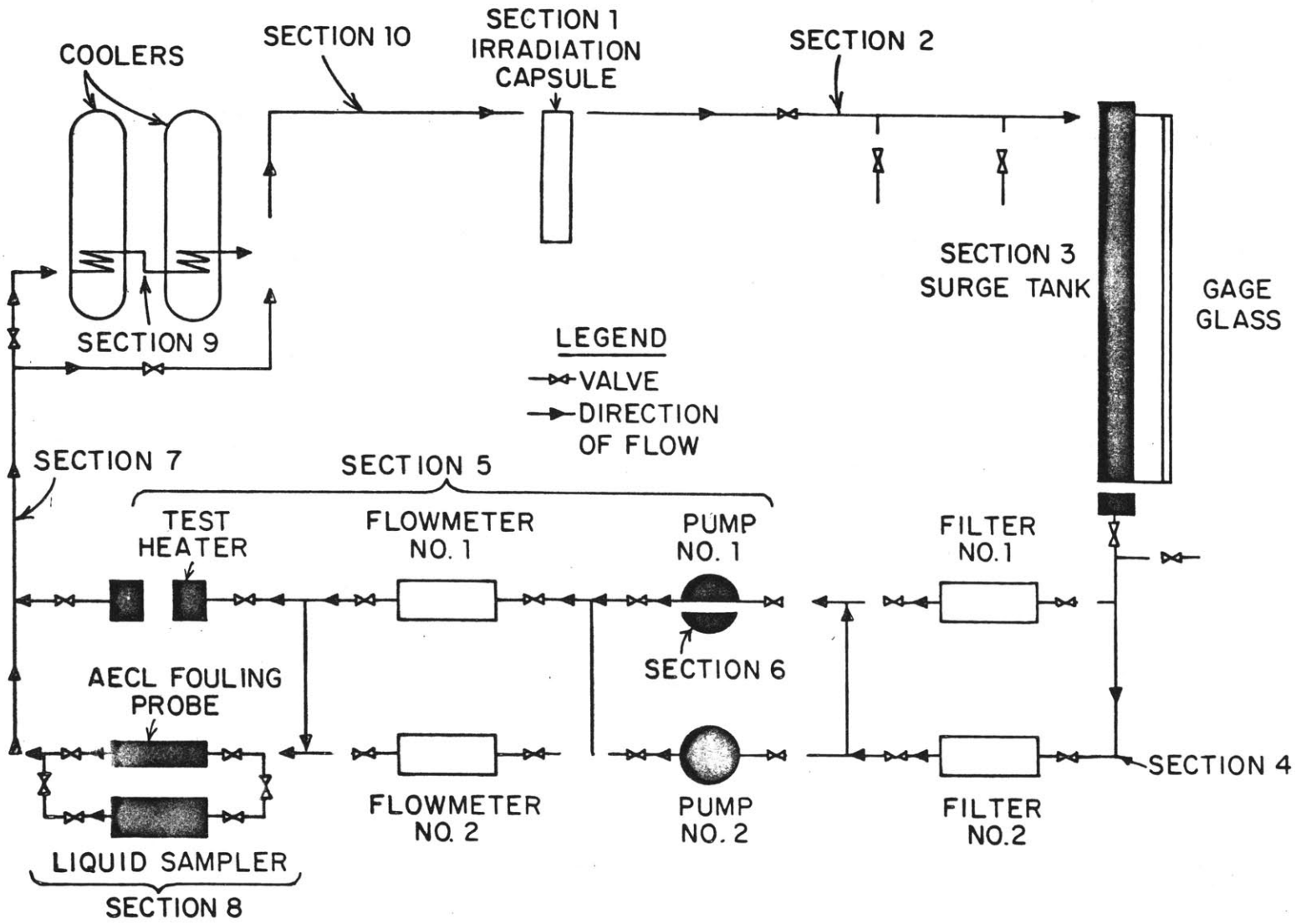

FIGURE A2.4 SCHEMATIC OF CIRCULATING VOLUME OF LOOP

The second and third methods of calculating M_o are somewhat interdependent, since a drain of the loop leaves a sizeable amount of residue and the amount of residue can only be calculated from a subsequent dilution-caused concentration change in the loop. The method based on the drain of the loop assumes that only the circulating mass in the loop is drained. At present there is no way of verifying such an assumption. Using this method, the circulating mass in the loop at the end of an irradiation is

$$M_{end} = M_{drain} + M_{residue} \qquad (A2.4)$$

M_{drain} was weighed and known fairly accurately. $M_{residue}$ was obtained by diluting the loop with fresh material and performing a dilution calculation:

$$M_{residue} = M_{added} \frac{(C_{added} - C_{diluted})}{(C_{diluted} - C_{residue})} \qquad (A2.5)$$

where

$C_{diluted}$ refers to the terphenyl concentration after dilution
C_{added} refers to the terphenyl concentration in the material added
$C_{residue}$ is assumed to be the same as the terphenyl concentration in the drained material.

$M_{residue}$ has a possible error introduced by the possible errors in terphenyl concentration. This error will be discussed shortly under the more general dilution calculation.

The third method of calculating the circulating coolant mass in the loop, that of measuring the concentration change after a dilution, is theoretically the most accurate, since no assumption of assignment of circulating and non-circulating columes need be made. Also, sections of the loop that may have void spaces would be taken into account by this method. However, in practice this method had quite a large error due to the possible errors in the measured concentrations, since most concentration changes were small. For the general dilution with a given mass of material, M_a, containing a concentration of the desired component, C_a, the circulating mass in the loop before dilution may be calculated as

$$M_{loop} = \frac{M_a(C_a - C_2)}{(C_2 - C_1)} \qquad (A2.6)$$

where

C_1 is the concentration of the desired component in the loop before dilution

C_2 is the concentration of the desired component in the loop after dilution.

Calculations based on Eq. (A2.6) were made using the change in terphenyl concentration across major dilutions during both irradiations. One calculation using the change in HB concentration was also made during the 610°F irradiation as a result of a dilution during the quasi-steady-state-HB period (1L159 et seq) over a weekend, when the reactor was shut down.

Just before the termination of the 610°F irradiation about six grams of terphenyl which had been tritiated by an exchange process by the Controls for Radiation, Inc. (Cambridge, Mass.) to an activity of about 10 mc/gram (A2.4) was added to the loop. Since the tritium background level in the loop was determined to be about 0.05 μc/gram (A2.4) this independent dilution method provided another means for calculating the circulating coolant mass in the loop. A sample of the coolant after addition of the tritiated terphenyl had been added and mixed was burned, and the water produced was analyzed for tritium content (about 15 μc/gm). The measured activities were stated to be accurate to ±5% (A2.4).

It should be possible to determine the circulating coolant mass in the system at any time from just one calculation using any of the methods described above because additions to and removals from the loop during the course of each irradiation are either weighed or determined by the change in levels of the feed and dump tank and surge tank. However, as will be shortly demonstrated, discrepancies arose when using these calculations and a mass balance on the system.

The circulating coolant mass in the loop at any time was defined by

$$M_{loop} = M_o + M^* \qquad (M_o \gg M^*) \qquad \text{(A2.7)}$$

M_o is an arbitrary level of mass and is set equal to M_{loop} at the time when M_{loop} is at its lowest level during the irradiation. Table A2.19 presents the results of the mass balance determinations of the circulating coolant mass in the loop during the 610°F irradiations in terms of M*.

TABLE A2.19

Relative Circulating Coolant Mass in Loop During the 610°F Irradiation of Santowax OMP

SAMPLE NUMBER	REACTOR MWH	ΔM, GRAMS	M*, GRAMS	COMMENTS
1L16	0		573	
1L17	18	−17	556	
1L18,19	58	−160	396	
1L21	95	−14	382	
1L22,23	148	−14	368	
1L24,25	172	−15	353	
1L26	178	−15	338	
	220	−50	288	NEW SAMPLER INSTALLATION
1L27	250	−15	273	
1L28	316	−15	258	
1L35	392	−15	243	
1L37	400	−72	171	
1L42	643	−15	156	
1L47	816	−15	141	
1L50	930	−16	125	
1L51	1076	−16	109	
1L52	1174	−18	91	
1L59	1472	−16	75	
1L62	1621	−75	0	
END TRANSIENT NO. 1				
1D1	1623	+850	850	AVG. FT AND ST
1L63	1659	−72	778	
	1710	−60	718	UNEXPLAINED ST DROP
1L66	1793	−16	702	
1L74	2163	−17	685	
1L82	2529	−17	668	
	2860	−100	568	UNEXPLAINED ST DROP
1L91	2869	−17	551	
1L92	2879	−17	534	
1L95	3075	−35	499	
1L99	3215	−74	425	
1L100	3219	−17	408	
1L111	3621	−17	391	
1L116	3839	−75	316	
1L117	3880	−75	241	
1L118	3887	−17	224	
END TRANSIENT NO. 2				
1D2	3891	+1100	1324	AVG. FT AND ST
1L120	3985	−315	1009	
1L121	3999	−321	688	
1L123	4083	−320	368	
1D3	4087	+841	1209	AVG. FT AND ST
1L124	4140	−317	892	
1L126	4243	−16	876	
1L131	4379	−317	559	
1D4	4426	+850	1409	AVG. FT AND ST
1L134	4476	−318	1091	
1D5	4520	−60	1031	PUMP REPLACEMENT
1L136	4621	−16	1015	

SAMPLE NUMBER	REACTOR MWH	ΔM, GRAMS	M*, GRAMS	COMMENTS
BEGIN QUASI-STEADY-STATE-HB				
1D6	4630	+282	1297	
1L137	4662	−317	980	
1D7	4678	+296	1276	
	4730	−60	1216	UNEXPLAINED ST DROP
1L146	4779	−320	896	
1D8	4830	+317	1213	
1L151	4874	−314	899	
1D9	4920	+308	1207	
1L152	4979	−317	890	
1D10	5028	+301	1191	
1L159	5179	−319	872	
1D11	5179	+332	1204	
1L160	5179	−317	887	
1D12	5233	+308	1195	
1L167	5381	−320	875	
1D13	5466	+334	1209	
1L172	5578	−316	893	
1D14	5623	+318	1211	
1L176	5668	−317	894	
1D15	5715	+340	1234	
1L180	5785	−318	916	
1D16	5804	+331	1247	
1L183	5886	−317	930	
1D17	5898	+339	1269	
1L186	6046	−317	952	
1D18	6131	+315	1267	
1L192	6196	−320	947	
END QUASI-STEADY-STATE-HB				
1D19	6196	−120	827	PUMP REPLACEMENT
1L195	6289	−21	806	
1D20	6442	0	806	FLOW THROUGH FLOWMETER 2
1L208	6741	−21	785	
1L214	6928	−79	706	
1D21	6934	+800	1506	AVG. FT AND ST
1L223	7074	−79	1427	
1D22	7180	+340	1767	
1L231	7317	−314	1453	
1D23	7347	+340	1793	
1L238	7526	−319	1474	
1D24	7546	+344	1818	
1L245	7723	−316	1502	
1D25	7792	+341	1843	
1L251	7880	−315	1528	
BEGIN STEADY-STATE-HB				
1D26	7882	+333	1861	
1L252	8030	−311	1550	
1D27	8049	+313	1863	
1L253	8180	−316	1547	

TABLE A2.19 (Concluded)

Relative Circulating Coolant Mass in Loop During the 610°F Irradiation of Santowax OMP

SAMPLE NUMBER	REACTOR MWH	ΔM, GRAMS	M*, GRAMS	COMMENTS
1D28	8189	+333	1880	
1L254	8336	−311	1569	
1D29	8340	+316	1885	
1L255	8480	−319	1566	
1D30	8490	+313	1879	
1L256	8627	−311	1568	
1D31	8642	+315	1883	
1L257	8781	−317	1566	
1D32	8787	+310	1876	
1L258	8928	−311	1565	
1D33	8932	+326	1891	
1L259	9081	−314	1577	
1D34	9086	+303	1880	
1L260	9231	−314	1566	
1D35	9234	+316	1882	
1L261	9381	−317	1565	
1D36	9388	+306	1871	
1L262	9530	−311	1560	
1D37	9533	+334	1894	
1L263	9683	−319	1575	
1D38	9688	+303	1878	
1L264	9831	−312	1566	
1D39	9836	+314	1880	
1L265	9979	−319	1561	
1D40	9986	+304	1865	
1L266	10130	−311	1554	
1D41	10132	+313	1867	
1L267	10280	−321	1546	
1D42	10284	+314	1860	
1L268	10428	−328	1532	
END STEADY-STATE-HB				
1D43	10442	+300	1832	
1L269	10579	−351	1481	
1D44	10589	+326	1807	
1L270	10730	−323	1484	
1L270.1	10735	−13	1471	
1L270.2	10746	−14	1457	
1L270.3	10749	−17	1440	
	10758	−100	1340	UNEXPLAINED ST DROP
1D45	10783	+317	1657	
1L271	10983	−321	1336	
1D46	10985	+326	1662	
1L272	11180	−336	1326	
1D47	11187	+337	1663	
1L273	11329	−336	1327	
1L274	11483	−335	992	
1L275	11538	−72	920	
1D48	11538	+6	926	TRITIUM ADDITION
1L276	11538	−335	591	
1L277	11538	−72	519	
1L278	11538	−2733		FINAL DRAIN
	11538	+3480		DILUTION

Some of the comments listed in Table A2.19 need explanation. Whenever a dilution was made via the feed and dump tank (FT), it was found that after the system had reached a temperature equilibrium again the surge tank (ST) level never rose as much as would be predicted from the calibrated volumes of each tank. For these dilutions the average of the feed tank and surge tank predictions of the increase in circulating mass was used, since this discrepancy has not been resolved at present.

Near the beginning of the 610°F irradiation there were sudden drops in the level of the surge tank for no apparent reason. It was felt that these drops were due to the sudden filling of some sections of the loop which had contained trapped gas. It was decided to assign one-half of the loss of mass in the surge tank to the "non-circulating" volume in the loop and the other half to circulating volume that had not quite been filled at the start of the irradiation (that is, had contained gas).

During the course of the 610°F irradiation there were also two pump failures which necessitated switching over to the spare pump. In these cases, the drop in the surge tank level was taken as indicative of the loss of circulating coolant mass.

The relative circulating coolant mass (M*) in the loop during the 750°F irradiation is tabulated in Table A2.20. The explanations of comments in Table A2.19 also apply for Table A2.20. During this irradiation there were extra losses of circulating mass incurred by the installation and removal of the AECL fouling probe at various intervals.

Thus, the tabulations of Tables A2.19 and A2.20 provided a means of comparing the results of the different methods of calculation via the circulating coolant mass constant, M_o. Table A2.21 summarizes the results of the calculations of M_o (and hence M_{loop}) for the 610°F irradiation. No formal error limits were assigned because, in most cases, they were unknown, but a discussion of the accuracy of the data presented in Table A2.21 follows. The first point to observe is that calculations using the data of Table A2.18 performed at the end of the first transient period and the middle of the steady-state-HB period differed by about 16%. One possible explanation of this discrepancy is that at the end of the first transient period there were sizeable gas pockets in the circulating volume. That there could be about 700 cc of gas space in the circulating volume at the end of the first transient period seems unreasonable. Another possible explanation is that

TABLE A2.20

Relative Circulating Coolant Mass in Loop During the 750°F Irradiation of Santowax OMP

SAMPLE NUMBER	REACTOR MWH	ΔM, GRAMS	M*, GRAMS	COMMENTS
2L1	0		875	
	28	−100	775	CLOSED OFF FLOWMETER 2
2L2	41	−10	765	
2G1,2	90	−26	739	
2L3	122	−9	730	
	123	−140	590	SAMPLE POSITION LEAK
	124	−335	255	CLOSED FILTER NO. 1
2G19	235	−19	236	
2L4	240	−10	226	
2D1	242	+619	845	AVG. OF FT AND ST
BEGIN TRANSIENT NO. 1				
2L5	253	−282	563	
	348	−100	463	UNEXPLAINED ST DROP
2L6	378	−11	452	
2L7	494	−12	440	
2L8	522	−23	417	
2L9	628	−108	309	
2L10	810	−14	295	
2L11	1056	−14	281	
END TRANSIENT NO. 1				
	1056	−281	0	SAMPLE POSITION LEAK
2D2	1075	+281	281	
2D3	1115	+266	547	AVG. OF FT AND ST
BEGIN TRANSIENT NO. 2				
2L12	1126	−12	535	
2L13	1406	−15	520	
2L14	1650	−31	489	
2L16	1936	−14	475	
2D4	2038	+30	505	AVG. OF FT AND ST
2L17	2040	−101	404	
END TRANSIENT NO. 2				
2D5	2042	+1200	1604	AVG. OF FT AND ST
	2056	−25	1579	FOULING PROBE INSTALLATION
2L18	2060	−299	1280	
	2060	−3	1277	FOULING PROBE INSTALLATION
2D6	2066	+323	1600	
	2110	−50	1550	FOULING PROBE LEAK
2L19	2145	−300	1250	
2D7	2150	+332	1582	
	2190	+335	1917	OPENED FILTER NO. 1
2L20	2250	−303	1614	
2D8	2253	+331	1945	
2L21	2253	−308	1637	
2D9	2253	+330	1967	
2L22	2278	−297	1670	
	2280	−335	1335	CLOSED FILTER NO. 1
BEGIN STEADY-STATE-HB				
2D10	2280	+312	1647	
2L23	2360	−355	1292	
2D11	2368	+342	1634	
	2412	−50	1584	FOULING PROBE LEAK
2L24	2424	−318	1266	
2D12	2427	+341	1607	
2L25	2520	−300	1307	
2D13	2526	+344	1651	
	2566	−50	1601	FOULING PROBE LEAK
2L26	2618	−308	1293	
	2620	−50	1243	FOULING PROBE LEAK
2D14	2623	+349	1592	
2L27	2707	−301	1291	
2D15	2712	+335	1626	
	2746	−50	1576	FOULING PROBE LEAK
2L28	2800	−303	1273	
2D16	2804	+364	1637	
2L29	2900	−300	1337	
2L30	2902	−26	1311	
2D17	2908	+356	1667	
2L31	3000	−298	1369	
2D18	3006	+366	1735	
	3199	−35	1700	FOULING PROBE OUT
2L32	3200	−339	1361	
2D19	3200	+325	1686	
2L33	3245	−301	1385	
2D20	3250	+312	1697	
2L34	3344	−378	1319	
2L35	3350	−26	1293	
2D21	3354	+291	1584	
2L36	3445	−324	1260	
2D22	3448	+332	1592	
2L37	3544	−302	1290	
2D23	3546	+301	1591	
2L38	3645	−296	1295	
2L39	3651	−27	1268	
2D24	3656	+303	1571	
2L40	3733	−343	1228	
END STEADY-STATE-HB				
2L41	3748	−3731		FINAL DRAIN
	3748	+3481		DILUTION (NO IN-PILE SECTION)

TABLE A2.21

Summary of Determinations of Circulating Mass Constant, M_o, for the 610°F Irradiation

Method	M_o, grams
Data of Table A2.18 at 9000 MWH (middle of steady-state-HB)	3700
Data of Table A2.18 at 1623 MWH (end of first transient)	4400
Measured drain and terphenyl dilution calculation on heel	3550
Measured drain and tritium dilution calculation on heel	2840
Tritium dilution at 11538 MWH	2770
Terphenyl dilution at 1623 MWH (end of first transient)	3420
Terphenyl dilution at 3891 MWH (end of second transient)	3620
HB dilution at 5179 MWH (quasi-steady-state HB)	3100

TABLE A2.22

Summary of Determinations of Circulating Mass Constant, M_o, for the 750°F Irradiation

Method	M_o, grams
Data of Table A2.18 at 3006 MWH (middle of steady-state-HB)	3170
Data of Table A2.18 at 2040 MWH (end of second transient)	3660
Measured drain and terphenyl dilution calculation on heel	3760
Terphenyl dilution at 2042 MWH (end of second transient)	4000

some of the material being fed into the loop via the feed and dump tank may not show up in the circulating volume, but in non-circulating volume, such as the space flowpath in the loop (possibly explaining the fact that surge tank rise was never as much as predicted from the feed tank change). Thus the mass balance of Table A2.19 would show an increasing amount of mass in the loop as more dilutions were made. This is currently being investigated.

The results obtained from the measured drain and the residue calculated from terphenyl dilution (about 30% of the total was residue) apparently agreed with the calculations of Table A2.18 during the steady-state-HB period. It is difficult to say whether such agreement is fortuitous or not since there is no way of telling whether drain material came from circulating or non-circulating volume. The drain and tritium dilution calculations did not agree as well with the calculations of Table A2.18, pointing out the difficulty of obtaining accuracy with dilution calculations with the present experimental error possible in the concentrations and activities. In fact, the results of all dilution calculations were estimated accurate to only ±20% because of the small concentration changes. Only one dilution method seems worth developing for the future – that of the tritium dilution. When only a small amount of highly active tritium is added to the loop (~6 grams in this case) the errors due to concentration change are diminished because of the very large dilution, but then there is a larger error possible in the fraction of the 6 grams which actually entered the circulating volume of the loop. Thus the error of the tritium dilution method was still ±20%. In the future, approximately 100 gram samples will be diluted in the loop in a compromise between concentration change and sample size.

For the steady-state-HB periods, the calculations using Table A2.18 are believed to be the most accurate, since by the time the steady-state-HB period began all the circulating volume that could be filled should have been filled with coolant. Thus, for calculations of small corrections in G values due to small changes in concentrations of components during the steady-state-HB period, M_o was set equal to 3700 ± 200 grams. During the transient periods, however, there remained the discrepancy between the "mass balance" and the

calculations of Table A2.18 at that time. It was arbitrarily decided to use the higher value of 4400 grams, equivalent to believing that M* should not have risen as much as given by the mass balance table between the transient and steady-state-HB periods (see discussion concerning feed tank dilution above). An error limit of ±16% was set on this value, however.

The results of all calculations for M_o during the 750°F irradiation are summarized in Table A2.22. Again there was a discrepancy between the calculations of Table A2.18 at the end of the second transient period and the same calculations made in the middle of the steady-state-HB period. This discrepancy amounted to about 13%. The drain and dilution calculations did not agree as well with the calculations using Table A2.18 for the 750°F irradiations, perhaps pointing out the fortuitous nature of the agreement during the 610°F irradiation. It was decided that the value of M_o calculated with the aid of Table A2.18 was the most accurate value for use in calculations during the steady-state-HB period. As with the 610°F transient periods, it was arbitrarily decided to use the calculations of Table A2.18 during the transient period (3660 gm), with a possible error of ±13% for this report.

A2.6 Least Squares Analysis of Data by Equations of the Form Y = a + bx (A2.5, A2.6)

In order to apply the method of least squares when fitting a set of data (y_j, x_j) by an equation of the form

$$Y = a + bx \tag{A2.8}$$

it is usually assumed that the only source of error lies in the dependent variable, Y, or at worst

$$\sigma^2(y_j) \gg \sigma^2(x_j) \tag{A2.9}$$

where

σ^2 denotes a variance

and

(y_j, x_j) denotes the j^{th} data point.

Attempts have been made to derive relations when both variables are subject to error (A2.7), but the equations recommended are both cumbersome

and not very general. It is felt that even when the relation (A2.9) is not valid the equations to be derived in this section yield better results than fitting the data by eye.

The quantity to be minimized is

$$\sum_{j=1}^{N} W_j (Y_j - y_j)^2 = \sum_{j=1}^{N} W_j (a + bx_j - y_j)^2 \qquad \text{(A2.10)}$$

where

N is the number of data points

W_j is a weighting factor to be applied to the j^{th} data point. Generally the weighting factor is chosen as the reciprocal of the variance of the j^{th} data point (each data point may have a different variance) (A2.5):

$$W_j = \frac{1}{\sigma^2(y_j)} \qquad \text{(A2.11)}$$

Upon setting the partial derivatives of Eq. (A2.10) with respect to a and b equal to zero and solving, there results

$$b = \frac{(\Sigma W_j)(\Sigma W_j x_j y_j) - (\Sigma W_j x_j)(\Sigma W_j y_j)}{(\Sigma W_j)(\Sigma W_j x_j^2) - (\Sigma W_j x_j)^2} \qquad \text{(A2.12)}$$

$$a = \overline{y} - b\overline{x} \qquad \text{(A2.13)}$$

where

$$\overline{y} = \frac{\Sigma W_j y_j}{\Sigma W_j} \quad \text{and} \quad \overline{x} \doteq \frac{\Sigma W_j x_j}{\Sigma W_j} \qquad \text{(A2.14)}$$

and the sums are over the N data points. The propagation of variances rule states that the variance of any quantity $Q(q_1, q_2, \ldots q_m)$ may be computed from

$$\sigma^2(Q) = \sum_{j=1}^{m} \left(\frac{\partial Q}{\partial q_j}\right)^2 \sigma^2(q_j) \qquad \text{(A2.15)}$$

Applying this relation to Eqs. (A2.12) and (A2.13) with y_j (and therefore W_j) the only variable with a variance, there results

$$\sigma^2(b) = \frac{1}{\Sigma W_j x_j^2 - \bar{x}^2 \Sigma W_j} \tag{A2.16}$$

$$\sigma^2(a) = \frac{1}{\Sigma W_j} + \bar{x}^2 \sigma^2(b) \tag{A2.17}$$

When computing the variance of the calculated value of y_j, Y_j, it must be remembered that the proper form of Eq. (A2.8) for this computation is

$$Y_j = a' + b(x_j - \bar{x}) \tag{A2.18a}$$

$$a' = a + b\bar{x} \tag{A2.18b}$$

The desired variance may be computed as

$$\sigma^2(Y_j) = \sigma^2(a) + x_j (x_j - 2\bar{x})\, \sigma^2(b) \tag{A2.19}$$

Standard deviations are given by the square roots of Eqs. (A2.16), (A2.17) and (A2.19). Confidence limits may be computed with the aid of Student's t (for N-2 degrees of freedom (A2.5)) as

$$\text{confidence limit} = \pm t \times (\text{standard deviation}) \tag{A2.20}$$

A table of Student's t may be found in reference (A2.8).

Another statistical quantity of interest is the correlation coefficient r defined as (A2.6):

$$r^2 = \frac{\Sigma W_j (Y_j - \bar{y})^2}{\Sigma W_j (y_j - \bar{y})^2} \tag{A2.21}$$

which may be written in terms of sums already formed as

$$r = \frac{(\Sigma W_j)(\Sigma W_j x_j y_j) - (\Sigma W_j x_j)(\Sigma W_j y_j)}{\left[(\Sigma W_j)\left(\Sigma W_j x_j^2\right) - (\Sigma W_j x_j)^2\right]^{0.5} \left[(\Sigma W_j)\left(\Sigma W_j y_j^2\right) - (\Sigma W_j y_j)^2\right]^{0.5}} \tag{A2.22}$$

Thus far nothing has been said about the calculation of the variance $\sigma^2(y_j)$ which is needed to compute the weighting factor W_j. In the commonly occurring case where the variance of each point y_j is the same (or in other words the absolute error in y is constant) the weighting factors

in Eqs. (A2.12), (A2.13) and (A2.14) may be replaced by ones and the variance $\sigma^2(y_j)$ may be estimated by

$$\sigma^2(y_j) = \frac{\Sigma(Y_j - y_j)^2}{N-2} \qquad \text{(A2.23)}$$

or, substituting,

$$\sigma^2(y_j) = \frac{\Sigma y_j^2 - A(\Sigma y_j) - B(\Sigma x_j y_j)}{N-2} \qquad \text{(A2.24)}$$

This relation assumes that only random errors contribute to variance of y_j, for the statistical method has no way of evaluating consistent errors. If these latter errors exist, their contribution to the total error must be calculated separately; and depending on the type of bias, the errors in the constants a and b may be affected in different ways. The propagation of variances rule may be used to include the errors due to bias. Equations (A2.16) and (A2.17) simplify to

$$\sigma^2(b) = \frac{\sigma^2(y_j)}{\left(\Sigma x_j^2 - N\bar{x}^2\right)} \qquad \text{(A2.25)}$$

$$\sigma^2(a) = \frac{\sigma^2(y_j)}{N} + \bar{x}^2\sigma^2(b) \qquad \text{(A2.26)}$$

Another commonly occurring case involves the change of variables $y = \ln z$ to obtain the form of Eq. (A2.8), and the variance $\sigma^2(z_j)$ constant for all data points. In this case, applying the propagation of variances (Eq. (A2.15)):

$$\sigma^2(y_j) = \frac{1}{y_j^2}\sigma^2(z_j) \qquad \text{(A2.27)}$$

and $\sigma^2(z_j)$ may be estimated from

$$\sigma^2(z_j) = \frac{\Sigma(Z_j - z_j)^2}{N-2} \qquad \text{(A2.28)}$$

As can be seen from the two cases above, the technique is to reduce

the problem, by a change of variables if necessary, to one in which the absolute error in the transformed variable is a constant for all data points.

A2.7 Statistics for Liquid Degradation Calculations

During transient periods of irradiation the organic coolant is assumed to degrade according to the power law (see Section 4.2).

$$-\frac{dC_i}{d\tau} = k_{i,n}[C_i]^n \qquad \text{(A2.29)}$$

where

C_i is the concentration of liquid component i

τ is the specific dose received by the coolant

k is the reaction constant

n is the reaction order.

Integrating this relation there results

$$-k_{i,n}\tau + a = \begin{cases} \dfrac{[C_i]^{1-n}}{1-n} & n \neq 1 \\ \ln C_i & n = 1 \end{cases} \qquad \text{(A2.30)}$$

where

"a" is a constant.

This form of the degradation relation is amenable to the method of least squares described in the previous section, but the weighting factors remain to be computed. Two possibilities were considered:

1. The absolute error (ΔC_i) in C_i is constant for all data points.
2. The relative error ($\Delta C_i / C_i$) in C_i is constant for all data points.

For a constant absolute error in C_i, the propagation of variances rule (Eq. (A2.15)) yields

$$\sigma^2\left(\frac{[c_{i,j}]^{1-n}}{1-n}\right) = [c_{i,j}]^{-2n}\,\sigma^2(c_{i,j}) \qquad \text{(A2.31)}$$

where

$c_{i,j}$ refers to the j^{th} measured value of the concentration of component i,

and $\sigma^2(c_{i,j})$ may be estimated by

$$\sigma^2(c_{i,j}) = \frac{\Sigma(C_{i,j} - c_{i,j})^2}{N-2} \qquad \text{(A2.32)}$$

where

N is the number of data points.

Thus the weighting factor for this case is

$$W_j = \frac{[c_{i,j}]^{2n}}{\sigma^2(c_{i,j})} \qquad \text{(A2.33)}$$

For a constant relative error in C_i it should be noted that the variable $\ln C_i$ has equal weighting for all data points. Applying the propagation of variance rule,

$$\sigma^2\left(\frac{[c_{i,j}]^{1-n}}{1-n}\right) = [c_{i,j}]^{2-2n}\,\sigma^2(\ln c_{i,j}) \qquad \text{(A2.34)}$$

and $\sigma^2(\ln c_{i,j})$ may be estimated by

$$\sigma^2(\ln c_{i,j}) = \frac{\Sigma(\ln C_{i,j} - \ln c_{i,j})^2}{N-2} \qquad \text{(A2.35)}$$

Thus, the weighting factor for this case is

$$W_j = \frac{[c_{i,j}]^{2n-2}}{\sigma^2(\ln c_{i,j})} \qquad \text{(A2.36)}$$

The G and G^* values for the organic component under consideration are defined as (see Section 4.2)

$$G(-i) = -\frac{dC_i}{d\tau} = 11.65\, k_{i,n}[C_i]^n \qquad \text{(A2.37)}$$

and

$$G^*(-i) = \frac{G(-i)}{C_i} \qquad \text{(A2.38)}$$

The variances of these quantities are calculated from the propagation of variances rule as

$$\sigma^2(G(-i)) = [C_i]^{2n}\, \sigma^2(k_{i,n}) \qquad \text{(A2.39)}$$

and

$$\sigma^2(G^*(-i)) = [C_i]^{2n-2}\, \sigma^2(k_{i,n}) \qquad \text{(A2.40)}$$

A2.8 Degradation Computer Program, MNDEG

MNDEG is an IBM 709/7090 FORTRAN program (for use with a 32 K storage) which applies a least squares fit to the concentration versus specific dose data during the transient period and determines G and G^* values for the data. A FORTRAN listing of the program is given in Table A2.23 and a logic flowsheet in Fig. A2.5.

The specific dose data are calculated from the period of reactor operation in MWH for each sample by the relation (see Section 4.2)

$$\tau_{j+1} - \tau_j = \frac{\bar{F}\bar{\rho}(MWH_{j+1} - MWH_j)}{\left(M_o + M_j^*\right)} \qquad \text{(A2.41)}$$

where

$\bar{F}$ is average dose rate factor for the in-pile section for the period MWH_j to MWH_{j+1}

$\bar{\rho}$ is the average density during this period

$(M_o + M_j^*)$ is the mass of circulating coolant in the loop

M_j^* is the relative mass of circulating coolant in the loop

j refers to the j^{th} sample

$j+1$ refers to the $j+1^{st}$ sample.

The program has the option of setting the specific dose back to zero after a dilution with fresh coolant, or letting it accumulate. If mass data are not given, the program will assume that the specific dose will be given as input instead of the reactor MWH and (Eq. (A2.41)) will not be used. This last option allows calculation to be performed on data from other laboratories.

Least squares analyses may be performed with four different weightings:

1. Equal weighting.

TABLE A2.23
FORTRAN LISTING OF MNDEG

```
*       LIST 8
*       LABEL
*       SYMBOL TABLE
CMNDEG
C       MNDEG HAS SUBPROGRAM MAIN IN FORTRAN, INT2D IN FAP
C       MAIN HAS 182 CARDS      6-1-63
        DIMENSION POWR(20),TTEST(31),EMWHMS(500),EMSTAR(500),TR(20),R(20,2
       10),EMWHR(20),TAU(500),DATE(100),EMWH(100),C(100),Y(100),CON (100),
       2G(100),ETAU(500),CONG(100),CCALC(100),GSTAR(100),CONGST(100),WT(4)
       3,NOWTS(4),FAC2(20),EMWHFA(20)
        NOT=2
        NIT=4
B       WT(1)=454645256060
B       WT(2)=512543336060
B       WT(3)=212262512543
B       WT(4)=212262336060
    45 READINPUTTAPE NIT,101,NPOWRS,(NOWTS(I),I=1,4),NBATCH,KPUNCH,KOVFR,
       1NR1,NR2,MSTAR,NFAC,NACC
   101 FORMAT(/(18I4))
        READINPUTTAPE NIT,102,FAC1,TBULK,EMZERO,EMWHC,(FAC2(I),EMWHFA(I),I
       1=1,NFAC)
   102 FORMAT(/(6E12.5))
        READINPUTTAPE NIT,102,(POWR(N),N=1,NPOWRS)
        READINPUTTAPE NIT,102,(TTEST(I),I=1,31)
        IF(MSTAR)37,37,36
    36 READINPUTTAPE NIT,102,(EMWHMS(I),EMSTAR(I),I=1,MSTAR)
        READINPUTTAPE NIT,102,(TR(J),(R(J,I),I=1,NR1),J=1,NR2),(EMWHR(I),I
       1=1,NR1)
        ETAU(1)=0.0
        DO 38 K=2,MSTAR
        IF(EMSTAR(K)-EMSTAR(K-1))65,65,66
    66 IF(NACC)67,67,65
    67 ETAU(K)=0.
        GO TO 38
    65 CALL INT2D(NFAC,1,EMWHFA,0,FAC2,(EMWHMS(K-1)+EMWHMS(K))*0.5,0,FAC3
       1)
        CALL INT2D(NR2,NR1,TR,EMWHR,R,TBULK,(EMWHMS(K-1)+EMWHMS(K))*0.5,RA
       1V)
        ETAU(K)=ETAU(K-1)+FAC3*RAV*(EMWHMS(K)-EMWHMS(K-1))/(EMZERO+EMSTAR(
       1K-1))
    38 CONTINUE
        WRITEOUTPUTTAPE NOT,105,EMZERO,EMWHC,(EMSTAR(I),EMWHMS(I),ETAU(I),
       1I=1,MSTAR)
        IF(KPUNCH)201,201,37
   201 PUNCH 105,EMZERO,EMWHC,(EMSTAR(I),EMWHMS(I),ETAU(I),I=1,MSTAR)
    37 DO 3 MBATCH=1,NBATCH
        READINPUTTAPE NIT,100
        WRITEOUTPUTTAPE NOT,100
   100 FORMAT(80H
       1                               )
        WRITEOUTPUTTAPE NOT,106,TBULK,EMZERO
        IF(KPUNCH)103,103,104
   103 PUNCH 100
        PUNCH 106,TBULK,EMZERO
   104 READINPUTTAPE NIT,300,NOPTS
   300 FORMAT(18I4)
        READINPUTTAPE NIT,107,(DATE(I),EMWH(I),C(I),I=1,NOPTS)
```

TABLE A2.23 (CONTINUED)

```
      IF(MSTAR)34,34,35
   34 DO 39 I=1,NOPTS
      TAU(I)=EMWH(I)
   39 CONTINUE
   35 DO 41 I=1,NOPTS
      DO 42 K=1,MSTAR
      IF(ABSF(EMWH(I)-EMWHMS(K))-1.0E-7)43,43,42
   43 TAU(I)=FTAU(K)
      GO TO 41
   42 CONTINUE
   41 CONTINUE
   40 EN=NOPTS
      DO 3 N=1,NPOWRS
      DO 2 M=1,4
      IF(NOWTS(M))200,200,2
  200 WRITEOUTPUTTAPE NOT,108,WT(M)
      IF(KPUNCH)109,109,110
  109 PUNCH 108,WT(M)
  110 IF(M-1)5,5,6
    5 POWER=0.0
      GO TO 7
    6 POWER=2.0*POWR(N)-4.0+FLOATF(M)
    7 SUMW=0.0
      SUMXW=0.0
      SUMYW=0.0
      SUMXYW=0.0
      SUMX2W=0.0
      SUMY2W=0.0
      DO 1 I=1,NOPTS
      IF(POWER)8,9,10
    8 WEIGHT=1.0/C(I)**(-POWER)
      GO TO 11
    9 WEIGHT=1.0
      GO TO 11
   10 WEIGHT=C(I)**POWER
   11 SUMW=SUMW+WEIGHT
      SUMXW=SUMXW+WEIGHT*TAU(I)
      SUMX2W=SUMX2W+WEIGHT*TAU(I)**2
      TEST=1.0-POWR(N)
      IF(ABSF(TEST)-1.0E-7)12,12,13
   12 Y(I)=LOGF(C(I))
      GO TO 14
   13 IF(TEST)15,15,16
   15 Y(I)=1.0/(C(I)**(-TEST))/TEST
      GO TO 14
   16 Y(I)=C(I)**TEST/TEST
   14 SUMYW=SUMYW+Y(I)*WEIGHT
      SUMXYW=SUMXYW+TAU(I)*Y(I)*WEIGHT
      SUMY2W=SUMY2W+Y(I)**2*WEIGHT
    1 CONTINUE
      SLOPE=(SUMXYW*SUMW-SUMXW*SUMYW)/(SUMW*SUMX2W-SUMXW**2)
      ENTCPT=(SUMYW-SLOPE*SUMXW)/SUMW
      SIG2EC=0.0
   23 DO 4 I=1,NOPTS
      IF(ABSF(TEST)-1.0E-7)17,17,18
   17 CCALC(I)=EXPF(ENTCPT+SLOPE*TAU(I))
      GO TO 19
   18 IF(TEST)20,20,21
   20 CCALC(I)=1.0/(TEST*(ENTCPT+SLOPE*TAU(I)))**(-1.0/TEST)
```

TABLE A2.23 (CONTINUED)

```
      GO TO 19
   21 CCALC(I)=(TFST*(ENTCPT+SLOPE*TAU(I)))**(1.0/TFST)
   19 IF(M-1)4,4,61
   61 IF(M-3)24,25,26
   24 SIG2EC=SIG2EC+(LOGF(CCALC(I)/C(I)))**2
      GO TO 4
   25 SIG2EC=SIG2EC+((LOGF(CCALC(I)/C(I)))**2+(CCALC(I)-C(I))**2)*0.5
      GO TO 4
   26 SIG2EC=SIG2EC+(CCALC(1)-C(I))**2
    4 CONTINUE
      SIG2EC=SIG2EC/(EN-2.0)
   22 SIG2E=(SUMY2W-ENTCPT*SUMYW-SLOPE*SUMXYW)/(EN-2.0)
      IF(SIG2E)52,53,53
   52 SIG2E=0.0
   53 SIG2P=(SUMY2W-SUMYW**2/SUMW)/(EN-1.0)
      RCORR=SQRTF(1.0-SIG2E*(EN-2.0)/SIG2P/(EN-1.0))
      IF(M-1)27,27,28
   27 SIG2=SIG2E
      GO TO 29
   28 SIG2=SIG2EC
   29 SIG2B=SIG2/(SUMX2W-SUMXW**2/SUMW)
      SIG2A=SIG2/SUMW+(SUMXW/SUMW)**2*SIG2B
      SIGB=SQRTF(SIG2B)
      SIGA=SQRTF(SIG2A)
      NFREE=NOPTS-2
      IF(NFREE-31)30,30,31
   31 NFREE=31
   30 DO 32 I=1,NOPTS
      CON(I)=TTEST(NFREE)*SQRTF(SIG2A+TAU(I)*(TAU(I)-2.0*SUMXW/SUMW)*SIG
     12B)
      IF(POWR(N))46,47,47
   46 CN=1.0/CCALC(I)**(-POWR(N))
      GO TO 51
   47 CN=CCALC(I)**POWR(N)
   51 G(I)=FAC1*SLOPE*CN
       GSTAR(I)=G(I)/CCALC(I)
      CONG(I)=TTEST(NFREE)*SIGB*CN*FAC1
      CONGST(I)=CONG(I)/CCALC(I)
   32 CONTINUE
      WRITEOUTPUTTAPE NOT,50,SLOPE,SIGB,ENTCPT,SIGA,RCORR,SIG2E,SIG2P,SI
     1G2EC,SUMW,SUMXW,SUMX2W,SUMXYW,SUMY2W,POWR(N),(DATE(I),TAU(I),Y(I),
     2CON(I),G(I),CONG(I),I=1,NOPTS)
      WRITEOUTPUTTAPE NOT,60,(DATE(I),GSTAR(I),CONGST(I),CCALC(I),I=1,NO
     1PTS)
      IF(KPUNCH)33,33,2
   33 PUNCH 50,SLOPE,SIGB,ENTCPT,SIGA,RCORR,SIG2E,SIG2P,SIG2EC,SUMW,SUMX
     1W,SUMX2W,SUMXYW,SUMY2W,POWR(N),(DATE(I),TAU(I),Y(I),CON(I),G(I),CO
     2NG(I),I=1,NOPTS)
      PUNCH 60,(DATE(I),GSTAR(I),CONGST(I),CCALC(I),I=1,NOPTS)
    2 CONTINUE
    3 CONTINUE
      IF(KOVER)44,44,45
   44 CALL EXIT
  105 FORMAT(1H1,15X3HM0=F6.0,31H GRAMS BASED ON CALCULATIONS ATF7.0,4H
     1MWH//26X2HM*,9X3HMWH,5X10HWATT-HR/GM/(F30.1,F12.1,F12.3))
   50 FORMAT(78H      SLOPE      S.D.(SLOPE)    INTERCEPT    S.D.(INTCP)  CO
     1RR. COEFF  SAMPLE VAR./1P6F13.5/3X9HPOP. VAR.,5X6HSIG2EC,8X4HSUMW,
     29X5HSUMXW,7X6HSUMX2W,7X6HSUMXYW/1P6E13.5/4X6HSUMY2W,5X10HPOWER OF
     3C/1P2E13.5///5X3HRUN,7X10HWATT-HR/GM,3X10HC**1-N/1-N,3X11HCONF. LI
```

TABLE A2.23 (CONTINUED)

```
   4M Y,7X1HG,7X11HCONF. LIM G/(4XA6,3X,1P5E13.5))
107 FORMAT(A6,2E12.5)
106 FORMAT(20X7HT BULK=F5.1,7H DFG. F,3X7HM ZERO=F6.1,6H GRAMS)
108 FORMAT(1H3,21X30HTHE TYPE OF WEIGHTING USED IS A6)
 60 FORMAT(1H0,4X3HRUN,11X2HG*,7X11HCON. LIM G*,4X7HC CALC./(4XA6,3X,1
   1P3E13.5))
    END
```

TABLE A2.23 (CONTINUED)

```
*       INT2D HAS 120 CARDS
*       FAP
        COUNT   120
      1 TTL     TWO DIMENSIONAL LINEAR INTERPOLATION FOR FORTRAN
        LBL     INT2D
        ENTRY   INT2D
        REM     THE FORTRAN CALLING SEQUENCE IS . . .
        REM     CALL INT2D(N1,N2,A,B,C,PA,PB,Q)
        REM
        REM     N1 IS THE NUMBER OF ELEMENTS IN A
        REM     N2 IS THE NUMBER OF ELEMENTS IN B
        REM     A IS THE FIRST INDEPENDENT VARIABLE  (2D EL MATRIX)
        REM     B IS THE SECOND INPEDENDENT VARIABLE  (1D MATRIX)
        REM     C IS THE DEPENDENT VARIABLE  (2D X N MATRIX)
        REM     PA IS THE PARTICULAR VALUE OF A
        REM     PB IS THE PARTICULAR VALUE OF B
        REM     Q IS THE ANSWER RETURNED BY THE SUBROUTINE
        REM
        REM     FOR 1D INTERPOLATION SET N2= TO COLUMN NO. OF C DESIRED,
        REM     SETB,PB=0
        REM
 INT2D  CLA*    1,4
        SUB     =01000000
        TZE     ONEELA                  ONLY ONE ELEMENT
        SXA     BACK,1                  SAVE INDEX REGISTERS
        SXA     BACK+1,2
        SXD     INT2D-2,4
        STD     N1LOOP
        CLA     3,4
        STA     NLOOP1+1
        STA     SETA
        ADD     =1
        STA     SETA1
        CLA     6,4
        STA     NLOOP1
        AXT     0,1
NLOOP1  CLA      PA
        FSB     **,1                    PA-A(L)
        TMI     *+8
        TXI     *+1,1,1                 FIND THE RIGHT A INTERVAL
N1LOOP  TXL     NLOOP1,1, N1-1
   OUT  TSX     $ERROR,4
        PZE     ALPHA                   ERROR IN DATA
        TXI     *+2,0,0
        PZE     INT2D-2,0,0
        TSX     $EXIT,4
        TXL     OUT,1,0
        STO     DATA
        CLA*    2,4
        SUB     =01000000
        TZE     1D
        NZT*    4,4                     2D OR 1D
        TRA     1D
        STD     N2LOOP
        CLA     4,4
        STA     NLOOP2+1
        STA     SETB
        ADD     =1
        STA     SETB1
        CLA     7,4
```

TABLE A2.23 (CONCLUDED)

```
        STA     NLOOP2
        AXT     0,2
NLOOP2  CLA      PB
        FSB     **,2
        TMI     *+4
        TXI     *+1,2,1                 FIND THE RIGHT B INTERVAL
N2LOOP  TXL     NLOOP2,2, N2-1
        TRA     OUT
        TXL     OUT,2,0
        STO     DATA+1
        SXD     IR2,2
        PXD     0,2
        AXT     2,2
 LOOP3  SSM
        XCA
        MPY     =024000000              FIND C ELEMENTS
        ARS     1
        ADD     5,4
        STA     SETC
        STA     1SETC
        ADD     =1
        STA     SETC1
  SETA  CLA     **,1
 SETA1  FSB     **,1                    A(L)-A(L-1)
        STO     Q+2,2
  SETC  CLA     **,1
 SETC1  FSB     **,1                    C(L,IR2)-C(L-1,IR2)
        FDP     Q+2,2
        FMP     DATA
 1SETC  FAD     **,1                    C(L,IR2)
        STO     Q+2,2
        NZT*    4,4                     1D OR 2D
        TRA     BACK-1
        CLA     IR2
        SUB     =01000000
        TIX     LOOP3,2,1
        LXD     IR2,2
  SETB  CLA     **,2
 SETB1  FSB     **,2                    B(K)-B(K-1)
        STO     DATA
        CLA     Q
        FSB     Q+1
        FDP     DATA
        FMP     DATA+1
        FAD     Q
        STO*    8,4                     ANSWER
  BACK  AXT     **,1
        AXT     **,2
        TRA     9,4
ONEELA  CLA*    5,4
        STO*    8,4
        TRA     9,4
    1D  AXT     1,2
        TRA     LOOP3
  DATA  BSS     2
     Q  BSS     2
   IR2  PZE
 ALPHA  BCI     5, EXTRAPOLATION IS NOT POSSIBLE
        OCT     777777777777
        END
```

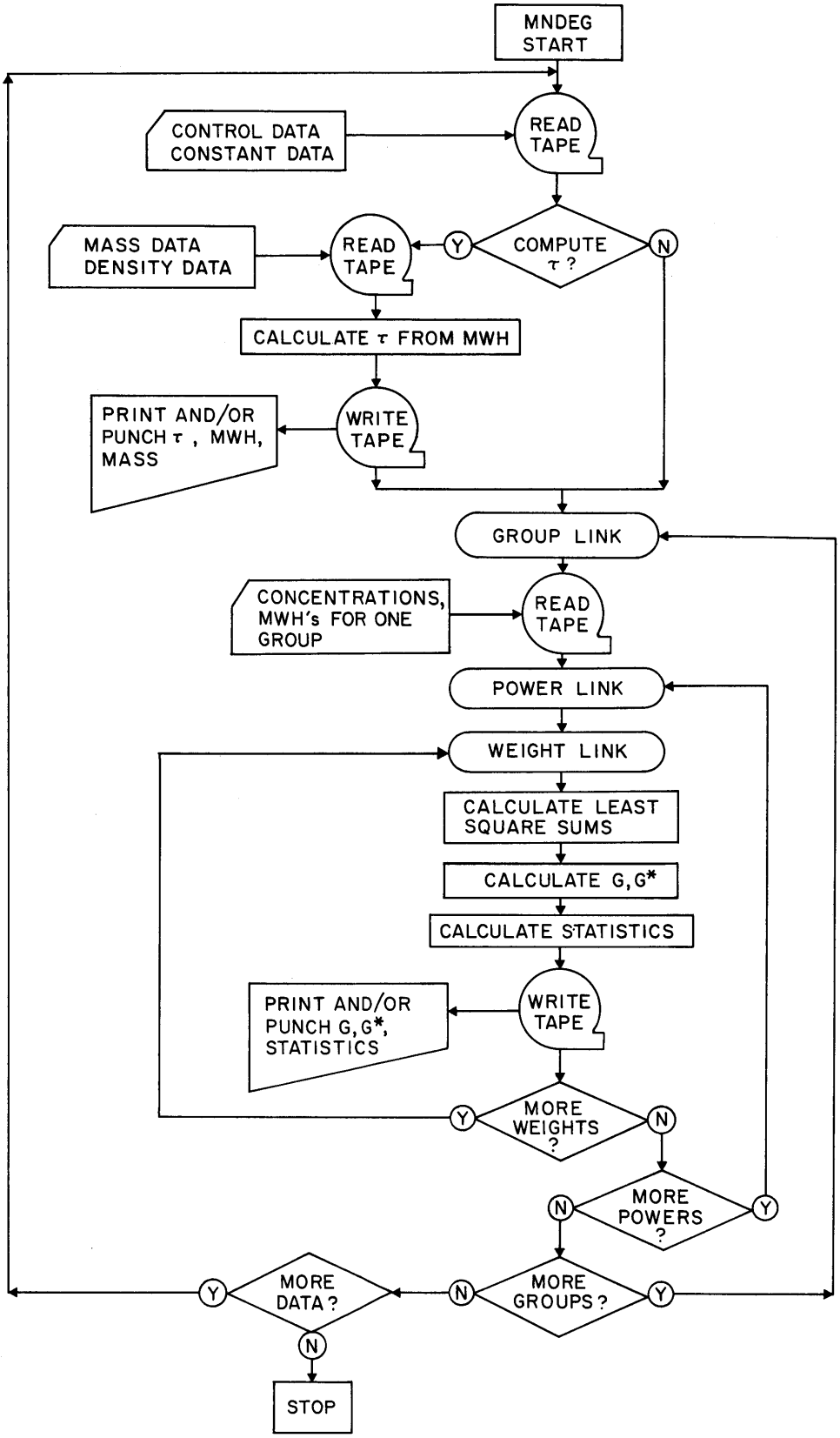

FIGURE A2.5 LOGIC FLOWSHEET FOR MNDEG

2. Weighting assuming a constant relative error ($\Delta C/C$) in the concentration data.
3. Weighting assuming a constant absolute error (ΔC) in the concentration data.
4. Weighting assuming the average of 2 and 3.

In the paragraphs that follow a brief description of how to use the program will be given; a sample input and sample output are given in Tables A2.24 and A2. 25, respectively, as an aid. Some familiarity with FORTRAN input/output format is assumed; for details, see the IBM 709/7090 FORTRAN reference manual (A2. 9).

The input is arranged as a series of tables, each headed by a card upon which any desired information may be placed. All fixed point data use I4 format and all floating point data E12.5 format. Alphanumeric data, used to describe the sample numbers, use A6 format.

The first table supplies control information for the program. It must contain the following information:

1. The number of powers, n, that will be used in the least squares analysis.
2. Four weighting control constants controlling the four possible weightings described above in the order
   i) Equal weighting
   ii) Weighting for constant relative error in C_i
   iii) Weighting for average of constant relative error and constant absolute error in C_i
   iv) Weighting for constant absolute error in C_i .
   For each possibility if the control is ≤ 0, that weighting will be used; if it is >0, that weighting will not be used.
   In the example given in Table A2. 24, only possibilities (ii) and (iv) are being considered.
3. The number of groups of samples to be analyzed.
4. A punch control. If the constant is ≤ 0, a punched record of the output will be given along with the printed record. If it is >0, only the printed record will be given.
5. A repeat control. After the computer has analyzed a certain number of groups of data with one set of "constant" data, it may be desired to change some of the "constants" before analyzing

TABLE A2.24
SAMPLE INPUT TO MNDEG

```
                                CONTROL TABLE
 2   1   0   1   0   1   0   0  10   2  37   2   0
                          CONVERSION FACTORS AND TBULK
11.65          610.          4180.          1623.          60.5          -2566.
55.8           16442.
                                POWERS TABLE
1.             2.
                      95 PER CENT CONFIDENCE LIMIT TABLE
12.706         4.303          3.182          2.776          2.571          2.447
2.365          2.306          2.262          2.228          2.201          2.179
2.160          2.145          2.131          2.120          2.110          2.101
2.093          2.086          2.080          2.074          2.069          2.064
2.060          2.056          2.052          2.048          2.045          2.042
1.95996
                    6-12-63 M* VERSUS MWH TABLE FOR 610 DEG RUN
0.             790.           18.            776.           58.            616.
95.            602.           148.           588.           172.           573.
178.           558.           220.           508.           250.           493.
316.           478.           392.           463.           400.           391.
643.           376.           816.           361.           930.           345.
1076.          329.           1174.          311.           1472.          295.
1621.          220.           1623.          1070.          1659.          998.
1710.          938.           1793.          922.           2164.          905.
2529.          888.           2860.          788.           2869.          771.
2879.          754.           3075.          719.           3215.          645.
3219.          628.           3621.          611.           3839.          536.
3880.          461.           3887.          444.           3891.          1544.
3985.          1229.
                  610 DEG RUN DENSITY TABLE     5-26-63
400.           0.9632         0.9899         0.9870         1.0114         0.997
0.993          0.993          0.999          0.999          1.01           700.
0.8231         0.8640         0.8590         0.8944         0.877          0.868
0.868          0.874          0.874          0.883          -0.001         1623.
1623.1         3891.          4150.          4575.          6233.          7880.
10730.         11540.
1              THIS IS TOTAL TERPHENYL TO 1ST DILUTION 2.15.63
 9
 1L27   250.          0.8992
 1L35   392.          0.8636
 1L37   400.          0.8615
 1L42   643.          0.7891
 1L50   930.          0.7285
 1L51   1076.         0.7142
 1L52   1174.         0.6681
 1L59   1472.         0.6253
 1L62   1621.         0.5987
```

TABLE A2.25
SAMPLE OUTPUT FROM MNDEG

M0= 4180. GRAMS BASED ON CALCULATIONS AT 1623. MWH

M*	MWH	WATT-HR/GM
790.0	0.	0.
776.0	18.0	0.188
616.0	58.0	0.606
602.0	95.0	1.006
588.0	148.0	1.582
573.0	172.0	1.843
558.0	178.0	1.909
508.0	220.0	2.370
493.0	250.0	2.703
478.0	316.0	3.439
463.0	392.0	4.291
391.0	400.0	4.381
376.0	643.0	7.166
361.0	816.0	9.164
345.0	930.0	10.489
329.0	1076.0	12.196
311.0	1174.0	13.350
295.0	1472.0	16.886
220.0	1621.0	18.668
1070.0	1623.0	0.
998.0	1659.0	0.366
938.0	1710.0	0.892
922.0	1793.0	1.759
905.0	2164.0	5.655
888.0	2529.0	9.517
788.0	2860.0	13.046
771.0	2869.0	13.144
754.0	2879.0	13.253
719.0	3075.0	15.406
645.0	3215.0	16.958
628.0	3219.0	17.003
611.0	3621.0	21.557
536.0	3839.0	24.044
461.0	3880.0	24.519
444.0	3887.0	24.602
1544.0	3891.0	0.
1229.0	3985.0	0.896

TABLE A2.25 (CONTINUED)

THIS IS TOTAL TERPHENYL TO 1ST DILUTION 2.15.63
T BULK=610.0 DEG. F M ZERO=4180.0 GRAMS

THE TYPE OF WEIGHTING USED IS REL.

SLOPE	S.D.(SLOPE)	INTERCEPT	S.D.(INTCP)	CORR. COEFF	SAMPLE VAR.
-2.55976E-02	7.37100E-04	-4.12171E-02	8.39292E-03	9.97110E-01	1.43587E-04
POP. VAR.	SIG2EC	SUMW	SUMXW	SUMX2W	SUMXYW
2.17707E-02	1.43584E-04	9.00000E 00	9.01289E 01	1.16685E 03	-3.35834E 01
SUMY2W	POWER OF C				
9.71040E-01	1.00000E 00				

RUN	WATT-HR/GM	C**1-N/1-N	CONF. LIM Y	G	CONF. LIM G
1L27	2.70324E 00	-1.06250E-01	1.58640E-02	-2.67038E-01	1.81858E-02
1L35	4.29085E 00	-1.46646E-01	1.37398E-02	-2.56403E-01	1.74615E-02
1L37	4.38087E 00	-1.49080E-01	1.36263E-02	-2.55813E-01	1.74213E-02
1L42	7.16562E 00	-2.36862E-01	1.06721E-02	-2.38213E-01	1.62227E-02
1L50	1.04887E 01	-3.16768E-01	9.48245E-03	-2.18788E-01	1.48999E-02
1L51	1.21964E 01	-3.36592E-01	1.01834E-02	-2.09430E-01	1.42626E-02
1L52	1.33497E 01	-4.03317E-01	1.10923E-02	-2.03337E-01	1.38477E-02
1L59	1.68855E 01	-4.69524E-01	1.52548E-02	-1.85742E-01	1.26494E-02
1L62	1.86681E 01	-5.12995E-01	1.77991E-02	-1.77457E-01	1.20852E-02

RUN	G*	CON. LIM G*	C CALC.
1L27	-2.98211E-01	2.03088E-02	8.95464E-01
1L35	-2.98211E-01	2.03088E-02	8.59803E-01
1L37	-2.98211E-01	2.03088E-02	8.57824E-01
1L42	-2.98211E-01	2.03088E-02	7.98804E-01
1L50	-2.98211E-01	2.03088E-02	7.33666E-01
1L51	-2.98211E-01	2.03088E-02	7.02286E-01
1L52	-2.98211E-01	2.03088E-02	6.81856E-01
1L59	-2.98211E-01	2.03088E-02	6.22853E-01
1L62	-2.98212E-01	2.03088E-02	5.95071E-01

THE TYPE OF WEIGHTING USED IS ABS.

SLOPE	S.D.(SLOPE)	INTERCEPT	S.D.(INTCP)	CORR. COEFF	SAMPLE VAR.
-2.57511E-02	7.25507E-04	-3.95807E-02	7.25845E-03	9.97246E-01	7.24037E-05
POP. VAR.	SIG2EC	SUMW	SUMXW	SUMX2W	SUMXYW
1.15174E-02	7.27351E-05	5.15582E 00	4.41391E 01	5.16062E 02	-1.50362E 01
SUMY2W	POWER OF C				
4.40770E-01	1.00000E 00				

RUN	WATT-HR/GM	C**1-N/1-N	CONF. LIM Y	G	CONF. LIM G
1L27	2.70324E 00	-1.06250E-01	1.34137E-02	-2.68967E-01	1.79216E-02
1L35	4.29085E 00	-1.46646E-01	1.15147E-02	-2.58193E-01	1.72037E-02
1L37	4.38087E 00	-1.49080E-01	1.14171E-02	-2.57595E-01	1.71639E-02
1L42	7.16562E 00	-2.36862E-01	9.19991E-03	-2.39770E-01	1.59762E-02
1L50	1.04887E 01	-3.16768E-01	9.47867E-03	-2.20105E-01	1.46659E-02
1L51	1.21964E 01	-3.36592E-01	1.08542E-02	-2.10636E-01	1.40349E-02
1L52	1.33497E 01	-4.03317E-01	1.21003E-02	-2.04472E-01	1.36242E-02
1L59	1.68855E 01	-4.69524E-01	1.68202E-02	-1.86677E-01	1.24385E-02
1L62	1.86681E 01	-5.12995E-01	1.94846E-02	-1.78302E-01	1.18805E-02

RUN	G*	CON. LIM G*	C CALC.
1L27	-3.00000E-01	1.99894E-02	8.96558E-01
1L35	-3.00000E-01	1.99894E-02	8.60644E-01
1L37	-3.00000E-01	1.99894E-02	8.58651E-01
1L42	-3.00000E-01	1.99894E-02	7.99233E-01

TABLE A2.25 (CONTINUED)

1L50	-3.00000E-01	1.99894E-02	7.33685E-01
1L51	-3.00000E-01	1.99894E-02	7.02121E-01
1L52	-3.00000E-01	1.99894E-02	6.81575E-01
1L59	-3.00000E-01	1.99894E-02	6.22258E-01
1L62	-3.00000E-01	1.99894E-02	5.94340E-01

THE TYPE OF WEIGHTING USED IS REL.

SLOPE	S.D.(SLOPE)	INTERCEPT	S.D.(INTCP)	CORR. COEFF	SAMPLE VAR.
-3.47283E-02	9.86531E-04	-1.01154E 00	9.86990E-03	9.97153E-01	1.36133E-04
POP. VAR.	SIG2EC	SUMW	SUMXW	SUMX2W	SUMXYW
2.09514E-02	1.34487E-04	5.15582E 00	4.41391E 01	5.16062E 02	-6.25705E 01
SUMY2W	POWER OF C				
9.00000E 00	2.00000E 00				

RUN	WATT-HR/GM	C**1-N/1-N	CONF. LIM Y	G	CONF. LIM G
1L27	2.70324E 00	-1.11210E 00	1.82397E-02	-3.31097E-01	2.22440E-02
1L35	4.29085E 00	-1.15794E 00	1.56575E-02	-3.00385E-01	2.01807E-02
1L37	4.38087E 00	-1.16077E 00	1.55247E-02	-2.98774E-01	2.00724E-02
1L42	7.16562E 00	-1.26727E 00	1.25099E-02	-2.54683E-01	1.71103E-02
1L50	1.04887E 01	-1.37268E 00	1.28889E-02	-2.13748E-01	1.43602E-02
1L51	1.21964E 01	-1.40017E 00	1.47593E-02	-1.96447E-01	1.31979E-02
1L52	1.33497E 01	-1.49678E 00	1.64537E-02	-1.85924E-01	1.24909E-02
1L59	1.68855E 01	-1.59923E 00	2.28718E-02	-1.58448E-01	1.06450E-02
1L62	1.86681E 01	-1.67029E 00	2.64948E-02	-1.46849E-01	9.86573E-03

RUN	G*	CON. LIM G*	C CALC.
1L27	-3.66001E-01	2.45890E-02	9.04634E-01
1L35	-3.48614E-01	2.34208E-02	8.61657E-01
1L37	-3.47677E-01	2.33579E-02	8.59342E-01
1L42	-3.21000E-01	2.15657E-02	7.93405E-01
1L50	-2.94074E-01	1.97567E-02	7.26853E-01
1L51	-2.81921E-01	1.89403E-02	6.96816E-01
1L52	-2.74267E-01	1.84260E-02	6.77896E-01
1L59	-2.53191E-01	1.70101E-02	6.25803E-01
1L62	-2.43748E-01	1.63756E-02	6.02463E-01

THE TYPE OF WEIGHTING USED IS ABS.

SLOPE	S.D.(SLOPE)	INTERCEPT	S.D.(INTCP)	CORR. COEFF	SAMPLE VAR.
-3.45091E-02	9.75637E-04	-1.01309E 00	8.47114E-03	9.97156E-01	6.85943E-05
POP. VAR.	SIG2EC	SUMW	SUMXW	SUMX2W	SUMXYW
1.05688E-02	6.71977E-05	3.17099E 00	2.31126E 01	2.39058E 02	-3.16649E 01
SUMY2W	POWER OF C				
5.15582E 00	2.00000E 00				

RUN	WATT-HR/GM	C**1-N/1-N	CONF. LIM Y	G	CONF. LIM G
1L27	2.70324E 00	-1.11210E 00	1.51814E-02	-3.28436E-01	2.19602E-02
1L35	4.29085E 00	-1.15794E 00	1.28987E-02	-2.98174E-01	1.99368E-02
1L37	4.38087E 00	-1.16077E 00	1.27885E-02	-2.96585E-01	1.98306E-02
1L42	7.16562E 00	-1.26727E 00	1.08908E-02	-2.53082E-01	1.69218E-02
1L50	1.04887E 01	-1.37268E 00	1.31546E-02	-2.12629E-01	1.42171E-02
1L51	1.21964E 01	-1.40017E 00	1.57084E-02	-1.95512E-01	1.30725E-02
1L52	1.33497E 01	-1.49678E 00	1.77230E-02	-1.85095E-01	1.23760E-02
1L59	1.68855E 01	-1.59923E 00	2.46750E-02	-1.57872E-01	1.05558E-02
1L62	1.86681E 01	-1.67029E 00	2.84241E-02	-1.46369E-01	9.78671E-03

TABLE A2.25 (CONCLUDED)

RUN	G*	CON. LIM G*	C CALC.
1L27	-3.63375E-01	2.42964E-02	9.03849E-01
1L35	-3.46230E-01	2.31500E-02	8.61203E-01
1L37	-3.45306E-01	2.30882E-02	8.58905E-01
1L42	-3.18977E-01	2.13278E-02	7.93416E-01
1L50	-2.92376E-01	1.95491E-02	7.27248E-01
1L51	-2.80360E-01	1.87457E-02	6.97360E-01
1L52	-2.72789E-01	1.82395E-02	6.78528E-01
1L59	-2.51931E-01	1.68449E-02	6.26646E-01
1L62	-2.42580E-01	1.62196E-02	6.03387E-01

more groups of data. This control provides the possibility. If it is ≤ 0, the computer, when it is finished analyzing the number of groups of data specified, will return to the very beginning of the program and start over. If it is >0, the computer will halt after completion of the analyses of the number of groups specified.

6. If density data are to be given to compute the specific dose from the reactor MWH, two constants must be given to specify the number of density data points to be given, since $\rho = \rho(\text{MWH}, T)$. The first gives the number of MWH elements to be supplied and the second the number of temperature elements to be supplied (see below for the description of the density input). If density data are not to be given, two zeros must be typed.
7. If the specific dose is to be computed, the number of elements in the M^*-MWH table to be supplied. If the specific dose is given as input a zero must be typed.
8. The number of elements in the F-MWH table to be supplied.
9. A control constant telling the computer whether to set the specific dose back to zero after a dilution with fresh coolant or not. If the constant is ≤ 0, the specific dose will be set back to zero; if it is >0, the specific dose will accumulate.

The second table supplies the following information:

1. The conversion factor between $k_{i,n}[C_i]^n$ and $G(-i)$ (11.65 in this work.
2. The bulk temperature at which the irradiation took place.
3. The circulating mass constant, M_o in Eq. (A2.41).
4. The reactor MWH at which the calculation of M_o was made.
5. The F-MWH table. The average dose rate factor for the in-pile section is considered as a function of the period of reactor operation in MWH and the table supplies this relationship in the form F_1, MWH_1, F_2, MWH_2 . . . .

The third table lists the powers, n, to be used in the least squares study of the concentration-specific dose data. In the example in Table A2.24 n = 1.0 and 2.0 were used.

The fourth table supplies Student's t data for use in the calculation of confidence limits. The data are to be supplied in the form t_1, t_2, . . . t_{30}, t_{31} where the subscript refers to the number of degrees of freedom

up to 30 and the 31st entry is for t_∞. The Student's t values for 95% confidence limits are given in Table A2.24.

The next two tables are to be given only if the specific dose is to be calculated from the reactor MWH. The first of these tables is the M^*-MWH table giving information in the order MWH_1, M_1^*, MWH_2, M_2^* . . . . Figure A2.6 shows how the entries are to be picked for the table. The M^* values are to be given after the step change, corresponding to

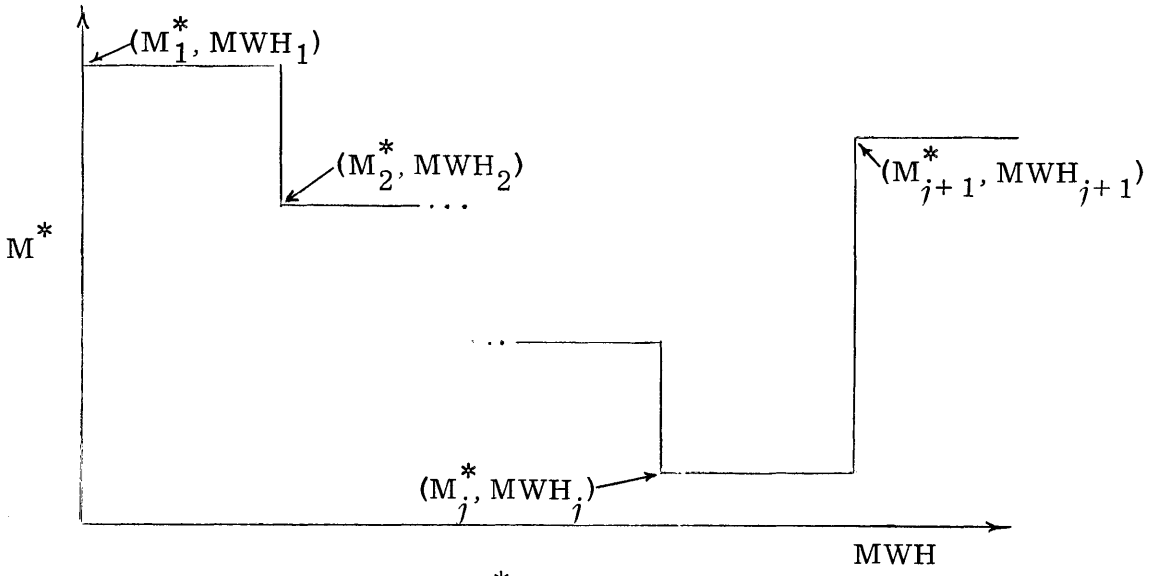

Figure A2.6 Schematic of M^* as a Function of Reactor MWH

after the sample has been taken (or other loss of material has occurred) or after a dilution with fresh material has been made. The second table gives the coolant density as a function of reactor MWH and temperature in the order T_1, ρ_{11}, ρ_{12}, $\cdots$ $\rho_{2,NR1}$, T_2, ρ_{21}, $\cdots$ $\rho_{2,NR1}$ $\cdots$ T_{NR2}, $\rho_{NR2,1}$ $\cdots$ $\rho_{NR2,NR1}$, MWH_1, MWH_2 $\cdots$ MWH_{NR1}; ρ_{ij} is the value of ρ at T_i, MWH_j, NR1 is the number of MWH entries and NR2 the number of temperature entries. The computer will linearly interpolate in both dimensions to calculate the density at a given temperature and MWH. The interpolation routine will not extrapolate and interpolates only on an open interval, so that the span of the table must be large enough to include all possible data. For instance, Table A2.24 lists −0.001 MWH as the first MWH entry to ensure that 0 MWH is inside the table.

Next, the groups of data are given the computer. Each group is headed by a "free" card upon which any desired information may be

punched, and the computer will re-print the information as a heading for the output. The second card contains the number of samples in the group to be analyzed. For each sample the following information must be given:

1. The sample number (A6 format).
2. The reactor MWH at which the sample was taken. This quantity must exactly correspond to one of the MWH entries in the M^*-MWH table. As stated above, if desired, the specific dose may be given here instead of the reactor MWH.
3. The concentration of the desired component in the sample, c_i. For each group of data the format must be as described.

If it is desired to change some of the "constants" in the input after a certain number of groups of data have been analyzed (the repeat control being selected above), the computer will return to the beginning again, and the format used must be as described above.

The output needs little explanation. First, if the conversion from MWH to watt-hr/gm was performed by the computer, a listing of the watt-hr/gm will be given each time there is a change in the value of M^*.

Following that tabulation, the results will be given for each weighting, W, for each power, n, for each set of samples to be analyzed. The type of weighting used is listed above each set of output, followed by the least squared slope and intercept, their standard deviations and various least squares sums. The power used is listed also for reference. The rest of the output is straightforward.

The loading time for MNDEG in an IBM type 7090 computer is 0.19 min and the running time is about 0.01 min per weighting per power per set of data to be analyzed (a set of data normally includes about ten data points).

A2.9 Corrections for Out-of-Pile Pyrolysis

There appears to be a general agreement at the various laboratories performing pyrolysis analyses that the terphenyl isomers pyrolyze according to a first order rate law (A2.10, A2.11, A2.12, A2.13):

$$-\frac{dC_i}{dt} = k_{p,i} C_i \qquad \text{(A2.42)}$$

where

t is the physical time elapsed at the pyrolysis temperature

k_p is the reaction constant.

Available data on first order rate constants are shown in Fig. A2.7. The data are assumed to obey the Arrhenius relation:

$$k_{p,i} = k^{o}_{p,i} \; e^{-\Delta E/RT} \qquad \text{(A2.43)}$$

A summary of the data used for this report is given in Table A2.26, and it may be seen that the isomer stability is para > meta > ortho.

TABLE A2.26

Pyrolysis Data for Terphenyls

Component	ΔE, kcal/mole	k_p at 610°F, hr^{-1}	k_p at 750°F, hr^{-1}
o-ϕ_3	73	1.2×10^{-7}	1.6×10^{-4}
m-ϕ_3	74	4.8×10^{-8}	6.8×10^{-5}
p-ϕ_3	74	2.5×10^{-8}	3.5×10^{-5}

For ortho-terphenyl the data obtained at Atomics International (A2.11, A2.14) were used. Kuper (A2.13) also reports pyrolysis data for ortho-terphenyl which generally agree with those obtained at AI, but seem to have a larger activation energy. The differences between the two results are perhaps indicative of the precision to which the pyrolysis measurements were made. For para-terphenyl the data of Houllier and Puig (A2.12) were used. For comparison the data of Wilkinson and Bates (A2.10) are shown, and again the precision of the results may be inferred from the differences in the data reported. Houllier and Puig also report preliminary results of measurements on meta-terphenyl which would indicate a much lower activation energy than those for para- and meta-terphenyl (A2.12). In another preliminary report (A2.15) their smoothed data for meta-terphenyl showed about the same activation energy as their measurements on para-terphenyl. Kuper (A2.13) also reports k_p data on meta-terphenyl

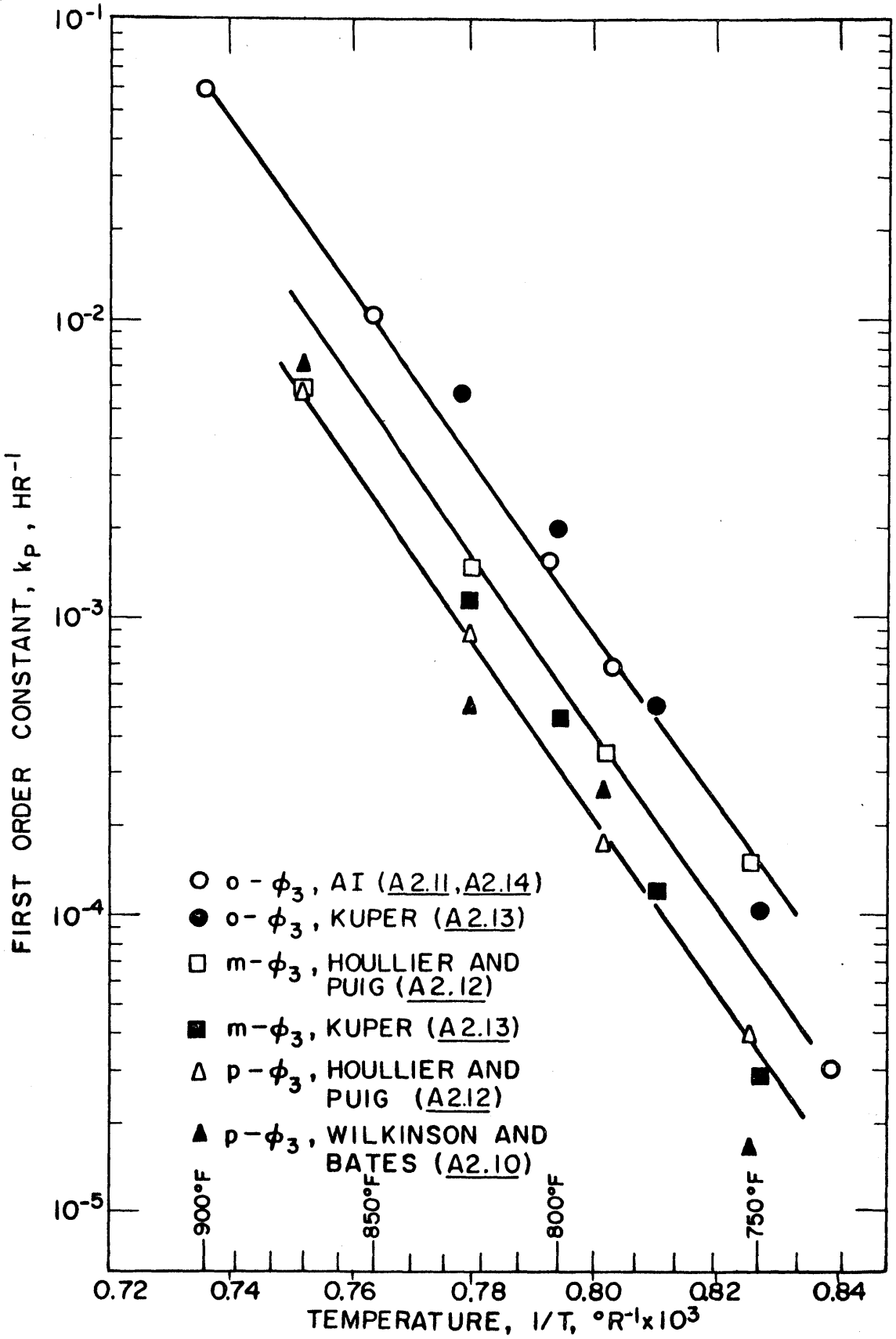

FIGURE A2.7 PYROLYSIS DATA FOR TERPHENYLS

which are somewhat lower than those obtained by Houllier and Puig, but show about the same activation energy as his own measurements on ortho-terphenyl. At any rate, it is certainly reasonable to expect an activation energy for meta-terphenyl about the same as for para- and ortho-terphenyl, so the best line having an activation energy equal to that of para-terphenyl was drawn through the data of Houllier and Puig, and this smoothed curve was used in the analysis of data in this report.

Preliminary calculations based on the data of Table A2.26 showed that out-of-pile pyrolysis for the 610°F irradiation contributed a negligible amount to the terphenyl degradation. For the 750°F irradiation out-of-pile pyrolysis contributed a small, but not negligible amount (~10%) to the terphenyl degradation, and so a method was developed for calculating its contribution.

During the transient periods of operation the time in hours at 750°F to which an irradiated sample was exposed was recorded. Using the first order law (Eq. (A2.42)), the number of grams of component i pyrolyzed in the out-of-pile section to the time of removal of the irradiated sample was written as

$$\delta_{p,i} = M_{out} C_i^o \left[1 - e^{-k_{p,i} t} \right] = M_{out} C_i^o (1-x) \qquad \text{(A2.44)}$$

where

M_{out} is the average circulating mass in the out-of-pile section during the period t = o to t = t

C_i^o is the initial concentration of component i.

Thus, if there were no out-of-pile pyrolysis, the concentration of component i in the irradiated sample would have been

$$C_i^{corr} = C_i^{measured} + \left(\frac{M_{out}}{M_{loop}} \right) C_i^o (1-x) \qquad \text{(A2.45)}$$

where

M_{loop} is the average total circulating coolant mass in the loop during the period t = o to t = t.

Based on the dimensions of the in-pile capsule given by Morgan and Mason (A2.1) and the circulating coolant mass given in Section A2.5 the ratio M_{out}/M_{loop} was found to be fairly independent of the DP concentration in the

circulating coolant and equal to about 0.93 for the transient periods of the 750°F irradiation.

The simple relation derived above applies as long as there is no dilution with unirradiated material. The simplest way to handle the dilution problem was to set the time equal to zero after each dilution and start with a new value of C_i^o based on a mass balance at the dilution. Thus, after the first dilution

$$\left(C_i^o\right)^{new} = \frac{\left(C_i^o\, e^{-k_{p,i}\, t_1}\right) M_b + M_a C_i^o}{M_b + M_a} \qquad (A2.46)$$

where

t_1 is the time elapsed (at 750°F) until the first dilution

C_i^o is the initial concentration of component i in the coolant

M_b is the circulating coolant mass before dilution

M_a is the number of grams of fresh material added.

The total correction to be added to a sample taken after the first dilution was thus

$$(\Delta C_i)^{pyrolysis} = \left(\frac{M_{out}}{M_{loop}}\right)\left[C_i^o\left(1 - e^{-k_{p,i}\, t_1}\right) - \left|\Delta C_i^{dilution}\right| + \left(C_i^o\right)^{new}\left(1 - e^{-k_{p,i}\, t_2}\right)\right] \qquad (A2.47)$$

where

t_1 is the time elapsed to the first dilution

t_2 is the time elapsed since the first dilution

and

$$\left|\Delta C_i^{dilution}\right| = \left(C_i^o\right)^{new} - C_i^o\, e^{-k_{p,i}\, t_1} \qquad (A2.48)$$

Applying these relations to the data of the transient periods of the 750°F irradiation and using the tabulated values of the measured sample analyses given in Section A2.3, the pyrolysis corrected data are given in Table A2.27.

During the steady-state-HB period of the 750°F irradiation, the correction for out-of-pile pyrolysis was much simpler. Since the out-of-pile circulating mass was approximately constant for the steady-state-HB period,

TABLE A2.27

Out-of-Pile Pyrolysis Corrected Concentration Data for Samples from the 750°F Irradiation of Santowax OMP

Sample Number	Measured Analyses				Corrected Analyses			
	o-ϕ_3	m-ϕ_3	p-ϕ_3	Total omp	o-ϕ_3	m-ϕ_3	p-ϕ_3	Total omp
2L5	10.4	53.0	27.0	90.4	10.6	53.4	27.1	91.1
2L6	9.9	51.0	26.4	87.3	10.1	51.6	26.6	88.3
2L7	8.8	48.2	25.9	82.9	9.1	49.1	26.1	84.3
2L9	7.3	45.7	24.2	77.2	7.8	46.8	24.4	79.0
2L10	7.5	42.0	22.1	71.6	8.1	43.4	22.5	74.0
2L11	6.3	37.0	19.7	63.0	7.1	38.9	20.2	66.2
2L12	6.9	38.4	20.6	65.9	7.6	40.1	21.0	68.7
2L13	6.0	34.5	19.2	59.7	7.0	36.7	19.8	63.5
2L14	4.6	29.8	15.3	49.7	5.8	32.4	16.0	54.2
2L16	3.5	25.7	14.0	43.2	5.0	28.9	14.9	48.8
2L17	3.1	24.2	13.8	41.1	4.6	27.6	14.8	47.0

Eq. (A2.42) was written as

$$-d(M_{out}C_i) = k_{p,i}\left(\frac{M_{out}}{M_{loop}}\right) M_{loop}C_i \; dt \qquad \text{(A2.49)}$$

The differential term $d(M_{out}C_i)$ may be related to a fictitious makeup rate necessary to keep the observed concentration C_i constant. Thus, upon integration, there resulted

$$\delta_{p,i} = k_{p,i}\left(\frac{M_{out}}{M_{loop}}\right) M_{loop}C_i \, \Delta t \qquad \text{(A2.50)}$$

where

$\delta_{p,i}$ is the makeup needed if there were out-of-pile pyrolysis alone acting on the coolant

Δt is the duration of the steady-state-HB period.

This makeup was subtracted from the actual makeup to obtain the pyrolysis corrected makeup. The results of corrections using Eq. (A2.50) are described in the next section.

A2.10 Calculations of G^* Values for Steady-State-HB Periods

This section presents details of the calculations of G^* values for the steady-state-HB periods. Attention is focused on the steady-state-HB period of the 610°F irradiation, and summaries of the calculations for all steady-state-HB periods are given.

A schematic flow chart of the makeup procedures used at the loop is given in Fig. A2.8. In part A of the figure the operations performed on a given loop sample are indicated. Before the ~300 gm sample was charged to the distillation column about 10 gm was set aside for various chemical and physical analyses. Products of the distillation procedure included the bottoms (~100 gm), cold trap (1-2 gm) and distillate (~200 gm). A sample of the distillate was set aside for various chemical and physical measurements before makeup of unirradiated Santowax OMP was added. Normally, more makeup than necessary (~250 gm) was added to insure filling of the dilution return capsule and about 300 gm were returned to the loop. Part B of the figure indicates schematically how the sampling and dilution procedures were performed at the loop. The

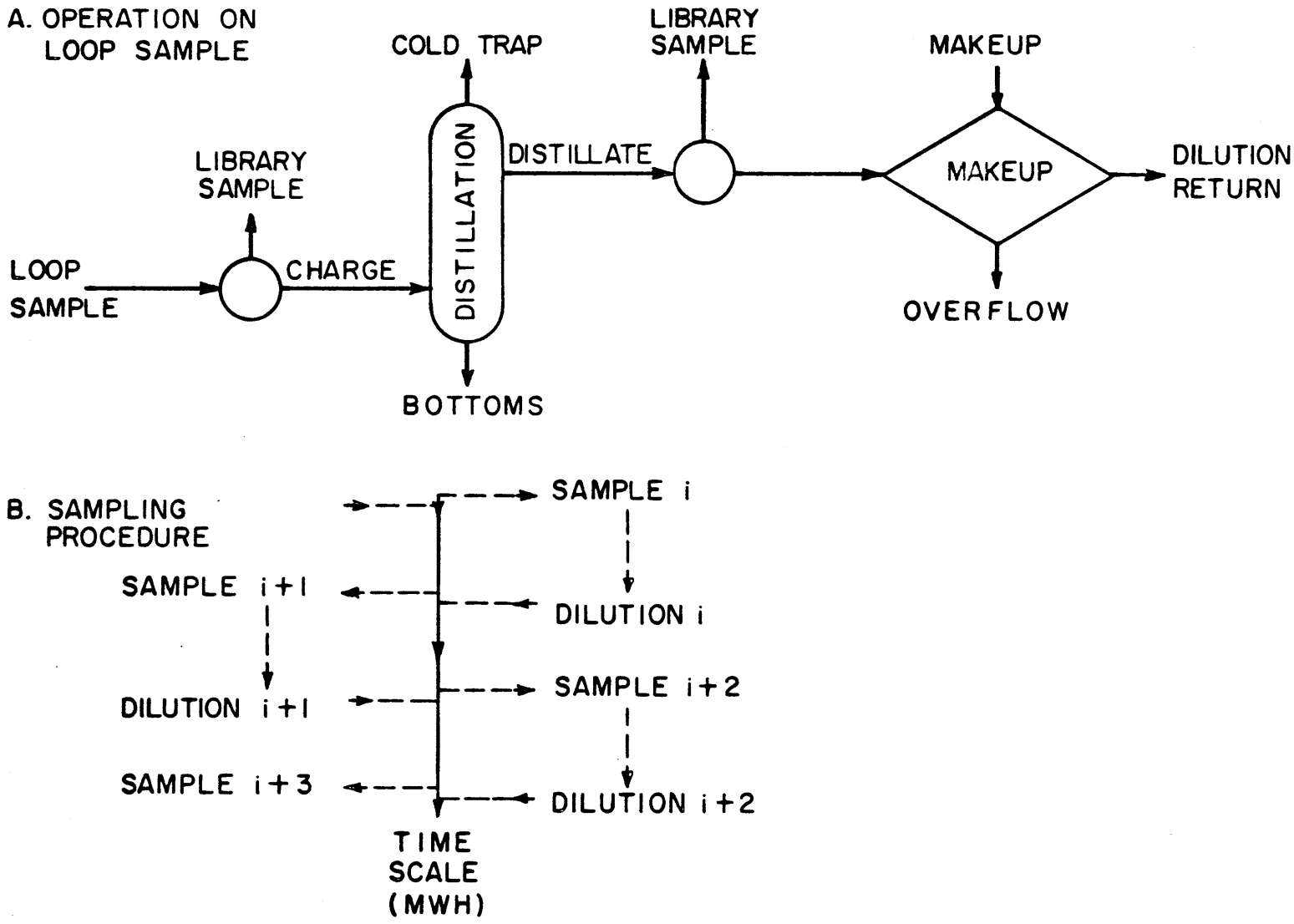

FIGURE A2.8 SCHEMATIC FLOW CHART OF MAKEUP PROCEDURE

period of time, normally measured in terms of reactor MWH, between the taking of samples was maintained approximately constant. Following loop sample i, the sample was taken at the loop, distilled, and makeup was added to the distillate. Sample $i+1$ was taken at the requisite time later, and, as soon as possible after that, the dilution return of sample i was fed back into the loop.

For the steady-state-HB period of the 610°F irradiation, a mass balance around the loop was begun just after sample 1L251 and terminated just after sample 1L268. In Section A2.3 the masses of each stream in part A of Fig. A2.8 are tabulated for each sample taken during the steady-state-HB period. The concentrations of the terphenyl isomers and of HB in each sample are also listed in Section A2.3. The amount of mass of each component removed from the loop during the period is given by

$$\text{mass of } i \text{ out} = \sum_j M_j^S C_{i,j}^S \qquad \text{(A2.51)}$$

where

M_j^S is the weight of the j^{th} loop sample

$C_{i,j}^S$ is the concentration of component i in the j^{th} loop sample.

However, as pointed out in Section 4.4.2, the concentration of each of the terphenyl isomers and of HB remained statistically constant during the steady-state-HB period, so that a simpler version of Eq. (A2.51) was used:

$$\text{mass of } i \text{ out} = \overline{C_i^S} \sum_j M_j^S \qquad \text{(A2.52)}$$

where

$\overline{C_i^S}$ is the average concentration of component i in loop samples from the steady-state-HB period.

Calculations using both methods differed negligibly.

The distillate analyses showed statistically constant concentrations of the terphenyls, and the same makeup was used throughout the steady-state-HB period, so that the amount of component i returned to the loop was calculated as

$$\text{mass of } i \text{ in} = \left[\overline{C_i^d}\,\Sigma\, M_j^d + \overline{C_i^m}\,\Sigma\, M_j^m\right]\left[\frac{\Sigma\, M_j^r}{\Sigma\, M_j^d + \Sigma\, M_j^m}\right] \qquad \text{(A2.53)}$$

where

d refers to distillate

m refers to makeup

r refers to dilution return.

The difference of Eqs. (A2.52) and (A2.53) provided the net number of grams of makeup or removal of component i during the steady-state-HB period.

The $G^*(-i)$ values for the terphenyl isomers were calculated from (see Section 4.2):

$$G(-i) = \frac{11.65[\text{net grams of } i \text{ makeup} + \Delta]}{\overline{F}\,\overline{\rho}[MWH_2 - MWH_1]} \qquad \text{(A2.54)}$$

$$\Delta = M^1_{loop}C^1 - M^2_{loop}C^2 \qquad \text{(A2.55)}$$

$$G^*(-i) = \frac{G(-i)}{\overline{C_i^L}} \qquad \text{(A2.56)}$$

where

1 refers to the start of the steady-state-HB period

2 refers to the end of the steady-state-HB period.

$\overline{C_i^L}$ is the loop average concentration of component i and may be calculated from the definition of $G(-i)$ (using the value calculated from Eq. (A2.54)) as

$$\overline{C_i^L} - \overline{C_i^S} = G(-i)\frac{\overline{F}\,\overline{\rho}}{\overline{M_{loop}}}\left\{\frac{\overline{\Delta MWH_S}}{2} - \overline{\Delta MWH_{SD}}\right\} \qquad \text{(A2.57)}$$

where

$\overline{\Delta MWH_S}$ is the average period, in MWH, between the taking of samples during the steady-state-HB period

$\overline{\Delta MWH_{SD}}$ is the average difference, in MWH, between the taking of samples and diluting with the dilution returns.

$\overline{C_i^L}$ was not equal to $\overline{C_i^S}$ during the steady-state-HB periods, as ΔMWH_{SD} was kept as close to zero as possible.

Because of the knowledge of the HB concentration during the steady-state-HB period it was also possible to calculate the production rates of HB and LIB. As explained in Section 4.4.2 these production rates were converted to an equivalent amount of terphenyl degradation. Equation (A2.54) still applies for the production rates of HB and LIB with "makeup" being replaced with "removal," and the signs in Eq. (A2.55) must be reversed. The concentration used in Eq. (A2.56) for these production rates was the loop average total omp concentration. The notation for these production rates is G(→HB), G(→LIB), G^*(→HB) and G^*(→LIB).

Using Eqs. (A2.52) to (A2.57) with the data for the 610°F irradiation steady-state-HB period tabulated in Section A2.3, an average in-pile dose rate factor, $\overline{F}$, of 57.6 (see Section 3.4) an average density at 610°F, $\overline{\rho}$, of 0.912 (see Section 5.2), the results are summarized in Table A2.28. M_{loop} was not needed for these calculations since C^1 equalled C^2 for all components studied.

An error analysis was performed on the G^* calculations listed in Table A2.28. For this analysis a standard deviation of ±2% was assigned to the average in-pile dose rate factor, $\overline{F}$ (see Section 3.4). The errors in loop average concentrations of the terphenyls were determined from the standard deviations of the mean values of the sample analyses and the possible consistent errors in analysis (see Section A2.1 for "f" factor error). The standard deviation in the grams of makeup (or grams removed) were determined from the standard deviations in the sample average concentrations and the standard deviation in the makeup analysis. For this latter analysis the deviations tabulated in Section A2.1 for individual sample analysis error were used. The errors in the average density and the sample weights were much smaller than the other errors considered and were neglected. Ninety-five percent confidence limits were assigned to the G^* values by multiplying the resulting total standard deviations by a factor of two.

G^* calculations for the quasi-steady-state-HB period of the 610°F irradiation were performed in a similar manner to those outlined above and the results are summarized in Table A2.29. No makeup analysis was available for this period, so the composition was assumed 95 w/o omp,

TABLE A2.28

Summary of G^* Calculations for the Steady-State-HB Period of the 610°F Irradiation

	Component						
	Total Coolant	o-ϕ_3	m-ϕ_3	p-ϕ_3	Total omp	HB	LIB
1. Sample avg. concentration (w/o)	100.0	5.9	37.0	18.1	61.0	33.2	5.8
2. Grams removed ($5361 \times C_i$)	5361	318	1983	968	3269	1778	314
3. Distillate avg. concentration (w/o)	100.0	9.2	56.2	25.7	91.1	0.0	8.9
4. Distillate grams to return	3222	295	1812	828	2935	0	287
5. Makeup concentration (w/o)	100.0	9.4	58.7	31.9	100.0	0.0	0.0
6. Makeup grams to return	3717	349	2184	1184	3717	0	0
7. Actual grams returned ([4.+6.]×[(3717+3222)/5366])	5366	498	3090	1556	5144	0	222
8. Net makeup (7.–2.)	5	180	1107	588	1875	–1778	–92
9. Δ Correction	–5	–0.3	–1.9	–0.9	–3.1	–1.7	–0.2
10. G(–i), G(→HB), G(→LIB) $(11.65/[\bar{F}\,\bar{p}\,\Delta MWH] = 8.71 \times 10^{-5}$	–	0.0157	0.0963	0.0511	0.163	0.155	0.008
11. Loop avg. concentration (w/o)	100.0	6.0	37.6	18.3	61.9	32.3	5.8
12. G^*(–i), G^*(→HB), G^*(→LIB)	–	0.26	0.26	0.28	0.26	0.25	0.01
13. Percent error in $\bar{F}$	–	±2	±2	±2	±2	±2	±2
14. Percent error in $\overline{C_i^L}$	–	±1	±0.4	±1	±0.7	–	–
15. Percent error in makeup	–	±3	±1.5	±4	±2	±0.1	±63
16. Total percent error	–	±4	±3	±5	±3	±2	±63
17. 95% confidence limits	–	±0.02	±0.02	±0.03	±0.02	±0.01	±0.01

TABLE A2.29

Summary of G^* Calculations for the Quasi-Steady-State-HB Period of the 610°F Irradiation

	Component			
	Total Coolant	Total omp	HB	LIB
1. Sample avg. concentration (w/o)	100.0	61.5	32.5	6.0
2. Grams removed ($4189 \times C_i$)	4189	2575	1360	254
3. Distillate avg. concentration (w/o)	100.0	90.9	0.0	9.1
4. Distillate grams to return	2071	1882	0	189
5. Makeup concentration (w/o)		95.0[a]	0.0	5.0
6. Makeup grams to return	3029	2874	0	155
7. Actual grams returned ([4.+6.]×[(2071+3029)/4121])	4121	3844	0	277
8. Net Makeup (7.−2.)	−68	1269	−1360	+23
9. Δ Correction[b]	68	−50.3	+204.0	−85.7
10. G(−omp), G(→HB), G(→LIB) $(11.65/[\bar{F}\,\bar{\rho}\,\Delta MWH] = 1.4 \times 10^{-4}$	—	0.171	0.162	0.009
11. Loop avg. concentration (w/o)	100.0	61.5	32.5	6.0
12. G^*(−omp), G^*(→LIB), G^*(→LIB)	—	0.28	0.26	0.02
13. 95% confidence limits	—	±0.05	±0.03	±0.03

a. No makeup analysis available; assumed 95 w/o omp, 5 w/o LIB.

b. M^1_{loop} = 5000 gm, M^2_{loop} = 4932 gm (see Section A2.5).

TABLE A2.30

Summary of G^* Calculations for the Steady-State-HB Period of the 750°F Irradiation

	Component						
	Total Coolant	o-ϕ_3	m-ϕ_3	p-ϕ_3	Total omp	HB	LIB
1. Sample avg. concentration (w/o)	100.0	5.9	34.9	18.4	59.2	33.3	7.5
2. Grams removed ($5077 \times C_i$)	5077	302	1771	932	3005	1695	377
3. Distillate avg. concentration (w/o)	100.0	9.7	54.3	28.0	92.0	0.0	8.0
4. Distillate grams to return	2596	252	1410	726	2388	0	208
5. Makeup concentration (w/o)	100.0	12.7	58.3	29.4	100.4	0.0	−0.4[a]
6. Makeup grams to return	2925	372	1705	860	2937	0	−12
7. Actual grams returned ([4.+6.]×[(2925+2596)/4973])	4973	561	2806	1429	4796	0	177
8. Net Makeup (7.−2.)	−104	259	1035	497	1791	−1695	−200
9. Δ Correction[b]	104	24.2	56.3	1.6	82.1	34.8	−12.9
10. $G(-i)$, $G(\rightarrow HB)$, $G(\rightarrow LIB)$ $(11.65/[\bar{F}\,\bar{\sigma}\,\Delta MWH] = 1.7 \times 10^{-4}$	—	0.0482	0.186	0.0848	0.319	0.282	0.037
11. Loop avg. concentration (w/o)	—	6.1	35.3	18.6	60.5	32.4	7.1
12. Total $G^*(-i)$, $G^*(\rightarrow HB)$, $G^*(\rightarrow LIB)$	—	0.79	0.52	0.45	0.53	0.47	0.06
13. 95% confidence limits on 12.	—	±0.07	±0.03	±0.03	±0.04	±0.02	±0.05
14. Out-of-pile pyrolysis, grams (see Eq. (A2.50))	—	31.8	80.6	22.5	134.9	—	—
15. Pyrolysis corrected $G^*(-i)$	—	0.70	0.48	0.43	0.49	—	—
16. 95% confidence limits on 15.[c]	—	±0.07	±0.03	±0.03	±0.04	—	—

a. Required to satisfy mass balance.

b. M^1_{loop} = 4820 gm, M^2_{loop} = 4716 gm (see Section A2.5).

c. Assumed same as for 13. since error in pyrolysis data unknown.

5 w/o LIB. Good control was not maintained on the HB concentration in the loop (see Section 4.4.2), and so corrections for changes in concentration during the period were not negligible (15% for HB). G^* calculations for the individual terphenyl isomers did not yield meaningful results; and in view of the large corrections needed for changes in concentrations during the period, only the calculations for total omp and HB are presented in this work.

For the steady-state-HB period of the 750°F irradiation, the same methods employed for the G^* calculations for the 610°F steady-state-HB period were used. The results are summarized in Table A2.30. One extra correction was applied to the 750°F irradiation data – for out-of-pile pyrolysis (see Section A2.9). The pyrolysis corrected $G^*(-i)$ values were calculated by subtracting the number of grams pyrolyzed in the out-of-pile section during the steady-state-HB period according to Eq. (A2.50) from the net makeup. The error limits assigned to the pyrolysis corrected $G^*(-i)$ values were the same as those assigned to the total $G^*(-i)$ values since the possible errors in the terphenyl pyrolysis data were unknown.

APPENDIX A3
PHYSICAL PROPERTY MEASUREMENTS

A3.1 Density Measurements – Theory

The densities of irradiated Santowax OMP samples were measured over the range 400-800°F by means of calibrated pycnometers. The details of the calibrations are given by Morgan and Mason(A3.1); only a recapitulation of their analysis will be given here.

During a measurement, the pycnometer containing a known weight of a sample is suspended in a constant temperature fused salt bath and pressurized with nitrogen to prevent boiling. The height in the capillary tube at any temperature is measured using a cathetometer. Each pycnometer has a height-to-volume calibration determined by the use of mercury in a 25°C water bath. From the known weight of a sample and the calculated volume, the sample density at any temperature may be determined. The calibration curves for the pycnometers used for the experiment are shown in Figure A3.1. The observed straight line relation between capillary height and pycnometer volume indicates a constant capillary thickness, so the calibration data were fit by least square straight lines. Table A3.1 gives the derived analytic relations for the pycnometer calibrations in the form

$$V = a + bH \qquad \text{(A3.1)}$$

where

V is the pycnometer volume, cc

H is the measured height in the pycnometer capillary tube, cm

a,b are constants.

An error analysis was performed on the calibration curve for pycnometer no. 7, which has the fewest data points to support it and thus should have the largest error. Using the relations derived in Section A2.6 for the statistics of a least squares analysis and assuming a measured height of 10 cm (most data fall between H = 5 and H = 10 cm), a standard deviation in the calculated value of V for pycnometer no. 7

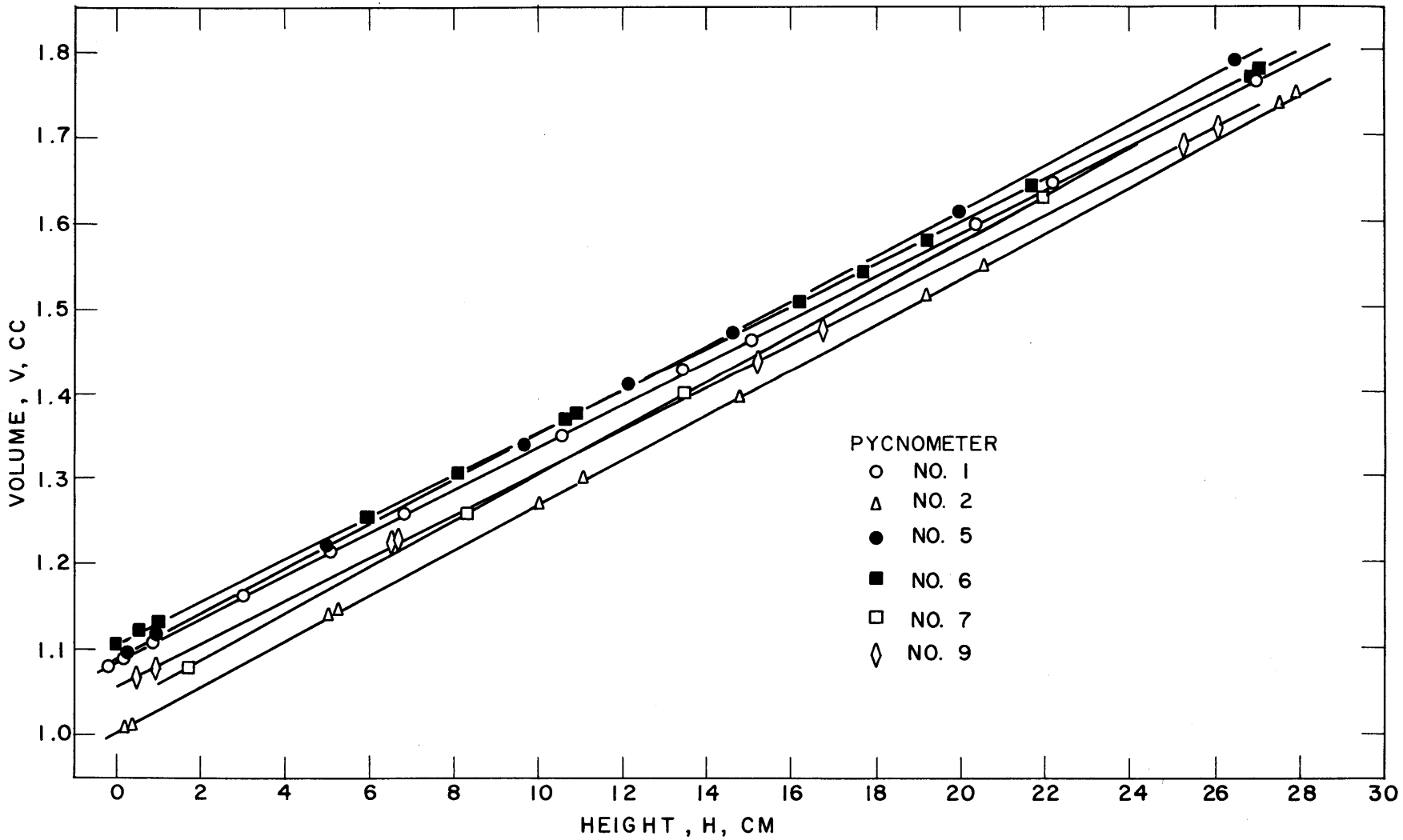

FIGURE A3.1 PYCNOMETER CALIBRATION CURVES

TABLE A3.1

Pycnometer Calibration Curves

Pycnometer Number	Calibration*
1	V = 1.084 + 0.02525H
2	V = 1.002 + 0.02667H
5	V = 1.087 + 0.02642H
6	V = 1.106 + 0.02488H
7	V = 1.034 + 0.02724H
9	V = 1.055 + 0.02514H

*V = volume, cc
H = height, cm

due to the error in the least squares fit was calculated to be 0.01 cc. Morgan and Mason (A3.1) report that the cathetometer can only be read to 0.005 cm. Assuming a maximum error of 0.01 cm at a height of 10 cm, the error in the calculated volume would be 0.0003 cc. The final error considered is the error in the temperature of the water bath. At 25°C mercury has a volume change per gram per degree of 1.34×10^{-6} cc/(g)(°C) (A3.2). A height of 10 cm usually requires about 18 g of mercury, so that even if as large an error as 1°C occurred in the bath, the error from this source would be considered to be negligible.

Thus, the error in the least squares fit to Eq. (A3.1) can be seen to be a reasonable approximation to the calibration error estimated above. Pycnometer no. 7 has a possible calibration error of about 0.001 cc or about 0.1% since the pycnometer volume is close to 1 cc. This error is considered a conservative error estimate for all pycnometer calibration curves.

In order to calculate the sample density at a given temperature, the following relation is used:

$$\rho(T) = \frac{W}{[a+bH(T)]} \qquad \text{(A3.2)}$$

where

$\rho(T)$ is the calculated density at the measured temperature, gm/cc

W is the sample weight, gm

a,b are the pycnometer calibration constants (Table A3.1)

H(T) is the measured height at the measured temperature, cm.

In addition to the calibration error, the error in the salt bath temperature becomes important for Santowax samples. From Section 5.2 it can be seen that a typical rate of change of density with temperature is 4×10^{-4} gm/(cc)(°F). Using an estimate of the salt bath temperature error of 2-3°F, the error in the measured density due to this source is 0.001 gm/cc. Also for Santowax, since the density is close to unity, the error in the measured sample weight is not insignificant in the calculation of the density, but contributes as much as a 0.0005 gm/cc error. Using the propagation of variances rule on Eq. (A3.2), a standard deviation

of ±0.002 gm/cc was calculated for a sample density at a given temperature.

Once a density-temperature plot has been prepared for a sample, the sample density as a function of temperature may be determined by fitting the data to the relation

$$\rho = A + BT \tag{A3.3}$$

This functional relation has been initially demonstrated as valid by Morgan and Mason (A3.1) and has since been found to be valid for all samples of both the 610°F and 750°F irradiations.

The conversion of sample height-temperature data to a smoothed curve of the form of Eq. (A3.3) is performed with the aid of the computer program VISDEN, which will be described in Section A3.3. An error analysis is performed by the computer solely on the least squares fit to Eq. (A3.3), and the error estimates given come fairly close to the error quoted above for a given density at a given temperature, the values ranging from almost zero to ±0.003 with most standard deviations around ±0.002 gm/cc.

In conclusion, the pycnometers are capable of measuring the densities of irradiated Santowax OMP samples to better than 0.5%

A3.2 Viscosity Measurements – Theory

Viscosities of irradiated Santowax OMP samples were determined by measuring efflux times in semi-micro capillary viscometers of the Ostwald type over the range 400-800°F. The theoretical details are described by Morgan and Mason (A3.1).

The measurement consists of placing a viscometer containing a known sample weight in the fused salt bath and pressurizing it with nitrogen to prevent boiling. At each temperature, the time for the liquid level to fall a measured distance is recorded. Because the weight of sample and the temperature are known, the total volume of sample in the viscometer may be calculated. Each viscometer has been calibrated using water in a 25°C water bath to obtain the constant, C_v, in the known relation for the viscometer

$$\frac{\mu}{\rho} = C_v t \tag{A3.4}$$

where

μ is the sample viscosity, centipoises

t is the efflux time, sec

C_v is the constant, (cp)(cc)/(gm)(sec).

C_v is linearly related to the sample volume, and by knowing the sample volume and density at a given temperature and measuring the efflux time, the viscosity may be determined from Eq. (A3.4). Figure A3.2 shows the calibration curves for the viscometers used in this experiment. The data have been fit to the relation

$$C_v = c + dV \tag{A3.5}$$

where

c,d are constants

and

V is the sample volume, cc

by the method of least squares, and Table A3.2 lists the analytic form of the calibration curves. The error-of-fit to the most often used viscometers, N302 and N306, determined by the relations developed in Section A2.6, amounts to about 1.5% and may be considered to include all errors of the calibration experiments, as in the case of the pycnometer calibration.

In order to calculate the sample viscosity at a given temperature, the following relation is used

$$\mu(T) = \frac{\rho(T)\, t(T)}{\left(c + d\,\frac{W}{\rho(T)}\right)} \tag{A3.6}$$

where

$\mu(T)$ is the calculated sample viscosity at the measured temperature, centipoises

W is the sample weight, gm

c,d are the viscometer calibration constants (Table A3.2)

t(T) is the measured efflux time at the measured temperature, sec

$\rho(T)$ is the calculated sample density at the measured temperature, gm/cc.

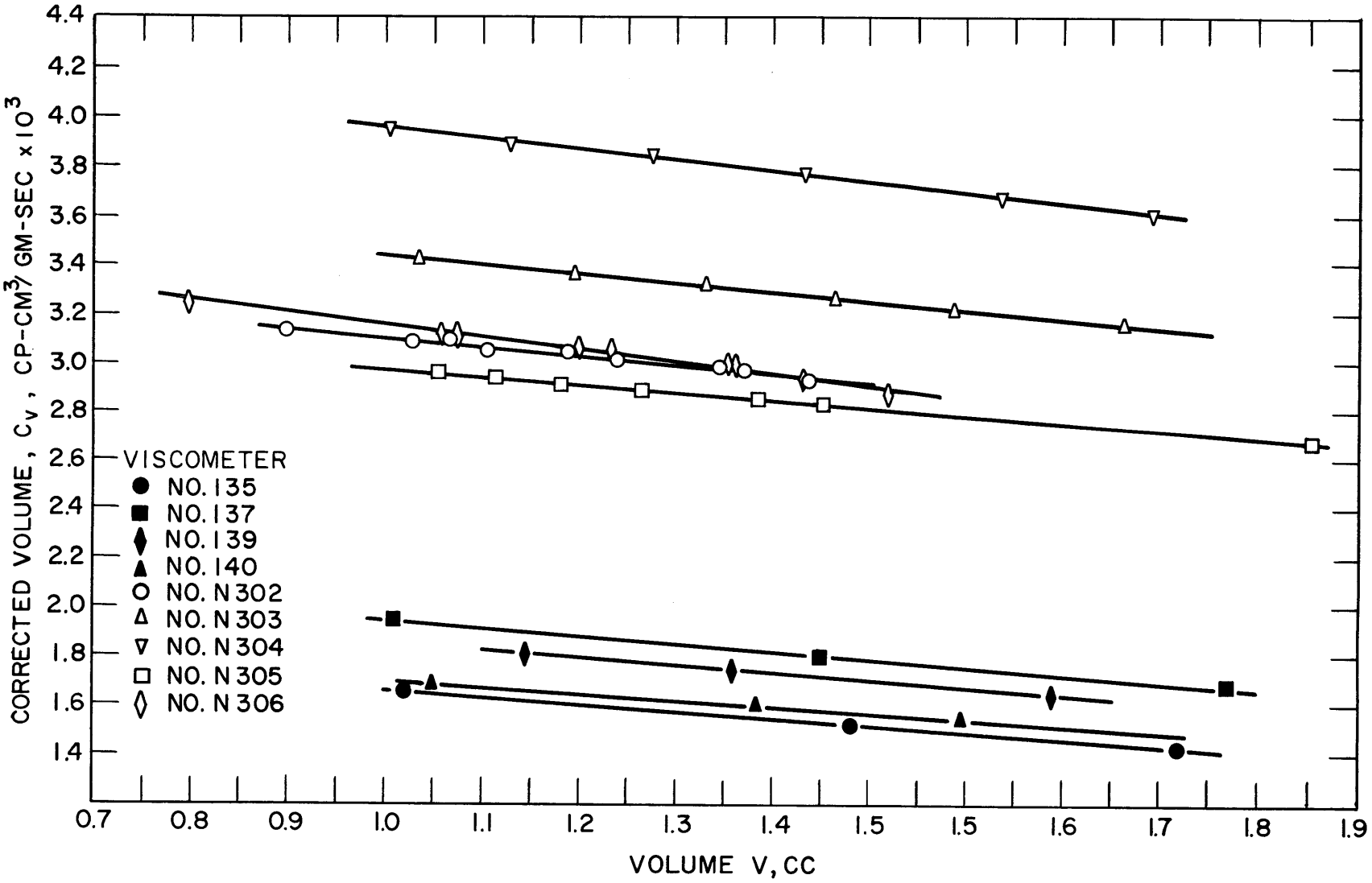

FIGURE A3.2 VISCOMETER CALIBRATION CURVES

TABLE A3.2

Viscometer Calibration Curves

Viscometer Number	Calibration* ($C_v \times 10^3$)
135	$C_v = 1.95 - 0.289V$
137	$C_v = 2.25 - 0.309V$
139	$C_v = 2.18 - 0.319V$
140	$C_v = 1.98 - 0.277V$
N302	$C_v = 3.48 - 0.378V$
N303	$C_v = 3.82 - 0.375V$
N304	$C_v = 4.39 - 0.433V$
N305	$C_v = 3.30 - 0.323V$
N306	$C_v = 3.67 - 0.506V$

*See Eq. (A3.5).

The sample density is obtained from a sample density measurement using the smoothed relation, Eq. (A3.3). A salt bath temperature error is much more important for the viscosity than the density. Based on the data presented in Section 5.3, this error amounts to about 1.5% for an error of 3°F. Considering this error and an error of 0.2% in the density, an error of 0.5% in the measured efflux time and an error of 1.5% in the calibration constants, the propagation of variances rule yields about ±2.5% as a total error in the calculated sample viscosity at a given temperature.

Another source of consistent error, which is difficult to evaluate, is the possibility of minute particles becoming trapped in the capillary part of a viscometer before filling with a sample. Usually, this results in giving the viscosity data an erroneous temperature slope. The best technique to eliminate this source of error is to measure all sample viscosities twice to check for reproducibility. In most cases, this was done.

Once a table of sample viscosities at various temperatures has been prepared, the data may be fit to the relation

$$\mu = \mu_o e^{\Delta E/RT} \tag{A3.7}$$

where

μ_o is a constant, cp

R is the gas constant, kcal/(mole)(°R)

ΔE is an "activation energy" for the viscous fluid, kcal/mole

T is the absolute temperature, °R.

Morgan and Mason (A3.1) have shown this functional relation to be valid for initial irradiated samples, and it has since been found valid for all samples of the 610°F and 750°F irradiations. The best fit is determined by the method of least squares applied to the logarithm of Eq. (A3.7), because ln μ is a linear function of 1/T.

The computer program VISDEN performs the complete data reduction from sample temperatures and efflux times using the equations and calibrations described above. The errors-of-fit determined by the computer agree quite well with the errors of the individual viscosity measurements calculated above, the values ranging from about ±1% to

±6% with most values near ±3%. Thus, the reported viscosity data are expected to be accurate to about ±3%.

A3.3 Density and Viscosity Computer Program, VISDEN

VISDEN is an IBM 709/7090 FORTRAN program (for use with a 32K storage) which reduces the density and viscosity data (taken at the fused salt bath) by means of the theory described in Sections A3.1 and A3.2 and produces as output the constants in the smoothed relations

$$\rho = A + BT \tag{A3.3}$$

$$\ln \mu = C + \frac{\Delta E}{RT} \tag{A3.8}$$

where C is equal to $\ln \mu_o$ in Eq. (A3.7) for each sample. It also has the facility of least squaring the data for a group of samples at a given temperature versus an independent variable, which could be reactor MWH, specific dose in (watt)(hr)/gm or some other desired variable. The purpose of this section is to briefly describe the program and how to utilize it via an example.

Table A3.3 gives the FORTRAN listing of VISDEN and a logic flowsheet of the program is presented in Fig. A3.3. An understanding of the use of the program is best given with the aid of an example, so Table A3.4 contains a sample input and Table A3.5 a sample output. Some knowledge of FORTRAN input/output format is presumed; for a detailed description, see reference (A3.3).

All fixed-point data are read in by I4 format, and all floating-point data in by E12.5 format. In addition, some alphanumeric data are used to label the sample numbers and the field description of these data is A6. The input is arranged as a series of tables, each headed by a card on which any desired information may be written, in order to help define the data.

The first table in the program provides the fixed-point control data for the program, and contains the following information:

1. A punch control. If the variable is ≤ 0, a punched copy of the output will be provided along with the printed copy; if it is > 0, then no punching will be done.

TABLE A3.3
FORTRAN LISTING OF VISDEN

```
*      LIST 8
*      LABEL
*      SYMBOL TABLE
CVISDEN
C      VISDEN HAS SUBPROGRAMS MAIN,LINLSQ(2) IN FORTRAN
C      MAIN HAS 174 CARDS      1-10-63
       COMMON SUMX,SUMY,SUMX2,SUMXY,SUMY2,SLOPE,ENTCPT,SIG2E,SIG2P,SIGA,S
      1IGB,RLIN,NOT,KPUNCH
       DIMENSION AD(20),BD(20),AV(20),BV(20),TEMPS(20),EMWH(200),TEMPR(20
      1),H(20),SAMPLE(200),TEMPM(20),TIME(20),RHO(20),SLOPER(200),ENTCPR(
      2200),SDSR(200),SDER(200),RHOP(200,20),EMU(20),TINV(20),Y(20),SLOPE
      3M(200),ENTCPM(200),SDSM(200),SDEM(200),EMUP(200,20),ACTE(200),YP(2
      400,20),TINVP(20)
       NIT=4
       NOT=2
   47  READINPUTTAPE NIT,1,KPUNCH,NDEN,NVIS,NBATCH,NTEMPS,KEND
    1  FORMAT(/(18I4))
       READINPUTTAPE NIT,2,(AD(I),BD(I),I=1,NDEN)
       READINPUTTAPE NIT,2,(AV(I),BV(I),I=1,NVIS)
       READINPUTTAPE NIT,2,FAC1,FAC2,(TEMPS(I),I=1,NTEMPS)
    2  FORMAT(/(6E12.5))
       DO 61 I=1,NTEMPS
       TINVP(I)=1.0/(FAC1+TEMPS(I))
   61  CONTINUE
       DO 46 J=1,NBATCH
       READINPUTTAPE NIT,3
    3  FORMAT(80H
      1                              )
       WRITEOUTPUTTAPE NOT,3
       IF(KPUNCH)4,4,5
    4  PUNCH 3
    5  READINPUTTAPE NIT,1,N,KLSQ
       DO 28 I=1,N
       READINPUTTAPE NIT,1,NRHO,NRHO1,NPYC,NMU,NMU1,NVISC0,NRHO2,NRHO3,NP
      1YC2,NMU2,NMU3,NVISC2
       READINPUTTAPE NIT,6,EMWH(I),GRHO,TEMPR(1),H(1),TEMPR(2),H(2),SAMPL
      1E(I),(TEMPR(K),H(K),K=3,NRHO),GMU,(TEMPM(K),TIME(K),K=1,NMU)
    6  FORMAT(6E12.5,A6/(6E12.5))
       NHIGH=NRHO
       DO 7 K=1,NRHO
       RHO(K)=GRHO/(AD(NPYC)+BD(NPYC)*H(K))
    7  CONTINUE
       IF(NRHO2)52,52,50
   50  NLOW=NRHO+1
       NHIGH=NRHO+NRHO2
       READINPUTTAPE NIT,60,GRHO,(TEMPR(K),H(K),K=NLOW,NHIGH)
   60  FORMAT(6E12.5)
       DO 51 K=NLOW,NHIGH
       RHO(K)=GRHO/(AD(NPYC2)+BD(NPYC2)*H(K))
   51  CONTINUE
       NHIGH=NRHO+NRHO3
       NRHO=NRHO+NRHO2
   52  CALL LINLSQ(NRHO1,NHIGH,TEMPR,RHO,-1)
       SLOPER(I)=SLOPE
       ENTCPR(I)=ENTCPT
       SDSR(I)=SIGB
       SDER(I)=SIGA
```

TABLE A3.3 (CONTINUED)

```
      DO 8 K=1,NTEMPS
      RHOP(I,K)=ENTCPR(I)+SLOPER(I)*TEMPS(K)
    8 CONTINUE
      IF(NMU)9,9,10
    9 SLOPEM(I)=0.0
      ENTCPM(I)=0.0
      GO TO 12
   10 NHIGH=NMU
      DO 11 K=1,NMU
      EMU(K)=(ENTCPR(I)+SLOPER(I)*TEMPM(K))*(AV(NVISCO)+BV(NVISCO)*GMU/(
     1ENTCPR(I)+SLOPER(I)*TEMPM(K)))*TIME(K)
      TINV(K)=1.0/(FAC1+TEMPM(K))
      Y(K)=LOGF(EMU(K))
   11 CONTINUE
      IF(NMU2)55,55,53
   53 NLOW=NMU+1
      NHIGH=NMU+NMU2
      READINPUTTAPE NIT,60,GMU,(TEMPM(K),TIME(K),K=NLOW,NHIGH)
      DO 54 K=NLOW,NHIGH
      EMU(K)=(ENTCPR(I)+SLOPER(I)*TEMPM(K))*(AV(NVISC2)+BV(NVISC2)*GMU/(
     1ENTCPR(I)+SLOPER(I)*TEMPM(K)))*TIME(K)
      TINV(K)=1.0/(FAC1+TEMPM(K))
      Y(K)=LOGF(EMU(K))
   54 CONTINUE
      NHIGH=NMU+NMU3
      NMU=NMU+NMU2
   55 CALL LINLSQ(NMU1,NHIGH,TINV,Y,-1)
      SLOPEM(I)=SLOPE
      ENTCPM(I)=ENTCPT
      SDSM(I)=SIGB
      SDEM(I)=SIGA
      ACTE(I)=FAC2*SLOPEM(I)
   12 DO 13 K=1,NTEMPS
      YP(I,K)=ENTCPM(I)+SLOPEM(I)*TINVP(K)
      EMUP(I,K)=EXPF(YP(I,K))
   13 CONTINUE
      WRITEOUTPUTTAPE NOT,14,SAMPLE(I)
   14 FORMAT(1H0,33X7HSAMPLE A6/ 8X5HTEMPD,5X7HDENSITY,4X6HTEMPMU,3X9HVI
     1SCOSITY,4X10H1/T DEG. A,6X6HLOGEMU)
      IF(KPUNCH)15,15,16
   15 PUNCH 14,SAMPLE(I)
   16 IF(NMU)26,26,56
   56 WRITEOUTPUTTAPE NOT,18,(TEMPS(K),RHOP(I,K),TEMPS(K),EMUP(I,K),TINV
     1P(K),YP(I,K),K=1,NTEMPS)
      IF(KPUNCH)57,57,58
   57 PUNCH 18,(TEMPS(K),RHOP(I,K),TEMPS(K),EMUP(I,K),TINVP(K),YP(I,K),K
     1=1,NTEMPS)
   58 IF(NRHO-NMU)20,17,23
   17 WRITEOUTPUTTAPE NOT,18,(TEMPR(K),RHO(K),TEMPM(K),EMU(K) ,TINV(K),Y
     1(K),K=1,NRHO)
   18 FORMAT(0PF14.1,0PF11.4,0PF10.1,0PF11.4,1PE16.5,0PF12.4)
      IF(KPUNCH)19,19,28
   19 PUNCH 18,(TEMPR(K),RHO(K),TEMPM(K),EMU(K),TINV(K),Y(K),K=1,NRHO)
      GO TO 28
   20 NV=NRHO+1
      WRITEOUTPUTTAPE NOT,18,(TEMPR(K),RHO(K),TEMPM(K),EMU(K) ,TINV(K),Y
     1(K),K=1,NRHO)
      WRITEOUTPUTTAPE NOT,21,(TEMPM(K),EMU(K),TINV(K),Y(K),K=NV,NMU)
   21 FORMAT(0PF35.1,0PF11.4,1PE16.5,0PF12.4)
```

TABLE A3.3 (CONTINUED)

```
      IF(KPUNCH)22,22,28
   22 PUNCH 18,(TEMPR(K),RHO(K),TEMPM(K),EMU(K),TINV(K),Y(K),K=1,NRHO)
      PUNCH 21,(TEMPM(K),EMU(K),TINV(K),Y(K),K=NV,NMU)
      GO TO 28
   23 ND=NMU+1
      WRITEOUTPUTTAPE NOT,18,(TEMPR(K),RHO(K),TEMPM(K),EMU(K) ,TINV(K),Y
     1(K),K=1,NMU)
      WRITEOUTPUTTAPE NOT,24,(TEMPR(K),RHO(K),K=ND,NRHO)
   24 FORMAT(F14.1,F11.4)
      IF(KPUNCH)25,25,28
   25 PUNCH 18,(TEMPR(K),RHO(K),TEMPM(K),EMU(K),TINV(K),Y(K),K=1,NMU)
      PUNCH 24,(TEMPR(K),RHO(K),K=ND,NRHO)
      GO TO 28
   26 WRITEOUTPUTTAPE NOT,24,(TEMPS(K),RHOP(I,K),K=1,NTEMPS),(TEMPR(K),R
     1HO(K),K=1,NRHO)
      IF(KPUNCH)27,27,28
   27 PUNCH 24,(TEMPS(K),RHOP(I,K),K=1,NTEMPS),(TEMPR(K),RHO(K),K=1,NRHO
     1)
   28 CONTINUE
      WRITEOUTPUTTAPE NOT,29,(SAMPLE(I),SLOPER(I),SDSR(I),ENTCPR(I),SDER
     1(I),I=1,N)
   29 FORMAT(1H1,3X6HSAMPLE,6X9HRHO SLOPE,3X10HS.D. SLOPE,3X11HR INTERCE
     1PT,2X11HS.D. INTCPT/(4XA6,3X,4F13.5))
      WRITEOUTPUTTAPE NOT,30
   30 FORMAT(1H1,3X6HSAMPLE,6X9HMU  SLOPE,3X10HS.D. SLOPE,3X11HM INTERCE
     1PT,2X11HS.D. INTCPT,2X11HACT. ENERGY)
      IF(KPUNCH)31,31,32
   31 PUNCH 29,(SAMPLE(I),SLOPER(I),SDSR(I),ENTCPR(I),SDER(I),I=1,N)
      PUNCH 30
   32 DO 36 I=1,N
      IF(SLOPEM(I))36,36,33
   33 WRITEOUTPUTTAPE NOT,34,SAMPLE(I),SLOPEM(I),SDSM(I),ENTCPM(I),SDEM(
     1I),ACTE(I)
   34 FORMAT(4XA6,3X,5F13.5)
      IF(KPUNCH)35,35,36
   35 PUNCH 34,SAMPLE(I),SLOPEM(I),SDSM(I),ENTCPM(I),SDEM(I),ACTE(I)
   36 CONTINUE
      IF(KLSQ)37,37,46
   37 WRITEOUTPUTTAPE NOT,38
   38 FORMAT(1H1,12H TEMPERATURE,2X11HIRRAD SLOPE,2X10HS.D. SLOPE,3X11HI
     1RRAD INTCP,2X11HS.D. INTCPT,2X11HCORR. COEF.)
      IF(KPUNCH)39,39,40
   39 PUNCH 38
   40 DO 45 I=1,NTEMPS
      CALL LINLSQ(1,N,EMWH,RHOP(1,I),-1)
      WRITEOUTPUTTAPE NOT,41,TEMPS(I),SLOPE,SIGB,ENTCPT,SIGA,RLIN
   41 FORMAT(6F13.5)
      IF(KPUNCH)42,42,43
   42 PUNCH 41,TEMPS(I),SLOPE,SIGB,ENTCPT,SIGA,RLIN
   43 CALL LINLSQ(1,N,EMWH,YP(1,I),-1)
      WRITEOUTPUTTAPE NOT,41,TEMPS(I),SLOPE,SIGB,ENTCPT,SIGA,RLIN
      IF(KPUNCH)44,44,45
   44 PUNCH 41,TEMPS(I),SLOPE,SIGB,ENTCPT,SIGA,RLIN
   45 CONTINUE
   46 CONTINUE
      IF(KEND)47,47,48
   48 CALL EXIT
      END
```

TABLE A3.3 (CONCLUDED)

```
*       LIST 8
*       LABEL
*       SYMBOL TABLE
        SUBROUTINE LINLSQ(N1,N2,X,Y,N3)
CLINLS2
C       LINLSQ(2) HAS 47 CARDS              7-26-63
        COMMON SUMX,SUMY,SUMX2,SUMXY,SUMY2,SLOPE,ENTCPT,SIG2E,SIG2P,SIGA,S
       1IGB,RLIN,NOT,KPUNCH
        DIMENSION X(300),Y(300)
        SUMX=0.0
        SUMY=0.0
        SUMX2=0.0
        SUMXY=0.0
        SUMY2=0.0
        EN=N2-N1+1
        DO 1 I=N1,N2
        IF(Y(I))12,11,12
   11   EN=EN-1.0
        GO TO 1
   12   SUMX=SUMX+X(I)
        SUMY=SUMY+Y(I)
        SUMX2=SUMX2+X(I)**2
        SUMXY=SUMXY+X(I)*Y(I)
        SUMY2=SUMY2+Y(I)**2
    1   CONTINUE
        DEN=EN*SUMX2-SUMX**2
        SLOPE=(EN*SUMXY-SUMX*SUMY)/DEN
        ENTCPT=(SUMY*SUMX2-SUMX*SUMXY)/DEN
        SIG2E=(SUMY2-ENTCPT*SUMY-SLOPE*SUMXY)/(EN-2.0)
        IF(SIG2E)9,9,10
    9   SIG2E=0.0
   10   SIG2P=(SUMY2-SUMY**2/EN)/(EN-1.0)
        SIGB=SQRTF(EN*SIG2E/DEN)
        SIGA=SQRTF(SUMX2*SIG2E/DEN)
        RLIN=SQRTF(1.0-SIG2E*(EN-2.0)/SIG2P/(EN-1.0))
        IF(N3)8,2,5
    2   WRITEOUTPUTTAPE NOT,3
    3   FORMAT(75H      SLOPE      S.D.(SLOPE)    INTERCEPT    S.D.(INTCP)  CO
       1RR. COEFF      SIG2E)
        IF(KPUNCH)4,4,5
    4   PUNCH 3
    5   WRITEOUTPUTTAPE NOT,6,SLOPE,SIGB,ENTCPT,SIGA,RLIN,SIG2E
    6   FORMAT(1P6E13.5)
        IF(KPUNCH)7,7,8
    7   PUNCH 6,SLOPE,SIGB,ENTCPT,SIGA,RLIN,SIG2E
    8   RETURN
        END
```

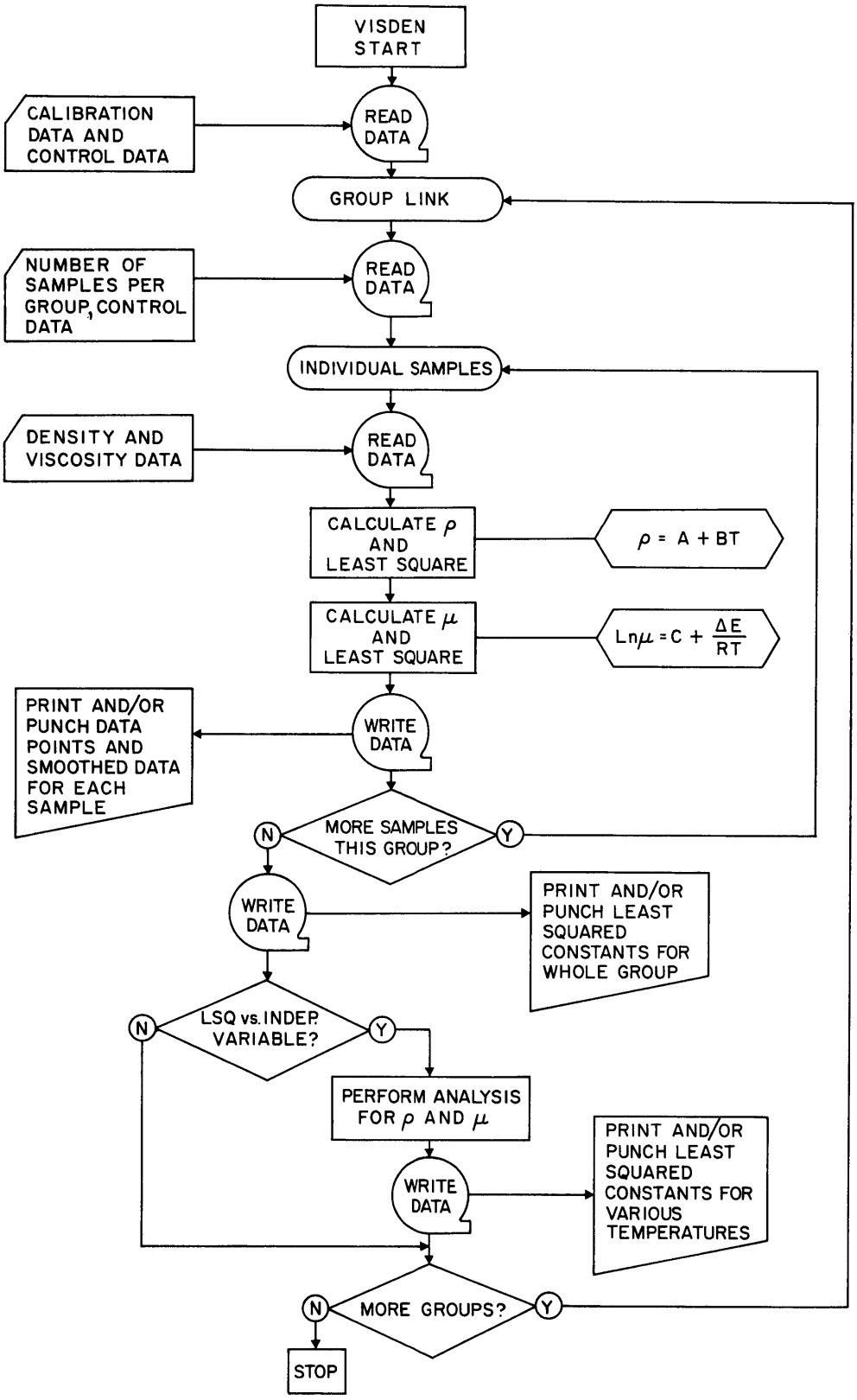

FIGURE A3.3 LOGIC FLOWSHEET FOR VISDEN

TABLE A3.4
SAMPLE INPUT TO VISDEN

```
                                CONTROL TABLE
  1   9  10   1   6
                              PYCNOMETER TABLE
 1.0844        0.025251      1.0019        0.026673      1.0743        0.026317
 0.            0.            1.0873        0.026417      1.1056        0.024875
 1.0336        0.027242      0.            0.            1.0554        0.025136
                              VISCOSIMETER TABLE
 0.            0.            0.0034844    -0.00037795    0.0038162    -0.00037462
 0.0043905    -0.00043289    0.0032978    -0.00032338    0.0036655    -0.00050559
 0.0022533    -0.00030861    0.0019514    -0.00028911    0.0021818    -0.00031907
 0.0019814    -0.00027667
                    TEMPERATURES AND CONVERSION FACTORS
 459.7         0.001104      400.          500.          600.          700.
 800.          1200.
1    DATA OF 610 DEG. F IRRADIATION TRANSIENT NO. 1   LSQ VERSUS MWH  5-21-63
                              NUMBER OF SAMPLES
  8
                                THIS IS 1L16
  5   1   1   5   1   4   5   5   2   5   5   7
 0.0           1.029         424.          0.028         494.          1.44          1L16
 565.          3.033         634.          4.73          687.          6.118
 1.3166        420.          222.1         480.          169.4         543.
 131.6         618.          105.4         705.          84.8
 1.029         389.          2.4           454.          3.615          542.
 5.427         632.          7.557         731.          10.233
 0.94          389.          475.6         454.          356.1          542.
 262.3         632.          199.6         731.          157.9
                                THIS 'S 1L27
  4   2   7   6   1   8
 250.          0.9961        623.          5.18          489.          1.39          1L27
 559.          2.795         698.          5.99          1.1365        422.
 537.5         502.6         388.9         576.3         304.2         657.
 242.9         723.6         207.3         768.6         191.
                                THIS IS 1L37
  6   1   2   5   2   5   0   0   0   5   5   4
 400.          0.9579        431.          0.223         494.          1.323         1L37
 576.          2.828         645.          4.428         730.          6.47
 770.          7.533         1.0545        466.          249.4         535.
 202.8         593.          170.8         654.          145.          677.
 137.8
 1.186         519.          169.9         560.          147.          615.
 124.6         666.          108.6         695.          103.
                                THIS IS 1L47
  6   2   5   5   1   9
 816.          1.1483        484.7         4.738         414.8         3.325         1L47
 557.          6.738         621.7         8.303         687.7         10.038
 752.8         11.860        1.1412        482.8         459.2         557.
 349.1         621.7         285.3         687.7         237.8         752.8
 202.8
                                THIS IS 1L50
  4   1   6
 930.          1.1561        451.2         4.238         485.5         4.968         1L50
 570.2         6.9           639.          8.703
                                THIS IS 1L51
  7   1   1   4   2   8
 1076.         1.3281        412.3         11.185        427.          11.505        1L51
```

TABLE A3.4 (CONCLUDED)

```
489.7          13.065         418.7          11.32          551.7          14.615
610.7          16.45          729.           19.925         1.1508         616.7
388.5          489.7          560.5          418.7          783.7          551.7
447.3
                                  THIS IS 1L59
 4   1   1   6   1   4   0   0   0   5   5   9
1472.          1.1582         485.           5.378          550.           6.79          1L59
617.           8.268          696.           10.333         1.1642         433.
388.7          496.           270.8          566.           202.5          617.
174.           645.           159.9          715.           131.1
0.8452         485.           599.           553.           455.7          617.
372.1          696.           297.2          793.           257.6
                                  THIS IS 1L62
 5   1   2   5   1   2   0   0   0   4   4   7
1621.          1.0757         498.           4.875          560.           6.01          1L62
650.           7.9            723.           9.593          747.           10.253
1.1904         482.           398.8          547.           307.9          604.
248.2          563.           218.3          680.           205.
0.8779         498.           609.1          560.           439.2          650.
320.4          747.           244.5
```

TABLE A3.5
SAMPLE OUTPUT FROM VISDEN

DATA OF 610 DEG. F IRRADIATION TRANSIENT NO. 1 LSQ VERSUS MWH 5-21-63

SAMPLE 1L16

TEMPD	DENSITY	TEMPMU	VISCOSITY	1/T DEG. A	LOGEMU
400.0	0.9610	400.0	0.8628	1.16320E-03	-0.1475
500.0	0.9152	500.0	0.5347	1.04199E-03	-0.6260
600.0	0.8695	600.0	0.3627	9.43663E-04	-1.0142
700.0	0.8238	700.0	0.2630	8.62292E-04	-1.3355
800.0	0.7781	800.0	0.2007	7.93840E-04	-1.6057
1200.0	0.5952	1200.0	0.0943	6.02519E-04	-2.3611
424.0	0.9483	420.0	0.8016	1.13675E-03	-0.2212
494.0	0.9181	480.0	0.5910	1.06417E-03	-0.5260
565.0	0.8863	543.0	0.4424	9.97307E-04	-0.8154
634.0	0.8548	618.0	0.3385	9.27902E-04	-1.0833
687.0	0.8306	705.0	0.2575	8.58590E-04	-1.3566
389.0	0.9654	389.0	0.8972	1.17827E-03	-0.1084
454.0	0.9369	454.0	0.6480	1.09445E-03	-0.4339
542.0	0.8974	542.0	0.4535	9.98303E-04	-0.7908
632.0	0.8550	632.0	0.3266	9.16003E-04	-1.1191
731.0	0.8072	731.0	0.2422	8.39842E-04	-1.4178

SAMPLE 1L27

TEMPD	DENSITY	TEMPMU	VISCOSITY	1/T DEG. A	LOGEMU
400.0	0.9714	400.0	0.9347	1.16320E-03	-0.0675
500.0	0.9248	500.0	0.5784	1.04199E-03	-0.5475
600.0	0.8781	600.0	0.3918	9.43663E-04	-0.9369
700.0	0.8315	700.0	0.2839	8.62292E-04	-1.2592
800.0	0.7849	800.0	0.2165	7.93840E-04	-1.5303
1200.0	0.5983	1200.0	0.1015	6.02519E-04	-2.2880
623.0	0.8480	422.0	0.8315	1.13417E-03	-0.1845
489.0	0.9297	502.6	0.5731	1.03918E-03	-0.5567
559.0	0.8976	576.3	0.4279	9.65251E-04	-0.8489
698.0	0.8323	657.0	0.3238	8.95496E-04	-1.1276
		723.6	0.2638	8.45094E-04	-1.3326
		768.6	0.2352	8.14133E-04	-1.4472

SAMPLE 1L37

TEMPD	DENSITY	TEMPMU	VISCOSITY	1/T DEG. A	LOGEMU
400.0	0.9664	400.0	1.0078	1.16320E-03	0.0077
500.0	0.9208	500.0	0.6302	1.04199E-03	-0.4617
600.0	0.8752	600.0	0.4306	9.43663E-04	-0.8426
700.0	0.8296	700.0	0.3142	8.62292E-04	-1.1577
800.0	0.7840	800.0	0.2410	7.93840E-04	-1.4228
1200.0	0.6016	1200.0	0.1149	6.02519E-04	-2.1639
431.0	0.9504	466.0	0.6851	1.08026E-03	-0.3782
494.0	0.9236	535.0	0.5360	1.00533E-03	-0.6236
576.0	0.8891	593.0	0.4365	9.49938E-04	-0.8289
645.0	0.8553	654.0	0.3573	8.97908E-04	-1.0292
730.0	0.8156	677.0	0.3348	8.79740E-04	-1.0943
770.0	0.7964	519.0	0.5932	1.02176E-03	-0.5222
		560.0	0.5012	9.80681E-04	-0.6908
		615.0	0.4111	9.30492E-04	-0.8890
		666.0	0.3472	8.88336E-04	-1.0578
		695.0	0.3233	8.66026E-04	-1.1291

TABLE A3.5 (CONTINUED)

SAMPLE 1L47

TEMPD	DENSITY	TEMPMU	VISCOSITY	1/T DEG. A	LOGEMU
400.0	0.9826	400.0	1.2002	1.16320E-03	0.1825
500.0	0.9361	500.0	0.7217	1.04199E-03	-0.3261
600.0	0.8896	600.0	0.4777	9.43663E-04	-0.7387
700.0	0.8432	700.0	0.3395	8.62292E-04	-1.0802
800.0	0.7967	800.0	0.2547	7.93840E-04	-1.3675
1200.0	0.6109	1200.0	0.1141	6.02519E-04	-2.1704
484.7	0.9471	482.8	0.7787	1.06101E-03	-0.2502
414.8	0.9772	557.0	0.5657	9.83574E-04	-0.5697
557.0	0.9075	621.7	0.4436	9.24727E-04	-0.8128
621.7	0.8788	687.7	0.3538	8.71536E-04	-1.0389
687.7	0.8490	752.8	0.2884	8.24742E-04	-1.2435
752.8	0.8199				

SAMPLE 1L50

TEMPD	DENSITY	TEMPMU	VISCOSITY	1/T DEG. A	LOGEMU
400.0	0.9769				
500.0	0.9342				
600.0	0.8916				
700.0	0.8490				
800.0	0.8064				
1200.0	0.6359				
451.2	0.9546				
485.5	0.9405				
570.2	0.9052				
639.0	0.8745				

SAMPLE 1L51

TEMPD	DENSITY	TEMPMU	VISCOSITY	1/T DEG. A	LOGEMU
400.0	0.9774	400.0	1.3522	1.16320E-03	0.3017
500.0	0.9345	500.0	0.8080	1.04199E-03	-0.2132
600.0	0.8916	600.0	0.5321	9.43663E-04	-0.6310
700.0	0.8487	700.0	0.3766	8.62292E-04	-0.9767
800.0	0.8059	800.0	0.2815	7.93840E-04	-1.2675
1200.0	0.6344	1200.0	0.1249	6.02519E-04	-2.0804
412.3	0.9717	616.7	0.5413	9.29023E-04	-0.6138
427.0	0.9660	489.7	0.8405	1.05330E-03	-0.1738
489.7	0.9390	418.7	1.2217	1.13843E-03	0.2002
418.7	0.9692	551.7	0.6475	9.88728E-04	-0.4346
551.7	0.9138				
610.7	0.8855				
729.0	0.8366				

SAMPLE 1L59

TEMPD	DENSITY	TEMPMU	VISCOSITY	1/T DEG. A	LOGEMU
400.0	0.9849	400.0	1.6498	1.16320E-03	0.5007
500.0	0.9432	500.0	0.9925	1.04199E-03	-0.0075
600.0	0.9016	600.0	0.6572	9.43663E-04	-0.4197
700.0	0.8599	700.0	0.4672	8.62292E-04	-0.7609
800.0	0.8182	800.0	0.3507	7.93840E-04	-1.0479
1200.0	0.6515	1200.0	0.1572	6.02519E-04	-1.8500
485.0	0.9492	433.0	1.4615	1.12020E-03	0.3795
550.0	0.9222	496.0	0.9870	1.04635E-03	-0.0131
617.0	0.8956	566.0	0.7121	9.74944E-04	-0.3395
696.0	0.8609	617.0	0.5957	9.28764E-04	-0.5181
		645.0	0.5392	9.05223E-04	-0.6177
		715.0	0.4253	8.51281E-04	-0.8550

TABLE A3.5 (CONCLUDED)

485.0	1.0794	1.05854E-03	0.0764
553.0	0.7930	9.87459E-04	-0.2320
617.0	0.6258	9.28764E-04	-0.4687
696.0	0.4785	8.65276E-04	-0.7371
793.0	0.3920	7.98276E-04	-0.9364

SAMPLE 1L62

TEMPD	DENSITY	TEMPMU	VISCOSITY	1/T DEG. A	LOGEMU
400.0	0.9934	400.0	1.8679	1.16320E-03	0.6248
500.0	0.9505	500.0	1.0791	1.04199E-03	0.0762
600.0	0.9076	600.0	0.6915	9.43663E-04	-0.3689
700.0	0.8647	700.0	0.4784	8.62292E-04	-0.7373
800.0	0.8218	800.0	0.3509	7.93840E-04	-1.0471
1200.0	0.6503	1200.0	0.1476	6.02519E-04	-1.9132
498.0	0.9503	482.0	1.1521	1.06191E-03	0.1416
560.0	0.9256	547.0	0.8596	9.93345E-04	-0.1513
650.0	0.8871	604.0	0.6718	9.40115E-04	-0.3978
723.0	0.8552	663.0	0.5716	8.90710E-04	-0.5593
747.0	0.8434	680.0	0.5316	8.77424E-04	-0.6319
		498.0	1.1407	1.04417E-03	0.1316
		560.0	0.7962	9.80681E-04	-0.2279
		650.0	0.5530	9.01144E-04	-0.5925
		747.0	0.3991	8.28706E-04	-0.9187

SAMPLE	RHO SLOPE	S.D. SLOPE	R INTERCEPT	S.D. INTCPT
1L16	-0.45725E-03	0.36360E-05	0.11439E 01	0.20574E-02
1L27	-0.46631E-03	0.32456E-05	0.11579E 01	0.19098E-02
1L37	-0.45605E-03	0.62800E-05	0.11489E 01	0.38911E-02
1L47	-0.46464E-03	0.63013E-05	0.11684E 01	0.38930E-02
1L50	-0.42626E-03	0.90010E-05	0.11474E 01	0.48737E-02
1L51	-0.42869E-03	0.36644E-05	0.11488E 01	0.19470E-02
1L59	-0.41672E-03	0.66673E-05	0.11516E 01	0.39484E-02
1L62	-0.42882E-03	0.51201E-05	0.11649E 01	0.32903E-02

SAMPLE	MU SLOPE	S.D. SLOPE	M INTERCEPT	S.D. INTCPT	ACT. ENERGY
1L16	0.39480E 04	0.46718E 02	-0.47398E 01	0.47054E-01	0.43586E 01
1L27	0.39604E 04	0.12424E 02	-0.46742E 01	0.11870E-01	0.43723E 01
1L37	0.38731E 04	0.81773E 02	-0.44975E 01	0.76632E-01	0.42759E 01
1L47	0.41965E 04	0.28713E 02	-0.46988E 01	0.26899E-01	0.46329E 01
1L51	0.42486E 04	0.99613E 02	-0.46402E 01	0.10578E-00	0.46904E 01
1L59	0.41926E 04	0.15594E 03	-0.43762E 01	0.14906E-00	0.46286E 01
1L62	0.45267E 04	0.16228E 03	-0.46406E 01	0.15407E-00	0.49974E 01

TEMPERATURE	IRRAD SLOPE	S.D. SLOPE	IRRAD INTCP	S.D. INTCPT	CORR. COEF.
0.40000E 03	0.16874E-04	0.27041E-05	0.96289E 00	0.26538E-02	0.93086E 00
0.40000E 03	0.46896E-03	0.18710E-04	-0.17716E-00	0.18496E-01	0.99604E 00
0.50000E 03	0.19658E-04	0.20290E-05	0.91629E 00	0.19913E-02	0.96950E 00
0.50000E 03	0.42988E-03	0.16508E-04	-0.64690E 00	0.16319E-01	0.99633E 00
0.60000E 03	0.22442E-04	0.15233E-05	0.86970E 00	0.14950E-02	0.98646E 00
0.60000E 03	0.39818E-03	0.18351E-04	-0.10280E 01	0.18141E-01	0.99473E 00
0.70000E 03	0.25225E-04	0.13856E-05	0.82310E 00	0.13598E-02	0.99107E 00
0.70000E 03	0.37194E-03	0.21820E-04	-0.13433E 01	0.21570E-01	0.99151E 00
0.80000E 03	0.28009E-04	0.17054E-05	0.77651E 00	0.16737E-02	0.98906E 00
0.80000E 03	0.34987E-03	0.25567E-04	-0.16086E 01	0.25274E-01	0.98691E 00
0.12000E 04	0.39145E-04	0.45518E-05	0.59014E 00	0.44672E-02	0.96175E 00
0.12000E 04	0.28819E-03	0.37986E-04	-0.23501E 01	0.37551E-01	0.95921E 00

2. The number of pycnometer calibrations to be expected.
3. The number of viscometer calibrations to be expected.
4. The number of groups of samples to be run.
5. The number of temperatures at which the smoothed densities and viscosities will be calculated and printed.
6. A repeat control. If the variable is ≤ 0, the computer, when it is finished analyzing the number of groups of data specified, will go all the way back to the beginning again for more data. In this way, if calibrations or other "constant" information change over the course of time, new calibration data may be read in to update the calibration tables before calculating densities and viscosities which depend on the new calibrations. If the variable is > 0, the computer will halt after completing the number of groups specified.

The second table supplies the pycnometer calibration data in the form of the constants a and b in Eq. (A3.1). The intercept and slope for each pycnometer are given in order, and in cases where no pycnometer number exists, zeroes are substituted. Thus there will be a one-to-one correspondence between the actual pycnometer number and the pycnometer number used by the computer to denote the same calibration curve.

The viscometer calibration curves are to be supplied in the third table using the form of Eq. (A3.5) in the same manner as the pycnometers, with one exception:- there is not a one-to-one correspondence between actual viscometer numbers and numbers assigned the viscometers by the computer since the numbers are so large. For the viscometers used in this experiment, the correspondence was established by means of Table A3.6.

The fourth table is the final table supplying "constant" information before the sample data begin. This table supplies:

1. The conversion of temperatures to degrees absolute (usually 459.7).
2. The gas constant (1.104×10^{-3} kcal/(mole)(°R)).
3. The list of temperatures at which the smoothed data are to be calculated.

TABLE A3.6

Correspondence of Actual Viscometer Numbers to Those Used by VISDEN

Actual Viscometer Number	VISDEN Viscometer Number
--	1
N302	2
N303	3
N304	4
N305	5
N306	6
137	7
135	8
139	9
140	10

For each group of samples to be supplied, the following data must also be given before giving the sample data:-

1. A "free" card upon which any desired information may be written. The computer will reprint the information on this card at the head of the output.
2. A control table listing first the number of samples in the group, and second, a control constant controlling least squaring with respect to an independent variable. If the control constant is ≤ 0, there will be least squaring; if it is > 0, there will not be any least squaring. In the example given, the period of reactor operation in MWH was supplied on the sample data cards and least squaring was requested for the six mentioned temperatures versus MWH.

The data for each sample are preceeded by another table of constants giving the following information:

1. The number of density data points in the density run (there is an allowance for re-run data to be included, as shown below).

2. The density data point number at which the computer will begin including the data for a least squares analysis. For example, Table A3.4 for sample 1L27 shows that the first density data point given the computer will be calculated but not used in smoothing the data, and the second and onward will be used for smoothing.
3. The pycnometer number.

4., 5., and 6. A repeat of 1-3 for viscosity data.

7. The number of density data points in a re-run which will be lumped together with the other data given. Thus, the program has provisions for one run and one re-run to be analyzed together.
8. The density data point in the re-run data at which least squaring will cease. Thus, for example, Table A3.4 shows sample 1L16 with a density re-run in which all five data points are to be included in the analysis.
9. The pycnometer number for the re-run data. If there is no re-run, type zeroes for items 7-9.

10., 11., and 12. A repeat of 7-9 for viscosity data.

After this heading, the observed sample data will be presented in the following order:

1. The value of the independent variable (such as reactor MWH) at the time the sample was taken.
2. The weight of sample placed in the pycnometer.
3. Temperature-height data given in the form T_1, H_1, T_2, H_2, T_3, H_3, . . . A minimum of the three data points is assumed. In addition, the first data card will also contain in columns 72-78 the sample number (A6 format).
4. Following immediately after the last density data point, the weight of sample placed in the viscometer.
5. Following immediately after item no. 4, the temperature-efflux time data in the form T_1, t_1, T_2, t_2 . . . A minimum of two data points is assumed if data are supplied. If it is desired to run just density data for a sample, the computer still searches for an imaginary viscosity run containing one

data point, so in this case, one must be careful to leave enough room on the data cards for this imaginary run. Table A3.4 shows this for sample 1L50, in which one blank card is placed at the end to leave enough room for the computer search.

6. Re-run density data (if any) starting on a new card with the sample weight and the temperature-height data in the form T_1, H_1, T_2, H_2 . . . As little as one data point may be given.
7. Re-run viscosity data (if any) starting on a new card with the sample weight and the temperature efflux time data in the form T_1, t_1, T_2, t_2 . . . As little as one data point may be given.

If it is desired to run more than one group of data, the proper heading for each group must precede each group as described above. Finally, if it is desired to supply new calibration or other "constant" data after a certain number of groups of data (the repeat control being selected above), the format must be as described from the very beginning of the input description.

The output listing, as shown by example in Table A3.5, is almost self-evident. First, the listing of the results for the individual samples are given. The smoothed densities and viscosities are listed, followed by the individual data points. For the viscosity, the values of $1/T$ and $\ln \mu$ are also given. Next, the tabulation of the least squared parameters of Eqs. (A3.3) and (A3.7) and their standard deviations are given. Finally, the least squared slopes and intercepts are given for the density and viscosity data at a given temperature versus an independent variable (in the example, reactor MWH), respectively.

The loading time for the program is 0.15 minutes on an IBM type 7090 computer and an average running time is about 0.01 minutes per sample.

A3.4 Tabulation of Results of Density and Viscosity Measurements

The results produced by VISDEN for all the samples analyzed during the course of this experiment are given in Table 3.7 for the 610°F irradiation of Santowax OMP and in Table A3.8 for the 750°F irradiation of Santowax OMP, in terms of the least squared parameters of Eqs. (A3.3) and (A3.7).

TABLE A3.7

Densities and Viscosities of Irradiated Santowax OMP Samples for the 610°F Irradiation

Sample Number	Density, $\rho = A + BT$ gm/cc		Viscosity, $\mu = \mu_o e^{\frac{\Delta E}{RT}}$, cp	
	A, gm/cc	B, gm/(cc)(°F) $\times 10^4$	μ_o, cp	ΔE, $\frac{\text{kcal}}{\text{gmole}(°R)}$
1L16	1.144	4.573	0.00874	43.6
1L27	1.158	4.663	0.00933	43.7
1L37	1.149	4.561	0.0111	42.8
1L47	1.168	4.646	0.00911	46.3
1L50	1.147	4.263	--	--
1L51	1.149	4.287	0.00966	46.9
1L59	1.152	4.167	0.0126	46.3
1L62	1.165	4.288	0.00965	50.0
1L63	1.157	4.250	0.0107	47.0
1L74	1.160	4.207	0.0137	47.3
1L91	1.163	3.972	0.0123	51.6
1L95	1.162	3.995	0.0170	48.4
1L99	1.165	4.022	0.0103	53.8
1L116	1.166	3.898	0.0163	52.5
1L120	1.164	3.997	0.00942	55.7
1L121	1.165	3.985	--	--
1L123	1.158	3.969	0.0123	53.0
1L124	1.157	3.990	0.00761	57.5
1L134	1.153	3.884	0.00935	54.0
1L151	1.157	4.156	0.0150	46.8
1L159	1.160	4.122	0.0165	46.3
1L172	1.159	4.124	0.0143	47.7
1L180	1.160	4.152	--	--
1L186	1.161	4.234	0.0117	49.3
1L192	1.162	4.200	0.0156	46.8
1L208	1.165	4.114	0.0164	47.1
1L214	1.162	4.003	0.0158	48.0
1L231	1.151	4.016	0.0123	49.0

TABLE A3.7 (Concluded)

Densities and Viscosities of Irradiated Santowax OMP Samples for the 610°F Irradiation

Sample Number	Density, $\rho = A + BT$ gm/cc		Viscosity, $\mu = \mu_o e^{\frac{\Delta E}{RT}}$, cp	
	A, gm/cc	B, gm/(cc)(°F) $\times 10^4$	μ_o, cp	ΔE, $\frac{\text{kcal}}{\text{gmole}(°R)}$
1L245	1.167	4.071	0.0174	46.5
1L252	1.156	4.055	0.0106	52.0
1L254	1.171	4.179	0.0161	45.8
1L256	1.161	3.994	0.0129	49.2
1L258	1.164	4.179	0.0134	47.8
1L260	1.168	4.079	0.0144	47.4
1L262	1.164	4.167	0.0102	51.9
1L264	1.170	4.269	0.0114	50.1
1L266	1.170	4.205	0.0137	47.8
1L268	1.168	4.158	--	--
1L270	1.171	4.297	0.0110	50.2
1L278	1.179	4.216	0.0118	50.9

TABLE A3.8

Densities and Viscosities of Irradiated Santowax OMP Samples for the 750°F Irradiation

Sample Number	Density, $\rho = A + BT$ gm/cc		Viscosity, $\mu = \mu_o e^{\frac{\Delta E}{RT}}$, cp	
	A, gm/cc	B, gm/(cc)(°F)$\times 10^4$	μ_o, cp	ΔE, $\frac{\text{kcal}}{\text{gmole}(°R)}$
750°F irradiation charge	1.158	4.791	0.00874	43.5
2L1	1.144	4.565	0.00921	43.3
2L2	1.146	4.518	0.00860	44.5
2L5	1.144	4.485	0.00995	43.5
2L6	1.157	4.641	0.0103	43.9
2L7	1.159	4.541	0.0110	43.2
2L9	1.165	4.509	0.0112	43.9
2L10	1.160	4.405	0.0128	44.0
2L11	1.173	4.373	0.0118	46.6
2L12	1.163	4.390	0.0135	44.4
2L13	1.180	4.475	0.0155	44.6
2L14	1.176	4.222	0.0155	46.0
2L16	1.178	4.124	0.0128	50.3
2L17	1.179	4.043	0.0148	50.1
2L18	1.178	4.335	0.0123	48.3
2L19	1.177	4.351	--	--
2L22	1.158	4.162	0.0125	46.5
2L24	1.165	4.209	0.0176	42.7
2L26	1.168	4.346	0.0122	47.0
2L28	1.162	4.245	0.0130	46.1
2L31	1.166	4.332	0.0126	46.5
2L33	1.163	4.278	0.0132	46.1
2L36	1.167	4.343	0.00919	51.0
2L40	1.166	4.273	0.0148	45.0
2L41	1.165	4.385	0.0133	45.4

A3.5 Specific Heat and Thermal Conductivity Data

Tabulations of the specific heat measurements made on irradiated Santowax OMP samples at the Monsanto Research Corporation (Dayton, Ohio) (A3.4) and at Grenoble, France (A3.5) are given in Tables A3.9 and A3.10, respectively.

Error limits of ±1% have been assigned to the measurements made at Grenoble (A3.6), but no error limits have been quoted for the Monsanto measurements. These latter measurements were made using drop calorimetry.

The heat content of each sample was determined at three temperatures and the specific heat determined from the derivative of the parabolic fit to the heat content-temperature curve. Since three points uniquely determine a parabola, no statistical estimate of the error involved in the measurements on one sample can be obtained. Since there seems to be no trend of the C_p data with irradiation (see Section 5.4), an estimate of the error of the Monsanto measurements can be computed from the RMS deviation of the smoothed values from the average at each temperature. Using this procedure, the maximum RMS deviation occurred at 400°F and was 3.5%. Thus, it seems reasonable to assign an error of ±4% to the data obtained for each of the samples by Monsanto.

The results of the thermal conductivity measurements on samples of the 610 and 750°F irradiation, as determined at Grenoble (A3.5), are given in Table A3.11. The results are stated accurate to ±2%.

A3.6 Number Average Molecular Weight Measurements – Theory

The number average molecular weight measurements made at M.I.T. use a Mechrolab Model 301A osmometer[1], a sketch of which is shown in Fig. A3.4. The instrument consists of two principal units – the sample chamber assembly and the control unit. The sample chamber assembly is a urethane-insulated housing consisting of a sample chamber, solvent cup, two thermistors, a thermostat, and six syringe guideholes and holders. The control unit is composed of a null indicator, a wheatstone bridge and a heater input control circuit. Two syringes in the

[1]Mechrolab, Inc., Mountain View, Calif.

TABLE A3.9

Specific Heat Measurements on Samples from the 610°F and 750°F Irradiations of Santowax OMP by Monsanto Research Corporation

Sample Number	Temperature, °C	Heat Content, $\frac{cal}{gm}$	Specific Heat, $\frac{cal}{(gm)(°C)}$, at		
			400°F	600°F	800°F
	204.4	101.8			
1L4	315.5	160.1	0.505	0.544	0.582
	425.7	222.1			
	204.3	85.1			
1L62	315.5	144.3	0.505	0.560	0.614
	426.7	209.5			
	204.4	83.9			
1L63	315.6	141.2	0.483	0.547	0.610
	426.5	205.4			
	204.5	78.4			
1L116	315.7	137.3	0.504	0.555	0.607
	426.7	201.8			
	204.4	82.1			
1L267	315.7	139.3	0.478	0.551	0.624
	426.7	204.6			
Charge material 750°F irradiation	204.4	98.7			
	315.6	157.4	0.501	0.556	0.610
	426.7	222.2			
	204.4	74.5			
2L17	315.6	139.6	0.531	0.556	0.582
	426.7	203.2			
	204.5	81.3			
2L37	315.7	141.6	0.521	0.563	0.606
	426.8	206.6			

TABLE A3.10

Specific Heat Measurements at Grenoble on a Sample from the 610°F Irradiation of Santowax OMP

Sample:- 1L195 (23.7 w/o) + 1L278 (76.3 w/o)

Temperature, °F	Specific Heat, $\frac{\text{cal}}{(\text{gm})(°\text{C})}$
374	0.490
504	0.527
608	0.551
651	0.561
766	0.595

TABLE A3.11

Thermal Conductivity Measurements on Samples of the 610°F and 750°F Irradiation of Santowax OMP at Grenoble

Sample Number	Temperature, °F	k, $\frac{\text{cal}}{(\text{cm})(\text{sec})(°\text{C})} \times 10^4$
1L192	446	2.95
	540	2.76
	615	2.66
1L278	435	3.24
	569	3.06
	662	2.96
Charge to 750°F irradiation	381	3.35
	540	3.20
	684	3.00

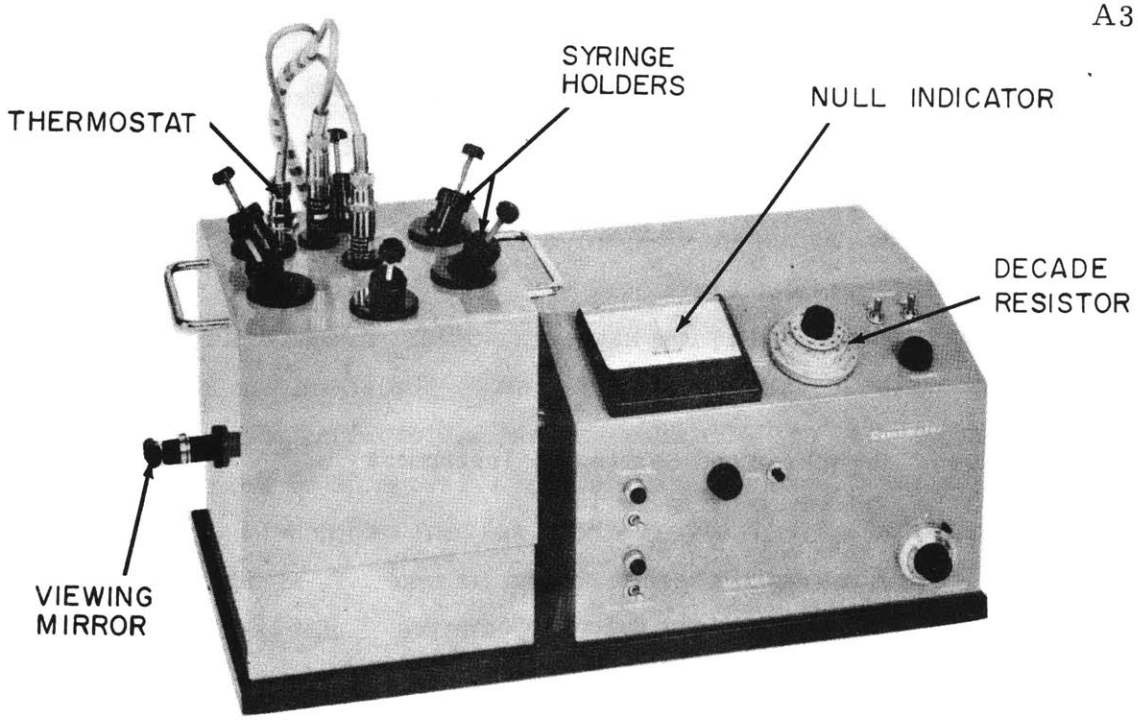

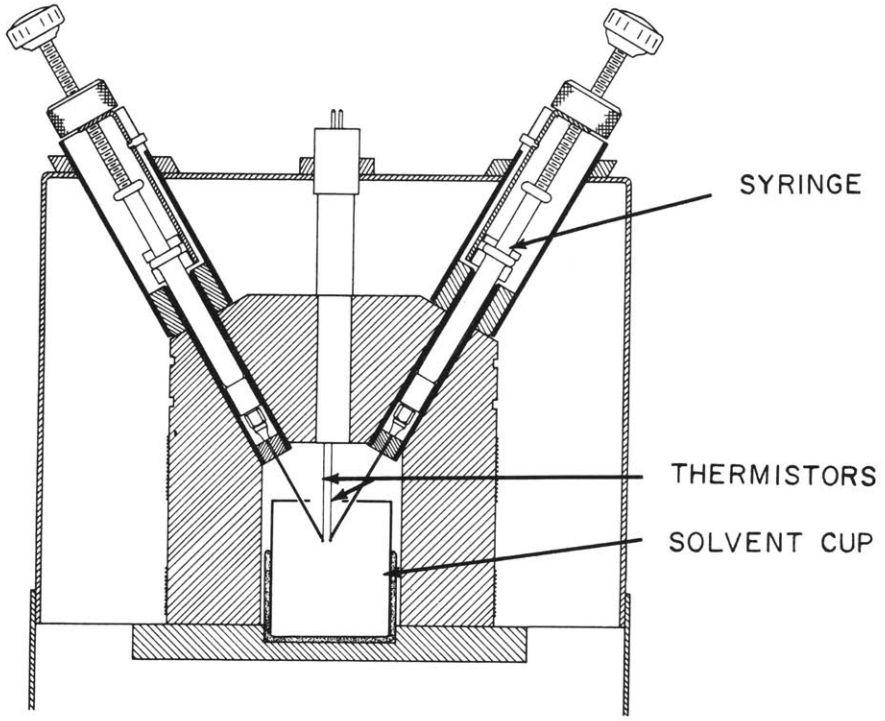

FIGURE A3.4 MECHROLAB MODEL 301A OSMOMETER

sample chamber assembly contain the solvent, and the other four hold standards if a calibration is in progress, or samples if molecular weights are being determined. One of the solvent syringes is used to place a solvent drop on the reference thermistor and the other is used to rinse the sample thermistor between measurements.

When a measurement is being made, a solvent drop is placed on the reference thermistor, and a solution drop is placed on the sample thermistor. The solvent cup contains solvent material to saturate the sample chamber atmosphere. Since the vapor pressure of the solution drop is lower than that of the solvent drop, solvent vapor will condense on the solution drop, causing its temperature to rise. In an ideal situation, the temperature rise is given by the Clausius-Clapeyron equation:

$$\Delta T = \frac{RT^2}{\lambda} \cdot \frac{c}{1000} \qquad \text{(A3.9)}$$

where

R is the gas constant

λ is the heat of vaporization per grams of solvent

c is the molality of the solution.

In the real case, the temperature rise will be somewhat smaller, due to heat losses, but ΔT and c are still related in a linear manner (A3.7). Thus, since the temperature rise increases the sample thermistor resistance in a linear manner, the change in thermistor resistance is directly proportional to the molality of the solution. A wheatstone bridge circuit is used to measure changes in the thermistor resistance. Pasternak et al. (A3.7) have found a linear relation between the resistance change, ΔR, and sample concentration to hold over the range 0.01 to 0.1 m.

The relation between ΔR and c for the instrument used was established through a series of calibration experiments in which three standards (diphenyl, triphenylmethane and p-terphenyl) were dissolved in reagent grade tetrahydrofuran (THF) at various concentrations. [1] These calibration experiments were performed periodically to check the calibration curve. A typical calibration curve is shown in Fig. A3.5. This curve was used for the samples of the 750°F irradiation. The data were fit to a linear relation by the method of least squares (see

1. THF was the solvent used for the molecular weight samples.

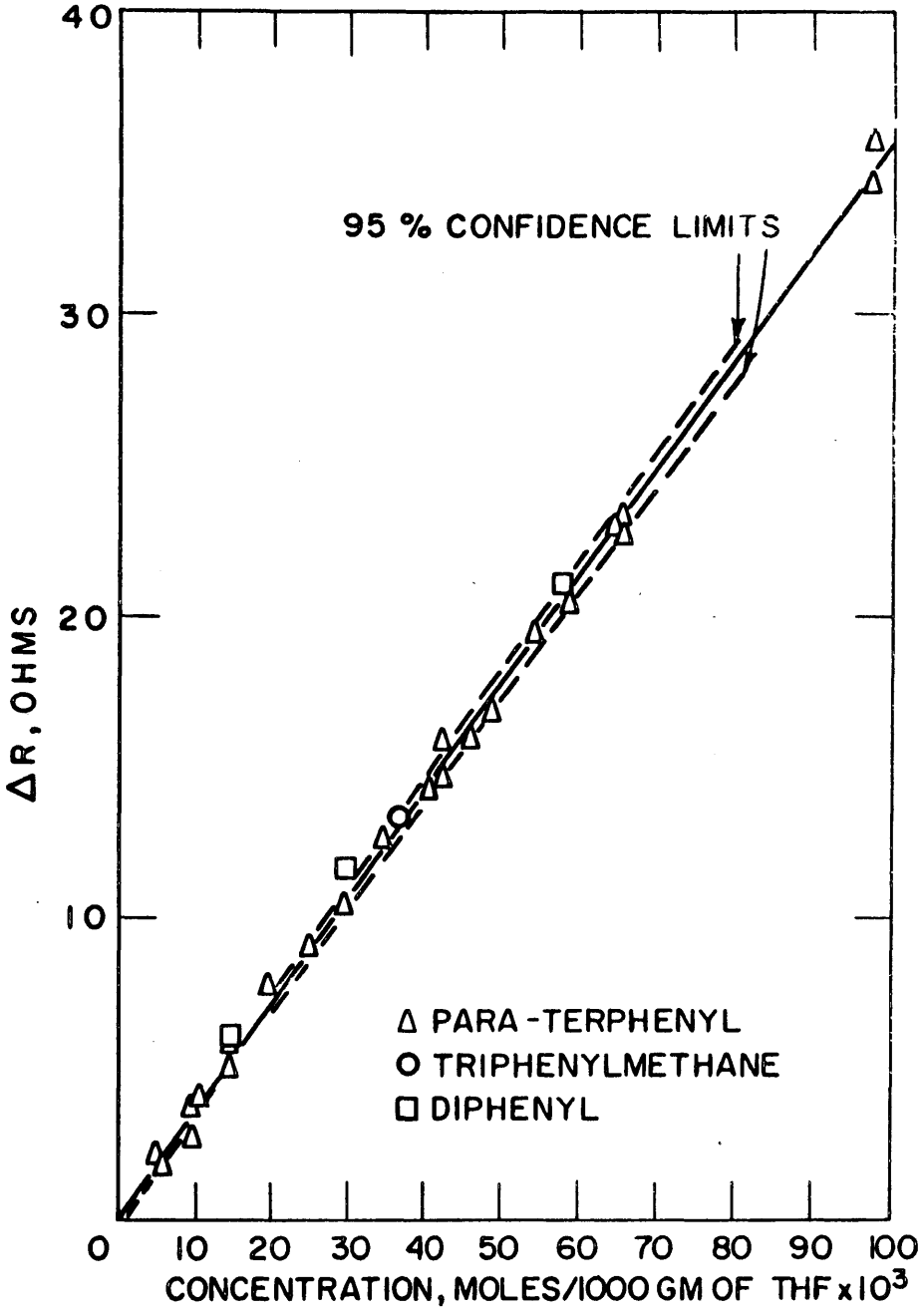

FIGURE A3.5 OSMOMETER CALIBRATION CURVE FOR 750°F IRRADIATION SAMPLES

Section A2.6) and the resulting equation for these data was

$$\Delta R = 0.23 + 354\,c \qquad \text{(A3.10)}$$

ΔR in ohms

c in moles/1000 g of THF

The intercept of the equation is not zero, even though the instrument was zeroed prior to each measurement. Subsequent calibrations, using dilute solutions (<0.01 m), showed the intercept to be zero, and so the osmometer seems to be non-linear for concentrations less than 0.01 m. Thus, all sample solutions were made with concentrations between 0.01 m and 0.1 m.

Once the calibration curve is obtained, the molality of a sample solution may be calculated from the measured resistance change of the sample thermistor. Knowing the molality and the number of grams of sample used to make up the solution, the number average molecular weight may be obtained from the relation

$$MW_N = \frac{W}{1000c} \qquad \text{(A3.11)}$$

where

W is the sample weight, grams

c is the calculated solution molality (Eq. (A3.10)).

This number average molecular weight is also defined by

$$MW_N = \frac{\Sigma C_i}{\Sigma C_i / A_i} \qquad \text{(A3.12)}$$

where

C_i is the weight fraction of component i in the mixture

and

A_i is the molecular weight of component i.

Analysis of the osmometer operation and sample preparation indicate two significant sources of error. These are insolubility effects and errors in the osmometer itself. When a dilute solution of an HB sample was placed in the path of a strong light, a Tyndall beam was easily observed, indicating a colloidal suspension of an insoluble fraction of the sample. This insoluble fraction has been estimated at about 2 w/o of the total sample. Equation (A3.12) may be split into the soluble and insoluble portions as follows:

$$MW_N = \frac{\Sigma C_i^{sol} + a}{\sum \frac{C_i^{sol}}{A_i} + \frac{a}{A_a}} \qquad (A3.13)$$

where a is the insoluble fraction, having a molecular weight of A_a. It can be seen from Eq. (A3.13) that if the molecular weight of the insoluble fraction is very large (about a factor of 100 higher) in comparison with the other A_i, the number average molecular weight calculated will be essentially correct, in spite of the insoluble fraction. If A_a is of the same order as the other A_i, an error of the order of the per cent insolubility will be committed in computing the number average molecular weight. However, if the insoluble fraction has a lower molecular weight than A_i, a large error in MW_N could result. Plus 2% is assumed as an error estimate for the error due to insolubility.

Significant osmometer errors are: the error in the calibration curve, and the random error in each measurement. A statistical analysis applied to the calibration curve shown in Fig. A3.5 gives a standard deviation of ±1.5% at the mean of the resistance readings measured. In the measurements on each sample, ΔR readings are taken until consecutive readings agree with ±1%.

Thus, applying the propagation of variances rule, the error in each number average molecular weight determined is estimated at +3% to −2%.

A3.7 Tabulation of Number Average Molecular Weight Data

The results of the number average molecular weight measurements made at M.I.T. and at the Monsanto Research Corporation (Everett, Mass.) for samples from the 610°F and 750°F irradiations are tabulated in Tables A3.12 and A3.13, respectively. The bottoms (HB) analyses were corrected for the small (usually less than 1 w/o) m- and p-terphenyl in the bottoms.

Using Eq. (A3.12), the uncorrected number average molecular weight of the bottoms may be written as

$$MW_N^{uncorrected} = \frac{\Sigma C_i + y}{\sum \frac{C_i}{A_i} + \frac{y}{230}} \qquad (A3.14)$$

TABLE A3.12

Number Average Molecular Weight, Coolant Melting Point and Carbon-Hydrogen Content of Samples from the 610°F Irradiation of Santowax OMP

SAMPLE NUMBER	NUMBER AVERAGE MOLECULAR WEIGHT				COOLANT MELTING POINT		C-H CONTENT	
	MIT ANALYSES		MONSANTO ANALYSES		INITIAL LIQUIDUS POINT, °F	FINAL LIQUIDUS POINT, °F	CARBON W/O	HYDROGEN W/O
	COOLANT	BOTTOMS	COOLANT	BOTTOMS				
1L16					167	340	93.8	6.2
1L24			238		165-169	333	94.2	5.9
1L27					145	322	94.1	6.1
1L28					135-145	329		
1L35			261				94.3	5.8
1L47			263				93.8	6.0
1L50			278		145	307	93.7	6.3
1L51			266		138-144	302	94.3	5.9
1L59					135-142	284		
1L62					134-138	280		
1L66			285				94.2	5.9
1L74					122-131	248-257		
1L82	296				100-109	282		
1L91							94.0	6.0
1L92					104-109	286		
1L99	346				113	270		
1L111							94.5	5.7
1L116			340		102	262		
1L120					77	282		
1L123					106	275		
1L134							94.3	5.9
1L137		834	321	660	82-104	277		
1L151		750		712	86-100	266		
1L152		806		690				
1L159		773		656	90-104	270		
1L160		762	303	679			93.9	6.1
1L167		774			86-108	230-259		
1L172		749		576				
1L176		832			97-104	268		
1L180		790						
1L183		820	312		81-93	273	94.3	5.9
1L192		836						
1L195					84-97	280		
1L214					86-97	275	94.2	5.9
1L231					90-102	289		
1L245					88-100	289		
1L251		682						
1L252		672			81-95	282	94.3	6.1
1L253		691	315					
1L254		679						
1L255		701					94.2	6.1

TABLE A3.12 (Concluded)
Number Average Molecular Weight, Coolant Melting Point and Carbon-Hydrogen Content of Samples from the 610°F Irradiation of Santowax OMP

SAMPLE NUMBER	NUMBER AVERAGE MOLECULAR WEIGHT				COOLANT MELTING POINT		C-H CONTENT	
	MIT ANALYSES		MONSANTO ANALYSES		INITIAL LIQUIDUS POINT, °F	FINAL LIQUIDUS POINT, °F	CARBON W/O	HYDROGEN W/O
	COOLANT	BOTTOMS	COOLANT	BOTTOMS				
1L256		697						
1L257		647	300					
1L258		658						
1L259		652						
1L260			307				94.1	6.1
1L261		646						
1L262	297	678						
1L263	309	712	670					
1L264	302	696						
1L265	304	752	276	611			94.2	5.9
1L266	296	751						
1L267	302	741						
1L268		705						
1L269		632		720				
1L270		652						
1L271		669						
1L272	325							
1L273	304							

A3.38

TABLE A3.13

Number Average Molecular Weight, Coolant Melting Point and Carbon-Hydrogen Content of Samples from the 750°F Irradiation of Santowax OMP

SAMPLE NUMBER	NUMBER AVERAGE MOLECULAR WEIGHT				COOLANT MELTING POINT		C-H CONTENT	
	MIT ANALYSES		MONSANTO ANALYSES		INITIAL LIQUIDUS POINT, °F	FINAL LIQUIDUS POINT, °F	CARBON W/O	HYDROGEN W/O
	COOLANT	BOTTOMS	COOLANT	BOTTOMS				
2L1	229		232		163	322	93.9	6.1
2L2	229							
2L3	236							
2L4	244							
2L5					144	325		
2L6	241							
2L7	240							
2L8	299							
2L9					100	264		
2L10	266							
2L11	280							
2L12	273							
2L13	301							
2L14	307							
2L17	341				<72(Room temp.)	261		
2L18	284	561	295	616			94.3	5.7
2L22	289	568	273	730	<81(Room temp.)	270	94.2	5.5
2L24	287	567	262					
2L25			265					
2L26	290	563	272	563	<82(Room temp.)	273		
2L28	276	586	279	594				
2L29			275					
2L31	282		271	580	<81(Room temp.)	273	93.3	5.8
2L32			274					
2L33	282	582	278					
2L36	287	587					94.2	5.9

where y is the weight fraction terphenyl in the bottoms sample and C_i is the weight fraction of component i (i not terphenyl). What is desired is the corrected value

$$MW_N^{corrected} = \frac{\Sigma C_i}{\sum \frac{C_i}{A_i}} \qquad (A3.15)$$

By combining Eqs. (A3.14) and (A3.15), remembering that $\Sigma C_i = 1$, there results

$$MW_N^{corrected} = \frac{1 - y}{\left[\frac{1}{MW_N^{uncorrected}} - \frac{1}{230}\right]} \qquad (A3.16)$$

Normally, the effect of the correction for terphenyls was to increase the MW_N of the HB fraction by about 3%.

A3.8 Tabulation of Coolant Melting Point Data

The initial and final liquidus points determined by a Fisher-Johns apparatus (A3.1) on samples of the 610°F and 750°F irradiations of Santowax OMP are given in Tables A3.12 and A3.13, respectively. For some of the samples, a melting range is given, due to the uncertainty in visual observation.

A3.9 Tabulation of Carbon-Hydrogen Content Data

The carbon-hydrogen content of irradiated Santowax OMP samples have been measured by the Monsanto Research Corporation (Everett, Mass.) using a standard combustion technique. The stated accuracy is ±0.5 w/o (A3.1). The results of these measurements for 610°F irradiation and 750°F irradiation samples are listed in Tables A3.12 and A3.13, respectively.

A3.10 Tabulation of Ash and Semi-Quantitative Emission Spectroscopy Analyses

The Monsanto Research Corporation (Dayton, Ohio) has performed ash and semi-quantitative emission spectroscopy analyses on irradiated samples of Santowax OMP, and the results of their analyses for 610°F

irradiation and 750°F irradiation samples are tabulated in Table A3.14. The conditions for ashing were 1000°C for 90 minutes, and the ash analyses have a probable accuracy of ±100 ppm.

TABLE A3.14

Ash and Semi-Quantitative Emission Spectroscopy Analyses

on Irradiated Santowax OMP Samples from the 610°F and 750°F Irradiations

Sample Number	Reactor MWH	Concentration of Inorganic Material, ppm (by wt.)											Ash ppm
		Al	Cr	Cu	Fe	Mg	Mn	Mo	Na	Ni	Si	Ti	
1L35	392	<2				<2		1-3			3-9		90
1L47	816	3-8		<2	1-2	4-12		<2	13-39	<3	15-150		400
1L50	930	1-4	1-4	<2	2-7	7-21	<1		6-17	<5	28-57		200
1L51	1076	<2	<2	<2	2-6	<2			<4		3-10		30
1L66	1793	1-3		<1	1-3	<1	trace	<1			2-5		20
1L91	2869	3-8		2-5	2-5	2-5		<3			14-42		80
1L116	3839	2-4			2-7	<3	<3		<3		2-7		15
1L134	4476	2-4		1-3	<2					<2	1-3		10
1L159	5179	2-6			2-6	<3	<3		3-8		8-24		70
1L180	5785	3-8		3-8	3-8	<3	<3		3-9		9-28		20
1L214	6928	2-4		2-7	2-7	<3	<3		2-4		2-7		5
1L265	9979	<2		<2	1-3	<2				<2	2-5	2-5	0
1L269	10579	<2		2-5	<2	<2	<2			<2	2-5		0
2L1	0	<3		<3	9-27	<3				2-7	3-9	<3	30
2L5	253	2-5		2-5	3-8	2-6				2-5	5-15		20
2L18	2060	<4		<4	4-13	<4				<4	18-45		50
2L22	2278	<3		<3	2-5	<3				<3	8-25		40
2L26	2618	<4		<4	2-6	<4				<4	11-32		10
2L31	3000	<4		<4	4-12	<4				2-6	8-23		20
2L32	3200	3-9		<4	4-12	<4				2-7	12-35		20
2L36	3445	<3		<3	3-9	<3				2-6	6-19		20

APPENDIX A4
HEAT TRANSFER

A4.1 Determination of Heat Transfer Coefficients – Theory

The techniques used in the report for determining heat transfer coefficients are, with minor modifications, the same as those reported by Swierzawski (A4.1) and Morgan and Mason (A4.2). This section summarizes the theory used.

The heat transfer coefficient determined was the local coefficient from the inside test heater wall to organic coolant, defined by

$$U = \frac{dQ_{in}}{dA\left(T_W^I - T_B\right)} \tag{A4.1}$$

where

dQ_{in} is the heat transfer rate into the coolant for a differential length of test heater, Btu/hr

dA is the differential inside wall surface through which the heat flows, ft^2

T_W^I is the temperature of the inside surface of the test heater wall at the differential element, °F

T_B is the coolant bulk temperature at the differential element, °F.

Morgan and Mason (A4.2) have shown that except near the electrodes of the test heater, the temperature difference is constant along the test heater length, and that dQ and dA can also be considered constant (see Fig. A4.1). Thus, Eq. (A4.1) is equivalent to the average heat transfer coefficient:

$$U = \frac{Q_{in}}{A\left(\overline{T_W^I} - \overline{T_B}\right)} \tag{A4.2}$$

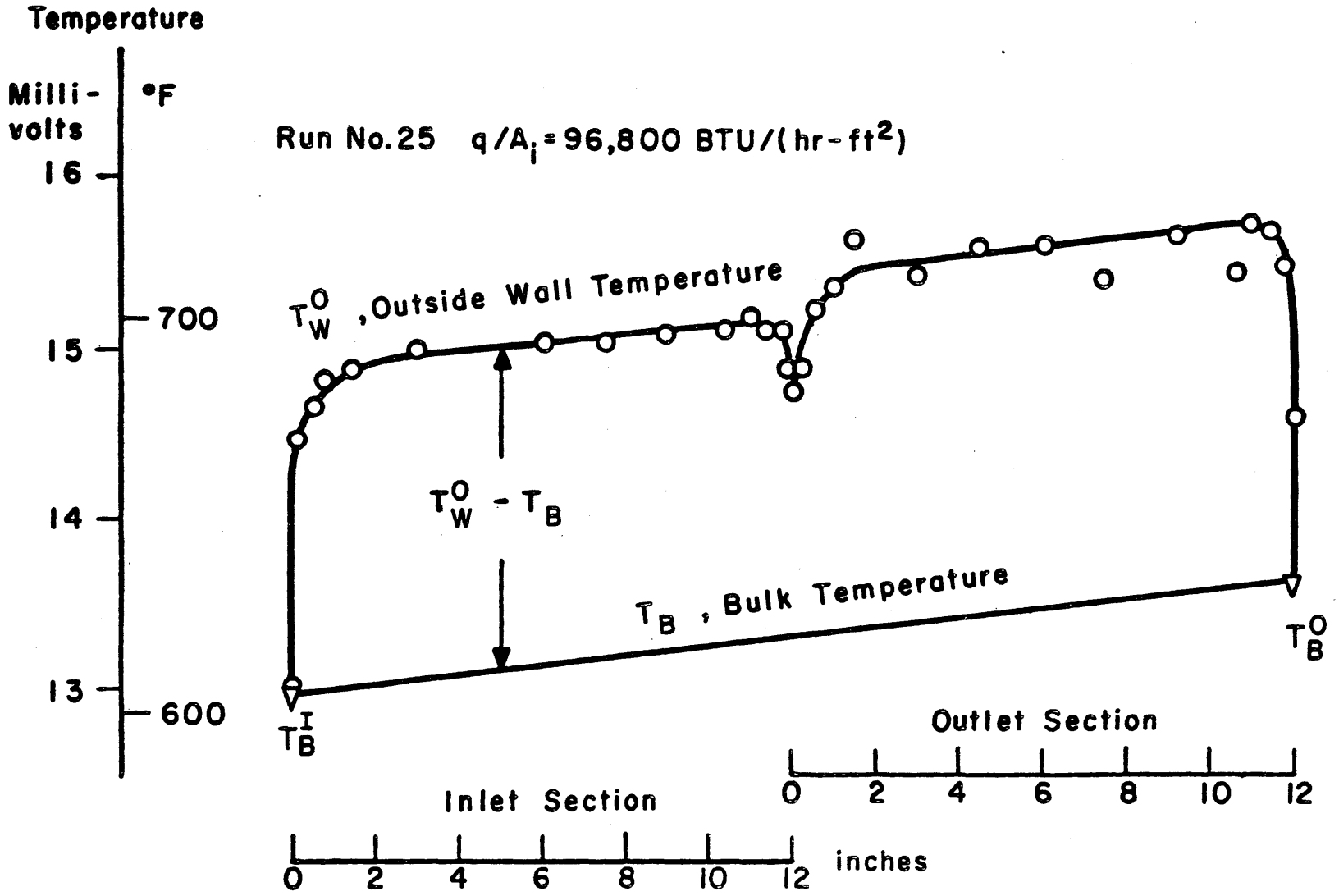

FIGURE A4.1 TYPICAL TEST HEATER TEMPERATURE PROFILE

Both the test heaters used for this report (TH5 and TH6) were divided electrically into two halves by the flow of current from the center electrodes to the end electrodes, so the analysis for the determination of $\left(\overline{T_W^I}-\overline{T_B}\right)$ and Q, which will be described, was applied to each section of the test heater separately. Normally, only the data for the upstream half heater were used in the correlation described below, since the downstream half heater wall thermocouples yield temperatures which were more scattered than those for the upstream half heater.

The thermocouples on the test heaters were attached by spot welding to the outside of the test heater walls. These thermocouples were calibrated relative to the bulk inlet immersion thermocouples with each of the test heaters in place in the hydraulic console. After the calibration experiment, TH6 was removed to provide a sampling position at the loop and TH5 was used initially for the heat transfer measurements. Unfortunately, two sources of error arise from these calibrations. First, the thermocouples were only calibrated to a wall temperature of 750°F and measurements were made to a wall temperature of 900°F, so that the curves had to be extrapolated. Second, on November 10, 1961, after about three months of operation, TH5 had to be removed and replaced by TH6 because of a coking accident. However, TH6 had previously been calibrated using the TH6 inlet immersion thermocouple, but was placed in the TH5 position on November 10, 1961. An unknown (but certainly less than 5%) error was introduced by the change as it was assumed that the response of the TH5 and TH6 inlet thermocouples was the same, and the previous TH6 calibrations were used for TH6.

For each section of the test heater, a smoothed curve was drawn through the corrected outside wall temperature profile and the average outside wall temperature, T_W^O, for each half section was calculated, but it was desired to have the average inside wall temperature, T_W^I. This temperature profile may be calculated from the theoretical relation (A4.2):

$$\overline{T_W^I} = \overline{T_W^O} - \frac{1}{k_s L}\left[\frac{Q}{2\pi\left[1-\left(\frac{r_I}{r_O}\right)^2\right]}\left(\left(\frac{r_I}{r_O}\right)^2 - 1 - 2\ln\frac{r_I}{r_O}\right) + \frac{Q_{loss}}{\pi}\ln\left(\frac{r_I}{r_O}\right)\right] \quad \text{(A4.3)}$$

where

k_s is the thermal conductivity at the test heater section evaluated at the average outside wall temperature, $\overline{T_W^O}$

L is the total test heater length (24 inches for this experiment)

r_I is the inner radius of the test heater section

r_O is the outer radius of the test heater section

Q is the heat produced in the half section of the test heater (see below)

Q_{loss} is the heat lost in the half section of the test heater (see below).

The data for k_s were taken from McAdams (A4.3) who shows a linear dependence of k_s on temperature. Equation (A4.3) differs from that derived by Morgan and Mason (A4.2) only in that the coefficient of Q_{loss} has been exactly doubled. This is because, for the reported calibrations, it was assumed that at infinite fluid velocity the inside and outside wall temperature were equal, which is true only if there is no heat loss. It was found easier to correct this error in Eq. (A4.3) than to change all of the calibrations. Substituting the dimensions of the test heaters into Eq. (A4.3), there results

$$\overline{T_W^I} = \overline{T_W^O} - \frac{1}{k_s L}\left[1.22\,Q - 4.61\,Q_{loss}\right] \qquad \text{(A4.4)}$$

with

k_s in Btu/(hr)(ft)(°F)

L in inches

Q, Q_{loss} in watts

$\overline{T_W^I}$, $\overline{T_W^O}$ in °F.

The average bulk temperature of the coolant in each half section was calculated from

$$\overline{T_B} = T_B^I + \frac{Q_{in}^U}{Q_{in}^U + Q_{in}^D}\left(T_B^O - T_B^I\right) \tag{A4.5}$$

$$\overline{T_B^U} = \frac{1}{2}\left(\overline{T_B} + T_B^I\right) \tag{A4.6}$$

$$\overline{T_B^D} = \frac{1}{2}\left(\overline{T_B} + T_B^O\right) \tag{A4.7}$$

where

T_B^I is the inlet bulk temperature

T_B^O is the outlet bulk temperature

Q_{in}^U is the heat transferred to the coolant in the upstream half of the test heater (see below)

Q_{in}^D is the heat transferred to the coolant in the downstream half of the test heater (see below)

$\overline{T_B^U}$ is the average bulk temperature in the upstream section of the test heater

$\overline{T_B^D}$ is the average bulk temperature in the downstream section of the test heater.

so that, with the aid of Eqs. (A4.4) and (A4.5), the desired temperature difference $\left(\overline{T_W^I} - \overline{T_B}\right)$ was calculated for each half of the test heaters from the measured temperature profile.

The heat transferred to the fluid for each half section of the test heater was calculated from

$$Q_{in} = \frac{\Delta V^2}{R} - Q_{loss} = Q - Q_{loss} \tag{A4.8}$$

where

ΔV is the measured voltage drop across the section

R is the resistance of the test heater section evaluated at the mean outside wall temperature

Q_{loss} is the heat loss in the test heater section evaluated at the mean outside wall temperature.

Test heater resistance and heat loss measurements as a function of temperature have been reported by Morgan and Mason (A4.2). The heat loss measurements have been corrected for the use of more recent specific heat data for the coolant. As a check on Eq. (A4.8), the heat input to the coolant for each half section was also calculated from

$$Q_{th}^{U} = 146.8\ G\rho C_p\left(\overline{T_B} - T_B^I\right) \tag{A4.9}$$

$$Q_{th}^{D} = 146.8\ G\rho C_p\left(T_B^O - \overline{T_B}\right) \tag{A4.10}$$

where

G is the volumetric flow rate of the coolant in the test heater

ρ is the coolant density evaluated at the mean bulk temperature of the half section, gm/cc

C_p is the coolant specific heat at the mean bulk temperature of the half section, cal/(gm)(°C)

T's in °F

Q_{th} in watts.

Knowing the temperature difference $\left(\overline{T_W^I} - \overline{T_B}\right)$, the heat input Q_{in} and the geometry of the test heater, the heat transfer coefficient was calculated from

$$U = \left[\frac{Q_{in}}{\left(\overline{T_W^I} - \overline{T_B}\right)}\right]\left[\frac{312.9}{DL}\right]\frac{Btu}{(hr)(ft^2)(°F)} \tag{A4.11}$$

where

D is the inner diameter of the test heater, inches

Q is in watts

$\overline{T_W^I}$, $\overline{T_B}$'s in °F

L is the total test heater length, inches.

Morgan and Mason (A4.2) estimated the over-all error in the measurement of U to be about 10% for measurements with Q/A larger than 100,000 Btu/(hr)(ft^2). As the heat flux is lowered below this value, uncertainties in the calibrations and heat losses become more important and may lead to larger errors.

A4.2 Determination of Flow Rates and Film Heat Transfer Coefficients

In Section A4.1, the equations used for the determination of the over-all heat transfer coefficient, U, from the inside of the test heater wall to the coolant were developed. It is desirable to know the film heat transfer coefficient, h_f, as a function of the coolant velocity, in order to develop dimensionless relations valid for other heat transfer geometries.

The coolant velocity was determined from the volumetric flow rate measured by a Potter turbine flowmeter (A4.2). Calibration experiments on the flowmeter were performed using water and methanol at room temperature, and the calibrations agreed closely with that supplied by the manufacturer. Morgan and Mason (A4.2) estimate that the combined effect of viscosity, density and elevated temperature on the flowmeter may produce an error of only about 1%, which is better than the accuracy with which the flowmeter can be read. The calibration used for the instrument was

$$G_{actual} = (1.05\, G_{measured} + 0.01) \text{ gpm} \tag{A4.12}$$

The velocity in the test heater was calculated from

$$v = 0.409 \frac{G_{actual}}{D^2} \text{ ft/sec} \tag{A4.13}$$

D in inches.

The film heat transfer coefficient, h_f, is equal to U if there is no scale on the heat transfer surface. One method of determining the scale resistance is due to Wilson (A4.2). The relation between U and h_f may be written as

$$\frac{1}{U} = \frac{1}{h_f} + R_s \tag{A4.14}$$

The film heat transfer coefficient is related to the fluid velocity by (A4.3):

$$h_f = a v^B (0.8<B<1.0) \tag{A4.15}$$

Thus, by plotting $1/U$ versus $1/v^B$ and extrapolating to infinite velocity, the scale resistance is given as the intercept. The computer program

MNHTR, described in Section A4.5, performs this analysis by fitting the set of data taken at different velocities on a given day to Eq. (A4.14) by the method of least squares (see Section A2.6), using the value of B determined by the computer for the over-all correlation of the heat transfer data. (U is assumed equal to h_f for a first approximation in the correlation. Corrections may be applied in further iterations if required.)

A second method is provided by the insertion of TH6 into the system after three months of operation (see above). Any change in U observed between the pre-coked TH5 and TH6 could be attributed to a scale buildup since very little change in physical properties occurred during the change-over. As reported in Section 6.4, no significant scale buildup has been observed by either method, so that h_f was equated to U for this work.

A4.3 Correlation of Heat Transfer Data

As reported in Section 6.2, the heat transfer rates were correlated with the physical properties of the coolant by an equation of the type:

$$Nu = ARe^{B}Pr^{C}\left(\frac{\mu}{\mu_W}\right)^{D} \qquad (A4.16)$$

where

$$Nu = \text{Nusselt number} = \frac{h_f D}{k}$$

$$Re = \text{Reynolds number} = \frac{Dv\rho}{\mu}$$

$$Pr = \text{Prandtl number} = \frac{C_p \mu}{k}.$$

μ is the viscosity evaluated at the inside wall surface temperature. All physical properties except μ_W were evaluated at the bulk fluid temperature. The heat transfer coefficient, h_f, and the fluid velocity, v, were measured at the loop, and the physical properties were determined from measurements made on samples from the loop. These data have been reported in Chapter 5 as a function of per cent degradation products in the coolant, but it is more convenient to know the physical properties as a function of the period of reactor operation in MWH (it is assumed that the properties do not change when the reactor is not operating), in order

to calculate the physical properties at the time of the heat transfer measurements. Figures A4.2, A4.3 and A4.4 show the density, viscosity, and thermal conductivity data, respectively, as a function of reactor MWH for the 610°F irradiation of Santowax OMP; and Figures A4.5, A4.6 and A4.7 show the same for the 750°F irradiation of Santowax OMP. For interpolation in temperature, the linear dependence of the properties reported in Chapter 5 was employed as follows:

$$\rho = a + bT \tag{A4.17}$$

$$\ln \mu = c + d/(T+460.) \tag{A4.18}$$

$$k = e + fT \tag{A4.19}$$

The specific heat measurements show no change with irradiation and the data of Chapter 5 may be used directly. The dependence on temperature was taken as

$$C_p = g + hT \tag{A4.20}$$

Thermal conductivity measurements were made only on three samples at two DP concentrations for the 610°F irradiation of Santowax OMP, and so the MWH dependence of these data was calculated from the variation of the DP concentration with MWH. The density and viscosity measurements, however, were made on many samples covering the entire periods of irradiation, so the MWH dependence could be determined directly from the measurements on each sample. These measurements are tabulated in Section A3.4 and the smoothed values at each temperature are shown on the figures. In order to calculate the viscosity at the inside wall surface temperature, the viscosity data listed in Section A3.4 were extrapolated to 1200°F.

A4.4 Statistics of Heat Transfer Correlations

Equation (A4.16) may be written in linear form by taking logarithms of both sides:

$$\ln Nu = \ln A + B \ln Re + C \ln Pr + D \ln \left(\frac{\mu}{\mu_W}\right) \tag{A4.21}$$

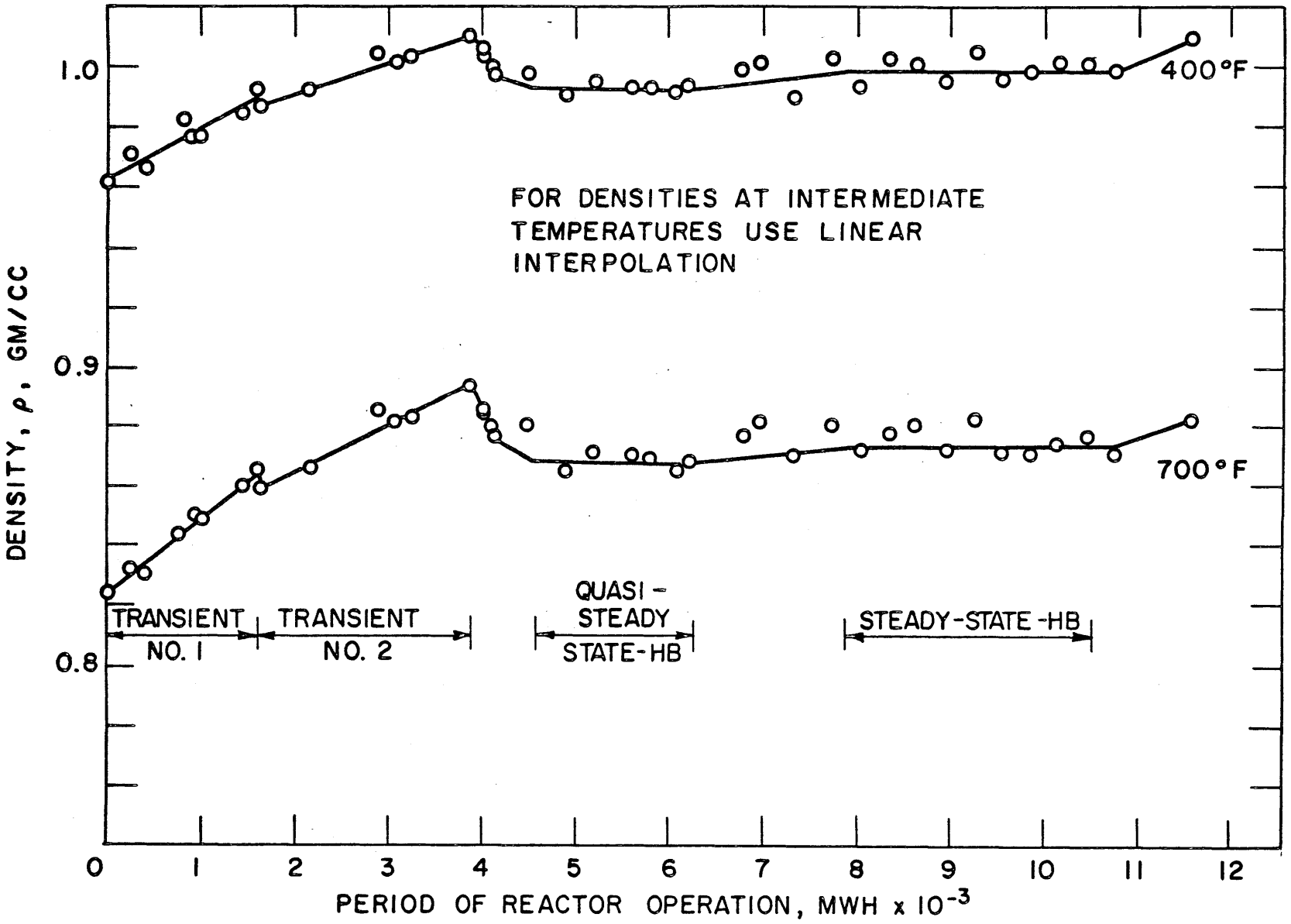

FIGURE A4.2 DENSITY OF IRRADIATED SANTOWAX OMP DURING THE 610°F IRRADIATION

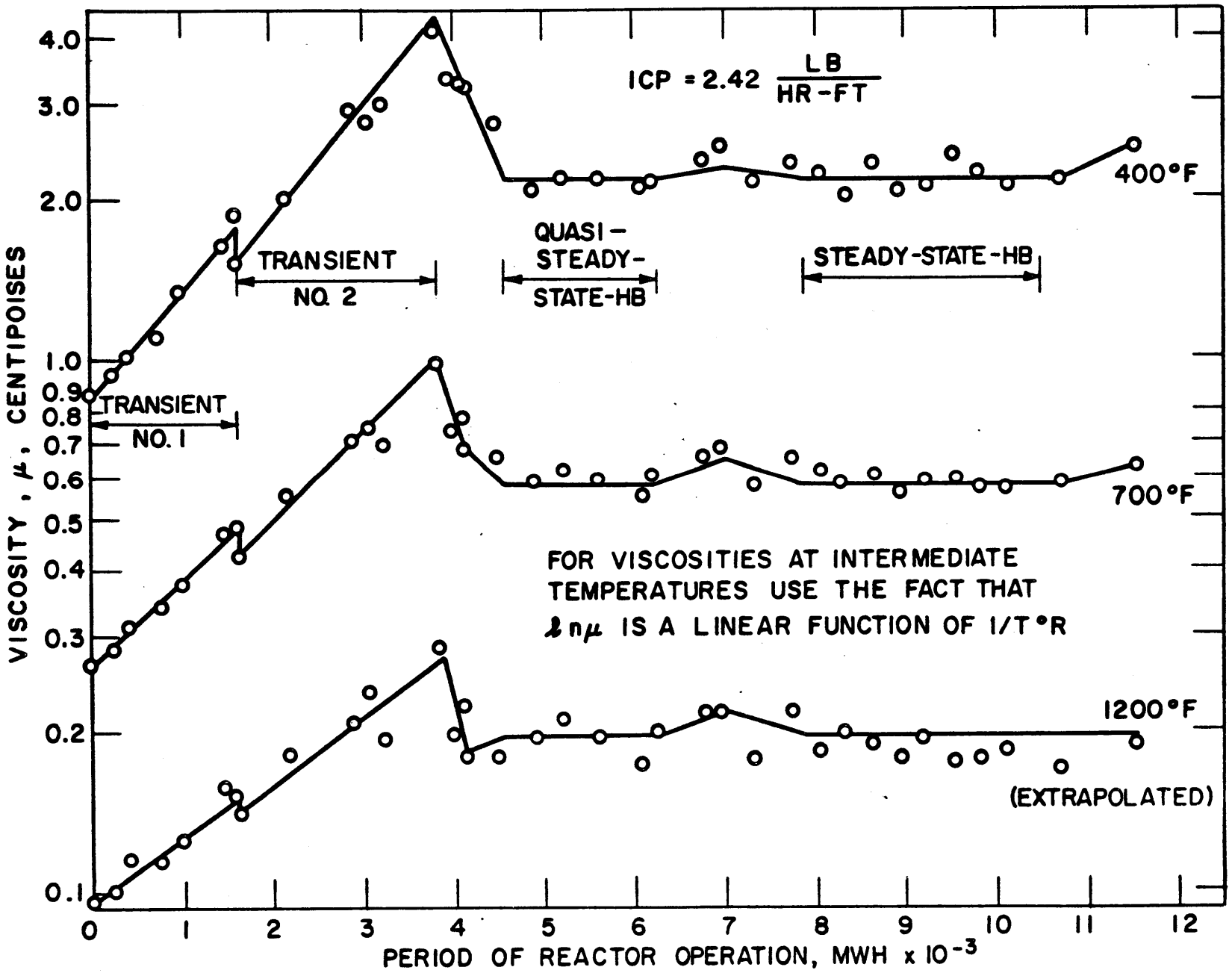

A4.11

FIGURE A4.3 VISCOSITY OF IRRADIATED SANTOWAX OMP DURING THE 610°F IRRADIATION

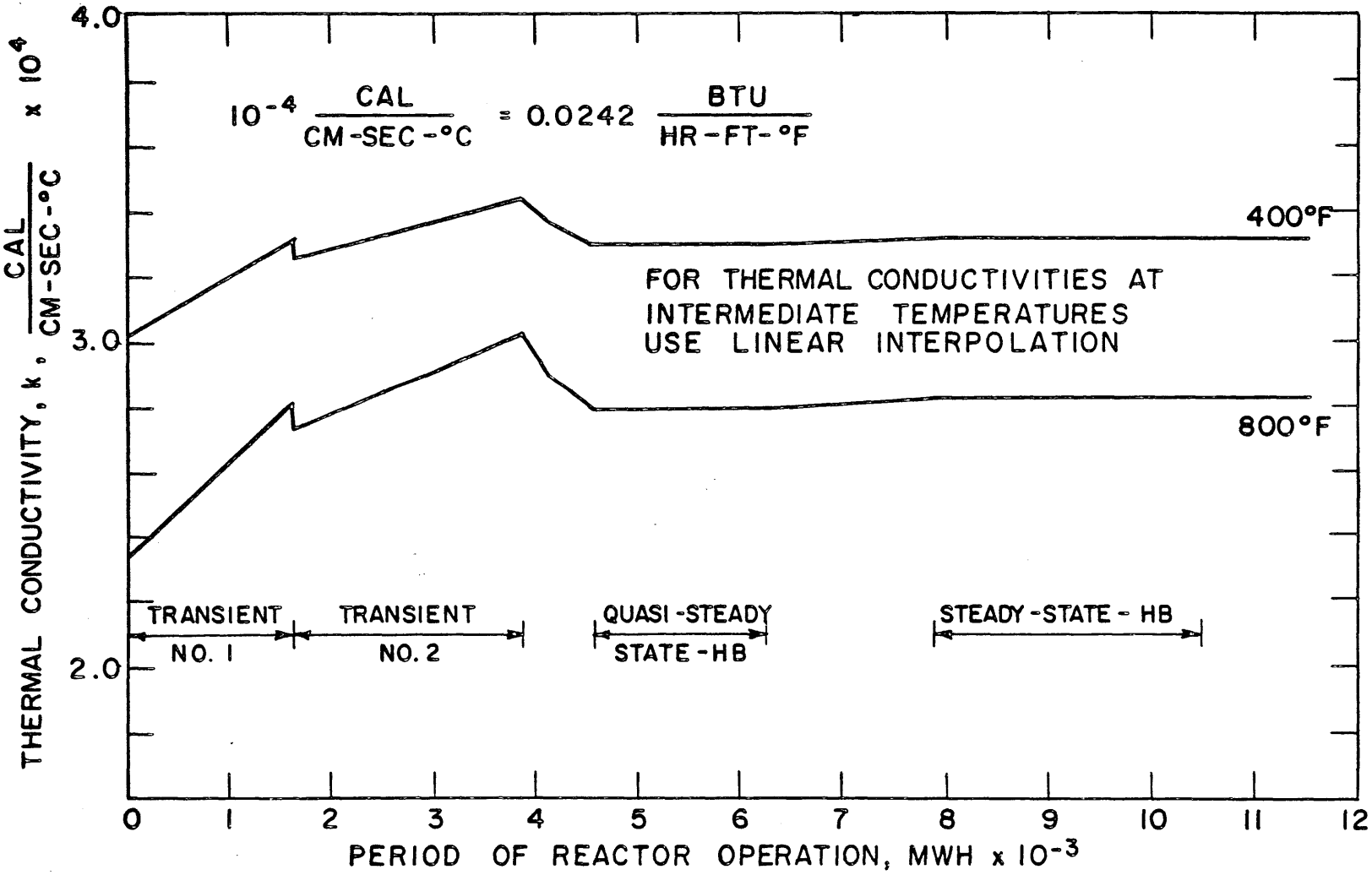

FIGURE A4.4 THERMAL CONDUCTIVITY OF IRRADIATED SANTOWAX OMP DURING THE 610°F IRRADIATION

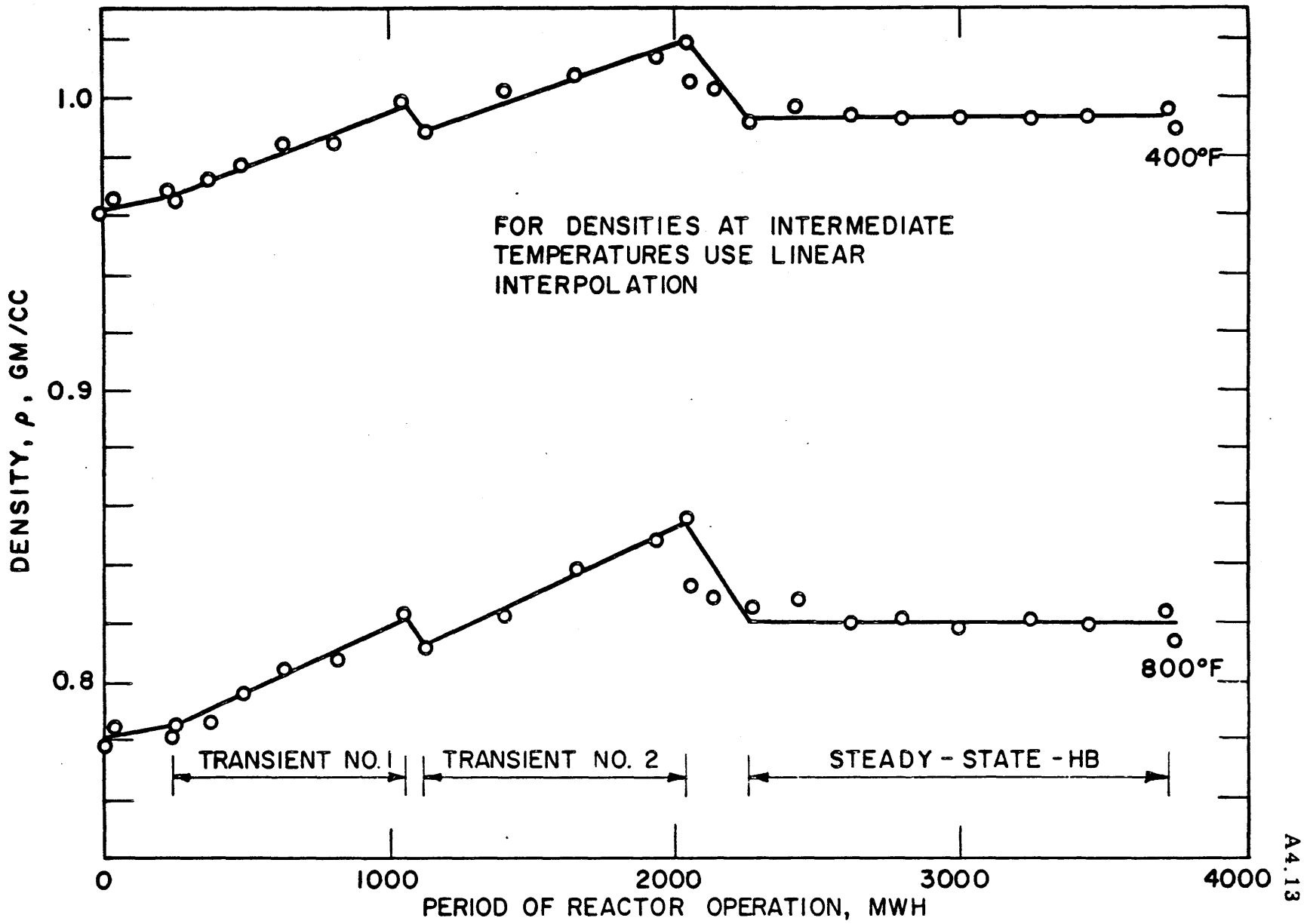

FIGURE A4.5 DENSITY OF IRRADIATED SANTOWAX OMP DURING THE 750°F IRRADIATION

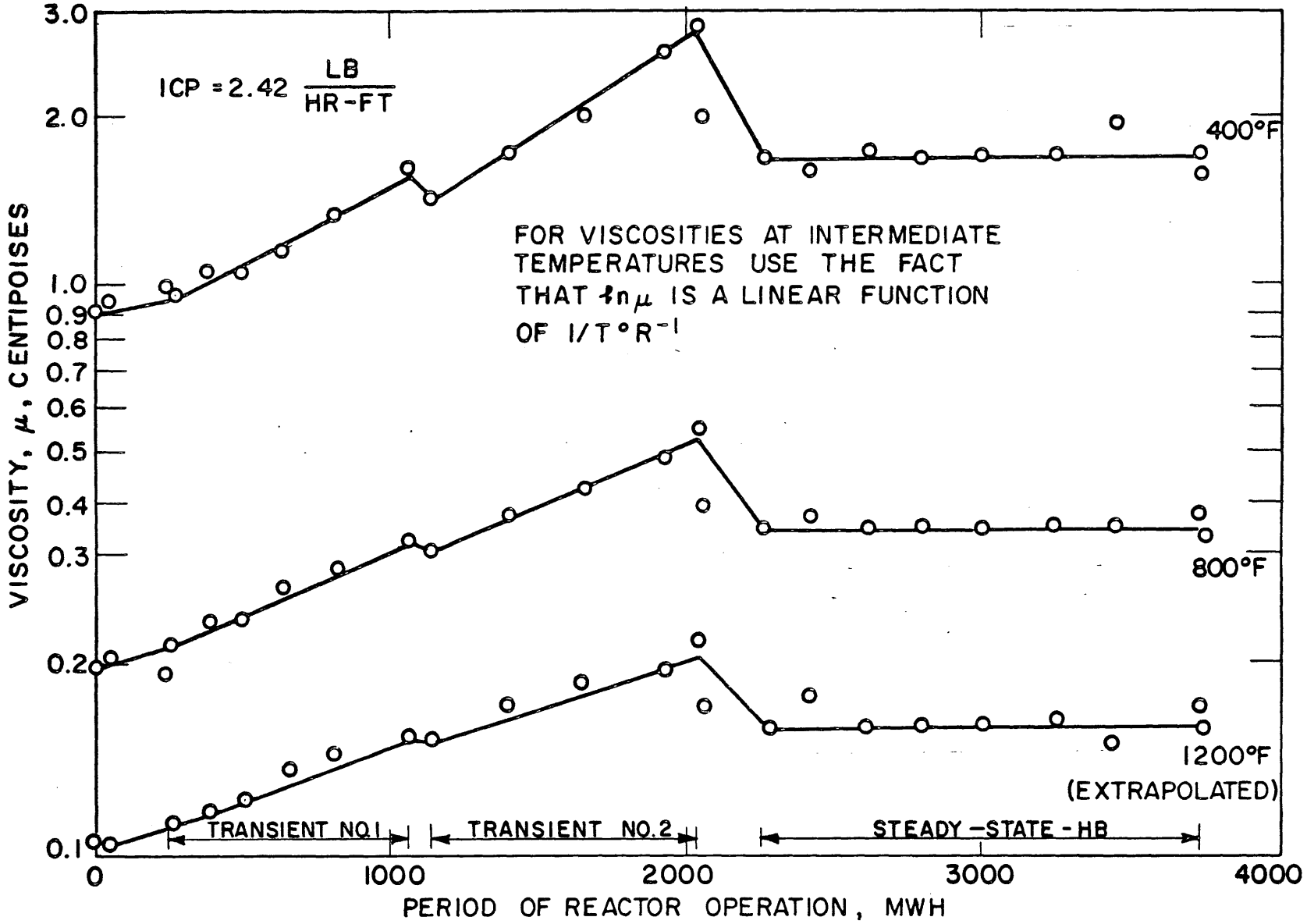

FIGURE A4.6 VISCOSITY OF IRRADIATED SANTOWAX OMP DURING THE 750°F IRRADIATION

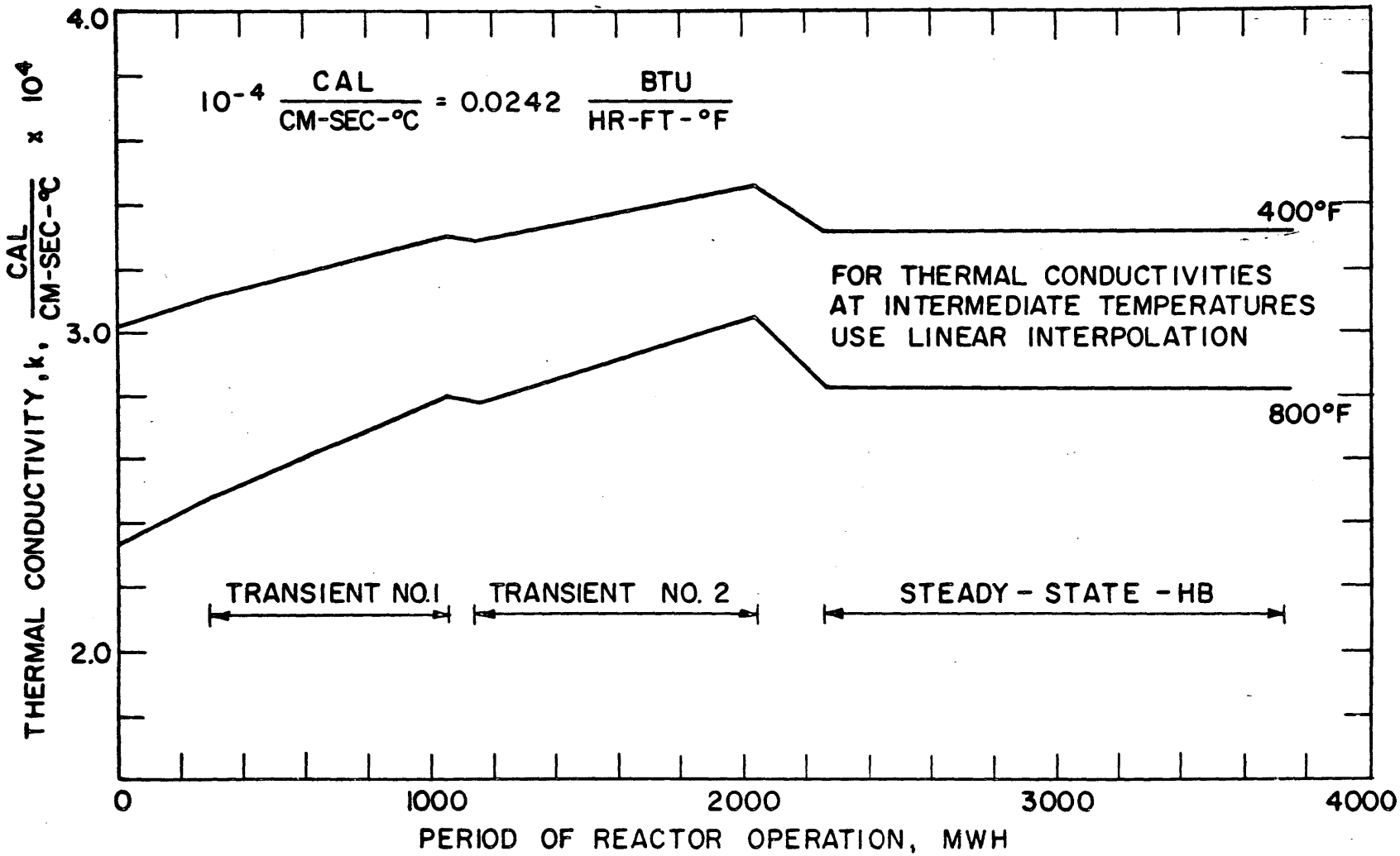

FIGURE A4.7 THERMAL CONDUCTIVITY OF IRRADIATED SANTOWAX OMP DURING THE 750°F IRRADIATION

or

$$Y = A' + Bx + Cz + Dw \tag{A4.22}$$

The variance in each measured value of Y, y_j, seems to be much larger than the variances in the measured values x_j, z_j, and w_j, since the measurement of h_f has the largest error, and the percentage error in the Nusselt number should be about the same for every measurement, so an unweighted least squares analysis may be applied to Eq. (A4.22). The quantity to be minimized is

$$\sum_{j=1}^{N} (Y_j - y_j)^2 = \sum_{j=1}^{N} (A' + Bx_j + Cz_j + Dw_j - y_j)^2 = \text{minimum} \tag{A4.23}$$

where N is the number of data points (y_j, x_j, z_j, w_j). Setting the partial derivative of Eq. (A4.23) with respect to A', B, C and D equal to zero, there results

$$NA' + (\Sigma x_j)B + (\Sigma z_j)C + (\Sigma w_j)D = \Sigma y_j \tag{A4.24}$$

$$(\Sigma x_j)A' + (\Sigma x_j^2)B + (\Sigma z_j x_j)C + (\Sigma w_j x_j)D = \Sigma y_j x_j \tag{A4.25}$$

$$(\Sigma z_j)A' + (\Sigma x_j z_j)B + (\Sigma z_j^2)C + (\Sigma w_j z_j)D = \Sigma y_j z_j \tag{A4.26}$$

$$(\Sigma w_j)A' + (\Sigma x_j w_j)B + (\Sigma z_j w_j)C + (\Sigma w_j^2)D = \Sigma y_j w_j \tag{A4.27}$$

This set of equations may be solved by Cramer's rule (A4.4) for A', B, C and D. The variance in y_j may be calculated directly from the fit, assuming only random errors contribute to the measurements, as

$$\sigma^2(y_j) = \frac{\Sigma (Y_j - y_j)^2}{N - 4} \tag{A4.28}$$

The correlation coefficient, r, is given by the relation (see Section A2.6)

$$r^2 = \frac{\Sigma (Y_j - \bar{y})^2}{\Sigma (y_j - \bar{y})^2} \tag{A.29}$$

The appropriate form of Eq. (A4.22) for the calculation of the variances of the parameters is

$$Y = A'' + B(x-\bar{x}) + C(z-\bar{z}) + D(w-\bar{w}) \tag{A4.30}$$

Using the propagation of variances treatment (y_j is the only variable with an error), there results

$$\Delta = \begin{vmatrix} (\Sigma x_j^2 - N\bar{x}^2) & (\Sigma x_j z_j - N\bar{x}\bar{z}) & (\Sigma x_j w_j - N\bar{x}\bar{w}) \\ (\Sigma x_j z_j - N\bar{x}\bar{z}) & (\Sigma z_j^2 - N\bar{z}^2) & (\Sigma z_j w_j - N\bar{z}\bar{w}) \\ (\Sigma x_j w_j - N\bar{x}\bar{w}) & (\Sigma z_j w_j - N\bar{z}\bar{w}) & (\Sigma w_j^2 - N\bar{w}^2) \end{vmatrix} \tag{A4.31}$$

$$\sigma^2(B) = \frac{\sigma^2(y_j)}{\Delta} \begin{vmatrix} (\Sigma z_j^2 - N\bar{z}^2) & (\Sigma z_j w_j - N\bar{z}\bar{w}) \\ (\Sigma z_j w_j - N\bar{z}\bar{w}) & (\Sigma w_j^2 - N\bar{w}^2) \end{vmatrix} \tag{A4.32}$$

$$\sigma^2(C) = \frac{\sigma^2(y_j)}{\Delta} \begin{vmatrix} (\Sigma x_j^2 - N\bar{x}^2) & (\Sigma x_j w_j - N\bar{x}\bar{w}) \\ (\Sigma x_j w_j - N\bar{x}\bar{w}) & (\Sigma w_j^2 - N\bar{w}^2) \end{vmatrix} \tag{A4.33}$$

$$\sigma^2(D) = \frac{\sigma^2(y_j)}{\Delta} \begin{vmatrix} (\Sigma x_j^2 - N\bar{x}^2) & (\Sigma x_j z_j - N\bar{x}\bar{w}) \\ (\Sigma x_j z_j - N\bar{x}\bar{z}) & (\Sigma z_j^2 - N\bar{z}^2) \end{vmatrix} \tag{A4.34}$$

$$\sigma^2(A') = \frac{\sigma^2(y_j)}{N} + \bar{x}\sigma^2(B) + \bar{z}\sigma^2(C) + \bar{w}\sigma^2(D) \tag{A4.35}$$

where

$$\bar{x} = \frac{\Sigma x_j}{N}, \quad \bar{z} = \frac{\Sigma z_j}{N}, \quad \bar{w} = \frac{\Sigma w_j}{N} \tag{A4.36}$$

Using the logarithmic relation between A' and A, the error in A may be calculated as

$$\sigma^2(A) = A^2\sigma^2(A') \tag{A4.37}$$

The error in the calculated value of the dependent variable, Y_j, may be calculated from

$$\sigma^2(Y_j) = \frac{\sigma^2(y_j)}{N} + (x_j-\bar{x})^2\sigma^2(B) + (z_j-\bar{z})^2\sigma^2(C) + (w_j-\bar{w})^2\sigma^2(D) \tag{A4.38}$$

and the root-mean-square deviation of the data may be calculated as the square root of Eq. (A4.28). Standard deviations are the square roots of the variances. Student's t may be used to calculate confidence limits (see Section A2.6).

Consistent errors in variables have to be taken into account separately and, depending on the bias, may affect the error in the parameters A, B, C and D in a different way (see Section A2.6).

The least squares analysis may still be applied in its entirety if the dependence on the variable (μ/μ_W) is assumed not to exist. In this case, every sum involving w_j is set to zero, except that Σw_j^2 is set to unity.

If a parameter is fixed instead of least squared, Eqs. (A4.24) to (A4.27) must be modified. The equation resulting from the partial derivative with respect to this parameter must not appear, and the fixed value of the parameter must be substituted into the other equations. The analysis of variance (Eqs. (A4.28) to (A4.38)) can no longer apply since the fixed parameter has an unknown error.

A4.5 Heat Transfer Computer Program, MNHTR

MNHTR is an IBM 709/7090 FORTRAN program (designed for a 32K storage) which correlates the heat transfer data measured at the loop using the relations derived in the preceding sections. The program has several options. First, the heat transfer coefficient may be based on the upstream half heater, the downstream half heater, or the average of the two. As noted in Section A4.1, data are usually based on the upstream half heater. Next, the heat input may be based on the voltage drop and the heat loss, Q_{in}, the calculated value from the temperature rise of the coolant, Q_{th}, or the average of the two. Third, the heat transfer coefficients calculated may be corrected for a given amount of scale resistance. Heat transfer data will be rejected on two counts: if the

difference between Q_{in} and Q_{th} is greater than a specified percentage, or if the scatter in the wall temperature data is too great. Finally, correlations of the data will be made using Eq. (A4.16) with any combination of A, B, C or D fixed or least squared. The parameter D has one special extra option – that of being set to zero in case no dependence on (μ/μ_W) is desired.

Table A4.1 gives the FORTRAN listing of the program and Fig. A4.8 gives the logic flowsheet of the program. Of particular note is the size of the program. It must use the special library subroutine DF2PM in order to fit into a 32K core. In the paragraphs that follow, a brief description of how to use the program will be given; a sample input and sample output are given in Tables A4.2 and A4.3 as an aid. Some familiarity with FORTRAN input/output format is assumed; for details, see the IBM FORTRAN reference manual (A4.5).

The input is arranged as a series of tables, each headed by a card upon which any desired information may be placed. All fixed-point data use I4 format and all floating-point data use E12.5 format. Alphanumeric data, used to describe run numbers, use A6 format.

The first table supplies control data for the program. It must contain the following information:

1. The number of groups of data to be run with the same "constant"data (to be described below).
2. The number of MWH entries to be supplied in the density-temperature-MWH table.
3. The number of temperature entries in the density-temperature-MWH table. In Table A4.2, the $\rho = \rho(T,MWH)$ plane is described by two temperature entries and seven MWH elements.
4. The number of MWH entries in the $\ln \mu - \frac{1}{(T+460.)} - MWH$ table.
5. The number of temperature entries in the $\ln \mu - \frac{1}{(T+460.)} - MWH$ table.
6. The number of entries in the specific heat-temperature-MWH table.
7. The number of temperature entries in the specific heat-temperature-MWH table.
8. The number of MWH entries in the thermal conductivity-temperature-MWH table.

TABLE A4.1
FORTRAN LISTING OF MNHTR

```
*       LIST 8
*       LABEL
*       SYMBOL TABLE
C       MNHTR HAS SUBPROGRAMS MAIN,RIT,HTLSQ,HTSUP,CRRL,WOT,LINLSQ IN
C       FORTRAN, INT2D IN FAP
C       MNHTR MUST USE DUMMY F2PM
C       MAIN HAS 178 CARDS      5-27-63
        COMMON SUMX,SUMY,SUMX2,SUMXY,SUMY2,SLOPE,FNTCPT,SIG2F,SIG2P,SIGA,S
       1IGB,RLIN,NOT,KPUNCH
        COMMON M,NR1,NR2,NEM1,NEM2,NCP1,NCP2,NEK1,NEK2,NRES1,NRES2,NQLOS1,
       1NQLOS2,NTCPLT,NTMCP1,NTMCP2,NGRAT,NGINT,MOVER,NCORRS,NIT,N,KA,KB,K
       2C,KD,KH,KQ,NFREE,NTH
        COMMON DIA,ERROR1,ERROR2,FAC1,FAC2,FAC3,FAC4,FAC5,FAC6,FAC7,FAC8,E
       1KWAL0,EKWAL1,A,AA,B,C,D,TR,R,EMWHR,TEM,EM,EMWHEM,TCP,CP,EMWHCP,TEK
       2,EK,EMWHEK,TRES,RESIS1,EMWHRE,TQLOS,QLOS,EMWHQL,TTMCPL,VTMCPL,VTCP
       3C,VTCPCR,XTCPL,GRATIO,EMWHGR,GINT,EMWHGI,SLOPE1,SLOPE2,ETCPT1,ETCP
       4T2,RCOR1,RCOR2,SIGA1,SIGA2,SIGB1,SIGB2,V,TWO1,TWO2,QA,QB,Q1,Q2,QLO
       5S1,QLOS2,TB,TB1,TB2,TWI1,TWI2,          QAREA1,QAREA2,H1,H2,H,RM
       6EAN,EMMEAN,EMWMEN,CPMEAN,EKMEAN,QINH,QIN,ERR,ENU,PR,RF,RATIO,DATE,
       7QINH1,QINH2,TTEST,VARE,VARP,RHEAT,X,Y,Z,W,COEF11,COEF12,COEF13,COE
       8F14, COEF15,COEF22,COEF23,COEF24,COEF25,COEF33,COEF34,COEF35,COEF4
       94,COEF45,RTEST,YSQ,ENTH,EMWHTH,RESIS2,VTCPL,TTCPL,EMWH,NREAD,KPUNC
        COMMON VARA,VARB,VARC,VARD
        COMMON C11,C12,C13,C14,C15,C22,C23,C24,C25,C33,C34,C35,C44,C45,C55
       1,E1,E2,E3,E4
        COMMON NRS,RSCALE,EMRS
        DIMENSION A(10),AA(10),B(10),C(10),D(10),TR(20),R(20,20),EMWHR(20)
       1,TEM(20),EM(20,20),EMWHEM(20),TCP(20),CP(20,20),EMWHCP(20),TEK(20)
       2,EK(20,20),EMWHEK(20),TRES(20),RESIS1(20,20),EMWHRE(20),TQLOS(20),
       3QLOS(20,20),EMWHQL(20),TTMCPL(20),VTMCPL(20),VTCPC(20),VTCPCR(20,2
       40),XTCPL(20),GRATIO(20),EMWHGR(20),GINT(20),EMWHGI(20),TTEST(31),K
       5A(10),KB(10),KC(10),KD(10),VARE(10),VARP(10),RHEAT(10),NFREE(10),V
       6TCPL(20),TTCPL(20),ENTH(20),EMWHTH(20),RESIS2(20,20)
        DIMENSION SLOPE1(300),SLOPE2(300),ETCPT1(300),ETCPT2(300),RCOR1(30
       10),RCOR2(300),SIGA1(300),SIGA2(300),SIGB1(300),SIGB2(300),V(300),T
       2WO1(300),TWO2(300),QA(300),QB(300),Q1(300),Q2(300),QLOS1(300),QLOS
       32(300),TB(300),TB1(300),TB2(300),TWI1(300),TWI2(300),QAREA1(300),Q
       4AREA2(300),H1(300),H2(300),H(300),RMEAN(300),EMMEAN(300),EMWMEN(30
       50),CPMEAN(300),EKMEAN(300),QINH(300),QIN(300),ERR(300),ENU(300),PR
       6(300),RF(300),RATIO(300),DATE(300),QINH1(300),QINH2(300),X(300),Y(
       7300),Z(300),W(300),EMWH(300),VARA(10),VARB(10),VARC(10),VARD(10)
D       DIMENSION C11(1),C12(1),C13(1),C14(1),C15(1),C22(1),C23(1),C24(1),
D      1C25(1),C33(1),C34(1),C35(1),C44(1),C45(1),C55(1),E1(1),E2(1),E3(1)
D      2,E4(1)
        DIMENSION RSCALE(20),EMRS(20)
     24 CALL RIT
        READINPUTTAPE NIT,1,NRS
        READINPUTTAPE NIT,200,(RSCALE(I),EMRS(I),I=1,NRS)
    200 FORMAT(6E12.5)
        DO 22 J=1,M
        READINPUTTAPE NIT,100
    100 FORMAT(80H1
       1                          )
        WRITEOUTPUTTAPE NOT,100
        CALL CLOCK(NOT)
        IF(KPUNCH)101,101,102
    101 PUNCH 100
```

TABLE A4.1 (CONTINUED)

```
102 READINPUTTAPE NIT,1,N,(KA(L),KB(L),KC(L),KD(L),L=1,NCORRS),KH,KQ
  1 FORMAT(/(18I4))
    WRITEOUTPUTTAPE NOT,10,J
    IF(KPUNCH)7,7,8
  7 PUNCH 10,J
  8 DO 13 I=1,N
    READINPUTTAPE NIT,2,EMWH(I),G,VOLT1,VOLT2,VTCPL(1),VTCPL(2),DATE(I
   1),(VTCPL(K),K=3,NTMCP1)
  2 FORMAT(6E12.5,A6/(6E12.5))
    NHALF=NTMCP1/2+1
    CALL INT2D(NTH,1,EMWHTH,0,ENTH,EMWH(I),0,ENTHC)
    IF(ENTHC)54,54,55
 55 READINPUTTAPE NIT,3,DIA,FAC4,FAC6,FAC7,FAC8
    READINPUTTAPE NIT,3,(VTCPC(J),(VTCPCR(J,K),K=1,NTMCP1),J=1,NTMCP2)
    READINPUTTAPE NIT,3,(TRFS(J),(RFSIS1(J,K),RFSIS2(J,K),K=1,NRFS1),J
   1=1,NRFS2),(EMWHRF(K),K=1,NRFS1)
    READINPUTTAPE NIT,3,(TQLOS(J),(QLOS(J,K),K=1,NQLOS1),J=1,NQLOS2),(
   1EMWHQL(K),K=1,NQLOS1)
  3 FORMAT(/(6E12.5))
 54 LLOW=1
    LHIGH=2
 53 DO 40 K=LLOW,LHIGH
    CALL INT2D(NTMCP2,K,VTCPC,0,VTCPCR,VTCPL(K),0,VTCPL(K))
    CALL INT2D(NTCPLT,1,VTMCPL,0,TTMCPL,VTCPL(K),0,TTCPL(K))
 40 CONTINUE
    IF(LLOW-1)62,62,63
 62 LLOW=3
    LHIGH=NTMCP1
    IF(VTCPL(3))50,50,51
 50 LLOW=NHALF+1
 51 IF(VTCPL(NHALF+1))52,52,53
 52 LHIGH=NHALF
    GO TO 53
 63 WRITEOUTPUTTAPE NOT,11,DATE(I),TTCPL(1),TTCPL(2),(TTCPL(K),K=LLOW,
   1LHIGH)
    IF(KPUNCH)12,12,14
 12 PUNCH 11,DATE(I),TTCPL(1),TTCPL(2),(TTCPL(K),K=LLOW,LHIGH)
 14 IF(VTCPL(3))60,60,61
 60 RCOR1(I)=-0.0
    GO TO 59
 61 CALL LINLSQ(3,NHALF,XTCPL,TTCPL,-1)
    SLOPE1(I)=SLOPE
    ETCPT1(I)=ENTCPT
    RCOR1(I)=RLIN
    SIGA1(I)=SIGA
    SIGB1(I)=SIGB
 59 IF(VTCPL(NHALF+1))56,56,57
 56 RCOR2(I)=-0.0
    GO TO 58
 57 CALL LINLSQ(NHALF+1,NTMCP1,XTCPL,TTCPL,-1)
    SLOPE2(I)=SLOPE
    ETCPT2(I)=ENTCPT
    RCOR2(I)=RLIN
    SIGA2(I)=SIGA
    SIGB2(I)=SIGB
 58 CALL INT2D(NGRAT,1,EMWHGR,0,GRATIO,EMWH(I),0,GRATP)
    CALL INT2D(NGINT,1,EMWHGI,0,GINT,EMWH(I),0,GINTP)
    G=GINTP+GRATP*G
    V(I)=FAC1*G/DIA**2
```

TABLE A4.1 (CONTINUED)

```
      TWO1(I)=ETCPT1(I)+SLOPE1(I)*XTCPL(2)*0.25
      TWO2(I)=ETCPT2(I)+SLOPE2(I)*XTCPL(2)*0.75
      CALL INT2D(NRES2,NRES1,TRES,EMWHRE,RESIS1,TWO1(I),EMWH(I),RES1)
      CALL INT2D(NRES2,NRES1,TRES,EMWHRE,RESIS2,TWO2(I),EMWH(I),RES2)
      QA(I)=VOLT1**2/RES1
      QB(I)=VOLT2**2/RES2
      CALL INT2D(NQLOS2,NQLOS1,TQLOS,EMWHQL,QLOS,TWO1(I),EMWH(I),QLOS1(I
     1))
      CALL INT2D(NQLOS2,NQLOS1,TQLOS,EMWHQL,QLOS,TWO2(I),EMWH(I),QLOS2(I
     1))
      Q1(I)=QA(I)-QLOS1(I)
      Q2(I)=QB(I)-QLOS2(I)
      TB(I)=TTCPL(1)+Q1(I)*(TTCPL(2)-TTCPL(1))/(Q1(I)+Q2(I))
      TB1(I)=(TTCPL(1)+TB(I))*0.5
      TB2(I)=(TTCPL(2)+TB(I))*0.5
      TWI1(I)=TWO1(I)-(FAC7*QA(I)+FAC8*QLOS1(I))/(EKWAL0+EKWAL1*TWO1(I))
     1/XTCPL(2)
      TWI2(I)=TWO2(I)-(FAC7*QB(I)+FAC8*QLOS2(I))/(EKWAL0+EKWAL1*TWO2(I))
     1/XTCPL(2)
      CALL INT2D(NCP2,NCP1,TCP,EMWHCP,CP,TB1(I),EMWH(I),CP1)
      CALL INT2D(NCP2,NCP1,TCP,EMWHCP,CP,TB2(I),EMWH(I),CP2)
      CALL INT2D(NR2,NR1,TR,EMWHR,R,TB1(I),EMWH(I),R1)
      CALL INT2D(NR2,NR1,TR,EMWHR,R,TB2(I),EMWH(I),R2)
      QINH1(I)=FAC3*G    *R1*CP1*(TB(I)-TTCPL(1))
      QINH2(I)=FAC3*G    *R2*CP2*(TTCPL(2)-TB(I))
      IF(KQ)73,4,5
   73 QAV1=QINH1(I)
      QAV2=QINH2(I)
      GO TO 6
    5 QAV1=Q1(I)
      QAV2=Q2(I)
      GO TO 6
    4 QAV1=(Q1(I)+QINH1(I))*0.5
      QAV2=(Q2(I)+QINH2(I))*0.5
    6 QAREA1(I)=FAC2*QAV1/DIA/XTCPL(2)
      QAREA2(I)=FAC2*QAV2/DIA/XTCPL(2)
      CALL INT2D(NRS,1,EMRS,0,RSCALE,EMWH(I),0,RS)
      H1(I)=QAREA1(I)/(TWI1(I)-TB1(I))
      H2(I)=QAREA2(I)/(TWI2(I)-TB2(I))
      H1(I)=H1(I)/(1.-RS*H1(I))
      H2(I)=H2(I)/(1.-RS*H2(I))
      H(I)=(H1(I)+H2(I))*0.5
      CALL INT2D(NR2,NR1,TR,EMWHR,R,TB(I),EMWH(I),RMEAN(I))
      CALL INT2D(NEM2,NEM1,TEM,EMWHEM,EM,1.0/(TB(I)+460.0),EMWH(I),EMMEA
     1N(I))
      EMMEAN(I)=EXPF(EMMEAN(I))
      CALL INT2D(NCP2,NCP1,TCP,EMWHCP,CP,TB(I),EMWH(I),CPMEAN(I))
      CALL INT2D(NEK2,NEK1,TEK,EMWHEK,EK,TB(I),EMWH(I),EKMEAN(I))
      QINH(I)=FAC3*G    *RMEAN(I)*CPMEAN(I)*(TTCPL(2)-TTCPL(1))
      QIN(I)=Q1(I)+Q2(I)
      ERR(I)=(QIN(I)-QINH(I))*100.0/QIN(I)
   13 CONTINUE
      CALL HTLSQ
      CALL WOT
      CALL CRRL
   22 CONTINUE
      IF(MOVER)23,23,24
   23 CALL EXIT
   10 FORMAT(34X10HBATCH NO.=I2/1H0,24X33HTEMPERATURE PROFILES FOR ALL R
```

TABLE A4.1 (CONTINUED)

```
     1UNS)
  11 FORMAT(1H A6,12F6.1/(13F6.1))
     END
```

TABLE A4.1 (CONTINUED)

```
*       LIST 8
*       LABEL
*       SYMBOL TABLE
        SUBROUTINE RIT
C       RIT HAS 68 CARDS                        7-26-62
        COMMON SUMX,SUMY,SUMX2,SUMXY,SUMY2,SLOPE,FNTCPT,SIG2E,SIG2P,SIGA,S
       1IGB,RLIN,NOT,KPUNCH
        COMMON M,NR1,NR2,NEM1,NEM2,NCP1,NCP2,NEK1,NEK2,NRES1,NRES2,NQLOS1,
       1NQLOS2,NTCPLT,NTMCP1,NTMCP2,NGRAT,NGINT,MOVER,NCORRS,NIT,N,KA,KB,K
       2C,KD,KH,KQ,NFREE,NTH
        COMMON DIA,ERROR1,ERROR2,FAC1,FAC2,FAC3,FAC4,FAC5,FAC6,FAC7,FAC8,F
       1KWAL0,FKWAL1,A,AA,B,C,D,TR,P,EMWHR,TEM,EM,EMWHEM,TCP,CP,EMWHCP,TEK
       2,EK,EMWHEK,TRES,RESIS1,EMWHRE,TQLOS,QLOS,EMWHQL,TTMCPL,VTMCPL,VTCP
       3C,VTCPCR,XTCPL,GRATIO,EMWHGR,GINT,EMWHGI,SLOPE1,SLOPE2,ETCPT1,ETCP
       4T2,RCOR1,RCOR2,SIGA1,SIGA2,SIGB1,SIGB2,V,TWO1,TWO2,QA,QB,Q1,Q2,QLO
       5S1,QLOS2,TB,TB1,TB2,TWI1,TWI2,          QAREA1,QAREA2,H1,H2,H,RM
       6EAN,EMMEAN,EMWMEN,CPMEAN,EKMEAN,QINH,QIN,ERR,ENU,PR,RE,RATIO,DATE,
       7QINH1,QINH2,TTEST,VARE,VARP,RHEAT,X,Y,Z,W,COEF11,COEF12,COEF13,COE
       8F14, COEF15,COEF22,COEF23,COEF24,COEF25,COEF33,COEF34,COEF35,COEF4
       94,COEF45,RTEST,YSQ,ENTH,EMWHTH,RESIS2,VTCPL,TTCPL
        DIMENSION A(10),AA(10),B(10),C(10),D(10),TR(20),R(20,20),EMWHR(20)
       1,TEM(20),EM(20,20),EMWHEM(20),TCP(20),CP(20,20),EMWHCP(20),TEK(20)
       2,EK(20,20),EMWHEK(20),TRES(20),RESIS1(20,20),EMWHRE(20),TQLOS(20),
       3QLOS(20,20),EMWHQL(20),TTMCPL(20),VTMCPL(20),VTCPC(20),VTCPCR(20,2
       40),XTCPL(20),GRATIO(20),EMWHGR(20),GINT(20),EMWHGI(20),TTEST(31),K
       5A(10),KB(10),KC(10),KD(10),VARE(10),VARP(10),RHEAT(10),NFREE(10),V
       6TCPL(20),TTCPL(20),ENTH(20),EMWHTH(20),RESIS2(20,20)
        DIMENSION SLOPE1(300),SLOPE2(300),ETCPT1(300),ETCPT2(300),RCOR1(30
       10),RCOR2(300),SIGA1(300),SIGA2(300),SIGB1(300),SIGB2(300),V(300),T
       2WO1(300),TWO2(300),QA(300),QB(300),Q1(300),Q2(300),QLOS1(300),QLOS
       32(300),TB(300),TB1(300),TB2(300),TWI1(300),TWI2(300),QAREA1(300),Q
       4AREA2(300),H1(300),H2(300),H(300),RMEAN(300),EMMEAN(300),EMWMEN(30
       50),CPMEAN(300),EKMEAN(300),QINH(300),QIN(300),ERR(300),ENU(300),PR
       6(300),RE(300),RATIO(300),DATE(300),QINH1(300),QINH2(300),X(300),Y(
       7300),Z(300),W(300)
        NOT=2
        NIT=4
        READINPUTTAPE NIT,1,M,NR1,NR2,NEM1,NEM2,NCP1,NCP2,NEK1,NEK2,NRES1,
       1NRES2,NQLOS1,NQLOS2,NTCPLT,NTMCP1,NTMCP2,NGRAT,NGINT,MOVER,NCORRS,
       2KPUNCH,NTH
      1 FORMAT(/(18I4))
        READINPUTTAPE NIT,2,DIA,ERROR1,ERROR2,FAC1,FAC2,FAC3,FAC4,FAC5,FAC
       16,FAC7,FAC8,FKWAL0,FKWAL1,RTEST,(A(L),B(L),C(L),D(L),L=1,NCORRS)
      2 FORMAT(/(6F12.5))
        READINPUTTAPE NIT,2,(TR(J),(R(J,I),I=1,NR1),J=1,NR2),(EMWHR(I),I=1
       1,NR1)
        READINPUTTAPE NIT,2,(TEM(J),(EM(J,I),I=1,NEM1),J=1,NEM2),(EMWHEM(I
       1),I=1,NEM1)
        READINPUTTAPE NIT,2,(TCP(J),(CP(J,I),I=1,NCP1),J=1,NCP2),(EMWHCP(I
       1),I=1,NCP1)
        READINPUTTAPE NIT,2,(TEK(J),(EK(J,I),I=1,NEK1),J=1,NEK2),(EMWHEK(I
       1),I=1,NEK1)
        READINPUTTAPE NIT,2,(TRES(J),(RESIS1(J,I),RESIS2(J,I),I=1,NRES1),J
       1=1,NRES2),(EMWHRE(I),I=1,NRES1)
        READINPUTTAPE NIT,2,(TQLOS(J),(QLOS(J,I),I=1,NQLOS1),J=1,NQLOS2),(
       1EMWHQL(I),I=1,NQLOS1)
        READINPUTTAPE NIT,2,(TTMCPL(I),VTMCPL(I),I=1,NTCPLT)
        READINPUTTAPE NIT,2,(ENTH(I),EMWHTH(I),I=1,NTH)
        READINPUTTAPE NIT,2,(VTCPC(J),(VTCPCR(J,I),I=1,NTMCP1),J=1,NTMCP2)
```

TABLE A4.1 (CONTINUED)

```
      READINPUTTAPE NIT,2,(XTCPL(I),I=1,NTMCPL)
      READINPUTTAPE NIT,2,(GRATIO(I),EMWHGR(I),I=1,NGRAT)
      READINPUTTAPE NIT,2,(GINT(I),EMWHGI(I),I=1,NGINT)
      READINPUTTAPE NIT,2,(TTEST(I),I=1,31)
      DO 3 L=1,NCORRS
      AA(L)=LOGF(A(L))
    3 CONTINUE
      RETURN
      END
```

TABLE A4.1 (CONTINUED)

```
*       LIST 8
*       LABEL
*       SYMBOL TABLE
        SUBROUTINE HTLSQ
C       HTLSQ HAS 133 CARDS     5-24-63
        COMMON SUMX,SUMY,SUMX2,SUMXY,SUMY2,SLOPE,ENTCPT,SIG2E,SIG2P,SIGA,S
       1IGB,RLIN,NOT,KPUNCH
        COMMON M,NR1,NR2,NEM1,NEM2,NCP1,NCP2,NEK1,NEK2,NRES1,NRES2,NQLOS1,
       1NQLOS2,NTCPLT,NTMCP1,NTMCP2,NGRAT,NGINT,MOVER,NCORRS,NIT,N,KA,KB,K
       2C,KD,KH,KQ,NFREE,NTH
        COMMON DIA,ERROR1,ERROR2,FAC1,FAC2,FAC3,FAC4,FAC5,FAC6,FAC7,FAC8,F
       1KWAL0,EKWAL1,A,AA,B,C,D,TR,R,EMWHR,TEM,EM,EMWHEM,TCP,CP,EMWHCP,TEK
       2,EK,EMWHEK,TRES,RESIS1,EMWHRE,TQLOS,QLOS,EMWHQL,TTMCPL,VTMCPL,VTCP
       3C,VTCPCR,XTCPL,GRATIO,EMWHGR,GINT,EMWHGI,SLOPE1,SLOPE2,ETCPT1,ETCP
       4T2,RCOR1,RCOR2,SIGA1,SIGA2,SIGB1,SIGB2,V,TWO1,TWO2,QA,QB,Q1,Q2,QLO
       5S1,QLOS2,TB,TB1,TB2,TWI1,TWI2,          QAREA1,QAREA2,H1,H2,H,RM
       6EAN,EMMEAN,EMWMEN,CPMEAN,EKMEAN,QINH,QIN,ERR,ENU,PR,RE,RATIO,DATE,
       7QINH1,QINH2,TTEST,VARE,VARP,PHEAT,X,Y,Z,W,COEF11,COEF12,COEF13,COE
       8F14, COEF15,COEF22,COEF23,COEF24,COEF25,COEF33,COEF34,COEF35,COEF4
       94,COEF45,RTEST,YSQ,ENTH,EMWHTH,RESIS2,VTCPL,TTCPL,EMWH,NREAD,KPUNC
        COMMON VARA,VARB,VARC,VARD
        COMMON C11,C12,C13,C14,C15,C22,C23,C24,C25,C33,C34,C35,C44,C45,C55
       1,E1,E2,E3,E4
        DIMENSION A(10),AA(10),B(10),C(10),D(10),TR(20),R(20,20),EMWHR(20)
       1,TEM(20),EM(20,20),EMWHEM(20),TCP(20),CP(20,20),EMWHCP(20),TEK(20)
       2,EK(20,20),EMWHEK(20),TRES(20),RESIS1(20,20),EMWHRE(20),TQLOS(20),
       3QLOS(20,20),EMWHQL(20),TTMCPL(20),VTMCPL(20),VTCPC(20),VTCPCR(20,2
       40),XTCPL(20),GRATIO(20),EMWHGR(20),GINT(20),EMWHGI(20),TTEST(31),K
       5A(10),KB(10),KC(10),KD(10),VARE(10),VARP(10),PHEAT(10),NFREE(10),V
       6TCPL(20),TTCPL(20),ENTH(20),EMWHTH(20),RESIS2(20,20)
        DIMENSION SLOPE1(300),SLOPE2(300),ETCPT1(300),ETCPT2(300),RCOR1(30
       10),RCOR2(300),SIGA1(300),SIGA2(300),SIGB1(300),SIGB2(300),V(300),T
       2WO1(300),TWO2(300),QA(300),QB(300),Q1(300),Q2(300),QLOS1(300),QLOS
       32(300),TB(300),TB1(300),TB2(300),TWI1(300),TWI2(300),QAREA1(300),Q
       4AREA2(300),H1(300),H2(300),H(300),RMEAN(300),EMMEAN(300),EMWMEN(30
       50),CPMEAN(300),EKMEAN(300),QINH(300),QIN(300),ERR(300),ENU(300),PR
       6(300),RE(300),RATIO(300),DATE(300),QINH1(300),QINH2(300),X(300),Y(
       7300),Z(300),W(300),EMWH(300),VARA(10),VARB(10),VARC(10),VARD(10)
D       DIMENSION C11(1),C12(1),C13(1),C14(1),C15(1),C22(1),C23(1),C24(1),
D      1C25(1),C33(1),C34(1),C35(1),C44(1),C45(1),C55(1),E1(1),E2(1),E3(1)
D      2,E4(1)
        NREAD=0
        KPUNC=1
D       Y1=0.0
D       X1=0.0
D       Z1=0.0
D       W1=0.0
D       C11=0.
D       C12=0.0
D       C13=0.0
D       C14=0.0
D       C15=0.0
D       C22=0.0
D       C23=0.0
D       C24=0.0
D       C25=0.0
D       C33=0.0
D       C34=0.0
D       C35=0.0
```

TABLE A4.1 (CONTINUED)

```
D       C44=0.0
D       C45=0.0
D       C55=0.0
D       E1=0.
D       E2=0.
D       E3=0.
D       E4=0.
        C11=N
        K=0
        DO 70 L=1,NCORRS
        IF(KD(L))71,70,71
   70   CONTINUE
        GO TO 72
   71   K=1
   72   DO 13 I=1,N
        IF(NREAD)800,800,801
  800   IF(ABSF(ERR(I))-ERROR1)6,6,5
    5   RE(I)=0.0
D       C11=C11-1.0
        GO TO 13
    6   NRTEST=0
        IF(RCOR2(I)-RTEST)7,8,8
    7   NRTEST=1
    8   IF(RCOR1(I)-RTEST)9,11,11
    9   IF(NRTEST)10,10,5
   10   NRTEST=-1
   11   IF(KH)1,14,3
    1   IF(NRTEST)2,2,12
    2   H(I)=H2(I)
        GO TO 4
    3   IF(NRTEST)2,12,12
   12   H(I)=H1(I)
        GO TO 4
   14   IF(NRTEST)2,4,12
    4   ENU(I)=FAC4*H(I)/EKMEAN(I)
        PR(I)=FAC5*CPMEAN(I)*EMMEAN(I)/EKMEAN(I)
        RE(I)=FAC6*V(I)*RMEAN(I)/EMMEAN(I)
  801   Y(I)=LOGF(ENU(I))
        X(I)=LOGF(RE(I))
        Z(I)=LOGF(PR(I))
        Y1=Y(I)
        X1=X(I)
        Z1=Z(I)
        IF(NREAD)802,802,803
  802   IF(K)61,61,60
   60   CALL INT2D(NEM2,NEM1,TEM,EMWHEM,EM,1.0/((TWI1(I)+TWI2(I))*0.5+460.
       10),EMWH(I),EMWMEN(I))
        EMWMEN(I)=EXPF(EMWMEN(I))
        RATIO(I)=EMMEAN(I)/EMWMEN(I)
  803   W(I)=LOGF(RATIO(I))
        W1=W(I)
D       C14=C14+W1
D       C24=C24+X1*W1
D       C34=C34+Z1*W1
D       C44=C44+W1**2
D       C45=C45+W1*Y1
        GO TO 62
   61   RATIO(I)=1.0
D  62   C12=C12+X1
```

TABLE A4.1 (CONTINUED)

```
D       C13=C13+Z1
D       C15=C15+Y1
D       C22=C22+X1**2
D       C23=C23+X1*Z1
D       C25=C25+X1*Y1
D       C33=C33+Z1**2
D       C35=C35+Z1*Y1
D       C55=C55+Y1**2
   13 CONTINUE
      IF(KPUNC)804,804,806
  804 PUNCH 805,(ENU(I),RE(I),PR(I),RATIO(I),H(I),V(I),DATE(I),I=1,N)
  805 FORMAT(32X17HSEMI-REDUCED DATA/(6E12.5,A6))
  806 CALL HTSUP
      RETURN
      END
```

TABLE A4.1 (CONTINUED)

```
*       LIST 8
*       LABEL
*       SYMBOL TABLE
        SUBROUTINE HTSUP
C       HTSUP HAS 190 CARDS     6-26-63
        COMMON SUMX,SUMY,SUMX2,SUMXY,SUMY2,SLOPE,ENTCPT,SIG2E,SIG2P,SIGA,S
       1IGB,RLIN,NOT,KPUNCH
        COMMON M,NR1,NR2,NEM1,NEM2,NCP1,NCP2,NEK1,NEK2,NRES1,NRES2,NQLOS1,
       1NQLOS2,NTCPLT,NTMCP1,NTMCP2,NGRAT,NGINT,NOVER,NCORRS,NIT,N,KA,KB,K
       2C,KD,KH,KQ,NEREF,NTH
        COMMON DIA,ERROR1,ERROR2,FAC1,FAC2,FAC3,FAC4,FAC5,FAC6,FAC7,FAC8,E
       1KWAL0,EKWAL1,A,AA,B,C,D,TR,R,EMWHR,TEM,EM,EMWHEM,TCP,CP,EMWHCP,TEK
       2,EK,EMWHEK,TRES,RESIS1,EMWHRE,TQLOS,QLOS,EMWHQL,TTMCPL,VTMCPL,VTCP
       3C,VTCPCP,XTCPL,GRATIO,EMWHGR,GINT,EMWHGI,SLOPE1,SLOPE2,ETCPT1,ETCP
       4T2,RCOR1,RCOR2,SIGA1,SIGA2,SIGB1,SIGB2,V,TWO1,TWO2,QA,QB,Q1,Q2,QLO
       551,QLOS2,TB,TB1,TB2,TWI1,TWI2,          QAREA1,QAREA2,H1,H2,H,RM
       6EAN,EMMEAN,EMWMEN,CPMEAN,EKMEAN,QINH,QIN,ERR,ENU,PR,RE,RATIO,DATE,
       7QINH1,QINH2,TTEST,VARE,VARP,PHEAT,X,Y,Z,W,COEF11,COEF12,COEF13,COE
       8F14, COEF15,COEF22,COEF23,COEF24,COEF25,COEF33,COEF34,COEF35,COEF4
       94,COEF45,RTEST,YSQ,ENTH,EMWHTH,RESIS2,VTCPL,TTCPL,EMWH,NREAD,KPUNC
        COMMON VARA,VARB,VARC,VARD
        COMMON C11,C12,C13,C14,C15,C22,C23,C24,C25,C33,C34,C35,C44,C45,C55
       1,E1,E2,E3,E4
        DIMENSION A(10),AA(10),B(10),C(10),D(10),TR(20),R(20,20),EMWHR(20)
       1,TEM(20),EM(20,20),EMWHEM(20),TCP(20),CP(20,20),EMWHCP(20),TEK(20)
       2,EK(20,20),EMWHEK(20),TRES(20),RESIS1(20,20),EMWHRE(20),TQLOS(20),
       3QLOS(20,20),EMWHQL(20),TTMCPL(20),VTMCPL(20),VTCPC(20),VTCPCP(20,2
       40),XTCPL(20),GRATIO(20),EMWHGR(20),GINT(20),EMWHGI(20),TTEST(31),K
       5A(10),KB(10),KC(10),KD(10),VARE(10),VARP(10),PHEAT(10),NEREF(10),V
       6TCPL(20),TTCPL(20),ENTH(20),EMWHTH(20),RESIS2(20,20)
        DIMENSION SLOPE1(300),SLOPE2(300),ETCPT1(300),ETCPT2(300),RCOR1(30
       10),RCOR2(300),SIGA1(300),SIGA2(300),SIGB1(300),SIGB2(300),V(300),T
       2WO1(300),TWO2(300),QA(300),QB(300),Q1(300),Q2(300),QLOS1(300),QLOS
       32(300),TB(300),TB1(300),TB2(300),TWI1(300),TWI2(300),QAREA1(300),Q
       4AREA2(300),H1(300),H2(300),H(300),RMEAN(300),EMMEAN(300),EMWMEN(30
       50),CPMEAN(300),EKMEAN(300),QINH(300),QIN(300),ERR(300),ENU(300),PR
       6(300),RE(300),RATIO(300),DATE(300),QINH1(300),QINH2(300),X(300),Y(
       7300),Z(300),W(300),EMWH(300),VARA(10),VARB(10),VARC(10),VARD(10)
D       DIMENSION C11(1),C12(1),C13(1),C14(1),C15(1),C22(1),C23(1),C24(1),
D      1C25(1),C33(1),C34(1),C35(1),C44(1),C45(1),C55(1),E1(1),E2(1),E3(1)
D      2,E4(1)
D       DIMENSION DETERM(5)
  806   DO 41 L=1,NCORRS
        II=1
        VARE(L)=0.0
        E1=AA(L)
        E2=B(L)
        E3=C(L)
        E4=D(L)
D       C112=C11
D       C212=C12
D       C312=C13
D       C412=C14
D       C152=C15
D       C222=C22
D       C322=C23
D       C422=C24
D       C252=C25
D       C332=C33
```

TABLE A4.1 (CONTINUED)

```
D       C432=C34
D       C352=C35
D       C442=C44
D       C452=C45
   131  IF(KA(L))120,120,130
D  130  C112=1.
D       C212=0.
D       C312=0.
D       C412=0.
        IF(II-1)900,900,120
D  900  C252=C252-C12*E1
D       C352=C352-C13*E1
D       C452=C452-C14*E1
   120  IF(KB(L))140,140,150
D  150  C212=0.
D       C222=1.
D       C322=0.
D       C422=0.
        IF(II-1)901,901,140
D  901  C152=C152-C12*E2
D       C352=C352-C23*E2
D       C452=C452-C24*E2
   140  IF(KC(L))160,160,170
D  170  C312=0.
D       C322=0.
D       C332=1.
D       C432=0.
        IF(II-1)902,902,160
D  902  C152=C152-C13*E3
D       C252=C252-C23*E3
D       C452=C452-C34*E3
   160  IF(KD(L))119,119,904
D  119  C412=0.
D       C422=0.
D       C432=0.
D       C442=1.
D       C452=0.
        IF(II-1)903,903,904
D  903  C152=C152-C14*E4
D       C252=C252-C24*E4
D       C352=C352-C34*E4
   904  IF(KA(L))701,701,700
D  700  C152=0.
   701  IF(KB(L))703,703,702
D  702  C252=0.
   703  IF(KC(L))611,611,704
D  704  C352=0.
D  611  C122=C212
D       C132=C312
D       C142=C412
D       C232=C322
D       C242=C422
D       C342=C432
        GO TO (610,121,141,161,104),II
D  610  S1=C332*C442-C342*C432
D       S2=C322*C442-C342*C422
D       S3=C322*C432-C332*C422
D       S4=C312*C442-C342*C412
D       S5=C312*C432-C332*C412
```

TABLE A4.1 (CONTINUED)

```
D      S6=C312*C422-C322*C412
D      RONIM1=C222*S1-C232*S2+C242*S3
D      RONIM2=C212*S1-C232*S4+C242*S5
D      RONIM3=C212*S2-C222*S4+C242*S6
D      RONIM4=C212*S3-C222*S5+C232*S6
D  613 DETERM(II)=C112*RONIM1-C122*RONIM2+C132*RONIM3-C142*RONIM4
       IF(II-1)614,614,615
  614  VARA(L)=0.
       VARB(L)=0.
       VARC(L)=0.
       VARD(L)=0.
  615  GO TO(100,101,102,103,104),II
D  100 C112=C152
D      C212=C252
D      C312=C352
D      C412=C452
       II=II+1
       GO TO 610
D  101 C112=C11
D      C212=C12
D      C312=C13
D      C412=C14
       GO TO 131
D  121 C122=C152
D      C222=C252
D      C322=C352
D      C422=C452
       II=II+1
       GO TO 610
D  102 C122=C12
D      C222=C22
D      C322=C23
D      C422=C24
       GO TO 131
D  141 C132=C152
D      C232=C252
D      C332=C352
D      C432=C452
       II=II+1
       GO TO 610
D  103 C132=C13
D      C232=C23
D      C332=C33
D      C432=C34
       GO TO 131
D  161 C142=C152
D      C242=C252
D      C342=C352
D      C442=C452
       II=II+1
       GO TO 610
  104  IF(KA(L))105,105,106
  105  AA(L)=DETERM(2)/DETERM(1)
  106  IF(KB(L))107,107,108
  107  B(L)=DETERM(3)/DETERM(1)
  108  IF(KC(L))109,109,110
  109  C(L)=DETERM(4)/DETERM(1)
  110  IF(KD(L))111,111,112
  112  D(L)=DETERM(5)/DETERM(1)
```

TABLE A4.1 (CONTINUED)

```
111 NFRFE(L)=C11
    NFREE(L)=NFREE(L)-3+KA(L)+KB(L)+KC(L)-KD(L)
    ENFREE=NFREE(L)
    DO 33 I=1,N
    IF(RE(I))33,33,34
 34 VARE(L)=VARE(L)+(AA(L)+B(L)*X(I)+C(L)*Z(I)+D(L)*W(I)-Y(I))**2
 33 CONTINUE
    VARE(L)=VARE(L)/ENFREE
 81 VARP(L)=(C55-C15**2/C11)/(C11-1.0)
    RHEAT(L)=SQRTF(1.0-VARE(L)*ENFREE/(C11-1.0)/VARP(L))
 41 CONTINUE
    RETURN
    END
```

TABLE A4.1 (CONTINUED)

```
*     LIST 8
*     LABEL
*     SYMBOL TABLE
      SUBROUTINE WOT
C     WOT HAS 102 CARDS       6-12-63
      COMMON SUMX,SUMY,SUMX2,SUMXY,SUMY2,SLOPE,ENTCPT,SIG2E,SIG2P,SIGA,S
     1IGB,RLIN,NOT,KPUNCH
      COMMON M,NR1,NR2,NEM1,NEM2,NCP1,NCP2,NEK1,NEK2,NRES1,NRES2,NQLOS1,
     1NQLOS2,NTCPLT,NTMCP1,NTMCP2,NGRAT,NGINT,MOVER,NCORRS,NIT,N,KA,KB,K
     2C,KD,KH,KQ,NFREE,NTH
      COMMON DIA,ERROR1,ERROR2,FAC1,FAC2,FAC3,FAC4,FAC5,FAC6,FAC7,FAC8,F
     1KWALO,EKWAL1,A,AA,B,C,D,TP,P,EMWHP,TEM,EM,EMWHEM,TCP,CP,EMWHCP,TEK
     2,EK,EMWHEK,TRES,RESIS1,EMWHRE,TQLOS,QLOS,EMWHQL,TTMCPL,VTMCPL,VTCP
     3C,VTCPCP,XTCPL,GRATIO,EMWHGR,GINT,EMWHGI,SLOPE1,SLOPE2,ETCPT1,ETCP
     4T2,RCOR1,RCOR2,SIGA1,SIGA2,SIGB1,SIGB2,V,TWO1,TWO2,QA,QB,Q1,Q2,QLO
     5S1,QLOS2,TB,TP1,TP2,TWI1,TWI2,          QAREA1,QAREA2,H1,H2,H,RM
     6EAN,EMMEAN,EMWMEN,CPMEAN,EKMEAN,QINH,QIN,ERR,ENU,PR,RE,RATIO,DATE,
     7QINH1,QINH2,TTEST,VARE,VARP,RHEAT,X,Y,Z,W,COEF11,COEF12,COEF13,COE
     8F14, COEF15,COEF22,COEF23,COEF24,COEF25,COEF33,COEF34,COEF35,COEF4
     94,COEF45,RTEST,YSQ,ENTH,EMWHTH,RESIS2,VTCPL,TTCPL,EMWH,NREAD,KPUNC
      COMMON VARA,VARB,VARC,VARD
      COMMON C11,C12,C13,C14,C15,C22,C23,C24,C25,C33,C34,C35,C44,C45,C55
     1,F1,F2,F3,F4
      DIMENSION A(10),AA(10),B(10),C(10),D(10),TP(20),P(20,20),EMWHP(20)
     1,TEM(20),EM(20,20),EMWHEM(20),TCP(20),CP(20,20),EMWHCP(20),TEK(20)
     2,EK(20,20),EMWHEK(20),TRES(20),RESIS1(20,20),EMWHRE(20),TQLOS(20),
     3QLOS(20,20),EMWHQL(20),TTMCPL(20),VTMCPL(20),VTCPC(20),VTCPCP(20,2
     40),XTCPL(20),GRATIO(20),EMWHGR(20),GINT(20),EMWHGI(20),TTEST(31),K
     5A(10),KB(10),KC(10),KD(10),VARE(10),VARP(10),RHEAT(10),NFREE(10),V
     6TCPL(20),TTCPL(20),ENTH(20),EMWHTH(20),RESIS2(20,20)
      DIMENSION SLOPE1(300),SLOPE2(300),ETCPT1(300),ETCPT2(300),RCOR1(30
     10),RCOR2(300),SIGA1(300),SIGA2(300),SIGB1(300),SIGB2(300),V(300),T
     2WO1(300),TWO2(300),QA(300),QB(300),Q1(300),Q2(300),QLOS1(300),QLOS
     32(300),TB(300),TB1(300),TB2(300),TWI1(300),TWI2(300),QAREA1(300),Q
     4AREA2(300),H1(300),H2(300),H(300),RMEAN(300),EMMEAN(300),EMWMEN(30
     50),CPMEAN(300),EKMEAN(300),QINH(300),QIN(300),ERR(300),ENU(300),PR
     6(300),RE(300),RATIO(300),DATE(300),QINH1(300),QINH2(300),X(300),Y(
     7300),Z(300),W(300),WILSON(300),HINV(300),EMWH(300),VARA(10),VARB(1
     80),VARC(10),VARD(10)
D     DIMENSION C11(1),C12(1),C13(1),C14(1),C15(1),C22(1),C23(1),C24(1),
D    1C25(1),C33(1),C34(1),C35(1),C44(1),C45(1),C55(1),E1(1),E2(1),E3(1)
D    2,E4(1)
      WRITEOUTPUTTAPE NOT,1
    1 FORMAT(1H1,28X25HDATA FOR LEFT HALF HEATER)
      WRITEOUTPUTTAPE NOT,2,(DATE(I),SLOPE1(I),SIGB1(I),ETCPT1(I),SIGA1(
     1I),RCOR1(I),I=1,N)
    2 FORMAT(1H5,5X3HRUN,9X6HSLOPE     S.D.(SLOPE)   INTERCEPT   S.D.(I
     1NTCP)  CORR. COEFF/(4XA6,3X,1P5E13.5))
      WRITEOUTPUTTAPE NOT,3,(DATE(I),V(I),QA(I),QLOS1(I),Q1(I),QINH1(I),
     1I=1,N)
    3 FORMAT(1H5,5X3HRUN,8X8HVELOCITY,7X1HQ,11X5HQLOST,8X4HQNET, 9X6HQ H
     1EAT/(4XA6,3X,1P5E13.5))
      WRITEOUTPUTTAPE NOT,4,(DATE(I),QAREA1(I),TWO1(I),TWI1(I),TB1(I),H1
     1(I),I=1,N)
    4 FORMAT(1H5,5X3HRUN,10X3HQ/A,9X3HTWO,11X3HTWI,9X5HTBULK,10X1HH/(4XA
     16,3X,1P5E13.5))
      WRITEOUTPUTTAPE NOT,5
    5 FORMAT(1H1,27X26HDATA FOR RIGHT HALF HEATER)
      WRITEOUTPUTTAPE NOT,2,(DATE(I),SLOPE2(I),SIGB2(I),ETCPT2(I),SIGA2(
```

TABLE A4.1 (CONTINUED)

```
     1I),RCOR2(I),I=1,N)
      WRITEOUTPUTTAPE NOT,3,(DATE(I),V(I),QB(I),QLOS2(I),Q2(I),QINH2(I),
     1I=1,N)
      WRITEOUTPUTTAPE NOT,4,(DATE(I),QAREA2(I),TWO2(I),TWI2(I),TB2(I),H2
     1(I),I=1,N)
      WRITEOUTPUTTAPE NOT,6
    6 FORMAT(1H1,21X37HMEAN PROPERTIES OF THE HEATER SECTION)
      WRITEOUTPUTTAPE NOT,7,(DATE(I),QIN(I),QINH(I),ERR(I),H(I),TB(I),I=
     11,N)
    7 FORMAT(1H5,5X3HRUN,6X47HQ ELECTRIC    Q THERMAL    ERROR Q/Q     M
     1EAN H,7X6HBULK T/(4XA6,3X,1P5E13.5))
      WRITEOUTPUTTAPE NOT,8,(DATE(I),RMEAN(I),EMMEAN(I),EMWMEN(I),CPMEAN
     1(I),EKMEAN(I),I=1,N)
    8 FORMAT(1H5,5X3HRUN,8X7HDENSITY,7X2HMU,12X3HMUW,10X2HCP,12X1HK/(4XA
     16,3X,1P5E13.5))
      WRITEOUTPUTTAPE NOT,9,(DATE(I),ENU(I),PR(I),RATIO(I),I=1,N)
    9 FORMAT(1H5,5X3HRUN,6X34HNUSSELT NO.  PRANDTL NO.    MU/MUW/(4XA6,3
     1X,1P3E13.5))
      WRITEOUTPUTTAPE NOT,12,(VARF(L),VARP(L),L=1,NCORRS),C11(1),C12(1),
     1C13(1),C14(1),C15(1),C22(1),C23(1),C24(1),C25(1),C33(1),C34(1),C35
     2(1),C44(1),C45(1),C55(1)
   12 FORMAT(1H1,30X21HMISCELLANEOUS NUMBERS/(6E13.5))
      IF(KPUNCH)10,10,11
   10 PUNCH 1
      PUNCH 2,(DATE(I),SLOPE1(I),SIGB1(I),ETCPT1(I),SIGA1(I),RCOR1(I),I=
     11,N)
      PUNCH 3,(DATE(I),V(I),QA(I),QLOS1(I),Q1(I),QINH1(I),I=1,N)
      PUNCH 4,(DATE(I),QAREA1(I),TWO1(I),TWI1(I),TB1(I),H1(I),I=1,N)
      PUNCH 5
      PUNCH 2,(DATE(I),SLOPE2(I),SIGB2(I),ETCPT2(I),SIGA2(I),RCOR2(I),I=
     11,N)
      PUNCH 3,(DATE(I),V(I),QB(I),QLOS2(I),Q2(I),QINH2(I),I=1,N)
      PUNCH 4,(DATE(I),QAREA2(I),TWO2(I),TWI2(I),TB2(I),H2(I),I=1,N)
      PUNCH 6
      PUNCH 7,(DATE(I),QIN(I),QINH(I),ERR(I),H(I),TB(I),I=1,N)
      PUNCH 8,(DATE(I),RMEAN(I),EMMEAN(I),EMWMEN(I),CPMEAN(I),EKMEAN(I),
     1I=1,N)
      PUNCH 9,(DATE(I),ENU(I),PR(I),RATIO(I),I=1,N)
      PUNCH 12,(VARF(L),VARP(L),L=1,NCORRS),C11(1),C12(1),C13(1),C14(1),
     1C15(1),C22(1),C23(1),C24(1),C25(1),C33(1),C34(1),C35(1),C44(1),C45
     2(1),C55(1)
   11 RETURN
      END
```

TABLE A4.1 (CONTINUED)

```
*       LIST A
*       LABEL
*       SYMBOL TABLE
        SUBROUTINE CRRL
C       CRRL HAS 137 CARDS      6-17-63
        COMMON SUMX,SUMY,SUMX2,SUMXY,SUMY2,SLOPE,ENTCPT,SIG2E,SIG2P,SIGA,S
       1IGB,RLIN,NOT,KPUNCH
        COMMON M,NR1,NR2,NEM1,NEM2,NCP1,NCP2,NEK1,NEK2,NRES1,NRES2,NQLOS1,
       1NQLOS2,NTCPLT,NTMCP1,NTMCP2,NGRAT,NGINT,MOVER,NCORRS,NIT,N,KA,KB,K
       2C,KD,KH,KQ,NFREE,NTH
        COMMON DIA,ERROR1,ERROR2,FAC1,FAC2,FAC3,FAC4,FAC5,FAC6,FAC7,FAC8,E
       1KWAL0,EKWAL1,A,AA,B,C,D,TR,R,EMWHR,TEM,EM,EMWHEM,TCP,CP,EMWHCP,TEK
       2,EK,EMWHEK,TRES,RESIS1,EMWHRE,TQLOS,QLOS,EMWHQL,TTMCPL,VTMCPL,VTCP
       3C,VTCPCR,XTCPL,GRATIO,EMWHGR,GINT,EMWHGI,SLOPE1,SLOPE2,ETCPT1,ETCP
       4T2,RCOR1,RCOR2,SIGA1,SIGA2,SIGB1,SIGB2,V,TWO1,TWO2,QA,QB,Q1,Q2,QLO
       5S1,QLOS2,TB,TB1,TB2,TWI1,TWI2,          QAREA1,QAREA2,H1,H2,H,RM
       6EAN,EMMEAN,EMWMEN,CPMEAN,EKMEAN,QINH,QIN,ERR,ENU,PR,RE,RATIO,DATE,
       7QINH1,QINH2,TTEST,VARE,VARP,RHEAT,X,Y,Z,W,COEF11,COEF12,COEF13,COE
       8F14, COEF15,COEF22,COEF23,COEF24,COEF25,COEF33,COEF34,COEF35,COEF4
       04,COEF45,RTEST,YSQ,ENTH,EMWHTH,RESIS2,VTCPL,TTCPL,EMWH,NREAD,KPUNC
        COMMON VARA,VARB,VARC,VARD
        COMMON C11,C12,C13,C14,C15,C22,C23,C24,C25,C33,C34,C35,C44,C45,C55
       1,E1,E2,E3,E4
        DIMENSION A(10),AA(10),B(10),C(10),D(10),TR(20),R(20,20),EMWHR(20)
       1,TEM(20),EM(20,20),EMWHEM(20),TCP(20),CP(20,20),EMWHCP(20),TEK(20)
       2,EK(20,20),EMWHEK(20),TRES(20),RESIS1(20,20),EMWHRE(20),TQLOS(20),
       3QLOS(20,20),EMWHQL(20),TTMCPL(20),VTMCPL(20),VTCPC(20),VTCPCR(20,2
       40),XTCPL(20),GRATIO(20),EMWHGR(20),GINT(20),EMWHGI(20),TTEST(31),K
       5A(10),KB(10),KC(10),KD(10),VARE(10),VARP(10),RHEAT(10),NFREE(10),V
       6TCPL(20),TTCPL(20),ENTH(20),EMWHTH(20),RESIS2(20,20)
        DIMENSION SLOPE1(300),SLOPE2(300),ETCPT1(300),ETCPT2(300),RCOR1(30
       10),RCOR2(300),SIGA1(300),SIGA2(300),SIGB1(300),SIGB2(300),V(300),T
       2WO1(300),TWO2(300),QA(300),QB(300),Q1(300),Q2(300),QLOS1(300),QLOS
       32(300),TB(300),TB1(300),TB2(300),TWI1(300),TWI2(300),QAREA1(300),Q
       4AREA2(300),H1(300),H2(300),H(300),RMEAN(300),EMMEAN(300),EMWMEN(30
       50),CPMEAN(300),EKMEAN(300),QINH(300),QIN(300),ERR(300),ENU(300),PR
       6(300),RE(300),RATIO(300),DATE(300),QINH1(300),QINH2(300),X(300),Y(
       7300),Z(300),W(300),WILSON(300),HINV(300),EMWH(300),VARA(10),VARB(1
       80),VARC(10),VARD(10)
D       DIMENSION C11(1),C12(1),C13(1),C14(1),C15(1),C22(1),C23(1),C24(1),
D      1C25(1),C33(1),C34(1),C35(1),C44(1),C45(1),C55(1),E1(1),E2(1),E3(1)
D      2,E4(1)
        XAV=C12/C11
        ZAV=C13/C11
        WAV=C14/C11
D       C22=C22-C12**2/C11
D       C23=C23-C12*C13/C11
D       C33=C33-C13**2/C11
        DO 2 L=1,NCORRS
D       C242=C24-C12*C14/C11
D       C342=C34-C13*C14/C11
D       C442=C44-C14**2/C11
        IF(KA(L))100,100,106
  100   IF(KB(L))101,101,106
  101   IF(KC(L))102,102,106
  102   IF(KD(L))106,103,104
D 103   C242=0.
D       C342=0.
D       C442=1.
```

TABLE A4.1 (CONTINUED)

```
  104 VARA(L)=VARF(L)/C11
D     DETERM=C22*(C33*C442-C342**2)-C23*(C23*C442-C342*C242)+C242*(C23*C
D    1342-C33*C242)
D     VB=(C33*C442-C342**2)/DETERM
      VARB(L)=VB*VARE(L)
D     VC=(C22*C442-C242**2)/DETERM
      VARC(L)=VC*VARE(L)
      IF(KD(L))106,106,105
D 105 VD=(C22*C33-C23**2)/DETERM
      VARD(L)=VD*VARE(L)
  106 N1=1
    3 IF(NFREE(L)-31)4,4,5
    5 NF=31
      GO TO 64
    4 NF=NFREE(L)
   64 A(L)=EXPF(AA(L))
      WRITEOUTPUTTAPE NOT,43
      IF(KPUNCH)45,45,46
   45 PUNCH 43
   46 DO 41 I=1,N
      HINV(I)=1.0/H(I)
      WILSON(I)=1.0/V(I)**B(L)
      IF(WILSON(I)-WILSON(I-1))39,39,49
   49 IF(I-N)41,50,50
   50 N2=I
      GO TO 40
   39 N2=I-1
   40 IF(N2-N1)42,41,42
   42 CALL LINLSQ(N1,N2,WILSON,HINV,-1)
      WRITEOUTPUTTAPE NOT,44,DATE(N1),DATE(N2 ),SLOPE,ENTCPT,SIGB,SIGA,R
     1LIN
      IF(KPUNCH)47,47,48
   47 PUNCH 44,DATE(N1),DATE(N2 ),SLOPE,ENTCPT,SIGB,SIGA,RLIN
   48 N1=I
   41 CONTINUE
   43 FORMAT(1H1,5X4HRUNS,5X64HWILSON SLOPE    INTERCEPT    S.D.(SLOPE)  S
     1.D.(INTCP)  CORR. COEFF)
   44 FORMAT(1XA6,1H-,A6,1P5E13.5)
      WRITEOUTPUTTAPE NOT,29
      IF(KPUNCH)33,33,34
   33 PUNCH 29
   34 DO 27 I=1,N
      IF(RE(I))27,27,65
   65 REB=RE(I)**B(L)
      PRC=PR(I)**C(L)
      IF(KD(L))7,6,7
    7 RATIOD=RATIO(I)**D(L)
      GO TO 8
    6 RATIOD=1.0
    8 CORREL=ENU(I)/RATIOD/PRC
   25 VARCOR=VARA(L)+VARB(L)*(X(I)-XAV)**2+VARC(L)*(Z(I)-ZAV)**2+VARD(L)
     1*(W(I)-WAV)**2
   26 SDCORR=TTEST(NF)*SQRTF(VARCOR)*CORREL
      WRITEOUTPUTTAPE NOT,30,DATE(I),HINV(I),WILSON(I),RE(I),CORREL,SDCO
     1RR
      IF(KPUNCH)28,28,27
   28 PUNCH 30,DATE(I),HINV(I),WILSON(I),RE(I),CORREL,SDCORR
   27 CONTINUE
      VARA(L)=SQRTF(VARA(L)+XAV**2*VARB(L)+ZAV**2*VARC(L)+WAV**2*VARD(L)
```

TABLE A4.1 (CONTINUED)

```
     1)*A(L)
      VARB(L)=SQRTF(VARB(L))
      VARC(L)=SQRTF(VARC(L))
      VARD(L)=SQRTF(VARD(L))
      RMS=SQRTF(VARE(L))*100.
      WRITEOUTPUTTAPE NOT,31,A(L),VARA(L),B(L),VARB(L),C(L),VARC(L),D(L)
     1,VARD(L),RMS,RHEAT(L)
      IF(KPUNCH)32,32,2
   32 PUNCH 31,A(L),VARA(L),B(L),VARB(L),C(L),VARC(L),D(L),VARD(L),RMS,R
     1HEAT(L)
    2 CONTINUE
      RETURN
   29 FORMAT(1H0,5X3HRUN,9X5H1.0/H,6X49H1.0/V**B     REYNOLDS NO  CORRELA
     1TION  CONF. LEVEL)
   30 FORMAT(4XA6,3X,1P5E13.5)
   31 FORMAT(6H5   NU=0PF7.5,1H$1PE11.4,6H*(RE**0PF7.5,1H$1PE11.4,7H)*(PR
     1**0PF7.5,1H$1PE11.4,2H)*//1X9H(MU/MUW**1PE11.4,1H$1PE11.4,12H)  RM
     2S DEV.=0PF6.3,23H 0/0  CORRELATION COEF=0PF6.4)
      END
```

TABLE A4.1 (CONTINUED)

```
*       LIST 8
*       LABEL
*       SYMBOL TABLE
        SUBROUTINE LINLSQ(N1,N2,X,Y,N3)
C       LINLSQ HAS 43 CARDS                    7-26-62
        COMMON SUMX,SUMY,SUMX2,SUMXY,SUMY2,SLOPE,ENTCPT,SIG2E,SIG2P,SIGA,S
       1IGB,RLIN,NOT,KPUNCH
        DIMENSION X(300),Y(300)
        SUMX=0.0
        SUMY=0.0
        SUMX2=0.0
        SUMXY=0.0
        SUMY2=0.0
        EN=N2-N1+1
        DO 1 I=N1,N2
   12   SUMX=SUMX+X(I)
        SUMY=SUMY+Y(I)
        SUMX2=SUMX2+X(I)**2
        SUMXY=SUMXY+X(I)*Y(I)
        SUMY2=SUMY2+Y(I)**2
    1   CONTINUE
        DEN=EN*SUMX2-SUMX**2
        SLOPE=(EN*SUMXY-SUMX*SUMY)/DEN
        ENTCPT=(SUMY*SUMX2-SUMX*SUMXY)/DEN
        SIG2E=(SUMY2-ENTCPT*SUMY-SLOPE*SUMXY)/(EN-2.0)
        IF(SIG2E)9,9,10
    9   SIG2E=0.0
   10   SIG2P=(SUMY2-SUMY**2/EN)/(EN-1.0)
        SIGB=SQRTF(EN*SIG2E/DEN)
        SIGA=SQRTF(SUMX2*SIG2E/DEN)
        RLIN=SQRTF(1.0-SIG2E*(EN-2.0)/SIG2P/(EN-1.0))
        IF(N3)8,2,5
    2   WRITEOUTPUTTAPE NOT,3
    3   FORMAT(75H      SLOPE      S.D.(SLOPE)    INTERCEPT    S.D.(INTCP)  CO
       1RR. COEFF      SIG2E)
        IF(KPUNCH)4,4,5
    4   PUNCH 3
    5   WRITEOUTPUTTAPE NOT,6,SLOPE,SIGB,ENTCPT,SIGA,RLIN,SIG2E
    6   FORMAT(1P6E13.5)
        IF(KPUNCH)7,7,8
    7   PUNCH 6,SLOPE,SIGB,ENTCPT,SIGA,RLIN,SIG2E
    8   RETURN
        END
```

TABLE A4.1 (CONTINUED)

```
*       INT2D HAS 120 CARDS
*       FAP
        COUNT   120
      1 TTL     TWO DIMENSIONAL LINEAR INTERPOLATION FOR FORTRAN
        LBL     INT2D
        ENTRY   INT2D
        REM     THE FORTRAN CALLING SEQUENCE IS . . .
        REM     CALL INT2D(N1,N2,A,B,C,PA,PB,Q)
        REM
        REM     N1 IS THE NUMBER OF ELEMENTS IN A
        REM     N2 IS THE NUMBER OF ELEMENTS IN B
        REM     A IS THE FIRST INDEPENDENT VARIABLE  (20 EL MATRIX)
        REM     B IS THE SECOND INPEDENDENT VARIABLE  (1D MATRIX)
        REM     C IS THE DEPENDENT VARIABLE  (20 X N MATRIX)
        REM     PA IS THE PARTICULAR VALUE OF A
        REM     PB IS THE PARTICULAR VALUE OF B
        REM     Q IS THE ANSWER RETURNED BY THE SUBROUTINE
        REM
        REM     FOR 1D INTERPOLATION SET N2= TO COLUMN NO. OF C DESIRED.
        REM     SETB,PB=0
        REM
 INT2D  CLA*    1,4
        SUB     =01000000
        TZE     ONEELA                  ONLY ONE ELEMENT
        SXA     BACK,1                  SAVE INDEX REGISTERS
        SXA     BACK+1,2
        SXD     INT2D-2,4
        STD     N1LOOP
        CLA     3,4
        STA     NLOOP1+1
        STA     SETA
        ADD     =1
        STA     SETA1
        CLA     6,4
        STA     NLOOP1
        AXT     0,1
NLOOP1  CLA      PA
        FSB     **,1                    PA-A(L)
        TMI     *+8
        TXI     *+1,1,1                 FIND THE RIGHT A INTERVAL
N1LOOP  TXL     NLOOP1,1, N1-1
   OUT  TSX     $ERROR,4
        PZE     ALPHA                   ERROR IN DATA
        TXI     *+2,0,0
        PZE     INT2D-2,0,0
        TSX     $EXIT,4
        TXL     OUT,1,0
        STO     DATA
        CLA*    2,4
        SUB     =01000000
        TZE     1D
        NZT*    4,4                     2D OR 1D
        TRA     1D
        STD     N2LOOP
        CLA     4,4
        STA     NLOOP2+1
        STA     SETB
        ADD     =1
        STA     SETB1
        CLA     7,4
```

TABLE A4.1 (CONCLUDED)

```
        STA     NLOOP2
        AXT     0,2
NLOOP2  CLA      PB
        FSB     **,2
        TMI     *+4
        TXI     *+1,2,1                 FIND THE RIGHT B INTERVAL
N2LOOP  TXL     NLOOP2,2, N2-1
        TRA     OUT
        TXL     OUT,2,0
        STO     DATA+1
        SXD     IR2,2
        PXD     0,2
        AXT     2,2
 LOOP3  SSM
        XCA
        MPY     =024000000              FIND C ELEMENTS
        ARS     1
        ADD     5,4
        STA     SETC
        STA     1SETC
        ADD     =1
        STA     SETC1
  SETA  CLA     **,1
 SETA1  FSB     **,1                    A(L)-A(L-1)
        STO     Q+2,2
  SETC  CLA     **,1
 SETC1  FSB     **,1                    C(L,IR2)-C(L-1,IR2)
        FDP     Q+2,2
        FMP     DATA
 1SETC  FAD     **,1                    C(L,IR2)
        STO     Q+2,2
        NZT*    4,4                     1D OR 2D
        TRA     BACK-1
        CLA     IR2
        SUB     =01000000
        TIX     LOOP3,2,1
        LXD     IR2,2
  SETB  CLA     **,2
 SETB1  FSB     **,2                    B(K)-B(K-1)
        STO     DATA
        CLA     Q
        FSB     Q+1
        FDP     DATA
        FMP     DATA+1
        FAD     Q
        STO*    8,4                     ANSWER
  BACK  AXT     **,1
        AXT     **,2
        TRA     9,4
ONEELA  CLA*    5,4
        STO*    8,4
        TRA     9,4
    1D  AXT     1,2
        TRA     LOOP3
  DATA  BSS     2
     Q  BSS     2
   IR2  PZE
 ALPHA  BCI     5, EXTRAPOLATION IS NOT POSSIBLE
        OCT     777777777777
        END
```

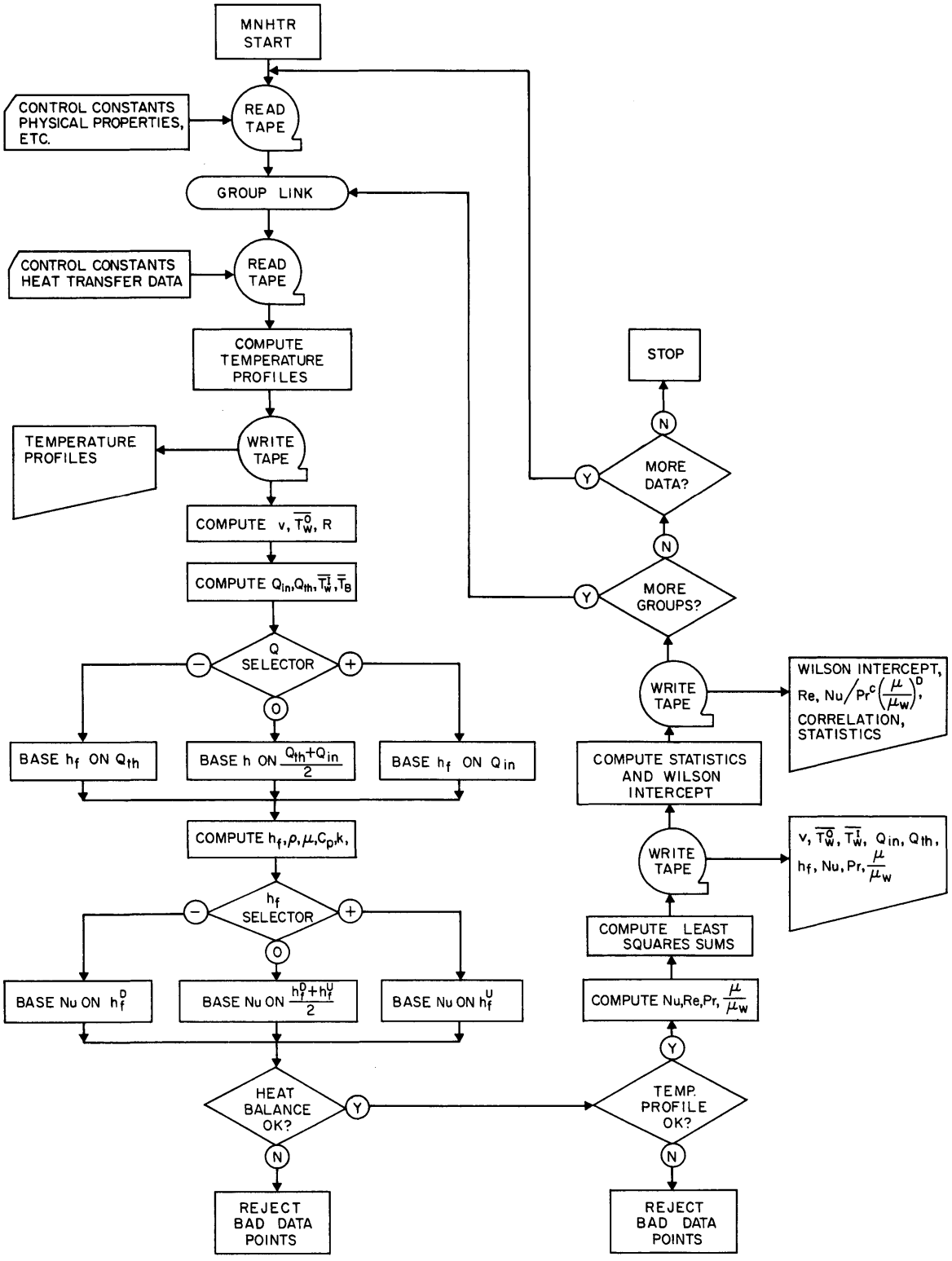

FIGURE A4.8 LOGIC FLOWSHEET FOR MNHTR

TABLE A4.2
SAMPLE INPUT TO MNHTR

```
                                CONSTANT DATA
  1   7   2   7   3   1   2   7   2   1   2   1   2  17  12  10   1   1
  1   2   0   1
                        GEOMETRY AND CONVERSION FACTORS
  0.207         100.0         0.00005       0.40856       312.86        146.78
  0.71345       100.0         1602.57       1.218948      -4.605158     8.5166667
  0.00416667    0.8           0.004         0.9           0.4           0.
  0.023         0.8           0.4           0.
        DENSITY= F(TEMP, MWH) TABLE FOR 750 DEG. F IRRADIATION, GM/CC
  400.          0.962         0.967         0.997         0.989         1.019
  0.993         0.993         800.          0.781         0.785         0.821
  0.812         0.854         0.820         0.820         -0.001        250.
  1060.         1120.         2040.         2260.         4000.
VISCOSITY= F(1./(T+460.), MWH) TABLE FOR 750 DEG. F IRRADIATION, MU IN CP
  0.60252E-3    -2.33         -2.24         -1.89         -1.89         -1.54
  -1.83         -1.83         0.79384E-3    -1.57         -1.5          -1.09
  -1.12         -0.65         -1.02         -1.02         1.16320E-3    -0.11
  -0.06         0.44          0.35          1.04          0.52          0.52
  -0.001        250.          1060.         1120.         2040.         2260.
  4000.
SPECIFIC HEAT= F(TEMP, MWH) TABLE FOR 750 DEG. F IRRADIATION, CAL/GM/DEG. C
  400.          0.5           800.          0.61          0.
THERMAL CONDUCTIVITY=F(T,MWH) TABLE FOR 750 IRR,(CAL/CM/SEC/DEG. C)*10**4
  400.          3.02          3.11          3.3           3.29          3.46
  3.32          3.32          800.          2.33          2.48          2.8
  2.78          3.05          2.83          2.83          -0.001        250.
  1060.         1120.         2040.         2260.         4000.
ELECTRICAL RESISTANCE AS A FUNCTION OF TEMPERATURE AND MWH TABLE  OHMS
  400.0         0.0279        0.0279        950.0         0.0339        0.0339
  0.
   HEAT LOSS AS A FUNCTION OF TEMPERATURE AND MWH TABLE  WATTS
  400.          55.           1200.         331.          0.
                THERMOCOUPLE TEMPERATURE-VOLTAGE TABLE
  400.0         8.31          450.0         9.43          500.0         10.57
  550.0         11.71         600.0         12.86         650.0         14.02
  700.0         15.18         750.0         16.35         800.0         17.53
  850.0         18.70         900.0         19.89         950.0         21.07
  1000.0        22.26         1050.0        23.44         1100.0        24.63
  1150.0        25.81         1200.0        26.98
                        750 DEG RUN TEST HEATER TABLE
  -1.0          0.
        THERMOCOUPLE CORRECTION TABLE FOR TH 6 RUN AT 750
  0.            0.            0.            -0.025        0.            0.045
  0.24          -0.015        -0.07         -0.05         -0.05         -0.07
  -0.10         10.           10.           10.           9.975         10.1
  10.045        10.24         9.985         9.93          9.95          9.95
  9.93          9.9           11.           11.           11.           11.
  11.1          11.065        11.24         11.025        10.98         10.99
  10.99         10.98         10.97         12.           12.           12.
  12.03         12.1          12.085        12.24         12.04         12.02
  12.025        12.025        12.02         12.01         13.           13.
  13.           13.05         13.1          13.11         13.34         13.06
  13.03         13.05         13.05         13.04         13.04         14.
  14.           14.           14.065        14.1          14.13         14.43
  14.07         14.055        14.07         14.07         14.055        14.06
  15.           15.           14.99         15.075        15.1          15.135
  15.44         15.08         15.07         15.083        15.083        15.07
```

TABLE A4.2 (CONTINUED)

```
15.065          16.             16.             15.985          16.08           16.1
16.14           16.44           16.085          16.08           16.09           16.09
16.08           16.065          17.             17.             16.98           17.08
17.1            17.14           17.45           17.085          17.08           17.095
17.095          17.08           17.065          30.             30.             29.98
30.08           30.75           30.14           30.97           30.085          30.08
30.095          30.095          30.08           30.065
                                THERMOCOUPLE DISTANCES TABLE
0.0             24.0            3.0             4.5             6.0             7.5
9.0             15.0            16.5            18.0            19.5            21.0
                            SLOPE OF G CALIBRATION CURVE TABLE
1.051           0.0
                          INTERCEPT OF G CALIBRATION CURVE TABLE
0.006           0.0
                          95 PER CENT CONFIDENCE LIMIT TABLE
12.706          4.303           3.182           2.776           2.571           2.447
2.365           2.306           2.262           2.228           2.201           2.179
2.160           2.145           2.131           2.120           2.110           2.101
2.093           2.086           2.080           2.074           2.069           2.064
2.060           2.056           2.052           2.048           2.045           2.042
1.95996
                                    RSCALE TABLE
 1
0.              0.
1                   SPECIAL RUNS AT CONSTANT FLOW  750 DEG RUN
                                CONTROL TABLE
 20   0   0   0   0   0   1   1   0   1   1
2425.           1.8             8.605           9.085           13.683          14.441          2-60
16.325          16.41           16.45           16.20           16.69           16.78
17.04           17.215          16.76           16.8
2425.           1.14            8.61            9.09            13.628          14.802          2-59
17.48           17.555          17.63           17.375          17.93           18.145
18.47           18.655          18.12           18.19
2425.           1.8             8.7             9.16            15.858          16.585          2-61
18.1975         18.3            18.3375         18.06           18.585          18.575
18.89           19.06           18.605          18.5775
2425.           1.14            8.705           9.16            15.6345         16.779          2-62
19.12           19.245          19.305          19.04           19.635          19.755
20.13           20.32           19.75           19.785
2425.           1.8             8.405           8.895           11.565          12.3275         2-63
14.48           14.5425         14.5925         14.3625         14.81           15.005
15.205          15.355          14.925          15.0025
2425.           1.14            8.48            8.91            11.575          12.731          2-64
15.795          15.79           15.91           15.65           16.155          16.42
16.725          16.845          16.385          16.456
3599.           1.805           8.8             9.28            11.585          12.384          2-107
14.7            14.765          14.83           14.595          15.045          15.25
15.46           15.625          15.17           15.2525
3599.           1.5             8.815           9.29            11.5915         12.55           2-106
15.25           15.30           15.37           15.125          15.61           15.835
16.095          16.2525         15.7675         15.865
3599.           1.12            8.85            9.3             11.5905         12.849          2-105
16.26           16.245          16.38           16.095          16.625          16.89
17.215          17.37           16.85           16.94
3599.           1.8             8.84            9.295           12.661          13.4525         2-110
15.5725         15.6475         15.6075         15.4825         15.945          16.08
16.33           16.485          16.025          16.1
3599.           1.51            8.88            9.31            12.626          13.569          2-109
16.02           16.09           16.16           15.92           16.42           16.58
```

TABLE A4.2 (CONCLUDED)

16.8525	17.025	16.5325	16.62			
3599.	1.12	8.89	9.32	12.624	13.867	2-108
16.975	17.	17.105	16.855	17.405	17.61	
17.95	18.11	17.585	17.6775			
3599.	1.81	8.8	9.285	13.809	14.5795	2-112
16.5	16.5975	16.645	16.4	16.88	16.9625	
17.24	17.415	16.94	16.95			
3599.	1.12	8.85	9.3	13.669	14.8885	2-111
17.705	17.77	17.865	17.615	18.17	18.375	
18.7	18.885	18.335	18.425			
3599.	1.8	8.905	9.36	14.8405	15.631	2-113
17.505	17.595	17.64	17.385	17.88	17.945	
18.245	18.435	17.935	17.965			
3599.	1.5	8.91	9.38	14.811	15.7615	2-114
17.935	18.04	18.085	17.825	18.36	18.455	
18.775	18.97	18.44	18.49			
3599.	1.12	8.925	9.39	14.761	16.001	2-115
18.685	18.8	18.87	18.61	19.2	19.36	
19.72	19.925	19.335	19.4			
3599.	1.8	8.91	9.38	15.792	16.5675	2-118
18.315	18.425	18.46	18.205	18.715	18.715	
19.04	19.22	18.73	18.74			
3599.	1.495	8.92	9.385	15.714	16.645	2-117
18.675	18.8	18.845	18.585	19.135	19.185	
19.515	19.715	19.18	19.215			
3599.	1.12	8.94	9.395	15.612	16.8325	2-116
19.355	19.495	19.56	19.29	19.885	20.01	
20.37	20.585	19.995	20.05			

TABLE A4.3
SAMPLE OUTPUT FROM MNHTR

SPECIAL RUNS AT CONSTANT FLOW 750 DEG RUN
BATCH NO.= 1

TEMPERATURE PROFILES FOR ALL RUNS

2-60	635.5	668.0	752.3	756.8	760.2	762.4	768.0	771.6	783.3	790.7	770.8	771.8
2-59	633.1	683.4	801.3	806.5	810.3	813.2	820.7	829.7	844.2	852.1	828.6	831.0
2-61	729.0	759.2	831.9	840.0	840.5	843.7	848.7	848.1	862.0	869.1	849.4	847.5
2-62	719.4	767.4	871.0	881.8	881.3	886.6	892.9	897.7	914.2	922.2	897.5	898.3
2-63	543.6	576.8	672.8	676.8	680.4	683.5	687.4	695.5	704.7	711.1	692.0	695.2
2-64	544.1	594.4	729.7	730.3	737.2	738.9	745.3	756.4	769.9	775.0	754.9	757.2
2-107	544.5	579.3	682.4	686.4	690.7	693.6	697.6	706.1	715.7	722.8	702.6	705.9
2-106	544.8	586.5	706.2	709.4	714.0	716.5	721.9	731.3	743.0	749.7	728.4	732.1
2-105	544.8	599.5	749.6	749.8	757.2	757.9	765.3	776.3	790.7	797.2	774.6	777.8
2-110	591.3	625.5	720.1	724.3	724.2	731.7	736.3	741.9	753.0	759.6	739.5	742.1
2-109	589.8	630.6	739.3	743.2	747.9	750.4	756.6	763.1	775.3	782.6	761.1	764.2
2-108	589.7	643.4	779.9	781.8	787.9	790.4	798.3	806.8	822.0	828.8	805.8	809.1
2-112	640.9	673.9	759.7	764.7	768.4	770.9	776.1	779.3	791.7	799.2	778.4	778.2
2-111	634.9	687.1	810.9	816.2	820.3	823.9	831.0	839.5	854.0	861.8	837.8	841.0
2-113	685.4	718.7	802.4	808.3	810.7	813.7	818.6	821.2	834.6	842.7	820.7	821.4
2-114	684.1	724.3	820.7	828.3	829.7	833.2	839.1	842.9	857.1	865.3	842.3	843.8
2-115	681.9	734.4	852.7	862.2	863.0	867.8	874.6	881.1	896.8	905.5	880.0	882.1
2-118	726.2	758.5	837.0	845.6	845.7	850.1	854.2	854.0	868.3	875.8	854.6	854.4
2-117	722.8	761.7	852.3	862.2	862.0	866.7	871.8	873.7	888.2	896.6	873.5	874.4
2-116	718.5	769.6	880.9	892.8	892.0	897.5	903.4	908.5	924.4	933.5	907.8	909.5

DATA FOR LEFT HALF HEATER

RUN	SLOPE	S.D.(SLOPE)	INTERCEPT	S.D.(INTCP)	CORR. COEFF
2-60	2.46328E 00	1.89553E-01	7.45152E 02	1.20631E 00	9.91238E-01
2-59	3.04059E 00	2.74942E-01	7.92165E 02	1.74972E 00	9.87946E-01
2-61	2.48546E 00	4.07699E-01	8.26048E 02	2.59458E 00	9.61939E-01
2-62	3.23347E 00	5.82626E-01	8.63321E 02	3.70781E 00	9.54579E-01
2-63	2.38570E 00	4.81125E-02	6.65875E 02	3.06186E-01	9.99391E-01
2-64	2.65541E 00	3.76550E-01	7.20337E 02	2.39635E 00	9.71114E-01
2-107	2.50690E 00	9.25463E-02	6.75108E 02	5.88961E-01	9.97961E-01
2-106	2.56011E 00	1.61621E-01	6.98239E 02	1.02855E 00	9.94076E-01
2-105	2.63041E 00	4.71934E-01	7.40157E 02	3.00337E 00	9.54913E-01
2-110	2.66018E 00	4.30382E-01	7.11352E 02	2.73893E 00	9.62921E-01
2-109	2.78429E 00	1.77797E-01	7.30761E 02	1.13149E 00	9.93942E-01
2-108	3.03263E 00	3.65940E-01	7.69461E 02	2.32883E 00	9.78871E-01
2-112	2.58898E 00	1.66254E-01	7.52445E 02	1.05803E 00	9.93869E-01
2-111	3.19403E 00	2.13580E-01	8.01290E 02	1.35921E 00	9.93359E-01
2-113	2.52322E 00	2.26627E-01	7.95588E 02	1.44225E 00	9.88105E-01
2-114	2.78062E 00	3.46736E-01	8.13530E 02	2.20661E 00	9.77479E-01
2-115	3.28964E 00	4.62027E-01	8.44333E 02	2.94032E 00	9.71667E-01
2-118	2.60266E 00	4.31406E-01	8.30903E 02	2.74545E 00	9.61178E-01
2-117	2.90870E 00	5.14433E-01	8.45560E 02	3.27383E 00	9.56176E-01
2-116	3.31431E 00	6.51232E-01	8.73451E 02	4.14441E 00	9.46720E-01

RUN	VELOCITY	Q	QLOST	QNET	Q HEAT
2-60	1.80953E 01	2.32655E 03	1.79177E 02	2.14737E 03	2.15402E 03
2-59	1.14813E 01	2.28964E 03	1.96591E 02	2.09305E 03	2.11865E 03
2-61	1.80953E 01	2.31394E 03	2.07131E 02	2.10681E 03	2.00261E 03
2-62	1.14813E 01	2.28478E 03	2.21539E 02	2.06324E 03	2.02183E 03
2-63	1.80953E 01	2.28203E 03	1.51665E 02	2.13037E 03	2.19494E 03
2-64	1.14813E 01	2.27792E 03	1.71013E 02	2.10691E 03	2.13042E 03
2-107	1.81454E 01	2.49282E 03	1.55102E 02	2.33771E 03	2.31585E 03
2-106	1.50889E 01	2.48089E 03	1.63192E 02	2.31770E 03	2.31256E 03

TABLE A4.3 (CONTINUED)

2-105	1.12809E 01	2.46429E 03	1.77799E 02	2.28649E 03	2.27870E 03
2-110	1.80953E 01	2.48312E 03	1.67923E 02	2.31520E 03	2.27941E 03
2-109	1.51892E 01	2.48826E 03	1.74876E 02	2.31339E 03	2.28768E 03
2-108	1.12809E 01	2.45984E 03	1.88742E 02	2.27110E 03	2.24086E 03
2-112	1.81955E 01	2.42650E 03	1.81953E 02	2.24454E 03	2.19936E 03
2-111	1.12809E 01	2.41090E 03	2.00057E 02	2.21085E 03	2.17272E 03
2-113	1.80953E 01	2.44896E 03	1.96701E 02	2.25226E 03	2.22000E 03
2-114	1.50889E 01	2.43572E 03	2.03424E 02	2.23230E 03	2.22697E 03
2-115	1.12809E 01	2.41655E 03	2.15104E 02	2.20144E 03	2.18002E 03
2-118	1.80953E 01	2.42250E 03	2.09049E 02	2.21345E 03	2.14177E 03
2-117	1.50388E 01	2.41469E 03	2.14739E 02	2.19995E 03	2.14688E 03
2-116	1.12809E 01	2.40142E 03	2.25201E 02	2.17622E 03	2.12325E 03

RUN	Q/A	TWO	TWI	TBULK	H
2-60	1.35231E 05	7.59932E 02	7.52761E 02	6.43156E 02	1.23381E 03
2-59	1.31810E 05	8.10408E 02	8.03802E 02	6.45012E 02	8.30091E 02
2-61	1.32676E 05	8.40961E 02	8.34490E 02	7.36133E 02	1.34892E 03
2-62	1.29932E 05	8.82721E 02	8.76691E 02	7.30810E 02	8.90675E 02
2-63	1.34160E 05	6.80190E 02	6.72542E 02	5.51483E 02	1.10821E 03
2-64	1.32683E 05	7.36269E 02	7.29115E 02	5.56073E 02	7.66768E 02
2-107	1.47218E 05	6.90149E 02	6.81648E 02	5.52769E 02	1.14229E 03
2-106	1.45957E 05	7.13600E 02	7.05358E 02	5.54710E 02	9.68861E 02
2-105	1.43992E 05	7.55939E 02	7.48135E 02	5.57815E 02	7.56578E 02
2-110	1.45800E 05	7.27313E 02	7.19182E 02	5.99480E 02	1.21803E 03
2-109	1.45686E 05	7.47467E 02	7.39486E 02	5.99550E 02	1.04108E 03
2-108	1.43022E 05	7.87657E 02	7.80138E 02	6.02563E 02	8.05419E 02
2-112	1.41350E 05	7.67979E 02	7.60440E 02	6.48706E 02	1.26506E 03
2-111	1.39228E 05	8.20454E 02	8.13411E 02	6.47301E 02	8.38169E 02
2-113	1.41836E 05	8.10728E 02	8.03444E 02	6.93289E 02	1.28761E 03
2-114	1.40579E 05	8.30214E 02	8.23143E 02	6.93626E 02	1.08541E 03
2-115	1.38636E 05	8.64071E 02	8.57348E 02	6.94420E 02	8.50906E 02
2-118	1.39392E 05	8.46519E 02	8.39634E 02	7.33809E 02	1.31720E 03
2-117	1.38542E 05	8.63012E 02	8.56288E 02	7.32052E 02	1.11515E 03
2-116	1.37047E 05	8.93336E 02	8.86902E 02	7.30632E 02	8.76995E 02

DATA FOR RIGHT HALF HEATER

RUN	SLOPE	S.D.(SLOPE)	INTERCEPT	S.D.(INTCP)	CORR. COEFF
2-60	-8.05104E-01	2.11774E 00	7.92119E 02	3.83832E 01	2.26479E-01
2-59	-8.68958E-01	2.50571E 00	8.52771E 02	4.54149E 01	1.90780E-01
2-61	-9.12292E-01	2.32195E 00	8.71636E 02	4.20843E 01	2.23707E-01
2-62	-1.03035E 00	2.73855E 00	9.24532E 02	4.96350E 01	2.19469E-01
2-63	-8.90035E-01	1.86774E 00	7.15703E 02	3.38520E 01	2.67974E-01
2-64	-8.80312E-01	2.16690E 00	7.78505E 02	3.92742E 01	2.19783E-01
2-107	-8.96076E-01	1.96206E 00	7.26731E 02	3.55615E 01	2.63943E-01
2-106	-8.74687E-01	2.14463E 00	7.52648E 02	3.88706E 01	2.29659E-01
2-105	-8.75729E-01	2.39565E 00	7.99068E 02	4.34201E 01	2.09571E-01
2-110	-8.71944E-01	2.05177E 00	7.62931E 02	3.71874E 01	2.42664E-01
2-109	-8.03056E-01	2.21142E 00	7.83728E 02	4.00809E 01	2.03604E-01
2-108	-7.83507E-01	2.47258E 00	8.28612E 02	4.48144E 01	1.80462E-01
2-112	-1.04524E 00	2.25432E 00	8.04174E 02	4.08586E 01	2.56949E-01
2-111	-8.78681E-01	2.50870E 00	8.62643E 02	4.54691E 01	1.99738E-01
2-113	-8.97431E-01	2.39358E 00	8.44273E 02	4.33826E 01	2.10519E-01
2-114	-8.75069E-01	2.47639E 00	8.66059E 02	4.48835E 01	2.09946E-01
2-115	-9.80382E-01	2.71959E 00	9.06774E 02	4.92913E 01	2.17112E-01
2-118	-8.54375E-01	2.40943E 00	8.76807E 02	4.36698E 01	1.83606E-01
2-117	-8.96389E-01	2.53028E 00	8.97437E 02	4.58602E 01	1.93512E-01
2-116	-9.60451E-01	2.76542E 00	9.34026E 02	5.01221E 01	2.00135E-01

TABLE A4.3 (CONTINUED)

RUN	Q/A	TWO	TWI	TBULK	H
2-60	1.50663E 05	7.77628E 02	7.69516E 02	6.59398E 02	1.36820E 03
2-59	1.46320E 05	8.37129E 02	8.29718E 02	6.70141E 02	9.16927E 02
2-61	1.80953E 01	2.55296E 03	2.12049E 02	2.34091E 03	2.22347E 03
2-62	1.14813E 01	2.51065E 03	2.29565E 02	2.28109E 03	2.23267E 03
2-63	1.80953E 01	2.53843E 03	1.58391E 02	2.38004E 03	2.45371E 03
2-64	1.14813E 01	2.49207E 03	1.80117E 02	2.31195E 03	2.33971E 03
2-107	1.81454E 01	2.75241E 03	1.62157E 02	2.59025E 03	2.56766E 03
2-106	1.50889E 01	2.73328E 03	1.71232E 02	2.56205E 03	2.55823E 03
2-105	1.12809E 01	2.69595E 03	1.87240E 02	2.50870E 03	2.50234E 03
2-110	1.80953E 01	2.72649E 03	1.74796E 02	2.55169E 03	2.51287E 03
2-109	1.51892E 01	2.71470E 03	1.82399E 02	2.53230E 03	2.50486E 03
2-108	1.12809E 01	2.67913E 03	1.98005E 02	2.48112E 03	2.44880E 03
2-112	1.81955E 01	2.68538E 03	1.87949E 02	2.49743E 03	2.44681E 03
2-111	1.12809E 01	2.63894E 03	2.09155E 02	2.42979E 03	2.38725E 03
2-113	1.80953E 01	2.68985E 03	2.02701E 02	2.48715E 03	2.45032E 03
2-114	1.50889E 01	2.68143E 03	2.10356E 02	2.47108E 03	2.46367E 03
2-115	1.12809E 01	2.65291E 03	2.23749E 02	2.42917E 03	2.40348E 03
2-118	1.80953E 01	2.67156E 03	2.14193E 02	2.45736E 03	2.37591E 03
2-117	1.50388E 01	2.65691E 03	2.21049E 02	2.43587E 03	2.37485E 03
2-116	1.12809E 01	2.63189E 03	2.33274E 02	2.39861E 03	2.33727E 03

RUN	VELOCITY	Q	QLOST	QNET	Q HEAT
2-60	1.80953E 01	2.57771E 03	1.85282E 02	2.39243E 03	2.39960E 03
2-59	1.14813E 01	2.52928E 03	2.05810E 02	2.32347E 03	2.35136E 03
2-61	1.47419E 05	8.55214E 02	8.47849E 02	7.51244E 02	1.52601E 03
2-62	1.43652E 05	9.05986E 02	8.99196E 02	7.54788E 02	9.94762E 02
2-63	1.49883E 05	6.99683E 02	6.91064E 02	5.68086E 02	1.21879E 03
2-64	1.45595E 05	7.62659E 02	7.54792E 02	5.81230E 02	8.38867E 02
2-107	1.63121E 05	7.10601E 02	7.01132E 02	5.70162E 02	1.24548E 03
2-106	1.61345E 05	7.36904E 02	7.27759E 02	5.75570E 02	1.06016E 03
2-105	1.57986E 05	7.83305E 02	7.74732E 02	5.85197E 02	8.33543E 02
2-110	1.60693E 05	7.47236E 02	7.38213E 02	6.16576E 02	1.32109E 03
2-109	1.59472E 05	7.69273E 02	7.60497E 02	6.19917E 02	1.13438E 03
2-108	1.56249E 05	8.14509E 02	8.06274E 02	6.29396E 02	8.83369E 02
2-112	1.57276E 05	7.85360E 02	7.76850E 02	6.65187E 02	1.40848E 03
2-111	1.53016E 05	8.46827E 02	8.39031E 02	6.73391E 02	9.23789E 02
2-113	1.56629E 05	8.28120E 02	8.19954E 02	7.09962E 02	1.42400E 03
2-114	1.55616E 05	8.50308E 02	8.42362E 02	7.13709E 02	1.20958E 03
2-115	1.52977E 05	8.89128E 02	8.81616E 02	7.20673E 02	9.50503E 02
2-118	1.54753E 05	8.61428E 02	8.53615E 02	7.49962E 02	1.49299E 03
2-117	1.53399E 05	8.81302E 02	8.73711E 02	7.51506E 02	1.25526E 03
2-116	1.51053E 05	9.16737E 02	9.09530E 02	7.56218E 02	9.85264E 02

MEAN PROPERTIES OF THE HEATER SECTION

RUN	Q ELECTRIC	Q THERMAL	ERROR 0/0	MEAN H	BULK T
2-60	4.53980E 03	4.55371E 03	-3.06407E-01	1.23381E 03	6.50839E 02
2-59	4.41652E 03	4.47023E 03	-1.21616E 00	8.30091E 02	6.56921E 02
2-61	4.44772E 03	4.22631E 03	4.97812E 00	1.34892E 03	7.43291E 02
2-62	4.34432E 03	4.25491E 03	2.05828E 00	8.90675E 02	7.42198E 02
2-63	4.51041E 03	4.64857E 03	-3.06309E 00	1.10821E 03	5.59325E 02
2-64	4.41886E 03	4.47012E 03	-1.16002E 00	7.66768E 02	5.68068E 02
2-107	4.92797E 03	4.88344E 03	-9.03501E-01	1.14229E 03	5.61020E 02
2-106	4.87975E 03	4.87074E 03	1.84502E-01	9.68861E 02	5.64618E 02
2-105	4.79520E 03	4.78105E 03	2.94963E-01	7.56578E 02	5.70871E 02
2-110	4.86689E 03	4.79230E 03	1.53259E 00	1.21803E 03	6.07613E 02
2-109	4.84569E 03	4.79260E 03	1.09555E 00	1.04108E 03	6.09273E 02
2-108	4.75222E 03	4.68980E 03	1.31339E 00	8.05419E 02	6.15386E 02

TABLE A4.3 (CONTINUED)

2-112	4.74197E 03	4.64628E 03	2.01794E 00	1.26506E 03	6.56507E 02
2-111	4.64064E 03	4.56021E 03	1.73304E 00	8.38169E 02	6.59731E 02
2-113	4.73941E 03	4.67051E 03	1.45382E 00	1.28761E 03	7.01213E 02
2-114	4.70338E 03	4.69090E 03	2.65319E-01	1.08541E 03	7.03158E 02
2-115	4.63061E 03	4.58389E 03	1.00899E 00	8.50906E 02	7.06901E 02
2-118	4.67082E 03	4.51794E 03	3.27296E 00	1.31720E 03	7.41464E 02
2-117	4.63581E 03	4.52205E 03	2.45408E 00	1.11515E 03	7.41284E 02
2-116	4.57483E 03	4.46097E 03	2.48889E 00	8.76995E 02	7.42803E 02

RUN	DENSITY	MU	MUW	CP	K
2-60	8.84512E-01	5.61885E-01	4.00324E-01	5.68981E-01	3.01272E 00
2-59	8.81882E-01	5.50516E-01	3.44759E-01	5.70653E-01	3.00527E 00
2-61	8.44527E-01	4.21119E-01	3.23966E-01	5.94405E-01	2.89947E 00
2-62	8.44999E-01	4.22448E-01	2.89377E-01	5.94104E-01	2.90081E 00
2-63	9.24092E-01	7.87031E-01	5.07507E-01	5.43814E-01	3.12483E 00
2-64	9.20311E-01	7.60125E-01	4.22746E-01	5.46219E-01	3.11412E 00
2-107	9.23359E-01	7.81706E-01	4.92308E-01	5.44280E-01	3.12275E 00
2-106	9.21803E-01	7.70577E-01	4.55612E-01	5.45270E-01	3.11834E 00
2-105	9.19098E-01	7.51788E-01	3.99993E-01	5.46990E-01	3.11068E 00
2-110	9.03208E-01	6.54103E-01	4.39420E-01	5.57093E-01	3.06567E 00
2-109	9.02489E-01	6.50148E-01	4.13116E-01	5.57550E-01	3.06364E 00
2-108	8.99845E-01	6.35895E-01	3.66833E-01	5.59231E-01	3.05615E 00
2-112	8.82061E-01	5.51279E-01	3.92059E-01	5.70539E-01	3.00578E 00
2-111	8.80667E-01	5.45384E-01	3.36452E-01	5.71426E-01	3.00183E 00
2-113	8.62726E-01	4.77457E-01	3.49339E-01	5.82833E-01	2.95101E 00
2-114	8.61884E-01	4.74598E-01	3.30902E-01	5.83368E-01	2.94863E 00
2-115	8.60265E-01	4.69173E-01	3.02278E-01	5.84398E-01	2.94405E 00
2-118	8.45317E-01	4.23344E-01	3.19595E-01	5.93902E-01	2.90171E 00
2-117	8.45395E-01	4.23564E-01	3.05552E-01	5.93853E-01	2.90193E 00
2-116	8.44738E-01	4.21711E-01	2.82584E-01	5.94271E-01	2.90007E 00

RUN	NUSSELT NO.	PRANDTL NO.	MU/MUW
2-60	2.92181E 02	1.06117E 01	1.40358E 00
2-59	1.97063E 02	1.04534E 01	1.59681E 00
2-61	3.31917E 02	8.63314E 00	1.29989E 00
2-62	2.19060E 02	8.65201E 00	1.45985E 00
2-63	2.53024E 02	1.36967E 01	1.55078E 00
2-64	1.75668E 02	1.33327E 01	1.79807E 00
2-107	2.60977E 02	1.36248E 01	1.58784E 00
2-106	2.21667E 02	1.34742E 01	1.69130E 00
2-105	1.73525E 02	1.32196E 01	1.87950E 00
2-110	2.83462E 02	1.18863E 01	1.48856E 00
2-109	2.42444E 02	1.18320E 01	1.57377E 00
2-108	1.88023E 02	1.16360E 01	1.73347E 00
2-112	3.00274E 02	1.04641E 01	1.40611E 00
2-111	1.99209E 02	1.03819E 01	1.62099E 00
2-113	3.11299E 02	9.42991E 00	1.36674E 00
2-114	2.62626E 02	9.38963E 00	1.43425E 00
2-115	2.06206E 02	9.31315E 00	1.55212E 00
2-118	3.23862E 02	8.66473E 00	1.32463E 00
2-117	2.74164E 02	8.66785E 00	1.38623E 00
2-116	2.15751E 02	8.64154E 00	1.49234E 00

MISCELLANEOUS NUMBERS

0.15178E-03	0.42030E-01	0.43241E-03	0.42030E-01	0.16012E-03	0.42030E-01
0.12031E-02	0.42030E-01	0.17082E-03	0.42030E-01	0.60846E-03	0.42030E-01
0.20000E 02	0.21009E 03	0.47303E 02	0.84380E 01	0.10976E 03	0.22085E 04
0.49625E 03	0.88092E 02	0.11540E 04	0.11245E 03	0.20204E 02	0.25934E 03

TABLE A4.3 (CONTINUED)

0.37537E 01 0.45958E 02 0.60317E 03

RUNS	WILSON SLOPE	INTERCEPT	S.D.(SLOPE)	S.D.(INTCP)	CORR. COEFF
2-60- 2-59	1.01783E-02	5.73876E-06	0.	0.	1.00000E 00
2-61- 2-62	9.84830E-03	-3.73301E-05	0.	0.	1.00000E 00
2-63- 2-64	1.03754E-02	8.20120E-05	0.	0.	1.00000E 00
2-107- 2-105	1.09257E-02	1.58729E-05	1.39613E-04	1.37567E-05	9.99918E-01
2-110- 2-108	1.03495E-02	4.26207E-06	9.84161E-05	9.68591E-06	9.99955E-01
2-112- 2-111	9.83345E-03	1.67375E-05	0.	0.	1.00000E 00
2-113- 2-115	9.77212E-03	8.50662E-06	2.90873E-04	2.86759E-05	9.99557E-01
2-118- 2-116	9.36115E-03	2.19247E-05	1.86886E-04	1.84402E-05	9.99801E-01

RUN	1.0/H	1.0/V**B	REYNOLDS NO	CORRELATION	CONF. LEVEL
2-60	8.10498E-04	7.90660E-02	4.56498E 04	8.66965E 01	7.37794E-01
2-59	1.20469E-03	1.17794E-01	2.94747E 04	5.89267E 01	4.90774E-01
2-61	7.41336E-04	7.90660E-02	5.81555E 04	1.09516E 02	1.87751E 00
2-62	1.12274E-03	1.17794E-01	3.68038E 04	7.21977E 01	8.07445E-01
2-63	9.02353E-04	7.90660E-02	3.40491E 04	6.58416E 01	8.64028E-01
2-64	1.30417E-03	1.17794E-01	2.22771E 04	4.63501E 01	8.39343E-01
2-107	8.75435E-04	7.88747E-02	3.43487E 04	6.80955E 01	8.76730E-01
2-106	1.03214E-03	9.27121E-02	2.89266E 04	5.81700E 01	8.07918E-01
2-105	1.32174E-03	1.19626E-01	2.21018E 04	4.59855E 01	8.30258E-01
2-110	8.20998E-04	7.90660E-02	4.00428E 04	7.93423E 01	6.45830E-01
2-109	9.60538E-04	9.21759E-02	3.37894E 04	6.80212E 01	5.35516E-01
2-108	1.24159E-03	1.19626E-01	2.55825E 04	5.32079E 01	6.45522E-01
2-112	7.90476E-04	7.86843E-02	4.66561E 04	8.97423E 01	8.07172E-01
2-111	1.19308E-03	1.19626E-01	2.91924E 04	5.97791E 01	5.11506E-01
2-113	7.76632E-04	7.90660E-02	5.23988E 04	9.81529E 01	1.26331E 00
2-114	9.21308E-04	9.27121E-02	4.39136E 04	8.29890E 01	8.03072E-01
2-115	1.17522E-03	1.19626E-01	3.31482E 04	6.54349E 01	5.80696E-01
2-118	7.59188E-04	7.90660E-02	5.79040E 04	1.06658E 02	1.80878E 00
2-117	8.96742E-04	9.29827E-02	4.81030E 04	9.02735E 01	1.21836E 00
2-116	1.14026E-03	1.19626E-01	3.62133E 04	7.11513E 01	7.99068E-01

NU=0.00720$ 1.0605E-03*(RE**0.87630$ 1.3129E-02)*(PR**0.51439$ 2.1832E-02)*

(MU/MUW** 0. $ 0.) RMS DEV.= 1.232 O/O CORRELATION COEF=0.9984

RUNS	WILSON SLOPE	INTERCEPT	S.D.(SLOPE)	S.D.(INTCP)	CORR. COEFF
2-60- 2-59	9.10540E-03	-8.74398E-05	0.	0.	1.00000E 00
2-61- 2-62	8.81017E-03	-1.27488E-04	0.	0.	1.00000E 00
2-63- 2-64	9.28170E-03	-1.29714E-05	0.	0.	1.00000E 00
2-107- 2-105	9.78925E-03	-8.64053E-05	8.62435E-05	1.03733E-05	9.99961E-01
2-110- 2-108	9.27422E-03	-9.27671E-05	4.52860E-05	5.44107E-06	9.99988E-01
2-112- 2-111	8.80196E-03	-7.37115E-05	0.	0.	1.00000E 00
2-113- 2-115	8.75722E-03	-8.31681E-05	2.22787E-04	2.68100E-05	9.99677E-01
2-118- 2-116	8.38835E-03	-6.58307E-05	1.35342E-04	1.62999E-05	9.99870E-01

RUN	1.0/H	1.0/V**B	REYNOLDS NO	CORRELATION	CONF. LEVEL
2-60	8.10498E-04	9.86160E-02	4.56498E 04	1.13589E 02	0.
2-59	1.20469E-03	1.41908E-01	2.94747E 04	7.70730E 01	0.
2-61	7.41336E-04	9.86160E-02	5.81555E 04	1.40140E 02	0.
2-62	1.12274E-03	1.41908E-01	3.68038E 04	9.24096E 01	0.
2-63	9.02353E-04	9.86160E-02	3.40491E 04	8.88207E 01	0.
2-64	1.30417E-03	1.41908E-01	2.22771E 04	6.23342E 01	0.
2-107	8.75435E-04	9.83981E-02	3.43487E 04	9.18059E 01	0.
2-106	1.03214E-03	1.14044E-01	2.89266E 04	7.83248E 01	0.
2-105	1.32174E-03	1.43921E-01	2.21018E 04	6.17837E 01	0.
2-110	8.20998E-04	9.86160E-02	4.00428E 04	1.05312E 02	0.

TABLE A4.3 (CONCLUDED)

2-109	9.60538E-04	1.13442E-01	3.37894E 04	9.02377E 01	0.
2-108	1.24159E-03	1.43921E-01	2.55825E 04	7.04514E 01	0.
2-112	7.90476E-04	9.81813E-02	4.66561E 04	1.17392E 02	0.
2-111	1.19308E-03	1.43921E-01	2.91924E 04	7.81265E 01	0.
2-113	7.76632E-04	9.86160E-02	5.23988E 04	1.26874E 02	0.
2-114	9.21308E-04	1.14044E-01	4.39136E 04	1.07221E 02	0.
2-115	1.17522E-03	1.43921E-01	3.31482E 04	8.44621E 01	0.
2-118	7.59188E-04	9.86160E-02	5.79040E 04	1.36540E 02	0.
2-117	8.96742E-04	1.14348E-01	4.81030E 04	1.15570E 02	0.
2-116	1.14026E-03	1.43921E-01	3.62133E 04	9.10576E 01	0.

NU=0.02104$ 0. *(RE**0.80000$ 0.)*(PR**0.40000$ 0.)*

(MU/MUW** 0. $ 0.) RMS DEV.= 2.079 0/0 CORRELATION COEF=0.9948

9. The number of temperature entries in the thermal conductivity-temperature-MWH table.
10. The number of MWH entries in the test heater resistance-temperature-MWH table.
11. The number of temperature entries in the test heater resistance-temperature-MWH table.
12. The number of MWH entries in the heat loss-temperature-MWH table.
13. The number of temperature entries in the heat loss-temperature-MWH table.
14. The number of entries in the millivolt-temperature table for the thermocouples.
15. The number of thermocouples being used for the temperature profile measurements, including inlet and outlet thermocouples and wall thermocouples. Five wall thermocouples in each half heater are used in this work.
16. The number of millivolt entries at which thermocouple corrections are to be given.
17. The number of entries in the slope of the flowmeter calibration curve-MWH table.
18. The number of entries in the intercept of the flowmeter calibration curve-MWH table.
19. A repeat control. If the constant is >0, the computer will begin from the beginning of the program again after completing analysis of the present group of data. If it is ≤ 0, the computer will halt upon completion of analysis of the present group of data. In this way, if more data are to be analyzed with different physical property or other "constant" data, the computer can be instructed to read in the new "constant" data.
20. The number of different dimensionless correlations to be performed by the computer.
21. A punch control. If the constant is ≤ 0, a punched record of the output will appear along with the pointed record. If it is >0, only the printed output will be given.
22. The number of entries in the test heater table (see below).

The second table must supply the following information:

1. The inner diameter of test heater.
2. The allowable error in per cent between Q_{in} and Q_{th}. The 100% in Table A4.2 is used so that no data should be rejected on account of the heat imbalance.
3. A constant unused at present, but room must be made for it.
4. The conversion factor used in Eq. (A4.12) for the calculation of fluid velocity from the volumetric flow rate. The value of 0.407 applies for D in inches, g in gpm and velocity in ft/sec.
5. The conversion factor used in Eq. (A4.10) in calculating the heat transfer coefficient U. The value of 312.9 applies for Q_{in} in watts, D in inches, L in inches, temperatures in °F and U in Btu/(hr)(ft^2)(°F).
6. The conversion factor used Eq. (A4.9) in calculating Q_{th}. The value of 146.8 applies for G in gpm, ρ in gm/cc, C_p in cal/(gm)(°C), T's in °F, Q_{in} in watts.
7. The conversion factor used to make the Nusselt number dimensionless. For an inner diameter of 0.207" (A4.2), h_f in $\frac{\text{Btu}}{(\text{hr})(\text{ft}^2)(°\text{F})}$, and k in $\frac{\text{cal}}{(\text{sec})(\text{cm})(°\text{C})} \times 10^4$, the Nusselt number is given by

$$\text{Nu} = 0.713 \frac{h_f}{k} \qquad \text{(A4.39)}$$

8. The conversion factor used to make the Prandtl number dimensionless. For μ in centipoises and k in $\frac{\text{cal}}{(\text{cm})(\text{sec})(°\text{C})} \times 10^4$, the Prandtl number is given by

$$\text{Pr} = 100 \frac{C_p \mu}{k} \qquad \text{(A4.40)}$$

9. The conversion factor used to make the Reynolds number dimensionless. For v in ft/sec, ρ in gm/cc, D = 0.207" and μ in centipoises, the Reynolds number is given by

$$\text{Re} = 1602 \frac{v\rho}{\mu} \qquad \text{(A4.41)}$$

10. The constant used in Eq. (A4.4) in front of Q. As stated in Section A4.1, this constant is 1.22 for the units used.

11. The constant used in Eq. (A4.4) in front of Q_{in}. As stated in Section A4.1, this constant is −4.61 for the units used.
12. and 13. The constants a and b in the relation $k_s = a + bT$ for the thermal conductivity of stainless steel. For the data of McAdams (A4.3)

$$k_s = 8.52 + 0.0042T \ \frac{\text{Btu}}{(\text{hr})(\text{ft})(°\text{F})} \qquad \text{(A4.42)}$$

14. The value of the correlation coefficient below which the temperature profile data are considered too scattered for the heat transfer coefficient to be meaningful. For five data points (the number of wall thermocouples used in each half heater), Spiegel (A4.6) tabulates that there is about one chance in twenty that a random set of points will yield a correlation coefficient of 0.8 in a linear least squares analysis, so r = 0.8 was chosen as the 95% confidence limit cutoff in the temperature profile data.
15. The values of A, B, C and D for each correlation to be performed by the computer. The computer will refer to the values given only if a given correlation is to have some parameter fixed. The selection of fixed parameters or least squared parameters will be given in a later table (see below). However, no matter what the choice below, values must be provided for every correlation to be performed.

The third table must supply the coolant density information for the program as a function of temperature and MWH. The program will perform a two-dimensional linear interpolation to obtain $\rho^* = \rho(T^*, MWH^*)$, where T* and MWH* are the values of the independent variables at which ρ is desired, so that a grid of values must be supplied. The order must be T_1, ρ_{11}, ρ_{12}, $\cdots$ $\rho_{1,NR1}$, T_2, ρ_{21}, ρ_{22} $\cdots$ $\rho_{2,NR1}$ $\cdots$ T_{NR2}, $\rho_{NR2,1} \cdots \rho_{NR2,NR1}$, MWH_1, MWH_2 $\ldots$ MWH_{NR1}; ρ_{ij} refers to the value of ρ at T_i, MWH_j and NR1 is the number of MWH entries, NR2 the number of temperature entries. The interpolation routine will not extrapolate and interpolates only on an open interval, so that the span of the table must be large enough to include all possible data. For instance, Table A4.2 lists −0.001 MWH as the first MWH entry to ensure

that 0 MWH is within the table.

The fourth table must supply the coolant viscosity information to the program in the same manner as the density table. The functional relation used is $\ln \mu = f\left(\frac{1}{(T+460)}, MWH\right)$. No matter what the units of μ, $\ln \mu$ may be fed directly into the program for immediately upon interpolation, the program will exponentiate the result.

The next two tables supply coolant specific heat and thermal conductivity information to the computer in the same manner as the density table. These tables supply $C_p = C_p(T,MWH)$, and $k = k(T, MWH)$, respectively. Notice that, in case there is to be no MWH dependence, there must still be one MWH entry, viz., 0 MWH, and the dependence on temperature will be given for this entry (see Table A4.2 for the C_p data).

The seventh table must give the electrical resistance of the test heater used. The electrical resistance is known to be a function of outside wall temperature (A4.2), but for the sake of generality, it is also assumed a function of reactor MWH. Also, the resistance of each half heater is given separately, even though it has been found that the resistances of each half heater are equal. Thus, the order of input is T_1, R^U_{11}, R^D_{11}, R^U_{12}, $R^D_{12} \cdots R^U_{1,NRES1}$, $R^D_{1,NRES1}$, T_2, R^U_{21}, $R^D_{21} \cdots R^U_{2,NRES1}$, $R^D_{2,NRES1} \cdots T_{NRES2} \cdots R^U_{NRES2,NRES1}$, $R^D_{NRES2,NRES1}$, MWH_1, $MWH_2 \ldots MWH_{NRES1}$. The superscript U refers to the upstream half heater and D refers to the downstream half heater; NRES1 is the number of MWH entries and NRES2 is the number of temperature entries. The same comments regarding interpolation and no MWH dependence apply.

The eighth table supplies the heat loss for a half section of the test heater (heat loss for each half assumed the same at a given temperature) as a function of outside wall temperature and reactor MWH in the same manner as the density table. No MWH dependence may be treated as discussed above.

The ninth table must supply the relation between the thermocouple millivolts and temperature. Chromel-alumel thermocouples have been used for the test heaters in this work. The input order must be T_1, mv_1, T_2, $mv_2 \ldots T_N$, mv_N where N is the number of pairs of entries in this table.

The tenth table is the test heater table and supplies the necessary means of taking into account a change in test heaters during the experiment. This table gives a constant, either +1.0 or −1.0, as a function of MWH. For each heat transfer data point to be analyzed, the computer will refer to the table. If it finds −1.0 corresponding to the MWH of this data point, it will assume that no change in test heaters has taken place. If it finds +1.0, it will assume a change in test heaters and will read in tables giving new information pertinent to the new test heater (see below). A typical profile of the table is shown in Fig. A4.9, with the test heater change indicated at data point $i + 1$. The length of the curve

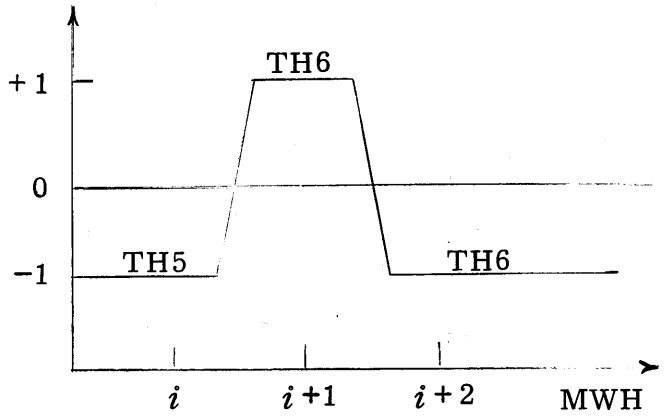

Figure A4.9 Graphic Picture of Test Heater Selector

at +1.0 should be small enough so that only the first data point with the new test heater will yield a +1.0 value when the table is searched (a new set of test heater data has to be read in for each data point giving a +1.0 value!). The order of input is C_1, MWH_1, C_2, MWH_2 . . . C_{NTH}, MWH_{NTH} where NTH is the number of pairs of entries in the test heater table.

The eleventh table gives the thermocouple corrections for the test heater being used. For each millivolt level, the table will supply the actual corrected reading of the thermocouples used in the test heater. The inlet and outlet thermocouples are listed first, then the wall thermocouples for the upstream half heater, then the wall thermocouples for the downstream half heater. Thus, using the thermocouple numbering system

and the wall thermocouples used in this work, the input order would be MV_1, mv_1^I, mv_1^O, mv_1^2, mv_1^3, mv_1^4, mv_1^5, mv_1^6, mv_M^9, mv_M^{10}, mv_M^{11}, mv_M^{12}, mv_M^{13}. For instance, when thermocouple j reads MV_i millivolts, the corrected reading would be mv_i^j millivolts.

The twelfth table supplies the positions of the thermocouples used (in inches for this work). The positions of the inlet and outlet thermocouples are given first and assumed to be located at 0 and L inches, respectively. This assumes no change in bulk temperature between the ends of the test heater and the actual location of the immersion thermocouples, which appears to be reasonable from the wall temperature profile of the test heater (see Fig. A4.1). The positions of the wall thermocouples used are then listed in order, from upstream to downstream, as in the previous table.

The thirteenth table gives the slope of the Potter flowmeter calibration curve as a function of MWH for the sake of generality. The input order must be $SLOPE_1$, MWH_1 . . . $SLOPE_{NG}$, MWH_{NG} where NG is the number of pairs of entries in this table. For no MWH dependence, only one pair of entries need be given.

The fourteenth table gives the intercept of the Potter flowmeter calibration curve as a function of MWH as in the preceding table.

The fifteenth table must supply Student's t for each degree of freedom as tabulated in reference (A4.7). The input order is t_1, t_2 . . . t_{30}, t_{31}, where the subscript refers to the number of degrees of freedom up to 30 and subscript 31 gives t_∞. Table A4.2 gives the 95% confidence limit Student's t table.

The sixteenth table supplies the scale resistance on the test heater wall as a function of MWH. The first card of this table must give the number of pairs of entries in the table and the remaining cards list the functional dependence in the order R_{S1}, MWH_1, R_{S2}, MWH_2 . . . $R_{S,NRS}$, MWH_{NRS}. As shown in Table A4.2, not only is no MWH dependence assumed, but R_S is given as 0. This is the normal situation; the table is included as a generality.

Next, the heat transfer data are to be given the computer, in groups. Within each group, data are usually taken on a given day, at several velocities, and it is important to order these data for the use of Wilson's method (see Section A4.2). The data for each day must be ordered with

the highest flow rate data point first, down to the lowest flow rate data point last. Each group is headed by a "free" card upon which any desired information may be typed, and the computer will head the output with this information. Also, before the actual data can be given, a control table must be given, containing the following information:

1. The number of data points to be analyzed in the present group.
2. For each correlation to be performed, control constants for the parameters A, B, C and D. The function of these control constants is to select whether the parameter will be least squared or fixed. Fixed values are given in the second input table (see above). Table A4.4 gives the use of the control constants.

TABLE A4.4

Use of Control Constants

for Least Squaring or Fixing Parameters A, B, C, D

Parameter	Value of Control Constant		
	< 0	$= 0$	> 0
A, B, C	Least square	Least square	Fix
D	Fix	No $\left(\frac{\mu}{\mu_W}\right)$ dependence	Least square

For instance, in Table A4.2, the first correlation has no $\left(\frac{\mu}{\mu_W}\right)$ dependence and will least square A, B, and C. The second correlation has no $\left(\frac{\mu}{\mu_W}\right)$ dependence and will least square A, fix B and C.

3. A control constant selecting which computed value of h_f to use in the correlation. If the constant is < 0, the value computed for the downstream half heater, h_f^D, will be used. If it is > 0, the value computed for the upstream half heater, h_f^U, will be used. If it equals 0, the average of h_f^U and h_f^D will be used.
4. A control constant selecting which computed heat input will be used in calculating h_f. If the constant is < 0, Q_{th} will be used. If the constant is > 0, Q_{in} will be used. If the constant equals 0, the average of Q_{in} and Q_{th} will be used.

For each data point, the following information must be supplied:

1. The reactor MWH at the time of the run.
2. The flowmeter reading, in gpm.
3. The voltage drop across the upstream half heater.
4. The voltage drop across the downstream half heater.
5. The inlet bulk temperature reading in millivolts.
6. The outlet bulk temperature reading in millivolts.
7. For the first card only, in column 73-78 an alphanumeric description of the run number.
8. The thermocouple readings in millivolts for the wall thermocouples being used, in the order upstream to downstream.

If a data point is the first one run on a new test heater (see test heater table above), immediately after the data for this point, four new tables must be read in. The first supplies new values of:

1. The inner diameter of the test heater.
2. The conversion factor to make the Nusselt number dimensionless (see Eq. (A4.38)).
3. The conversion factor to make the Reynolds number dimensionless (see Eq. A4.40)).

4. and 5. The constants used in front of Q and Q_{loss} in Eq. (A4.4).

The second new table must supply new thermocouple correction data in the same manner as previously described. The third table must give the electrical resistance of the new test heater in the manner previously described. The last new table must give the heat losses from the new test heater in the manner described above.

If it is desired to use new physical property or other constant data after a given number of groups of data (the repeat control being selected above), the computer will return to the very beginning to send in more data and the format must be as described above.

The output needs a little explanation. The first output table lists the temperature profile for each data point. The inlet and outlet temperature are given first, followed by the wall temperatures in the order upstream to downstream.

The next three output tables list results for the upstream half heater (called right half heater) in the same manner as for the upstream half heater.

The mean properties of the test heater as a whole occupy the next three output tables. The only item needing explanation is the column marked "ERROR 0/0" under which the difference between Q_{in} and Q_{th} (based on Q_{in} being correct) is given in per cent.

The table marked "MISCELLANEOUS NUMBERS" lists least squares sums and may be disregarded. The format for the output is given in the subroutine WOT.

For each correlation performed by the computer, the results of Wilson's method applied to each set of data taken on a given day are listed first. The computer gives the least squared slope and intercept together with their standard deviations for each set. (The velocity power dependence is the value of B given by the correlation.) The intercept is the quantity of interest, being equal to the scale resistance (units $(ft^2)(hr)(°F)/Btu$ for this work). Next, the values of $1/h_f$ (equal to 1/U unless a scale resistance is used in the input), $1/v^B$, Re, $Nu/(Pr^C)\left(\frac{\mu}{\mu_W}\right)^D$ and the confidence limits on the latter are listed for each data point. Finally, the over-all correlation of the data is given. The dollar sign is used to signify ± and a standard deviation will be given only if it makes sense, i.e., all parameters least squared. The root-mean-square deviation of the data from the correlation is given in per cent, and the correlation coefficient is also listed.

The loading time for MNHTR in a 7090 type computer is 0.23 minutes and the running time about 0.001 minutes per data point analyzed and for each correlation assumed.

A4.6 Tabulation of Heat Transfer Data

Some of the results produced by MNHTR for all the heat transfer data taken during the course of this experiment, are given in Tables A4.5-A4.10. Tables A4.5 and A4.6 list the results obtained with TH5 at nominal heat fluxes of 200,000 $Btu/(hr)(ft^2)$ and 100,000 $Btu/(hr)(ft^2)$, respectively, during the 610°F irradiation of Santowax OMP. Table A4.7 gives the results obtained with TH6 during the 610°F irradiation of Santowax OMP. Table A4.8 gives the results obtained with TH6 at a nominal heat flux of 130,000 $Btu/(hr)(ft^2)$ during the 750°F irradiation of Santowax OMP and the special runs at constant flow during the 750°F

irradiation are listed in Tables A4.9 and A4.10.

In each table, MU/MUW stands for (μ/μ_W).

A4.7 Tests of the Effect of Hypothetical Scale Resistance on Heat Transfer Correlations

The Nusselt number defined in this work is based on the overall heat transfer coefficient from inside wall to bulk fluid, U. No evidence of any scale resistance on the wall was found, but an investigation of the effect of hypothetical scale resistance on the heat transfer correlations was still pursued.

The relation between U and h_f is given by

$$\frac{1}{U} = \frac{1}{h_f} + R_S \tag{A4.43}$$

$$h_f = av^B \qquad (0.8 < B < 1.0) \tag{A4.44}$$

It can easily be shown for the correlation of results obtained on a single day, when R_S and the physical properties of the coolant would be constant, that a scale resistance would only increase the power dependence of h_f on velocity over that determined for U. Assume that the least squares correlation of the data for a single day yielded

$$U = Cv^D \tag{A4.45}$$

By substitution of the definition of U by Eq. (A4.43) there results

$$h_f = Cv^D \left[\frac{1}{1 - R_S Cv^D}\right] \tag{A4.46}$$

This is an equation of a curve on log-log paper, but if h_f were to be least squared for a power, B, according to Eq. (A4.45), an inspection of Eq. (A4.46) shows that the power dependence would be greater than D.

However, if there were a hypothetical buildup of scale resistance with time, it might be thought possible to obtain a lower Reynolds number power dependence for h_f than for U, since the lower Reynolds number data were, in general, obtained at later times during the irradiation (due to

TABLE A4.5
HEAT TRANSFER DATA FROM TH5 DURING THE 610 DEG. F IRRADIATION OF SANTOWAX OMP
NOMINAL Q/A= 200,000 BTU/HR/FT**2

RUN	REACTOR MWH	VELOCITY FT/SEC	HT COEF, U BTU/HR/FT**2 /DEG. F	NUSSELT NO.	REYNOLDS NO.	PRANDTL NO.	MU/MUW
12	0.	24.6	2415.	653.	101220.	7.12	1.32
13	0.	22.5	2189.	594.	93791.	7.05	1.35
14	0.	20.1	1913.	519.	84181.	7.02	1.40
15	0.	17.6	1659.	451.	74150.	6.99	1.46
16	0.	15.1	1444.	394.	64495.	6.91	1.53
34	442.	21.2	1919.	498.	74350.	8.12	1.44
35	442.	19.1	1741.	453.	67899.	8.03	1.48
36	442.	17.1	1573.	411.	61544.	7.95	1.52
37	442.	15.1	1377.	360.	54465.	7.93	1.60
38	442.	13.1	1210.	317.	48051.	7.82	1.68
44	658.	21.1	1834.	467.	68517.	8.65	1.47
45	658.	19.1	1666.	426.	62759.	8.57	1.51
46	658.	17.1	1489.	381.	56671.	8.51	1.56
47	658.	15.1	1329.	341.	50677.	8.42	1.63
48	658.	13.1	1160.	298.	44471.	8.34	1.71
59	935.	20.9	1722.	429.	61818.	9.34	1.49
60	935.	18.1	1523.	381.	54411.	9.23	1.56
61	935.	16.1	1363.	341.	48886.	9.15	1.63
62	935.	14.1	1190.	298.	43181.	9.08	1.71
63	935.	12.1	1040.	261.	37583.	8.97	1.81
69	1127.	20.9	1721.	422.	57472.	9.94	1.53
70	1127.	18.6	1538.	377.	51585.	9.87	1.58
71	1127.	16.1	1330.	327.	45206.	9.77	1.67
72	1127.	13.6	1143.	282.	38791.	9.63	1.79
73	1127.	11.5	973.	240.	33263.	9.52	1.92
79	1355.	20.6	1618.	389.	52321.	10.63	1.57
80	1355.	18.6	1466.	353.	47839.	10.52	1.63
81	1355.	16.1	1299.	314.	42181.	10.35	1.71
82	1355.	14.1	1137.	275.	37023.	10.32	1.80
83	1355.	12.1	990.	240.	32513.	10.12	1.92
89	1580.	20.5	1566.	370.	47966.	11.40	1.60
90	1580.	18.1	1392.	329.	42884.	11.27	1.67
91	1580.	16.1	1246.	295.	38591.	11.15	1.74
92	1580.	13.6	1049.	249.	33315.	10.94	1.88
93	1580.	11.6	917.	218.	28843.	10.80	2.00
99	1984.	20.6	1566.	372.	46325.	11.96	1.58
100	1984.	18.1	1383.	329.	41043.	11.87	1.66
101	1984.	16.1	1243.	296.	36859.	11.77	1.73
102	1984.	13.8	1117.	266.	31709.	11.73	1.83
103	1984.	11.6	993.	237.	27030.	11.58	1.92
109	2212.	20.5	1503.	354.	41819.	13.10	1.63
110	2212.	18.1	1334.	315.	37402.	12.95	1.70
111	2212.	16.1	1204.	284.	33583.	12.84	1.77

TABLE A4.6
HEAT TRANSFER DATA FROM TH5 DURING THE 610 DEG. F IRRADIATION OF SANTOWAX OMP
NOMINAL Q/A= 100,000 BTU/HR/FT**2

RUN	REACTOR MWH	VELOCITY FT/SEC	HT COEF, U BTU/HR/FT**2 /DEG. F	NUSSELT NO.	REYNOLDS NO.	PRANDTL NO.	MU/MUW
28	280.	20.7	1836.	482.	75903.	7.82	1.21
29	280.	18.1	1607.	423.	66815.	7.78	1.24
30	280.	15.6	1403.	370.	57972.	7.73	1.28
31	280.	13.1	1199.	316.	48727.	7.73	1.33
32	280.	11.1	1014.	268.	41672.	7.66	1.39
33	280.	8.6	804.	213.	32508.	7.62	1.49
39	446.	20.6	1811.	468.	70110.	8.32	1.22
40	446.	18.1	1598.	413.	61932.	8.28	1.25
41	446.	15.1	1364.	353.	51928.	8.24	1.30
42	446.	12.1	1095.	284.	41896.	8.19	1.37
43	446.	8.6	793.	206.	30340.	8.06	1.50
49	662.	20.5	1707.	433.	64577.	8.87	1.24
50	662.	18.1	1515.	384.	57151.	8.85	1.27
51	662.	15.1	1283.	326.	48064.	8.79	1.32
52	662.	12.1	1043.	265.	38790.	8.74	1.39
53	662.	8.6	769.	197.	28231.	8.56	1.51
54	893.	20.1	1618.	403.	58776.	9.44	1.25
55	893.	18.1	1469.	365.	52538.	9.50	1.28
56	893.	16.1	1323.	329.	47129.	9.43	1.32
57	893.	13.1	1092.	273.	38882.	9.32	1.38
58	893.	8.6	749.	188.	26108.	9.13	1.56
64	1030.	20.1	1517.	372.	54555.	10.06	1.26
65	1030.	17.1	1336.	328.	46938.	9.96	1.30
66	1030.	14.1	1119.	275.	39156.	9.86	1.36
67	1030.	11.6	945.	233.	32656.	9.74	1.42
68	1030.	8.6	733.	181.	24424.	9.65	1.54
74	1342.	20.0	1494.	357.	48489.	11.06	1.30
75	1342.	17.6	1334.	319.	43014.	10.99	1.33
76	1342.	15.1	1151.	276.	37579.	10.81	1.38
77	1342.	12.1	949.	228.	30216.	10.77	1.47
78	1342.	8.6	695.	168.	22056.	10.52	1.63
84	1568.	20.0	1452.	342.	45025.	11.78	1.32
85	1568.	17.1	1274.	300.	38990.	11.65	1.36
86	1568.	14.1	1071.	252.	32246.	11.61	1.43
87	1568.	11.6	886.	209.	26783.	11.51	1.51
88	1568.	8.6	682.	161.	20305.	11.28	1.66
94	1976.	20.0	1449.	342.	42931.	12.44	1.30
95	1976.	17.1	1256.	297.	37200.	12.30	1.35
96	1976.	14.1	1061.	251.	30941.	12.20	1.41
97	1976.	11.6	882.	209.	25449.	12.19	1.50
98	1976.	8.6	680.	162.	19394.	11.90	1.66
104	2204.	19.8	1402.	329.	39417.	13.38	1.33
105	2204.	17.1	1217.	286.	34335.	13.27	1.37
106	2204.	14.1	1021.	240.	28333.	13.26	1.44
107	2204.	11.6	864.	203.	23536.	13.14	1.54
108	2204.	8.6	652.	154.	17676.	12.98	1.70
120	2572.	19.6	1350.	313.	34218.	15.16	1.35
121	2572.	17.1	1170.	272.	30084.	15.05	1.40
122	2572.	14.1	993.	231.	24920.	14.99	1.47
123	2572.	11.6	844.	196.	20769.	14.81	1.57

TABLE A4.7
HEAT TRANSFER DATA FROM TH6 DURING THE 610 DEG. F IRRADIATION OF SANTOWAX OMP
NOMINAL Q/A= 100,000 BTU/HR/FT**2

RUN	REACTOR MWH	VELOCITY FT/SEC	HT COEF, U BTU/HR/FT**2 /DEG. F	NUSSELT NO.	REYNOLDS NO.	PRANDTL NO.	MU/MUW
18	0.	19.1	1777.	483.	80537.	6.98	1.42
19	0.	17.1	1580.	431.	72653.	6.94	1.47
20	0.	15.1	1393.	380.	64595.	6.90	1.54
21	0.	13.1	1227.	336.	56726.	6.83	1.61
135	3120.	19.2	1062.	241.	26393.	18.98	1.32
136	3120.	16.6	939.	213.	23006.	18.84	1.36
137	3120.	14.1	819.	186.	19634.	18.75	1.42
138	3120.	11.6	696.	158.	16274.	18.62	1.50
139	3120.	8.6	536.	122.	12275.	18.31	1.67
140	3528.	19.2	1119.	253.	25849.	19.40	1.43
141	3528.	16.6	982.	222.	22494.	19.28	1.49
142	3528.	14.1	855.	194.	19217.	19.18	1.57
143	3528.	11.6	726.	165.	15994.	18.97	1.68
144	3528.	8.6	546.	124.	12078.	18.64	1.92
145	3578.	19.0	1040.	233.	22473.	21.93	1.49
146	3578.	16.6	920.	206.	19781.	21.78	1.54
147	3578.	14.1	804.	180.	16853.	21.71	1.63
148	3578.	11.6	676.	151.	13992.	21.52	1.75
149	3578.	8.6	511.	115.	10562.	21.15	1.99
150	3820.	18.8	987.	219.	20059.	24.17	1.52
151	3820.	16.6	889.	197.	17913.	23.92	1.58
152	3820.	14.1	775.	172.	15389.	23.67	1.67
153	3820.	11.6	648.	144.	12764.	23.48	1.80
154	3820.	8.6	492.	110.	9645.	23.06	2.05
155	3830.	19.5	1104.	246.	21929.	23.07	1.99
156	3830.	19.4	1079.	240.	21388.	23.48	1.90
157	3830.	19.2	1041.	231.	20964.	23.68	1.77
160	3830.	19.0	1030.	229.	20589.	23.84	1.64
158	3830.	16.6	910.	203.	18391.	23.37	1.89
159	3830.	14.1	792.	176.	15837.	23.07	2.04
161	3982.	19.3	1105.	247.	22984.	21.79	1.46
162	3982.	16.6	966.	216.	19882.	21.62	1.53
163	3982.	14.1	851.	191.	17051.	21.43	1.61
164	3982.	11.6	719.	161.	14049.	21.39	1.74
165	3982.	8.6	547.	123.	10726.	20.81	1.96
166	4135.	19.6	1163.	265.	28714.	17.79	1.46
167	4135.	16.6	1017.	232.	24691.	17.54	1.53
168	4135.	14.1	890.	203.	21189.	17.37	1.60
169	4135.	11.6	754.	172.	17417.	17.38	1.72
170	4135.	8.6	571.	131.	13242.	16.97	1.95
171	4820.	19.3	1185.	278.	35445.	14.51	1.38
172	4820.	16.6	1035.	243.	30737.	14.41	1.43
173	4820.	14.1	897.	211.	26223.	14.35	1.49
174	4820.	11.6	763.	180.	21649.	14.29	1.58
175	4820.	8.6	591.	140.	16376.	14.03	1.73
176	4820.	20.3	1326.	313.	38588.	14.09	1.69
177	4820.	17.1	1134.	268.	33047.	13.88	1.79
178	5068.	19.4	1218.	286.	35785.	14.46	1.37
179	5068.	16.6	1066.	251.	30778.	14.39	1.42
180	5068.	14.1	926.	218.	26302.	14.31	1.48
181	5068.	11.6	782.	184.	21753.	14.24	1.56
182	5068.	8.6	599.	141.	16346.	14.05	1.72
183	5372.	19.4	1218.	286.	35630.	14.51	1.37

TABLE A4.7 (CONTINUED)

RUN	REACTOR MWH	VELOCITY FT/SEC	HT COEF, U BTU/HR/FT**2 /DEG. F	NUSSELT NO.	REYNOLDS NO.	PRANDTL NO.	MU/MUW
184	5372.	16.6	1058.	249.	30660.	14.44	1.42
185	5372.	14.1	923.	217.	26179.	14.37	1.48
186	5372.	11.6	777.	183.	21721.	14.25	1.56
187	5372.	8.6	603.	143.	16410.	14.01	1.71
188	5558.	19.4	1202.	282.	35534.	14.55	1.37
189	5558.	16.6	1043.	245.	30620.	14.45	1.42
190	5558.	14.1	910.	214.	26122.	14.39	1.48
191	5558.	11.6	775.	183.	21843.	14.18	1.56
193	5558.	8.6	595.	141.	16440.	13.98	1.71
194	5950.	19.7	1242.	292.	36317.	14.47	1.37
195	5950.	16.6	1066.	251.	30731.	14.41	1.42
196	5950.	14.1	943.	222.	26290.	14.31	1.48
197	5950.	11.6	794.	187.	21856.	14.18	1.56
198	5950.	8.6	615.	145.	16485.	13.95	1.70
199	6090.	19.4	1199.	282.	35802.	14.45	1.38
200	6090.	16.6	1042.	245.	30799.	14.38	1.43
201	6090.	14.1	915.	215.	26256.	14.33	1.49
202	6090.	11.6	773.	182.	21807.	14.20	1.58
203	6090.	8.6	595.	140.	16437.	13.99	1.74
204	6340.	19.5	1270.	298.	35460.	14.66	1.36
205	6340.	16.6	1105.	260.	30357.	14.59	1.41
206	6340.	14.1	965.	227.	25869.	14.54	1.47
207	6340.	11.6	815.	192.	21484.	14.42	1.55
208	6340.	8.6	627.	148.	16249.	14.15	1.70
209	6462.	19.4	1268.	298.	34543.	14.97	1.35
210	6462.	16.6	1104.	259.	29618.	14.93	1.41
211	6462.	14.1	961.	226.	25457.	14.78	1.46
212	6462.	11.6	811.	191.	21070.	14.69	1.54
213	6462.	8.6	629.	149.	15961.	14.40	1.68
215	6782.	18.0	1163.	273.	30884.	15.53	1.38
216	6782.	16.1	1058.	248.	27621.	15.53	1.40
217	6782.	13.6	919.	216.	23458.	15.45	1.46
218	6782.	11.1	768.	181.	19334.	15.31	1.54
219	6782.	8.6	610.	144.	15163.	15.14	1.69
220	6790.	19.4	1194.	280.	32996.	15.66	1.36
221	6790.	16.6	1037.	243.	28369.	15.59	1.41
222	6790.	14.1	911.	214.	24206.	15.52	1.47
223	6790.	11.6	762.	179.	20235.	15.30	1.54
224	6790.	8.6	597.	141.	15328.	15.00	1.68
225	7333.	20.0	1166.	272.	34378.	15.48	1.36
226	7333.	16.6	1015.	238.	29059.	15.23	1.41
227	7333.	14.1	886.	208.	24696.	15.22	1.47
228	7333.	11.6	750.	176.	20556.	15.06	1.55
229	7333.	8.6	568.	134.	15437.	14.87	1.71
230	7739.	19.7	1173.	273.	35689.	14.69	1.39
231	7739.	14.1	898.	210.	26044.	14.43	1.42
232	8007.	18.7	1032.	233.	25374.	18.89	1.57
233	8007.	16.5	924.	208.	22423.	18.86	1.64
234	8007.	14.1	810.	183.	19234.	18.79	1.73
235	8007.	11.6	685.	155.	15876.	18.72	1.87
236	8007.	8.6	527.	119.	11892.	18.53	2.12
237	8007.	5.9	374.	85.	8298.	18.22	2.51
239	8007.	9.9	388.	84.	7540.	31.68	1.36
241	8016.	19.7	1201.	280.	36417.	14.40	1.38
242	8016.	18.5	1141.	266.	34343.	14.34	1.40

TABLE A4.7 (CONTINUED)

RUN	REACTOR MWH	VELOCITY FT/SEC	HT COEF, U BTU/HR/FT**2 /DEG. F	NUSSELT NO.	REYNOLDS NO.	PRANDTL NO.	MU/MUW
243	8016.	16.6	1029.	240.	31026.	14.25	1.44
244	8016.	14.1	898.	210.	26195.	14.32	1.50
245	8016.	11.6	769.	180.	21908.	14.11	1.58
246	8016.	8.6	598.	140.	16618.	13.82	1.71
247	8740.	19.7	1171.	273.	36355.	14.42	1.39
248	8740.	18.6	1109.	258.	34461.	14.37	1.40
249	8740.	16.6	1012.	236.	30943.	14.29	1.44
250	8740.	14.0	889.	208.	26329.	14.22	1.50
251	8740.	11.6	756.	177.	21992.	14.06	1.58
252	8740.	8.6	584.	137.	16563.	13.86	1.72
253	8887.	19.5	1175.	274.	36050.	14.39	1.39
254	8887.	18.1	1063.	248.	33510.	14.38	1.41
255	8887.	16.1	991.	231.	29867.	14.35	1.46
256	8887.	14.1	893.	208.	26470.	14.19	1.50
257	8887.	12.1	784.	183.	22842.	14.12	1.56
258	8887.	9.1	624.	146.	17446.	13.92	1.69
259	8994.	19.4	1168.	272.	35965.	14.36	1.39
260	8994.	17.1	1039.	242.	31908.	14.27	1.43
261	8994.	15.1	947.	221.	28137.	14.29	1.47
262	8994.	13.6	870.	203.	25485.	14.21	1.49
263	8994.	11.1	733.	171.	21105.	14.03	1.59
264	8994.	8.1	566.	133.	15651.	13.81	1.75
265	9285.	19.6	1176.	274.	36082.	14.45	1.39
266	9285.	17.8	1086.	253.	32915.	14.39	1.42
267	9285.	14.8	941.	219.	27495.	14.32	1.48
268	9285.	12.3	805.	188.	23235.	14.11	1.55
269	9285.	10.7	717.	168.	20486.	13.94	1.62
270	9285.	8.4	585.	137.	16038.	13.96	1.72
276	9386.	17.7	1065.	249.	32990.	14.29	1.42
275	9386.	15.6	961.	224.	29197.	14.27	1.47
274	9386.	12.9	813.	190.	24221.	14.19	1.54
273	9386.	10.7	697.	163.	20268.	14.07	1.62
272	9386.	8.4	576.	135.	16179.	13.86	1.74
271	9386.	5.9	429.	101.	11640.	13.54	1.95
286	9541.	20.0	1132.	256.	28472.	18.11	1.49
285	9541.	17.6	1019.	231.	25152.	18.04	1.55
284	9541.	15.9	933.	212.	22857.	17.94	1.60
283	9541.	14.2	850.	193.	20615.	17.84	1.66
282	9541.	13.3	799.	181.	19291.	17.79	1.70
281	9541.	12.0	731.	166.	17501.	17.70	1.76
280	9541.	10.1	632.	144.	14851.	17.56	1.87
279	9541.	8.7	564.	128.	12896.	17.43	1.96
278	9541.	6.5	435.	99.	10078.	16.73	2.18
277	9541.	5.0	342.	78.	8023.	16.43	2.45
292	9741.	17.9	1086.	253.	33016.	14.42	1.42
291	9741.	15.3	956.	223.	28415.	14.33	1.47
290	9741.	12.6	809.	189.	23593.	14.22	1.54
289	9741.	10.7	709.	166.	20324.	14.04	1.61
288	9741.	8.3	584.	137.	16037.	13.89	1.73
287	9741.	5.8	433.	102.	11472.	13.61	1.95
298	10000.	19.1	1145.	267.	35368.	14.37	1.39
297	10000.	15.4	959.	224.	28549.	14.35	1.47
296	10000.	13.3	852.	199.	24905.	14.22	1.52
295	10000.	11.8	777.	182.	22337.	14.14	1.57
294	10000.	9.1	623.	146.	17452.	13.91	1.69

TABLE A4.7 (CONCLUDED)

RUN	REACTOR MWH	VELOCITY FT/SEC	HT COEF, U BTU/HR/FT**2 /DEG. F	NUSSELT NO.	REYNOLDS NO.	PRANDTL NO.	MU/MUW
293	10000.	6.9	496.	116.	13429.	13.72	1.84
299	10160.	13.6	870.	203.	25377.	14.27	1.51
300	10160.	10.1	680.	159.	19243.	14.00	1.64
322	11340.	19.3	1079.	246.	26911.	18.80	1.68
323	11340.	17.0	951.	216.	23091.	19.24	1.74
324	11340.	14.1	825.	188.	19622.	18.77	1.84
325	11340.	10.0	605.	139.	14716.	17.93	1.87
326	11340.	7.6	458.	105.	10862.	18.29	1.70

TABLE A4.8

HEAT TRANSFER DATA FROM TH6 DURING THE 750 DEG. F IRRADIATION OF SANTOWAX OMP

NOMINAL Q/A= 130,000 BTU/HR/FT**2

RUN	REACTOR MWH	VELOCITY FT/SEC	HT COEF, U BTU/HR/FT**2 /DEG. F	NUSSELT NO.	REYNOLDS NO.	PRANDTL NO.	MU/MUW
2-5	37.	21.8	1954.	569.	115430.	5.93	1.19
2-4	37.	17.1	1533.	446.	90253.	5.94	1.25
2-3	37.	15.1	1364.	397.	79993.	5.92	1.28
2-2	37.	13.1	1202.	350.	69350.	5.92	1.31
2-1	37.	11.0	1026.	299.	58082.	5.93	1.37
2-6	286.	21.8	1894.	524.	108080.	6.03	1.22
2-7	286.	18.8	1633.	451.	93107.	6.05	1.25
2-8	286.	15.4	1362.	377.	76667.	6.04	1.30
2-9	286.	12.0	1078.	298.	59377.	6.05	1.38
2-10	286.	10.5	929.	250.	47526.	6.50	1.40
2-14	476.	19.6	1664.	448.	88970.	6.49	1.23
2-13	476.	17.4	1485.	399.	78935.	6.49	1.26
2-12	476.	15.0	1282.	345.	68032.	6.49	1.30
2-11	476.	12.8	1110.	298.	58085.	6.51	1.34
2-19	582.	21.4	1798.	477.	92477.	6.74	1.21
2-18	582.	17.4	1461.	387.	75224.	6.75	1.26
2-17	582.	15.1	1283.	340.	65245.	6.75	1.30
2-16	582.	12.8	1098.	291.	55432.	6.76	1.36
2-15	582.	10.4	852.	223.	42837.	7.01	1.51
2-24	813.	21.3	1738.	446.	82602.	7.38	1.23
2-23	813.	18.6	1525.	392.	72074.	7.39	1.26
2-22	813.	15.6	1291.	331.	60418.	7.39	1.31
2-21	813.	13.0	1094.	281.	50199.	7.40	1.36
2-20	813.	10.5	911.	234.	40553.	7.40	1.43
2-26	830.	20.5	1494.	358.	53711.	10.26	1.27
2-27	830.	11.5	895.	215.	30805.	10.05	1.45
2-31	974.	20.9	1671.	420.	75346.	7.84	1.24
2-30	974.	15.5	1261.	317.	56113.	7.81	1.31
2-29	974.	12.9	1054.	265.	46402.	7.85	1.38
2-28	974.	10.6	891.	224.	38355.	7.84	1.45
2-36	1165.	21.1	1647.	411.	73621.	8.00	1.23
2-35	1165.	18.1	1424.	355.	63078.	8.03	1.27
2-34	1165.	15.3	1145.	284.	51569.	8.23	1.37
2-33	1165.	12.7	1035.	258.	44208.	8.04	1.38
2-32	1165.	10.4	864.	215.	36051.	8.03	1.45
2HT41	1367.	20.5	1555.	380.	64624.	8.77	1.26
2HT40	1367.	18.3	1390.	340.	57771.	8.78	1.29
2HT39	1367.	15.5	1196.	292.	48941.	8.78	1.34
2HT38	1367.	12.6	986.	241.	39671.	8.77	1.41
2HT37	1367.	10.5	840.	205.	33019.	8.78	1.48
2HT46	1562.	19.5	1436.	345.	56101.	9.54	1.29
2HT45	1562.	17.1	1275.	306.	49066.	9.56	1.32
2HT44	1562.	15.1	1140.	274.	43294.	9.56	1.36
2HT43	1562.	12.5	963.	231.	35792.	9.57	1.43
2HT42	1562.	10.6	825.	198.	30325.	9.57	1.50
2HT51	1838.	17.7	1243.	289.	42373.	11.25	1.31
2HT50	1838.	16.0	1131.	263.	38252.	11.27	1.34
2HT49	1838.	13.9	1004.	233.	33296.	11.24	1.39
2HT48	1838.	11.3	834.	194.	27038.	11.25	1.46
2HT47	1838.	8.9	660.	153.	21296.	11.24	1.57
2-53	1992.	15.1	1041.	240.	34953.	11.63	1.33
2-52	1992.	8.9	638.	147.	20390.	11.71	1.51
2-58	2365.	20.9	1524.	375.	67136.	8.64	1.25

TABLE A4.8 (CONCLUDED)

RUN	REACTOR MWH	VELOCITY FT/SEC	HT COEF, U BTU/HR/FT**2 /DEG. F	NUSSELT NO.	REYNOLDS NO.	PRANDTL NO.	MU/MUW
2-57	2365.	17.5	1292.	318.	56339.	8.64	1.30
2-56	2365.	15.2	1133.	279.	48776.	8.64	1.34
2-55	2365.	12.7	961.	236.	40754.	8.63	1.40
2-54	2365.	10.5	828.	204.	33792.	8.61	1.47
2-78	2534.	20.5	1534.	378.	66178.	8.60	1.26
2-77	2534.	19.1	1434.	353.	61589.	8.61	1.28
2-76	2534.	16.1	1227.	302.	51863.	8.61	1.33
2-75	2534.	13.1	1001.	246.	42171.	8.61	1.41
2-74	2534.	10.7	831.	205.	34367.	8.62	1.49
2-83	2947.	18.2	1341.	330.	58651.	8.61	1.30
2-82	2947.	15.9	1206.	297.	51200.	8.61	1.33
2-81	2947.	13.0	1008.	248.	41810.	8.62	1.40
2-80	2947.	10.7	831.	205.	34407.	8.62	1.48
2-88	3338.	20.8	1490.	367.	66915.	8.63	1.27
2-87	3338.	18.3	1325.	326.	58972.	8.61	1.30
2-86	3338.	15.7	1159.	285.	50660.	8.60	1.35
2-85	3338.	13.3	1008.	248.	42987.	8.61	1.40
2-84	3338.	10.6	817.	201.	34118.	8.61	1.49
2-93	3530.	20.8	1475.	363.	67000.	8.62	1.27
2-92	3530.	18.1	1305.	321.	58266.	8.62	1.31
2-91	3530.	15.7	1155.	284.	50690.	8.62	1.35
2-90	3530.	13.0	977.	241.	41948.	8.62	1.41
2-89	3530.	10.7	814.	200.	34381.	8.62	1.50
2-123	3678.	20.8	1503.	370.	67097.	8.61	1.27
2-122	3678.	18.1	1334.	328.	58554.	8.60	1.30
2-121	3678.	15.3	1152.	284.	49326.	8.61	1.35
2-120	3678.	13.2	998.	246.	42532.	8.61	1.41
2-119	3678.	10.7	828.	204.	34486.	8.60	1.49

TABLE A4.9
SPECIAL RUNS AT CONSTANT FLOW USING TH6
750 DEG. F IRRADIATION OF SANTOWAX OMP
NOMINAL Q/A= 130,000 BTU/HR/FT**2

RUN	REACTOR MWH	VELOCITY FT/SEC	HT COEF, U BTU/HR/FT**2 /DEG. F	NUSSELT NO.	REYNOLDS NO.	PRANDTL NO.	MU/MUW
2-60	2425.	18.1	1234.	292.	45650.	10.61	1.40
2-59	2425.	11.5	830.	197.	29475.	10.45	1.60
2-61	2425.	18.1	1349.	332.	58156.	8.63	1.30
2-62	2425.	11.5	891.	219.	36804.	8.65	1.46
2-63	2425.	18.1	1108.	253.	34049.	13.70	1.55
2-64	2425.	11.5	767.	176.	22277.	13.33	1.80
2-107	3599.	18.1	1142.	261.	34349.	13.63	1.59
2-106	3599.	15.1	969.	222.	28927.	13.47	1.69
2-105	3599.	11.3	757.	174.	22102.	13.22	1.88
2-110	3599.	18.1	1218.	283.	40043.	11.89	1.49
2-109	3599.	15.2	1041.	242.	33789.	11.83	1.57
2-108	3599.	11.3	805.	188.	25583.	11.64	1.73
2-112	3599.	18.2	1265.	300.	46656.	10.46	1.41
2-111	3599.	11.3	838.	199.	29192.	10.38	1.62
2-113	3599.	18.1	1288.	311.	52399.	9.43	1.37
2-114	3599.	15.1	1085.	263.	43914.	9.39	1.43
2-115	3599.	11.3	851.	206.	33148.	9.31	1.55
2-118	3599.	18.1	1317.	324.	57904.	8.66	1.32
2-117	3599.	15.0	1115.	274.	48103.	8.67	1.39
2-116	3599.	11.3	877.	216.	36213.	8.64	1.49

TABLE A4.10
SPECIAL RUNS AT CONSTANT FLOW USING TH6
750 DEG. F IRRADIATION OF SANTOWAX OMP
NOMINAL Q/A= 45,000 BTU/HR/FT**2

RUN	REACTOR MWH	VELOCITY FT/SEC	HT COEF, U BTU/HR/FT**2 /DEG. F	NUSSELT NO.	REYNOLDS NO.	PRANDTL NO.	MU/MUW
2-65	2425.	18.1	838.	187.	27239.	16.68	1.23
2-67	2425.	15.1	724.	162.	22937.	16.54	1.28
2-66	2425.	11.5	576.	129.	17609.	16.41	1.35
2-68	2425.	18.1	806.	178.	24137.	18.58	1.29
2-69	2425.	15.1	686.	152.	20269.	18.47	1.34
2-70	2425.	11.6	551.	122.	15666.	18.35	1.41
2-71	2425.	18.1	934.	213.	33181.	14.01	1.22
2-73	2425.	15.1	804.	183.	27957.	13.88	1.25
2-72	2425.	11.7	645.	147.	21688.	13.86	1.31
2-96	3599.	18.1	835.	186.	26456.	17.12	1.25
2-95	3599.	15.0	706.	157.	22050.	17.06	1.29
2-94	3599.	11.3	553.	123.	16691.	16.94	1.37
2-99	3599.	18.1	900.	202.	29457.	15.60	1.21
2-98	3599.	15.1	761.	171.	24476.	15.61	1.25
2-97	3599.	11.3	592.	133.	18393.	15.54	1.32
2-100	3599.	18.1	922.	210.	32822.	14.15	1.19
2-101	3599.	15.1	784.	178.	27527.	14.07	1.22
2-102	3599.	11.3	613.	140.	20667.	14.02	1.29
2-104	3599.	18.1	987.	228.	37422.	12.61	1.24
2-103	3599.	11.3	669.	154.	23182.	12.68	1.35

the increase in the coolant viscosity) than the higher Reynolds number data. A buildup of scale would tend to give a greater increase in the Nusselt numbers (converting from U to h_f) at the lower Reynolds numbers than at the higher Reynolds numbers, thus lowering the power dependence for h_f over that found for U. Two tests were thus applied to the measured heat transfer data. Using the data obtained at a nominal heat flux of 10^5 Btu/(hr)(ft^2) with TH5 during the 610°F irradiation (see Table A4.6), least squares analyses were applied using h_f under two conditions:

1. A constant $R_S = 1 \times 10^{-4}$ (hr)(ft^2)(°F)/Btu over the period that these data were obtained. This scale resistance amounted to a maximum of 10% in the measured overall resistance to heat transfer during this period.
2. A linear increase in R_S from zero to 1×10^{-4} (hr)(ft^2)(°F)/Btu over the period that these data were obtained.

The first test caused the least squares value of B to increase from 0.93 (Table 6.3 in Section 6.3.1) to 1.04, and the second test caused an increase to 0.99.

Thus, it was concluded that the effect of any scale resistance on the heat transfer walls would be to increase the Reynolds number power dependence above the values reported in this work.

APPENDIX A5

REFERENCES

A5. 1 References for Chapter 1

(1. 1) R. O. Bolt and J. G. Carroll, editors, Radiation Effects on Organic Materials, Chapter 8, Academic Press, New York, 1963.

(1. 2) S. Berg et al. ,"Irradiations of Santowax OMP at the Curtiss-Wright Research Reactor," NAA-SR-TDR-5892, Atomics International, Canoga Park, Calif. , January, 1961.

(1. 3) R. H. J. Gercke, "Surface Film Formation in Organic Reactors," NAA-SR-memo-7328 (Rev. 1), Atomics International, Canoga Park, Calif. , May, 1962.

(1. 4) D. T. Morgan and E. A. Mason, "The Irradiation of Santowax OMP in the M. I. T. In-Pile Loop," parts I and II, MITNE-21 (IDO-11, 104) and MITNE-22 (IDO-11, 105), Dept. of Nuclear Engineering, M. I. T. , Cambridge, Mass. , May, 1962.

(1. 5) T. H. Bates, W. G. Burns et al. , "The Radiation and Thermal Stability of Some Potential Organic Moderator Coolants, part II: Pile Irradiation of Para-Terphenyl and Santowax R," AERE C/R 2185, Atomic Energy Research Establishment, Harwell, England, July, 1959.

(1. 6) T. H. Bates, W. G. Burns et al. , "The Radiation and Thermal Stability of Some Potential Organic Moderator Coolants, part V: Pile and Electron Irradiation of Biphenyl, Orthoterphenyl, Metaterphenyl, and Pile Irradiation of Santowax R to High HBR Content," AERE-R 3743, Atomic Energy Research Establishment, Harwell, England, March, 1962.

(1.7) M. Van der Venne, "Behaviour of Organic Coolants at High Temperature and Under Pile-Radiations," EUR/C/3463/62 e, Brussels, September, 1962.

(1.8) R. T. Keen et al., "Radiolysis Products of Polyphenyl Coolants, part I: In-Pile Loop Irradiations," NAA-SR-4355, Atomics International, Canoga Park, Calif., March, 1962.

(1.9) J. F. Zack, Jr., S. Berg and N. M. Ewbank, "In-Pile Capsule Experiments to determine the Effect of Fast Neutrons on the Radiolytic Decomposition Rate of Terphenyls," NAA-SR-7395, Atomics International, Canoga Park, Calif., May, 1963.

(1.10) Annual Technical Progress Report, AEC Unclassified Programs, Fiscal year 1961, Section III-C, NAA-SR-6370, Atomics International, Canoga Park, Calif., August, 1961.

(1.11) R. W. Wilkinson and T. H. Bates, "The Radiation and Thermal Stability of Some Potential Organic Moderator Coolants, part III: Thermal Stability of Para-Terphenyl and Santowax R," AERE-M 412, Atomic Energy Research Establishment, Harwell, England, August, 1959.

(1.12) Annual Technical Progress Report, AEC Unclassified Programs, Fiscal Year 1962, Section III-C, NAA-SR-7400, Atomics International, Canoga Park, Calif., August, 1962.

(1.13) A. Houllier and J. R. Puig, "Stabilité Thermique et Radiolytique des Triphényles," Énergie Nucléaire, 4, no. 5, pp. 343-351, October, 1962.

(1.14) D. G. Kuper, "Organic Coolant Degradation Studies," IDO-16851, Phillips Petroleum Co., Idaho Falls, Idaho, March, 1963.

(1.15) T. H. Bates, W. G. Burns, et al., "The Radiation and Thermal Stability of Some Potential Organic Moderator Coolants, part VI: The Effect of Temperature on the Radiolysis of Biphenyl, Isopropyl Biphenyl, Metaterphenyl and Santowax R," AERE-R 3989, Atomic Energy Research Establishment, Harwell, England, August, 1962.

(1. 16) R. O. Bolt et al., "Relative Effects of Fast Neutrons and Gamma Rays on the Radiolysis of Polyphenyls," California Research AEC Report No. 23, California Research Corporation, Richmond, Calif., June, 1963.

(1. 17) Organic Coolant Reactor Program, Quarterly Report, July 1 - September 30, 1961, IDO-16734, Phillips Petroleum Co., Idaho Falls, Idaho, December, 1961.

(1. 18) M. Van der Venne, "In-Pile Radiolysis of Terphenyls at High Temperature," EUR/C/2368/63 e, Brussels, May, 1963.

(1. 19) R. H. J. Gercke and C. A. Trilling, "A Survey of the Decomposition Rates of Organic Reactor Coolants," NAA-SR-3835, Atomics International, Canoga Park, Calif., June, 1959.

(1. 20) R. W. Bowring and D. A. Garton, "Measurement of the Density of 'Santowax R,' Para-, Meta-, and Ortho-Terphenyl, Diphenyl and Dowtherm A," AERE R/R 2762, Atomic Energy Research Establishment, Harwell, England, December, 1958.

(1. 21) R. H. J. Gercke and G. Asanovich, "Thermo-Physical Properties of Irradiated Polyphenyl Coolants, part I: Density and Viscosity," NAA-SR-4484, Atomics International, Canoga Park, Calif., December, 1960.

(1. 22) R. W. Bowring, G. L. Christie and D. A. Garton, "Measurement of the Viscosity of Santowax 'R', Para-, Meta- and Ortho-Terphenyl, Diphenyl and Dowtherm 'A'," AERE-R 3309, Atomic Energy Research Establishment, Harwell, England, July, 1960.

(1. 23) R. Bessouat et al., "Études Thermiques sur les Caloporteurs Organiques," paper presented at the 7th Nuclear Congress, Rome, June, 1962.

(1. 24) R. W. Bowring, D. A. Garton and H. G. Norris, "Measurement of the Specific Heats of Santowax 'R', Para-, Meta- and Ortho-Terphenyl, Diphenyl and Dowtherm 'A'," AEEW-R 38, Atomic Energy Establishment, Winfrith, England, December, 1960.

(1. 25) H. Ziebland and J. T. A. Burton, "Transport Properties of Some Organic Heat Transfer Fluids," J. Chem and Eng. Data, 6, no. 4, pp. 579-583, October, 1961.

(1.26) Annual Technical Progress Report, AEC Unclassified Programs, Fiscal Year 1961, Section III-C, NAA-SR-6370, Atomics International, Canoga Park, Calif., August, 1961.

(1.27) E.R.G. Eckert and R.M. Drake, Heat and Mass Transfer, 2nd ed., Ch. 8, McGraw-Hill Book Co., New York, 1959.

A5.2 References for Chapter 2

(2.1) D.T. Morgan and E.A. Mason, "The Irradiation of Santowax OMP in the M.I.T. In-Pile Loop," MITNE-21 (IDO-11, 104) and MITNE-22 (IDO-11, 105), Department of Nuclear Engineering, M.I.T., Cambridge, Mass., May, 1962.

(2.2) "Organic Cooled Power Reactor Study," TID-8501, prepared by Bechtel Corporation and Atomics International, March, 1959.

A5.3 References for Chapter 3

(3.1) T.H. Bates, W.G. Burns et al., "The Radiation and Thermal Stability of Some Potential Organic Moderator Coolants, part II: Pile Irradiation of Para-Terphenyl and Santowax R," AERE C/R 2185, Atomic Energy Research Establishment, Harwell, England, July, 1959.

(3.2) S. Berg et al., "Irradiations of Santowax OMP at the Curtiss-Wright Research Reactor: The Effect of Fast Neutrons on Organic Coolants," NAA-SR-TDR-5892, Atomics International, Canoga Park, Calif., January, 1961.

(3.3) D.T. Morgan and E.A. Mason, "The Irradiation of Santowax OMP in the M.I.T. In-Pile Loop, parts I and II, MITNE-21 (DIO-11, 104) and MITNE-22 (IDO-11, 105), Department of Nuclear Engineering, M.I.T., Cambridge, Mass., May, 1962.

(3.4) G.L. Woodruff, "Calorimetric Dosimetry in the M.I.T. Reactor," S.M. Thesis in Nuclear Engineering, M.I.T., Cambridge, Mass., January, 1963.

(3.5) G.C. Nullens, "Calorimetric Measurements in the Central Fuel Position of the MITR at 2 MW," S.M. Thesis in Nuclear Engineering, M.I.T., Cambridge, Mass., August, 1963.

(3. 6) E. Sefchovich-Itzcovich, "Neutron Dose Rates in the M. I. T. Reactor," S. M. Thesis in Nuclear Engineering, M. I. T., Cambridge, Mass., January, 1962.

A5. 4 References for Chapter 4

(4. 1) D. T. Morgan and E. A. Mason, "The Irradiation of Santowax OMP in the M. I. T. In-Pile Loop," parts I and II, MITNE-21 (IDO-11, 104) and MITNE-22 (IDO-11, 105), Department of Nuclear Engineering, M. I. T., Cambridge, Mass., May, 1962.

(4. 2) T. H. Bates, W. G. Burns et al., "The Radiation and Thermal Stability of Some Potential Organic Moderator Coolants, part I: Electron Irradiation of Para-Terphenyl and Santowax R," AERE C/R 2121, Atomic Energy Research Establishment, Harwell, England, May, 1957.

(4. 3) Annual Technical Progress Report, AEC Unclassified Programs, Fiscal Year 1961, Section III-C, NAA-SR-6370, Atomics International, Canoga Park, Calif., August, 1961.

(4. 4) R. Bessouat et al., "Études Thermiques sur les Caloporteurs Organiques," paper presented at the 7th Nuclear Congress, Rome, June, 1962.

(4. 5) T. H. Bates, W. G. Burns et al., "The Radiation and Thermal Stability of Some Potential Organic Moderator Coolants, part V: Pile and Electron Irradiation of Biphenyl, Ortho-terphenyl, Metaterphenyl, and Pile Irradiation of Santowax R to High HBR Content," AERE-R 3743, Atomic Energy Research Establishment, Harwell, England, March, 1962.

(4. 6) R. T. Keen et al., "Radiolysis Products of Polyphenyl Coolants, part I: In-Pile Loop Irradiations," NAA-SR-4355, Atomics International, Canoga Park, Calif., March, 1962.

(4. 7) M. Van der Venne, "Behaviour of Organic Coolants at High Temperature and Under Pile-Radiations," EUR/C/3463/62 e, Brussels, September, 1962.

(4.8) W. D. Mackintosh, "The Electron Irradiation of the Potential Organic Coolant for Power Reactors, Santowax O-M," paper presented at the Third Conference on Nuclear Reactor Chemistry, Gatlinburg, Tenn., October, 1962.

(4.9) J. G. Zack, Jr., S. Berg and N. M. Ewbank, "In-Pile Capsule Experiments to determine the Effect of Fast Neutrons on the Radiolytic Decomposition Rate of Terphenyls," NAA-SR-7395, Atomics International, Canoga Park, Calif., May, 1963.

(4.10) R. W. Wilkinson and T. H. Bates, "The Radiation and Thermal Stability of Some Potential Organic Moderator Coolants, part III: Thermal Stability of Para-Terphenyl and Santowax-R," AERE-M 412, Atomic Energy Research Establishment, Harwell, England, August, 1959.

(4.11) Annual Technical Progress Report, AEC Unclassified Programs, Fiscal Year 1962, Section III-C, NAA-SR-7400, Atomics International, Canoga Park, Calif., August, 1962.

(4.12) A. Houllier and J. R. Puig, "Stabilité Thermique et Radiolytique des Triphényles," Énergie Nucléaire, 4, no. 5, pp. 343-351, October, 1962.

(4.13) D. G. Kuper, "Organic Coolant Degradation Studies," IDO-16851, Phillips Petroleum Co., Idaho Falls, Idaho, March, 1963.

(4.14) M. Van der Venne, "In-Pile Radiolysis of Terphenyls at High Temperature," EUR/C/2368/63 e, Brussels, May, 1963.

(4.15) W. G. Burns et al., "The Radiation and Thermal Stability of Some Potential Organic Moderator Coolants, part VI: The Effect of Temperature on the Radiolysis of Biphenyl, Isopropyl Biphenyl, Metaterphenyl and Santowax R," AERE-R 3989, Atomic Energy Research Establishment, Harwell, England, August, 1962.

(4.16) Organic Coolant Reactor Program, Quarterly Report, July 1-September 30, 1961, IDO-16734, Phillips Petroleum Co., Idaho Falls, Idaho, December, 1961.

(4.17) R. O. Bolt et al., "Relative Effects of Fast Neutrons and Gamma Rays on the Radiolysis of Polyphenyls," California Research AEC Report No. 23, California Research Corp., Richmond, Calif., June, 1963.

(4.18) R.D. Evans, The Atomic Nucleus, McGraw-Hill Book Co., New York, 1955.

(4.19) W.N. Bley, "An In-Pile Loop Study of the Performance of Polyphenyl Reactor Coolant," NAA-SR-2470, Atomics International, Canoga Park, Calif., September, 1958.

(4.20) C.F. Walther and F. Rossillion, Centre D'Études Nucléaires de Grenoble, France, personal communication to Prof. E.A. Mason, June 26, 1961.

(4.21) R.H.J. Gercke and C.A. Trilling, "A Survey of the Decomposition Rates of Organic Reactor Coolants," NAA-SR-3835, Atomics International, Canoga Park, Calif., June, 1959.

(4.22) S. Berg et al., "Irradiations of Santowax OMP at the Curtiss-Wright Research Reactor," NAA-SR-TDR-5892, Atomics International, Canoga Park, Calif., January, 1961.

(4.23) A.R. Anderson and R.J. Waite, "The Calorimetric Measurement of Energy Absorption from Reactor Radiation in BEPO," AERE C/R 2253, Atomic Energy Research Establishment, Harwell, England, March, 1960.

(4.24) T.H. Bates, W.G. Burns et al., "The Radiation and Thermal Stability of Some Potential Organic Moderator Coolants, part II: Pile Irradiation of Para-Terphenyl and Santowax R," AERE C/R 2185, Atomic Energy Research Establishment, Harwell, England, July, 1959.

A5.5 References for Chapter 5

(5.1) D.T. Morgan and E.A. Mason, "The Irradiation of Santowax OMP in the M.I.T. In-Pile Loop," parts I and II, MITNE-21 (IDO-11, 104) and MITNE-22 (IDO-11, 105), Department of Nuclear Engineering, M.I.T., Cambridge, Mass., May, 1962.

(5.2) R.H.J. Gercke and G. Asanovich, "Thermo-Physical Properties of Irradiated Polyphenyl Coolants, part I: Density and Viscosity," NAA-SR-4484, Atomics International, Canoga Park, Calif., December, 1960.

(5.3) W.N. Bley, "An In-Pile Loop Study of the Performance of Polyphenyl Reactor Coolants," NAA-SR-2470, Atomics International, Canoga Park, Calif., September, 1958.

(5.4) S. Elberg, Centre D'Études Nucléaires de Grenoble, France, personal communication to W.N. Bley, March 11, 1963.

(5.5) R. Bessouat et al., "Études Thermiques sur les Caloporteurs Organiques," paper presented at the 7th Nuclear Congress, Rome, June, 1962.

(5.6) R.W. Bowring and D.A. Garton, "Measurement of the Density of 'Santowax R', Para-, Meta-, and Ortho-Terphenyl, Diphenyl and Dowtherm A," AERE R/R 2762, Atomic Energy Research Establishment, Harwell, England, December, 1958.

(5.7) T.H. Bates, W.G. Burns et al., "The Radiation and Thermal Stability of Some Potential Organic Moderator Coolants, part V: Pile and Electron Irradiation of Biphenyl, Orthoterphenyl, Metaterphenyl, and Pile Irradiation of Santowax R to High HBR Content," AERE-R 3743, Atomic Energy Research Establishment, Harwell, England, March, 1962.

(5.8) Quarterly Technical Progress Report, AEC Unclassified Programs, October - December 1961, Section III-C, NAA-SR-6999, Atomics International, Canoga Park, Calif., February, 1962.

(5.9) R.W. Bowring, G.L. Christie and D.A. Garton, "Measurement of the Viscosity of Santowax 'R', Para-, Meta- and Ortho-Terphenyl, Diphenyl and Dowtherm 'A'," AERE-R 3309, Atomic Energy Research Establishment, Harwell, England, July, 1960.

(5.10) W.H. Yanko, Monsanto Research Corporation, Dayton, Ohio, personal communications to B.J. Gudzinowicz, April 8, 1963, June 11, 1963 and June 18, 1963.

(5.11) H. Mondin, Centre D'Études Nucléaires de Grenoble, France, personal communication to Prof. E.A. Mason, May 14, 1963.

(5.12) R.W. Bowring, D.A. Garton and H.F. Norris, "Measurement of the Specific Heats of Santowax 'R', Para-, Meta- and Ortho-Terphenyl, Diphenyl and Dowtherm 'A'," AEEW-R 38, Atomic Energy Establishment, Winfrith, England, December, 1960.

(5. 13) Annual Technical Progress Report, AEC Unclassified Programs, Fiscal Year 1962, Section III-C, NAA-SR-7400, Atomics International, Canoga Park, Calif., August, 1962.

(5. 14) H. Ziebland and J. T. A. Burton, "Transport Properties of Some Organic Heat Transfer Fluids," J. Chem.and Eng. Data, 6, no. 4, pp. 579-583, October, 1961.

(5. 15) Annual Technical Progress Report, AEC Unclassified Programs, Fiscal year 1961, Section III-C, NAA-SR-6370, Atomics International, Canoga Park, Calif., August, 1961.

(5. 16) Annual Technical Progress Report, AEC Unclassified Programs, Fiscal Year 1960, Section III-C, NAA-SR-5350, Atomics International, Canoga Park, Calif., August, 1960.

(5. 17) R. H. J. Gercke, "Surface Film Formation in Organic Reactors," NAA-SR-memo-7328 (Rev. 1), Atomics International, Canoga Park, Calif., May, 1962.

(5. 18) G. T. Furukawa et al., "Calorimetric Properties of Diphenyl Ether from 0 - 570°K," J. Res. Nat. Bur. Standards, 46, no. 3, March, 1951.

A5. 6 References for Chapter 6

(6. 1) D. T. Morgan and E. A. Mason, "The Irradiation of Santowax OMP in the M. I. T. In-Pile Loop," parts I and II, MITNE-21 (IDO-11, 104) and MITNE-22 (IDO-11, 105), Department of Nuclear Engineering, M. I. T., Cambridge, Mass., May, 1962.

(6. 2) W. H. McAdams, Heat Transmission, 3rd ed., Ch. 9, McGraw-Hill Book Co., New York, 1954.

(6. 3) E. R. G. Eckert and R. M. Drake, Heat and Mass Transfer, 2nd ed., Ch. 8, McGraw-Hill Book Co., New York, 1959.

(6. 4) J. P. Stone, C. T. Ewing and R. R. Miller, "Heat Transfer Studies on Some Stable Organic Fluids in a Forced Convection Loop," J. Chem. and Eng. Data, 7, no. 4, pp. 519-529, October, 1962.

(6. 5) R. Bessouat et al., "Études Thermiques sur les Caloporteurs Organiques," paper presented at the 7th Nuclear Congress, Rome, June, 1962.

(6. 6) M. Silverberg and D. A. Huber, "Forced Convection Heat Transfer Characteristics of Polyphenyl Reactor Coolants," NAA-SR-2796, Atomics International, Canoga Park, Calif., January, 1959.

(6. 7) R. H. J. Gercke, "Surface Film Formation in Organic Reactors," NAA-SR-memo-7328 (Rev. 1), Atomics International, Canoga Park, Calif., May, 1962.

(6. 8) Excerpts from AECL Progress Reports, October 1 - December 31 1962, PR-CM-32 (Section 7) and PR-RRD-32, Chemistry and Metallurgy Division, AECL, Chalk River, Ontario.

(6. 9) A. R. Bancroft, AECL Chemistry and Metallurgy Division, Chalk River, Ontario, personal communication to W. N. Bley, December 4, 1962.

(6. 10) D. H. Charlesworth, AECL Chemistry and Metallurgy Division, Chalk River, Ontario, personal communication to Prof. E. A. Mason, May 9, 1963.

A5. 7 References for Appendix A1

(A1. 1) G. L. Woodruff, "Calorimetric Dosimetry in the M. I. T. Reactor," S. M. Thesis in Nuclear Engineering, M. I. T., Cambridge, Mass., January, 1963.

(A1. 2) D. T. Morgan and E. A. Mason, "The Irradiation of Santowax OMP in the M. I. T. In-Pile Loop," parts I and II, MITNE-21 (IDO-11, 104) and MITNE-22 (IDO-11, 105), Department of Nuclear Engineering, M. I. T., Cambridge, Mass., May, 1962.

(A1. 3) G. C. Nullens, "Calorimetric Measurements in the Central Fuel Position of the MITR at 2 MW," S. M. Thesis in Nuclear Engineering, M. I. T., Cambridge, Mass., August, 1963.

(A1. 4) G. H. Kaiz, "Measurement of the Gamma Ray Spectra and its Relative Intensity at the M. I. T. Reactor," S. B. Thesis in Physics, M. I. T., Cambridge, Mass., June, 1960.

(A1. 5) Reference Manual, 709/7090 FORTRAN Programming System, IBM publication, 1961.

(A1. 6) A. Turrichia, "Dose Rate Measurements by Means of Adiabatic Calorimeters and a Miniature Ionization Chamber," S. M. Thesis in Nuclear Engineering, M. I. T., Cambridge, Mass., January, 1962.

(A1. 7) H. Etherington, Editor, Nuclear Engineering Handbook, p. 2-2, McGraw-Hill Book Co., New York, 1958.

(A1. 8) S. Untermeyer and J. T. Weills, "Heat Generation in Irradiated Uranium," AECD-3454, 1952.

(A1. 9) E. Sefchovich-Itzcovich, "Neutron Dose Rates in the M. I. T. Reactor," S. M. Thesis in Nuclear Engineering, M. I. T., Cambridge, Mass., January, 1962.

(A1. 10) J. B. Trice et al., "A Series of Thermal, Epithermal and Fast Neutron Flux Measurements in the MTR," ORNL-CF-55-10-140, Oak Ridge National Laboratory, Oak Ridge, Tenn., October, 1955.

(A1. 11) B. E. Watt, "Energy Spectrum of Neutrons from Thermal Fission of U^{235}," Phys. Rev., 87, p. 1037, 1957.

(A1. 12) R. Dahlberg et al., "Measurements of Some Resonance Activation Integrals," J. Nuc. Eng., 14, no. 1, p. 53, April, 1961.

(A1. 13) R. J. Howerton, "Tabulated Neutron Cross Sections, 0.001 - 14.5 Mev," UCRL 5226, University of California Radiation Laboratory, May, 1959.

(A1. 14) T. O. Passell and R. L. Heath, "Cross Sections of Threshold Reactions for Fission Neutrons: Nickel as a Fast Flux Monitor," J. Nuc. Sci. and Eng., 10, pp. 308-315, August, 1961.

(A1. 15) L. Gonzales, J. Rapaport and J. J. Van Loef, "Ni^{58} (n, p) Co^{58} Cross Section for Neutrons of Energies Between 2.2 and 3.6 Mev," Phys. Rev., 120, no. 4, p. 1319, 1960.

(A1. 16) I. L. Preiss and R. W. Fink, "New Isotopes of Cobalt; Activation Cross Sections of Nickel, Cobalt, and Zinc for 14.8 Mev Neutrons," Nuc. Phys., 15, pp. 326-336, 1960.

(A1. 17) "Reactor Development Program Progress Report," ANL-6580, Argonne National Laboratory, Argonne, Ill., June, 1962.

(A1. 18) J. F. Barry, "The Cross Section of the ^{58}Ni (n, p) ^{58}Co Reaction for Neutrons in the Energy Range 1.6 to 14.7 MeV," J. Nuc. Energy, 16, no. 10, pp. 467-472, October, 1962.

(A1. 19) R. E. Bullock and R. G. Moore, "Odd-Even Dependence of Nuclear Level Density Parameters," Phys. Rev., 119, pp. 721-731, 1960.

(A1. 20) D. J. Hughes and R. B. Schwartz, "Neutron Cross Sections," BNL 325, Brookhaven National Laboratory, Upton, N. Y., July, 1958.

(A1. 21) B. P. Bayhurst and R. J. Prestwood, "(n, 2n), (n, p) and (n,α) Excitation Functions of Several Nuclei from 7. 0 to 19. 8 Nev," LA 2493, Los Alamos Scientific Laboratory, Los Alamos, N. M., 1961.

(A1. 22) J. Moteff, "Neutron Flux and Spectrum Measurement with Radioactivants," Nucleonics, 20, no. 12, pp. 56-60, December, 1962.

(A1. 23) I. S. Sokolnikoff and R. M. Redheffer, Mathematics of Physics and Modern Engineering, Ch. 9, McGraw-Hill Book Co., New York, 1958.

(A1. 24) K. Parker, "Neutron Cross-Sections of Carbon in the Energy Range 0. 025 eV - 15 MeV," AWRE O-71/60, Atomic Weapons Research Establishment, Aldermaston, England, August, 1961.

(A1. 25) K. Parker, "Neutron Cross-Sections of Beryllium in the Energy Range 0. 025 eV - 15 MeV," AWRE O-27/60, Atomic Weapons Research Establishment, Aldermaston, England, September, 1960.

A5. 8 References for Appendix A2

(A2. 1) D. T. Morgan and E. A. Mason, "The Irradiation of Santowax OMP in the M. I. T. In-Pile Loop," parts I and II, MITNE-21 (IDO-11, 104) and MITNE-22 (IDO-11, 105), Department of Nuclear Engineering, M. I. T., Cambridge, Mass., May, 1962.

(A2. 2) J. H. TeStrake, "Separation and Recycle of Irradiated Coolant in M. I. T. Organic Loop," S. B. Thesis in Chemical Engineering, M. I. T., Cambridge, Mass., May, 1962.

(A2. 3) M. Tomlinson, AECL Chemistry and Metallurgy Division, Chalk River, Ontario, personal communication to Prof. E. A. Mason, June 19, 1963.

(A2. 4) P. F. Russo, Controls for Radiation, Inc., Cambridge, Mass., personal communications to W. N. Bley, February 19, 1963 and March 12, 1963.

(A2. 5) H. S. Mickley, T. K. Sherwood and C. E. Reed, Applied Mathematics in Chemical Engineering, 2nd ed., Ch. 2, McGraw-Hill Book Co., New York, 1957.

(A2. 6) M. R. Spiegel, Theory and Problems of Statistics, Schaum's Outline Series, Schaum Publishing Co., New York, 1961.

(A2. 7) A. Wald, "The Fitting of Straight Lines if Both Variables are Subject to Error," Ann. Math. Stat., pp. 284-300, September, 1940.

(A2. 8) C. D. Hodgman, Editor, Standard Mathematical Tables, 12th ed., Chemical Rubber Publishing Co., Cleveland, Ohio, 1959.

(A2. 9) Reference Manual, 709/7090 FORTRAN Programming System, IBM publication, 1961.

(A2. 10) R. W. Wilkinson and T. H. Bates, "The Radiation and Thermal Stability of Some Potential Organic Moderator Coolants, part III: Thermal Stability of Para-Terphenyl and Santowax-R," AERE-M 412, Atomic Energy Research Establishment, Harwell, England, August, 1959.

(A2. 11) Annual Technical Progress Report, AEC Unclassified Programs, Fiscal Year 1962, Section III-C, NAA-SR-7400, Atomics International, Canoga Park, Calif., August, 1961.

(A2. 12) A. Houllier and J. R. Puig, "Stabilité Thermique et Radiolytique des Triphényles," Énergie Nucléaire, 4, no. 5, pp. 343-351, October, 1962.

(A2. 13) D. G. Kuper, "Organic Coolant Degradation Studies," IDO-16851, Phillips Petroleum Co., Idaho Falls, Idaho, March, 1963.

(A2. 14) Quarterly Technical Progress Report, AEC Unclassified Programs, October-December 1962, Section III-B, NAA-SR-8080, Atomics International, Canoga Park, Calif., February, 1963.

(A2. 15) J. R. Puig, D. Rosier and A. Houllier, "Radiolyse et Pyrolyse des Triphēnyles Á Haute Temperature," paper presented at the 7th Nuclear Congress, Rome, June, 1962.

A5. 9 References for Appendix A3

(A3. 1) D. T. Morgan and E. A. Mason, "The Irradiation of Santowax OMP in the M. I. T. In-Pile Loop," parts I and II, MITNE-21 (IDO-11, 104) and MITNE-22 (IDO-11, 105), Department of Nuclear Engineering, M. I. T., Cambridge, Mass., May, 1962.

(A3. 2) C. D. Hodgman, Editor, Handbook of Chemistry and Physics, 44th ed., Chemical Rubber Publishing Co., Cleveland, Ohio, 1962.

(A3. 3) Reference Manual, 709/7090 FORTRAN Programming System, IBM publication, 1961.

(A3. 4) W. H. Yanko, Monsanto Research Corporation, Dayton, Ohio, personal communications to B. J. Gudzinowicz, April 8, 1963, June 11, 1963 and June 18, 1963.

(A3. 5) S. Elberg, Centre D'Études Nucléaires de Grenoble, France, personal communication to W. N. Bley, March 11, 1963.

(A3. 6) H. Mondin, Centre D'Etudes Nucleaires de Grenoble, France, personal communication to Prof E. A. Mason, May 14, 1963.

(A3. 7) R. Pasternak, P. Brady and H. Ermantrant, "An Instrument for the Fast and Precise Determination of Molecular Weights," paper presented at the ACHEMA 13th Chemical Engineering Congress, Frankfort am Main, June, 1961.

A5. 10 References for Appendix A4

(A4. 1) T. J. Swierzawski, "Effect of In-Pile Irradiation on Heat Transfer Character of Santowax OMP," S. M. Thesis in Nuclear Engineering, M. I. T., Cambridge, Mass., January, 1962.

(A4. 2) D. T. Morgan and E. A. Mason, "The Irradiation of Santowax OMP in the M. I. T. In-Pile Loop," parts I and II, MITNE-21 (IDO-11, 104) and MITNE-22 (IDO-11, 105), Department of Nuclear Engineering, M. I. T., Cambridge, Mass., May, 1962.

(A4. 3) W. H. McAdams, Heat Transmission, 3rd ed., McGraw-Hill Book Co., New York, 1954.

(A4. 4) I. S. Sokolnikoff and R. M. Redheffer, Mathematics of Physics and Modern Engineering, Appendix A, McGraw-Hill Book Co., New York, 1958.

(A4. 5) Reference Manual, 709/7090 FORTRAN Programming System, IBM publication, 1961.

(A4. 6) M. R. Spiegel, Theory and Problems of Statistics, Schaum's Outline Series, Schaum Publishing Co., New York, 1961.

(A4. 7) C. D. Hodgman, Editor, Standard Mathematical Tables, 12th ed., Chemical Rubber Publishing Co., Cleveland, Ohio, 1959.

APPENDIX A6
NOMENCLATURE

A = constant.

A = inside surface area of test heater wall, ft^2.

A_j = atomic or molecular weight of species j.

A_i = chromatograph area of component i.

Act = absolute activity per atom of flux detectors, dis/sec. Appears also with subscript B (bare foil) and subsequent Cd (cadmium covered foil).

a = constant.

B = constant.

b = constant.

C = constant.

C, C_i = concentration of component i in a mixture, wt % or weight fraction. Subscript i refers most frequently to ortho-, meta-, para- or total terphenyl.

$C_{i,j}$ = calculated concentration of component i in sample j.

C, C_b = measured count rate of a detector and of the background respectively, dis/sec.

$C_1 \ldots C_6$ = number of carbon atoms in a radiolytic gas component.

C_p, C_p^j = specific heat of material j, cal/(gm)(^oC).

C_v = viscometer calibration constant, (centipoises)(cc)/(gm)(sec).

c = constant.

$c_{i,j}$ = measured concentration of component i in sample j.

c = molarity of a component in solution, gm/1000 gm solvent.

D = constant.

D = total absorbed dose, watt-hr.

D = inner diameter of test heater, inches.

DP = degradation products. That fraction of the irradiated coolant which is not terphenyls.

d = constant.

E = neutron energy, ev or Mev.

E_c = cadmium cutoff energy, ev.

E_{eff} = effective threshold energy of a threshold detector, Mev.

E_{th} = actual threshold energy of a threshold detector, Mev.

ΔE = activation energy, kcal/mole.

e = constant.

F, F_T = total in-pile dose rate factor, (watt)(hr)(cm^3)/(MWH)(gm).

F_N = in-pile dose rate factor due to fast neutron interactions, (watt)(hr)(cm^3)/(MWH)(gm).

F_γ = in-pile dose rate factor due to gamma ray interactions, (watt)(hr)(cm^3)/(MWH)(gm).

f = constant.

f = fraction of operating power after reactor shutdown.

f_i = "f" factor for gas chromatograph measurements on component i.

f_N = fraction of absorbed dose due to fast neutron interactions.

f_γ = fraction of absorbed dose due to gamma ray interactions.

$G(-i)$ = radiolytic decomposition yield of component i in the coolant, expressed as molecules of component i degraded/100 ev absorbed in the total coolant, where i refers to ortho-terphenyl (o-ϕ_3), meta-terphenyl (m-ϕ_3), para-terphenyl (p-ϕ_3) or total terphenyl (omp).

$G(\rightarrow HB)$ = radiolytic production yield of HB in the coolant, expressed as equivalent molecules of omp degraded to form HB/100 ev absorbed in the total coolant.

$G(\rightarrow LIB)$ = radiolytic production yield of LIB in the coolant, expressed as equivalent molecules of omp degraded to form LIB/100 ev absorbed in the total coolant.

$G^*(-i) = G(-i)/C_i$

$G^*(\rightarrow HB) = G(\rightarrow HB)/C_{omp}$.

$G^*(\rightarrow LIB) = G(\rightarrow LIB)/C_{omp}$.

$G_N(-i)$ = decomposition yield of component i in the coolant for fast neutron interactions.

$G_\gamma(-i)$ = decomposition yield of component i in the coolant for gamma ray interactions.

$G(\text{gas } i)$ = radiolytic gas generation yield for gaseous component i, expressed as molecules of gaseous component i generated per 100 ev absorbed in the total coolant. Subscript i refers to hydrogen (H_2); methane (C_1); ethane and ethylene (C_2); propane and propylene (C_3); butanes and butenes (C_4); pentanes, pentenes, hexanes and hexenes (C_{5+6}); benzene, toluene and xylene (Aromatics); or total gas.

$G_N(\text{total gas})$ = total radiolytic gas generation yield for fast neutron interactions.

G_γ (total gas) = total radiolytic gas generation yield for gamma ray interactions.

G = volumetric flow rate, gallons/min.

g = constant.

g_i = average fraction of neutron energy lost per collision with nuclide i, equal to $2A_i/(A_i + 1)^2$. Subscript i refers to hydrogen (H), carbon (C), beryllium (Be) or aluminum (Al).

g(E) = attenuation factor.

H = height of fluid in pycnometer, cm.

HB = high boilers. Those fractions of irradiated coolant having higher boiling points than that of para-terphenyl.

h = constant.

h_f = film coefficient of convective heat transfer, $Btu/(hr)(ft^2)(^oF)$.

I_i = energy transfer integral for nuclide i, watts/atom. Subscript i refers to hydrogen (H), carbon (C) beryllium (Be) or aluminum (Al).

I(E) = intensity of gamma field, $photons/(cm^2)(sec)(Mev)$.

K = constant.

K = conversion factor, 0.0387 $(watt)(^oC)(min)/(^oF)(cal)$.

k = thermal conductivity of the irradiated coolant, $cal/(cm)(sec)(^oC)$.

k_s = thermal conductivity of stainless steel test heater tube, $Btu/(hr)(ft)(^oF)$.

$k_{i,n}$ = n^{th} order liquid degradation reaction constant for component i. in the coolant, gm/(watt)(hr).

$k_{p,i}$ = first order pyrolytic reaction constant for component i in the coolant, hr^{-1}.

L = length of test heater, inches.

L_L = distance of the bottom of the in-pile capsule from the reactor core center, inches.

L_U = distance of the top of the in-pile capsule from the reactor core center, inches.

L_T = distance of the top of the in-pile assembly from the reactor core center, inches.

LIB = low and intermediate boilers. Those fractions of the irradiated coolant having boiling points equal to or less than those of the terphenyls (w/o DP – w/o HB = w/o LIB).

M = mass of coolant, grams.

M,M_{loop} = circulating mass of coolant in the loop, grams.

M_o = circulating mass constant, grams, defined by $M_{loop} = M_o + M^*$.

M^* = relative circulating mass of coolant in the loop, grams, set equal to zero at that time during the irradiation when there is the least amount of circulating coolant in the loop.

M_{out} = the amount of circulating coolant in the out-of-pile section of the loop, grams.

MW_N = number average molecular weight, grams/gram mole.

MWH = period of reactor operation, megawatt-hours.

N = number of data points in a group.

N = number of atoms in a flux detector.

N_i = number of atoms per gram of nuclide i.

N_o = Avagadro's number, molecules/gram mole.

N(E) = number of photons of energy E per fission and per Mev emitted on fission and by fission product decay.

Nu = Nusselt number = UD/k.

n = reaction order.

omp = ortho-, meta-, and para-terphenyl.

P = reactor power level, MW.

Pr = Prandtl number, $C_p\mu/k$.

p = constant.

p = pressure, psia.

Q = electrical heat generated in a half section of a test heater, watts.

Q_{loss} = heat loss from a half section of a test heater, watts.

$Q_{in} = Q - Q_{loss}$ = net heat input to coolant in a half section of a test heater, watts and Btu/hr.

Q_{th} = heat gain by coolant in a half section of a test heater, watts, measured by temperature rise of coolant.

q = constant.

R = universal gas constant, kcal/(gram mole)(^{o}R).

R = electrical resistance of a half section of a test heater, ohms.

ΔR = electrical resistance change in the sample thermistor during a number average molecular weight measurement, ohms.

R_S = scale resistance to heat transfer, (hr)(ft^2)(^{o}F)/Btu.

Re = Reynolds number, $Dv\rho/\mu$.

R_T^j = total dose rate in material j, watts/gm. Subscript j refers to Santowax OMP (SW), polyethylene (PE), polystyrene (PS), carbon (C), beryllium (Be) or aluminum (Al).

R_N^j = fast neutron dose rate in material j, watts/gm.

R_γ^j = gamma ray dose rate in material j, watts/gm.

R_{th}^j = thermal neutron dose rate in material j, watts/gm.

R_{Cd} = cadmium ratio.

r = correlation coefficient.

r = radius, inches.

S = conversion factor, 1.6×10^{-43}(cm^2)(watt)(sec)/(barn)(ev).

s = gas solubility, (std. cc)/(gm)(psia).

T = irradiation time for flux detectors, min.

T = temperature, ^{o}F and ^{o}R.

T_B = bulk temperature of coolant in test heater, ^{o}F.

T_B^I = inlet bulk temperature of coolant to test heater, ^{o}F.

T_B^O = outlet bulk temperature of coolant from test heater, ^{o}F.

T_W^O = outside wall temperature of test heater, ^{o}F.

T_W^I = inside wall temperature of test heater, ^{o}F.

t = time.

t = Student's t.

U = heat transfer coefficient, Btu/(hr)(ft^2)(^oF), from inside test heater wall to bulk coolant.

V = volume, cc.

$V_{i,\ rem}^{undis}$ = volume of undissolved gaseous component i removed from the loop via gas samples, std. cc.

$V_{i,\ rem}^{dis}$ = volume of dissolved gaseous component i removed from the loop via liquid samples, std. cc.

$V_{i,\ accum}^{undis}$ = volume of undissolved gaseous component i accumulated in the loop, std. cc.

$V_{i,\ accum}^{dis}$ = volume of dissolved gaseous component i accumulated in the loop, std. cc.

ΔV = voltage drop through a half section of a test heater, volts.

v = velocity, ft/sec.

W = sample or detector weight, grams.

W_j = statistical weighting factor to be applied to data point j.

$w = \ln (\mu/\mu_W)$.

w/o = weight percent.

X_i = weight of component i in a chromatograph sample.

$X(E)$ = fission neutron spectrum, n/(cm^2)(sec)(ev).

x = volume per unit length of in-pile capsule, cc/inch.

$x = \ln Re$.

x_j = j^{th} data point for independent variable.

Y_j = calculated value of dependent variable at data point x_j.

y_j = measured value of dependent variable at data point x_j.

y = surge tank gage glass level, inches.

$y = \ln Nu$.

Z_i = atomic charge of nuclide i.

Z_j = calculated value, $\ln Y_j$.

z_j = measured value, $\ln y_j$.

$z = \ln Pr$.

β = beta radiation.

γ = gamma radiation.

Δ = correction factor for G value calculations in steady-state-HB periods, grams.

δ = correction factor for G value calculations in steady-state-HB periods, grams.

$\delta_{p,i}$ = grams of component i in the coolant pyrolyzed in the out-of-pile section.

ϵ = counting efficiency for flux detectors.

κ_a = pair production energy absorption coefficient, cm^{-1}.

λ = disintegration constant for a flux detector, min^{-1}.

μ = total linear absorption coefficient, cm^{-1}.

μ = viscosity, centipoises (cp).

μ_o = constant, cp.

μ_W = coolant viscosity measured at the inside test heater wall temperature, cp.

ρ = density, gm/cc.

Σ = summation sign.

σ, σ^2 = standard deviation and variance respectively.

σ = neutron cross section, barns.

σ_a = Compton linear absorption coefficient, cm^{-1}.

σ_s = elastic scattering neutron cross section, barns.

$\overline{\sigma_{eff}}$ = effective threshold neutron cross section, barns.

σ_{res} = resonance component of neutron cross section, barns.

$\sigma_{1/v}$ = 1/v component of neutron cross section, barns.

σ_{2200} = 2200 meter/sec neutron absorption cross section, barns.

τ = specific dose absorbed by irradiated coolant, watt-hr/gm coolant.

$\phi(E)$ = neutron flux per unit energy, $n/(cm^2)(sec)(ev)$.

$\phi(\geqslant E)$ = integrated fast neutron flux above energy E, $n/(cm^2)(sec)$.

ϕ_o = epithermal neutron flux constant, $n/(cm^2)(sec)$.

ϕ_{2200} = 2200 meter/sec neutron flux, $n/(cm^2)(sec)$.

$\sim$ = approximately.